DEFORMATIONSPROZESSE IN DER ERDE I

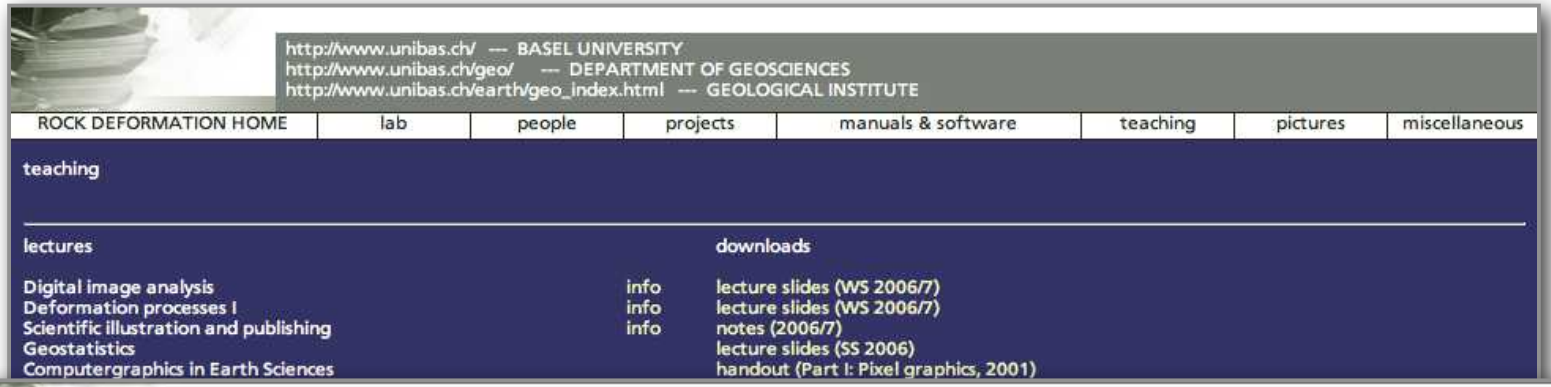

www.unibas.ch/earth/micro/teaching

THEMEN

1	1. Nov. 2006	VL	Introduction - History
2	8. Nov. 2006	VL	Principles of experimental rock deformation
3	15. Nov. 2006	P	Deformation experiment in the brittle field
4	22. Nov. 2006	VL	Mechanics: stress - strain - material properties
5	29. Nov. 2006	VL+P	Data reduction
6	6. Dez. 2006	VL	Failure criteria - Mohr Coulomb - Griffith
7	13. Dez. 2006		fällt aus - Themen für Essays
8	20. Dez. 2006		MIDTERM
9	10. Jan. 2007	VL	Friction - Earth quakes
10	17. Jan. 2007	P	Grain size - Fractals - shape
11	24. Jan. 2007	VL	Brittle - Ductile
12	31. Jan. 2007	P	Cataclasis - Healing - Faulting - B/D
13	7. Feb. 2007	VL	Flow laws - Deformation mechanism maps
14	14. Feb. 2007	Ue	Final Discussion EVALUATION
	7. März 2007		Abgabe Essay

I
Intro - History

Processes

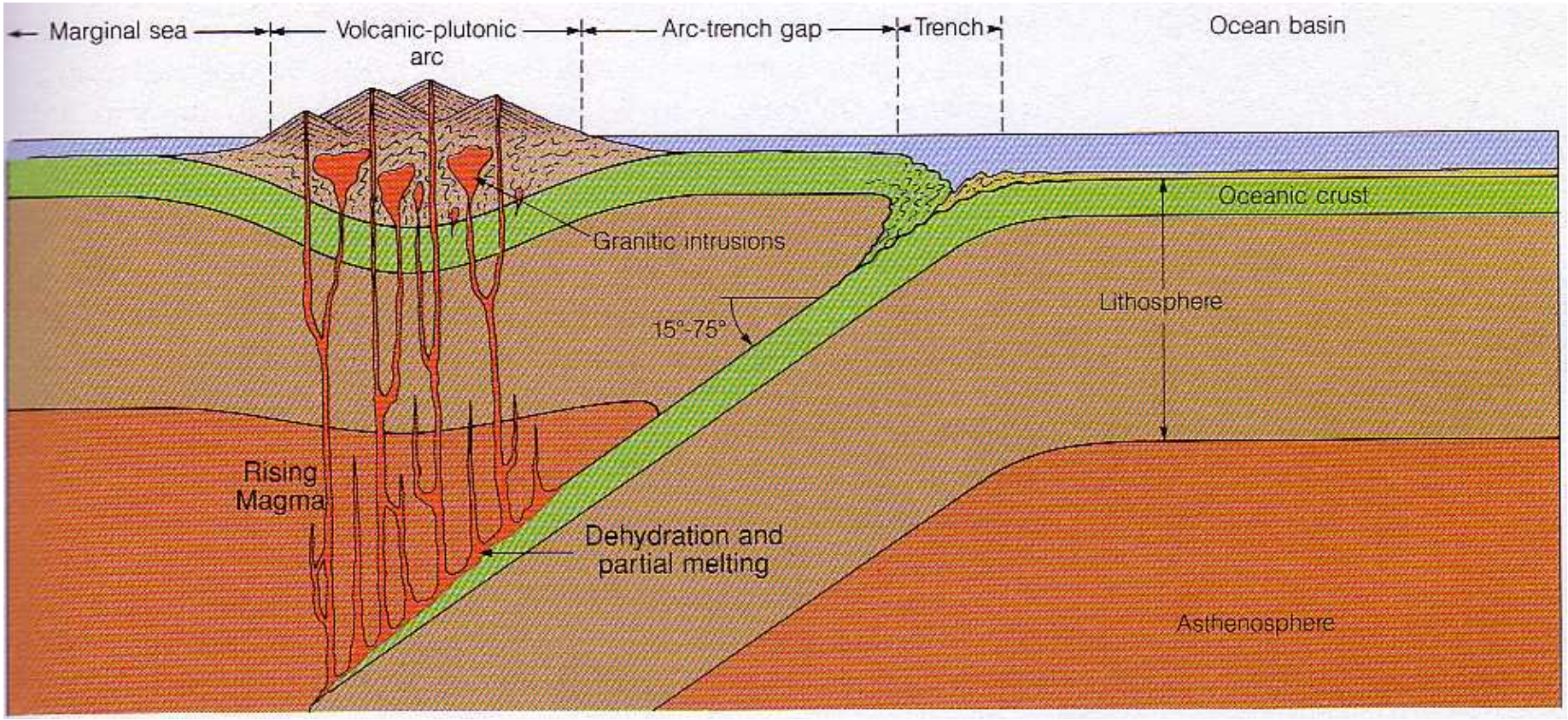
Marginal sea
Volcanic-plutonic arc
Arc-trench gap
Trench
Ocean basin
Oceanic crust
Granitic intrusions
15°-75°
Lithosphere
Rising Magma
Dehydration and partial melting
Asthenosphere

Properties

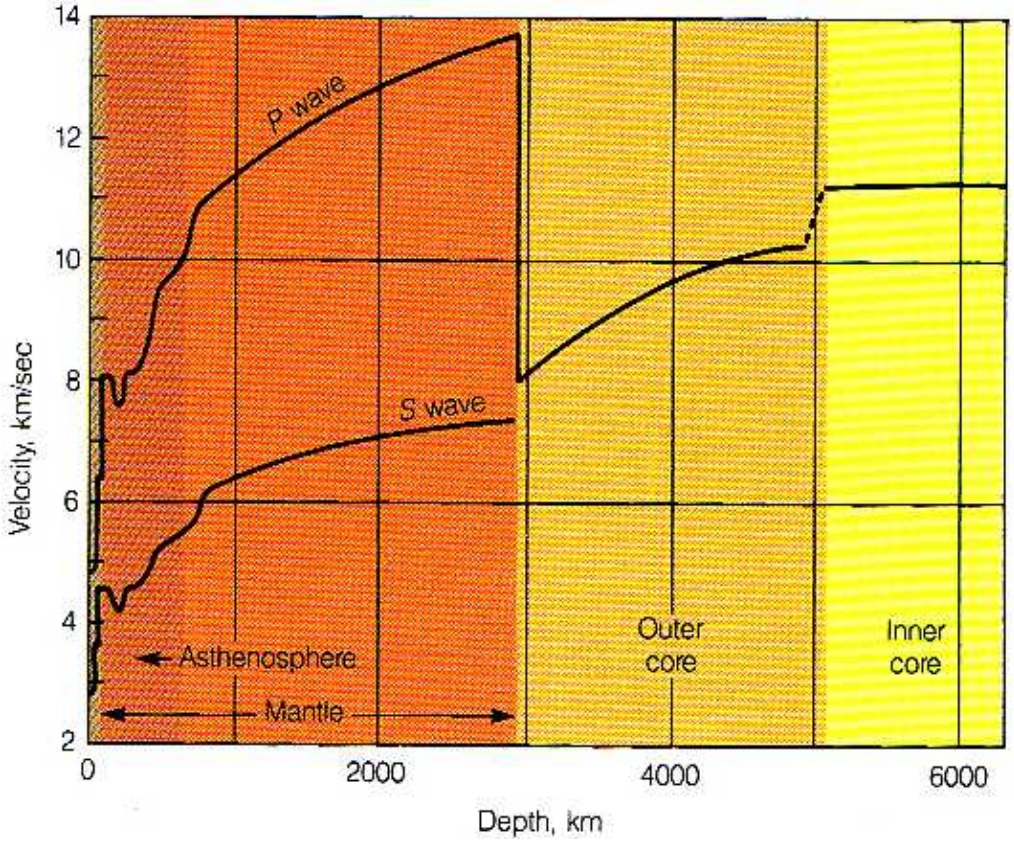
14
12
10
8
6
4
2
Velocity, km/sec
P wave
S wave
Asthenosphere
Mantle
Outer core
Inner core
0
2000
4000
6000
Depth, km

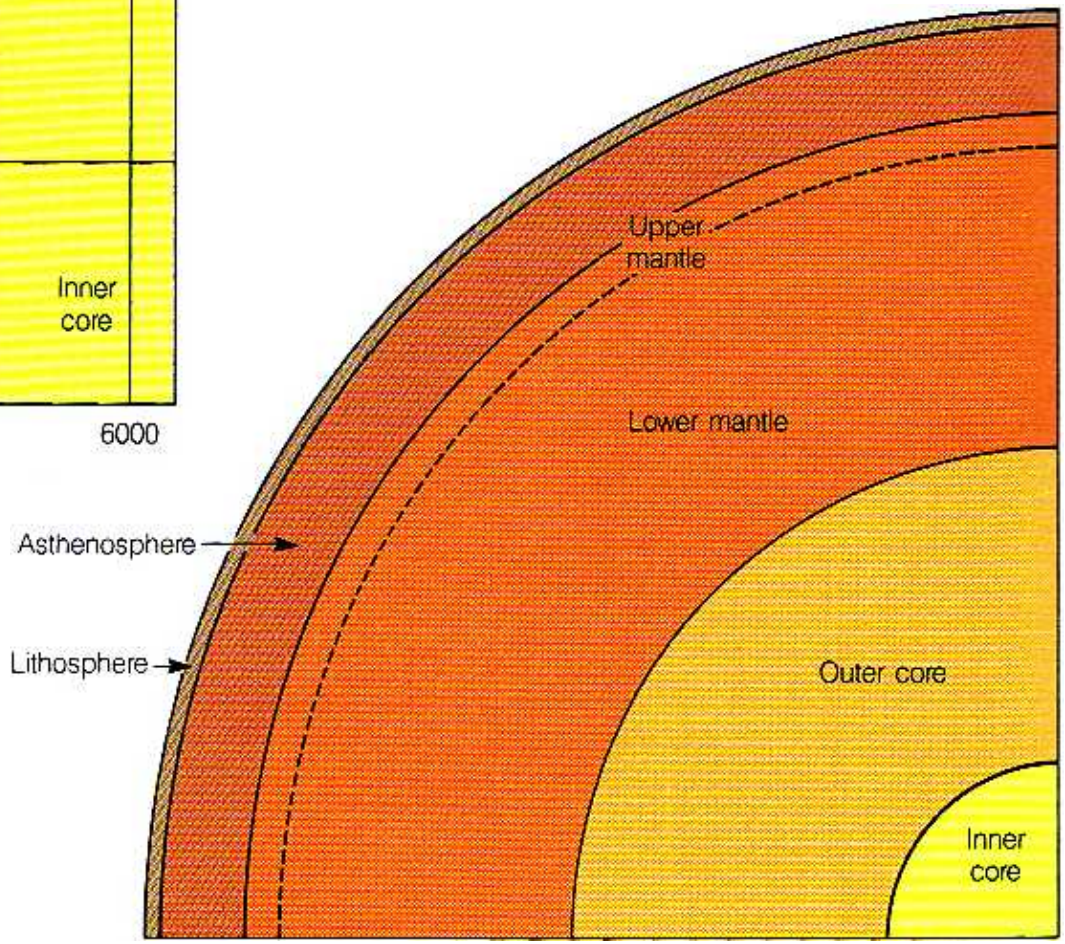
Upper mantle
Lower mantle
Asthenosphere
Lithosphere
Outer core
Inner core

Crustal section

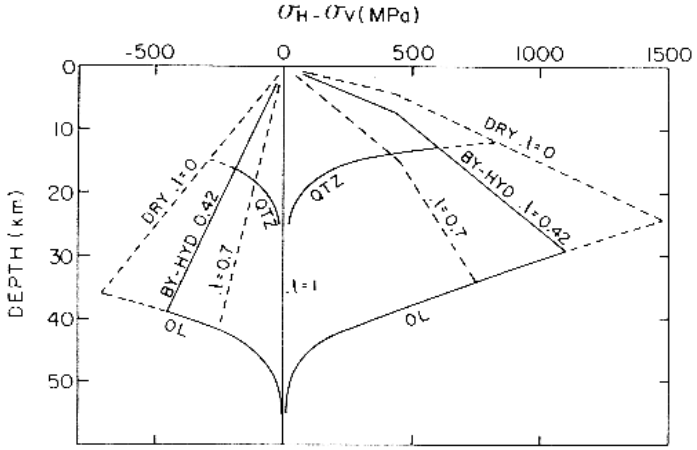

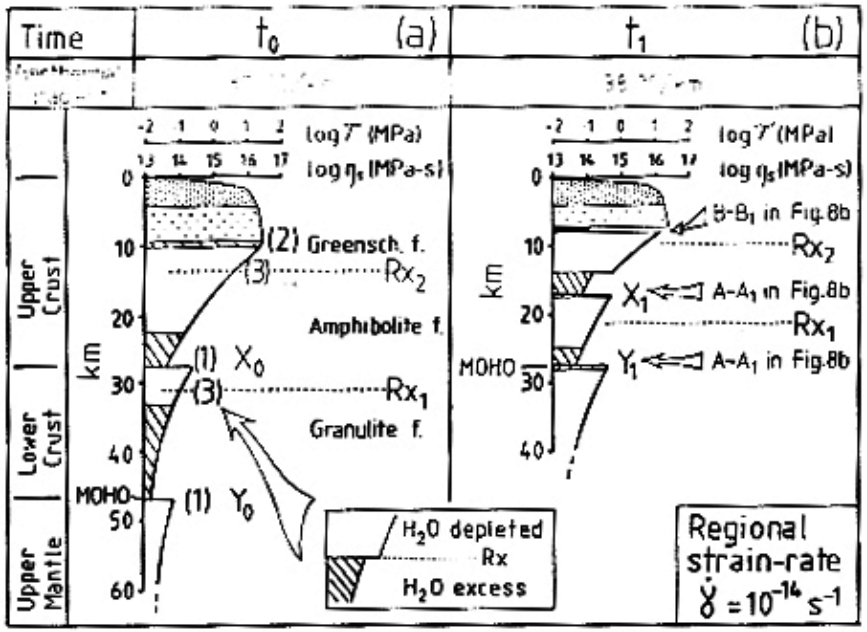

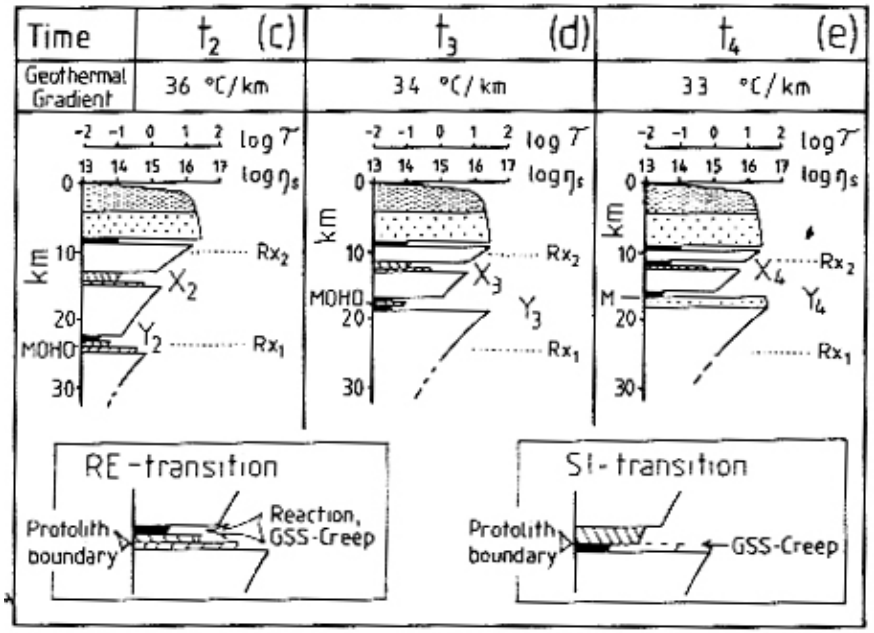

EXTRAPOLATION

Natural and experimental microstructures of deformed rocks look very much alike; microstructures form a link between nature and experiment, between natural and experimental rock deformation. It is on the basis of this similarity that we are confident that mechanical data obtained in the laboratory can be extrapolated to nature, and that inspection of natural microstructures may guide us towards meaningful experiments.

Terminology:
Deformation mechanisms describe how bulk rocks deform in response to pressure, temperature stress level, strain rate, pore pressure etc.
One or more phases and one or more processes may be involved

Example:
The deformation mechanisms called "Pressure solution" involves (at least) three processes: solution of material, transport of solute from source to sink, precipitation of material.

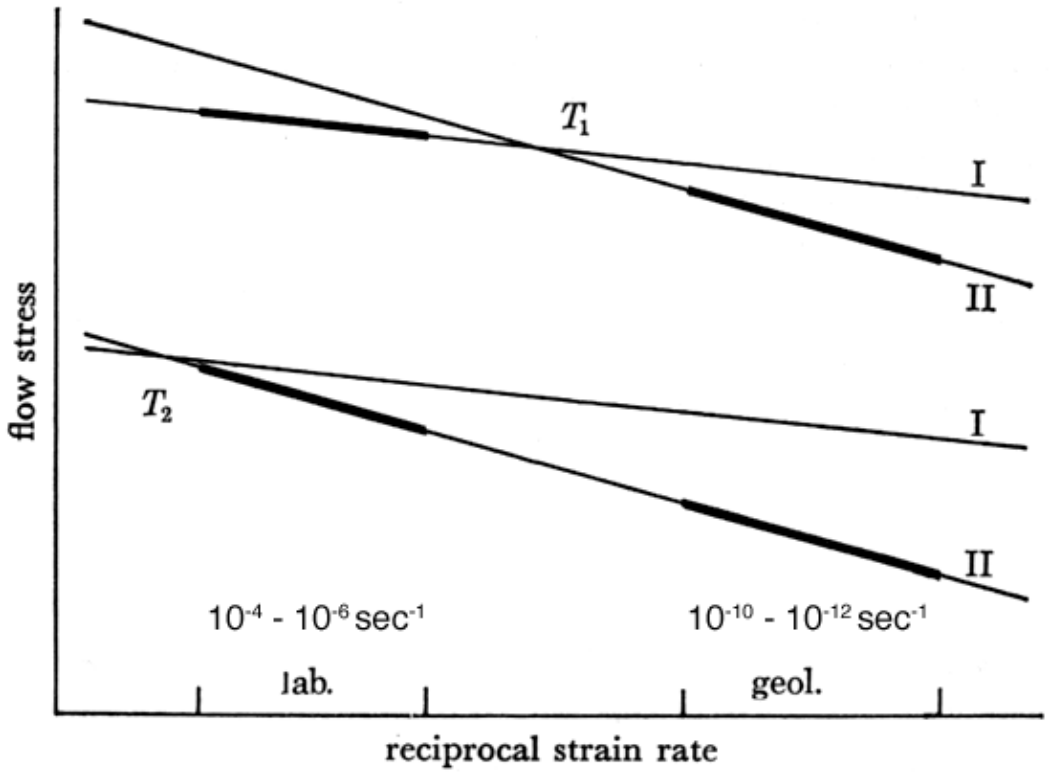

I, II = processes

T1 low deformation temperature

T2 high deformation temperature

Problem of extrapolation:
Strain rate dependence of a deformation mechanisms (DM) at two different temperatures, T, where T1 < T2. The DM is composed of two processes, I and II, which show different strain rate dependencies. At (low) natural strain rates, process II is more competitive, requiring lower flow stress than process I. At (high) laboratory strain rates and high temperatures, the same is true. But at (high) laboratory strain rates and low temperatures, process I outweighs process II. In this case, extrapolation of high T experiments yields correct predictions for natural flow stresses, whereas low T experiment predict natural flows stresses which are too high.

Theodore von Karman, 1881 - 1963

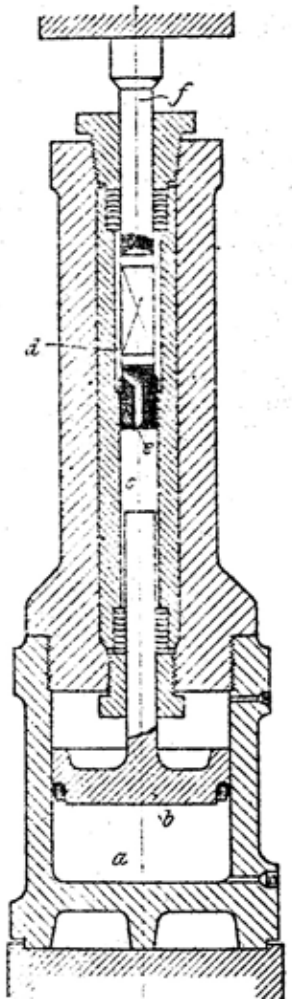

David Tressel Griggs, 1911 - 1974

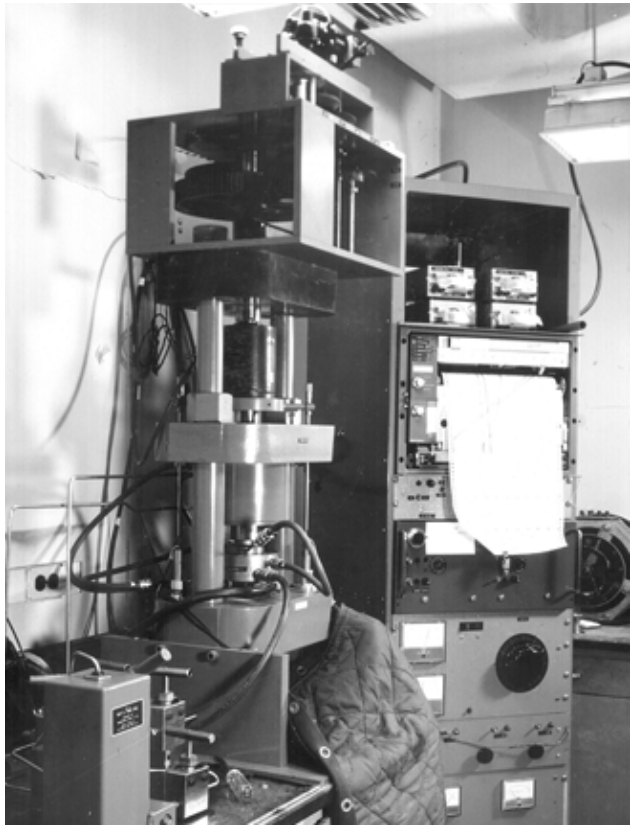

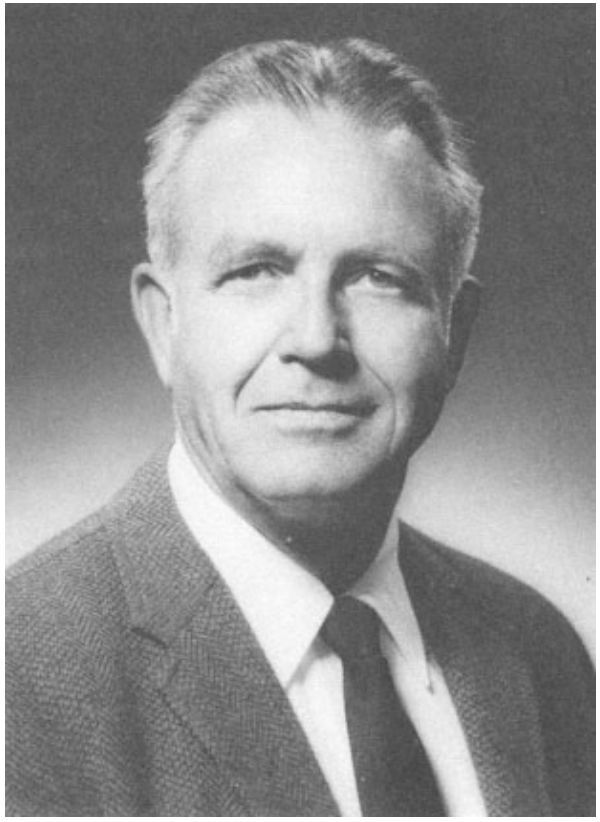

Frances Robertson Handin, 1923 - 2006

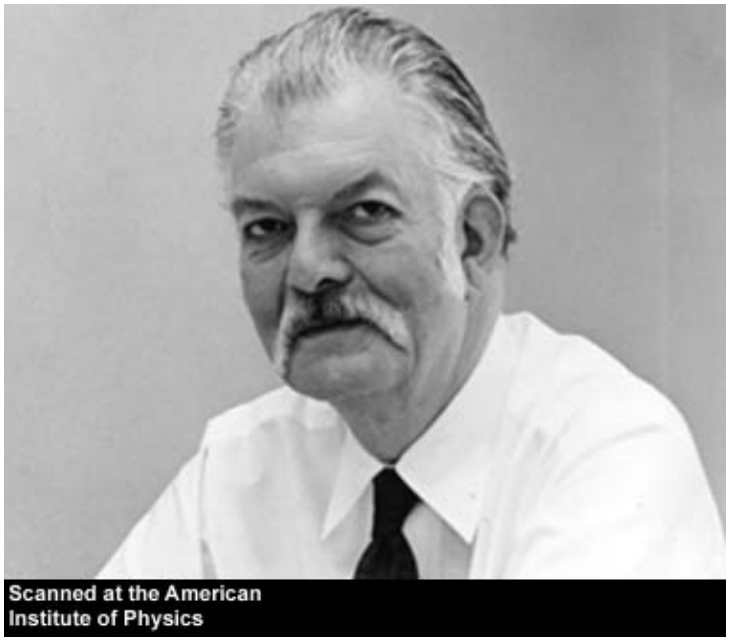

http://geoweb.tamu.edu/tectono/facilities/facilities.html

Mervyn Silas Paterson, 1925 -

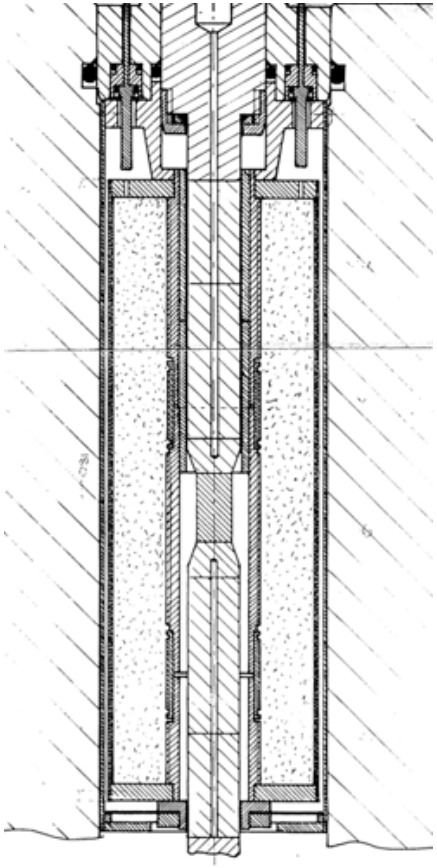

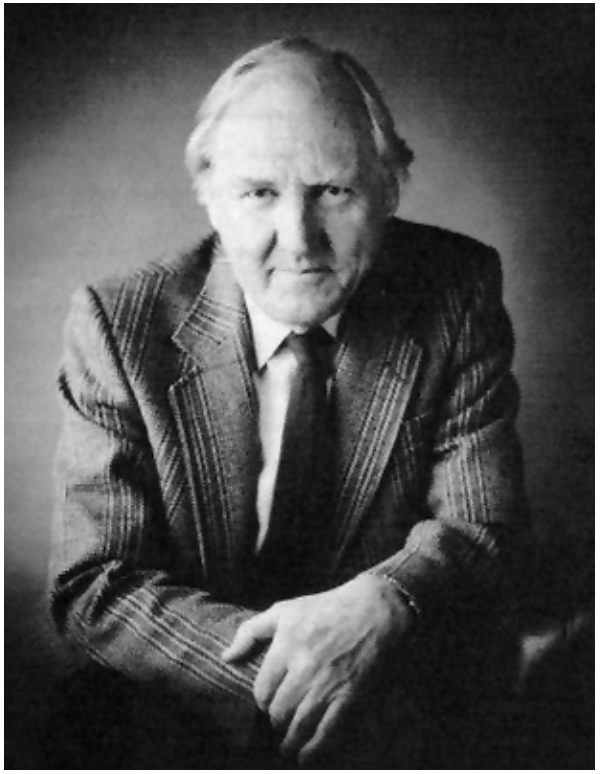

Jan Tullis, 1943 -

Holger Stünitz, 1956 -

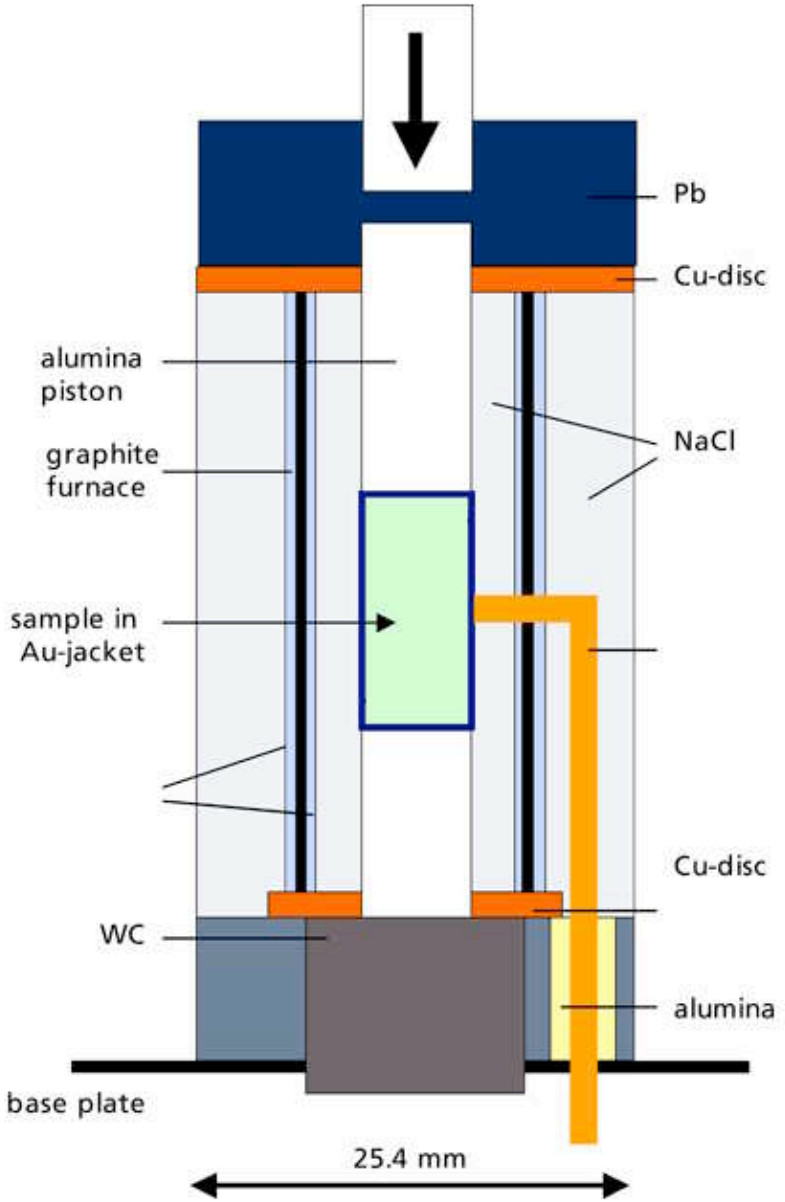

Schematic of deformation apparatus

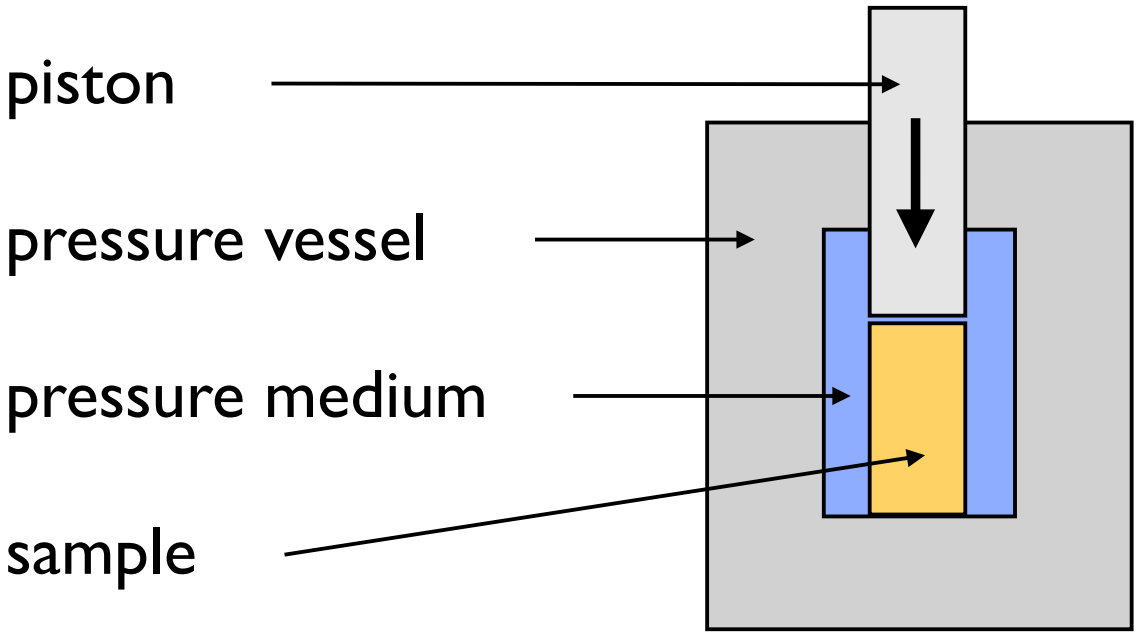

Controlled variables:

- confining pressure
- temperature
- displacement rate or load

States of stress (Mohr cirlcle)

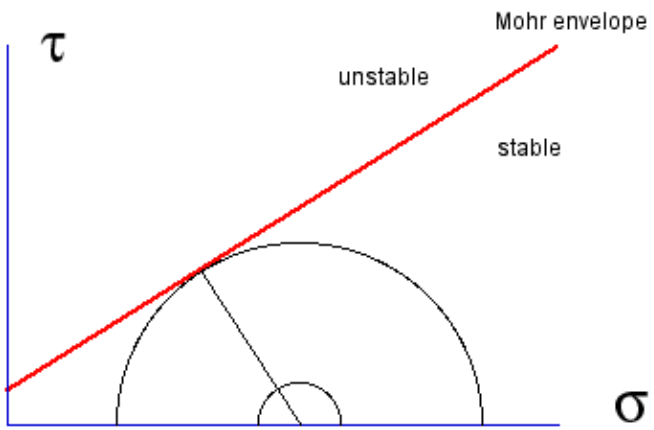

in rock deformation:

compressive > 0 tensile < 0

$\sigma 1 \geq \sigma 2 \geq \sigma 3$

shear component	τ
normal component	σ
mean stress	$\sigma = 1/3 \cdot \sigma ii$
confining pressure	$pc = \sigma 3$
differential stress	$\Delta\sigma = \sigma 1 - \sigma 3$

Loading

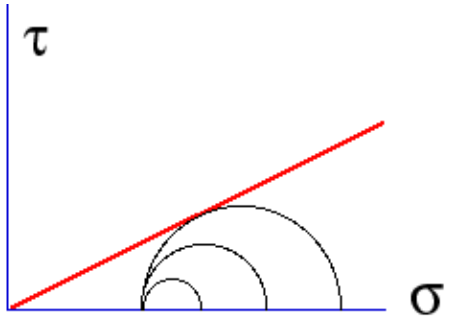

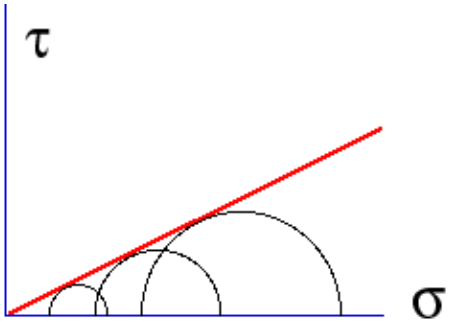

experimental

proportional (nature)

Types of experiments

Triaxial compression $\sigma1 > \sigma2 = \sigma3$ $\sigma1, \sigma2, \sigma3 > 0$	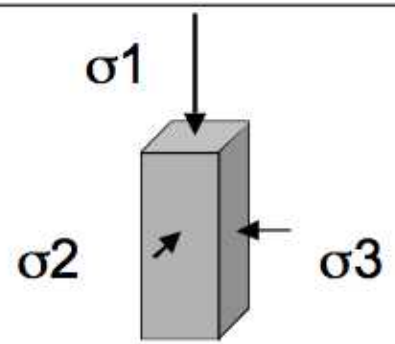
Uniaxial compression $\sigma1 > 0$ $\sigma2 = \sigma3 = 0$	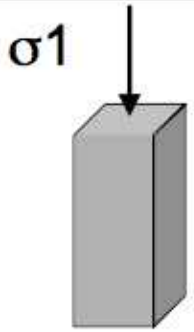
Extension $\sigma1 = \sigma2 > \sigma3$ $\sigma1, \sigma2, \sigma3 > 0$	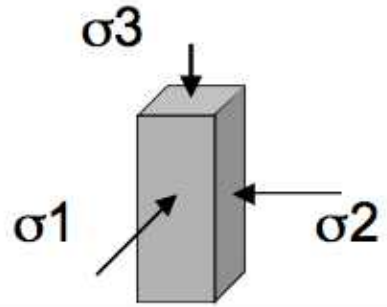
Tensile $\sigma1 = \sigma2 = 0$ $\sigma3 < 0$	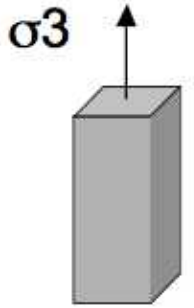

Types of experiments

Shearing	 split cylinder: 45° or 30° precut
Torsion	 solid or hollow cylinder
Friction	 rock plates
Fracture	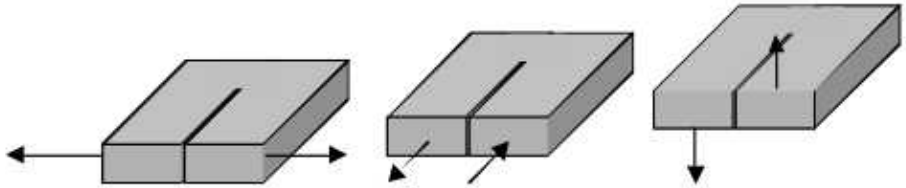
Brazil	 circular disc

GAS DEFORMATION APPARATUS

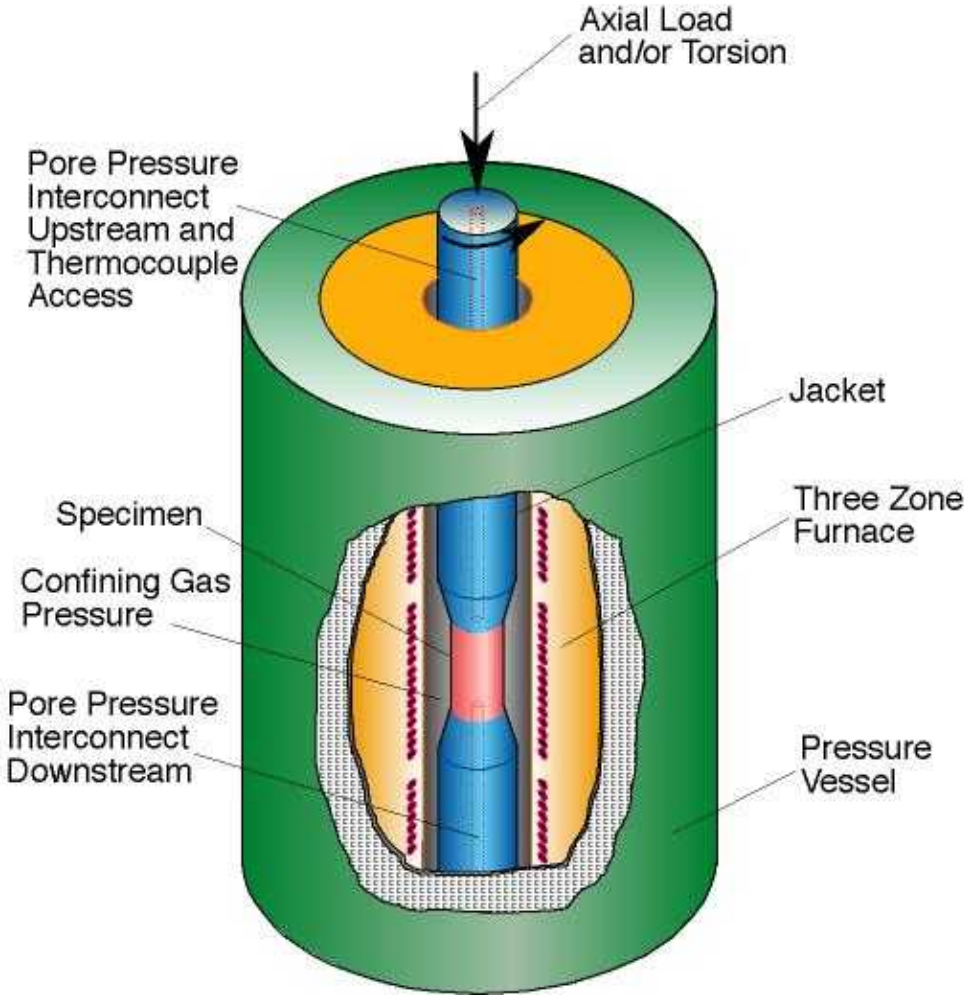

Description:

Paterson-type gas apparatus for triaxial deformation and torsion experiments under high pressure - high temperature conditions

Specifications:

Sample size: 10 x 20 mm
Temperature: < 1300°C
Confining Pressure: < 500 MPa (gas)
Axial load: < 100 kN
Stiffness (frame): 2 MN/mm
Strain rate range: 10-7 to 10-1 s-1
Torque: < 1000 Nm
Pore pressure: < 500 MPa

Features: Axial and/or torsional load
Pore pressure servo control
Permeability measurement system
Internal force, torque and displacement sensors

POTSDAM Experimental Rock Deformation Laboratory
http://www.gfz-potsdam.de/pb3/pg32/

CREEP APPARATUS

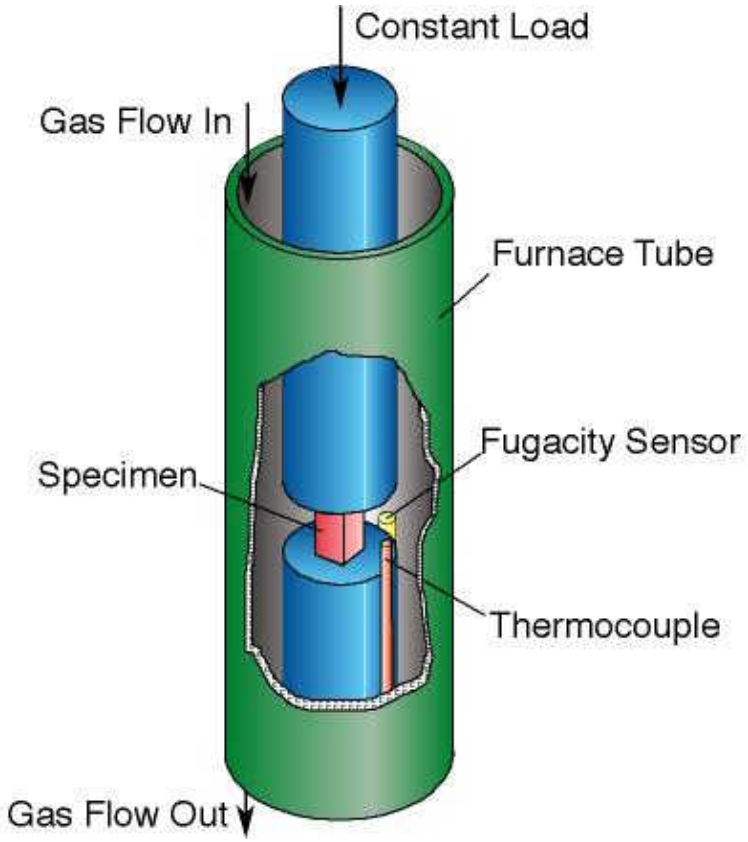

Description:
Dead-load-type uniaxial creep rig for high temperature creep test under controlled chemical environment.

Specifications:
Sample size: 3 x 3 x 6 mm
Temperature: < 1400°C
Confining Pressure: 0.1 MPa
Axial load: < 1 kN
Stiffness (frame): 3 MN/mm
Strain rate range: 10-8 to 10-4 s-1

Features:
Oxygen-fugacity control
Frictionless loading
High displacement accuracy

POTSDAM Experimental Rock Deformation Laboratory
http://www.gfz-potsdam.de/pb3/pg32/

CONVERSIONS

	Pa	bar	Torr	atm (phys)	at (tech)
Pa	1	10^{-5}	$7.5 \cdot 10^{-3}$	$9.87 \cdot 10^{-6}$	$1.02 \cdot 10^{-5}$
bar	10^{5}	1	750	0.987	1.02
Torr	133	$1.33 \cdot 10^{-3}$	1	$1.32 \cdot 10^{-3}$	$1.36 \cdot 10^{-3}$
atm (phys)	101'330	1.0133	760	1	1.033
at (tech)	98'100	0.981	736	0.968	1

1 MPa = 10 bar	**1kb = 100 MPa**

[force] = 1 N = 1 kg m s^{-2}	**[stress] = 1 Pa = 1 kg m^{-1} s^{-2}**

TYPICAL MECHANICAL DATA

rock type	strength (MPa) pc = 0 ~ surface conditions	strength (MPa) pc = 100 MPa ~ 3-4 km depth
igneous rocks	100 - 200	500 - 800
calcite rocks, marbles	50 - 100	200 - 300
high porosity sedimentary rocks	10 - 50	
dolomites, quartzites (low porosity)	≤ 300	500 - 1000

GENERAL EFFECT OF VARIABLES ON STRENGTH

factor	change	influence on strength
confining pressure	+	+
temperature	+	-
strain rate	+	+
pore pressure	+	-

Deformationsprozesse in der Erde I (2)

Experimental rock deformation

1) Coulomb Law of Failure

2) Anderson's Theory of Faulting

3) Byerlee's Law

Common types of deformation experiments

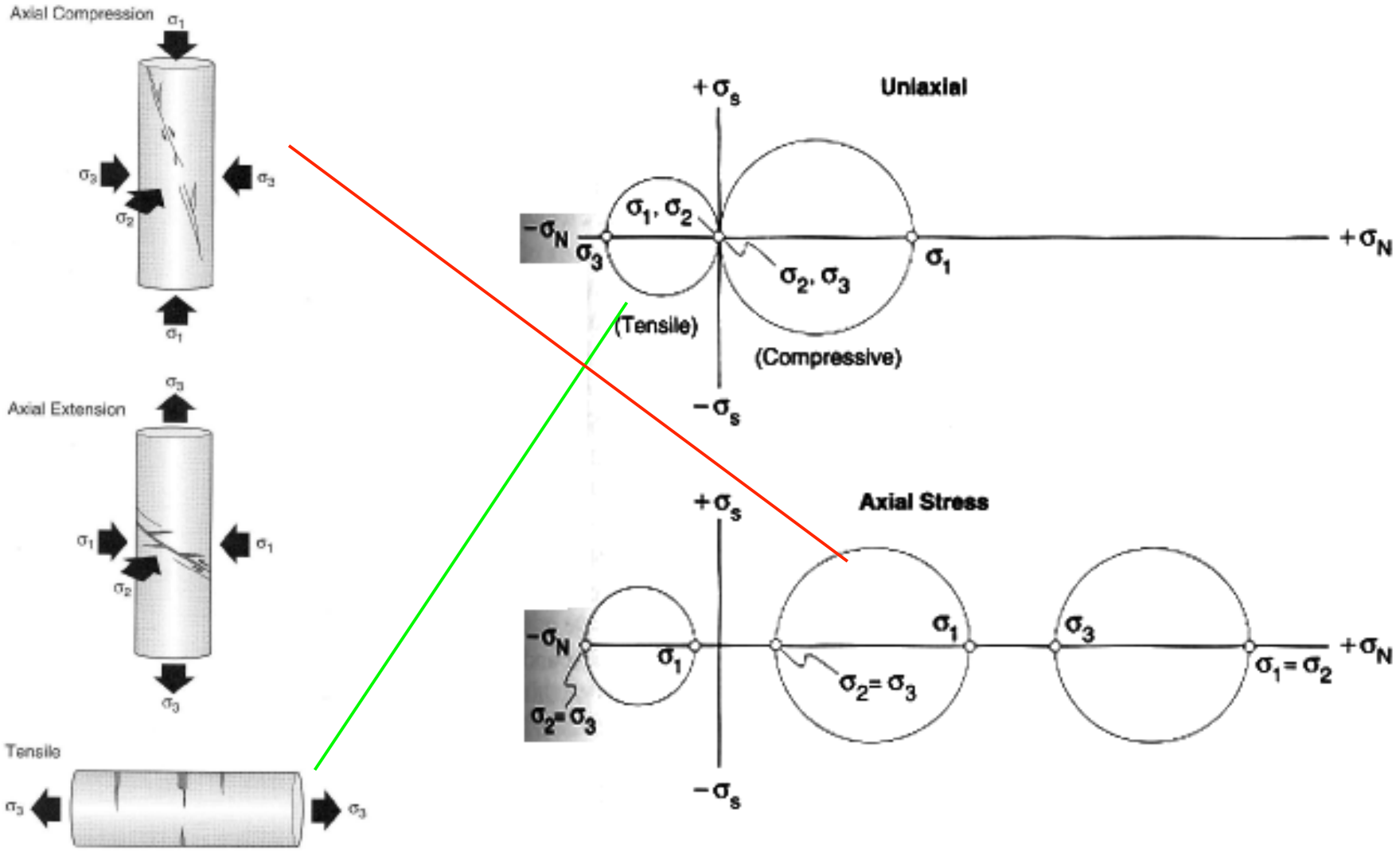

Rock rheology (mechanical behavior of rocks)

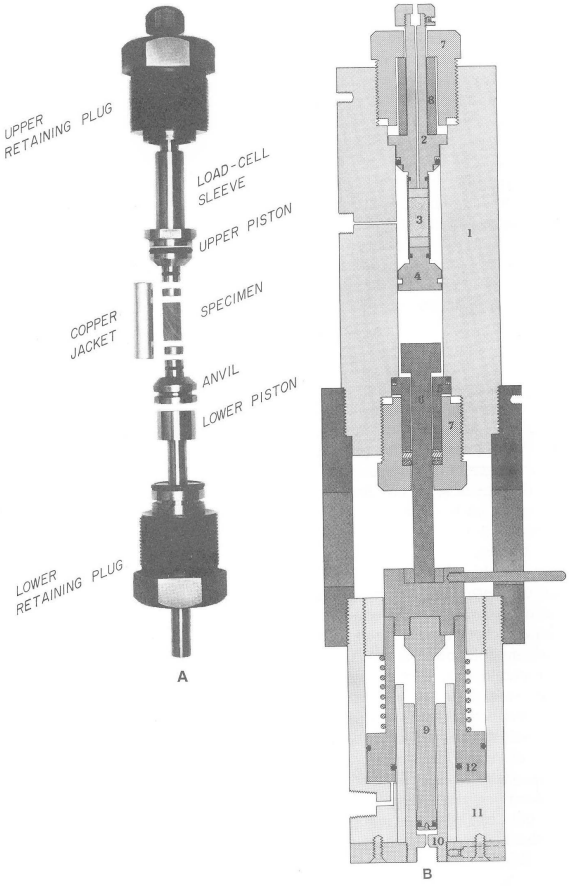

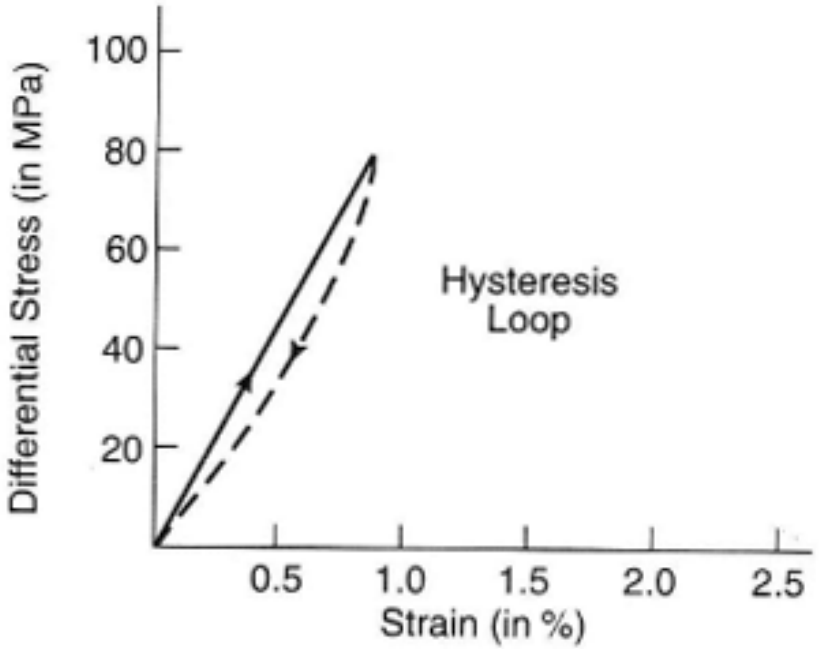

Figure 3.32 When the load is removed from an elastically deforming specimen, the specimen will return to its original length. The return is along a looping path, signifying a time lag in recovery.

Elastic strain: deformation and recovery = instantaneous

Compressive strength tests: The Goal

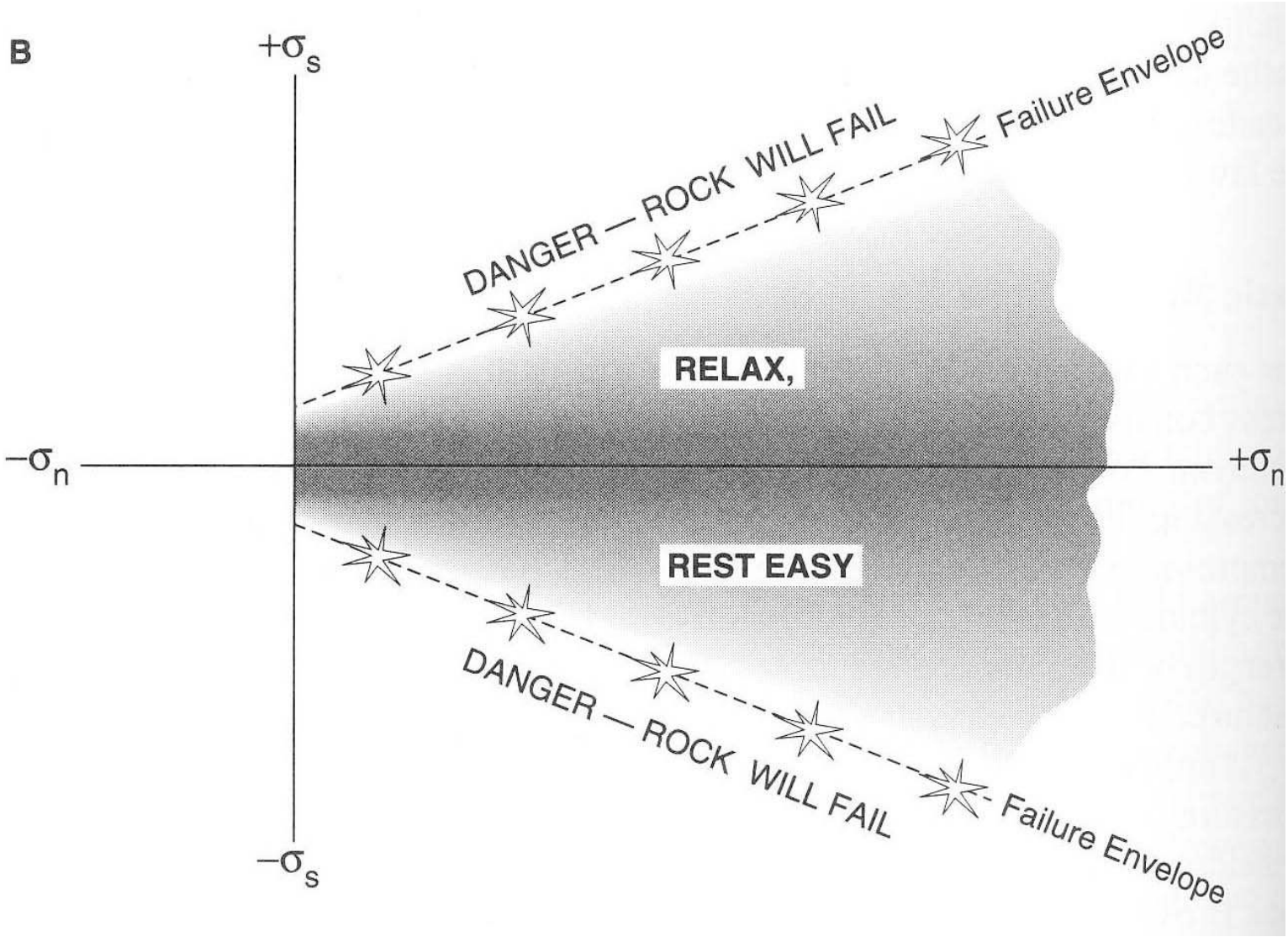

Compressive strength tests: The Approach

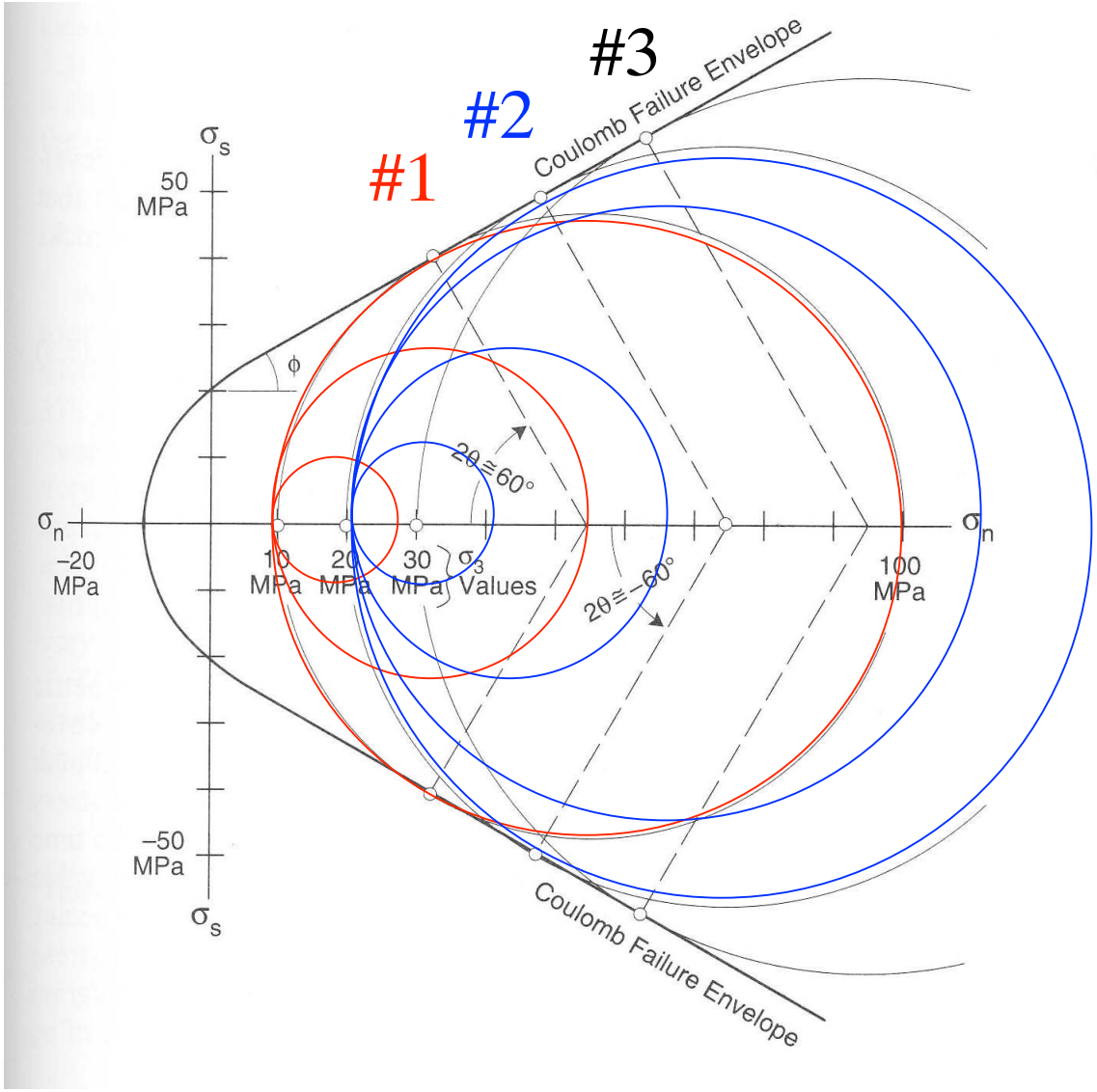

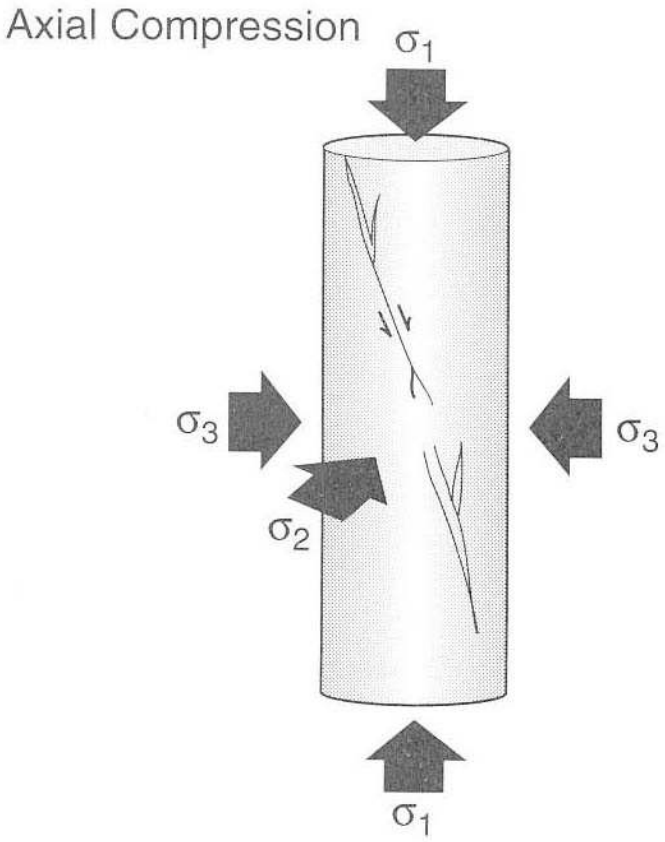

Compressive strength tests: The results

Linear envelope of failure; fractures form at angles of 25 to 35° from σ1- very consistent!

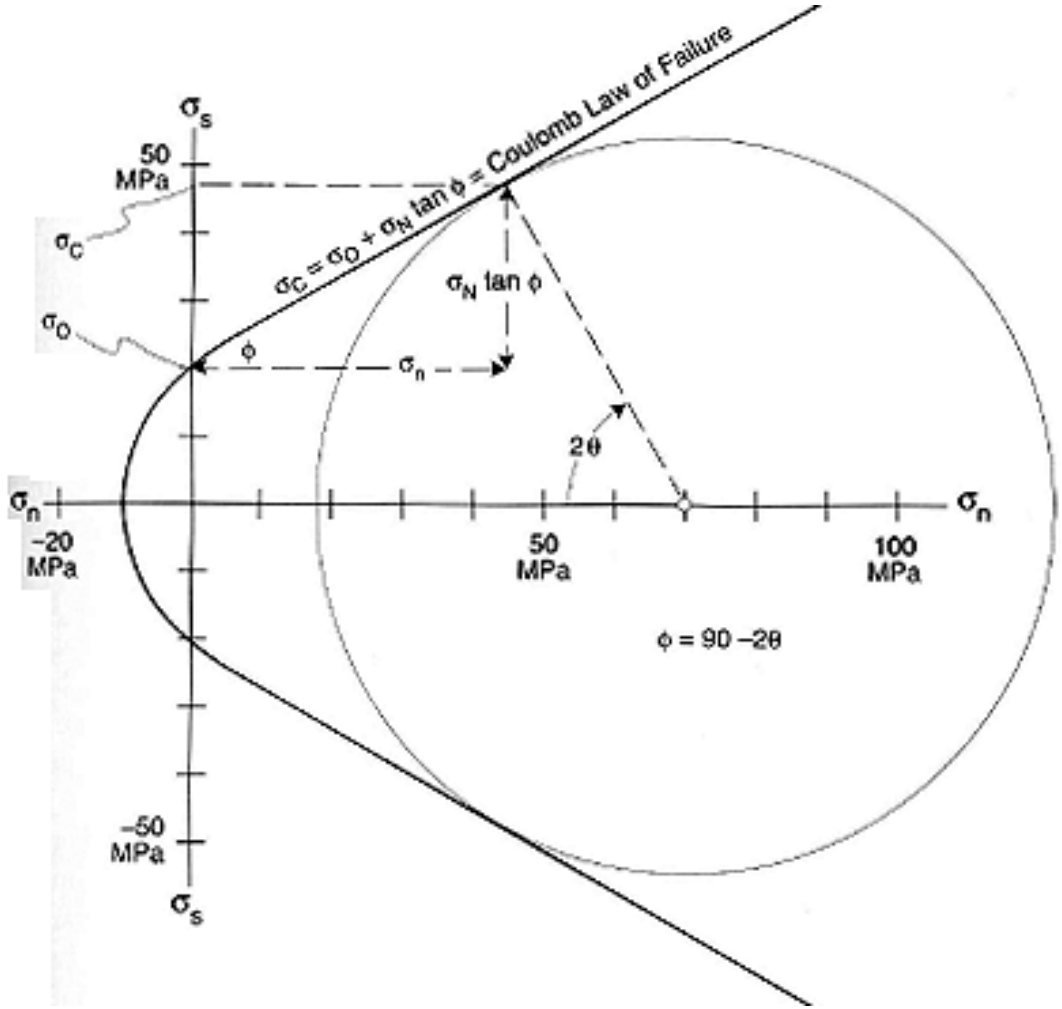

Coulomb's Law of Failure

$\sigma_c = \sigma_0 + \tan\varphi(\sigma_n)$

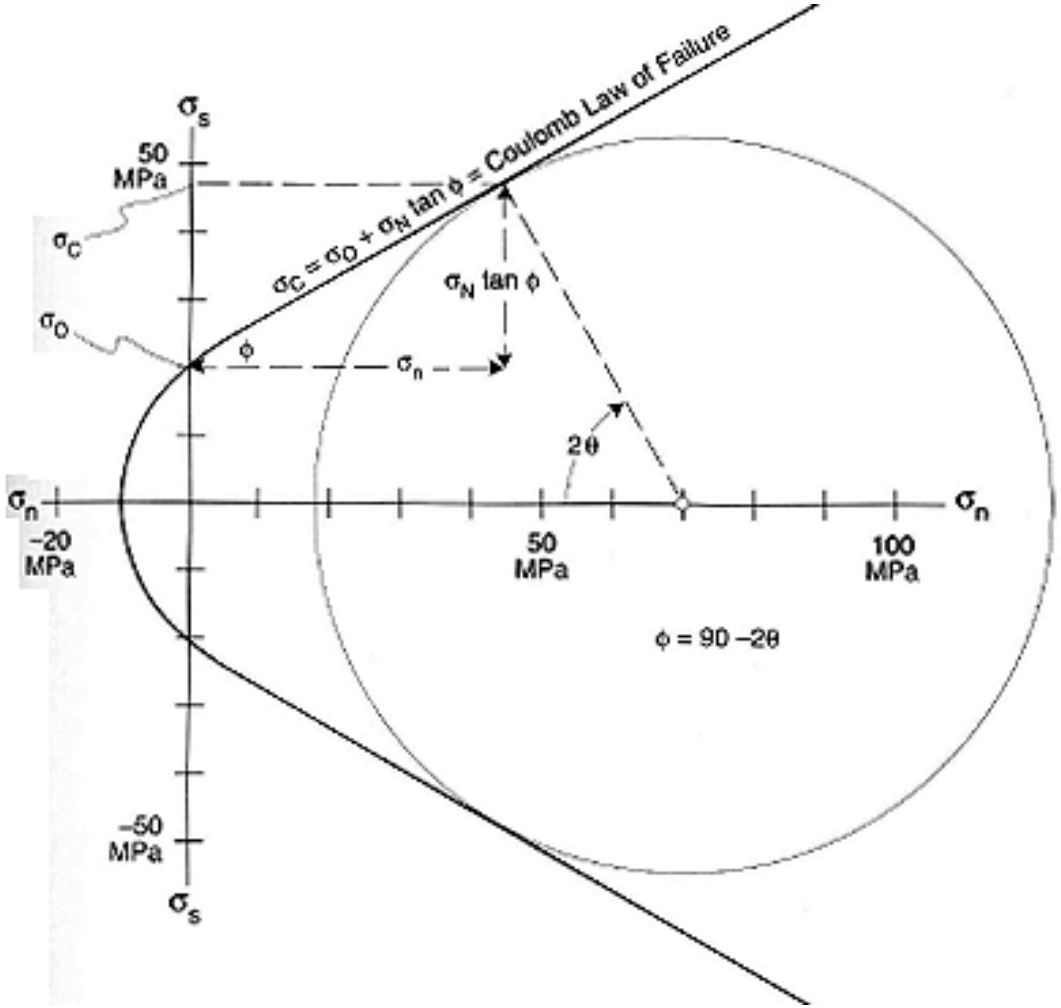

σ_c = critical shear stress required for failure

σ_0 = cohesive strength

$\tan\varphi$ = coefficient of internal friction ($\varphi = 90 - 2\theta$)

σ_N = normal stress

Tensile strength tests with no confining pressure

Approach: Similar to compressive strength tests

Results: (1) Fracture oriented parallel to $\sigma 1$ ($\theta = 0$)

(2) Rocks weaker in tension than in compression

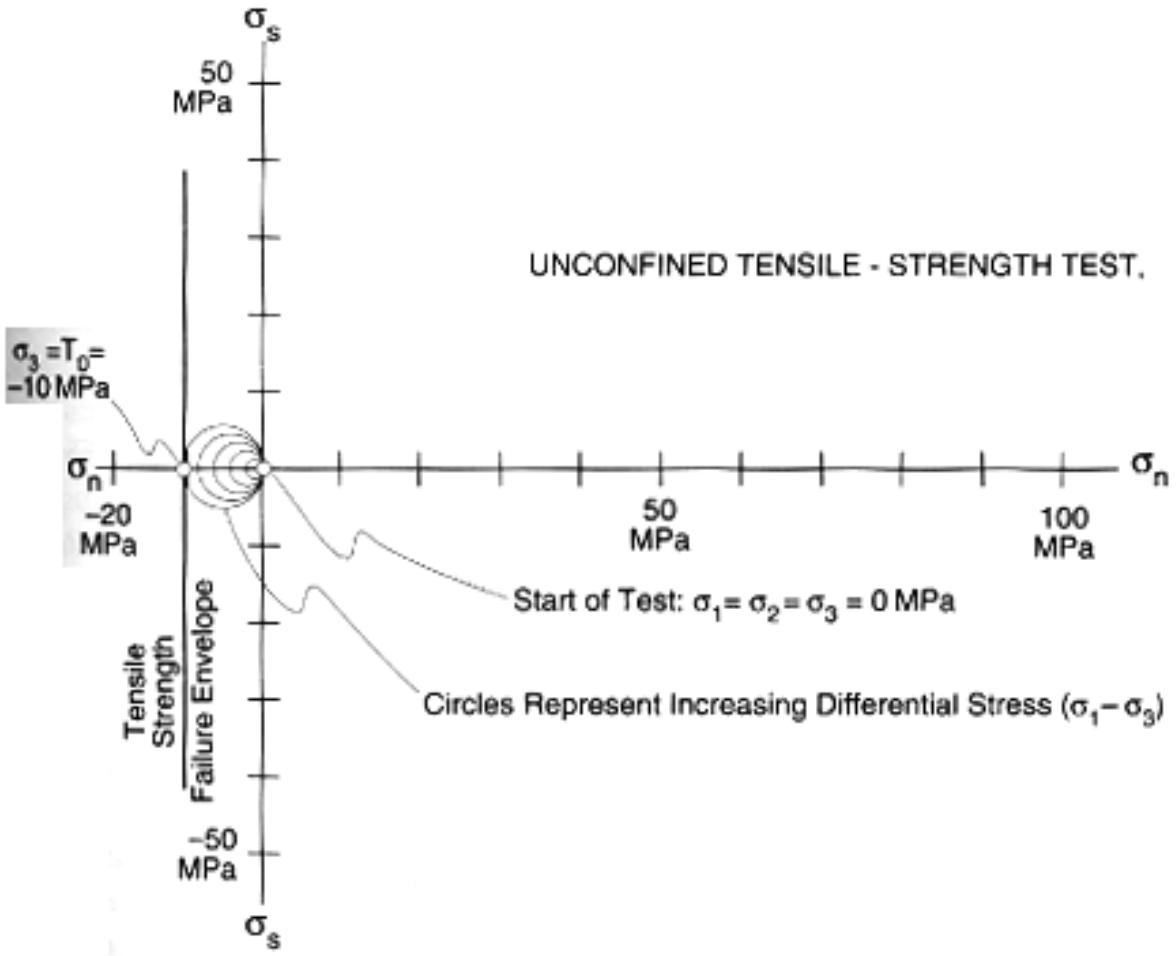

Tensile + Compressive strength tests

Result: Failure envelope is parabolic $0° < \theta < 30°$

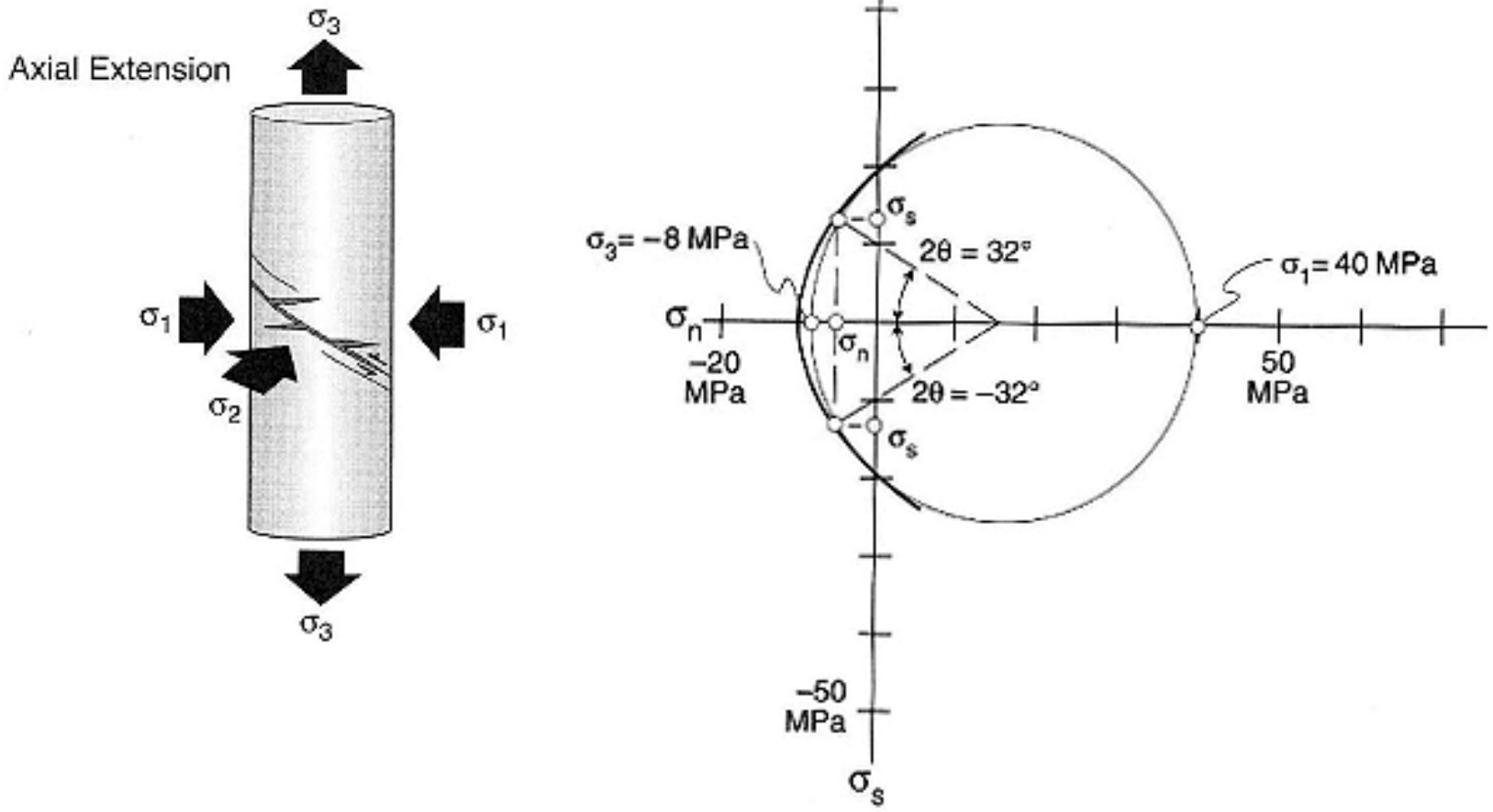

Failure envelopes for different rocks: note that slope of envelope is similar for most rocks

$\sigma_c = \sigma_0 + \tan\varphi(\sigma_n)$

σ_c = critical shear stress required for failure

σ_0 = cohesive strength

$\tan\varphi$ = coefficient of internal friction

σ_N = normal stress

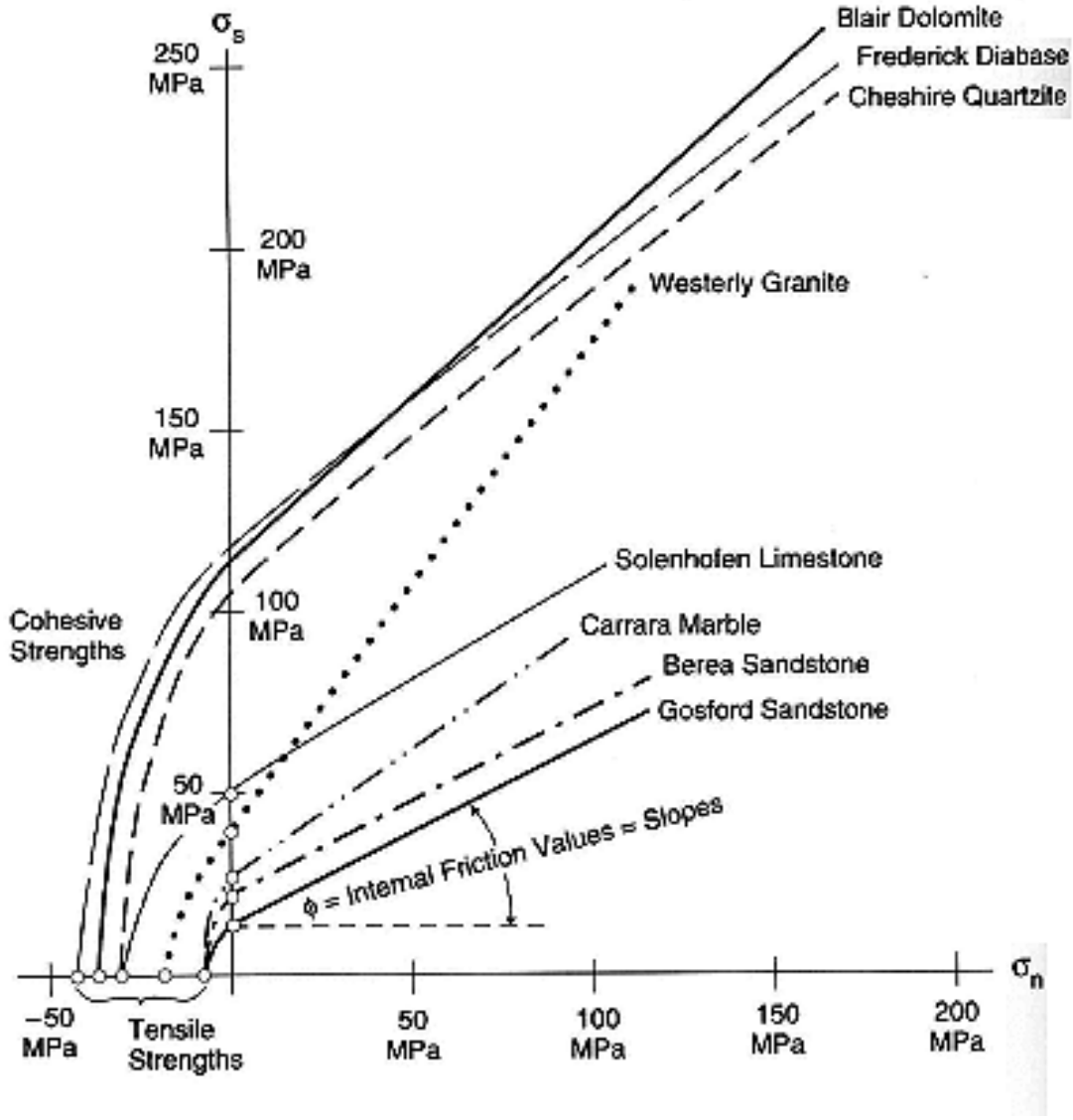

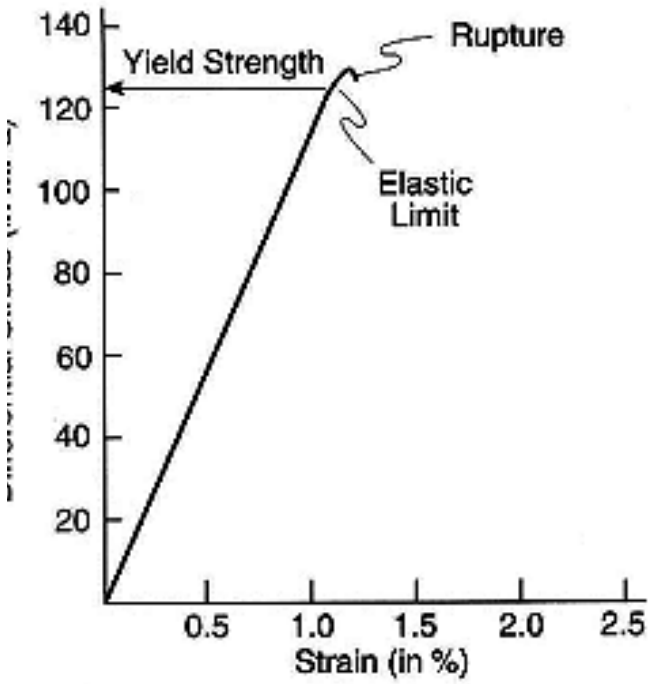

Elastic limit:
There is no longer a linear relationship between stress and strain.
Rock behaves in a different manner

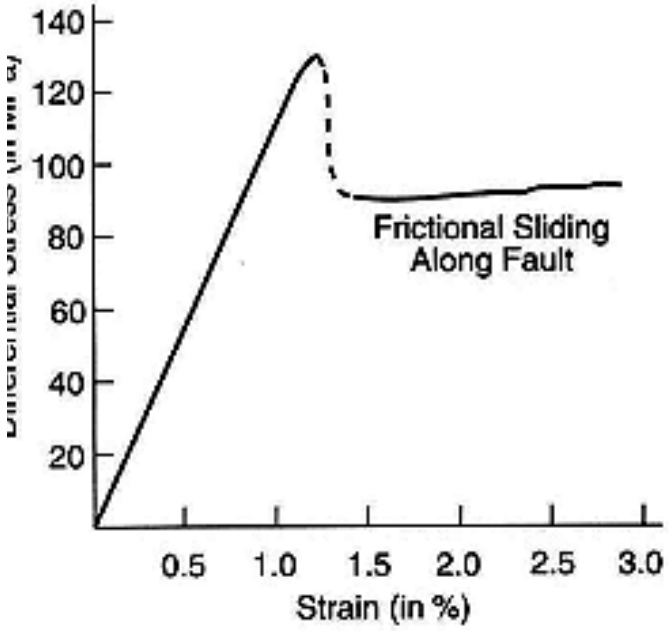

Yield strength:
The differential stress at which the rock is no longer behaving in an elastic fashion

Anderson's Theory of Faulting

The Earth's surface is a free surface (contact between rock and atmosphere), and cannot be subject to shear stress. As the principal stress directions are directions of zero shear stress, they must be parallel (2 of them) and perpendicular (1 of them) to the Earth's surface.

Combined with an angle of failure of 30 degrees from $\sigma 1$, this gives:

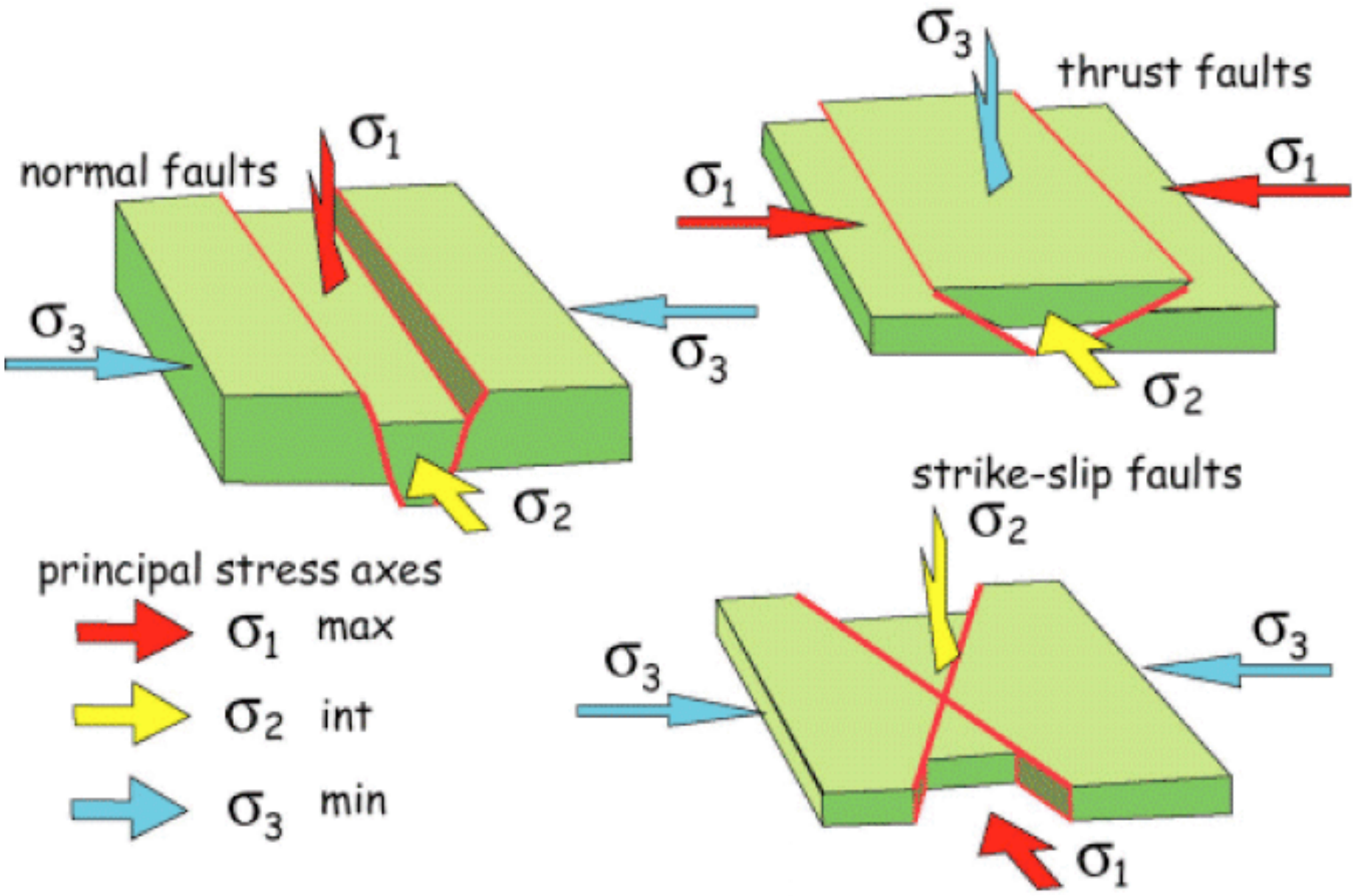
normal faults
σ1
σ3
σ3
σ2
thrust faults
σ3
σ1
σ1
σ2
strike-slip faults
σ2
σ3
σ3
σ1
principal stress axes
σ1 max
σ2 int
σ3 min

2

Types of deformation (brittle-ductile) Types of testing

Deformationsprozesse in der Erde I (2)

Types of deformation(brittle-ductile) Types of testing

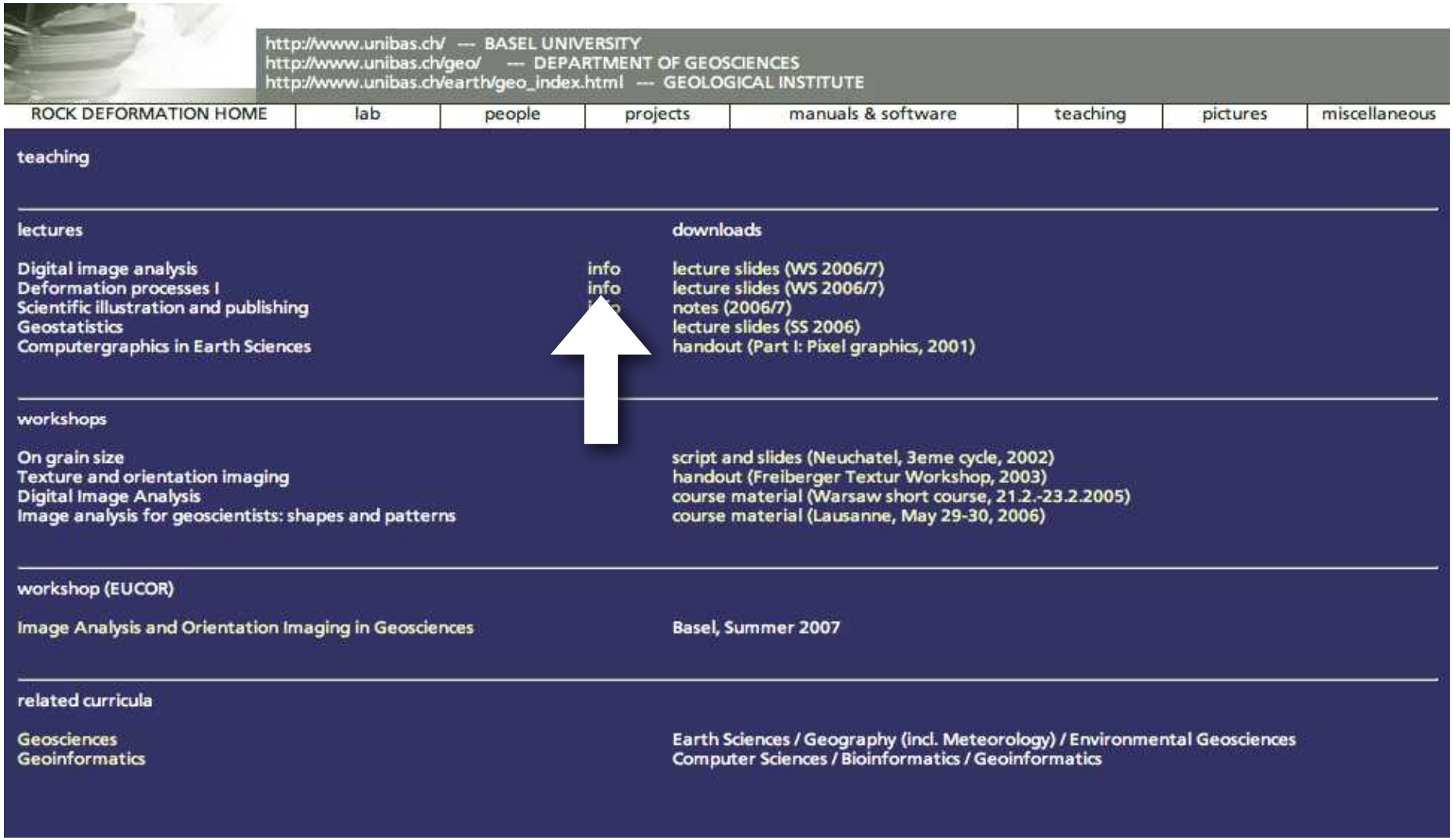

www.unibas.ch/earth/micro/teaching

SPRÖDDEFORMATION - BRITTLE DEFORMATION

Elastizität (augenblicklich - instantaneous)

$\neq f(t)$ (keine Zeitabhängigkeit)

$$\varepsilon = C \cdot \sigma$$

Deformation = Materialeigenschaft · Druck

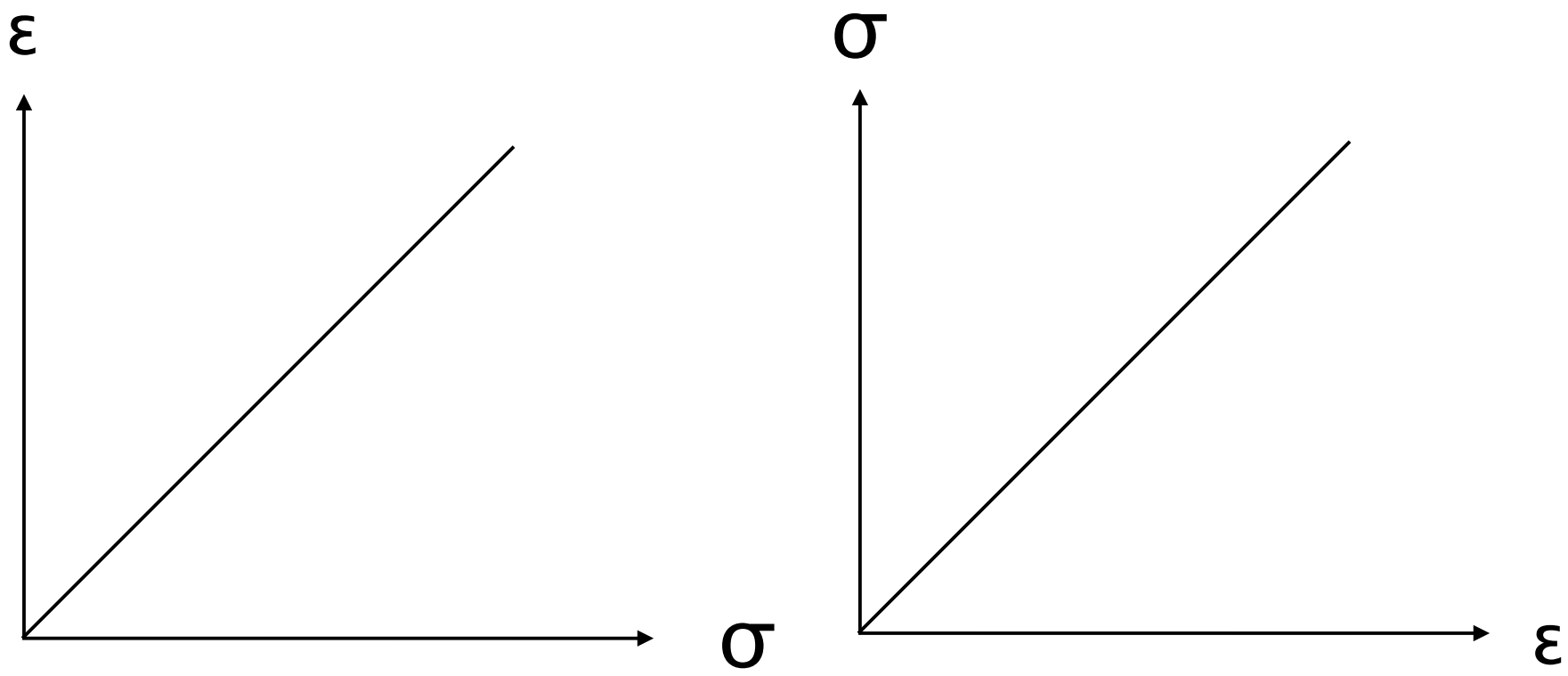
ε
σ
σ
ε

DUKTILE DEFORMATION-DUCTILE DEFORMATION

Plastizität

= f(t) (Zeitabhängigkeit)

$$\dot{\varepsilon} = \frac{\delta\varepsilon}{\delta t} = A \cdot \sigma$$

Deformation
-änderung = Materialeigenschaft · Druck

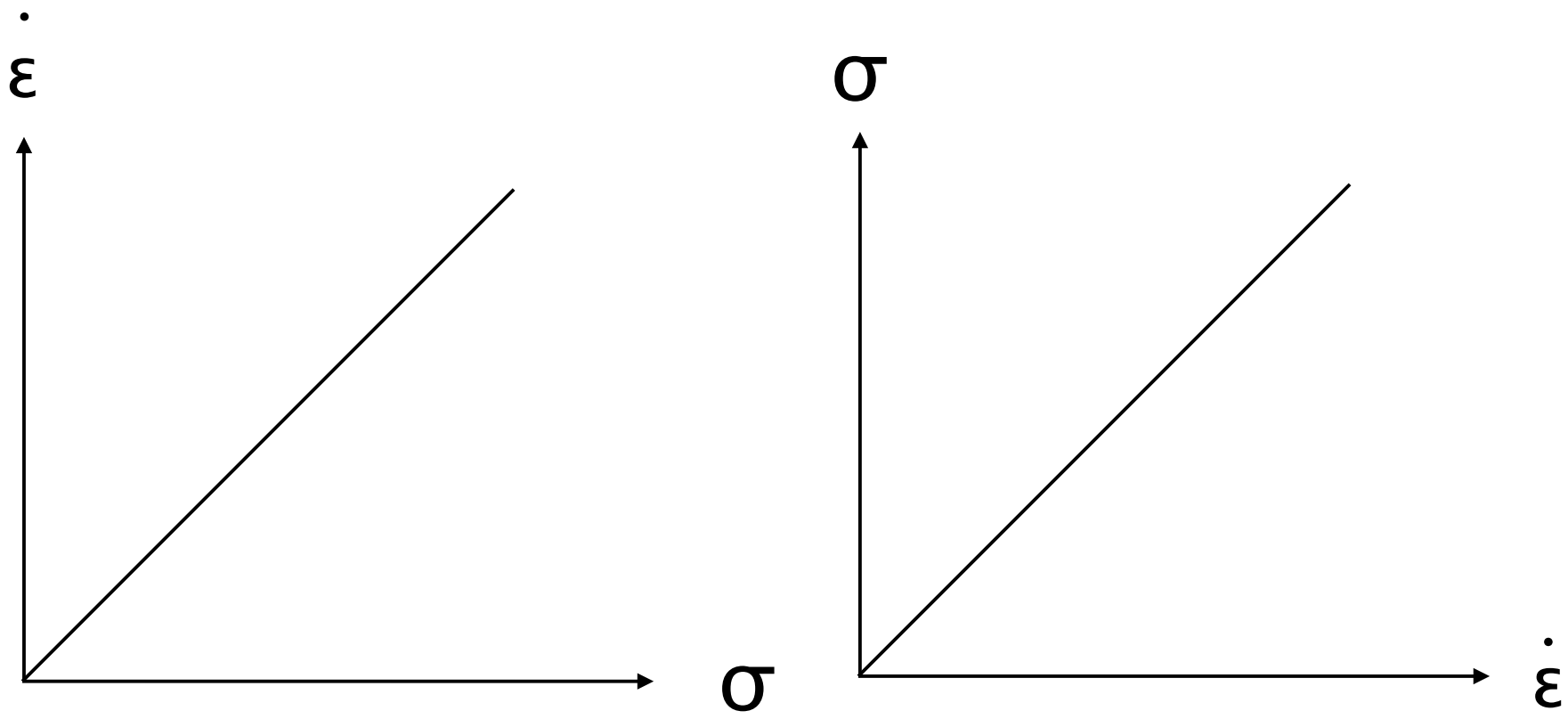
$\dot{\varepsilon}$
σ
σ
$\dot{\varepsilon}$

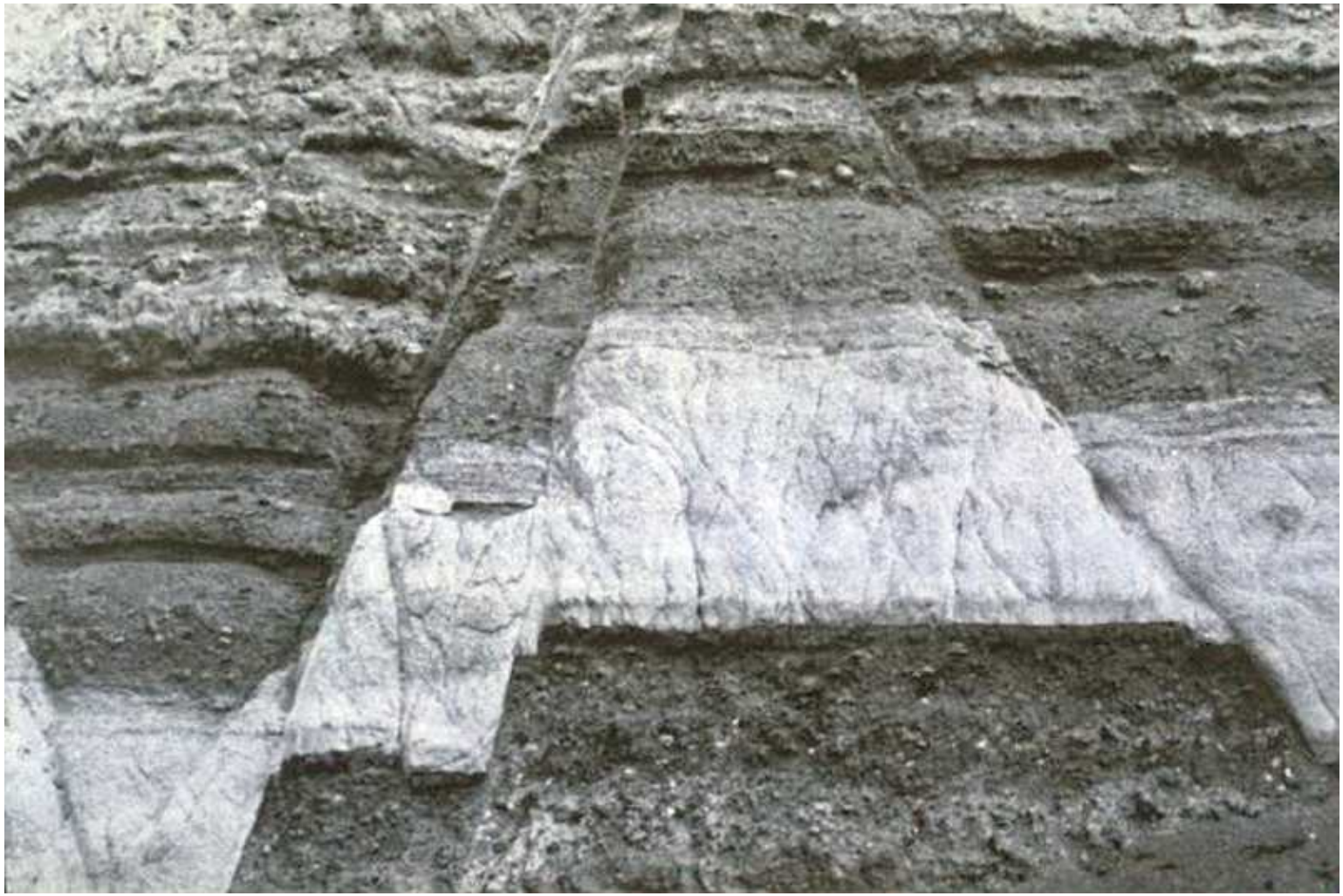

Image courtesy of R.A. Nelson
http://ic.ucsc.edu/~casey/eart150/Lectures/faultmechanics/thrst&nrmlflts.stefano/

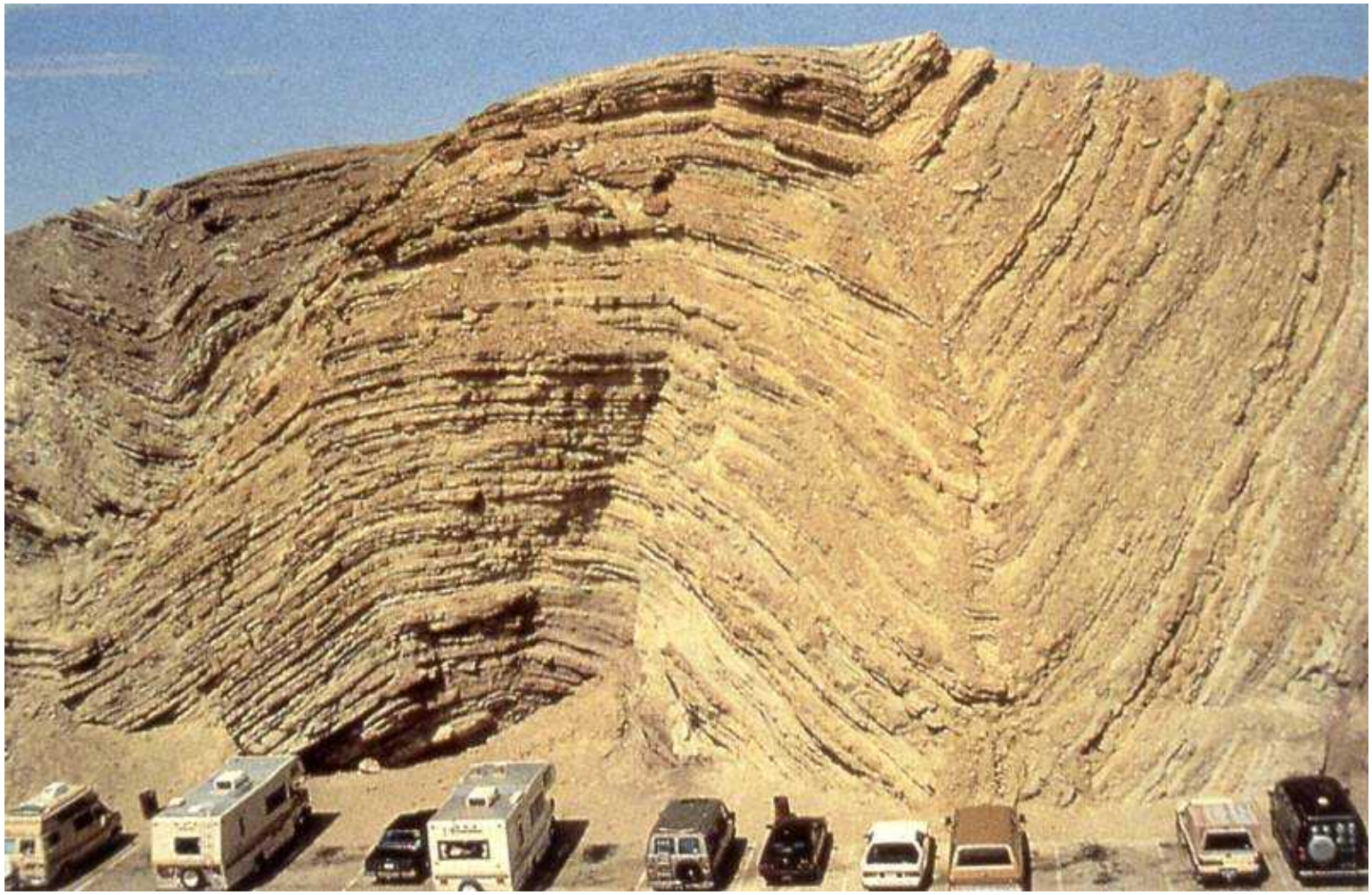

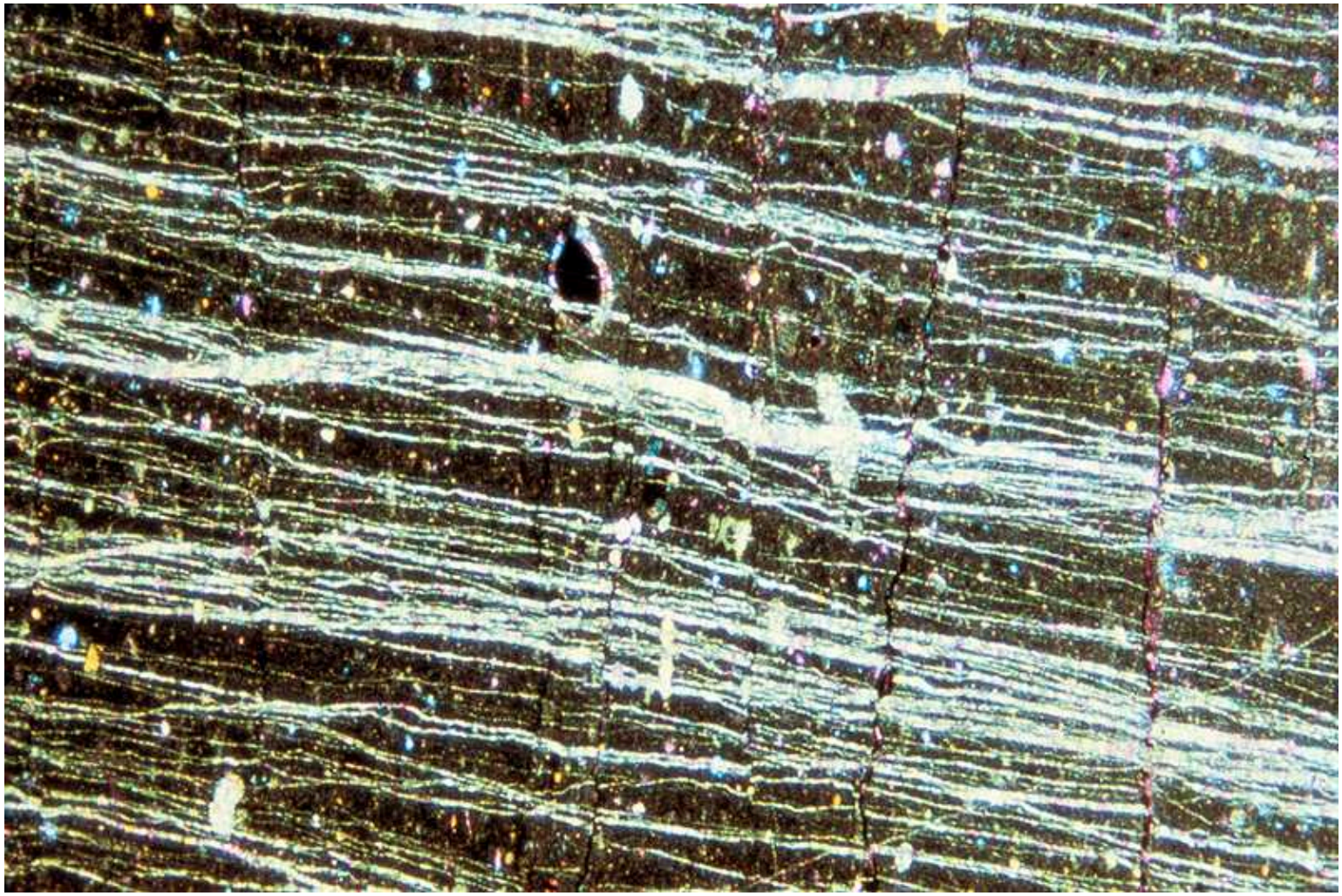

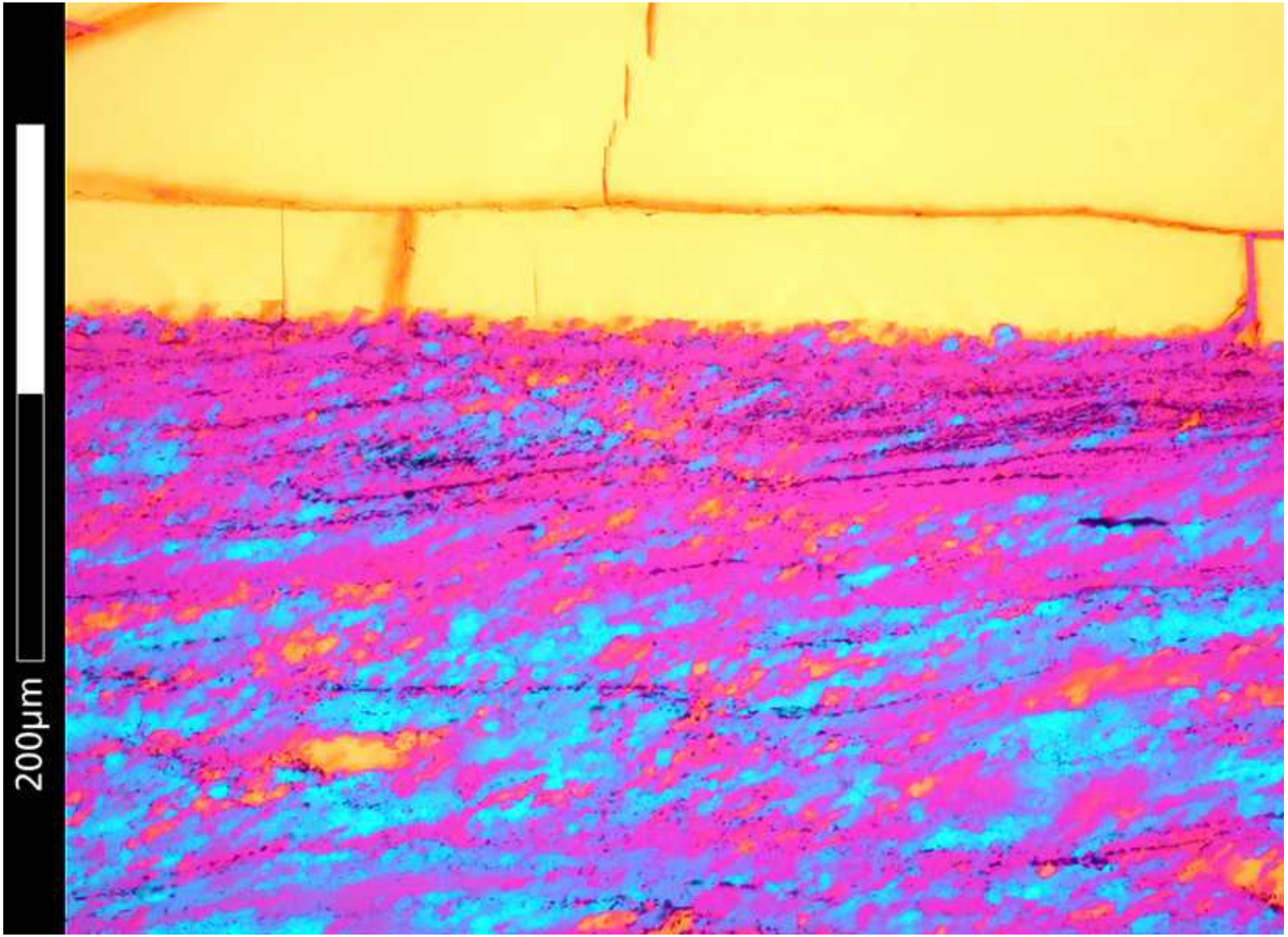
200µm

types of tests

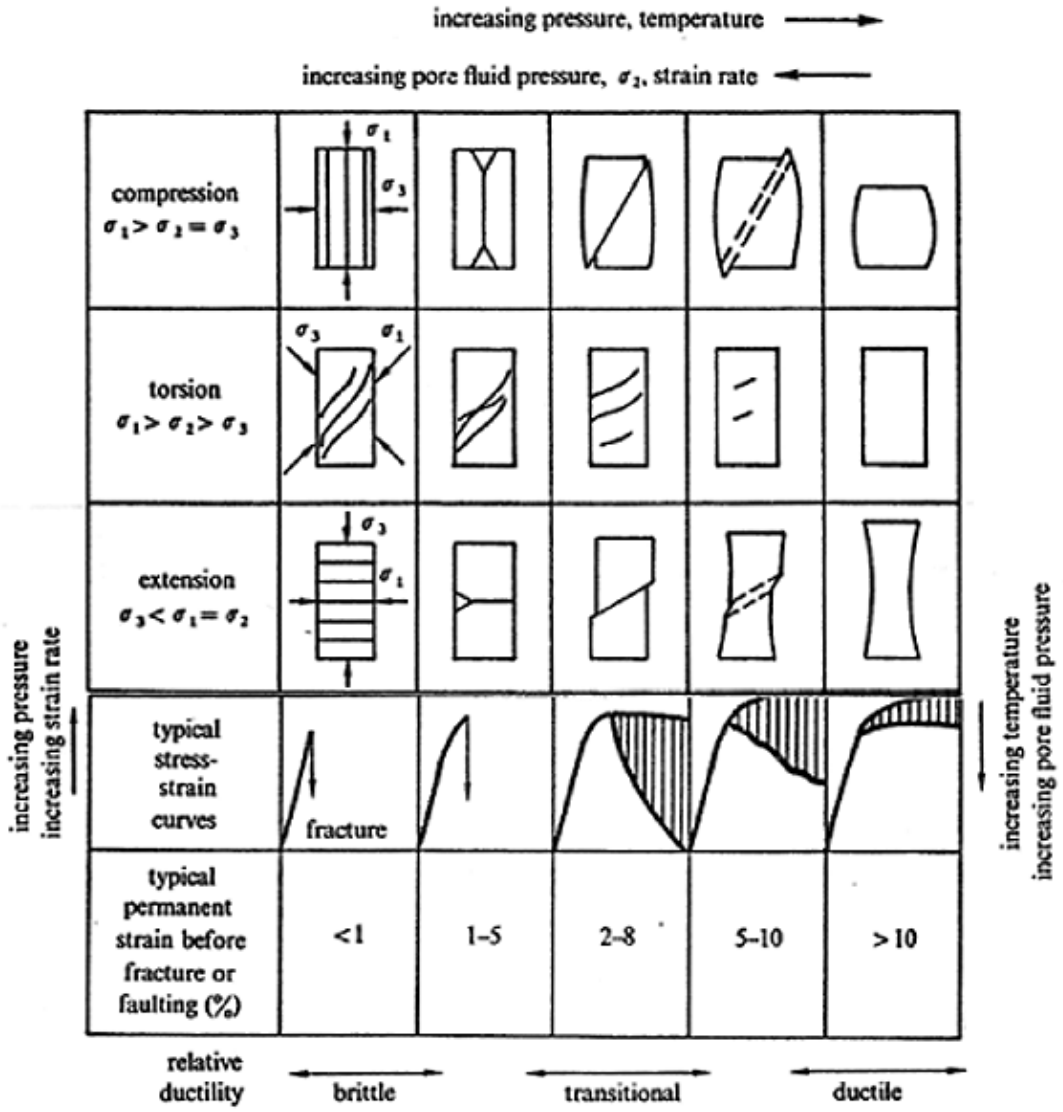

types of tests

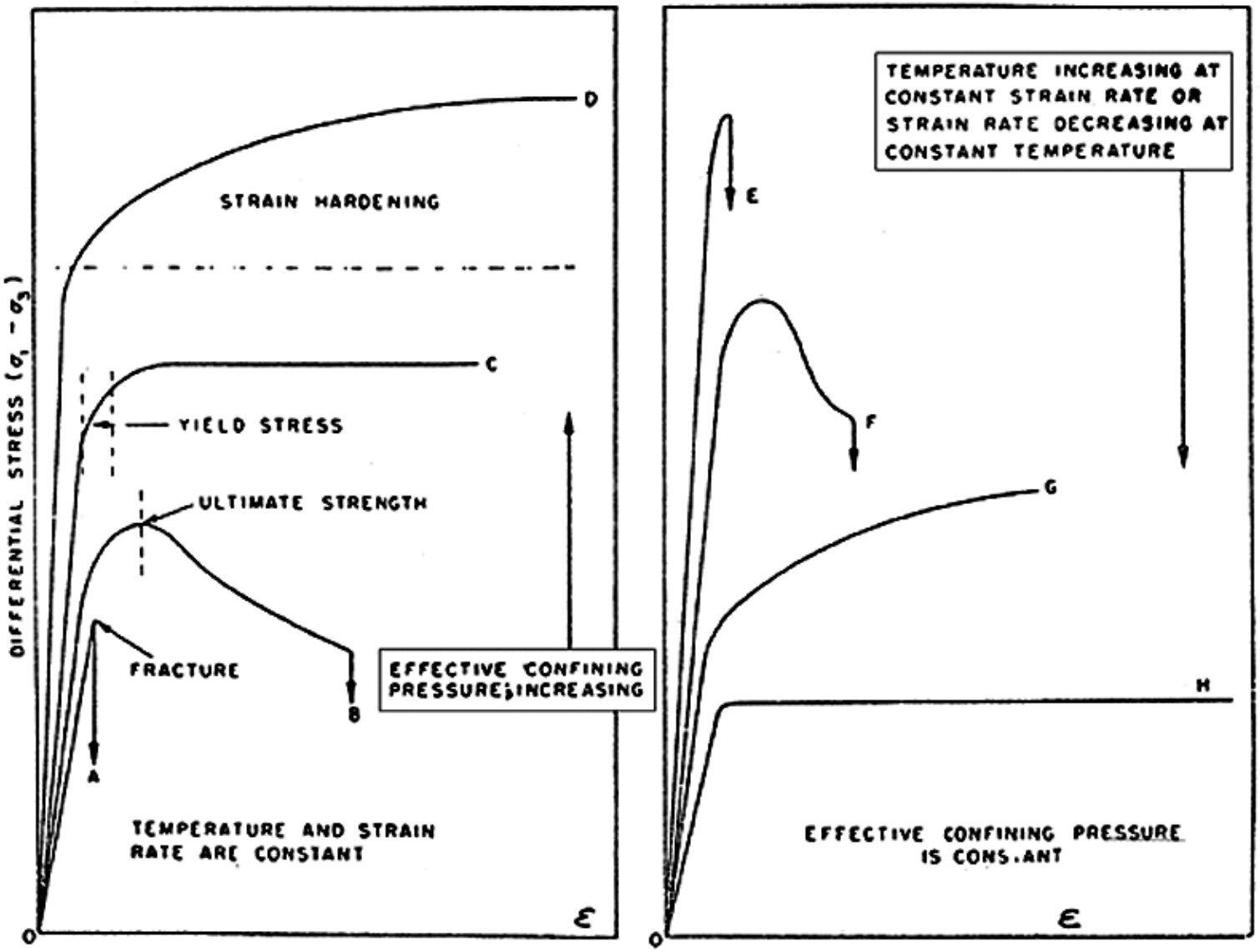

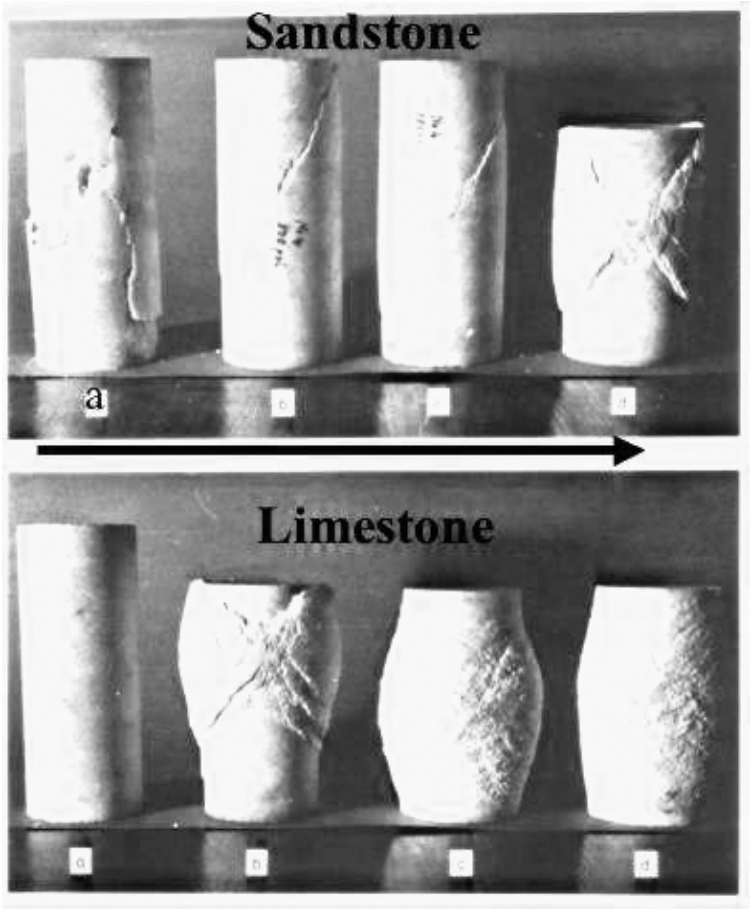
Sandstone
a
Limestone

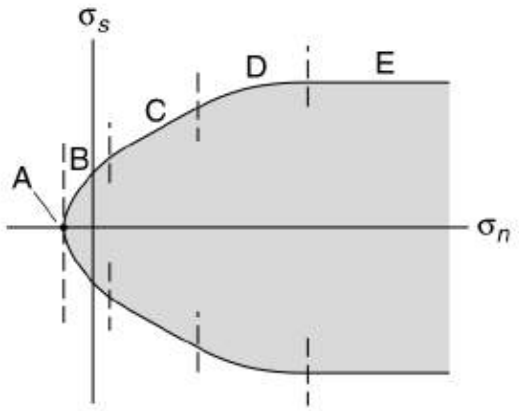

Composite failure envelope

A: Tensile failure criterion
B: Mohr (parabolic) failure criterion
C: Coulomb (straight-line) failure criterion
D: Brittle-plastic transition
E: von Mises plastic yield criterion

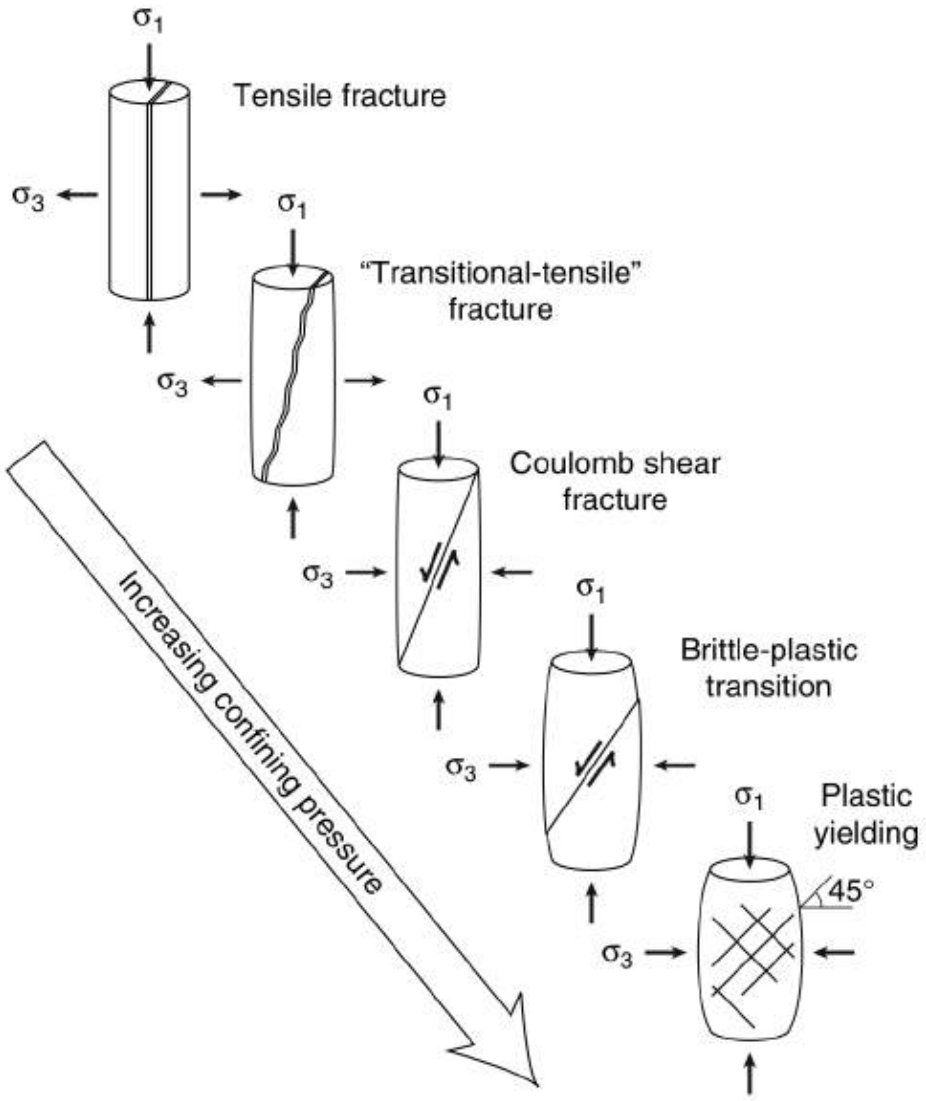

http://ic.ucsc.edu/~casey/eart150/Lectures/BrittleDef/brittleDef.html

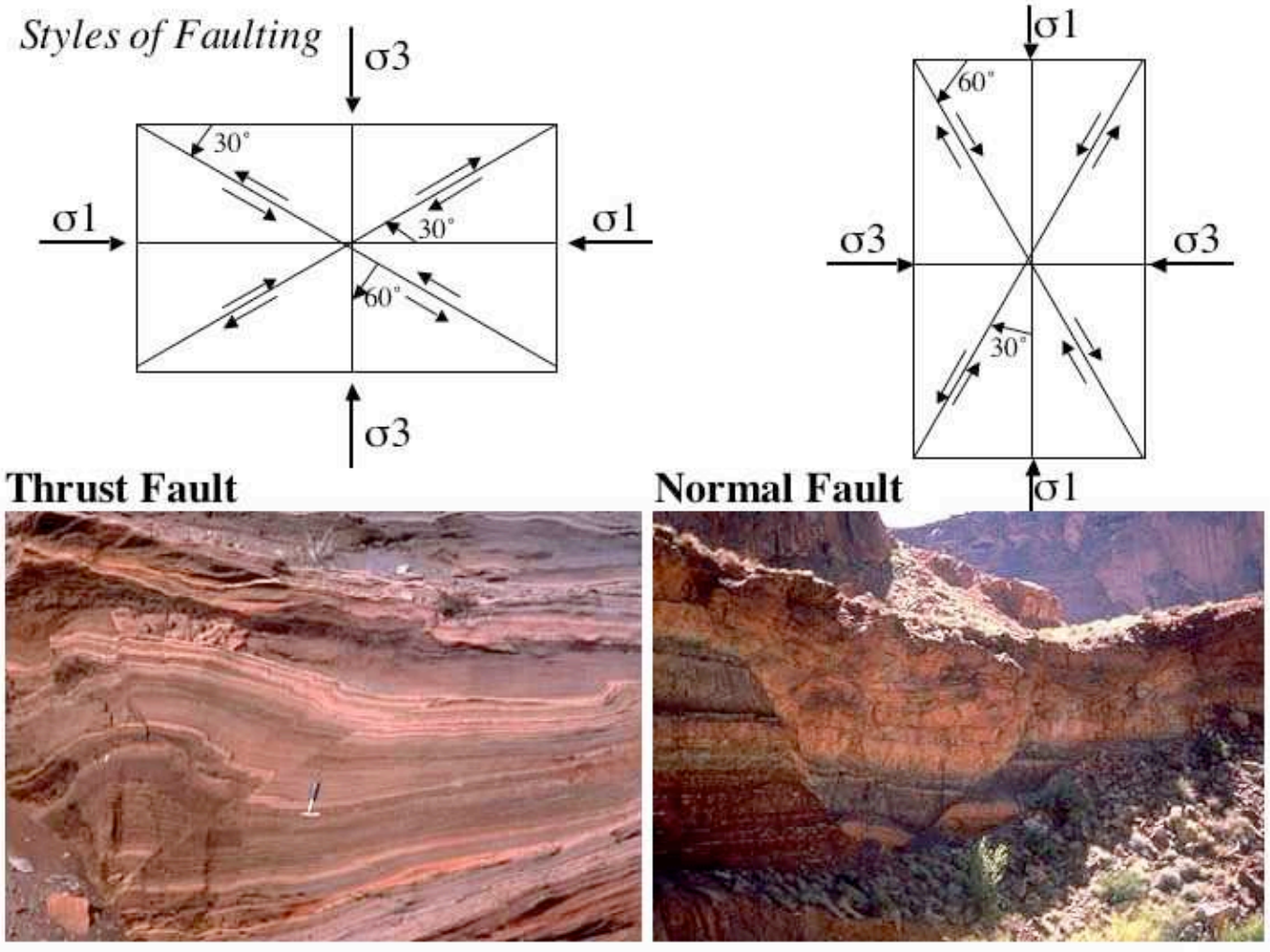

http://ic.ucsc.edu/~casey/eart150/Lectures/faultmechanics/thrst&nrmlflts.stefano/

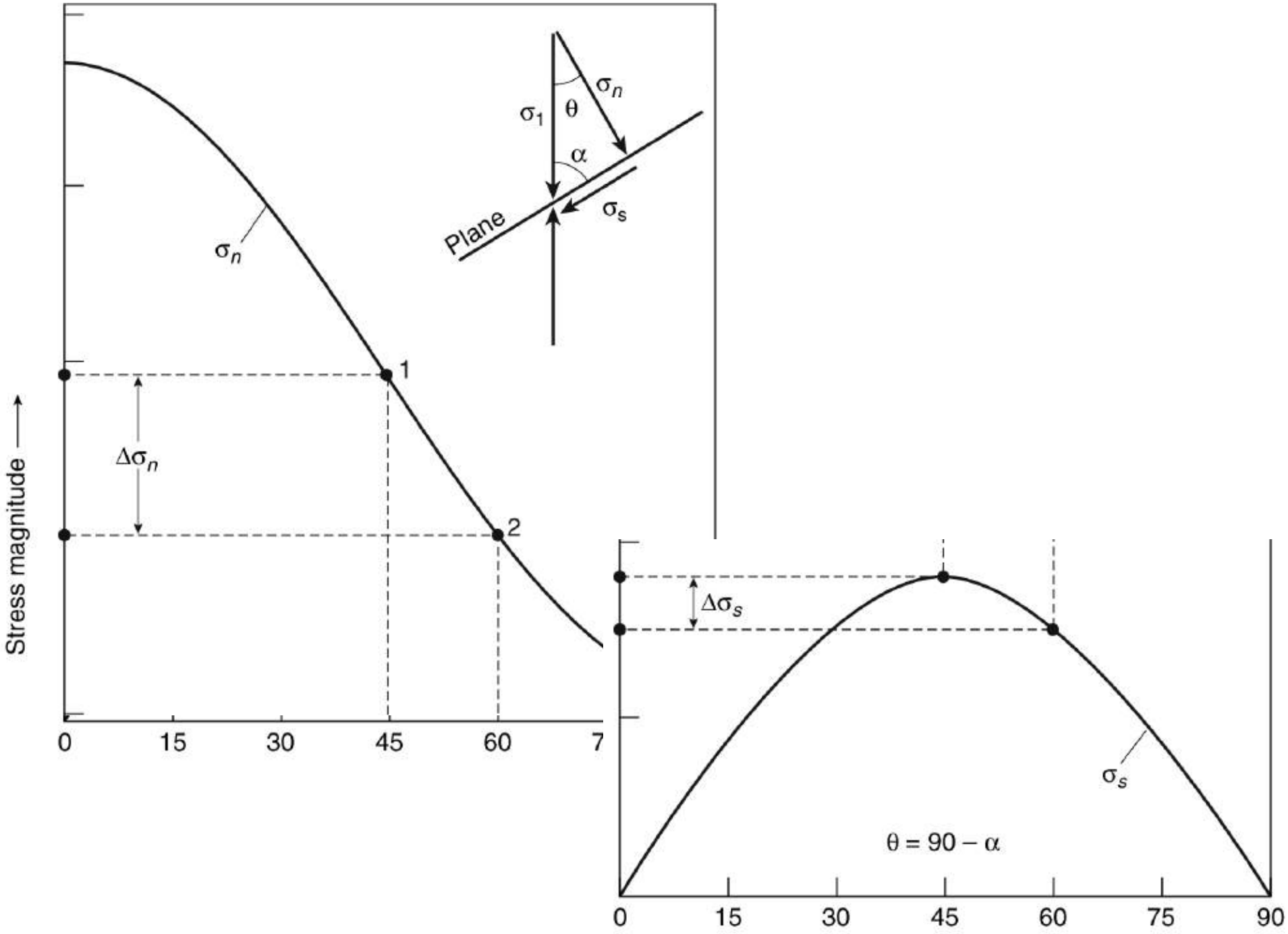
Stress magnitude
σ_n
$\Delta\sigma_n$
1
2
0
15
30
45
60
7
σ_1
θ
σ_n
α
Plane
σ_s
$\Delta\sigma_s$
σ_s
$\theta = 90 - \alpha$
0
15
30
45
60
75
90

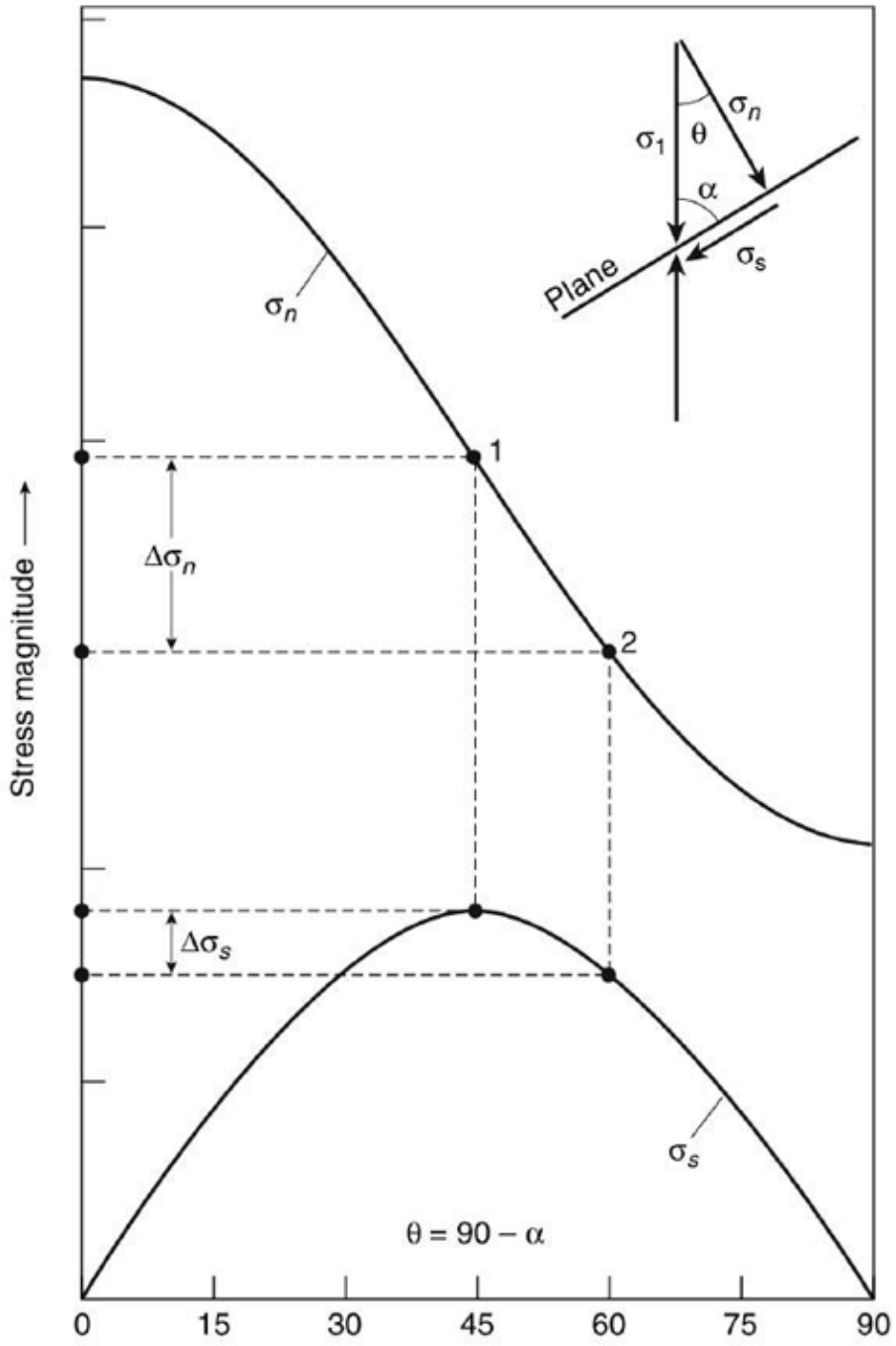
Stress magnitude
σ_n
σ_1
θ
α
Plane
σ_s
1
2
$\Delta\sigma_n$
$\Delta\sigma_s$
$\theta = 90 - \alpha$
0
15
30
45
60
75
90

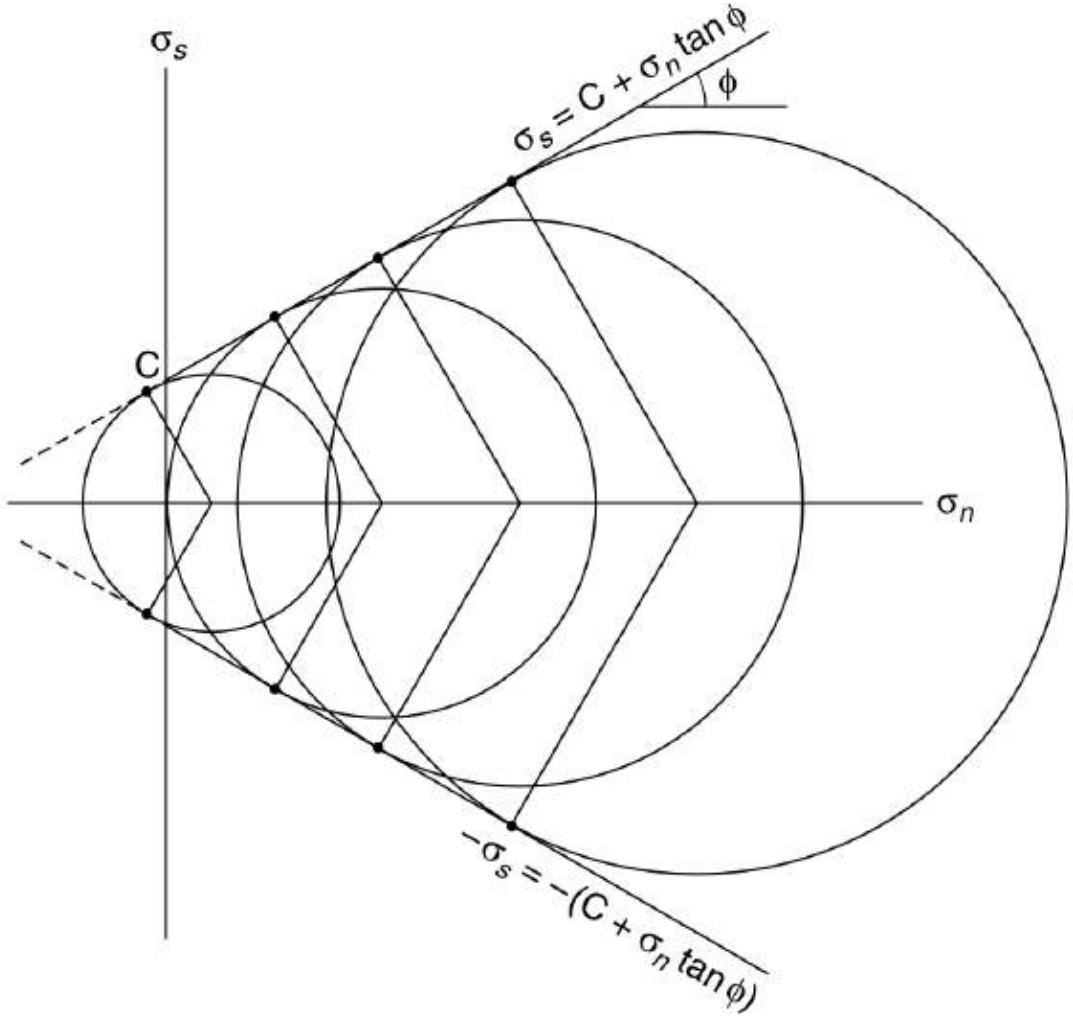
σ_s
$\sigma_s = C + \sigma_n \tan\phi$
ϕ
C
σ_n
$-\sigma_s = -(C + \sigma_n \tan\phi)$

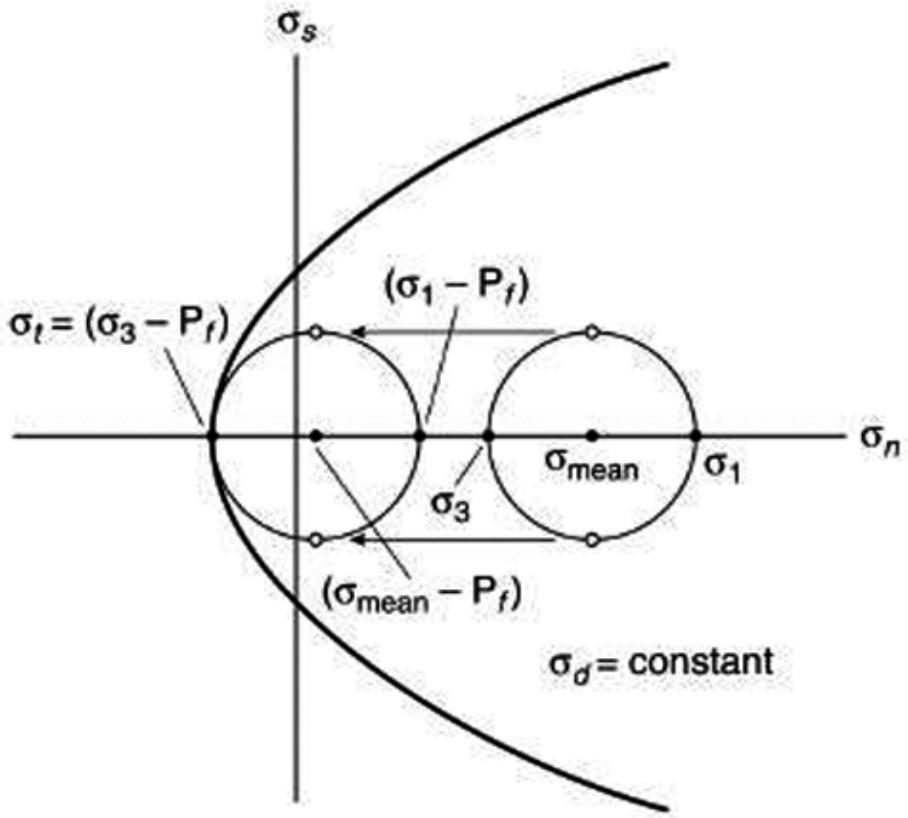

FIGURE 6.27 A Mohr diagram showing how an increase in pore pressure moves the Mohr circle toward the origin. The increase in pore pressure decreases the mean stress (σ_{mean}), but does not change the magnitude of differential stress $(\sigma_1 - \sigma_3)$. In other words, the diameter of the Mohr circle remains constant, but its center moves to the left.

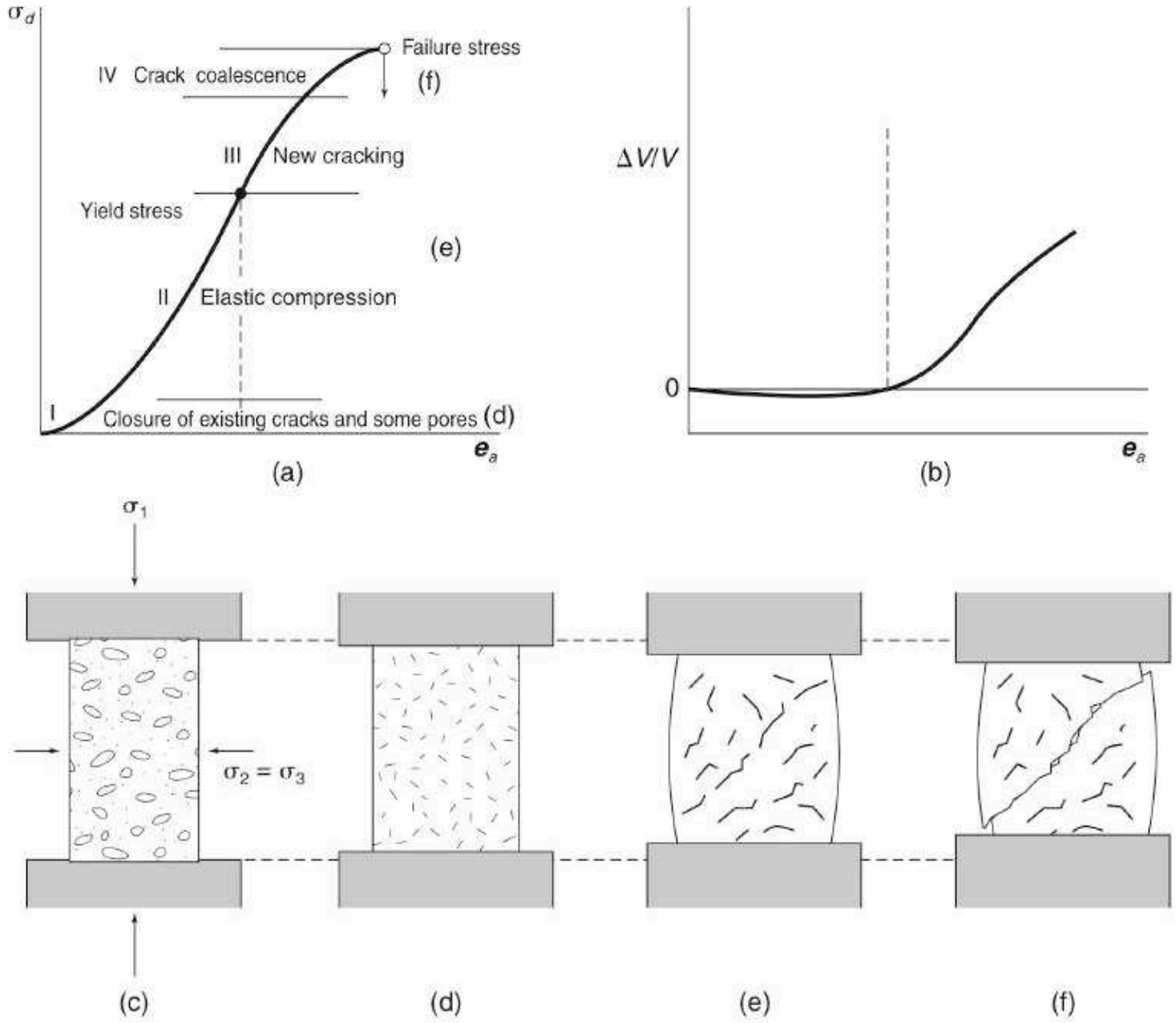
σ_d
Failure stress
IV Crack coalescence
(f)
III New cracking
Yield stress
(e)
II Elastic compression
I
Closure of existing cracks and some pores
(d)
e_a
(a)
$\Delta V/V$
0
e_a
(b)
σ_1
$\sigma_2 = \sigma_3$
(c)
(d)
(e)
(f)

DEFORMATIONSPROZESSE IN DER ERDE I

Repetitorium

1 - Einführung, Geschichte der exp. Gesteinsverformung
2 - Verformungsarten (Spröd - duktil), Typen v. Experimenten
3 - Experiment (Labor), Datenauswertung (rigPrep)
4 - Datenauswertung (rigC4), versch. Masse für Verformung
5 - Karman, Reibungsgesetze (Amonton, Euler), Coulomb-Mohr
6 - Griffith, Reibung in der Tiefe (Byerlee's Regel)

1 Crustal section

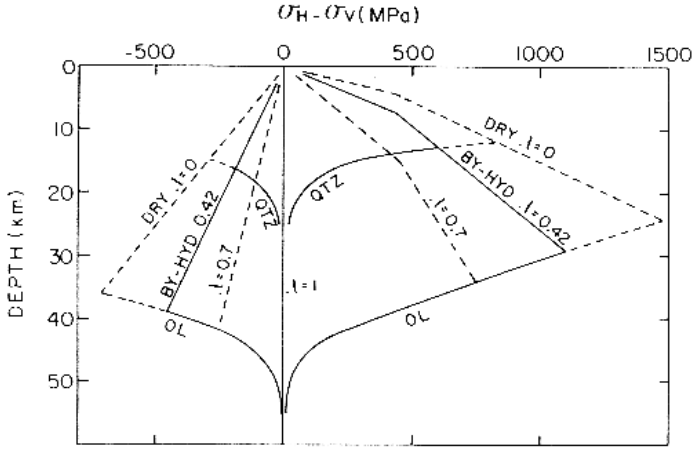

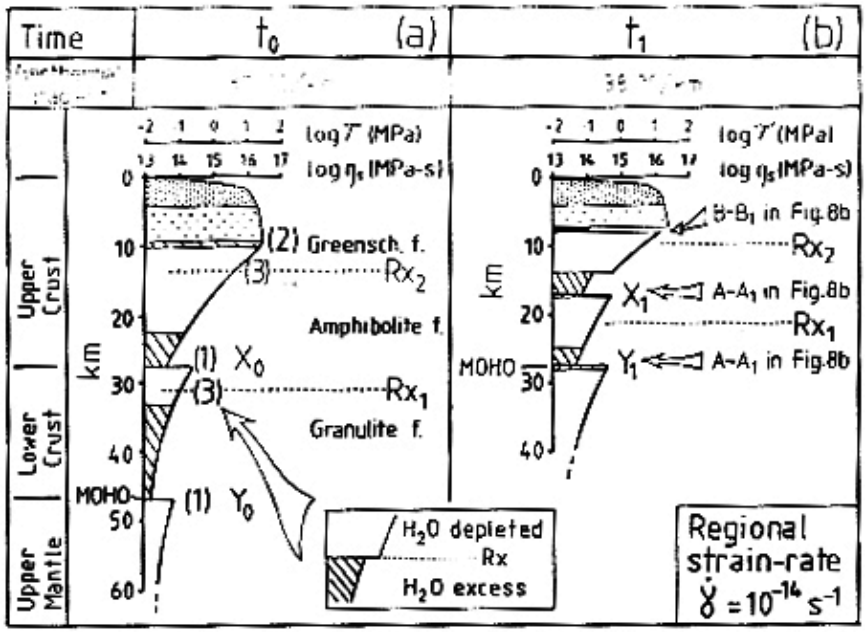

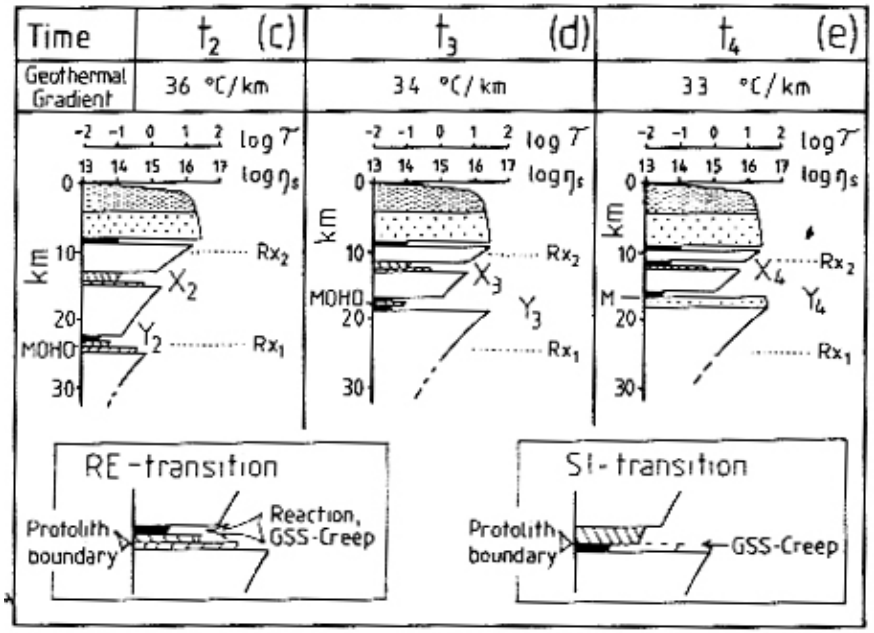

1 States of stress (Mohr cirlcle)

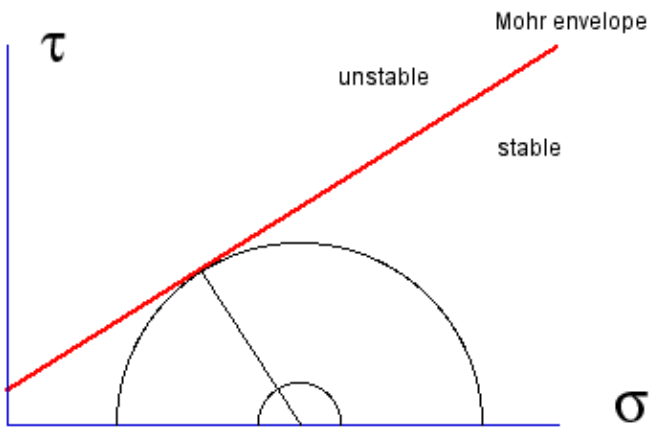

in rock deformation:

compressive > 0 tensile < 0

$\sigma 1 \geq \sigma 2 \geq \sigma 3$

shear component	τ
normal component	σ
mean stress	$\sigma = 1/3 \cdot \sigma ii$
confining pressure	$pc = \sigma 3$
differential stress	$\Delta\sigma = \sigma 1 - \sigma 3$

Loading

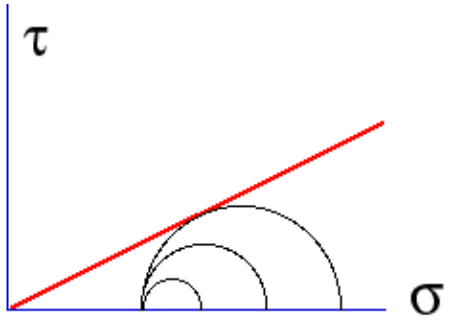

experimental

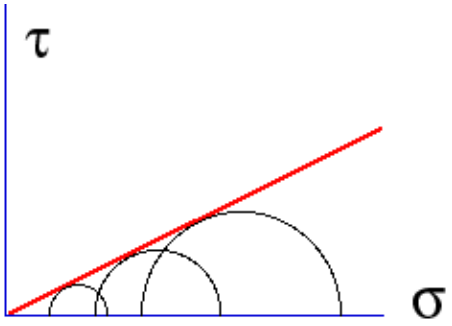

proportional (nature)

TYPICAL MECHANICAL DATA

rock type	strength (MPa) pc = 0 ~ surface conditions	strength (MPa) pc = 100 MPa ~ 3-4 km depth
igneous rocks	100 - 200	500 - 800
calcite rocks, marbles	50 - 100	200 - 300
high porosity sedimentary rocks	10 - 50	
dolomites, quartzites (low porosity)	≤ 300	500 - 1000

GENERAL EFFECT OF VARIABLES ON STRENGTH

factor	change	influence on strength
confining pressure	+	+
temperature	+	-
strain rate	+	+
pore pressure	+	-

2 types of tests

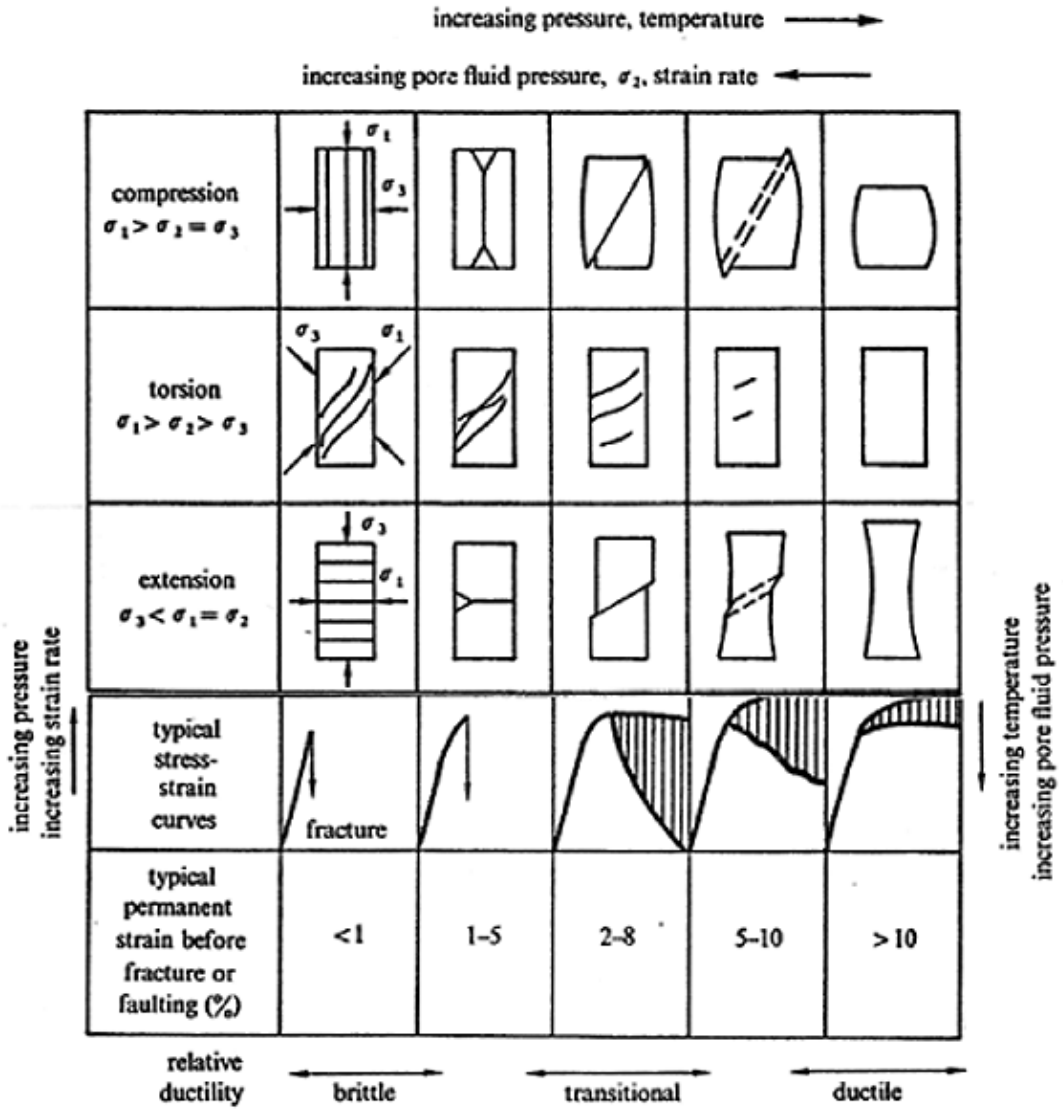

2 types of tests

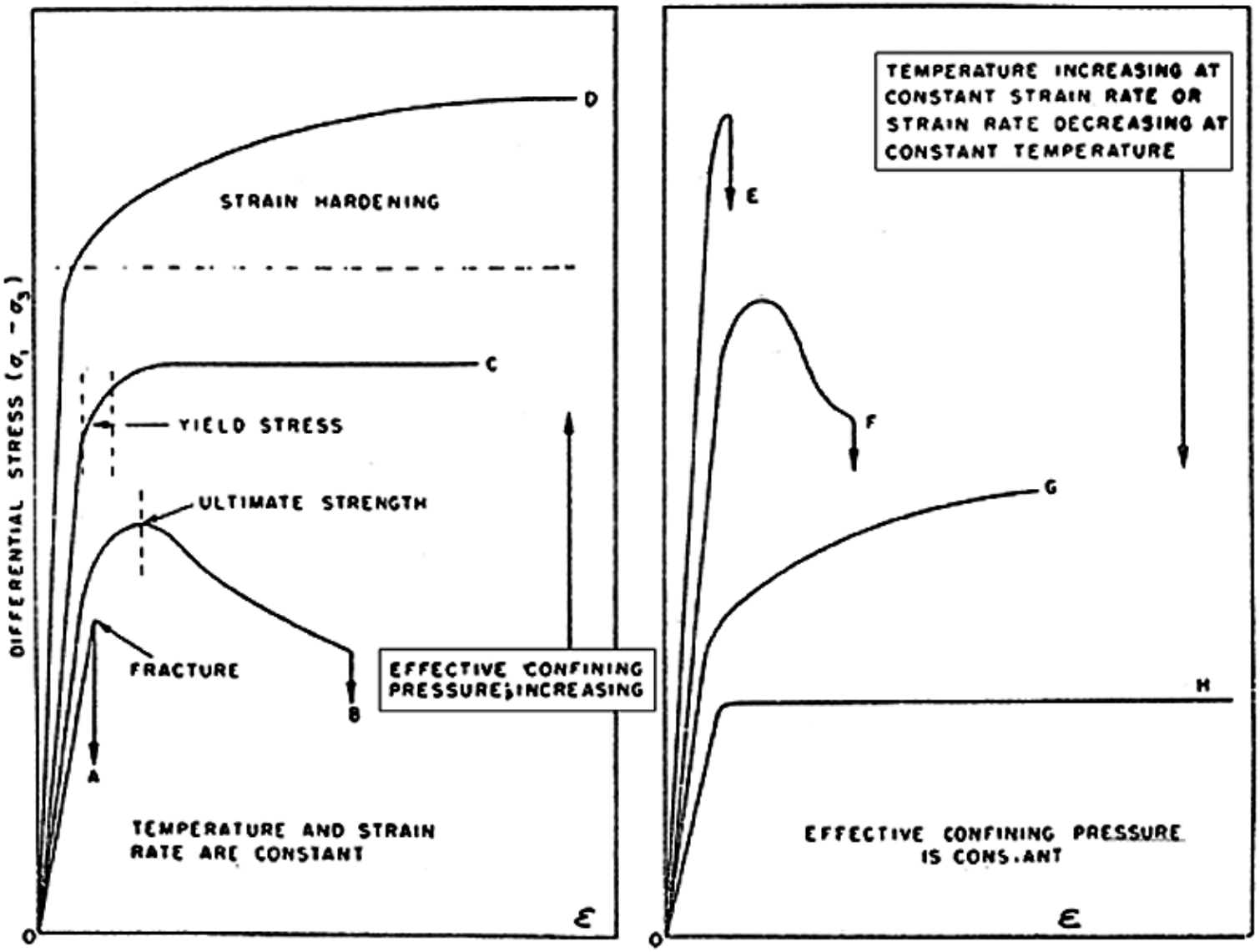

2

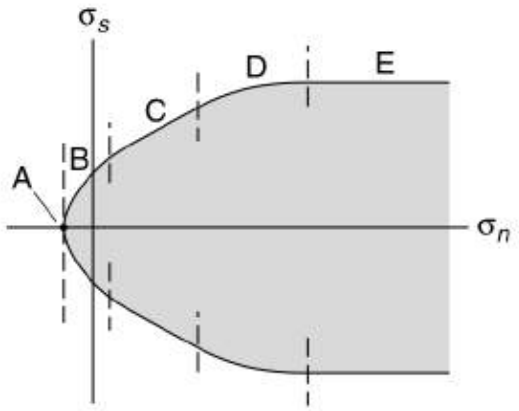

Composite failure envelope

A: Tensile failure criterion
B: Mohr (parabolic) failure criterion
C: Coulomb (straight-line) failure criterion
D: Brittle-plastic transition
E: von Mises plastic yield criterion

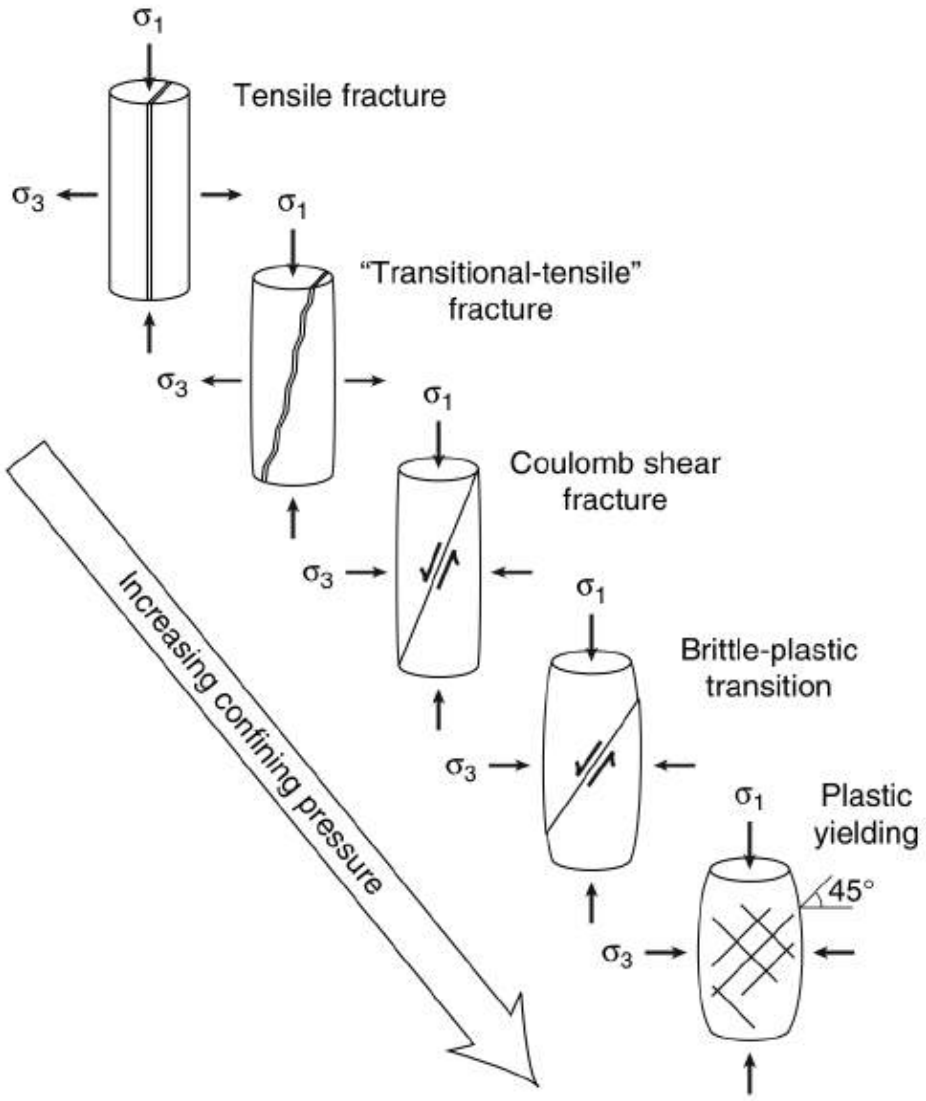

http://ic.ucsc.edu/~casey/eart150/Lectures/BrittleDef/brittleDef.html

3

```
*1---- rig distortion: d -> dc

        do i=1,n
        dc(i) = d(i)-f(i)*distor
        enddo
```

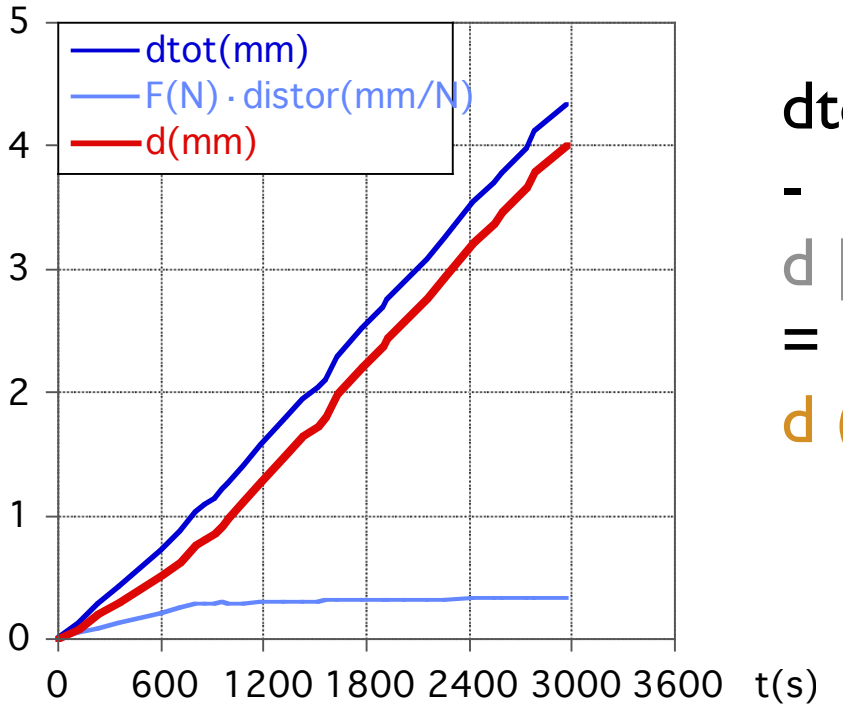

dtot(mm)

-

d [=(F(N) ·distor]

=

d (mm)

3

```
*2---- friction: f -> f*

        do i = 1,n
        fc(i) = f(i)-d(i)*friction
        enddo
```

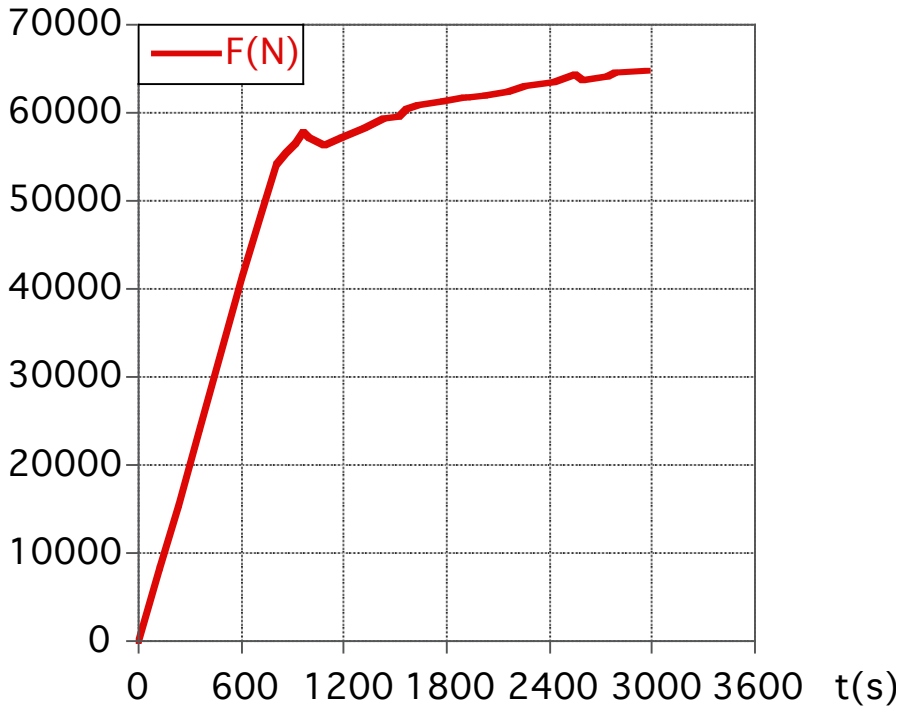

3

```
*3a---- displacement to strain: dc -> e

        do i = 1,n
        e(i) = dc(i) / slen
        enddo
```

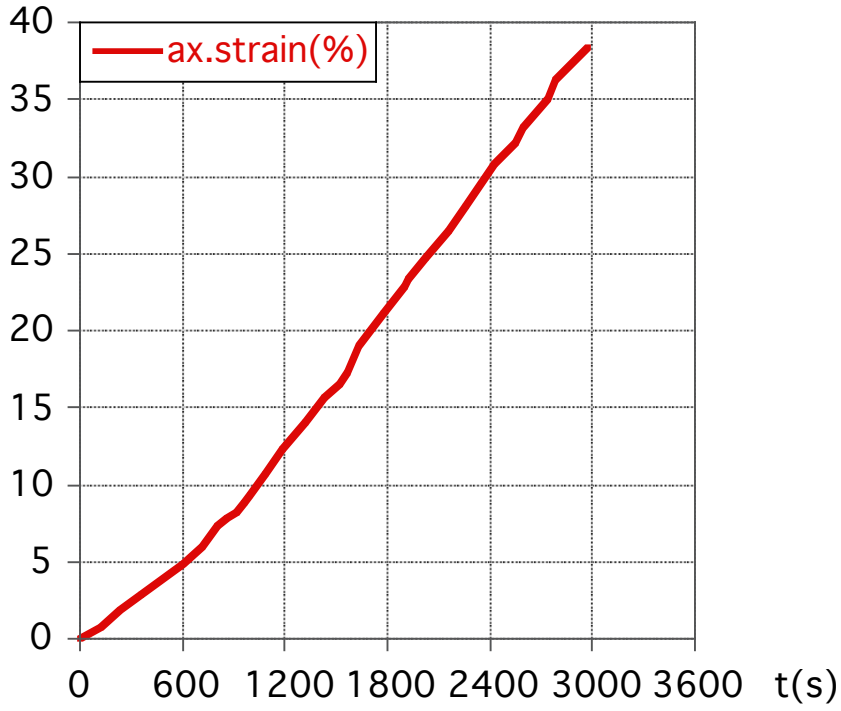

3

```
*4---- load to (axial) differential stress: fc -> s
*      correction for increasing sample diameter
*      correction for changing confining pressure
      do i=1,n
      s(i)    = fc(i) * (1. - e(i)) / area
      sig(i)  = s(i) - p(i)
      enddo
```

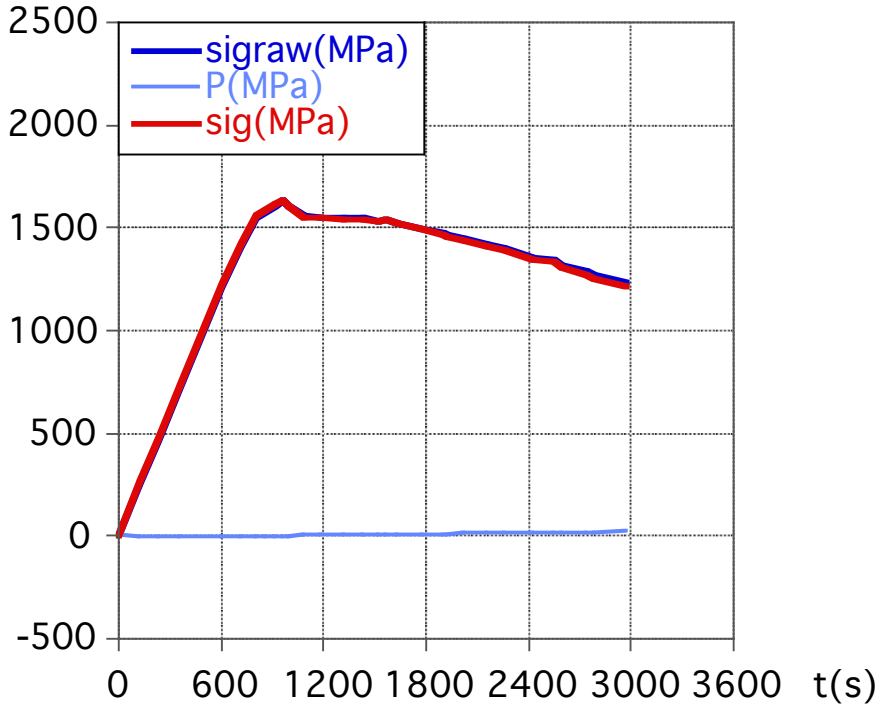

3

$\Delta\sigma = f(e(\%))$

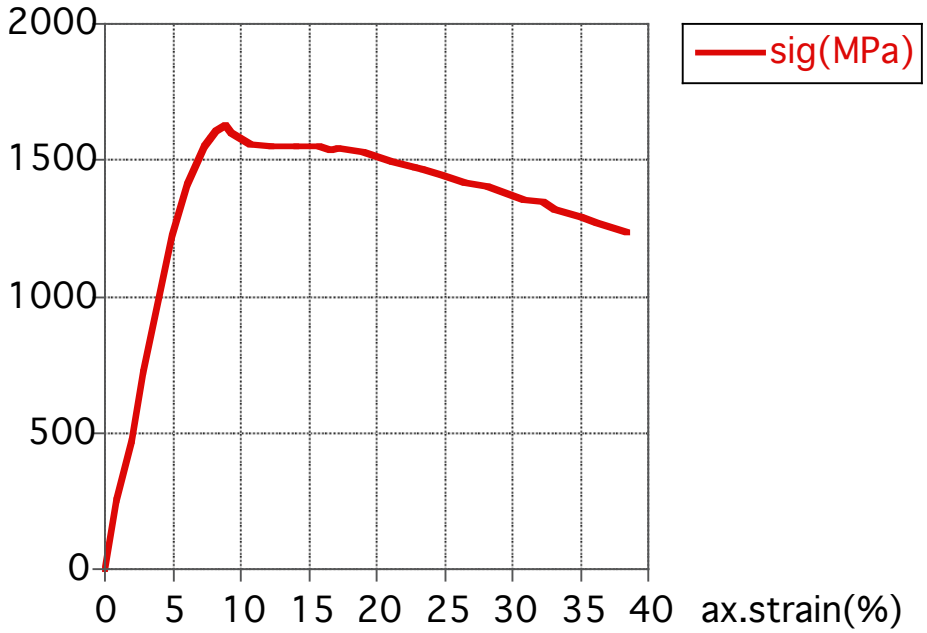

differential stress =
f(engineering strain)

4 Measures for mean strain / strain magnitude

es = oct

strain magnitude = octahedral shear strain

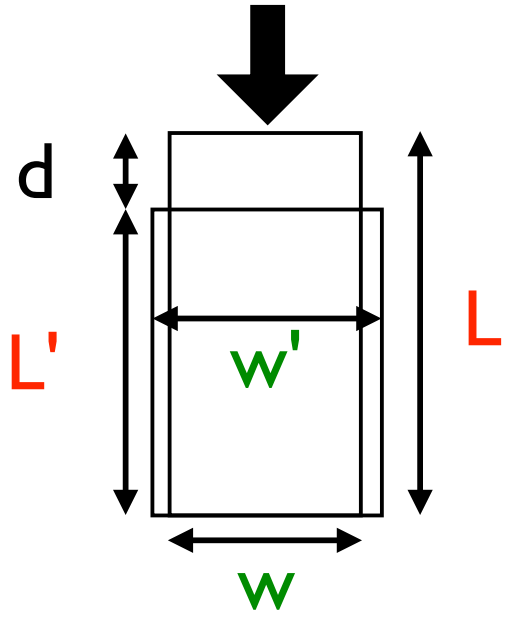

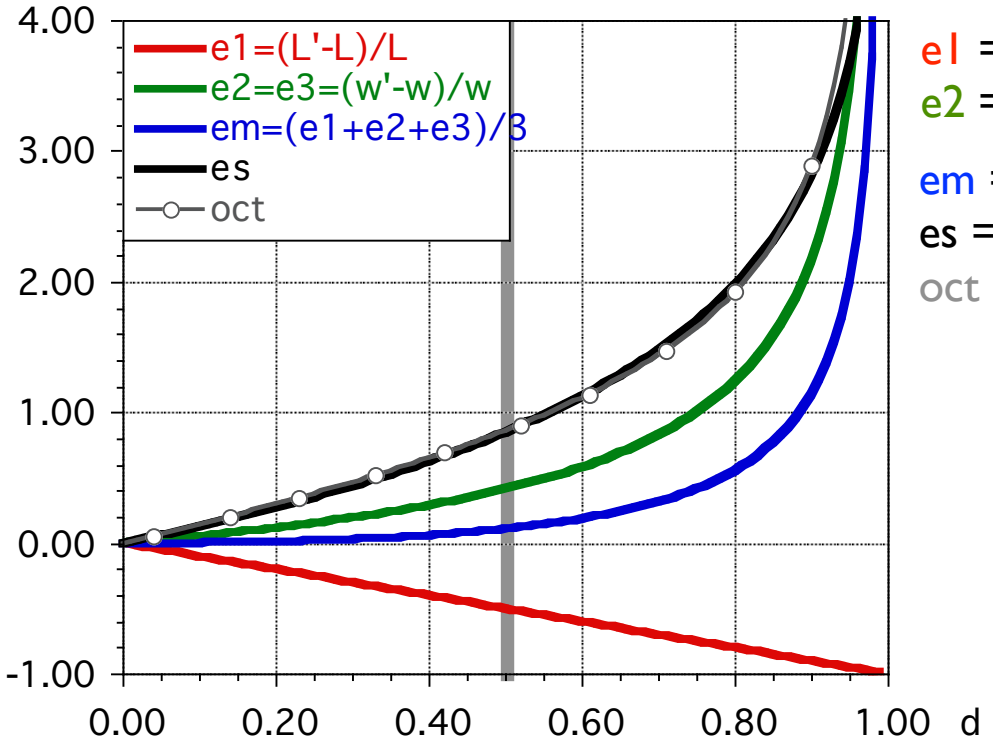

e1 = 1-dim strain

e2 = 1-dim strain

em = 3-dim strain

es = 3-dim strain

oct = 3-dim strain

at d /L = 0.5:

axial strain e1= -0.50, radial strain e2,e3 = 0.41, R = 2.83

mean strain em = 0.11, εs = 0.85, oct.shear strain oct = 0.86

4

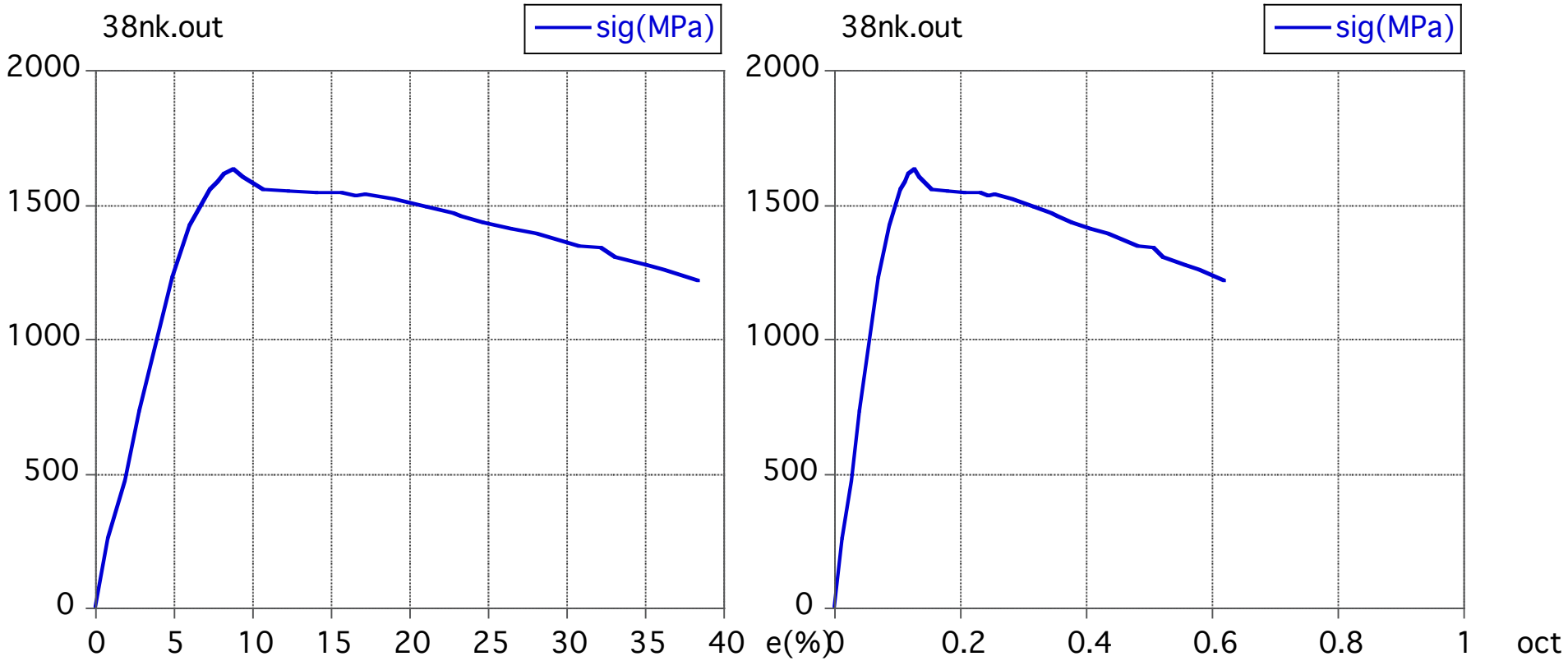

38nk.out:

stress = f(strain)

stress = f(oct. shear strain)

4

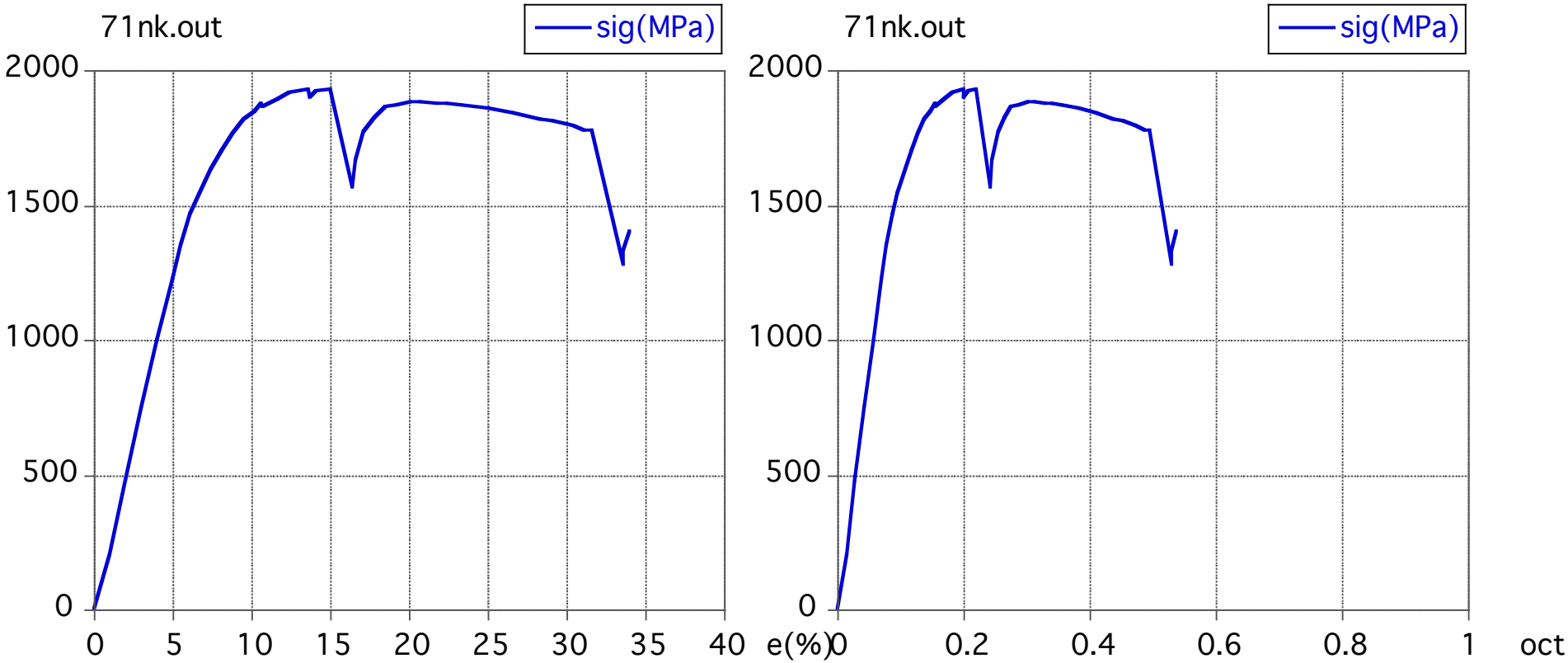

71nk.out:

stress = f(strain)

stress = f(oct. shear strain)

4

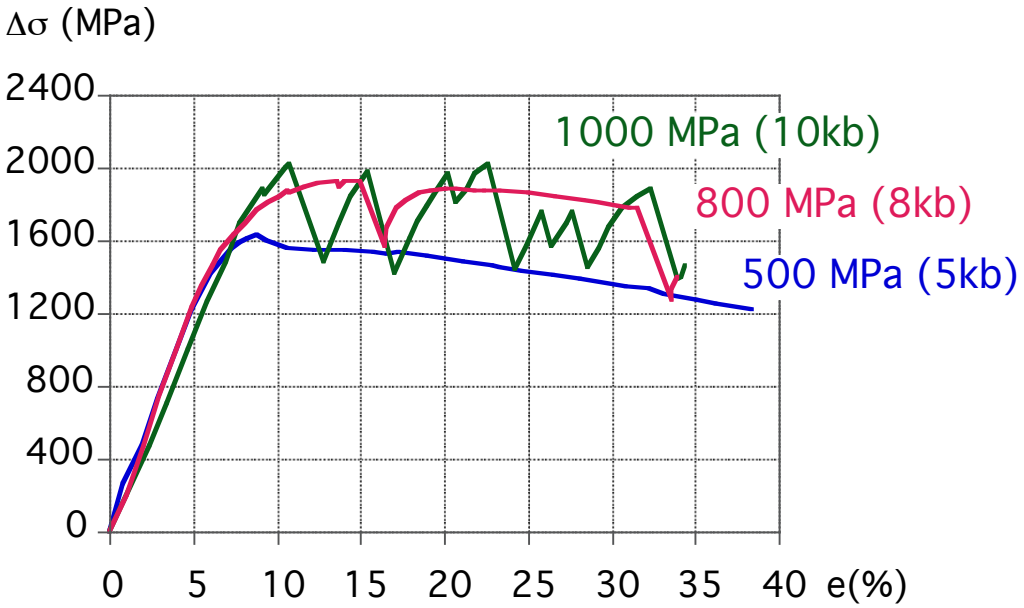

sample	confining pressure (MPa)	max. differential stress (MPa)
38nk	500	1634
60nk	1000	2022
71nk	800	1931

4

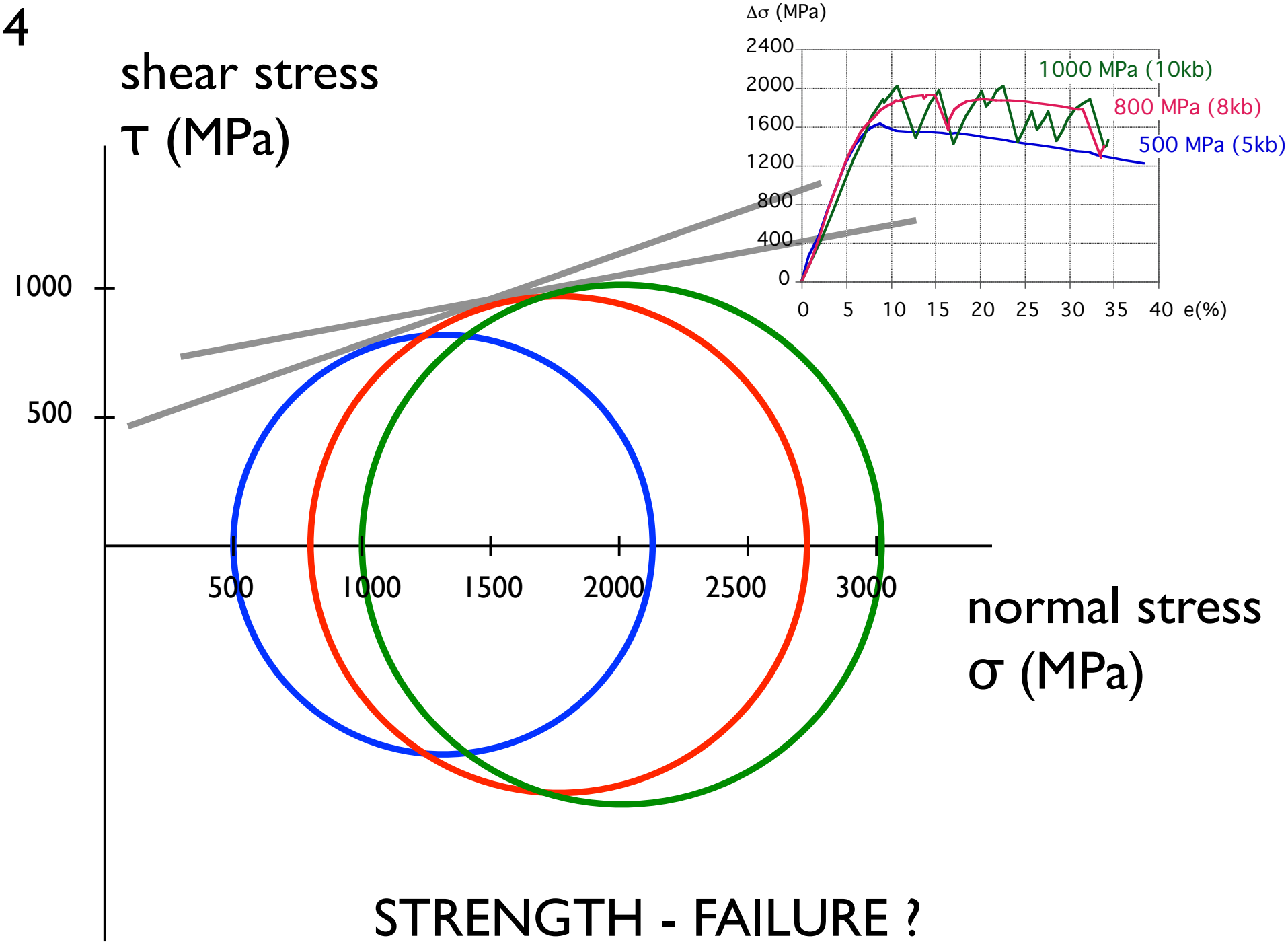

STRENGTH - FAILURE ?

5

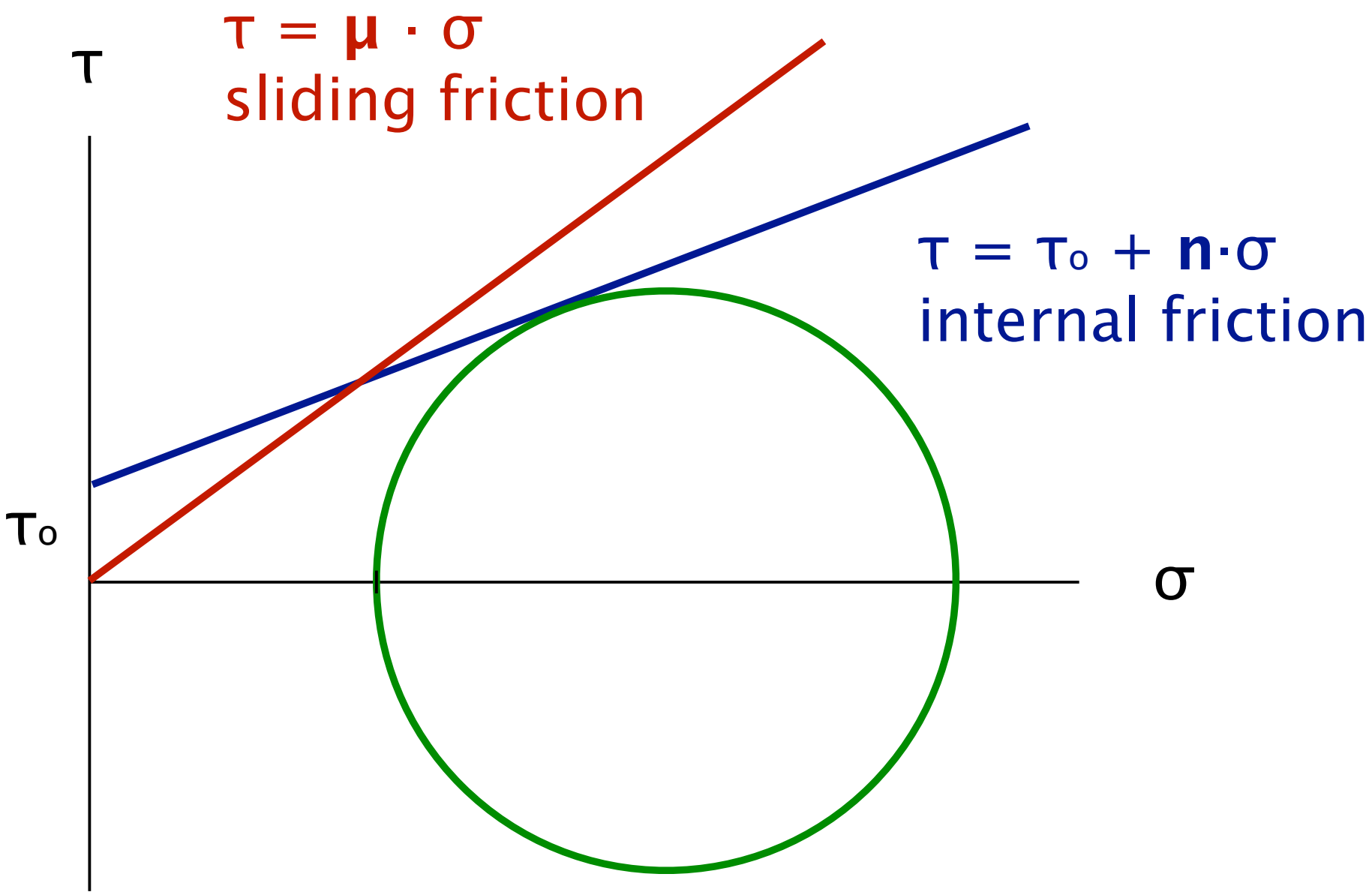

5

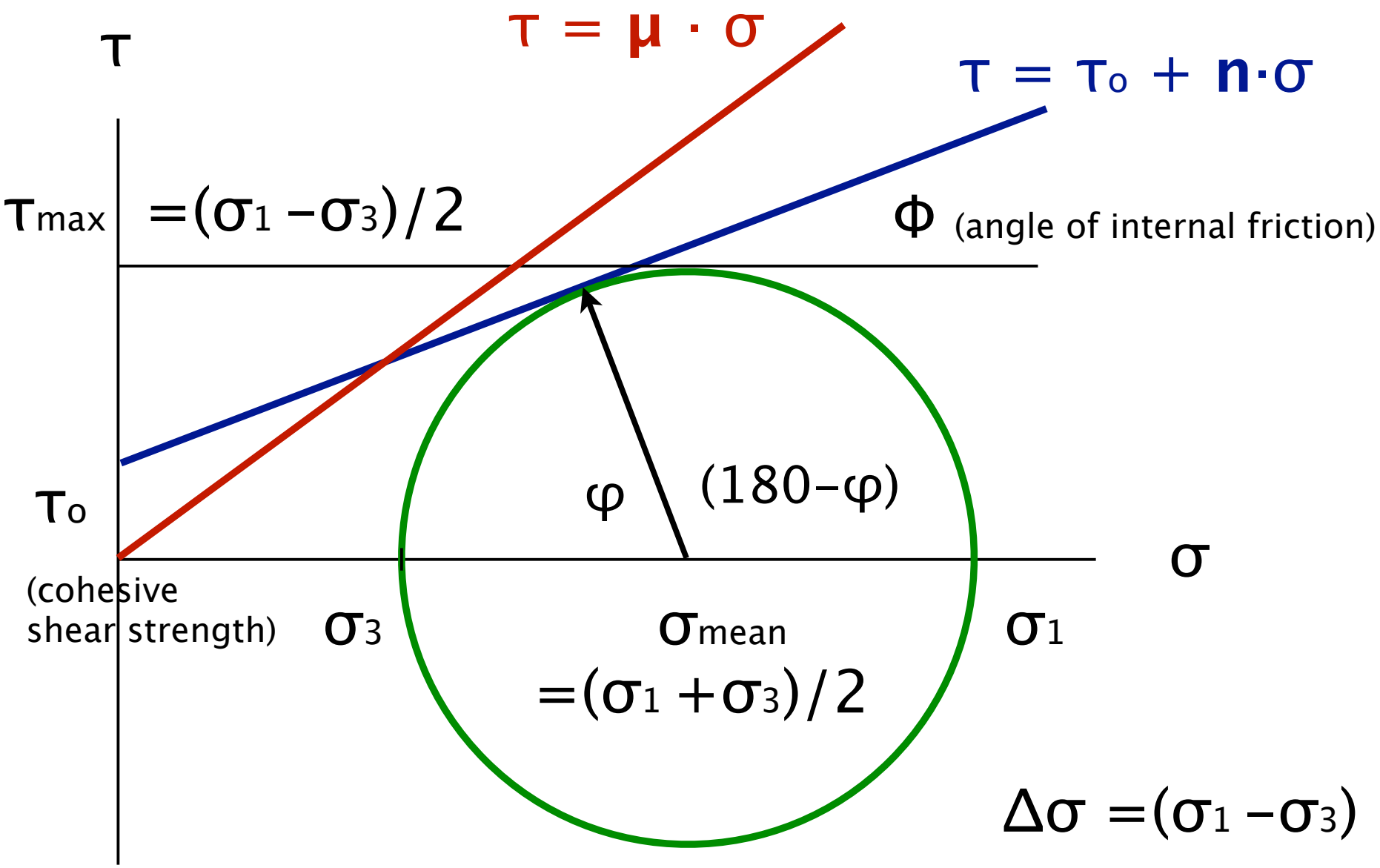
τ
τ = μ · σ
τ = τo + n·σ
τmax =(σ1 −σ3)/2
Φ (angle of internal friction)
τo
(cohesive
shear strength)
φ
(180−φ)
σ
σ3
σmean
=(σ1 +σ3)/2
σ1
Δσ =(σ1 −σ3)

5

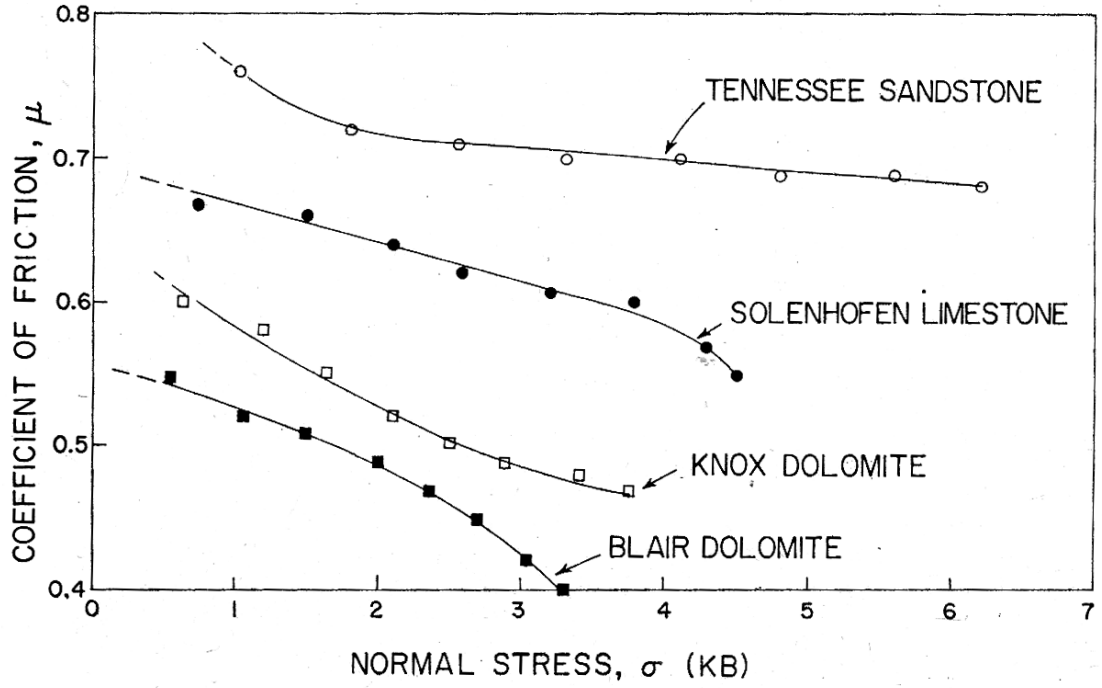

Coefficients of sliding friction on 45° saw cuts in four rocks as functions of normal stress.

TABLE 2. Cohesive Strengths and Coefficients of Internal and Sliding Friction of Some Rock under 1 kb Confining Pressure

Rock	Cohesive Strength τ_0 kb	Coefficient of Internal Friction n	Coefficient of Sliding Friction μ
Blair Dolomite	0.45	1.00	0.40
Lueders Limestone	0.15	0.53	0.60
Solenhofen Limestone	1.05	0.53	0.62
Tennessee Sandstone	0.50	0.84	0.70

τ_0 = cohesive strength
$n = \tan(\Phi)$ = coefficient of internal friction
Φ = angle of internal friction
θf = angle between shear fracture and $\sigma 1$
μ = coefficient of sliding friction ($\tau = \mu \cdot \sigma$)

6

Force at:
C = Initital...
D = Maximum...
G = Residual...
.... Friction

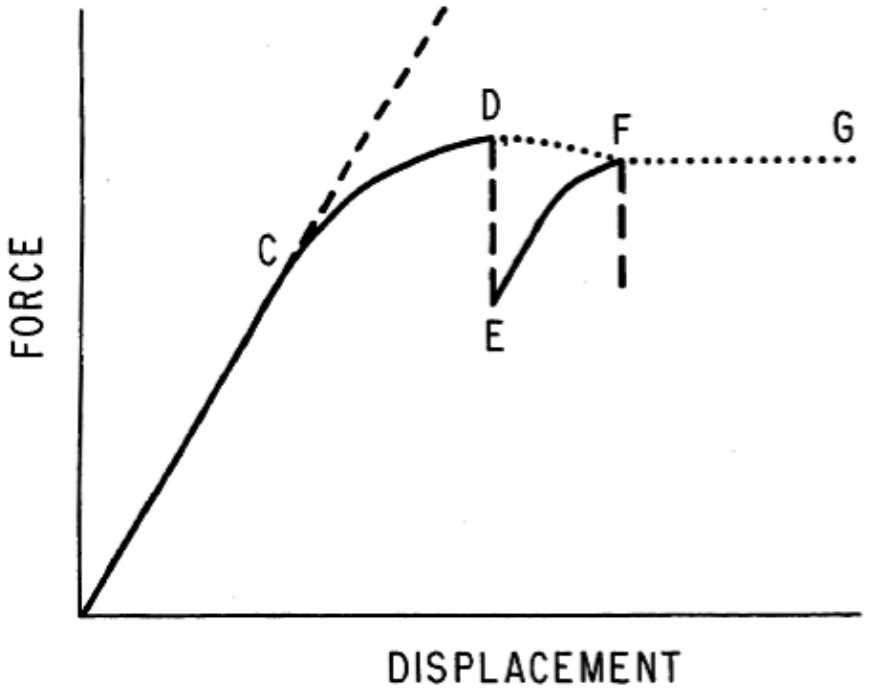

fig. 1 and fig. 2 (Byerlee, 1978)

6

0 - 2 GPa
(0 - 20 kb)
up to 80 km

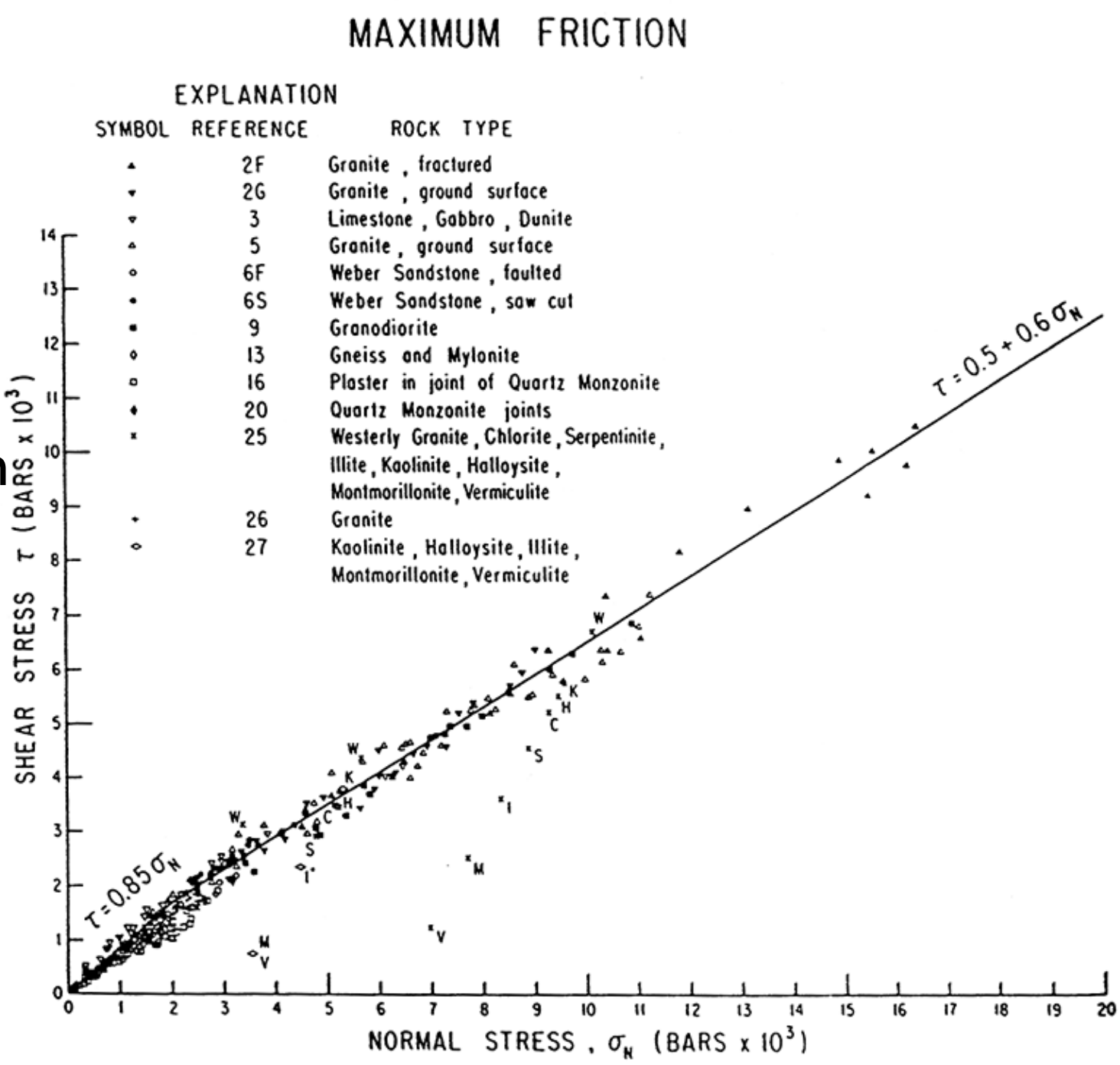

fig. 7 (Byerlee, 1978)

3
Deformation experiment - brittle field

Deformationsprozesse in der Erde I (3)

Deformation experiment - brittle field

Griggs apparatus:

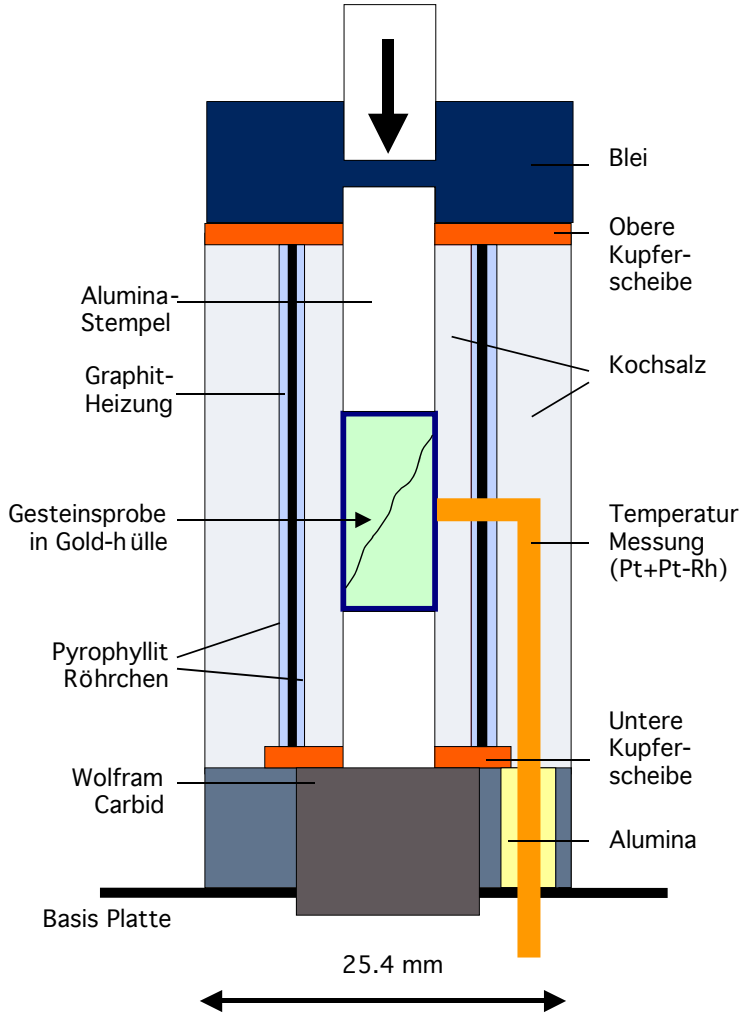

Deformed sample:

Mechanical data:

load(t), displacement(t) ⇨ stress = f(strain)

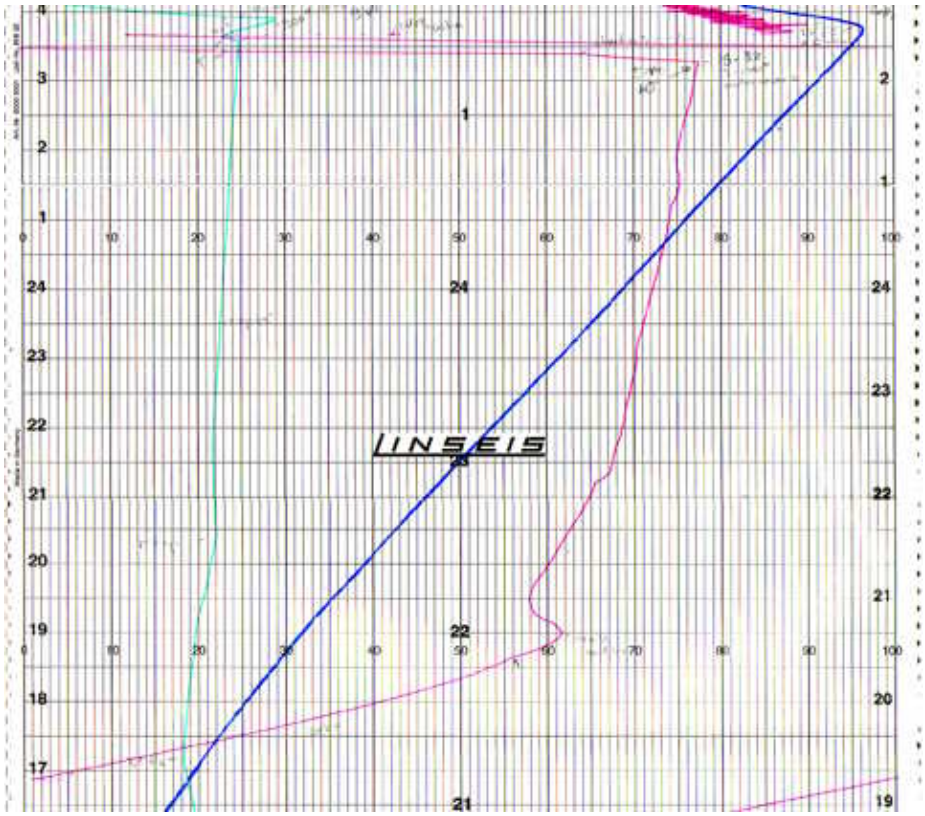

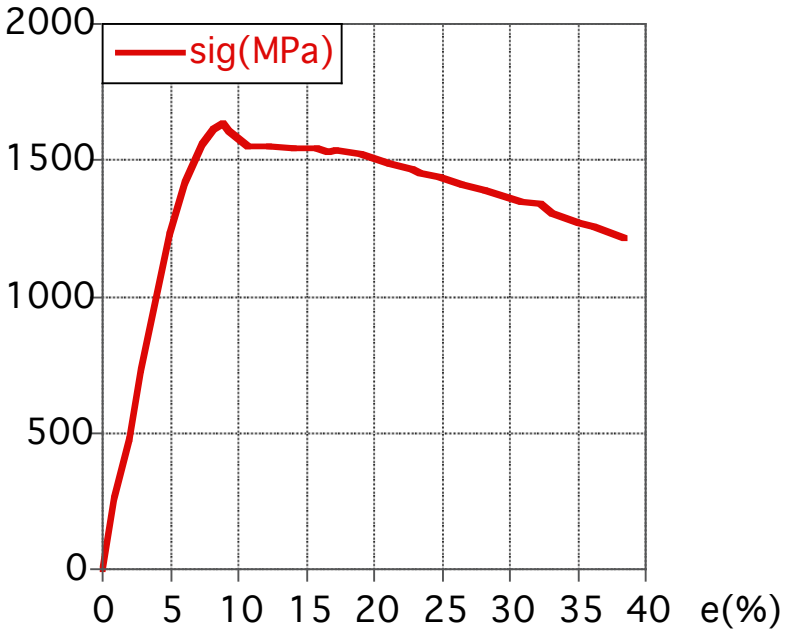

Strip chart rig2

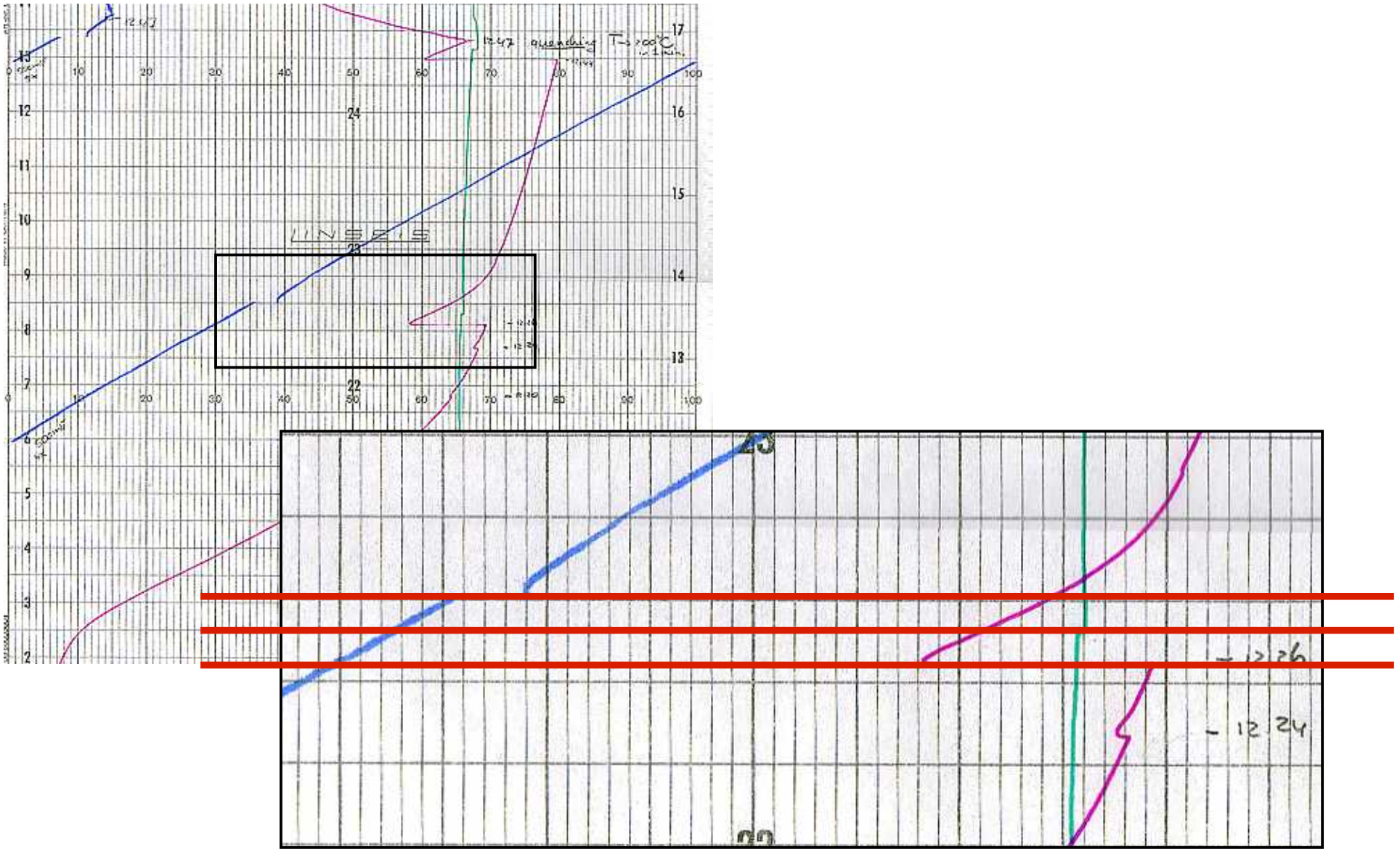

Create input file (test.inp) - Record data

```
38NK
sdia(mm)    slen
6.416,  10.44
d0(chartdiv)    d0(chartdiv)   p0(chartdiv)   f0(chartdiv)
-0.20000    0.0000  20.600  0.0000
chspeed(s/chdiv)  convd(mm/chdiv)  convp(MPa/chdiv)  convf(N/chdiv)
120., 0.050431187, 4.2, 440.69
distor  friction
5.0486E-6,  0.0
n
29
t(i) d(i)  p(i) f(i)
0.80000 2.5000  19.400  18.900
1.8000  5.5000  19.800  35.300
2.8000  8.3000  19.000  54.800
4.8000  14.300  18.600  94.000
5.8000  17.300  18.900  110.30
6.5000  20.500  19.300  122.90
7.0000  21.700  19.500  125.90
7.4000  22.600  19.600  128.50
7.8000  24.100  19.800  131.20
8.1000  25.100  20.100  129.80
8.8000  27.700  21.000  127.80
9.7000  31.100  21.600  129.90
10.800  35.000  22.000  132.40
11.700  38.500  21.900  134.80
12.500  40.300  21.800  135.10
12.800  41.700  21.800  137.00
13.400  45.400  21.900  138.30
14.600  49.800  22.200  139.20
15.600  53.400  22.400  140.10
15.800  54.500  22.500  140.10
16.700  57.400  22.700  140.80
17.800  61.100  23.000  141.80
18.600  64.500  23.200  143.00
20.000  70.200  23.700  144.10
21.000  73.200  23.300  146.10
21.400  75.000  23.800  144.70
22.600  79.000  24.200  145.60
23.000  81.500  24.500  146.50
24.600  86.000  24.900  147.10
```

```
t(i) d(i)  p(i) f(i)
0.8000   2.5000   19.400   18.900
1.8000   5.5000   19.800   35.300
2.8000   8.3000   19.000   54.800
4.8000   14.300   18.600   94.000
5.8000   17.300   18.900   110.30
6.5000   20.500   19.300   122.90
7.0000   21.700   19.500   125.90
7.4000   22.600   19.600   128.50
7.8000   24.100   19.800   131.20

... etc.
```

Create input file (test.inp) - Record data

Rock Deformation & Structure Analysis

http://www.unibas.ch/earth/micro/index.html

compmathheads Adam Riese Power for a...mple z-test Uni Basel VPN Digitizing Tablets AlpConFoto

www.unibas.ch/earth/micro/software/rig/rig.html

ROCK DEFORMATION HOME | lab | pe

- software
- orientation imaging | c-axis analysi
- image analysis | microstructu
- grain size analysis | conversion of
- grain size simulations | simulations o
- stress-strain calculation | data conversi
- lazy macros | macros for N

Display a menu

stress-strain calculation for solid medium deformation apparatus

INPUT

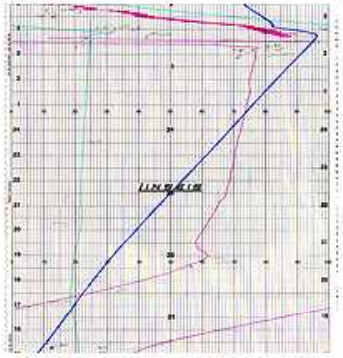

Stripchart with load diplacement recordings

OUTPUT

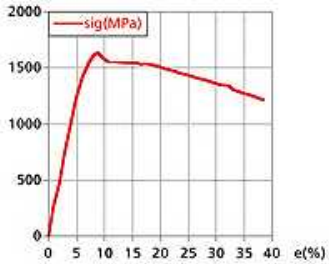

Converted stress strain plot

The rig programs are designed to convert run records of a Griggs-type deformation apparatus to stress strain plots and other type of derived mechanical data.

The input data can be

- displacement, load (chart units)
- time, displacement, confining pressure, load (chart units)

Available programs are

- rigC and rigC2 for axial compression (input: d,f)
- rigC4 for axial compression (input: t,d,p,f)
- rigS and rigS2 for shearing (input: d,f)
- rigS4 for shearing (input: t,d,p,f)

Sources (Fortran 77 text files):
rigC.for (MacOS9)
rigS.for (MacOS9)
rigC2.f (MacOSX)
rigS2.f (MacOSX)
rigC4.f (MacOSX)
rigS4.f (MacOSX)
rigPrep.f (MacOSX)

Compiled versions:
rigC.sea.hqx (MacOS9)
rigS.sea.hqx (MacOS9)
rigC2.exec (MacOSX)
rigS2.exec (MacOSX)
rigC4.exec (MacOSX)
rigS4.exec (MacOSX)
rigPrep.exec (MacOSX)

Test files - INPUT:
testC2.inp - for rigC and rigC2 (d,f input)
testS2.inp - for rigS and rigS2 (d,f input)
testC4.inp - for rigC4 (t,d,p,f input)
testS4.inp - for rigS4 (t,d,p,f input)
Example files - OUTPUT:
testC2.out - from rigC2
testS2.out - from rigS2
testC4.out - from rigC4
testS4.out - from rigS4

Manuals:
rig manual 1
how to run rigC, rigC2 and rigC4 (convert data of axial compression experiment)

to force download, do this:
- on Mac - press Alt key
- on Linux - press Shift key

(last update: 2004-november-21)

(e-mail for more info)

Data:

38nk
5kb 300° 10-4 rig2

60nk
10kb 300° 10-4 rig1

71nk
8kb 300° 10-4 rig2

Prepare input data for riXi4

Terminal
./rigPrep

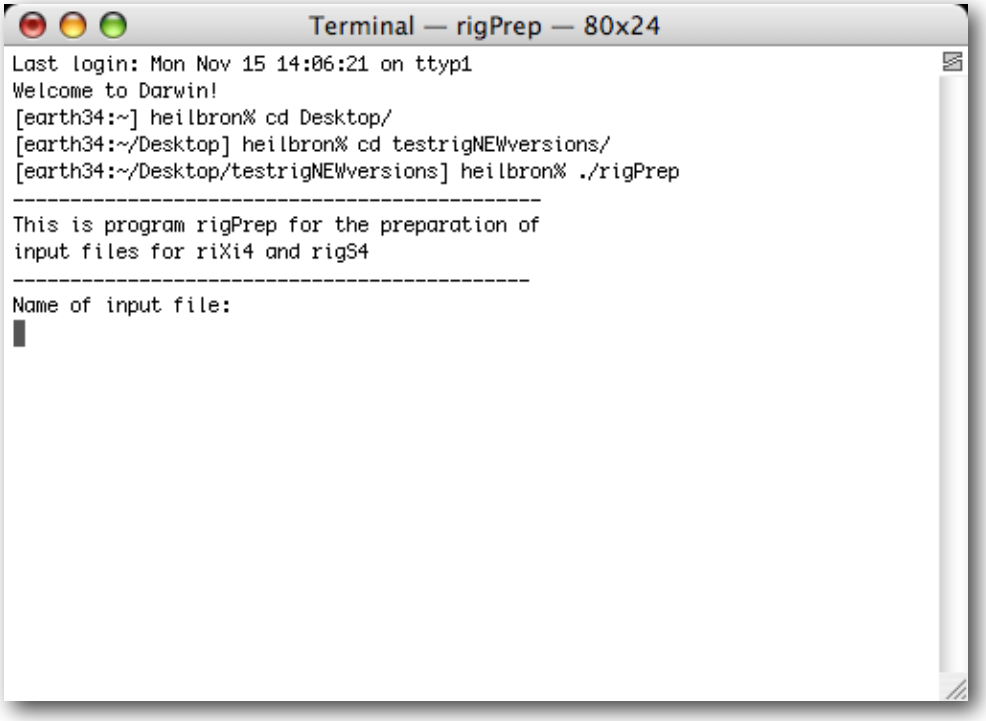

result: header of input file

Run program rigPrep
./rigPrep

```
-------------------------------------------
This is program rigPrep for the preparation of
input files for riXi4 and rigS4
-------------------------------------------
Name of input file:
71nk.4in
File header (max=60 characters):
71 nk 8kb, 300deg, 10-4s-1
Data of axial (1) or shear (2) experiment:
1
Apparatus: rig1 (1) or rig2 (2):
2
sample diameter (mm):
6.383
sample length (mm):
10.538
Chart speed in cm/minute
.5
Displacement record setting:
500mV full scale (1), 1V full scale (2)
1
Confining pressure setting:
2V full scale (2), 5V full scale (5)
5
Load (=force) record setting:
1V full scale (1), 2V full scale (2), 5V full scale (5)
5
T0 = time at hitpoint (chart units)
.2
D0 = displacment at hitpoint (chart units)
58.5
P0 = pressure at hitpoint (chart units)
67
F0 = load at hitpoint (chart units)
4
Number of readings (T,D,P,F) max = 200
1
Input of t(i),d(i), p(i), f(i)
T( 1) --- point no  1
1
D( 1)
1
P( 1)
1
F( 1)
1
------------ done ---------------
```

Result of rigPrep

Example: 71nk.4in

```
71 nk 8kb, 300deg, 10-4s-1
sample diameter(mm)  sample length(mm)
      6.3830      10.5380
t0(chartdiv)  d0(chartdiv)  p0(chartdiv)  f0(chartdiv)
      0.2000      58.5000      67.0000      4.0000
chspeed(s/div)  convd(mm/div)  convp(MPa/div)  convf(N/div)
   0.12000E+03   0.25215E-01   0.12581E+02   0.11017E+04
apparatus distortion(mm/N)  friction(N)
   0.50486E-05   0.00000E+00
number of readings
     1
t(i),d(i), p(i), f(i)
      1.0000       1.0000       1.0000       1.0000
```

71nk

	0 t	1 d	2 p	3 f
1	1.0000	63.900	66.900	10.000
2	2.0000	70.000	66.600	18.000
3	3.0000	76.000	66.300	26.100
4	4.0000	81.700	66.000	33.900
5	5.0000	87.400	65.900	41.200
6	5.5000	90.400	65.800	45.000
7	6.0000	94.100	65.700	48.900
8	6.5000	96.900	65.600	51.500
9	7.0000	100.50	65.400	54.500
10	7.5000	104.20	65.300	57.100
11	8.0000	107.60	65.300	59.600
12	8.5000	110.80	65.300	61.600
13	9.0000	114.00	65.300	63.000
14	9.4000	116.30	65.300	64.400

copy-paste additional points from Kaleidagraph

Finished example: 71nk.4in

```
71 nk 8kb, 300deg, 10-4s-1
sample diameter(mm)  sample length(mm)
      6.3830     10.5380
t0(chartdiv)  d0(chartdiv)  p0(chartdiv)  f0(chartdiv)
      0.2000     58.5000     67.0000      4.0000
chspeed(s/div)  convd(mm/div)  convp(MPa/div)  convf(N/div)
   0.12000E+03   0.25215E-01   0.12581E+02   0.11017E+04
apparatus distortion(mm/N)  friction(N)
   0.50486E-05   0.00000E+00
number of readings
    42
t(i),d(i), p(i), f(i)
1.000  63.90  66.90  10.000
2.000  70.00  66.60  18.000
3.000  76.00  66.30  26.100
4.000  81.70  66.00  33.900
5.000  87.40  65.90  41.200
5.500  90.40  65.80  45.000
6.000  94.10  65.70  48.900
6.500  96.90  65.60  51.500
7.000  100.5  65.40  54.500
7.500  104.2  65.30  57.100
8.000  107.6  65.30  59.600
8.500  110.8  65.30  61.600

...

etc.
```

displacement - conf.pressure - load (chart units): 71nk.4in

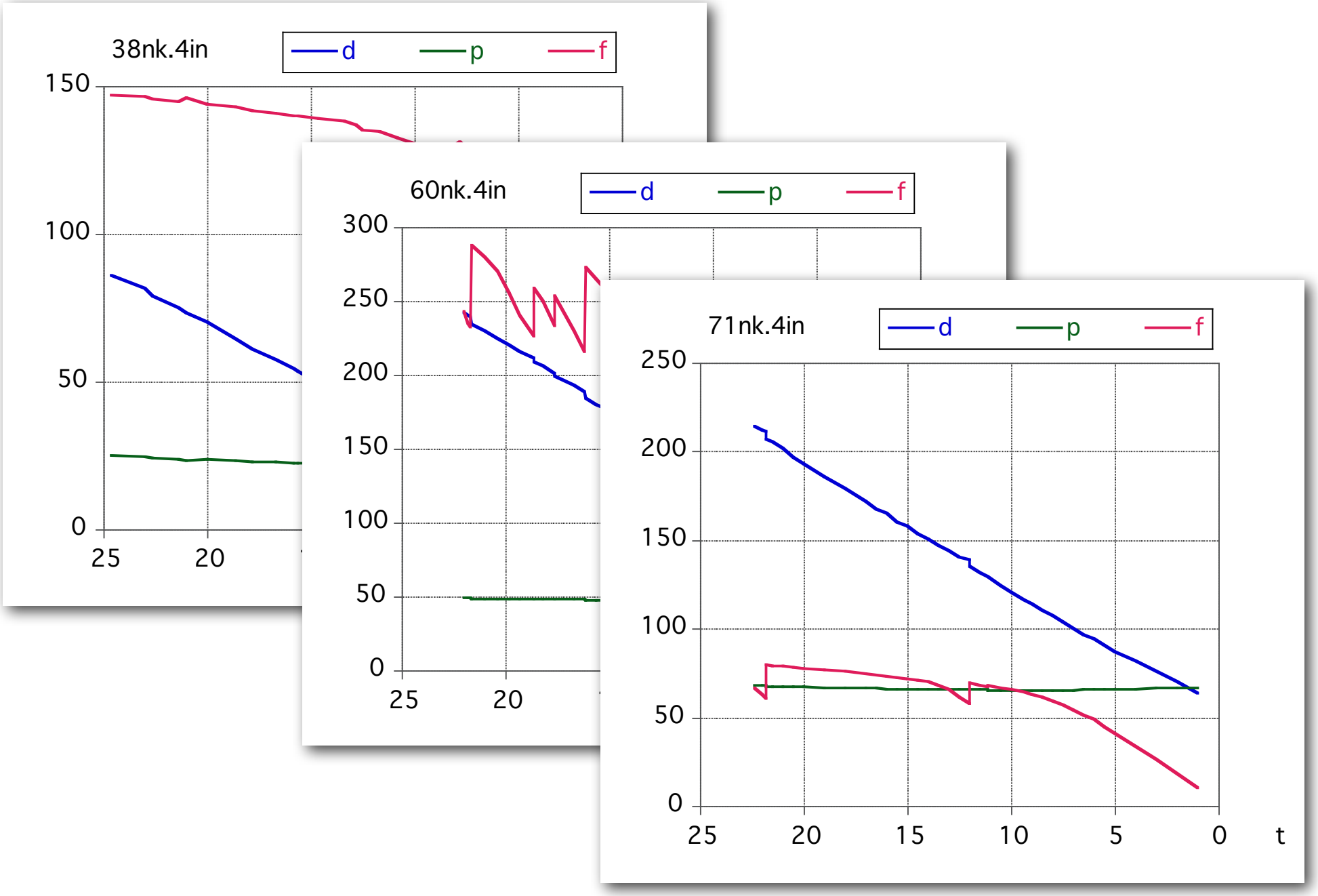

Program riXi4

```
*-----------------------------------------------------------------------
*   Program riXi4 (Fortran 77)
*-----------------------------------------------------------------------
*   For rig1 and rig2 (Basel):
*   Data: time (t) - displacement (d) - confing pressure (p) - force (f)

*   The idea of this program is to read

*      ALL the sample specifications
*      ALL the necessary conversion factors and rig settings
*      ALL the calibrations
*      N, the number of (digitized) data points, and
*      T(N), D(N) = time and displacement in chart units
*      P(N), F(N) = pressure and load in chart units

*   from a pre-existing input file.

*   If this file does not exist, it has to be generated using
*   e.g., Edit II or and text editor.

*   This input file is meant to be explicite, no implicit
*   conversions or assumptions are "hidden" in the program

*   Upon reading, the chart units are converted to
*   real t(n), d(n), f(n) and p(n), where t is in seconds,
*   d is in millimeters, p is in MPa and f is in Newtons.

*   1. The displacement is corrected (rig stiffness); this correction can be zero.
*   2. The load is corrected (friction); this correction can be zero.
*      There is no separate jacket correction.
*   3. The strain is calulated assuming zero volume change and
*      homogeneous deformation (cylinder).
*   4. The differential stress is calculated for increasing sample diameter
*      assuming that the cross-sectional area = f(sample strain).
*      Differential stress is corrected for changes of the confining pressure.
*   5. Between consecutive points, strain rate and rate of strain magnitude
*      are calculated.

*   The output file contains a list of
*      t(n)   time (s)
*      f(n)   load, raw  (N)
*      d(n)   displacement, raw (mm)
*      fc(n)  load, corrected  (N)
*      dc(n)  displacement, corrected (mm)
*      e(n)   axial strain dl/l0 (%)
*      s(n)   differential stress (MPa)
*      o(n)   strain magnitude (%)
*      et(n)  strain rate (multiples of 10-6 s-1)
*      ot(n)  rate of strain magnitude (multiples of 10-6 s-1)

*   From this file various plots can be generated
*   e.g., using Kaleidagraph

*   This program has been developed from rigC,
*   which has been compiled (copied and pasted) from
*   various precursors (RIGCX etc.) written for the Griggs
*   apparatus at Brown Univ. and from another one (RIG) written for
*   the Heard apparatus at ETH Zürich.

*   Brown, August 2001  RH
*   Basel, November 2004 RH
```

Input file (test.inp) - Conversion factors

```
38NK
sdia(mm)    slen
6.416,  10.44
d0(chartdiv)    d0(chartdiv)   p0(chartdiv)   f0(chartdiv)
-0.20000    0.0000  20.600  0.0000
chspeed(s/chdiv)  convd(mm/chdiv)  convp(MPa/chdiv)  convf(N/chdiv)
120., 0.050431187, 4.2, 440.69
distor  friction
5.0486E-6,  0.0
n
29
t(i) d(i)  p(i) f(i)
0.80000 2.5000  19.400  18.900
1.8000  5.5000  19.800  35.300
```


```
38NK
sdia(mm)   slen
6.416,   10.44
d0(chartdiv)   d0(chartdiv)   p0(chartdiv)   f0(chartdiv)
-0.20000   0.0000   20.600   0.0000
chspeed(s/chdiv) convd(mm/chdiv) convp(MPa/chdiv) convf(N/chdiv)
120., 0.050431187, 4.2, 440.69
distor   friction
5.0486E-6,   0.0
n
29
```

Program riXi4.f (Fortran77 source code) step 0

```
do k=1,n
i=n+1-k

t(i+1)= (t(i)-t0)*chspeed  ! convert T to s
d(i+1)= (d(i)-d0)*convd    ! convert D to mm
p(i+1)= (p(i)-p0)*convp    ! convert P to MPa
f(i+1)= (f(i)-f0)*convf    ! convert F to N

enddo
```

Program riXi4.f (Fortran77 source code) step 1

```
*1---- rig distortion: d -> dc

      do i=1,n
      dc(i) = d(i)-f(i)*distor
      enddo
```

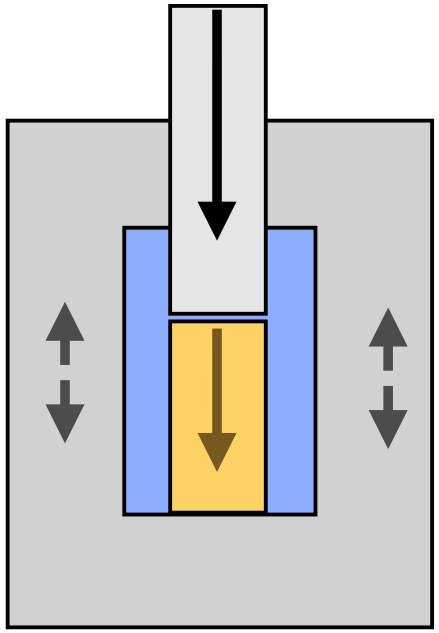

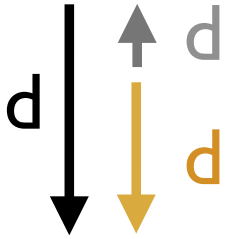

Total displacement d of piston
- distortion d of apparatus
= net displacement d of sample

$$d - d = d$$

K = stiffness of apparatus

$$d = K \cdot F$$

for rig2:

$K = 5.0486 \cdot 10\text{-}6$ mm/N

Program riXi4.f (Fortran77 source code) step 1

```
*1---- rig distortion: d -> dc

      do i=1,n
      dc(i) = d(i)-f(i)*distor
      enddo
```

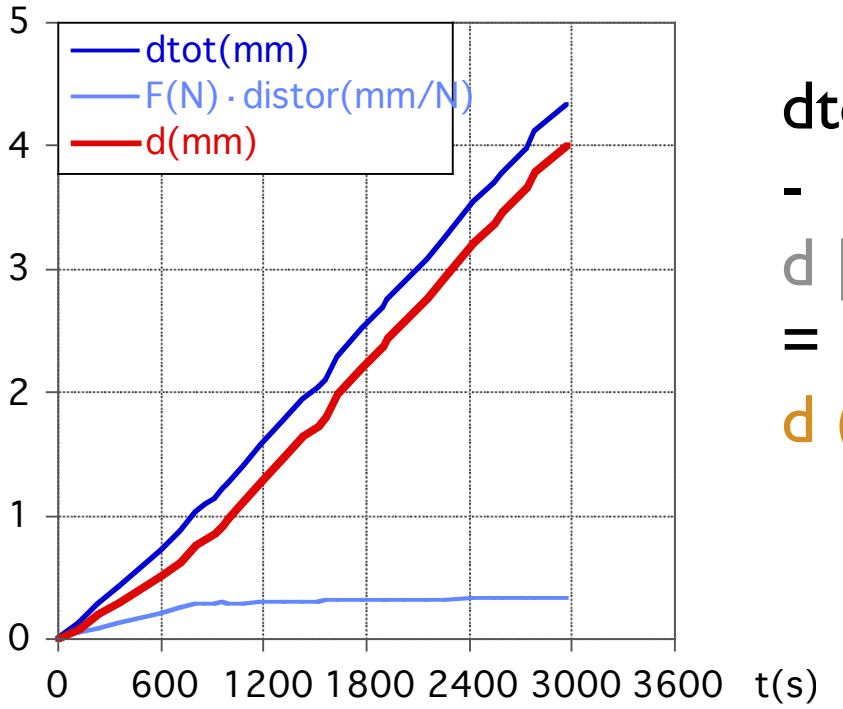

dtot(mm)

-

d [=(F(N) ·distor]

=

d (mm)

Program riXi4.f (Fortran77 source code) step 2

```
*2---- friction: f -> f*

      do i = 1,n
      fc(i) = f(i)-d(i)*friction
      enddo
```

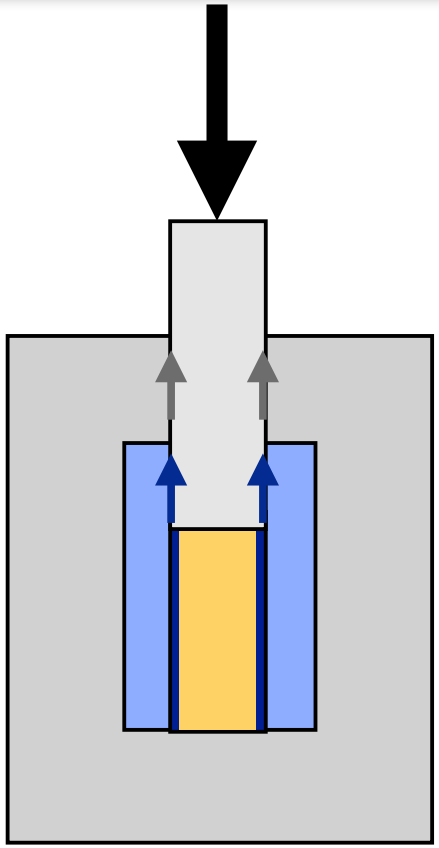

applied load

friction supports load

cross sectional area
of jacket supports load

(riXi4: no jacket correction)

Program riXi4.f (Fortran77 source code) step 2

```
*2---- friction: f -> f*

      do i = 1,n
      fc(i) = f(i)-d(i)*friction
      enddo
```

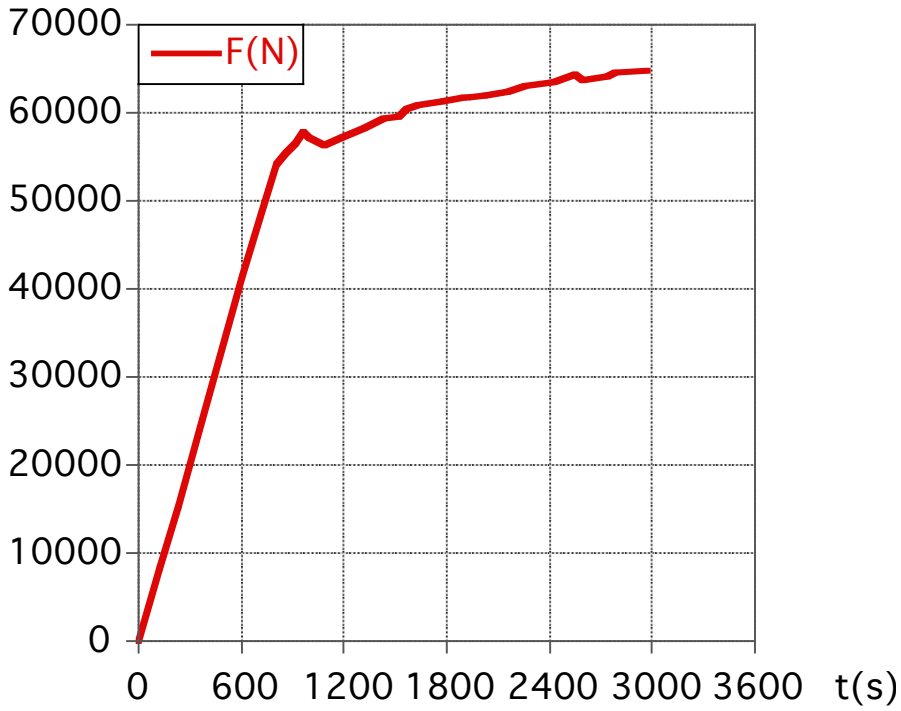

Program riXi4.f (Fortran77 source code) step 3

```
*3a---- displacement to strain: dc -> e

        do i = 1,n
        e(i) = dc(i) / slen
        enddo
```

engineering strain:

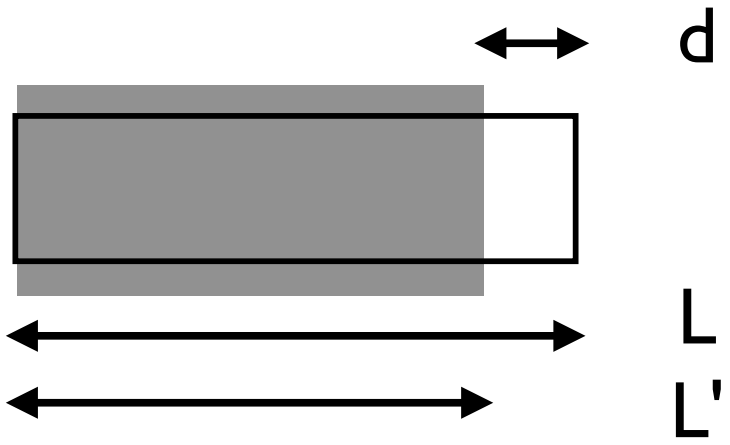

$e(\%) = 100 \cdot (L'-L) / L$

$e(\%) = 100 \cdot \Delta L / L$

Note:

if $L' < L$ (shortening) $\Delta L < 0$:

But in rock deformation, shortening is positive:

$e(\%) = 100 \cdot (-\Delta L) / L$

$e(\%) = 100 \cdot (L-L') / L$

Program riXi4.f (Fortran77 source code) step 3

```
*3a---- displacement to strain: dc -> e

        do i = 1,n
        e(i) = dc(i) / slen
        enddo
```

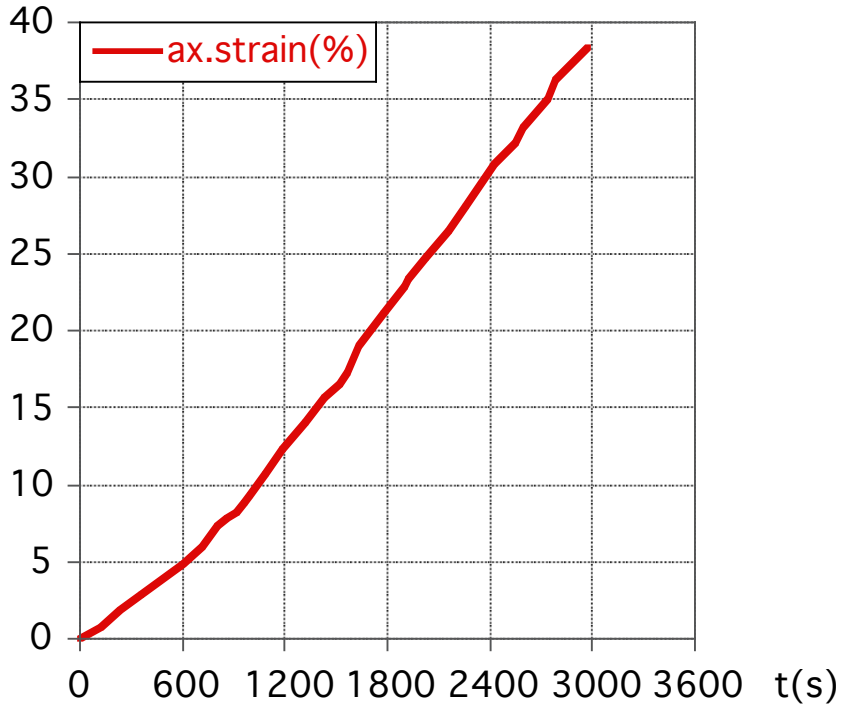

Program riXi4.f (Fortran77 source code) step 3

```
*3b---- strain magnitude, octahedral shear strain

        do i = 1,n
       es(i)= smag(e(i))
       o(i) = octshear(e(i))
       enddo
```

engineering strain:

$e(\%) = 100 \cdot (-\Delta L) / L$

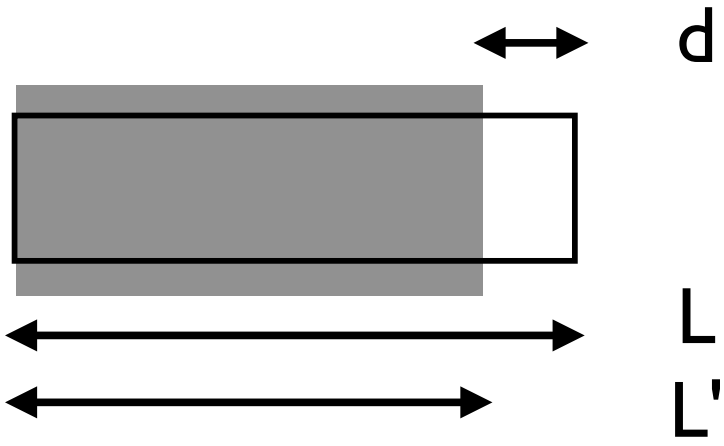

natural / logarithmic strain:

$\varepsilon_{1,2,3} = \ln(L'/L)$

strain magnitude / intensity parameter (deviator):

$\varepsilon s = 1/\sqrt{3} \cdot \sqrt{[\,(\varepsilon 1-\varepsilon 2)^2 + (\varepsilon 2-\varepsilon 3)^2 + (\varepsilon 3-\varepsilon 1)^2\,]}$

Program riXi4.f (Fortran77 source code) step 3

```
*3b---- strain magnitude, octahedral shear strain

        do i = 1,n
       es(i)= smag(e(i))
       o(i) = octshear(e(i))
       enddo
```

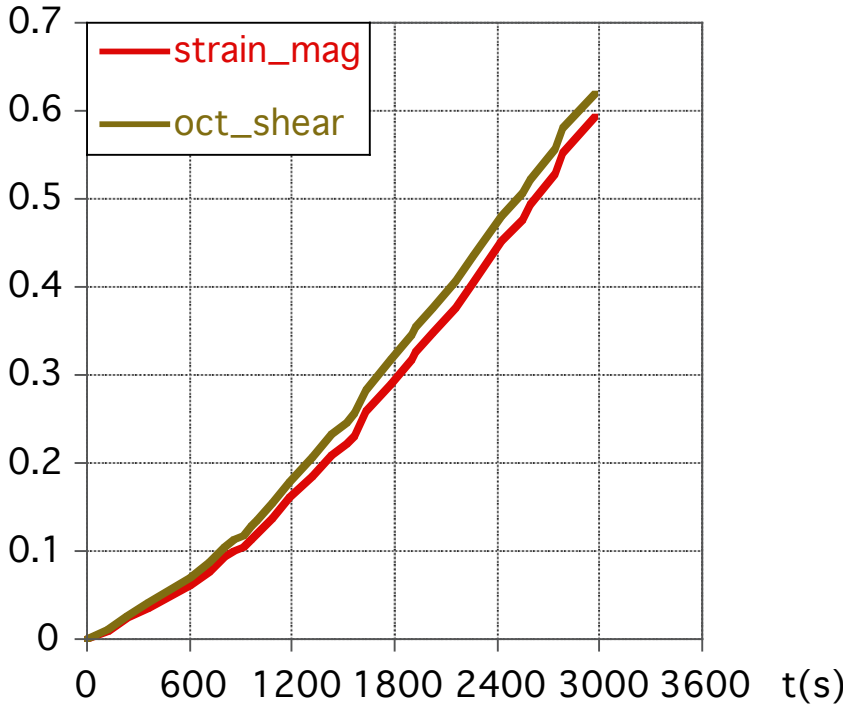

Program riXi4.f (Fortran77 source code) step 4

```
*4---- load to (axial) differential stress: fc -> s
*      correction for increasing sample diameter
*      correction for changing confining pressure

       r = 0.5 * sdia
       area = 3.14159 * r*r     !r in mm2
*                                N/mm2 = MPa since  N/m2 = Pa
       do i=1,n
       s(i)    = fc(i) * (1. - e(i)) / area
       sig(i)  = s(i) - p(i)
       enddo
```

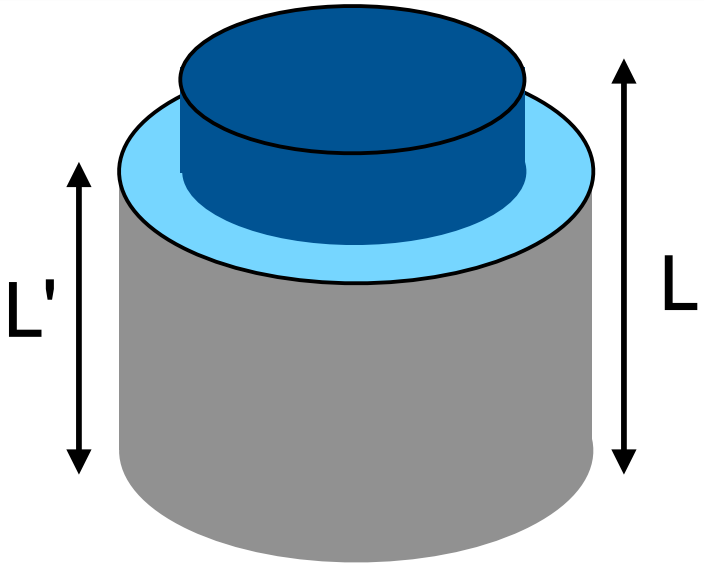

for constant volume:

$L \cdot area = L' \cdot area'$

$area' = area \cdot L/L'$

$L/L' = L/(L-\Delta L) = 1/(1-e)$

Program riXi4.f (Fortran77 source code) step 4

```
*4---- load to (axial) differential stress: fc -> s
*      correction for increasing sample diameter
*      correction for changing confining pressure
      do i=1,n
      s(i)    = fc(i) * (1. - e(i)) / area
      sig(i)  = s(i) - p(i)
      enddo
```

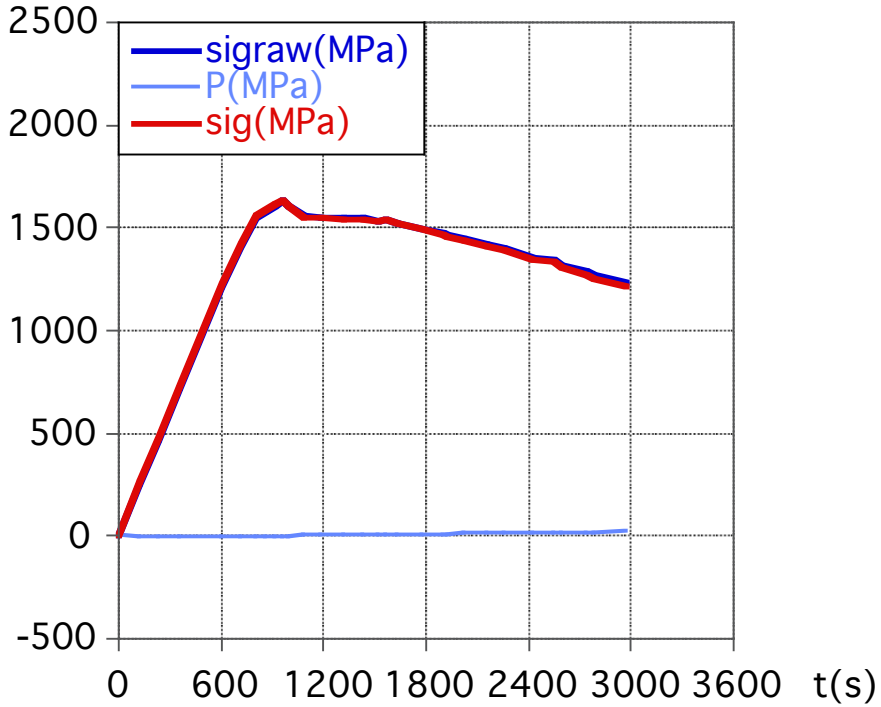

Program riXi4.f (Fortran77 source code) step 5

```
*5--- strain rates between two consecutive points
        do i=1,n-1
        j=i+1
        tdif=t(j)-t(i)
        if(tdif.ne.0.) et(j) = (e(j)-e(i))/tdif
        if(tdif.ne.0.) est(j) = (es(j)-es(i))/tdif
        if(tdif.ne.0.) ot(j) = (o(j)-o(i))/tdif
        enddo
```

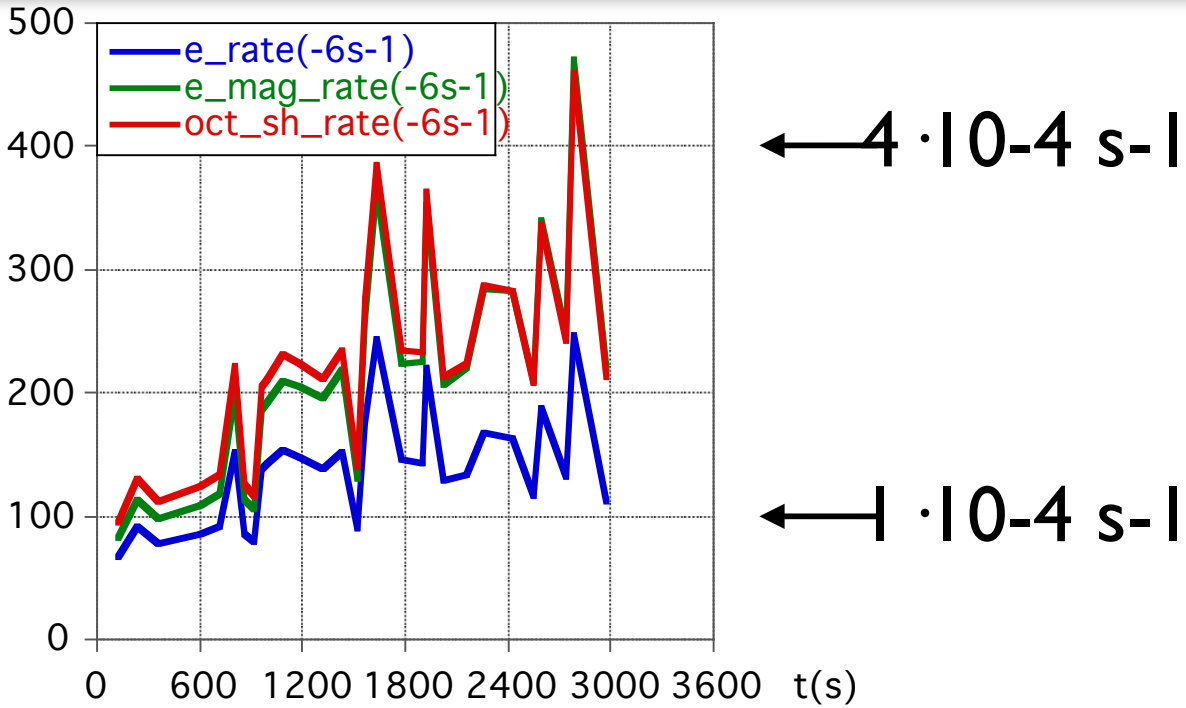

Running riXi4

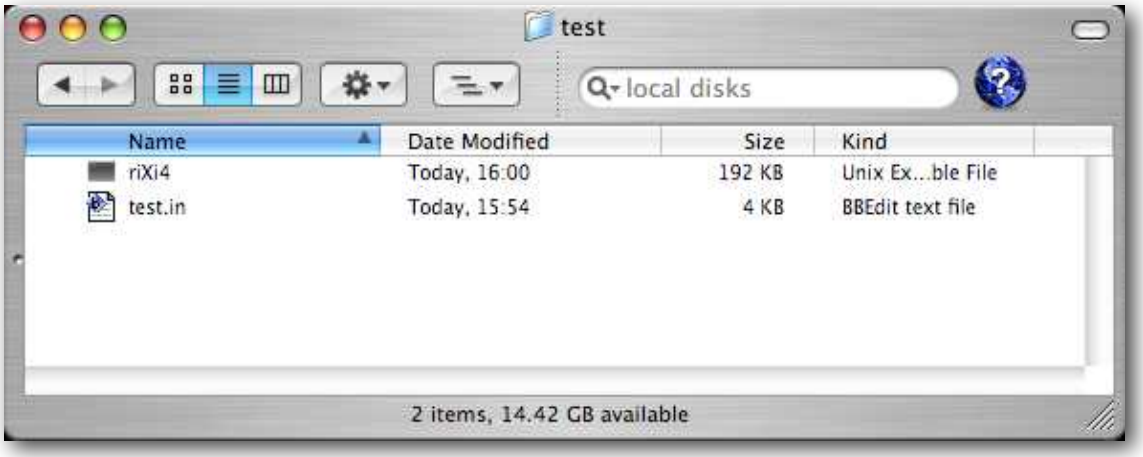

MacOSX:
arrange folder

use Terminal:
run riXi4
(type ./riXi4)

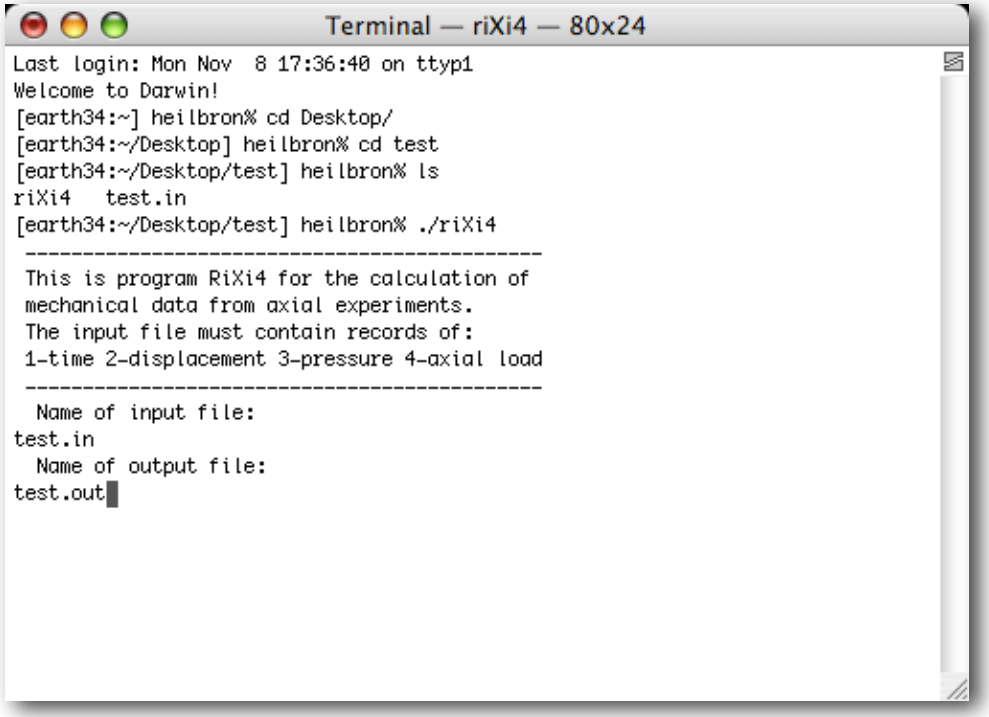

Running riXi4

dialogue:

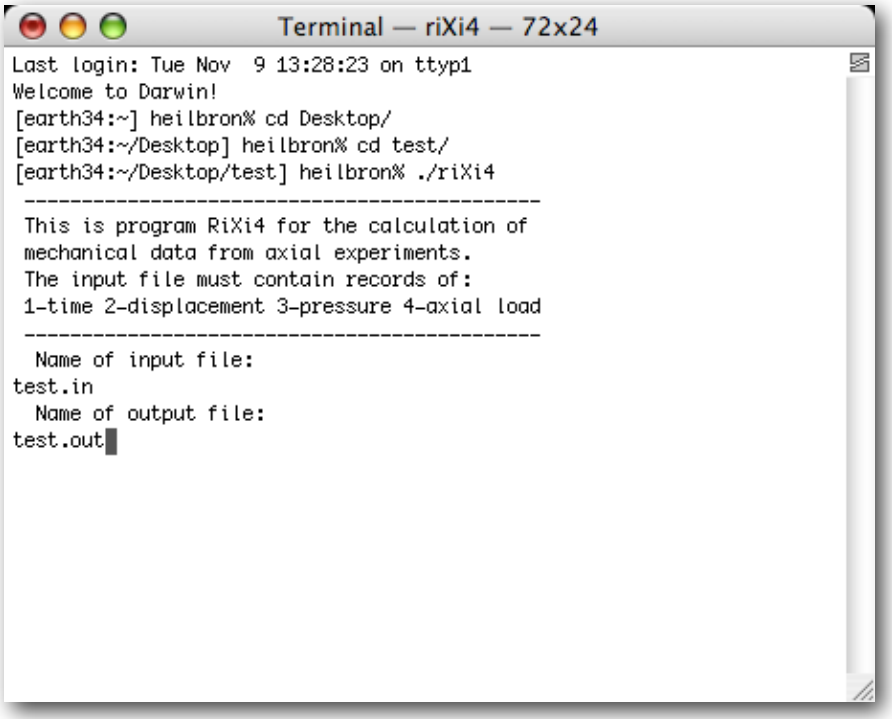

output on screen:

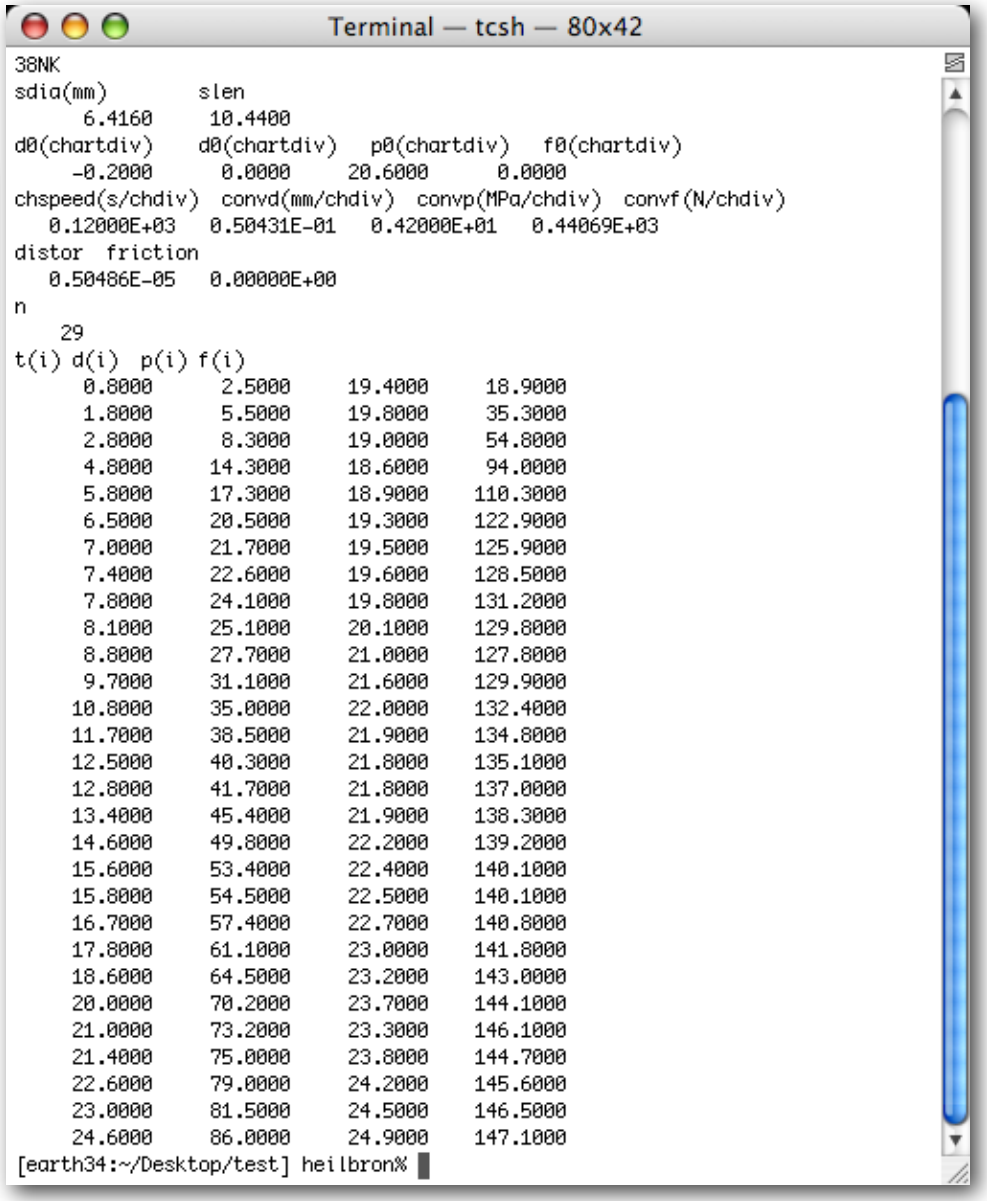

Use Kaleidagraph to plot results

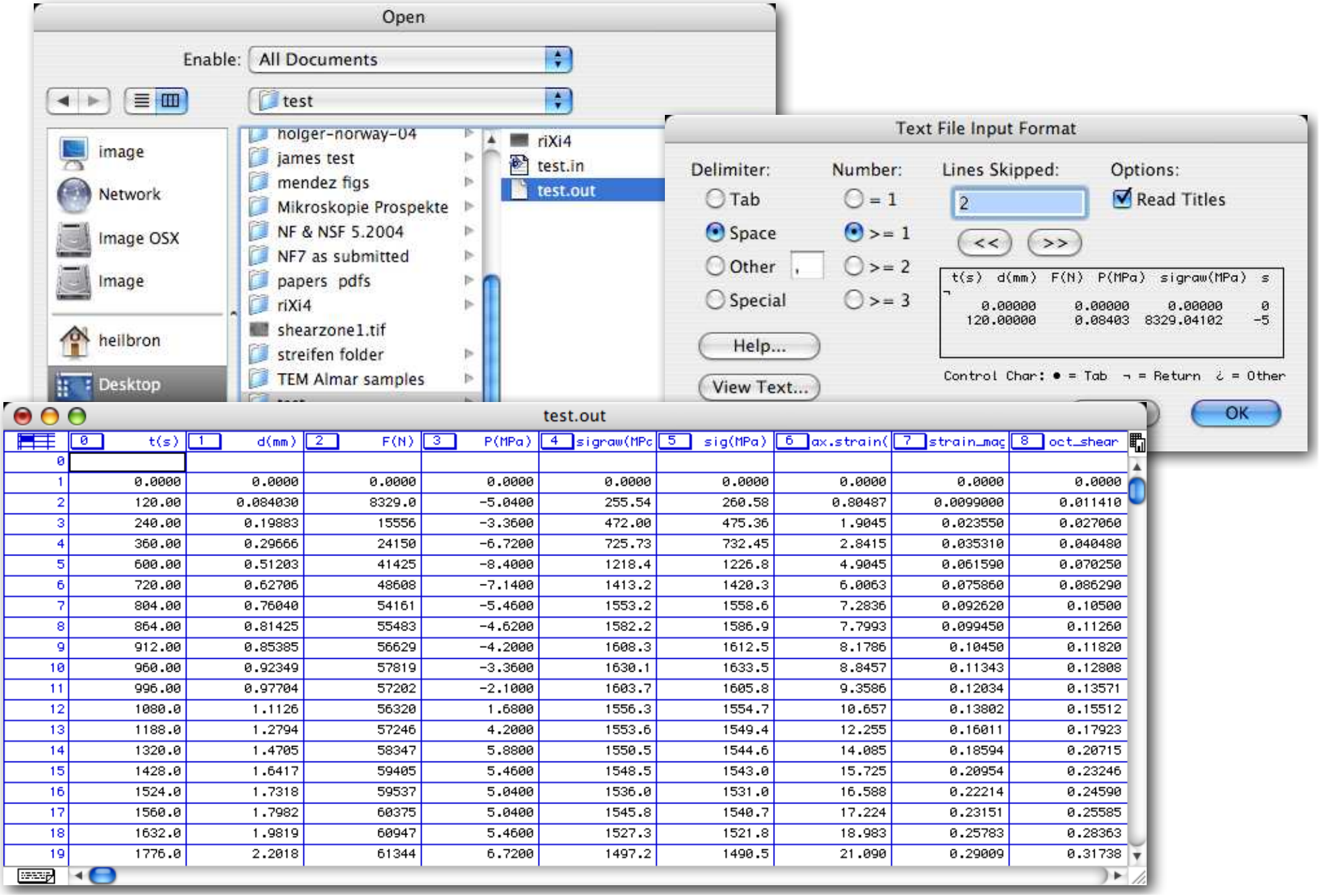

	0 t(s)	1 d(mm)	2 F(N)	3 P(MPa)	4 sigraw(MPc	5 sig(MPa)	6 ax.strain(	7 strain_mag	8 oct_shear
0									
1	0.0000	0.0000	0.0000	0.0000	0.0000	0.0000	0.0000	0.0000	0.0000
2	120.00	0.084030	8329.0	-5.0400	255.54	260.58	0.80487	0.0099000	0.011410
3	240.00	0.19883	15556	-3.3600	472.00	475.36	1.9045	0.023550	0.027060
4	360.00	0.29666	24150	-6.7200	725.73	732.45	2.8415	0.035310	0.040480
5	600.00	0.51203	41425	-8.4000	1218.4	1226.8	4.9045	0.061590	0.070250
6	720.00	0.62706	48608	-7.1400	1413.2	1420.3	6.0063	0.075860	0.086290
7	804.00	0.76040	54161	-5.4600	1553.2	1558.6	7.2836	0.092620	0.10500
8	864.00	0.81425	55483	-4.6200	1582.2	1586.9	7.7993	0.099450	0.11260
9	912.00	0.85385	56629	-4.2000	1608.3	1612.5	8.1786	0.10450	0.11820
10	960.00	0.92349	57819	-3.3600	1630.1	1633.5	8.8457	0.11343	0.12808
11	996.00	0.97704	57202	-2.1000	1603.7	1605.8	9.3586	0.12034	0.13571
12	1080.0	1.1126	56320	1.6800	1556.3	1554.7	10.657	0.13802	0.15512
13	1188.0	1.2794	57246	4.2000	1553.6	1549.4	12.255	0.16011	0.17923
14	1320.0	1.4705	58347	5.8800	1550.5	1544.6	14.085	0.18594	0.20715
15	1428.0	1.6417	59405	5.4600	1548.5	1543.0	15.725	0.20954	0.23246
16	1524.0	1.7318	59537	5.0400	1536.0	1531.0	16.588	0.22214	0.24590
17	1560.0	1.7982	60375	5.0400	1545.8	1540.7	17.224	0.23151	0.25585
18	1632.0	1.9819	60947	5.4600	1527.3	1521.8	18.983	0.25783	0.28363
19	1776.0	2.2018	61344	6.7200	1497.2	1490.5	21.090	0.29009	0.31738

Use Kaleidagraph to plot results

$\Delta\sigma = f(e(\%))$

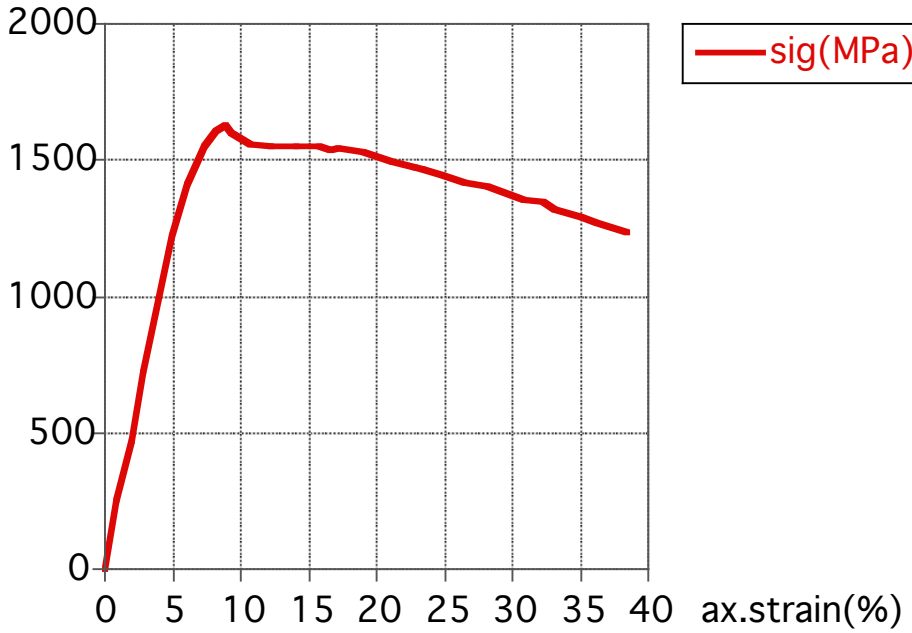

differential stress = f(engineering strain)

$\Delta\sigma = f(\varepsilon s)$

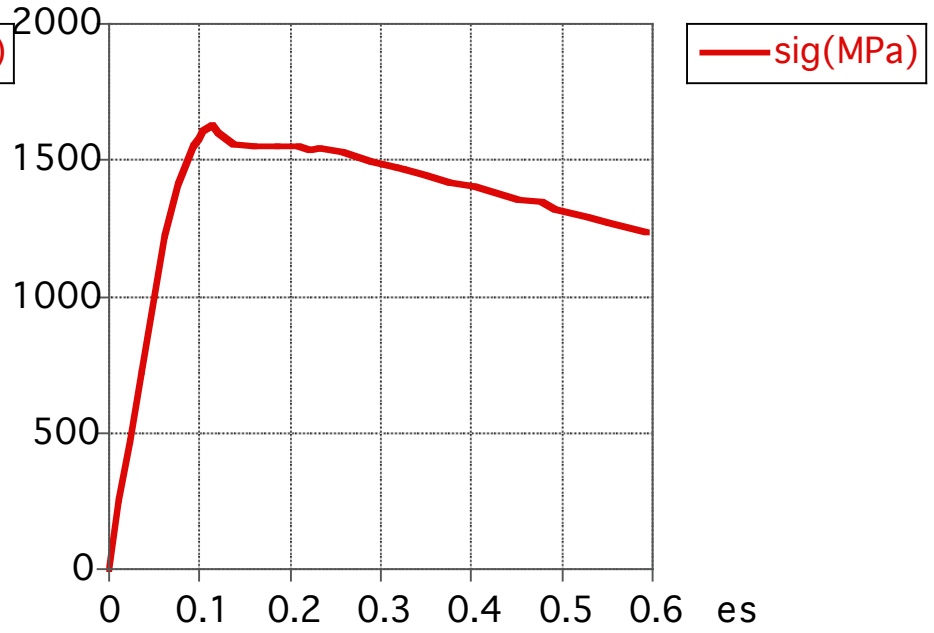

differential stress = f(strain magnitude)

Use Kaleidagraph to plot results

axial regime 3

w858

thin line w/r axial strain
heavy line w/r oct. shear strain

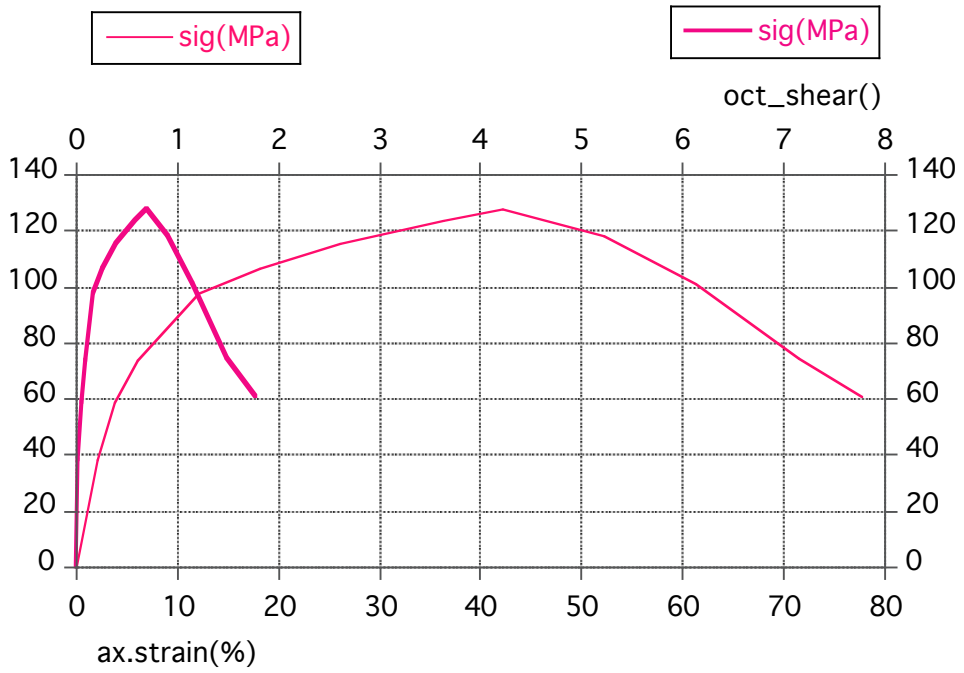

Use Kaleidagraph to plot results

axial regime 3

w858

thin line w/r axial strain
heavy line w/r oct. shear strain

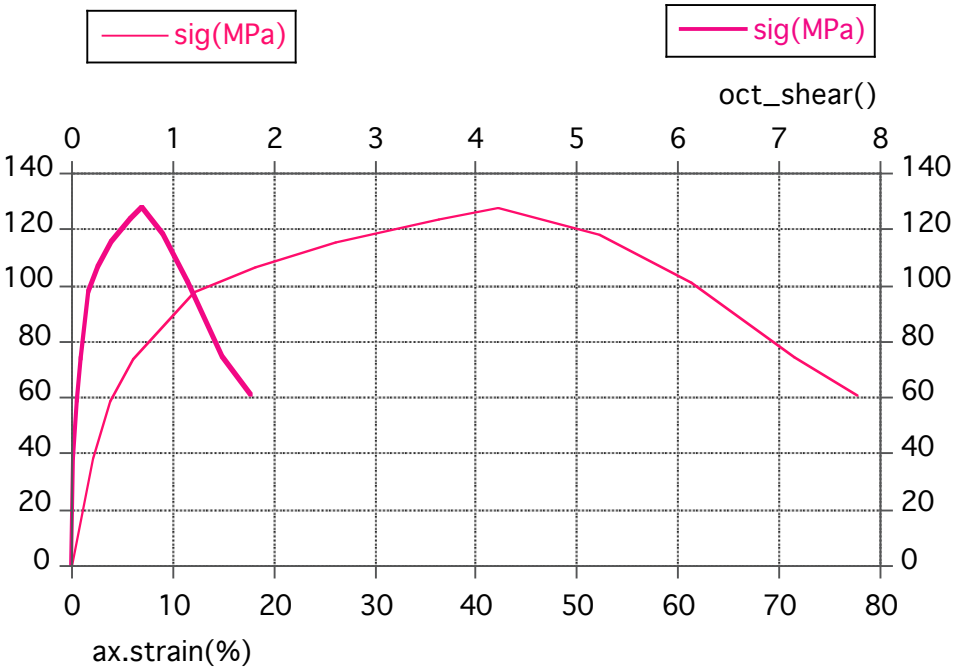

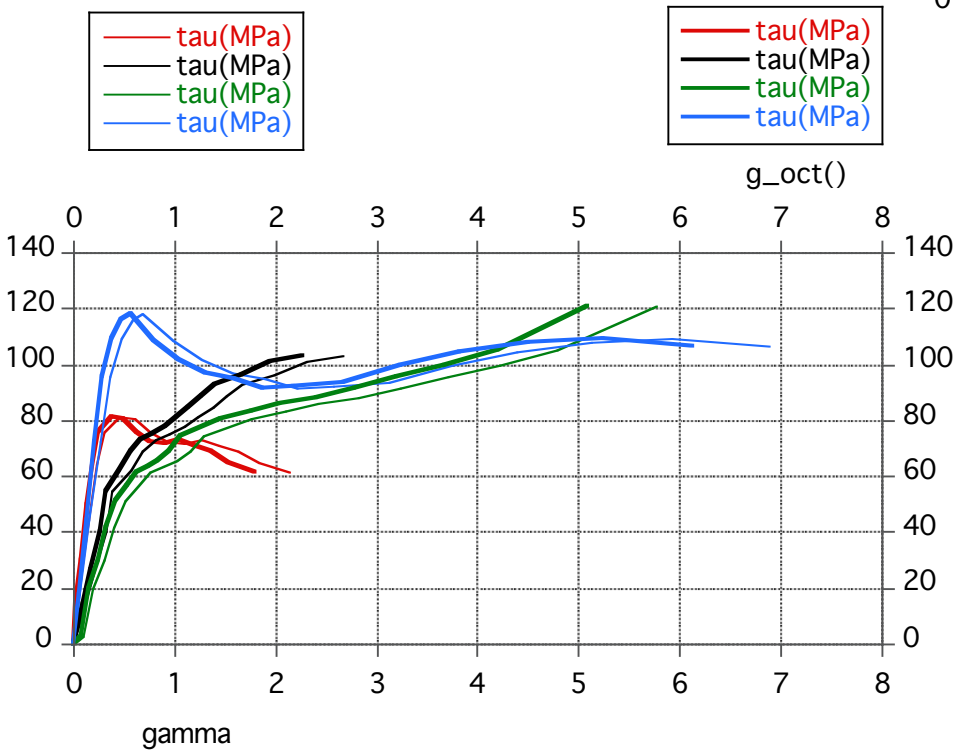

shear regime 3

w920
w1010
w935
w965

thin line w/r gamma
heavy line w/r oct. shear strain

4

Mechanical data - strain measures

Deformationsprozesse in der Erde I (4)

Mechanical data - strain measures

Rock Deformation & Structure Analysis

http://www.unibas.ch/earth/micro/index.html

Google

compmathheads Adam Riese Powe

http://www.uniba
http://www.uniba
http://www.uniba

ROCK DEFORMATION HOME | lab | p

- software
- orientation imaging | c-axis analy
- image analysis | microstruct
- grain size analysis | conversion
- grain size simulations | simulations
- stress-strain calculation | data conve
- lazy macros | macros for

Display a menu

www.unibas.ch/earth/micro/software/rig/rig.html

stress-strain calculation for solid medium deformation apparatus

INPUT

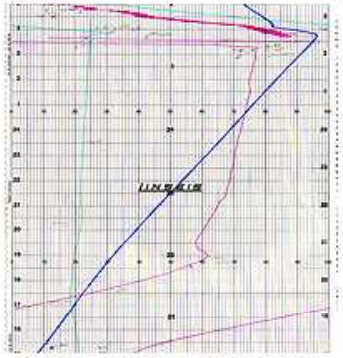

Stripchart with load diplacement recordings

OUTPUT

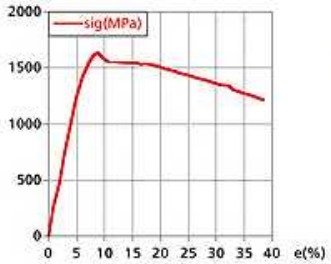

Converted stress strain plot

The rig programs are designed to convert run records of a Griggs-type deformation apparatus to stress strain plots and other type of derived mechanical data.

The input data can be

- displacement, load (chart units)
- time, displacement, confining pressure, load (chart units)

Available programs are

- rigC and rigC2 for axial compression (input: d,f)
- rigC4 for axial compression (input: t,d,p,f)
- rigS and rigS2 for shearing (input: d,f)
- rigS4 for shearing (input: t,d,p,f)

Sources (Fortran 77 text files):
rigC.for (MacOS9)
rigS.for (MacOS9)
rigC2.f (MacOSX)
rigS2.f (MacOSX)
rigC4.f (MacOSX)
rigS4.f (MacOSX)
rigPrep.f (MacOSX)

Compiled versions:
rigC.sea.hqx (MacOS9)
rigS.sea.hqx (MacOS9)
rigC2.exec (MacOSX)
rigS2.exec (MacOSX)
rigC4.exec (MacOSX)
rigS4.exec (MacOSX)
rigPrep.exec (MacOSX)

Test files - INPUT:
testC2.inp - for rigC and rigC2 (d,f input)
testS2.inp - for rigS and rigS2 (d,f input)
testC4.inp - for rigC4 (t,d,p,f input)
testS4.inp - for rigS4 (t,d,p,f input)
Example files - OUTPUT:
testC2.out - from rigC2
testS2.out - from rigS2
testC4.out - from rigC4
testS4.out - from rigS4

Manuals:
rig manual 1
how to run rigC, rigC2 and rigC4 (convert data of axial compression experiment)

to force download, do this:
- on Mac - press Alt key
- on Linux - press Shift key

(last update: 2004-november-21)

(e-mail for more info)

38nk.out:
displacement(mm) deltaP(MPa) force(N)

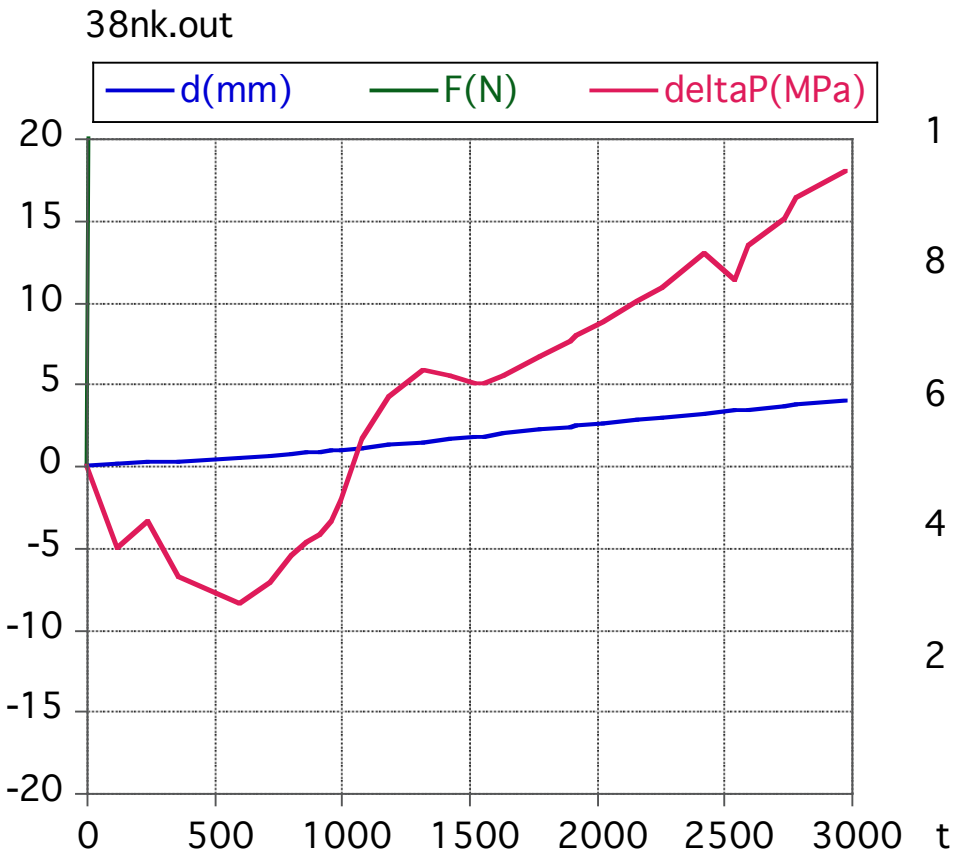

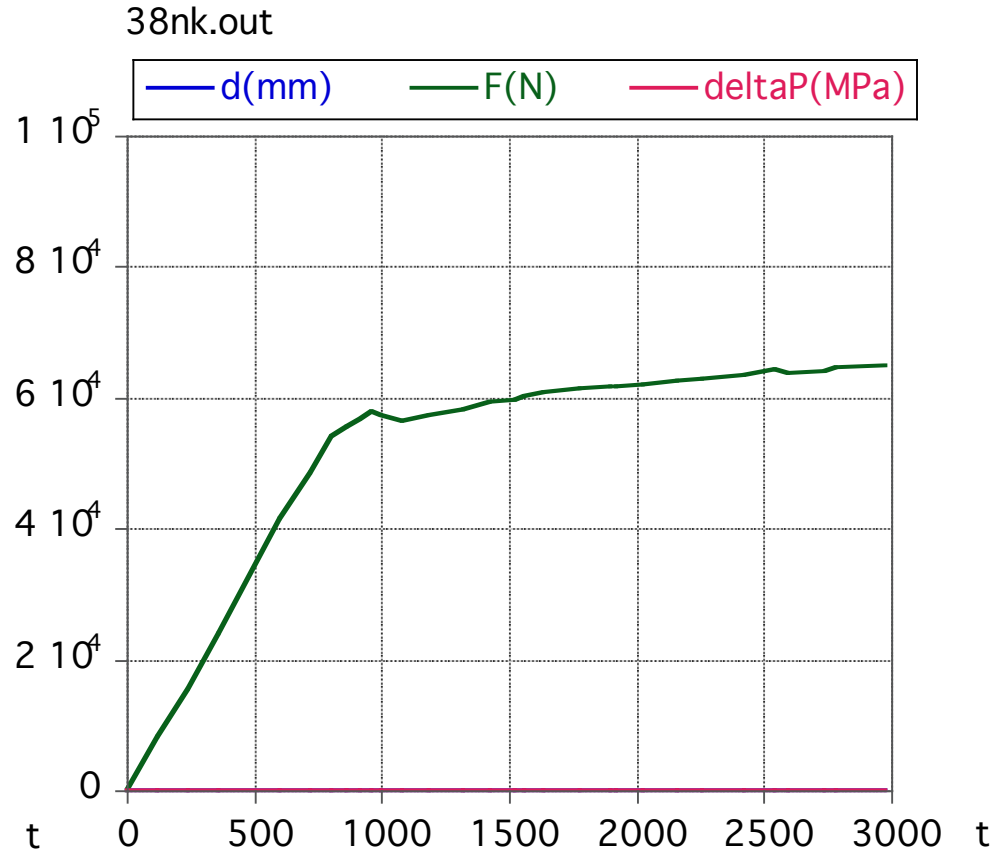

71nk.out:
displacement(mm) deltaP(MPa) force(N)

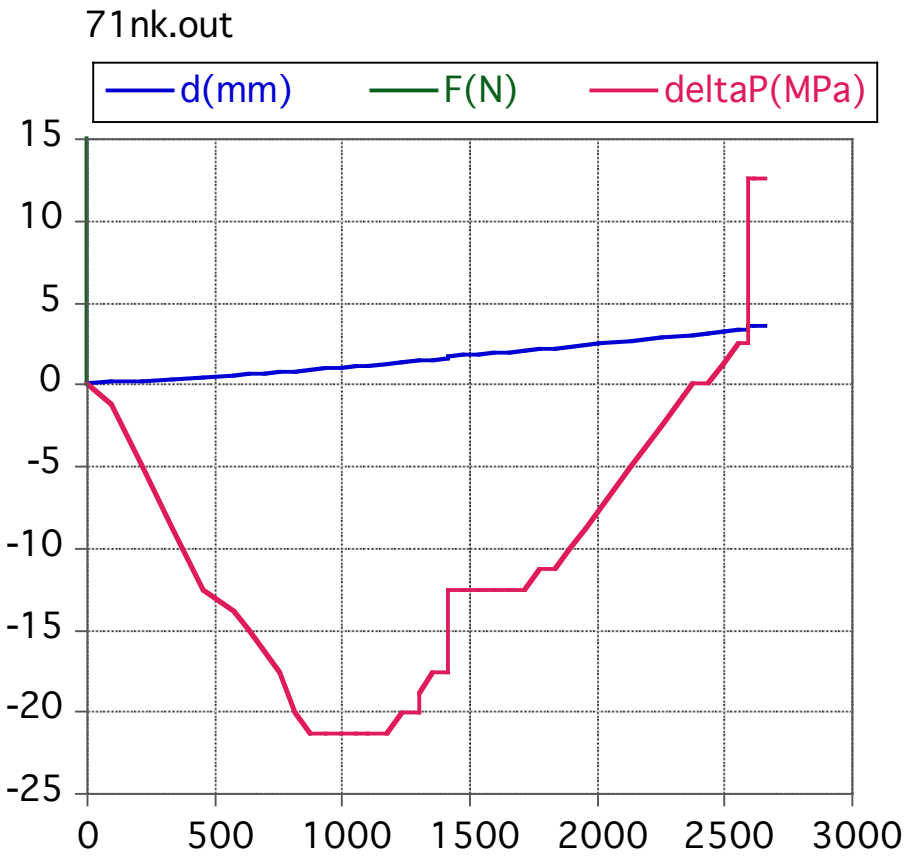

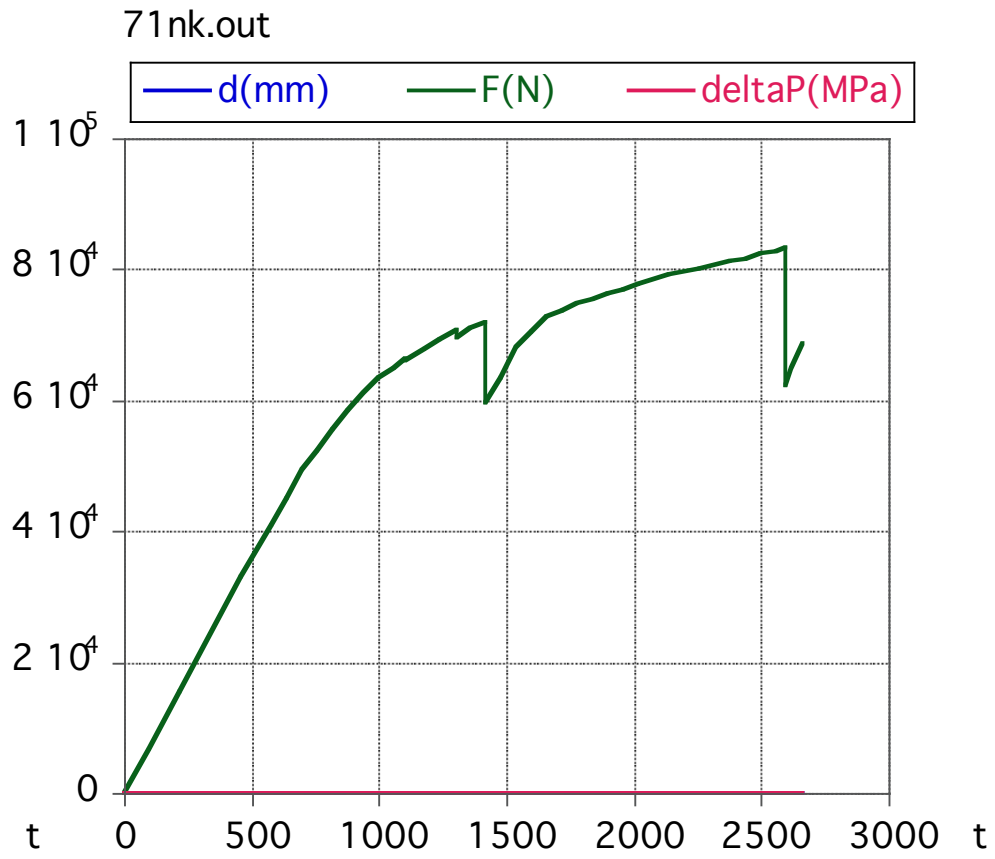

38nk.out:

stress = f(strain)

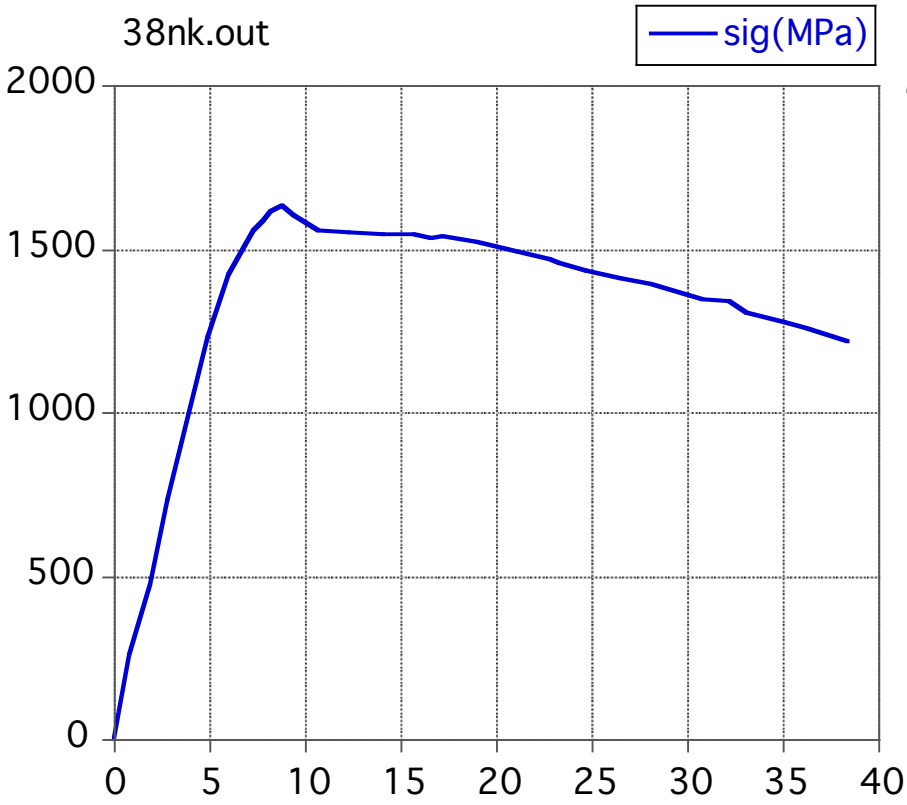

stress = f(oct. shear strain)

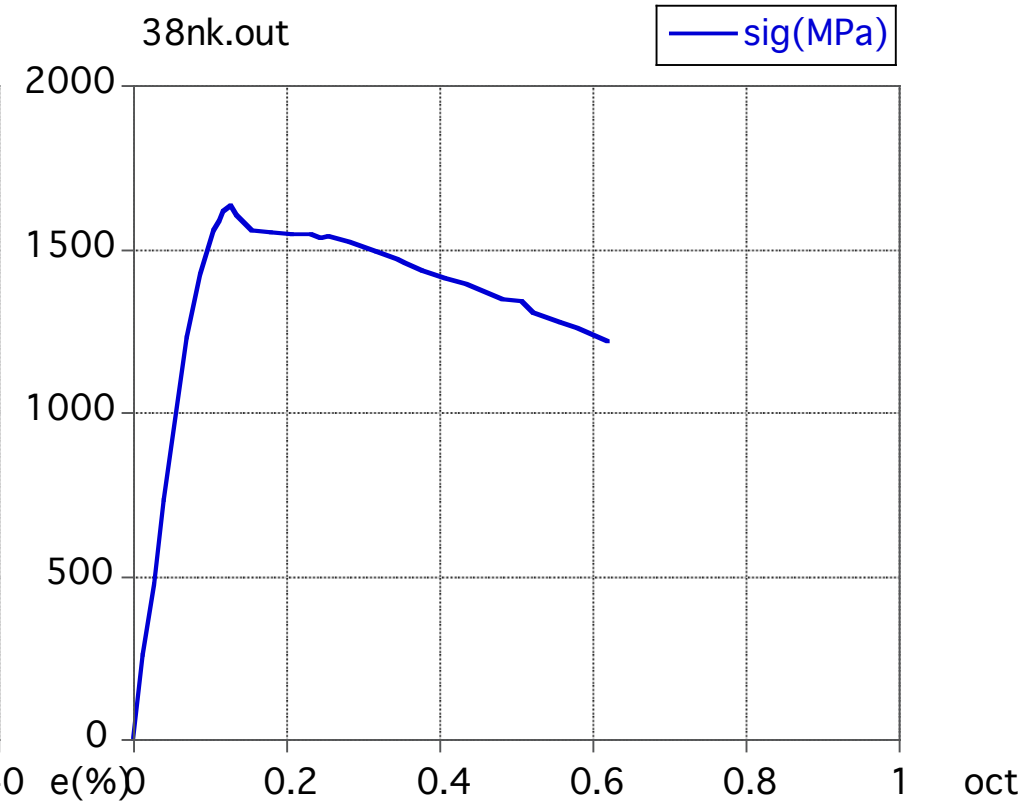

71nk.out:

stress = f(strain)

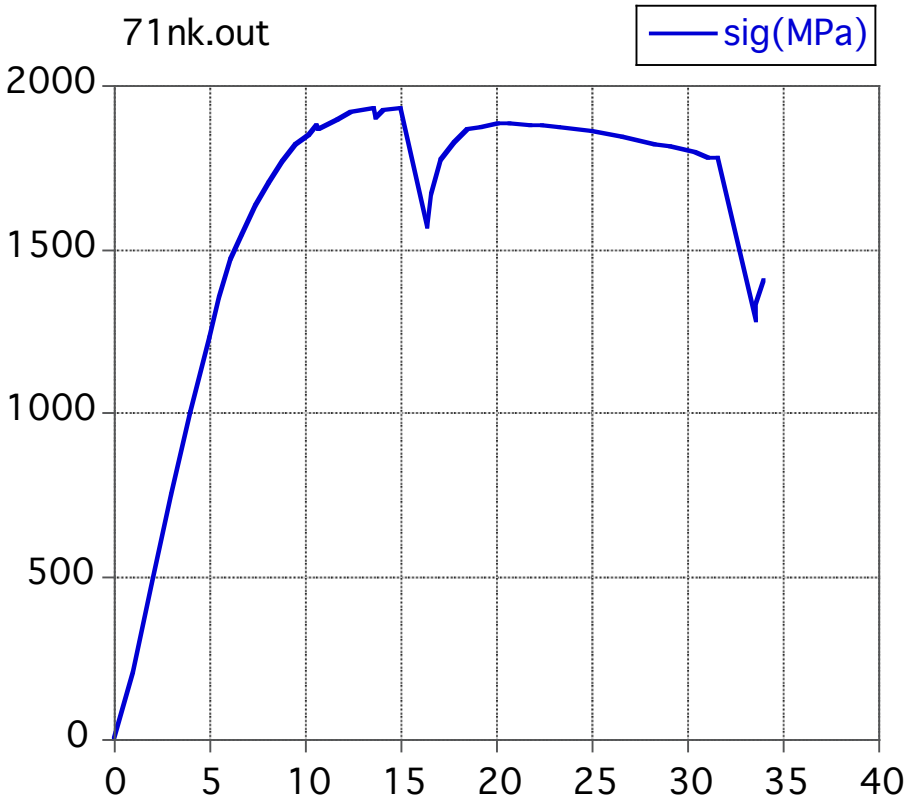

stress = f(oct. shear strain)

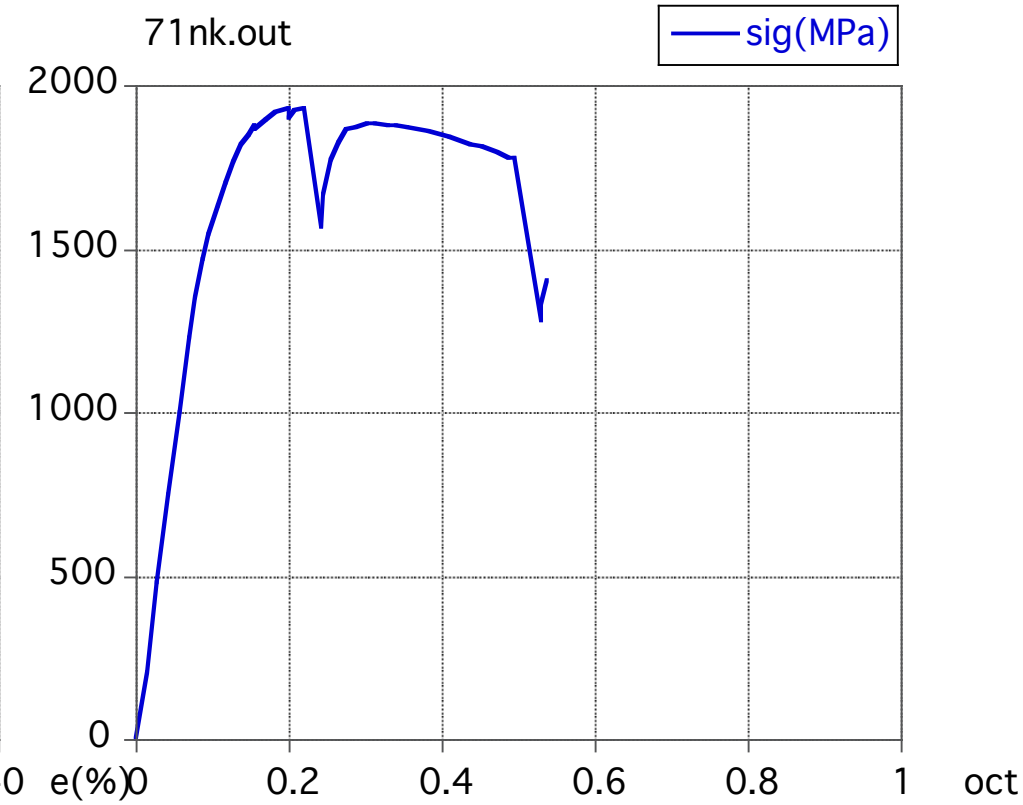

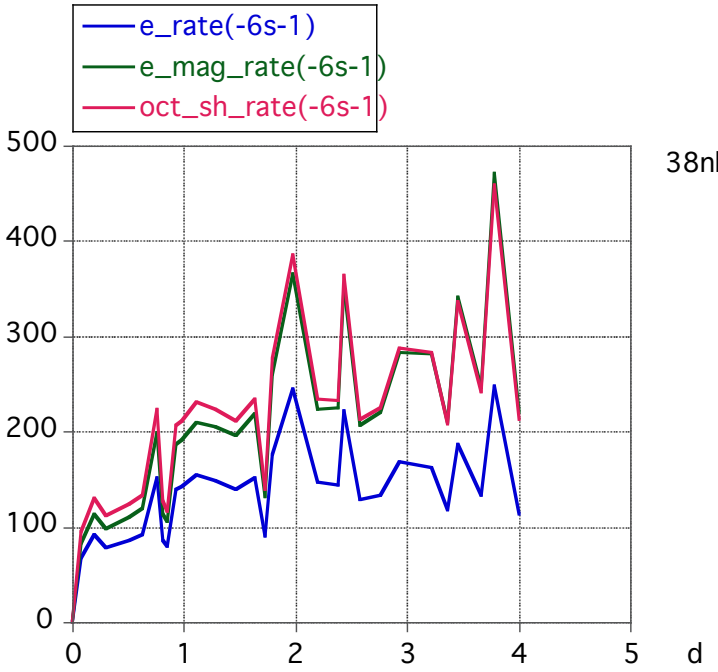

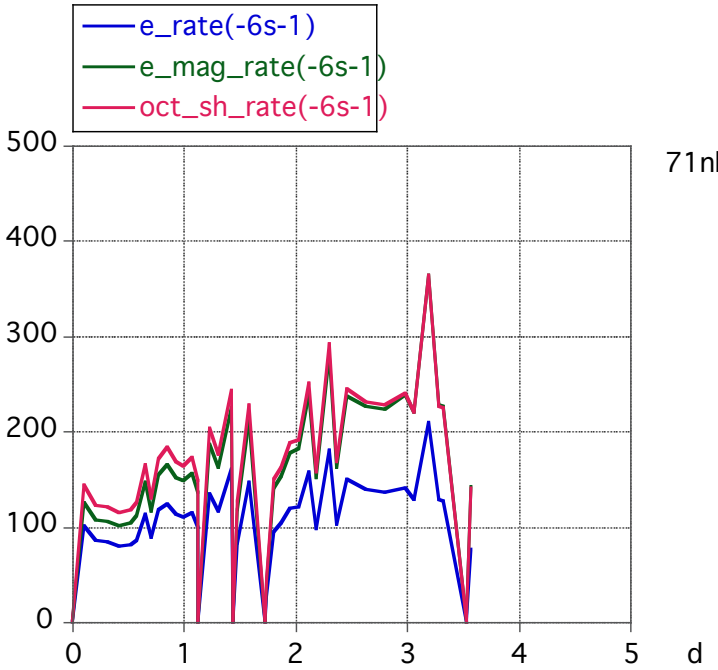

"strain rates":

- axial strain
- strain magnitude
- octahedral shear strain

"strain rates":

- axial strain
- strain magnitude
- octahedral shear strain

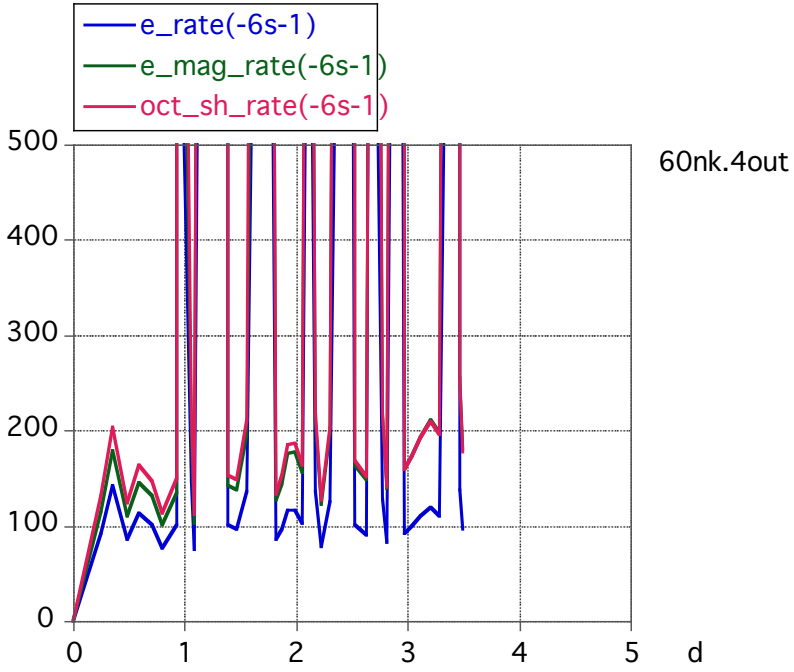

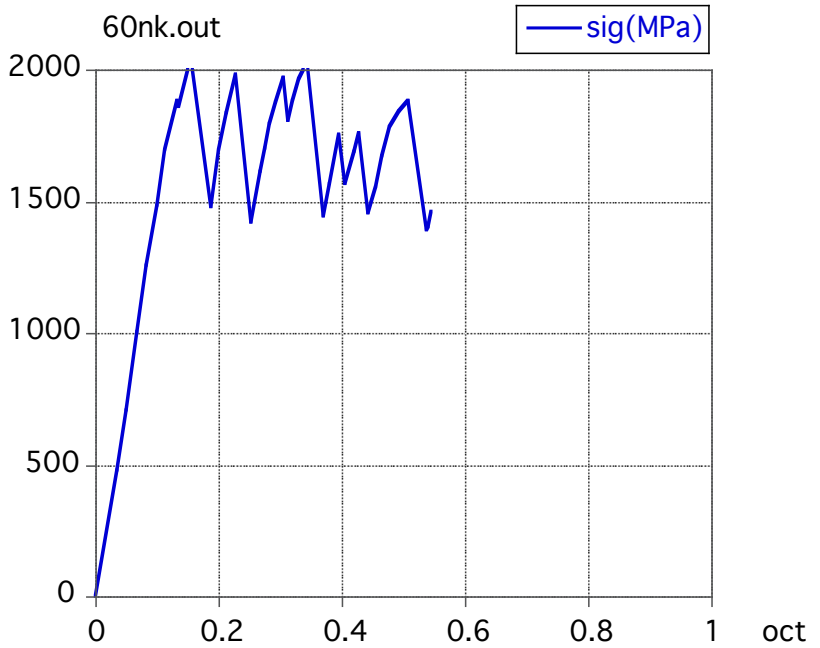

Measures for strain

need "universal" strain measure to:

.. consider 3 dimensions
(influence of $\sigma 2$)

.. compare shearing and axial experiments
(γ vs. $\varepsilon(\%)$)

.. formulate failure criterion
(breaking strength = f(confining pressure))

.. formulate flow law
(flow stress = f(p, T, $\dot{\varepsilon}$, ..., ε?, ...))

Measures for strain

strain ellipse:

3 axes:

1+e1
1+e2
1+e3

matrix:

e11 e12 e13
e21 e22 e23
e31 e32 e33

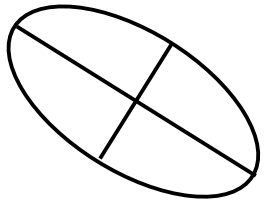

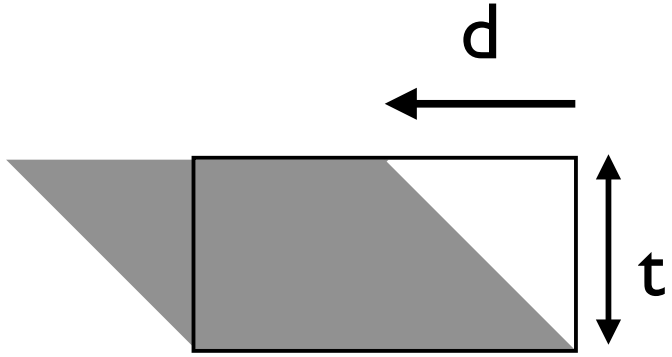

simple shear: e2 = 0

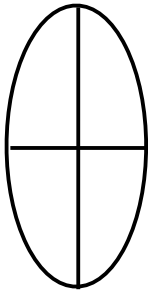

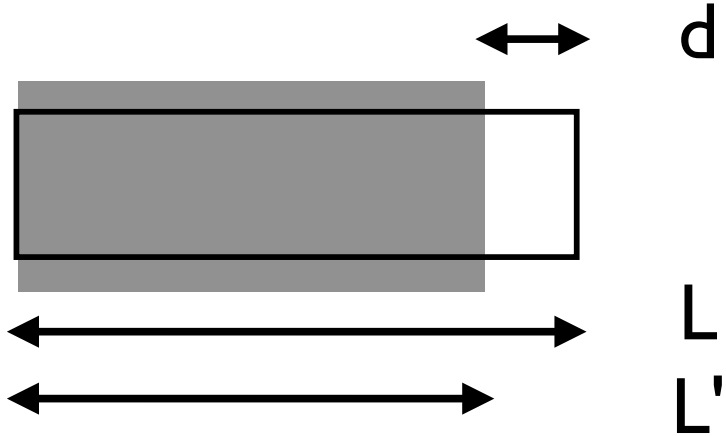

axial compression: e2 = e3

Types of strain

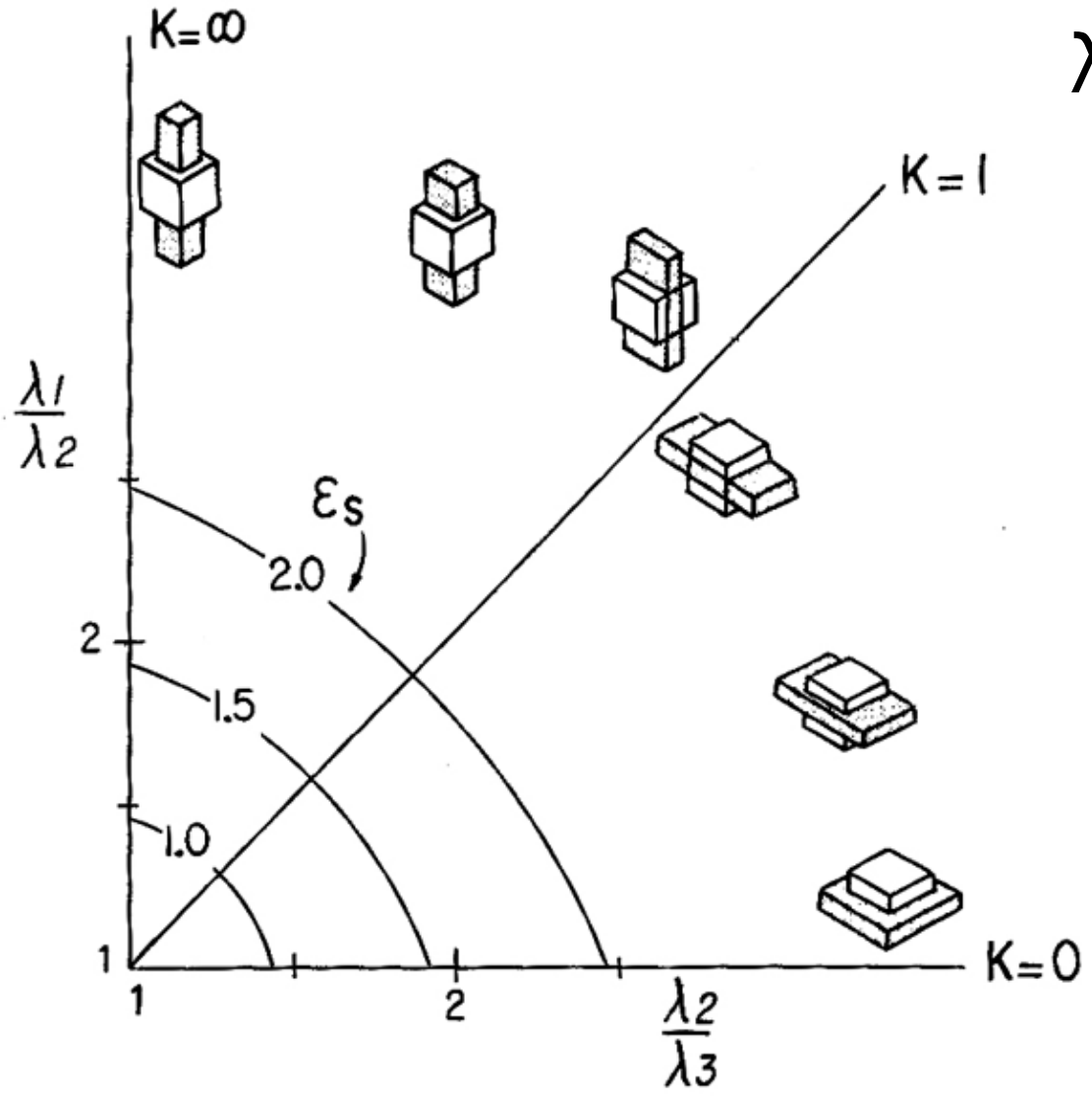

es = strain magnitude

$\lambda = (1+e)2$

Measures for strain and elongation (axial compression)

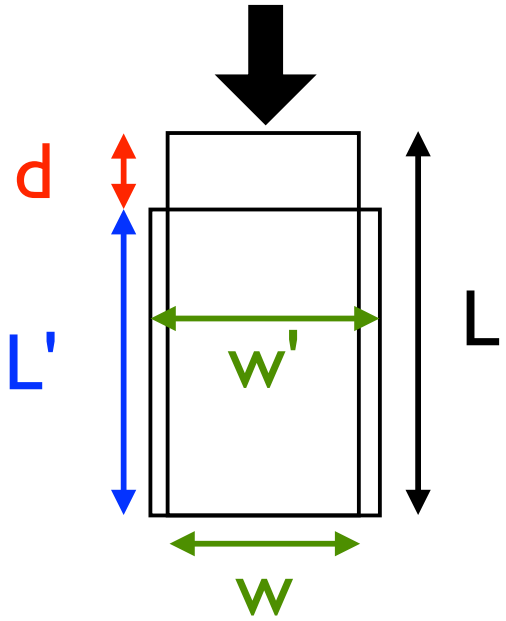

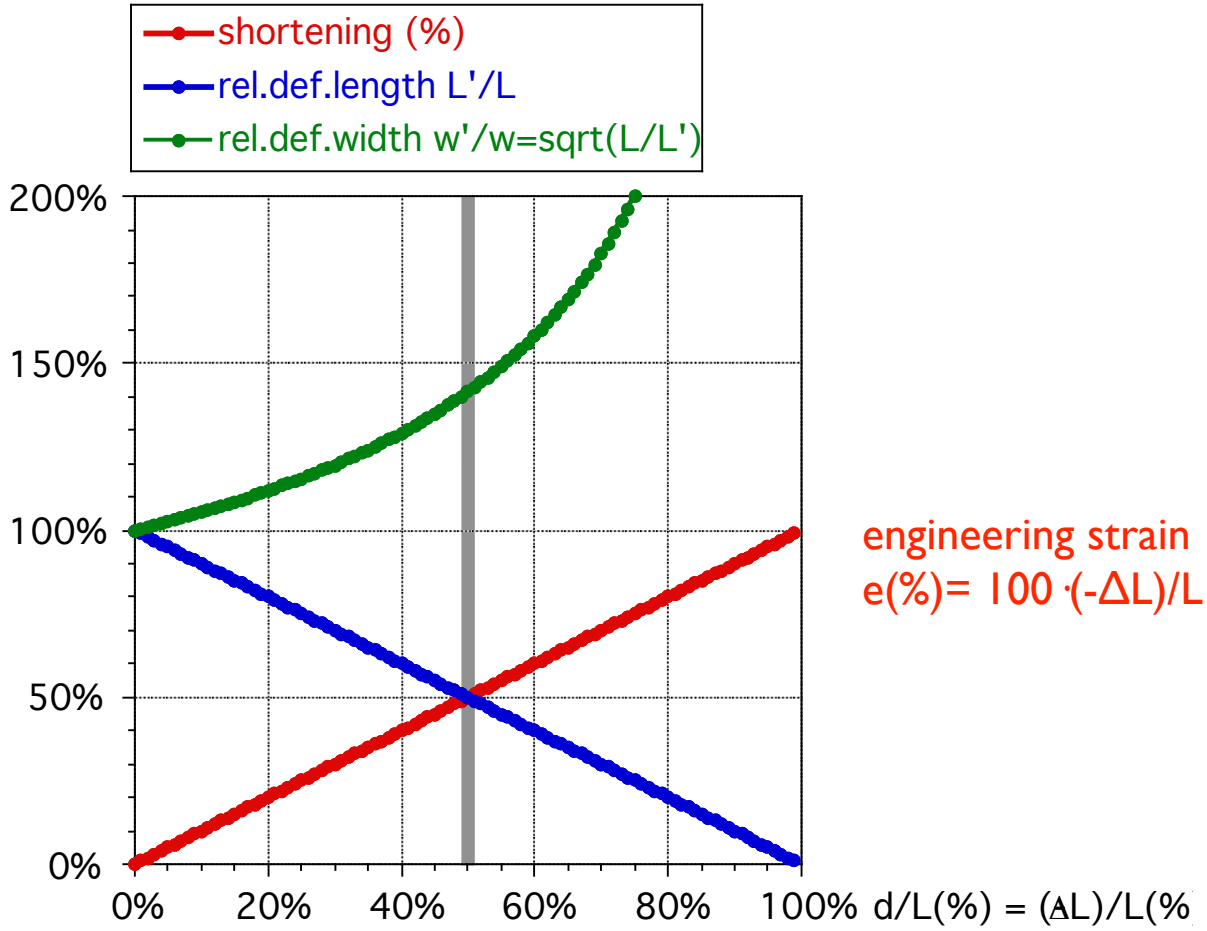

engineering strain
e(%)= 100 ·(-ΔL)/L

at d /L = 0.5
(i.e., at (-ΔL)/L = 0.5 or e(%) = 50%):
strain e(%) = 50%, def. length L'/L = 50%, def. width w'/w = 141%

Measures for elongation and strain (axial compression)

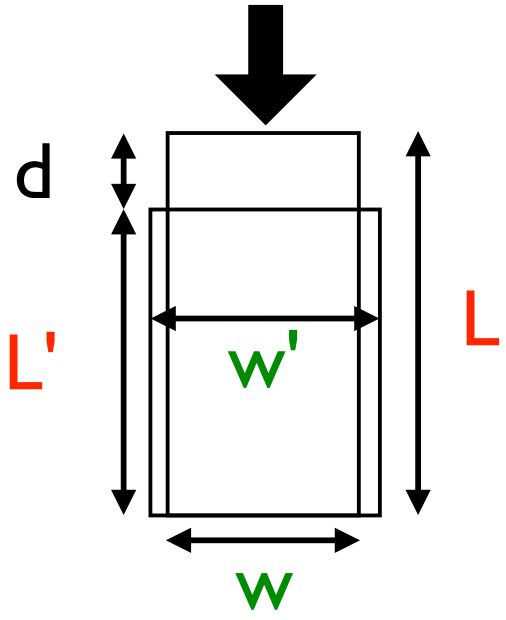

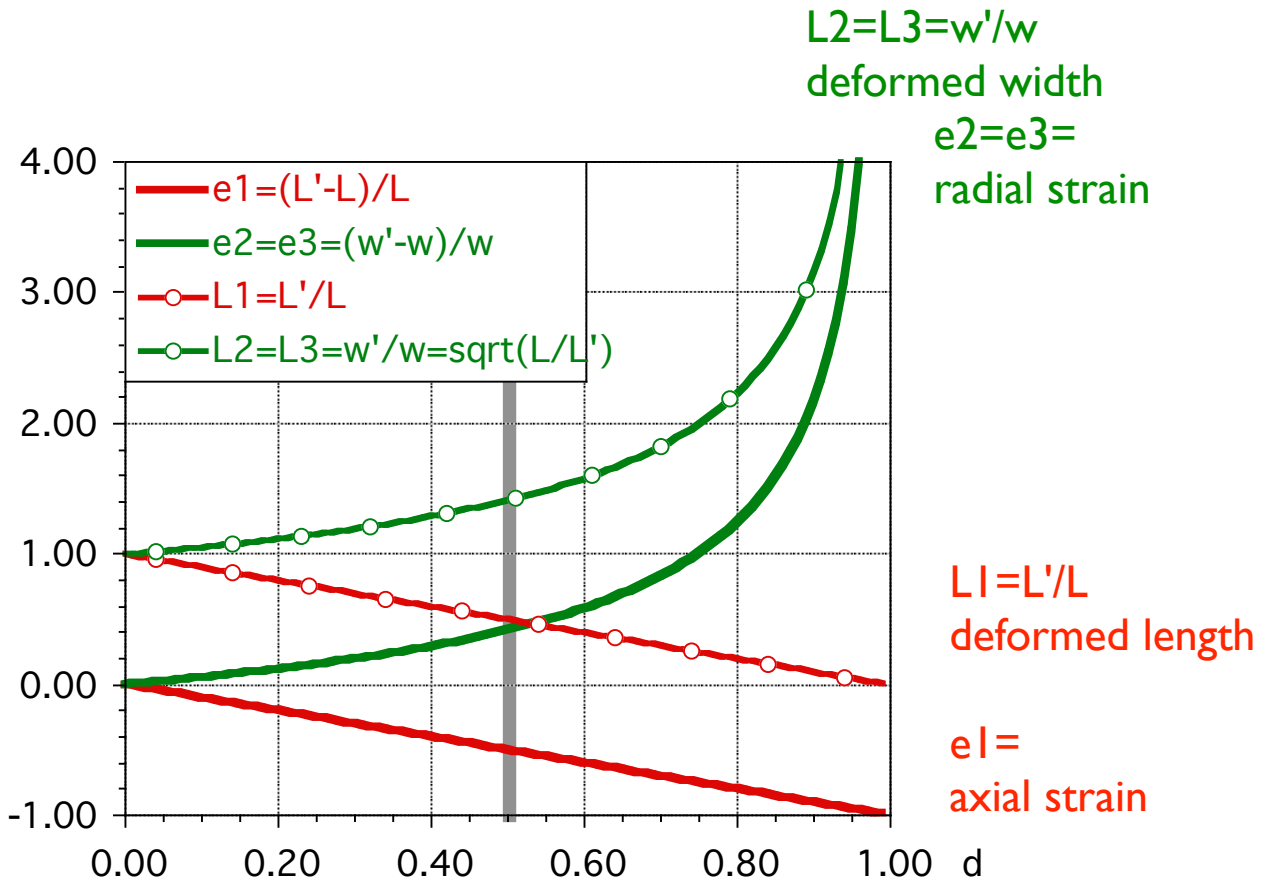

at d /L = 0.5:
axial strain e1 = -0.50, radial strain e2 = 0.41,
axial elongation L1 = 0.50, radial elongation L2 = 1.41

Measures for (natural/true) strain (axial compression)

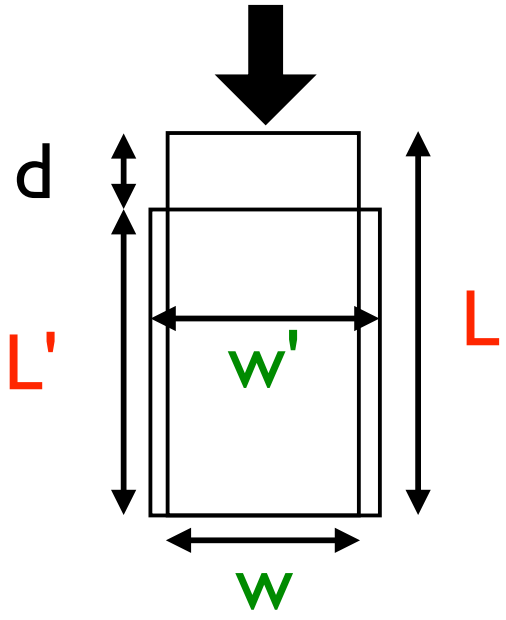

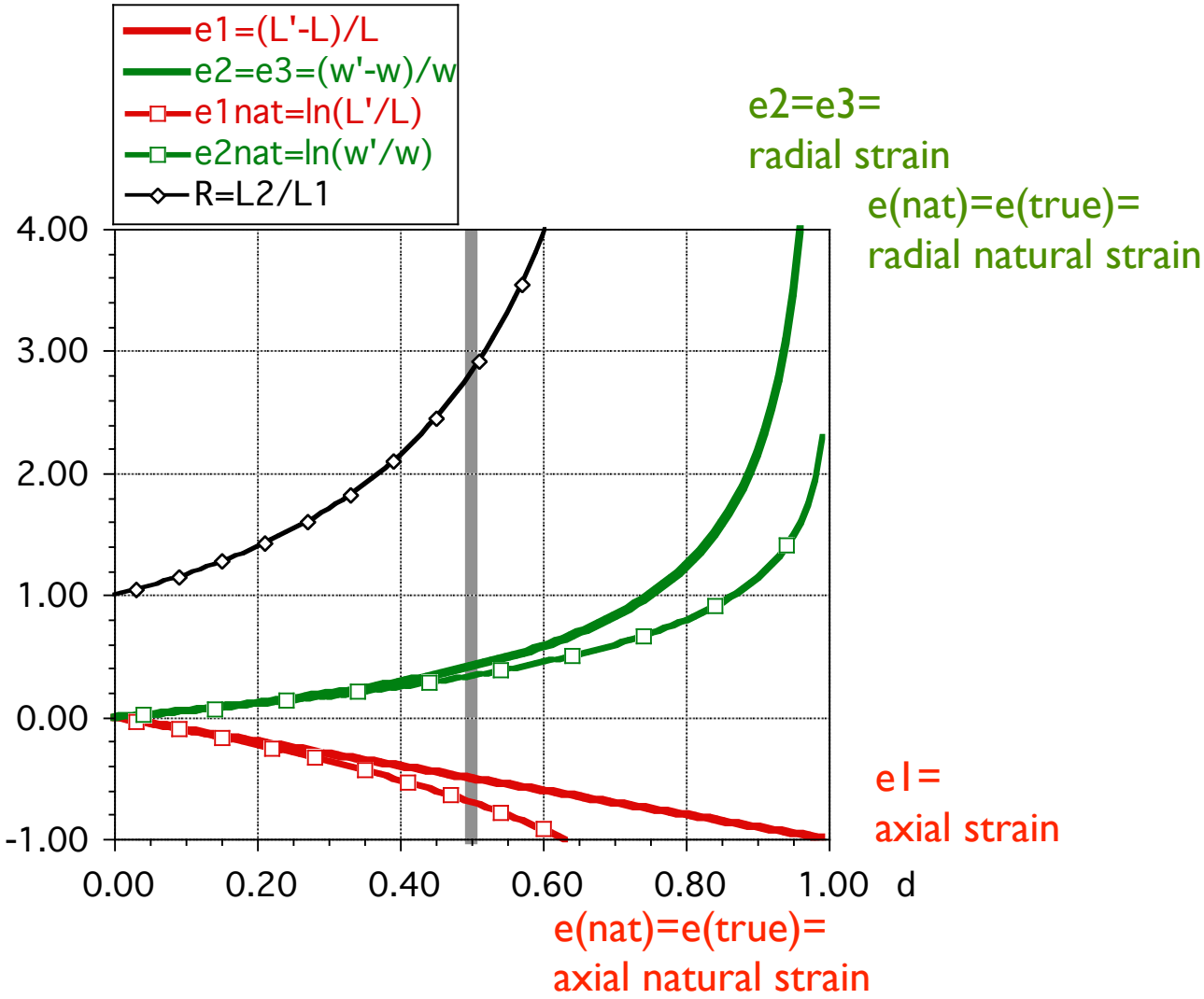

at d /L = 0.5:

axial strain e1= -0.50, radial strain e2,e3 = 0.41, R = 2.83

axial natural strain ε1= -0.69, radial natural strain ε1 = 0.35

Measures for mean strain / strain magnitude

es = oct

strain magnitude = octahedral shear strain

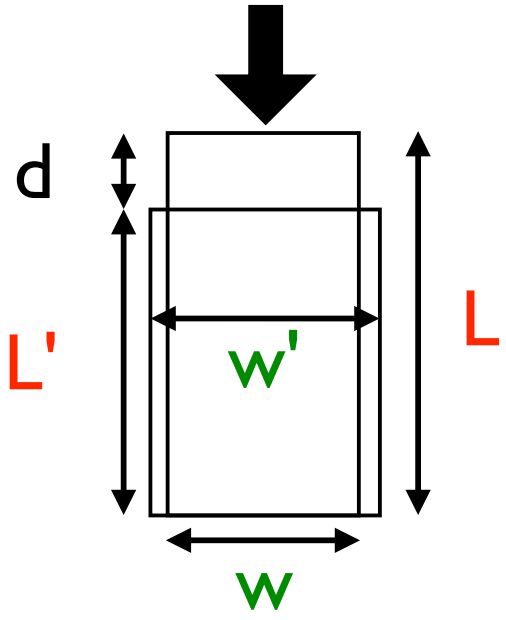

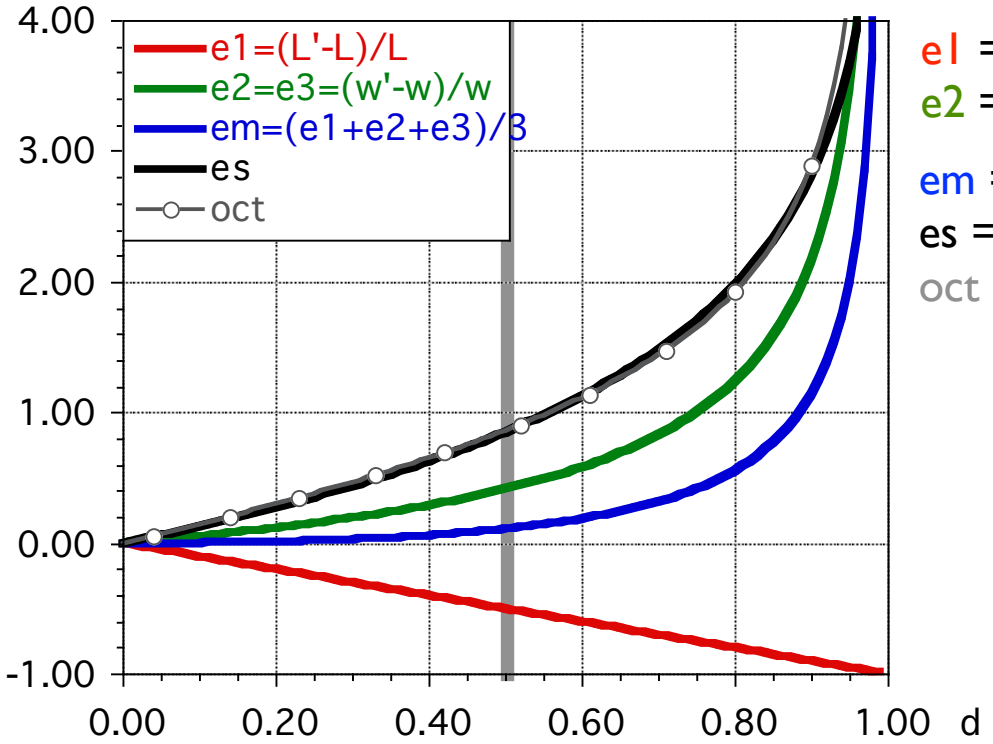

e1 = 1-dim strain

e2 = 1-dim strain

em = 3-dim strain

es = 3-dim strain

oct = 3-dim strain

at d /L = 0.5:

axial strain e1= -0.50, radial strain e2,e3 = 0.41, R = 2.83

mean strain em = 0.11, εs = 0.85, oct.shear strain oct = 0.86

Measures for strain (simple shear)

shear strain γ = d/t

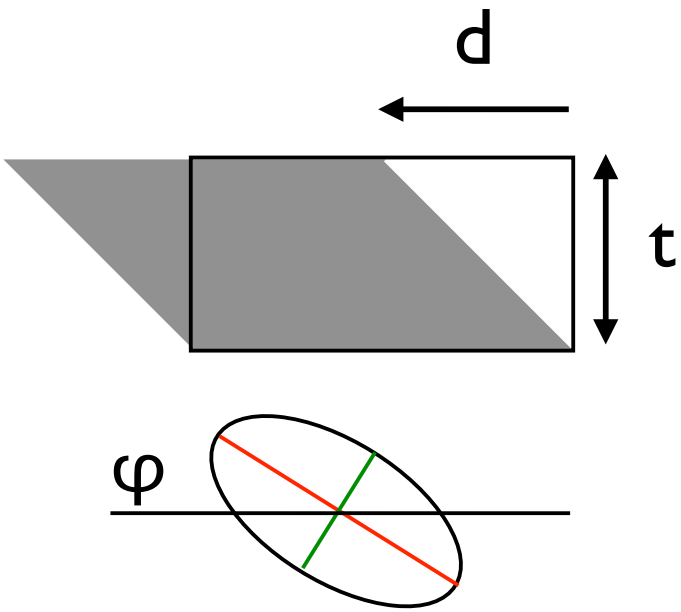

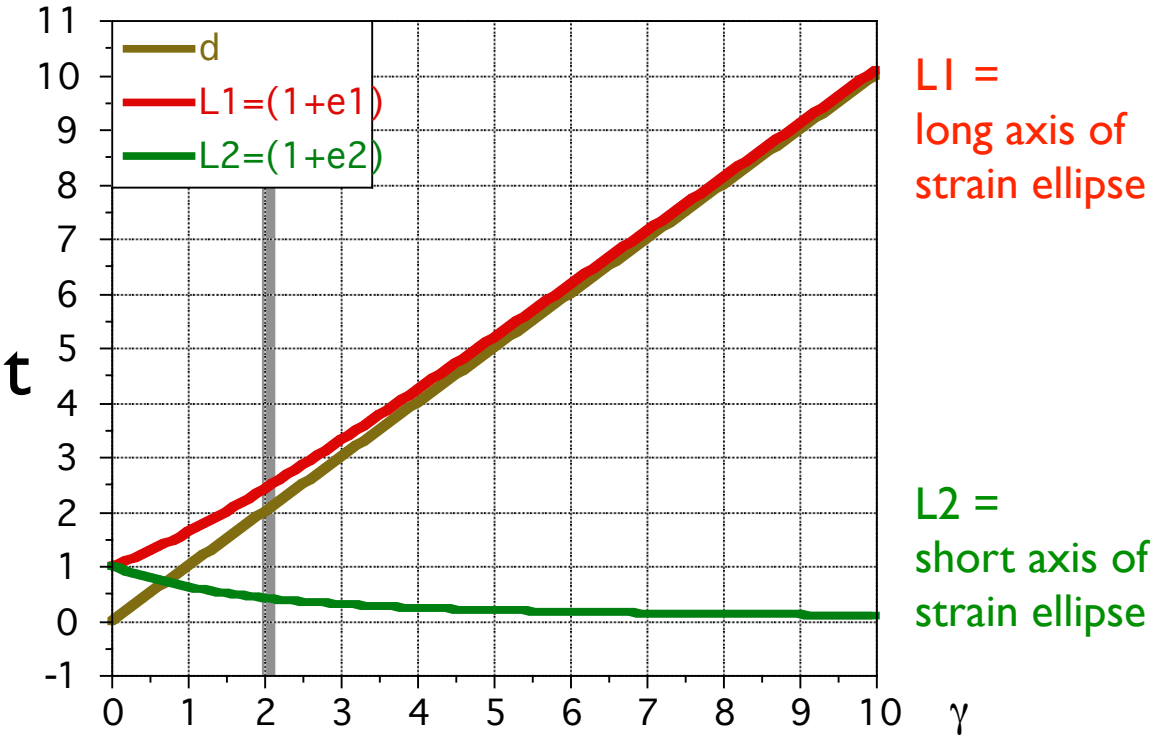

L1 = long axis of strain ellipse

L2 = short axis of strain ellipse

at shear strain γ = 2:

long axis a = 2.41, short axis b = 0.41, angle φ = 33°

R = a / b = 5.83

Measures for strain (simple shear)

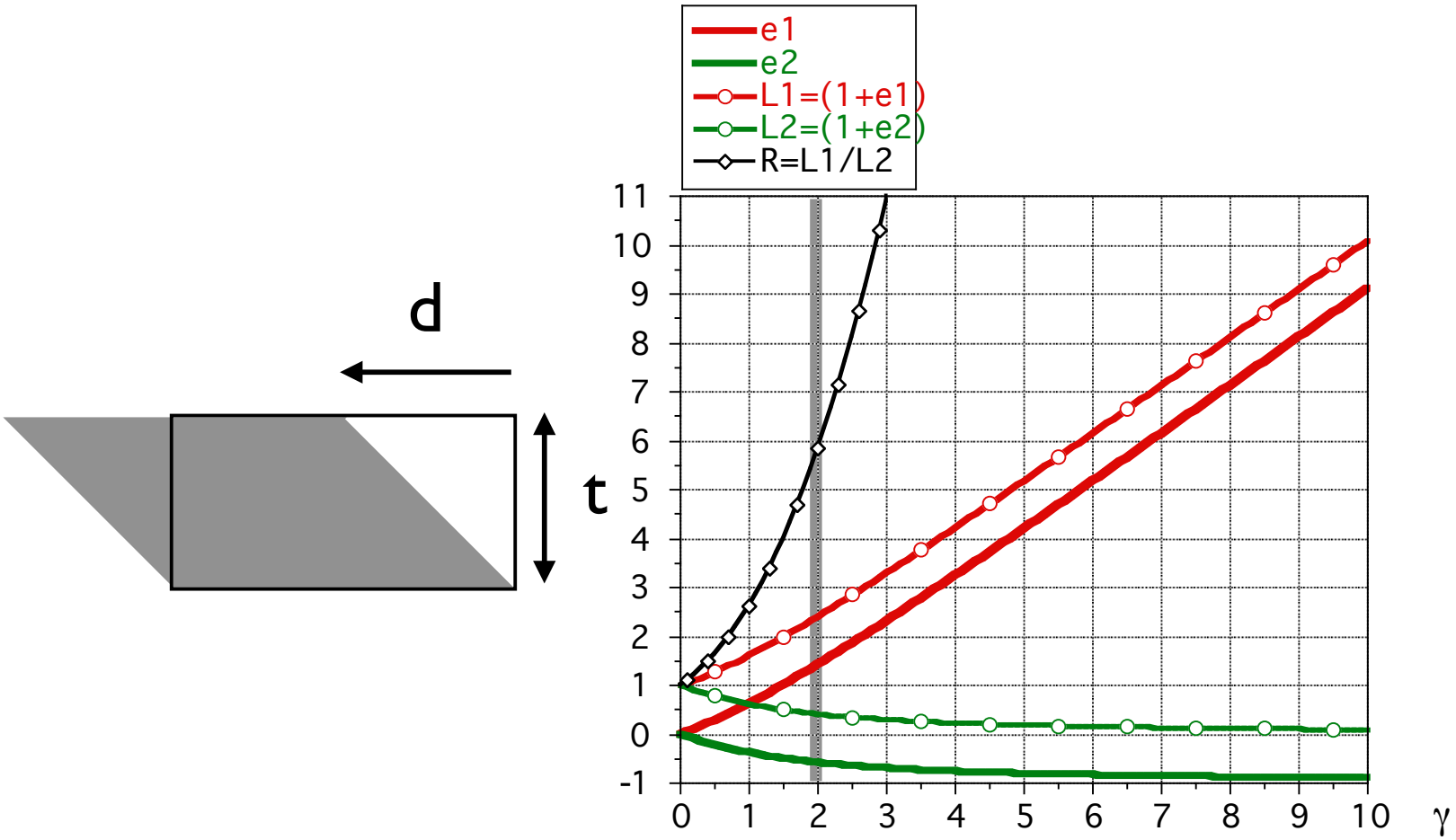

at shear strain γ = 2:

strains: e1 = 1.41, e2 = -0.59, R = 5.83

long axis (strain ellipse)= 2.41, short axis (strain ellipse) = 0.41

```
*    function smag      strain mag from shortening strain delta_l/l0
      function smag(del)
      smag = 0.
      if(del.le.0.0) go to 100
      e    = 1.-del
      e1   = alog(e)
      e2   = alog(sqrt(1./e))
      e3   = e2
      e1e2 = e1-e2
      e2e3 = e2-e3
      e3e1 = e3-e1
      oct  = (e1e2*e1e2)+(e2e3*e2e3)+(e3e1*e3e1)
      smag= 0.57735*sqrt(oct)
100    return
      end
```

```
*    function oct   octahedral shear strain from shortening strain delta_l/l0
      function oct(del)
      oct = 0.
      if(del.le.0.0) go to 100
      e1   = 1.-del
      e2   = sqrt(1./e1)
      e1   = e1-1.
      e2   = e2-1.
      e3   = e2
      e12 = e1-e2
      e23 = e2-e3
      e31 = e3-e1
      oct  = (e12*e12)+(e23*e23)+(e31*e31)
      oct = 0.66667*sqrt(oct)
100   return
      end
```

engineering strain:

$e(\%) = 100 \cdot (-\Delta L) / L$

natural / logarithmic strain:

$\varepsilon_{1,2,3} = \ln(L'/L)$

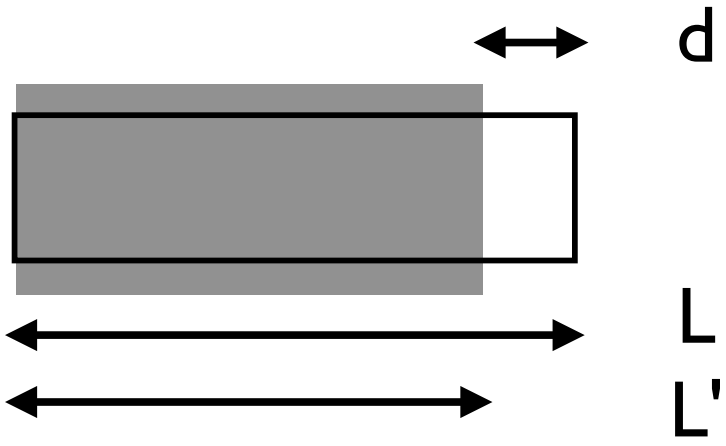

strain magnitude / intensity parameter (deviator):

$\varepsilon s = 1/\sqrt{3} \cdot \sqrt{[\ (\varepsilon 1-\varepsilon 2)^2 + (\varepsilon 2-\varepsilon 3)^2 + (\varepsilon 3-\varepsilon 1)^2\ ]}$

Measures for strain (simple shear)

es ≠ oct

strain magnitude ≠ octahedral shear strain

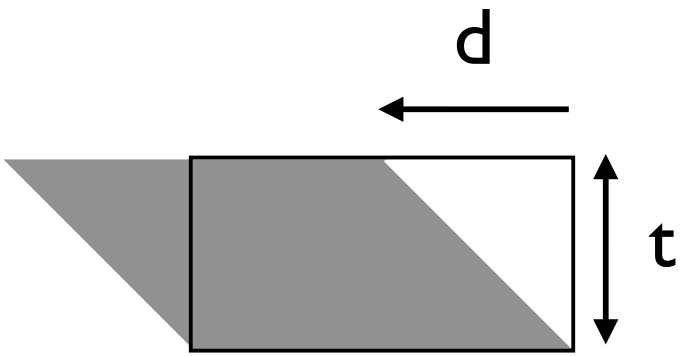

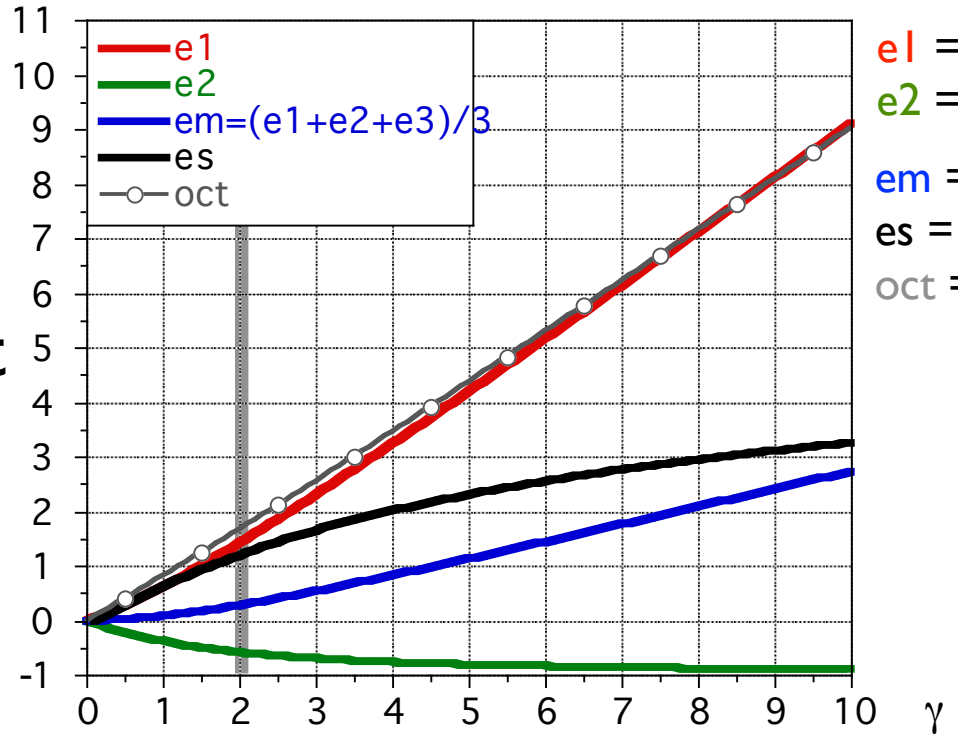

e1 = 1-dim strain
e2 = 1-dim strain

em = 3-dim strain
es = 3-dim strain
oct = 3-dim strain

at shear strain γ = 2:

strains: e1 = 1.41, e2 = -0.59, R = 5.83

mean strain = 0.28, εs = 1.20, oct.shear strain = 1.68

Measures for strain derived for d and γ

(axial)

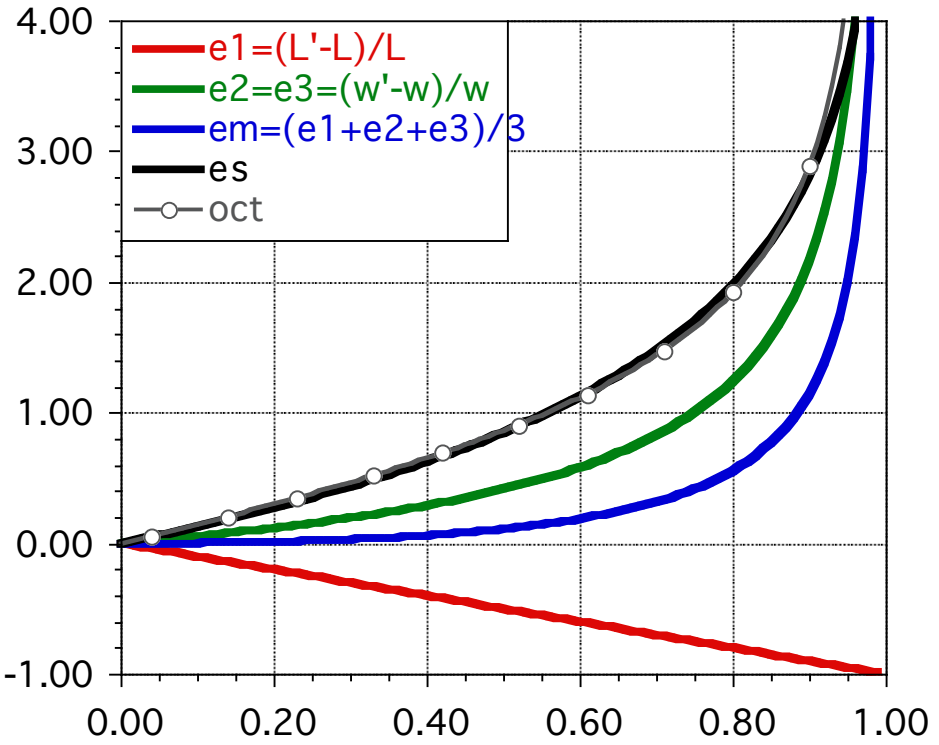

(simple shear)

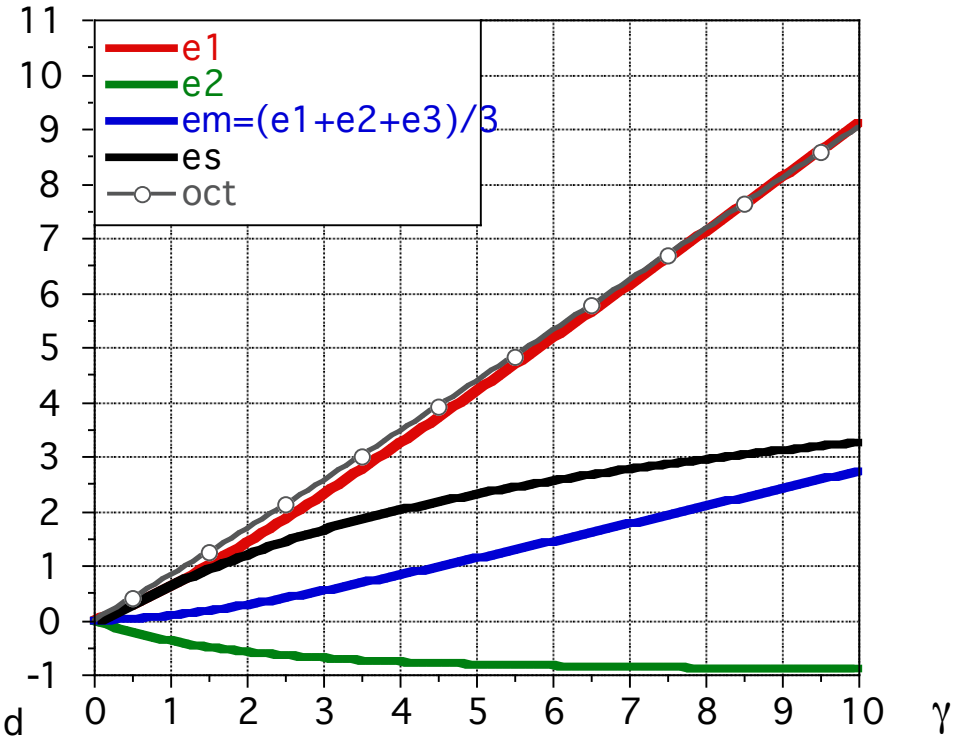

e1 = 1-dim strain
e2 = 1-dim strain
em = 3-dim strain
es = 3-dim strain
oct = 3-dim strain

d and γ in terms of deviatoric strain measures

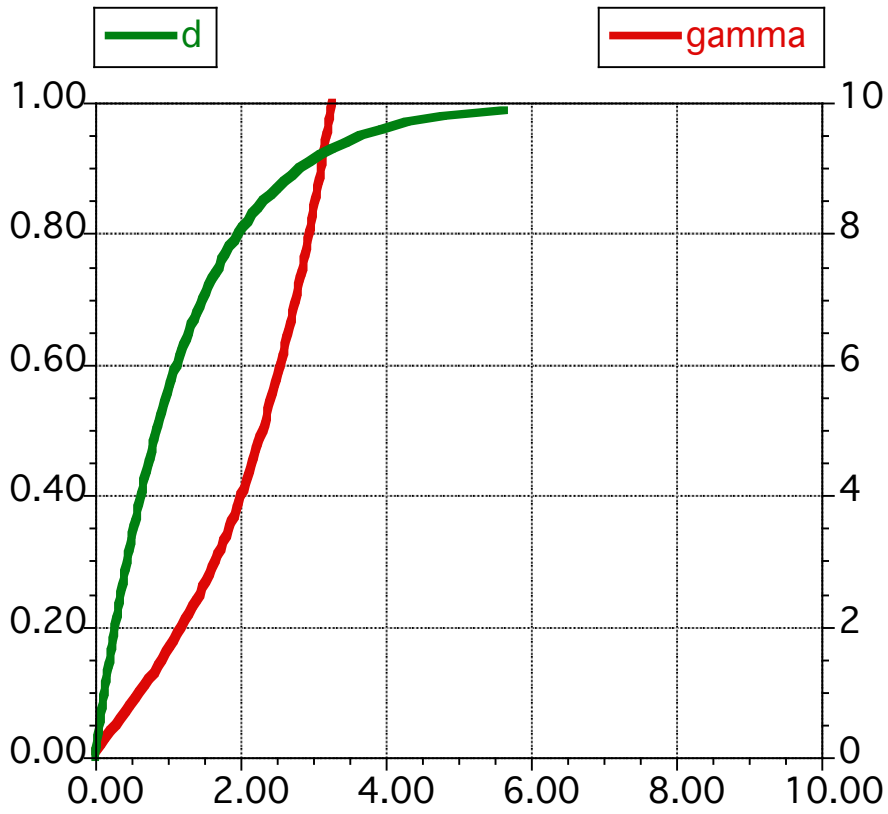

strain magnitude

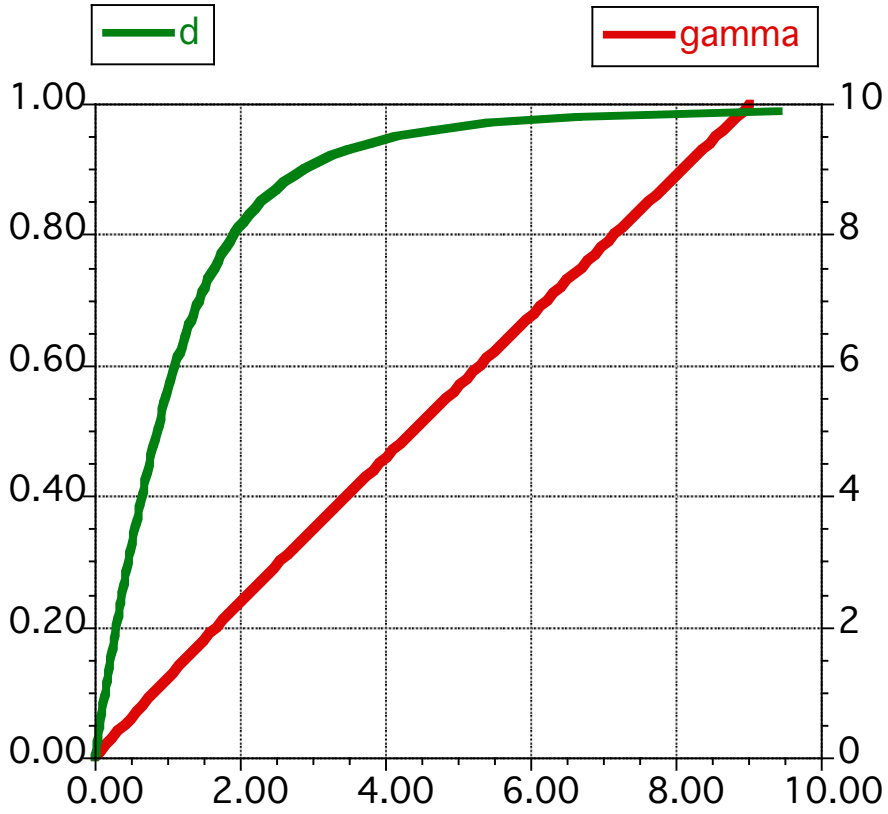

octahedral shear strain

STRENGTH

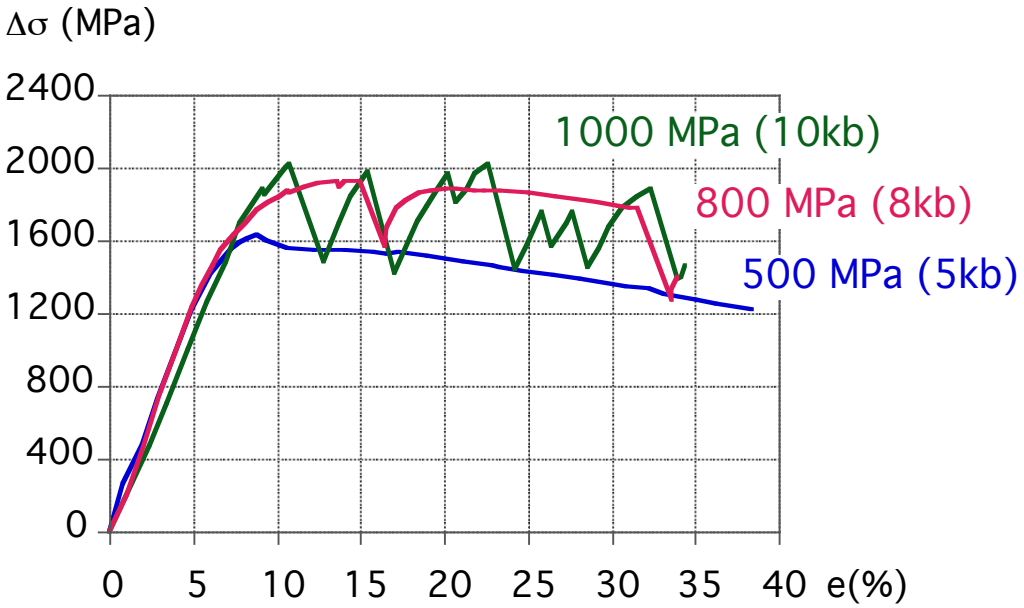

sample	confining pressure (MPa)	max. differential stress (MPa)
38nk	500	1634
60nk	1000	2022
71nk	800	1931

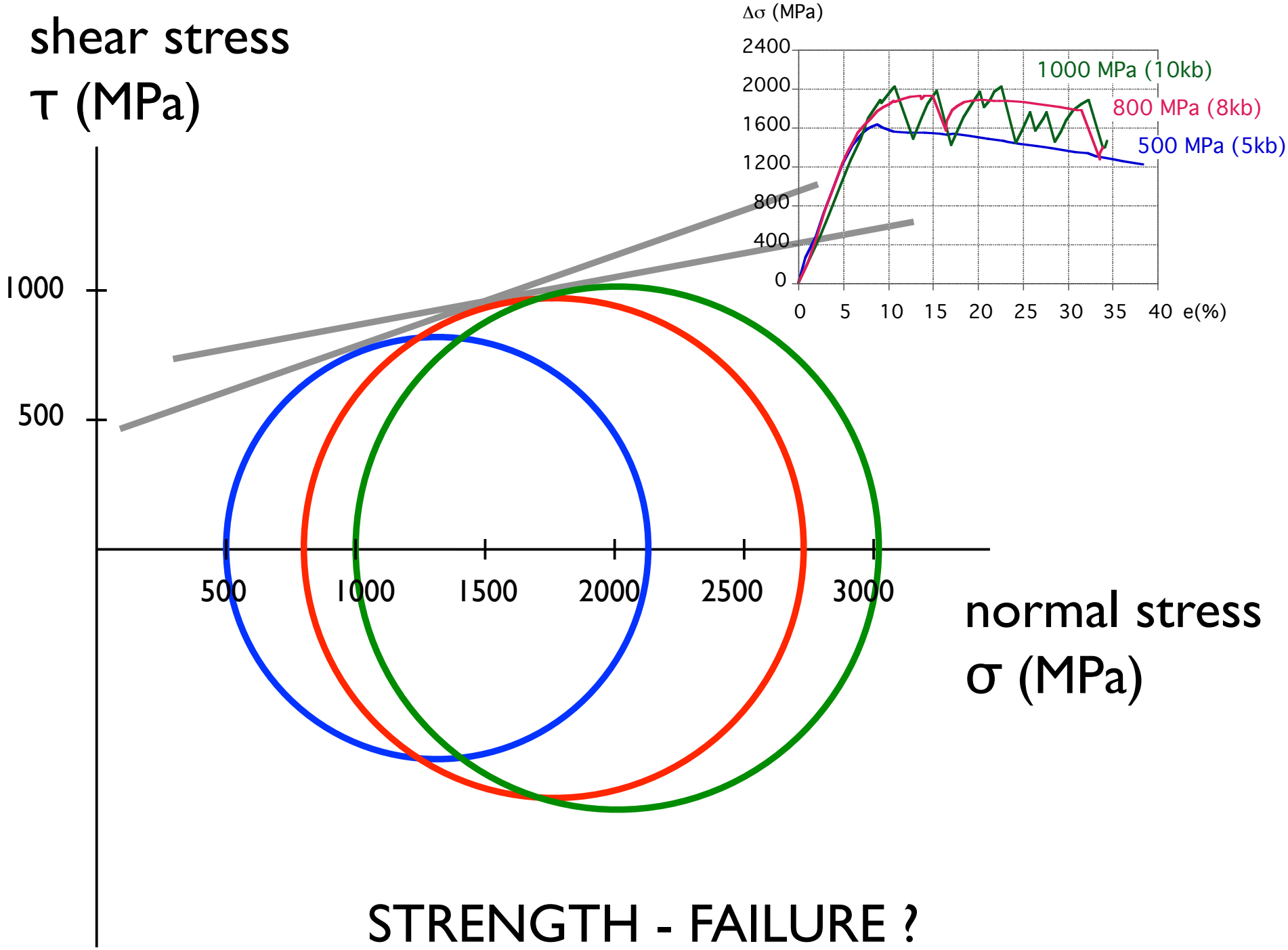
shear stress
τ (MPa)
1000
500
500
1000
1500
2000
2500
3000
normal stress
σ (MPa)
Δσ (MPa)
2400
2000
1600
1200
800
400
0
0
5
10
15
20
25
30
35
40
e(%)
1000 MPa (10kb)
800 MPa (8kb)
500 MPa (5kb)
STRENGTH - FAILURE ?

5
Coulomb-Mohr

Deformationsprozesse in der Erde (5)

Coulomb-Mohr, Friction and the strength of rocks

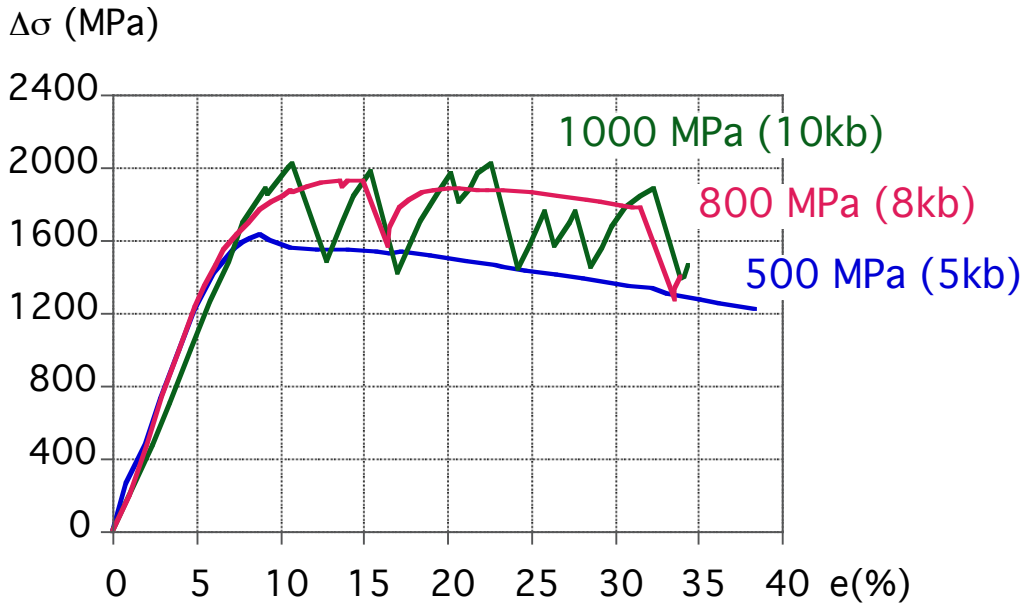

sample	confining pressure (MPa)	max. differential stress (MPa)
38nk	500	1634
60nk	1000	2022
71nk	800	1931

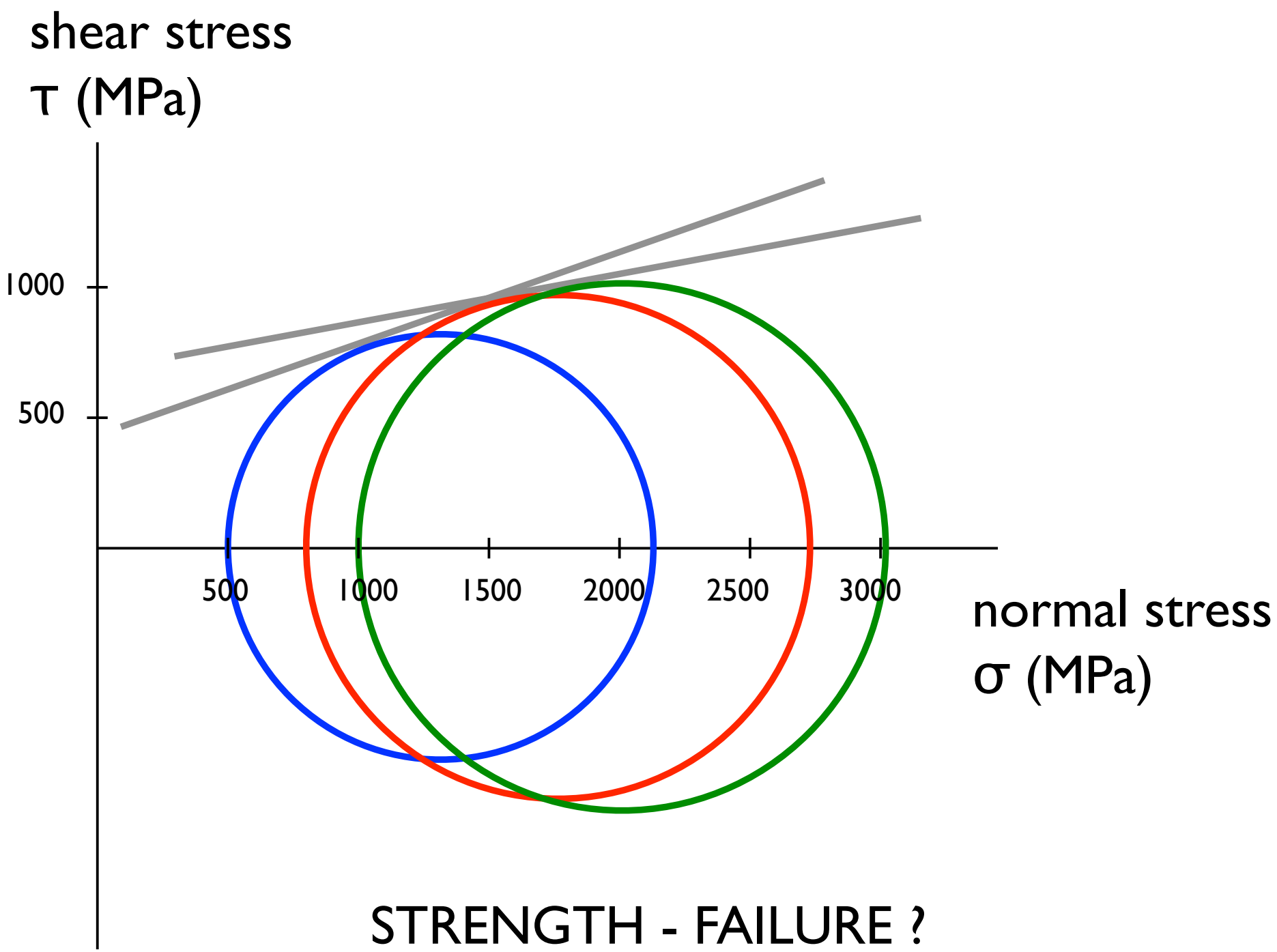

STRENGTH - FAILURE ?

Coulomb - Mohr failure criterion

ZEITSCHRIFT
DES
VEREINES DEUTSCHER INGENIEURE.

Nr. 42. Sonnabend, den 21. Oktober 1911. Band 55.

Inhalt:

Festigkeitsversuche unter allseitigem Druck. Von Th. v. Kármán (hierzu Textblatt 29) . . . 1749
Kerchove- und Gleichstrom-Dampfmaschine. Von G. Doederlein (Schluß) . . . 1758
Elektrisches Schweißen. Von B. Loewenherz (Schluß) . . . 1763
Entwicklung und Aussichten des Stahlbandantriebes Von L. Silberberg . . . 1768
Fehler bei Wehrbauten in Eisenbeton. Dansville- und Austin-Damm. Von Ziegler . . . 1773
Posener B.-V.: Versammlung der Ostdeutschen Bezirksvereine des Vereines deutscher Ingenieure vom 11. bis 13. August 1911. — Rheingau-B.-V. — Siegener B.-V. . . . 1777
Bücherschau: Lord Kelvin. Vorlesungen über Molekulardynamik. Von B. Weinstein — Transformers. Von H. Bohle und D. Robertson. — Elementarmechanik für Maschinentechniker. Von R. Vogdt. — Einflußlinien für die Berechnung paralleler Vierendeel-Träger. Von W. St. Ritter v. Balicki. — Bei der Redaktion eingegangene Bücher 1777
Zeitschriftenschau . . . 1780
Rundschau: Vierzylinder-Heißdampf-Verbundlokomotive für Gebirgstrecken der österreichischen Staatsbahnen. — Fahrbarer Bockkran für 150 t mit 2 Auslegern. — Rechenuhr. — Verschiedenes . . . 1783
Patentbericht . . . 1787
Zuschriften an die Redaktion: Flüssige Brennstoffe für Kraftbetrieb . 1788
Angelegenheiten des Vereines: Mitteilungen über Forschungsarbeiten, Heft 106. — Internationale Industrie- und Gewerbeausstellung in Turin 1911 . . . 1788

(hierzu Textblatt 29)

Festigkeitsversuche unter allseitigem Druck.

Von Dr. **Th. v. Kármán** in Göttingen.

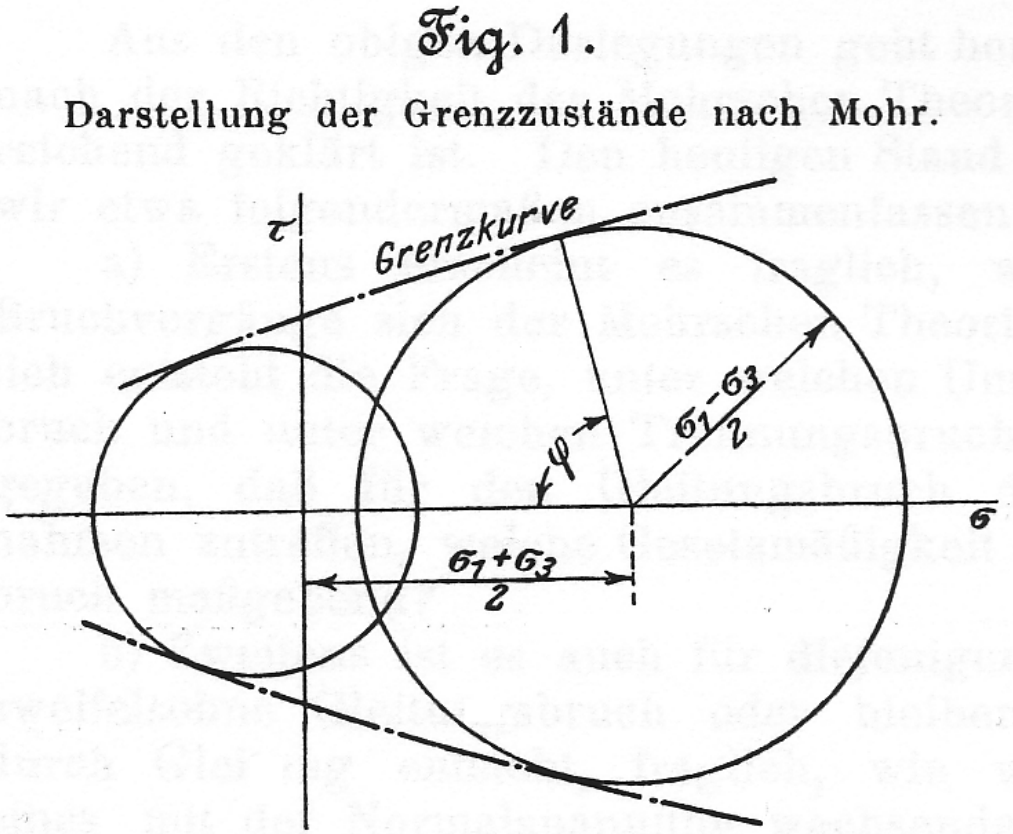

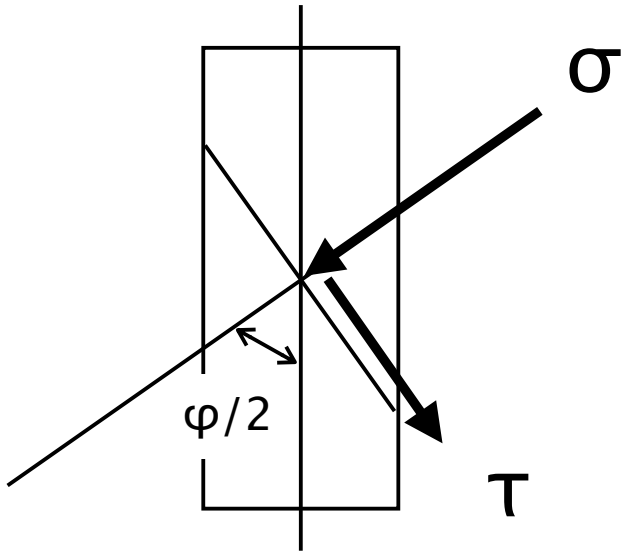

φ = 2·Winkel zwischen σ (Flächennormale) und σ1

(180−φ) = 2·Winkel zwischen τ (Fläche) und σ1

Fig. 5.

Formänderungskurve des Marmors beim Versuch unter allseitigem Druck.

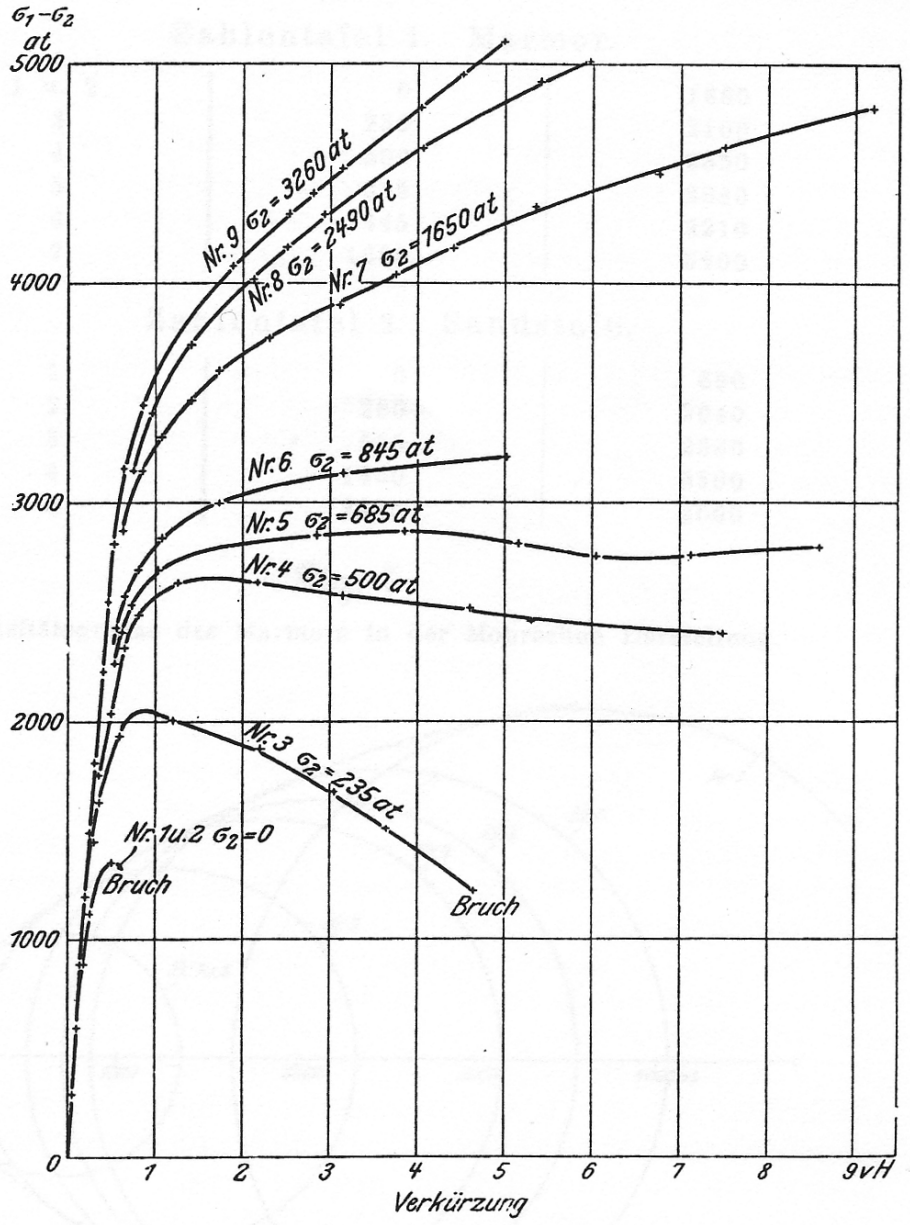

Fig. 7.

Elastizitätsgrenze des Marmors in der Mohrschen Darstellung.

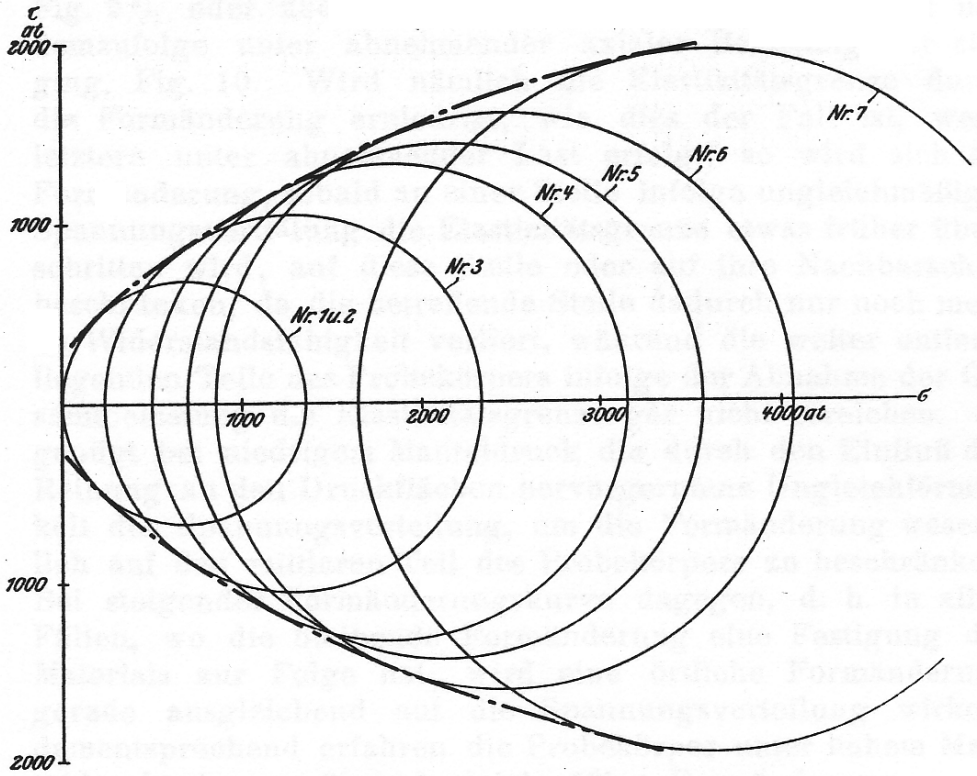

Fig. 5.

Formänderungskurve des Marmors beim Versuch unter allseitigem Druck.

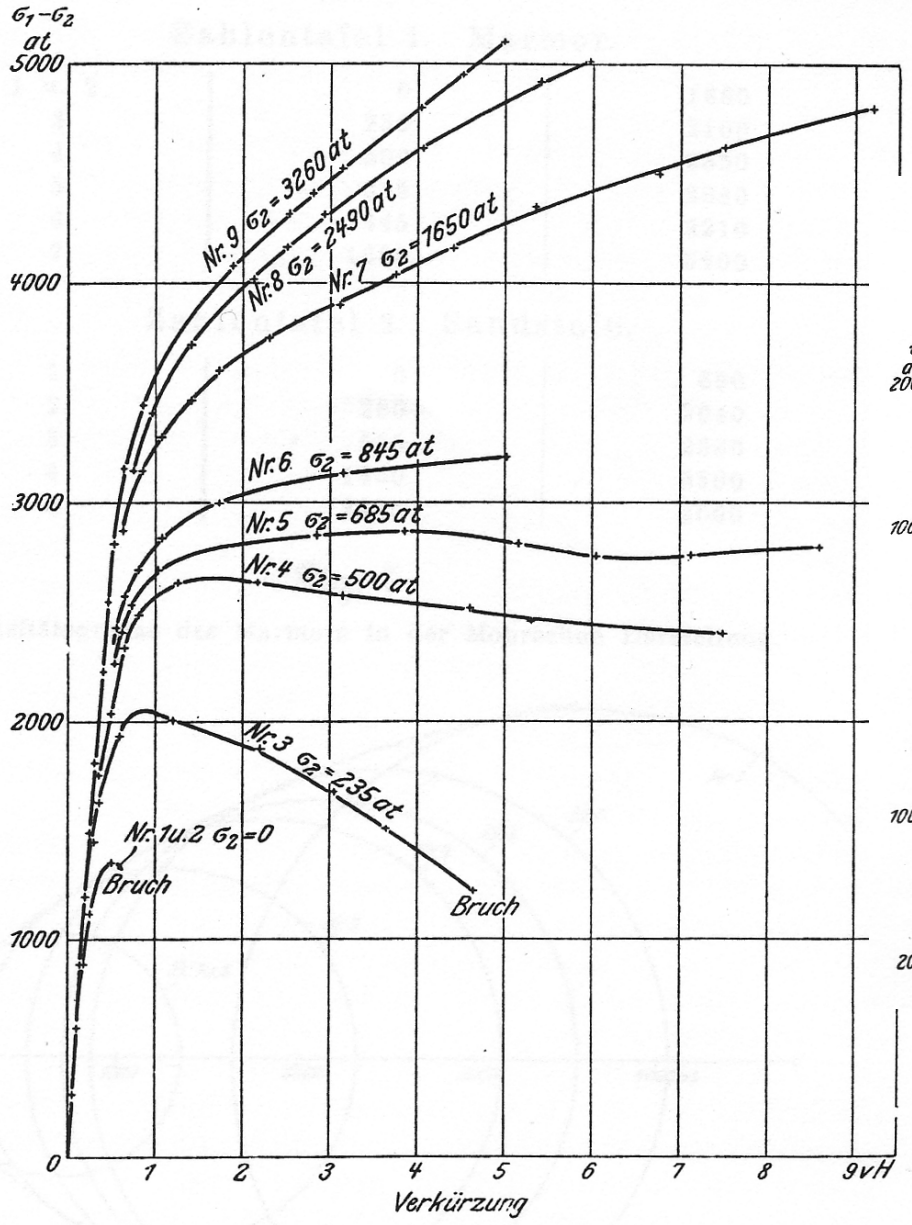

Fig. 8.

Kurven gleicher bleibender Dehnung bei Marmor in der Mohrschen Darstellung.

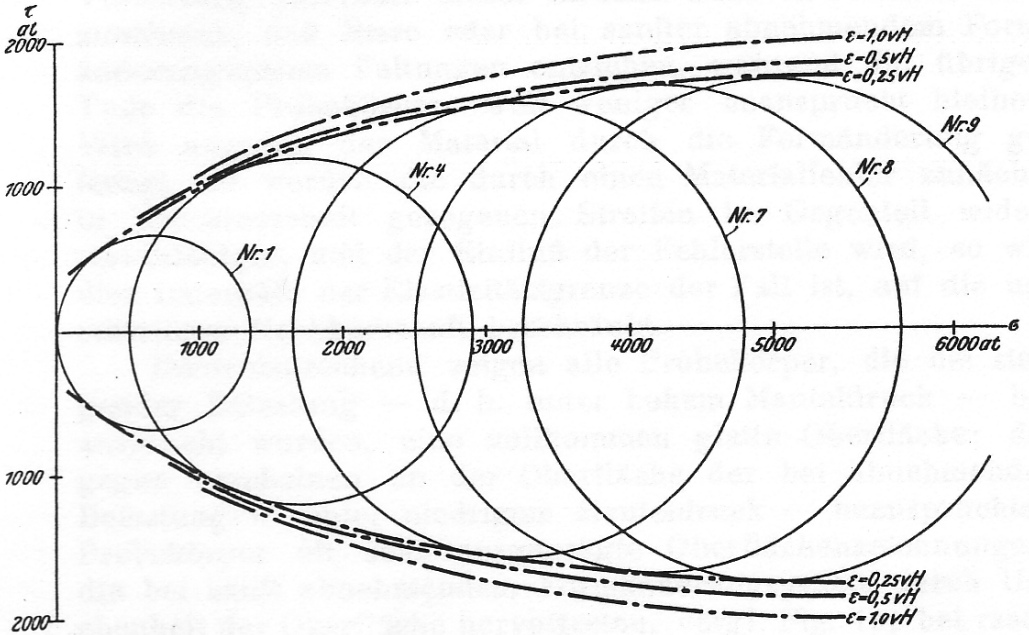

5
Friction

Deformationsprozesse in der Erde (5)

Friction

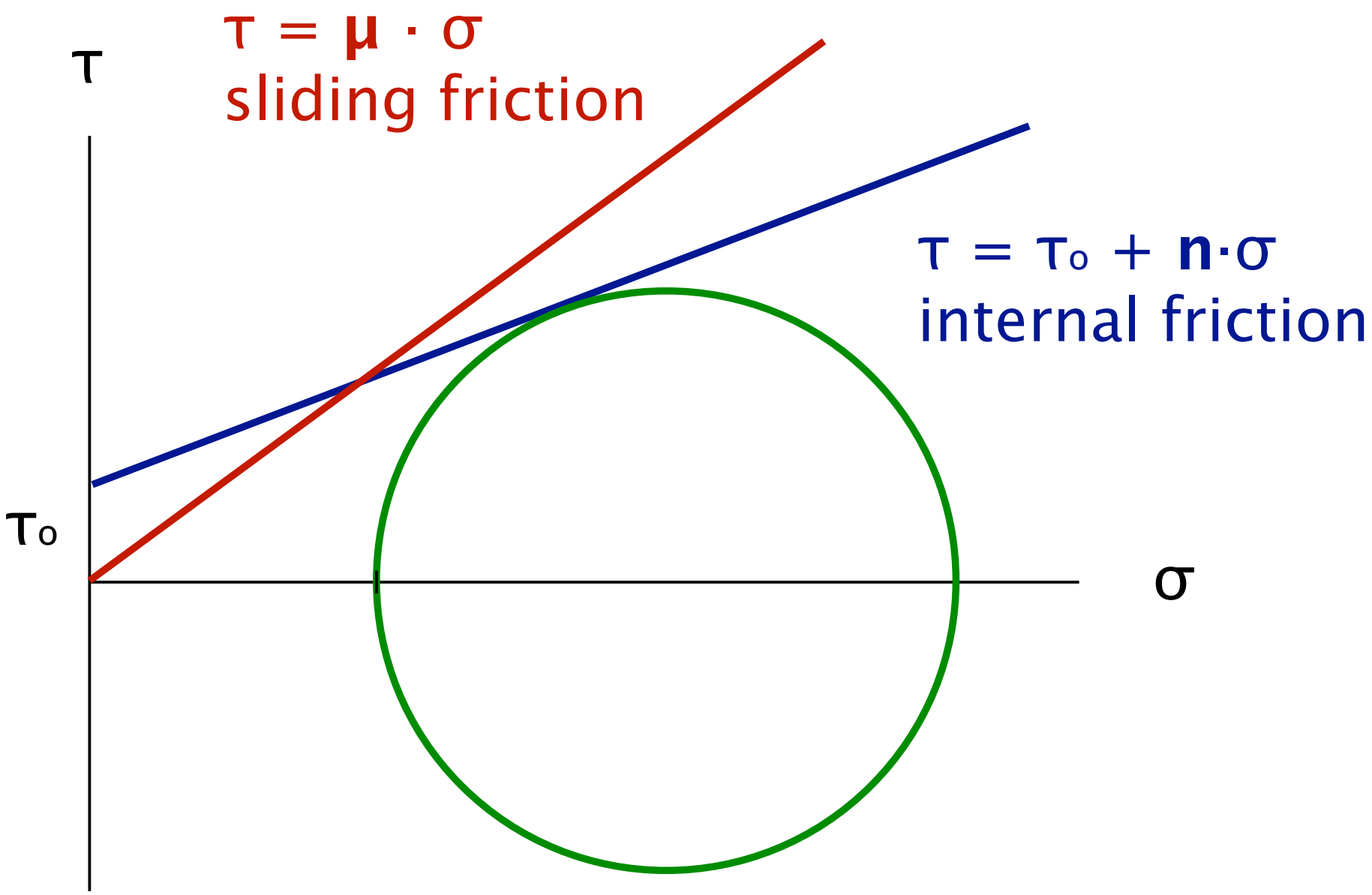

Friction

Law of Leonardo da Vinci: Friction is independent of the area of contact

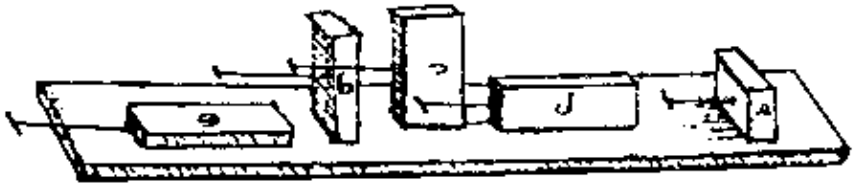

Leonardo Da Vinci (1452-1519)

Leonardo da Vinci stated the two basic laws of friction 200 years before Newton even defined what force is.

Da Vinci simply stated that:

1. the areas in contact have no effect on friction.
2. if the load of an object is doubled, its friction will also be doubled.

sliding block on conveyor belt: friction is independent of the area of contact

http://www.nano-world.org/frictionmodule/content/

Friction

Law of Amontons: Frictional force F proportional to load L

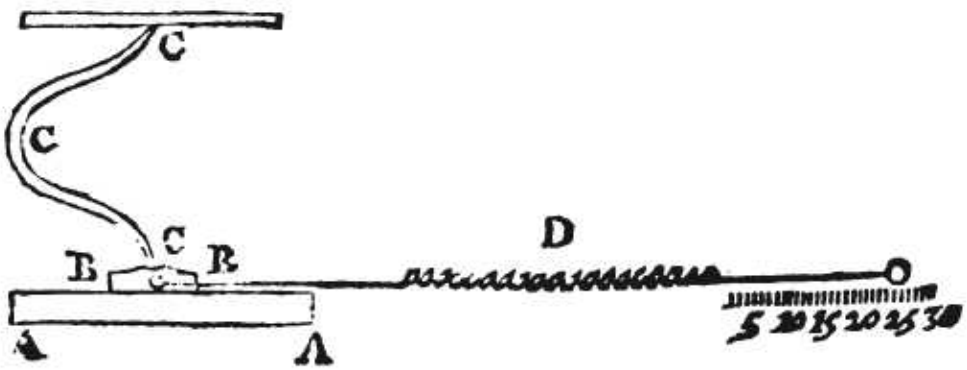

Versuchsaufbau von G. Amontons zur Messung der kinetischen Reibkraft. Die Reibung zwischen den Oberflächen A und B wird mittels der Auslenkung einer Feder D gemessen. Die Feder C dient der Einstellung der Normalkraft.

(De la résistance causée dans les machines (1699) in Memoires de l'Académie des Sciences.)

Guillaume Amontons (1663-1705)

Guillaume Amontons rediscovered the two basic laws of friction that had been discovered by Leonardo Da Vinci, and he also came up with an original set of theories. He believed that friction was predominately a result of the work done to lift one surface over the roughness of the other, or from the deforming or the wearing of the other surface. For several centuries after Amontons' work, scientists believed that friction was due to the roughness on the surfaces.

sliding block on conveyor belt: friction is proportional to the weight

http://www.nano-world.org/frictionmodule/content/

Friction

Law of Coulomb: Friction is independent on the velocity

Charles August Coulomb (1736-1806)

He added to the second law of friction; "strength due to friction is proportional to compressive force", "although for large bodies friction does not follow exactly this law". Coulomb published the work referring to Amontons. The second law of friction is known as the "Amontons-Coulomb Law" referring to work done by the two scientists in 1699 and 1785 respectively.

The Amontons-Coulomb law of friction holds for many different material combinations and geometries but unlike Newton's first law, nothing fundamental can be derived from it.

sliding block on conveyor belt: friction is independent of the velocity

http://www.nano-world.org/frictionmodule/content/

Friction

Law of Euler: Static friction is greater than sliding friction

Leonhard Euler (1707-1783)

introduced the model of rigid interlocking asperities as the cause of frictional resistance.

used the relation between inclination angle α and friction coefficient μ:

$$F_H = mg\sin\alpha = F_r = \mu F_N = \mu mg\cos\alpha \qquad \sin\alpha = \mu\cos\alpha \qquad \mu = \tan\alpha$$

found that the friction coefficient is velocity-independent

distinguished between static and kinetic friction

found that static friction is always larger than kinetic friction

Friction

Tomlinson mechanism: Stick-Slip - cause of dissipation

- squeaky door
- violine strings
- earth quakes

F. Philip Bowden and David Tabor (1950)

Bowden and Taylor gave a physical explanation for the laws of friction. They determined that the true area of contact is a very small percentage of the apparent contact area. The true contact area is formed by the asperities. As the normal force increases, more asperities come into contact and the average area of each asperity contact grows.

The frictional force was shown to be dependent on the true contact area—a much more intuitively satisfying argument than what the Amontons-Coulomb law allows. Bowden and Tabor argued that within these asperities all of the dynamics of friction take place.

model of friction at the atomic level: stick-slip

http://www.nano-world.org/frictionmodule/content/

Friction

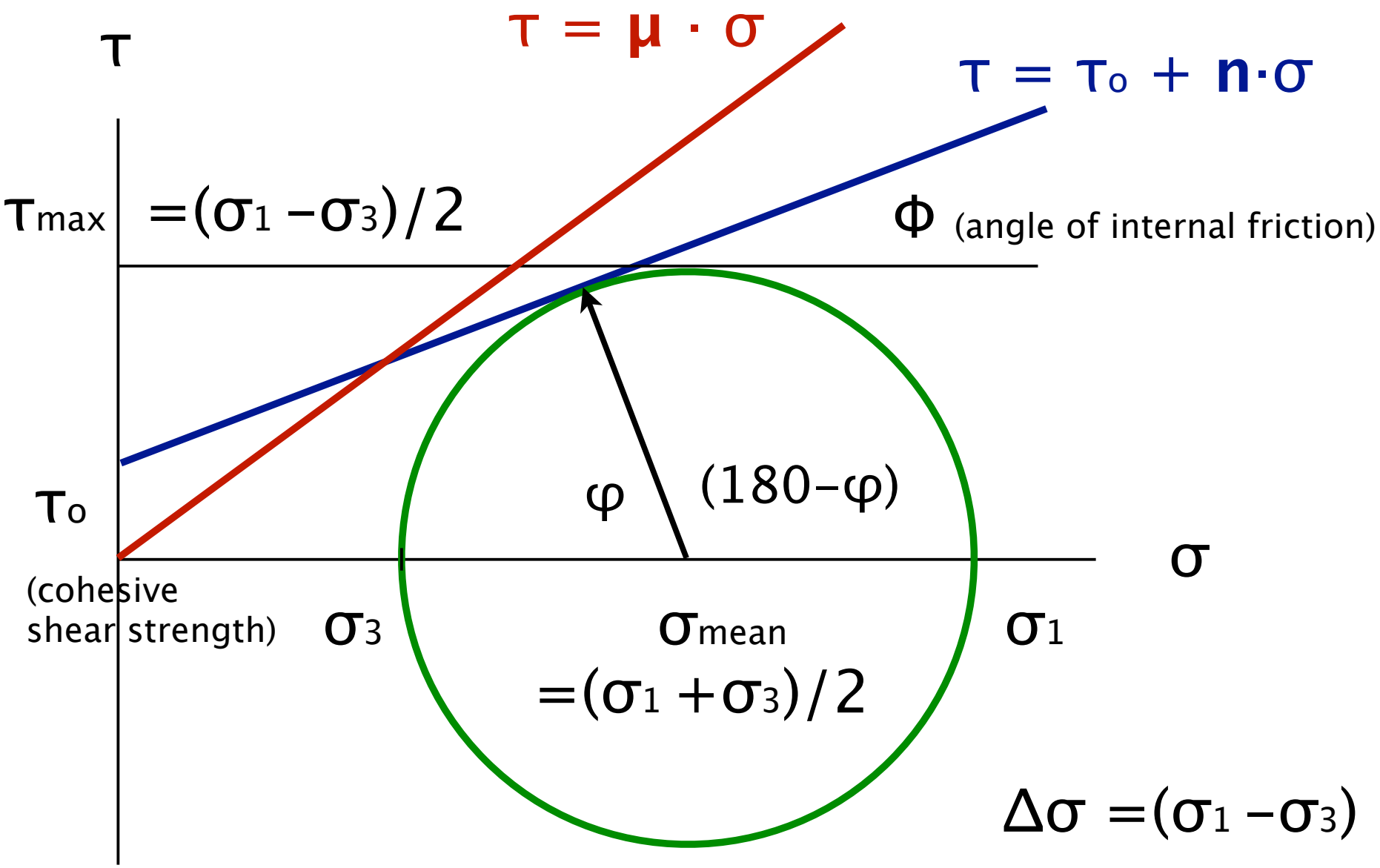
τ
τ = μ · σ
τ = τo + n·σ
τmax =(σ1 −σ3)/2
Φ (angle of internal friction)
τo
(cohesive
shear strength)
φ
(180−φ)
σ
σ3
σmean
=(σ1 +σ3)/2
σ1
Δσ =(σ1 −σ3)

Friction

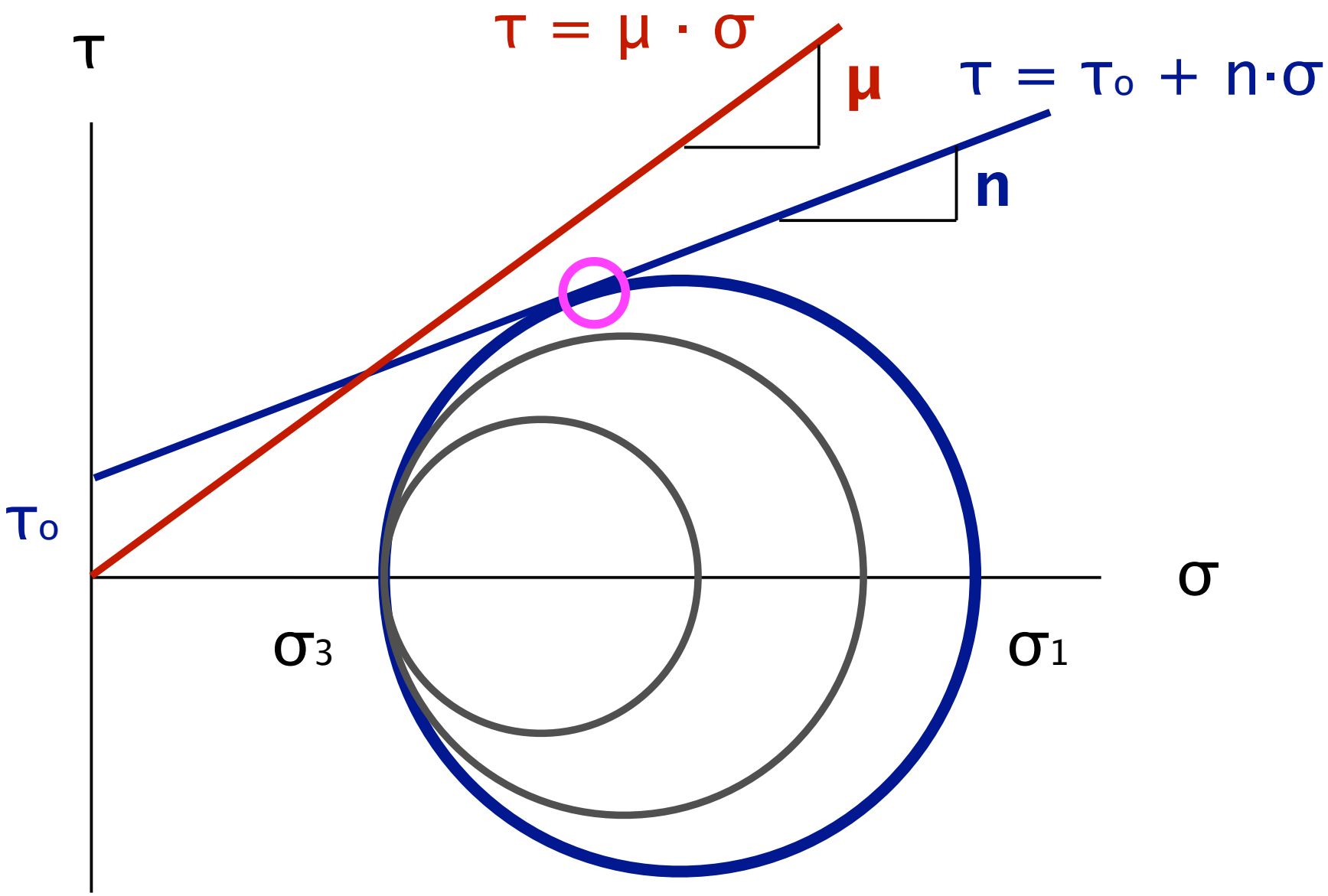

Friction

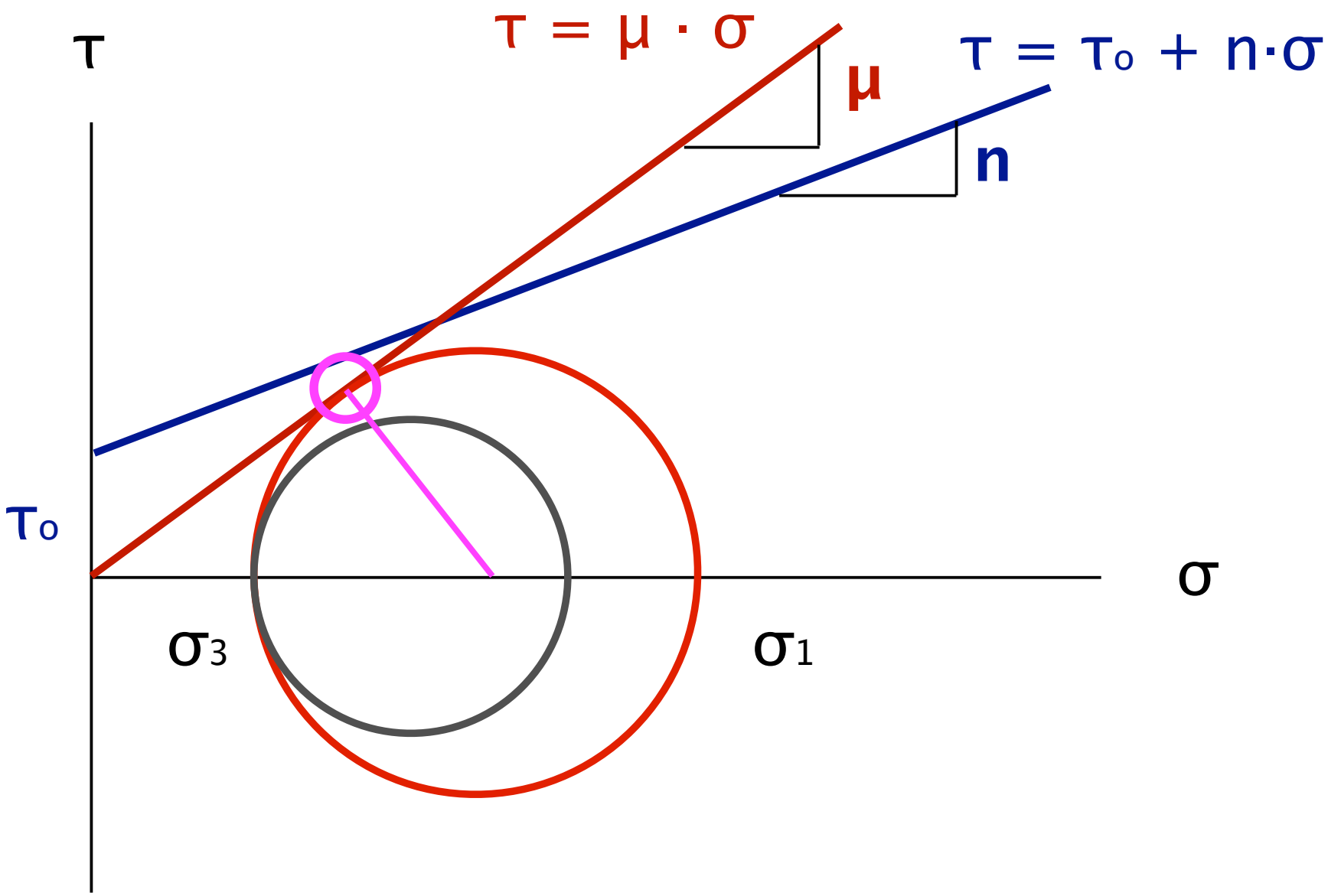

Friction

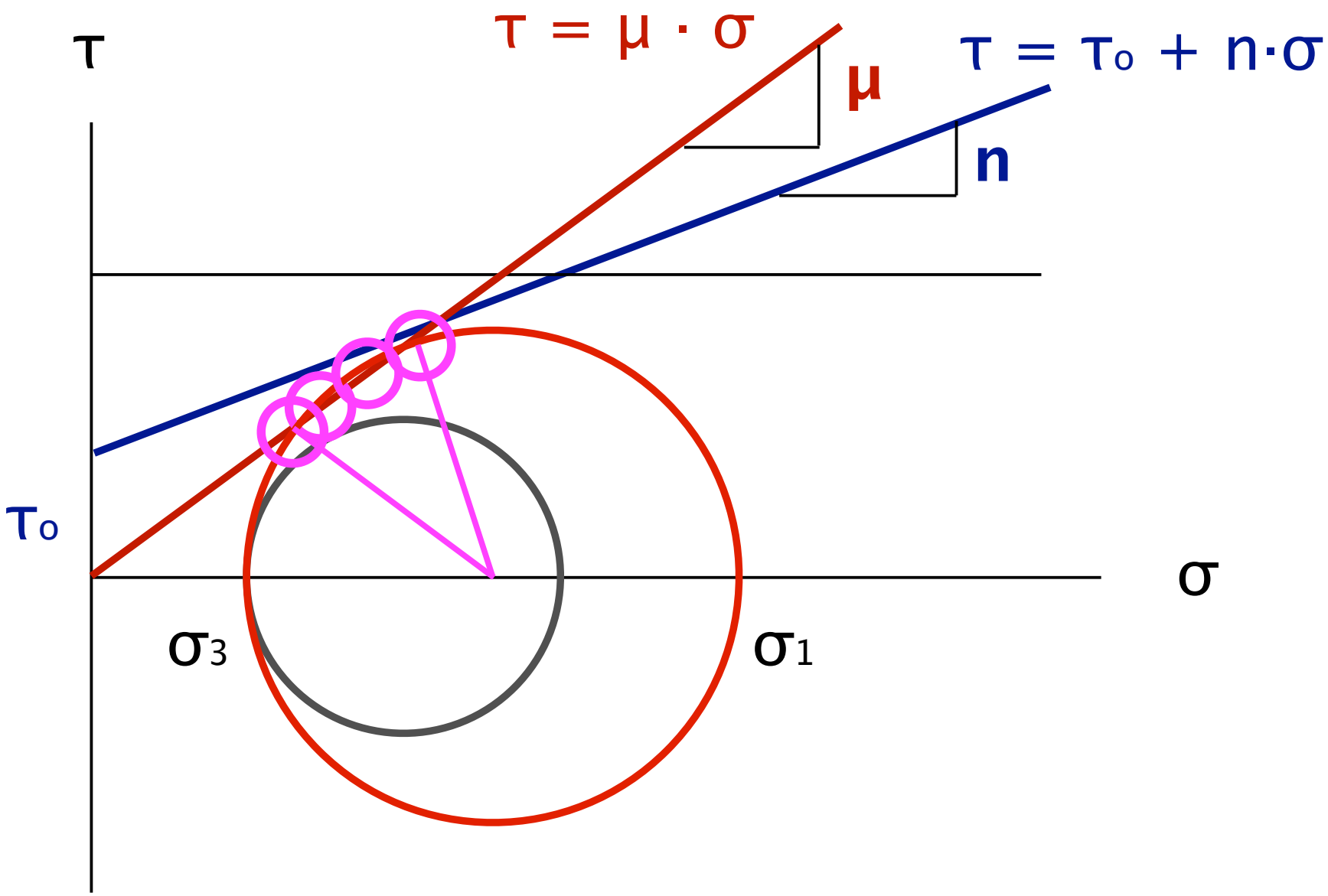

Friction

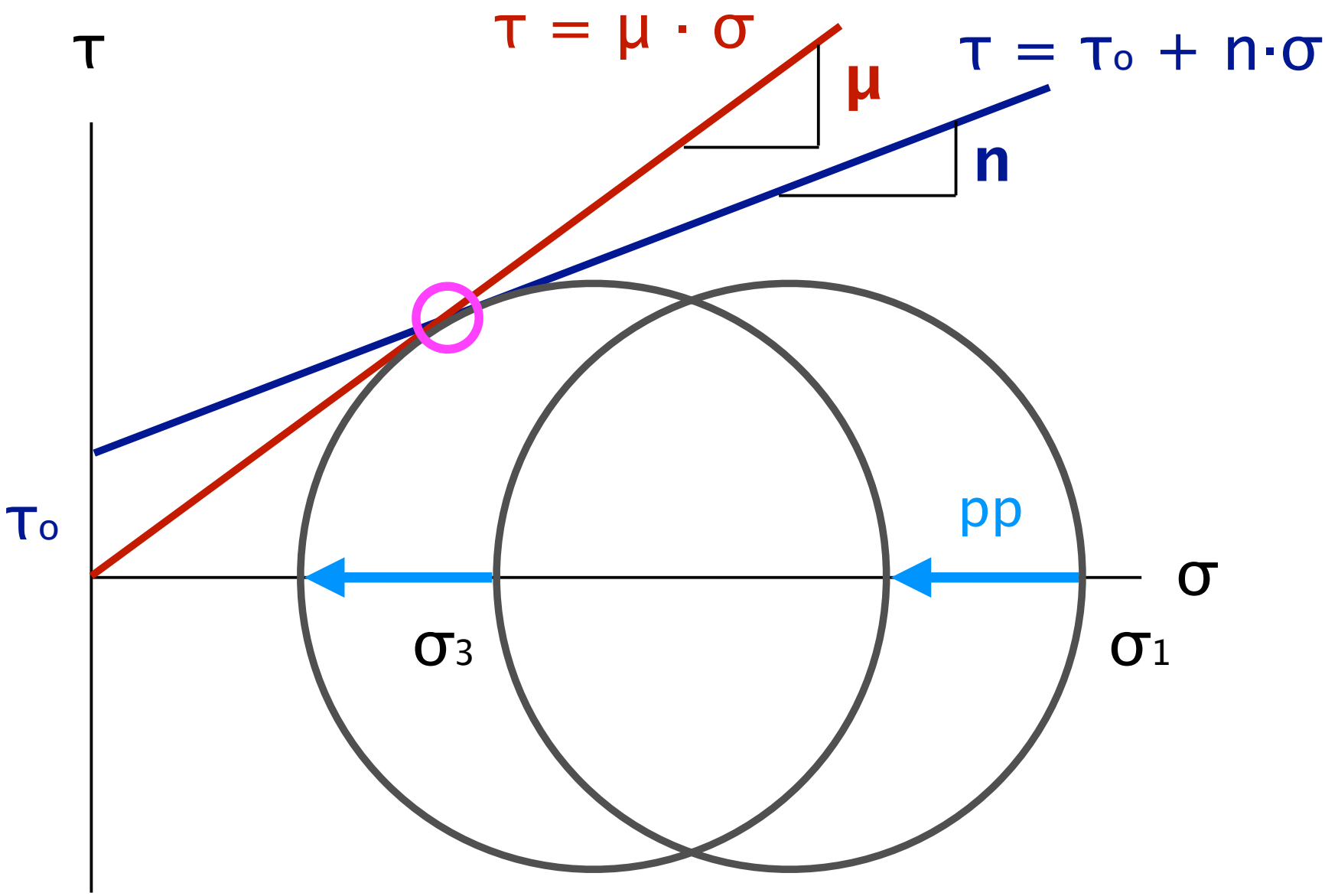

Coulomb - Mohr failure criterion

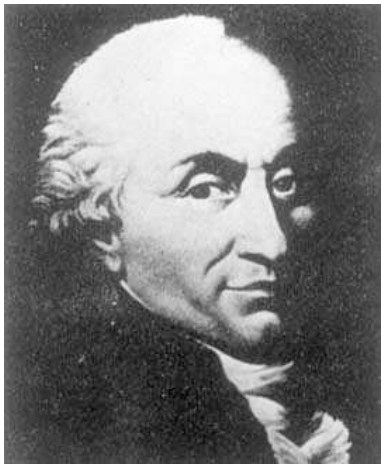

Charles Augustin de Coulomb
1736 - 1806

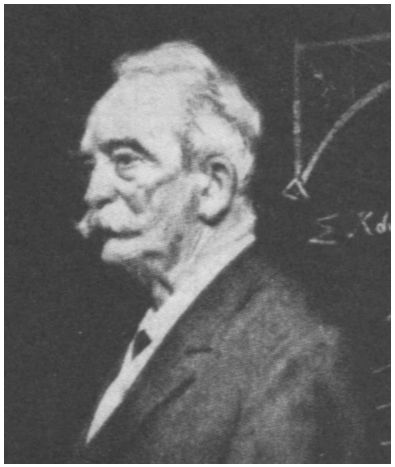

Christian Otto Mohr
1835 - 1918

JOURNAL OF GEOPHYSICAL RESEARCH VOL. 74, NO. 22, OCTOBER 15, 1969

On the Coulomb-Mohr Failure Criterion

JOHN HANDIN

Center for Tectonophysics, Texas A&M University
College Station, Texas 77843

Coulomb's criterion for the shear fracture of a brittle material is that total shearing resistance is the sum of the cohesive shear strength (independent of direction) and the product of the effective normal stress and the coefficient of internal friction (a constant independent of normal stress). Mohr generalized this criterion by extending it to a three-dimensional state of stress, and by allowing for a variable coefficient. The coefficients of internal and external (sliding) friction are not the same in general. Both tend to decrease with increasing normal stress, and their relative magnitudes may determine if failure occurs by new shear fracturing or by slip on pre-existing cohesionless surfaces like joints in rocks.

Coulomb's [1776] problem was the shear fracture in a prism of isotropic material under uniaxial compression σ_1 (compressive stresses counted positive). He wrote down the equations for the shear stress τ and normal stress σ on a plane inclined at an angle, say θ, to the loading direction. He assumed that 'la cohésion se mesure par la résistance que les corps solides opposent à la désunion directe de leur parties', and 'je suppose ici que l' adhérence oppose une egalé résistance, soit que la force soit dirigée parallèlment ou perpendiculairement au plan de rupture.' He then solved for the value of θ for which the uniaxial stress (compressive breaking strength) would be a minimum, and he found, of course, that $\theta = 45°$.

During the following two centuries, writers of authority have erroneously stated that Coulomb proceeded no further. For example, in the first edition of his widely known book on faulting *Anderson* [1942] ascribed the notion of internal friction to Navier. *Jaeger* [1962] repeated this mistake. In one edition of his great book, *The Earth*, *Jeffreys* [1952] in turn credits Anderson with this concept!

In fact, however, Coulomb went on to say 'je supposerai ici que la résistance dûe au frottement [sic] est proportionelle a la pression comme l'a trouvé M. Amontons.' He then added the cohesive shear strength, which is now commonly denoted as τ_0, to the frictional shearing resistance $n\sigma$, where n is the coefficient of internal friction, and obtained the equation

$$\tau = \tau_0 + n\sigma.$$

Coulomb then differentiated the uniaxial compressive stress with respect to θ to find the minimum value, and showed that

$$\theta_f = \pm 45° \mp \phi/2,$$

where ϕ = the angle of internal friction, n = $\tan \phi$, and θ_f = the angle between a potential shear fracture and σ_1.

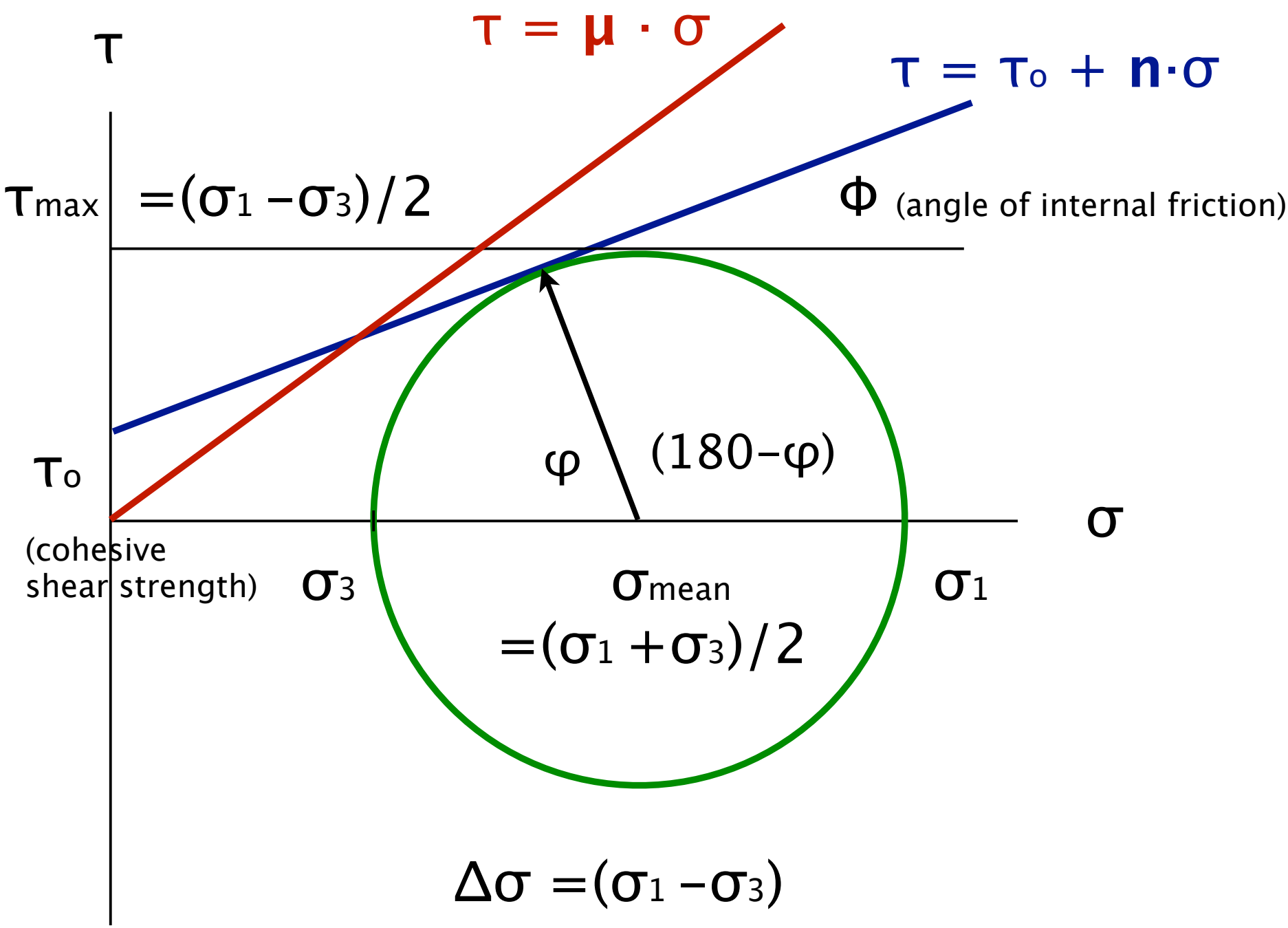
τ
τ = μ · σ
τ = τo + n·σ
τmax =(σ1 −σ3)/2
Φ (angle of internal friction)
τo
(cohesive
shear strength)
φ
(180−φ)
σ
σ3
σmean
=(σ1 +σ3)/2
σ1
Δσ =(σ1 −σ3)

maximum stress ratio τ/σ

$$\sigma = (\sigma 1+\sigma 3) + (\sigma 1-\sigma 3) \cdot \cos(\theta)$$

$$\tau = (\sigma 1-\sigma 3) \cdot \sin(\theta)$$

Kaleidagraph:

example:
σ1 = 3
σ2 = 1

create series: 0 to 180 in c1

c2=0.5*(3+1)+0.5*(3-1)*cos(c1)
c3=0.5*(3-1)*sin(c1)
c4=c3/c2
c0=0.5*c1

Theta	2*Theta	Sigma n	Tau	Tau/Sigma
c0	c1	c2	c3	c4
0.0000	0.0000	3.0000	0.00000	0.0000
10.000	20.000	2.9397	0.34202	0.11635
20.000	40.000	2.7660	0.64279	0.23239
30.000	60.000	2.5000	0.86603	0.34641
40.000	80.000	2.1736	0.98481	0.45307
50.000	100.00	1.8264	0.98481	0.53922
60.000	120.00	1.5000	0.86603	0.57735
70.000	140.00	1.2340	0.64279	0.52092
80.000	160.00	1.0603	0.34202	0.32257
90.000	180.00	1.0000	0.00000	0.00000

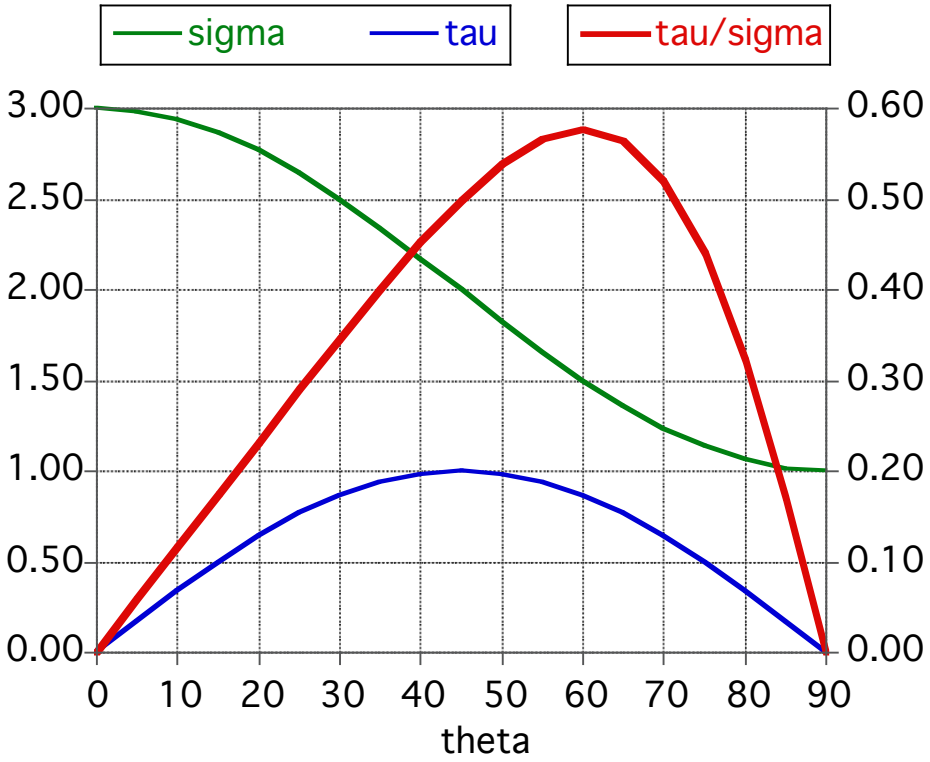

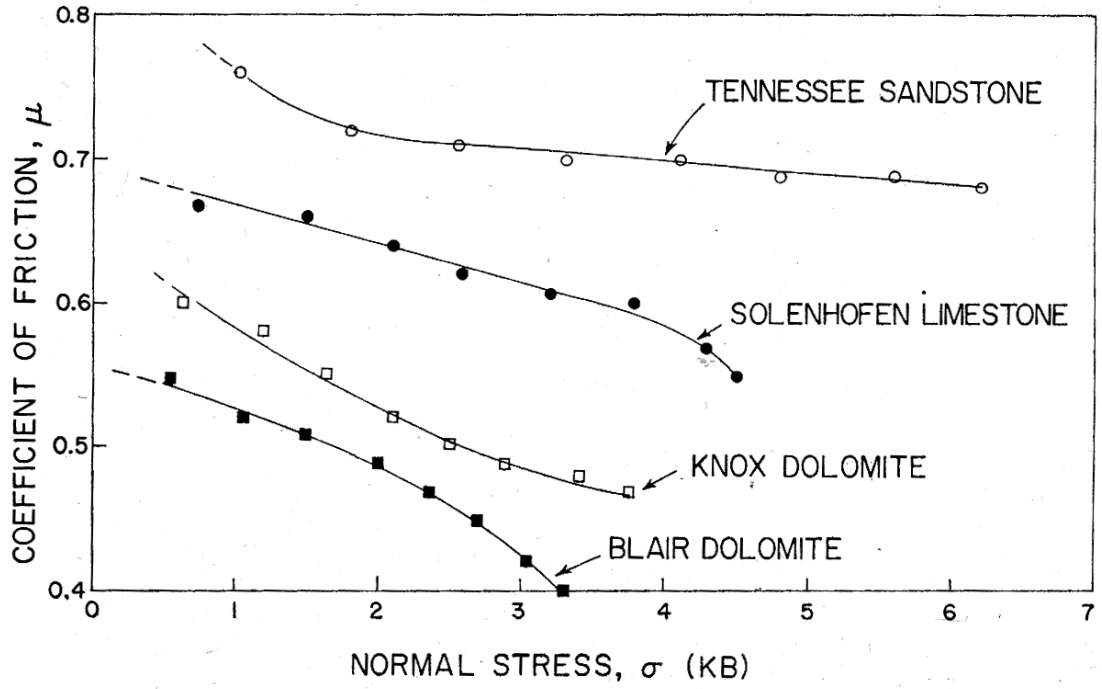

Coefficients of sliding friction on 45° saw cuts in four rocks as functions of normal stress.

TABLE 2. Cohesive Strengths and Coefficients of Internal and Sliding Friction of Some Rock under 1 kb Confining Pressure

Rock	Cohesive Strength τ_0 kb	Coefficient of Internal Friction n	Coefficient of Sliding Friction μ
Blair Dolomite	0.45	1.00	0.40
Lueders Limestone	0.15	0.53	0.60
Solenhofen Limestone	1.05	0.53	0.62
Tennessee Sandstone	0.50	0.84	0.70

τ_0 = cohesive strength
$n = \tan(\Phi)$ = coefficient of internal friction
Φ = angle of internal friction
θ_f = angle between shear fracture and σ_1
μ = coefficient of sliding friction ($\tau = \mu \cdot \sigma$)

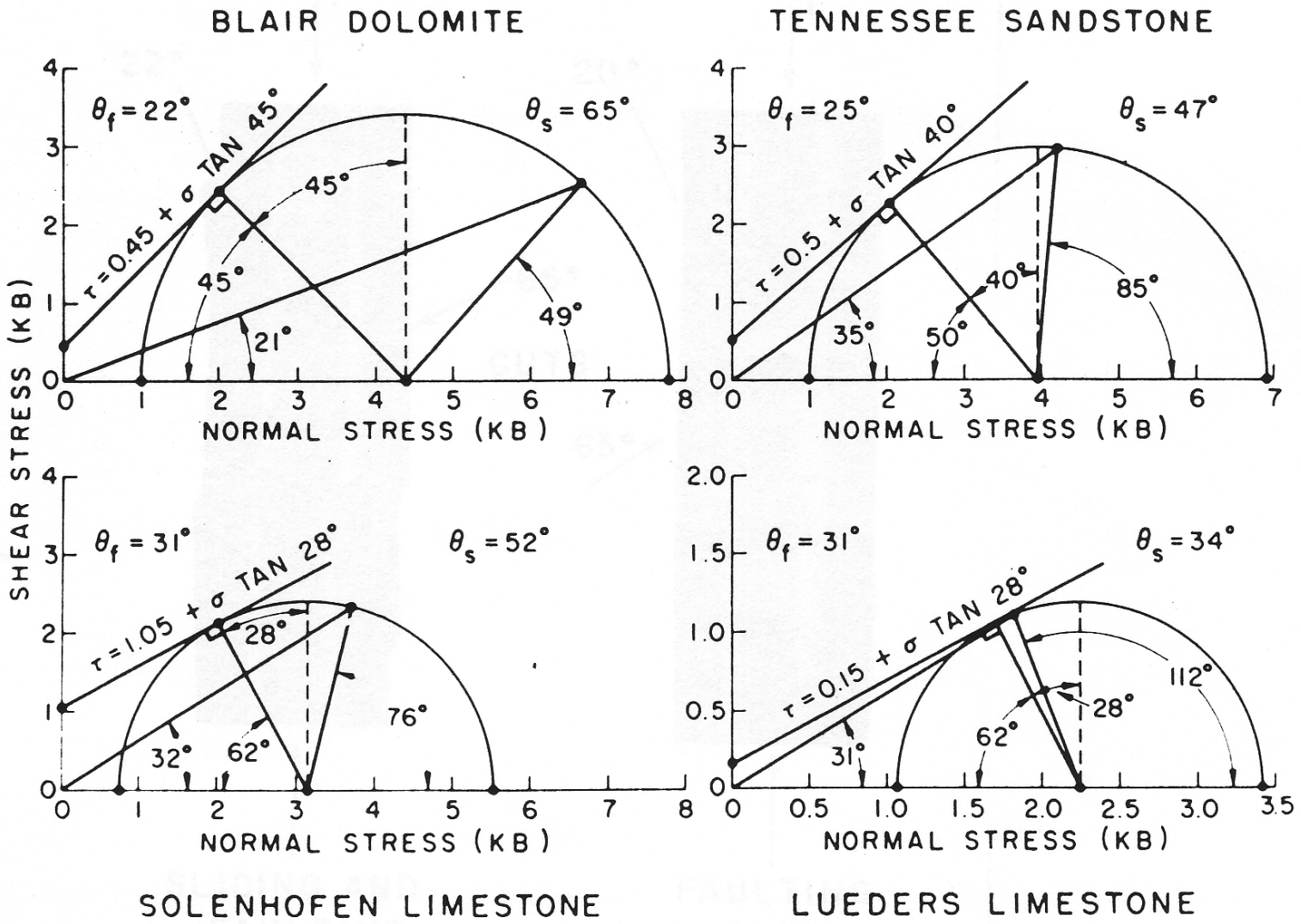

Fig. 2. Mohr envelopes and sliding lines for some rocks.

n = tan(Φ) = coefficient of internal friction
μ = coefficient of sliding friction ($\tau = \mu \cdot \sigma$)

τo = cohesive strength
θf = angle between shear fracture and σ1
θs = angle of sliding friction

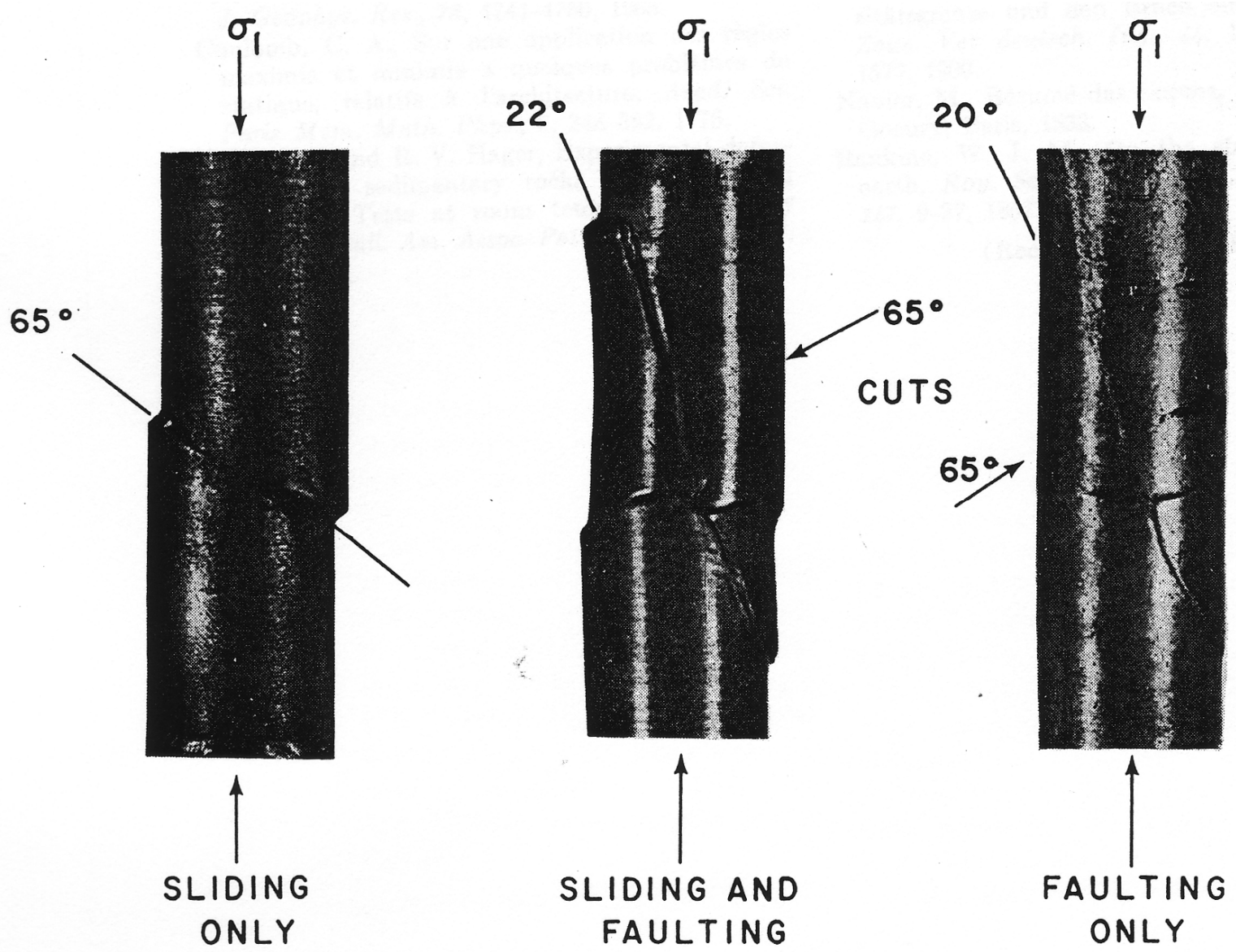

Fig. 3. Blair dolomite specimens with 65° saw cuts.

6
Brittle deformation at depth

Deformationsprozesse in der Erde (6)

Brittle deformation at depth

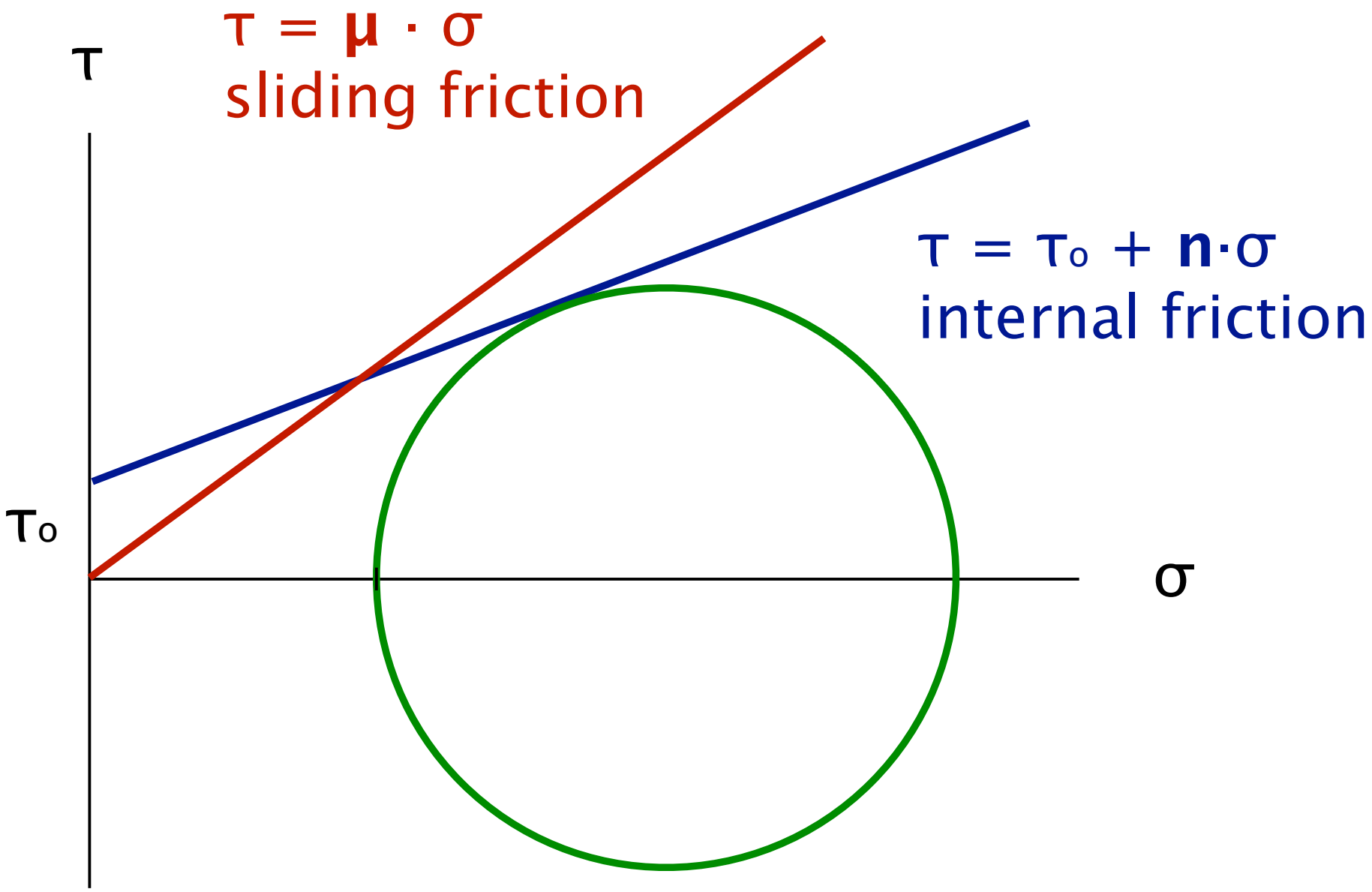

Measured coefficients of sliding friction

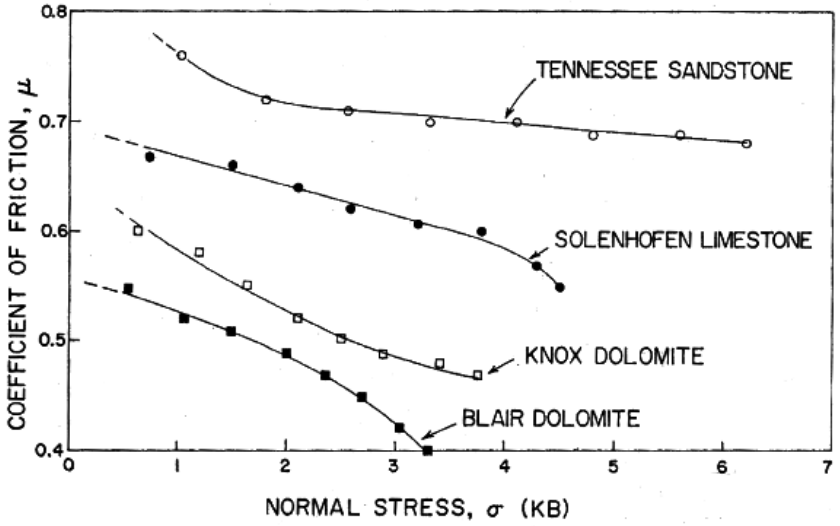

Rock	Coefficient of Sliding Friction μ
Blair Dolomite	0.40
Lueders Limestone	0.60
Solenhofen Limestone	0.62
Tennessee Sandstone	0.70

Handin (1969)

Byerlee's ~~law~~ rule

$\mu = \tau / \sigma n$ (from $\tau = \mu \cdot \sigma$)

$\mu = B + A / \sigma n$ (from $\tau = A + B \cdot \sigma$)

μ = coefficient of sliding friction

(Byerlee, 1978)

$\mu = 0.85 \cdot \sigma n$ (for $\sigma n < 200$ MPa)

$\mu = 0.5 + 0.6 \cdot \sigma n$ (for 200 MPa $< \sigma n < 2000$ MPa)

Friction

AB spring
v = velocity
m = mass

Force at:
C = Initital...
D = Maximum...
G = Residual...
.... Friction

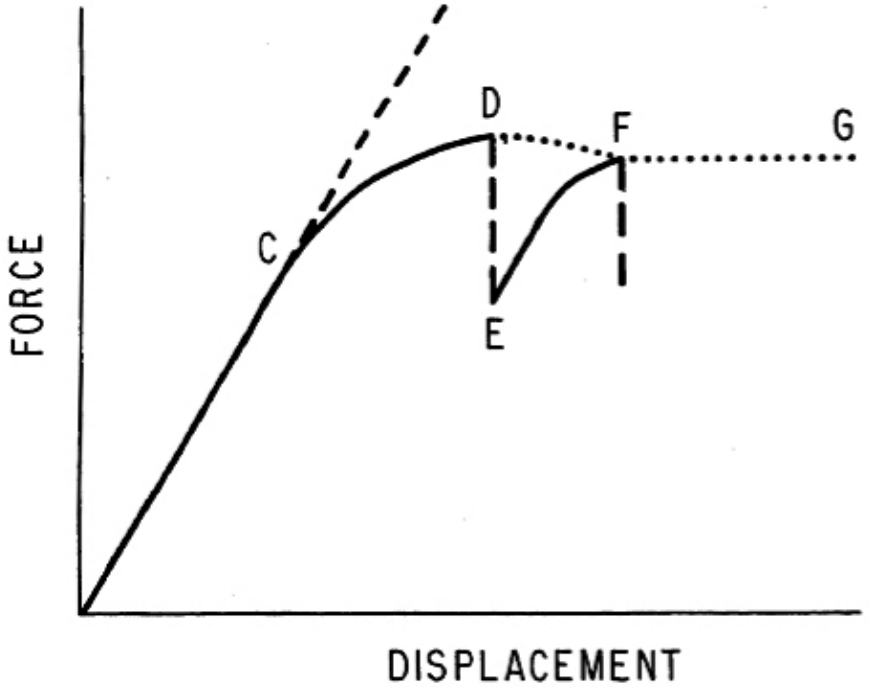

fig. 1 and fig. 2 (Byerlee, 1978)

Maximum Friction
0 - 5 MPa
(0 - 50 bar)

surface

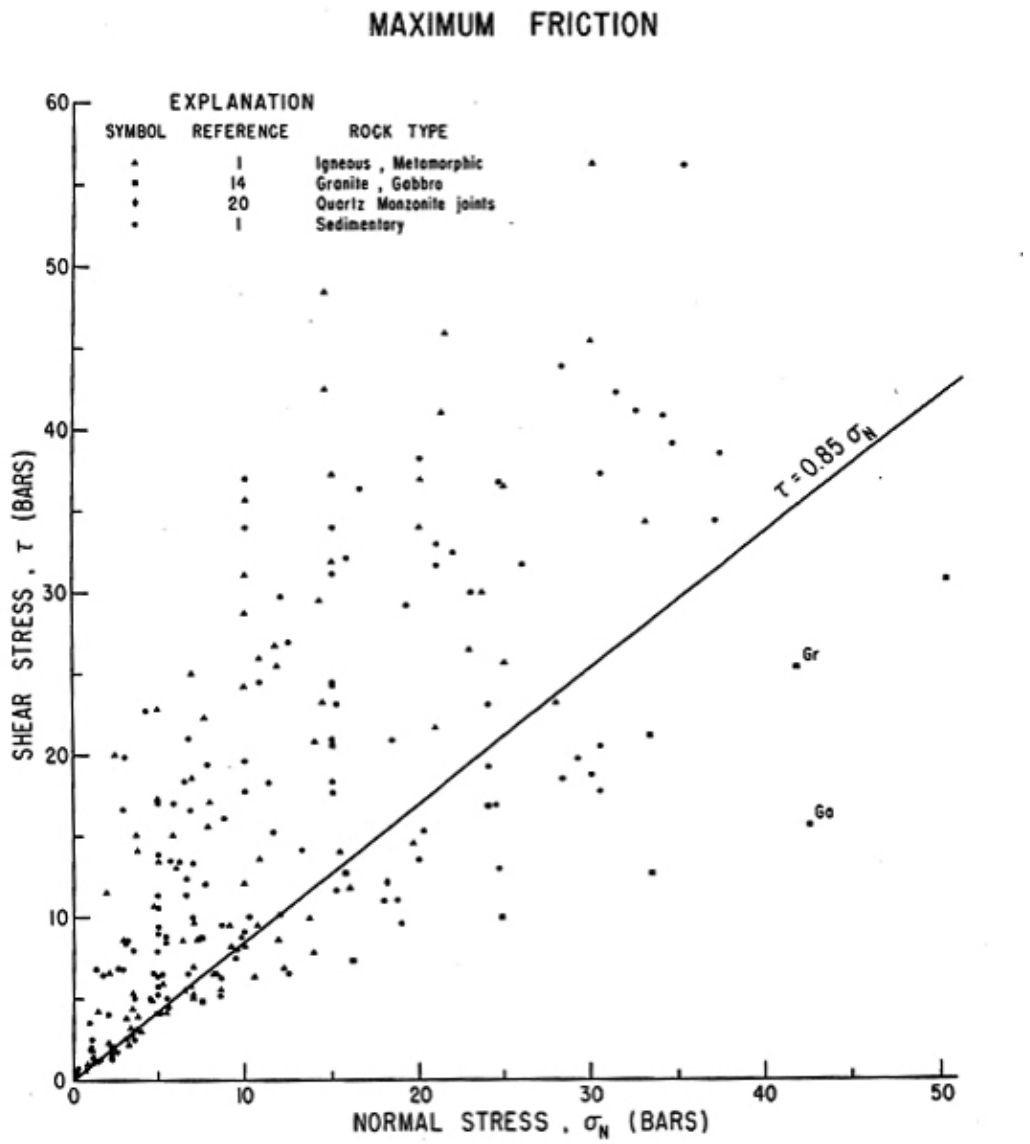

fig. 3 (Byerlee, 1978)

Initial Friction
0 - 100 MPa
(0 - 1000 bar)

up to 4 km

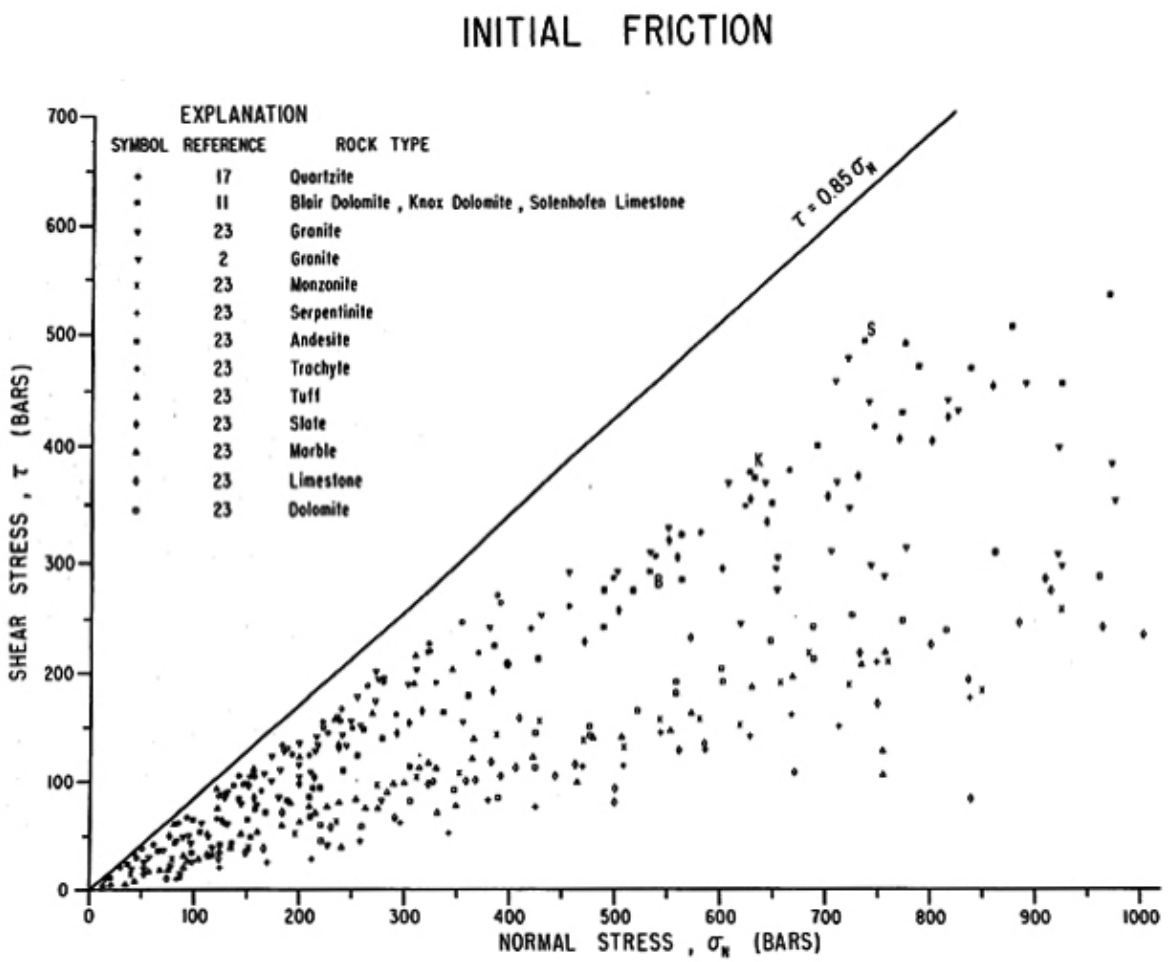

fig. 4 (Byerlee, 1978)

Maximum Friction
0 - 100 MPa
(0 - 1000 bar)

up to 4 km

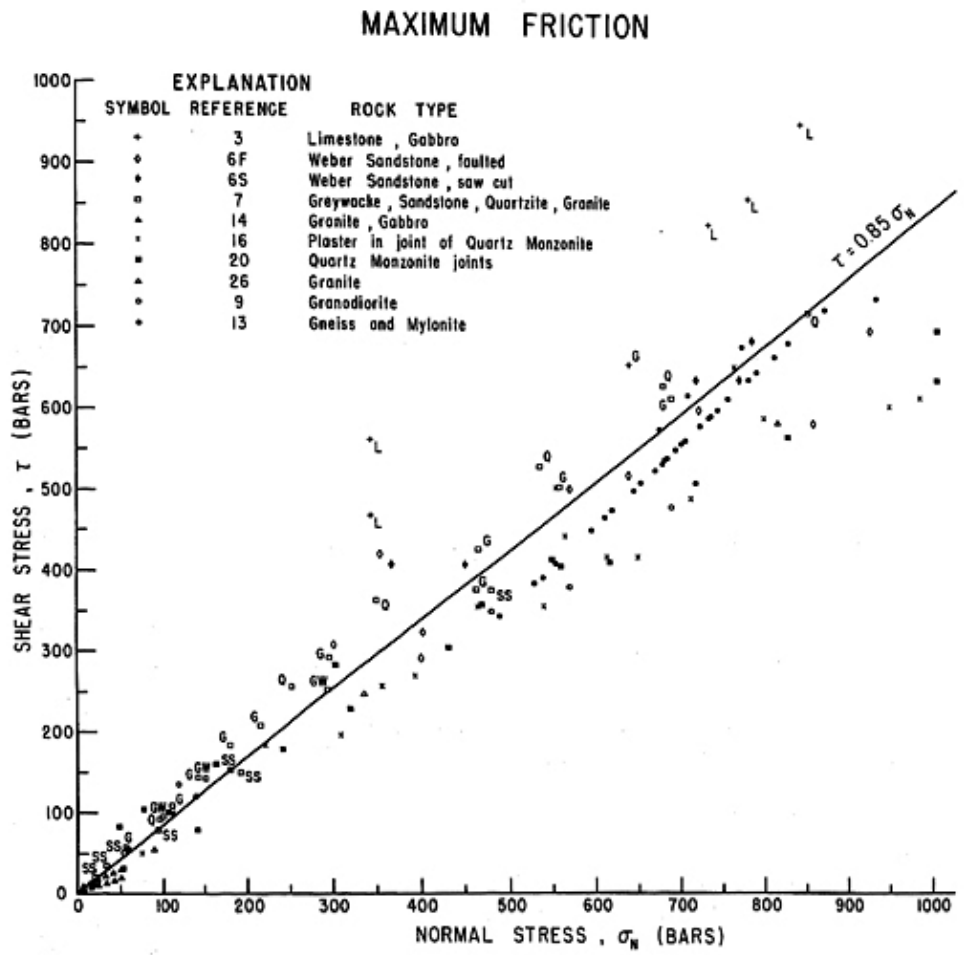

fig. 5 (Byerlee, 1978)

Initial Friction
0 - 2 GPa
(0 - 20 kb)

up to 80 km

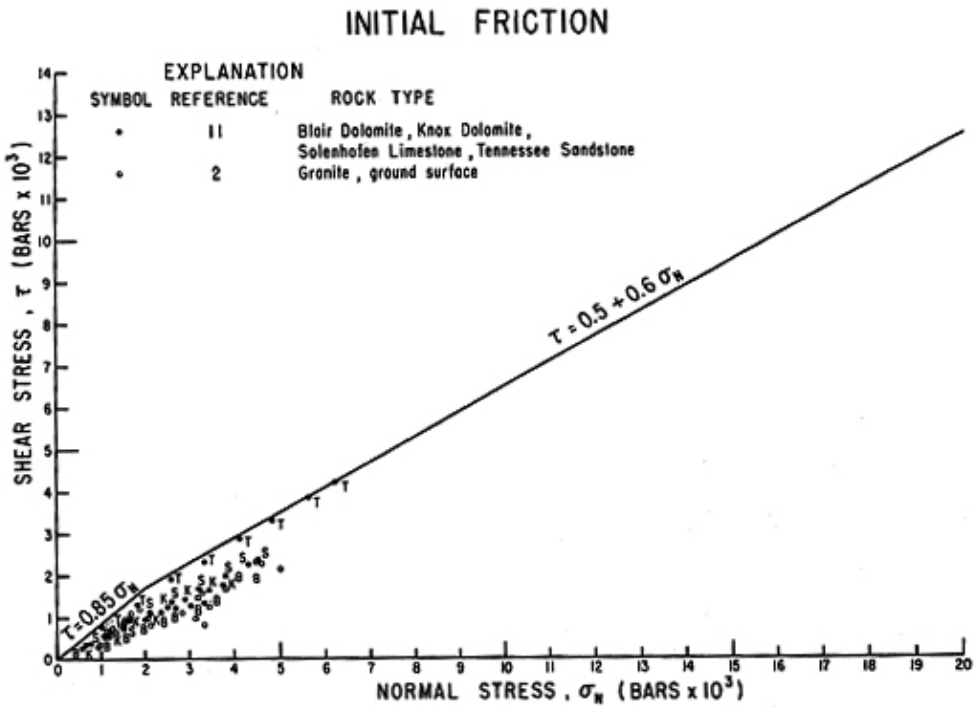

fig. 6 (Byerlee, 1978)

Friction
0 - 2 GPa
(0 - 20 kb)

up to 80 km

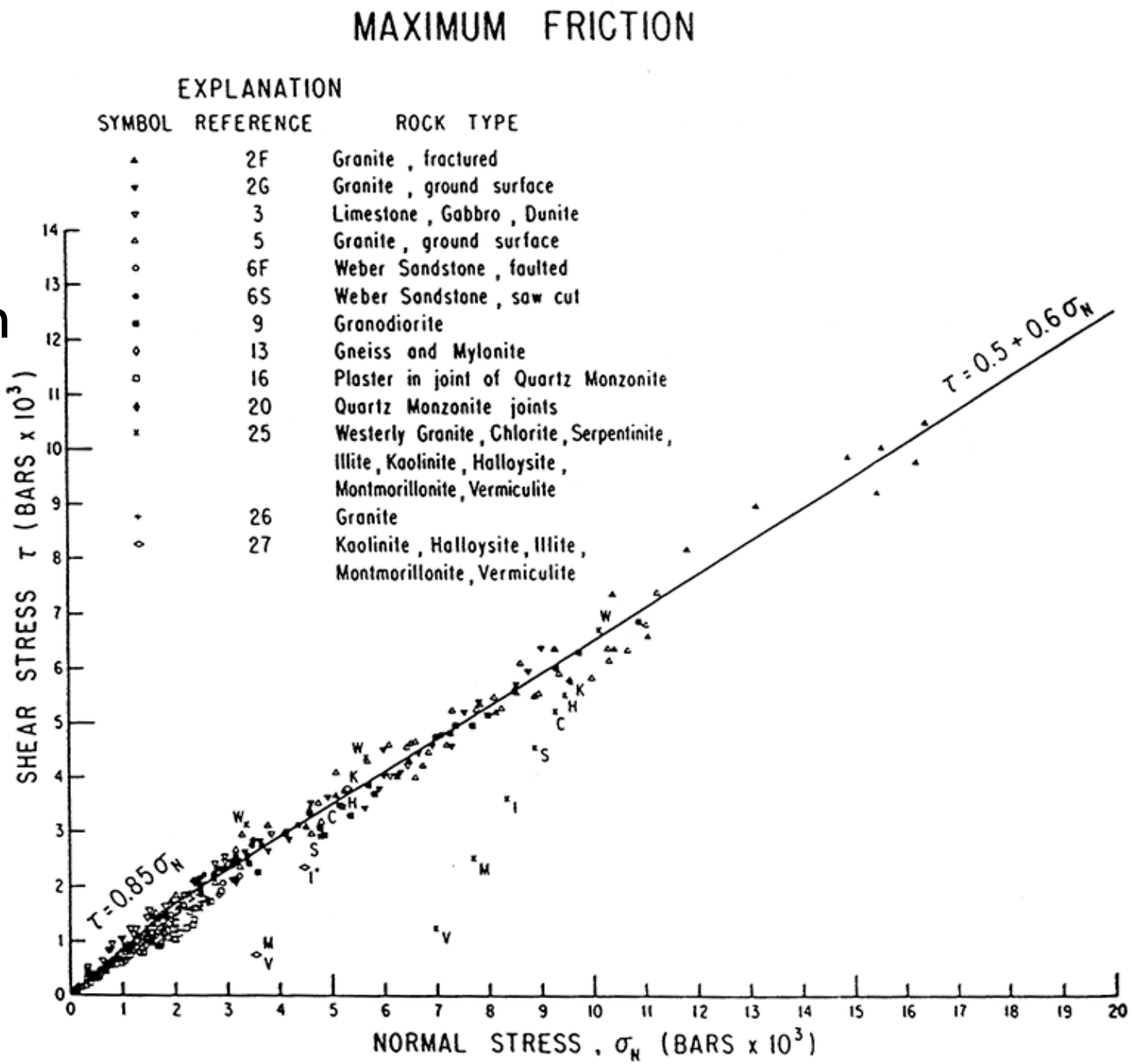

fig. 7 (Byerlee, 1978)

Depth profiles of stength

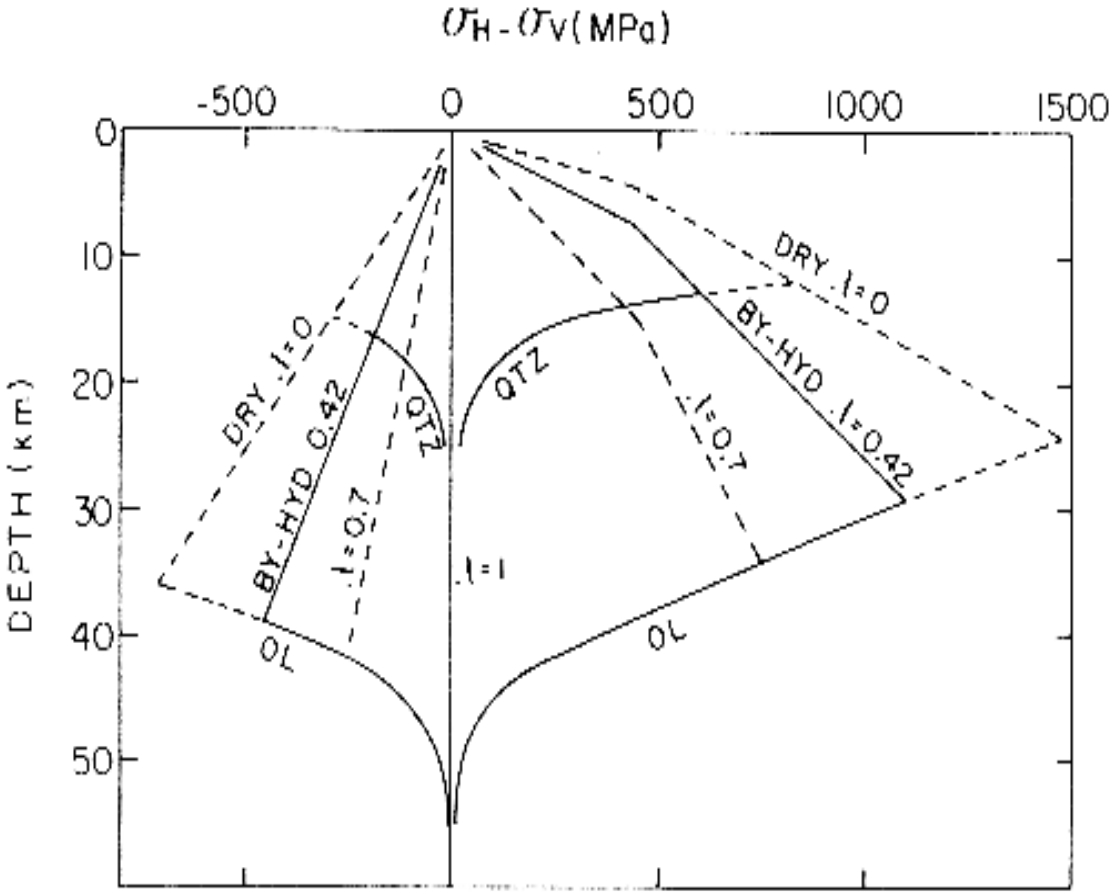

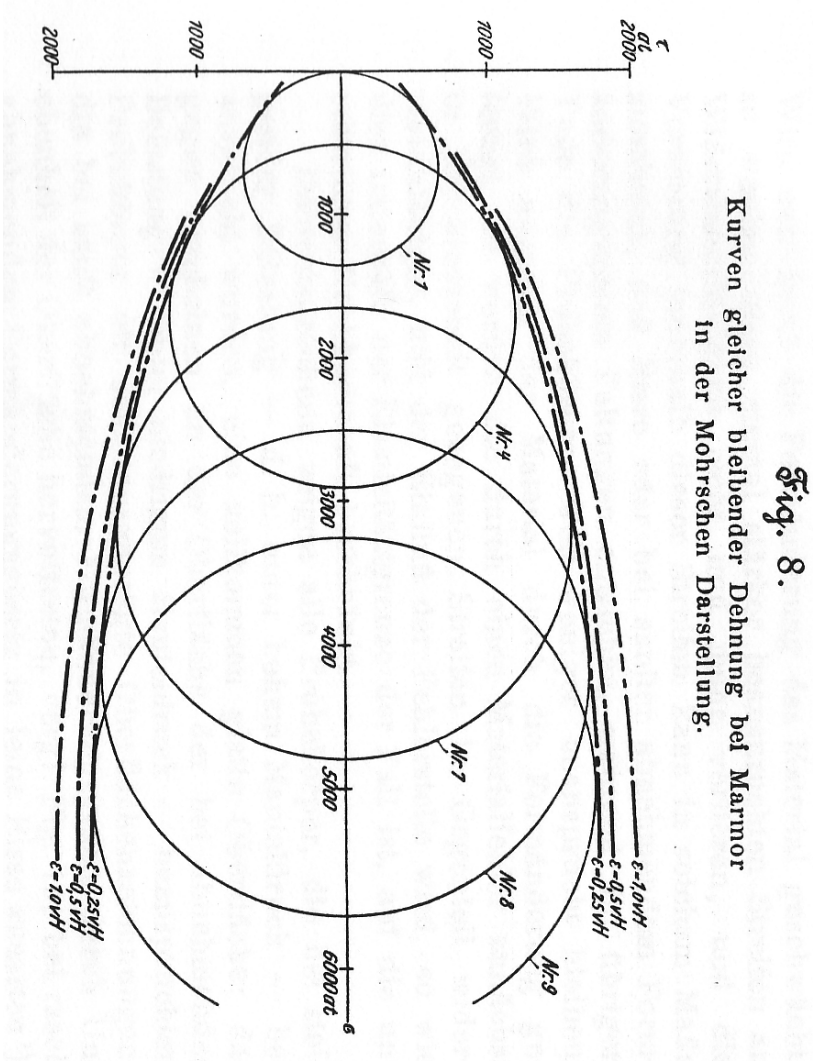

Fig. 8.
Kurven gleicher bleibender Dehnung bei Marmor in der Mohrschen Darstellung.

Fracture process

nature
macro

experiment
micro

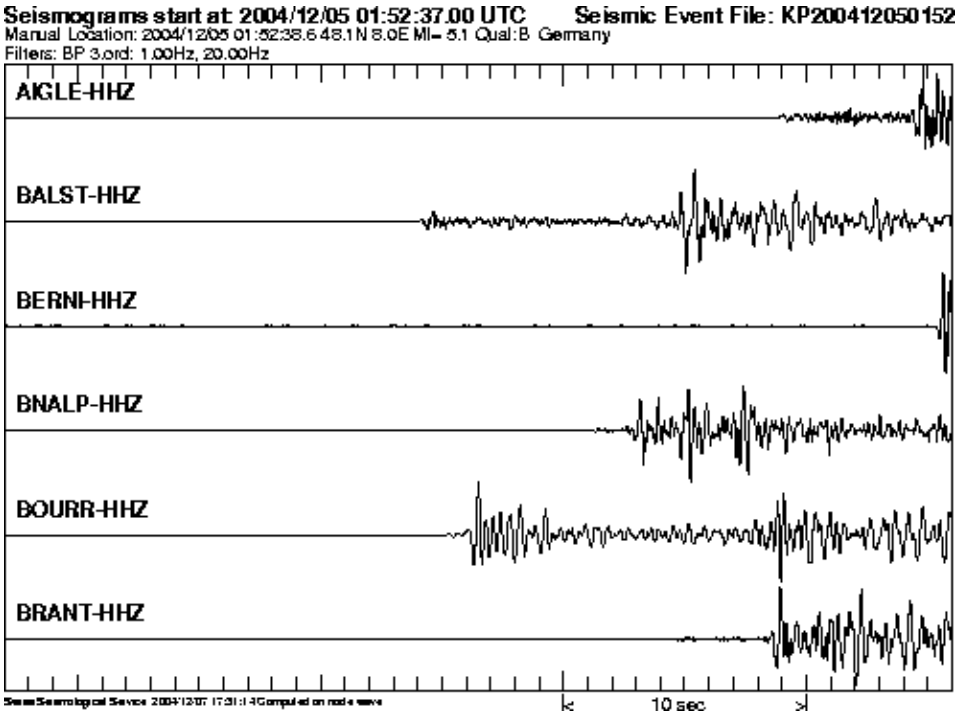

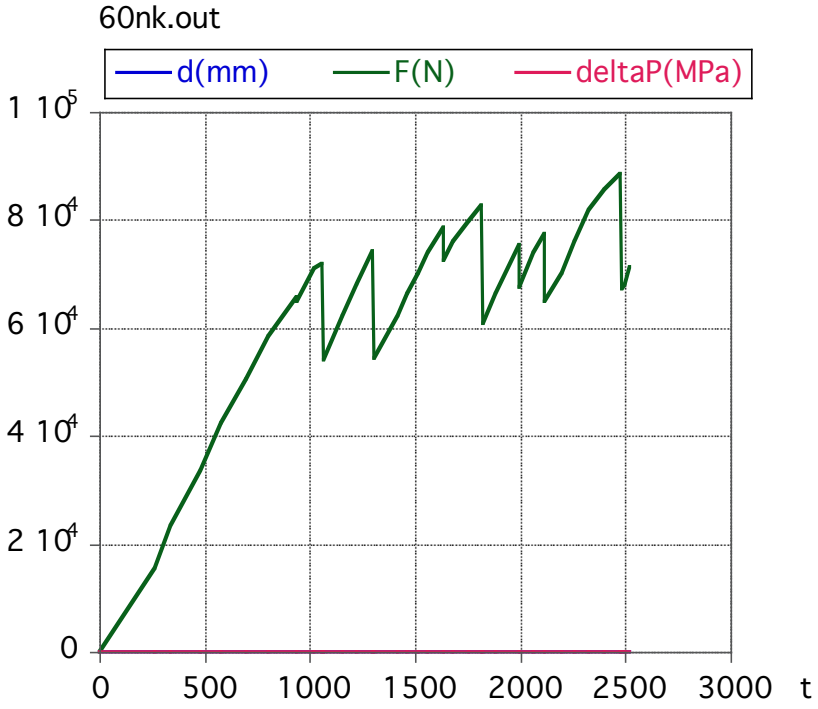

Fracture process in experiments

in stress strain curve:

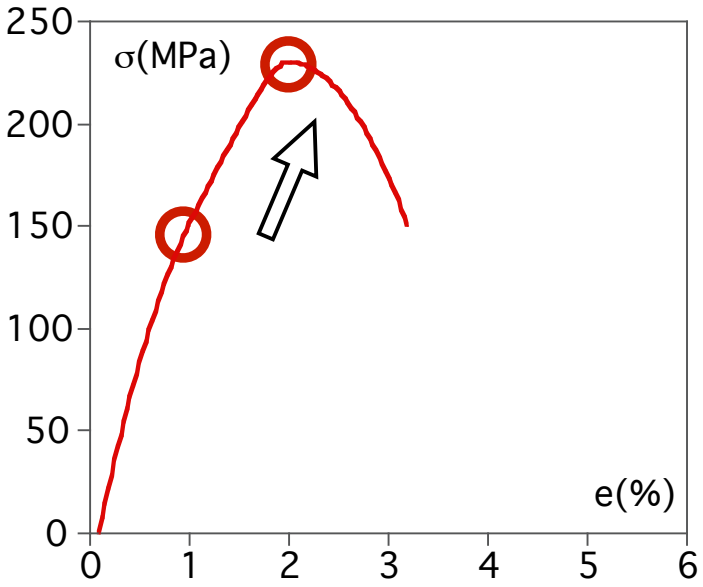

in Mohr space:
(no strain, no time)

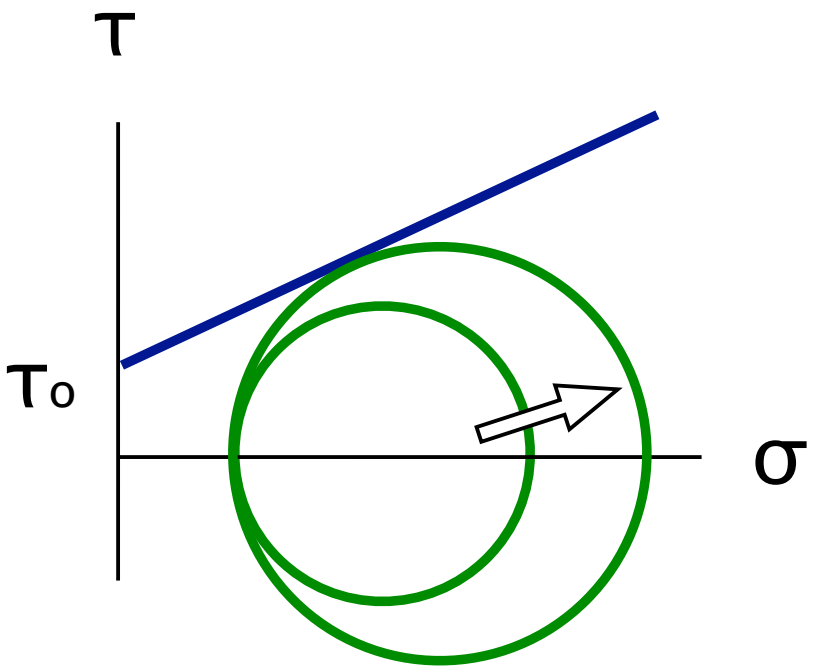

Fracture process in experiments

Mechanisms of brittle fracture

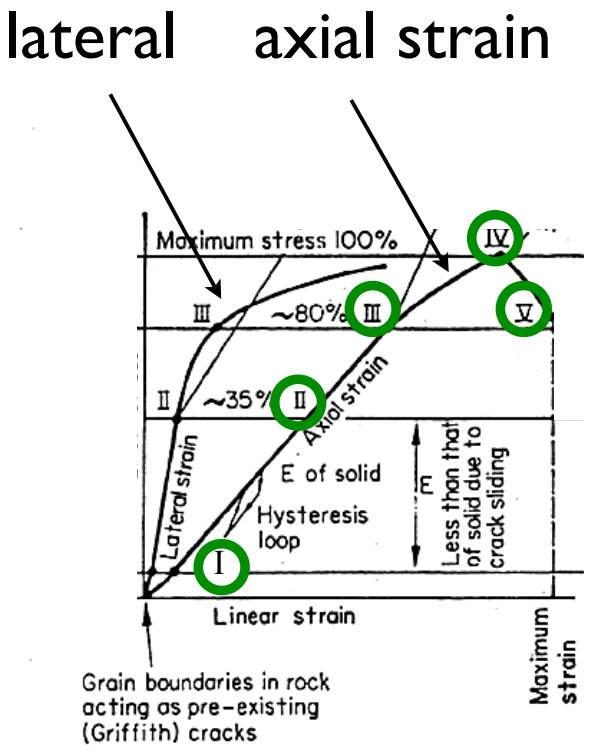

points on curve:

I. crack closure

II. fracture initiation

III. critical energy release

IV. strength failure

V. rupture

Fracture process in experiments

Mechanisms of brittle fracture

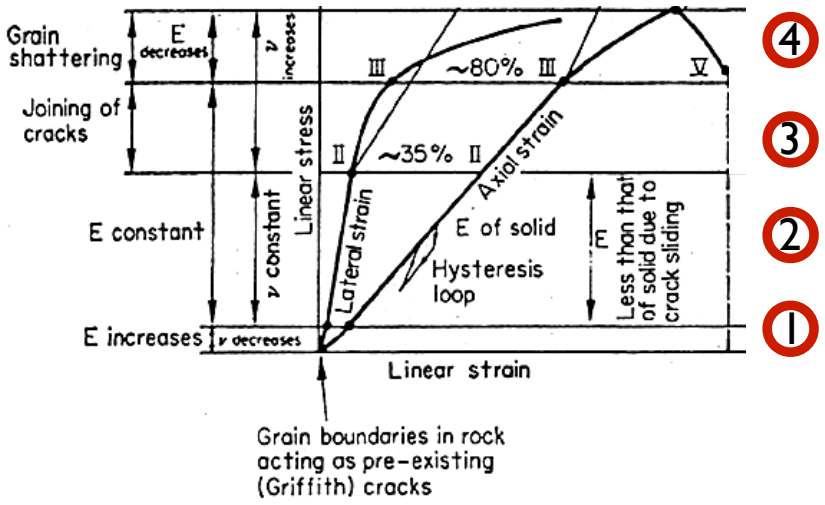

segments of curve (stages):

1. closing of cracks
2. linear elastic deformation
3. stable fracture propagation
4. unstable fract. propagation

Mechanisms of brittle fracture

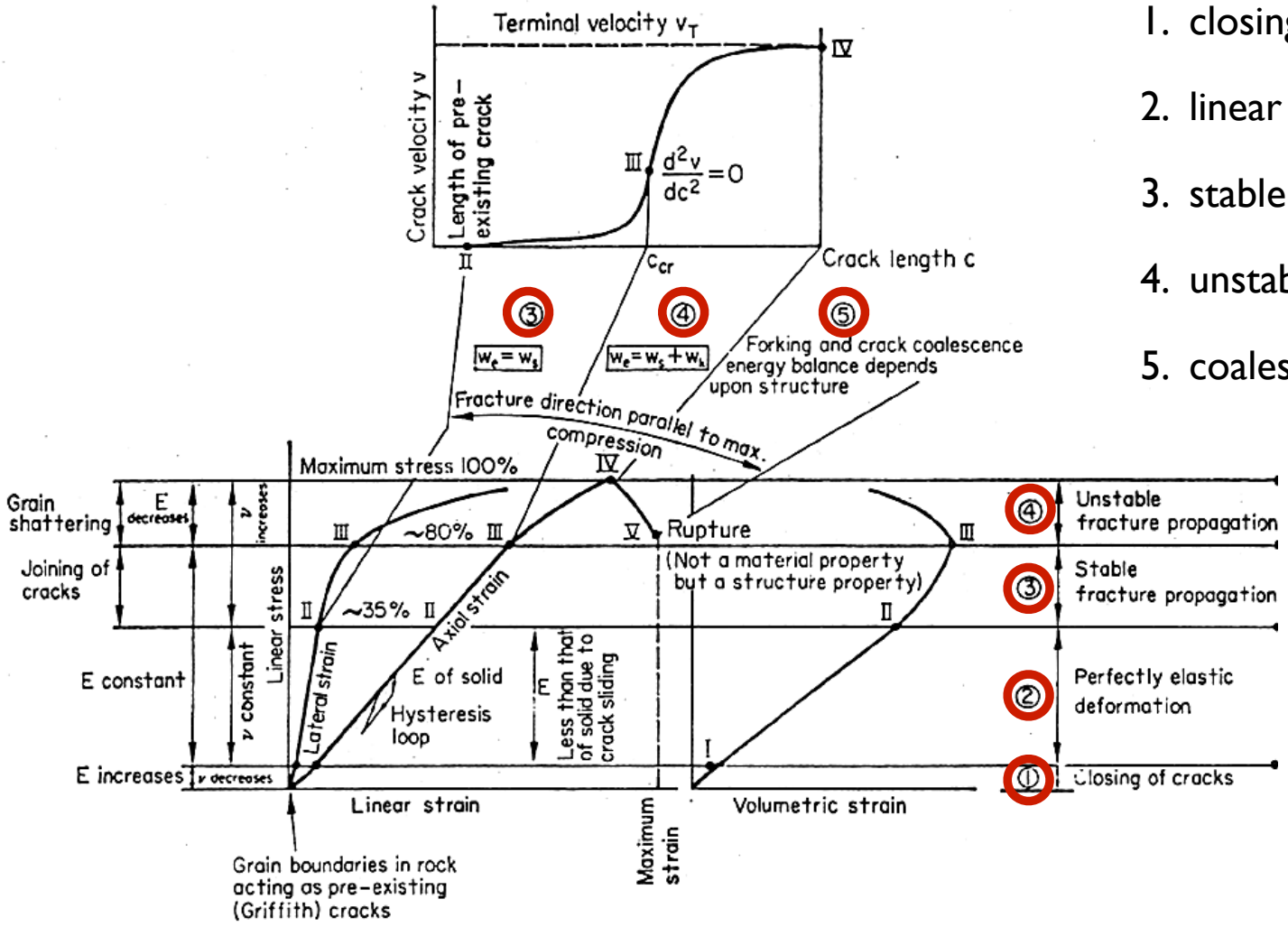

1. closing of cracks
2. linear elastic deformation
3. stable fracture propagation
4. unstable fract. propagation
5. coalescence of cracks

Precursors

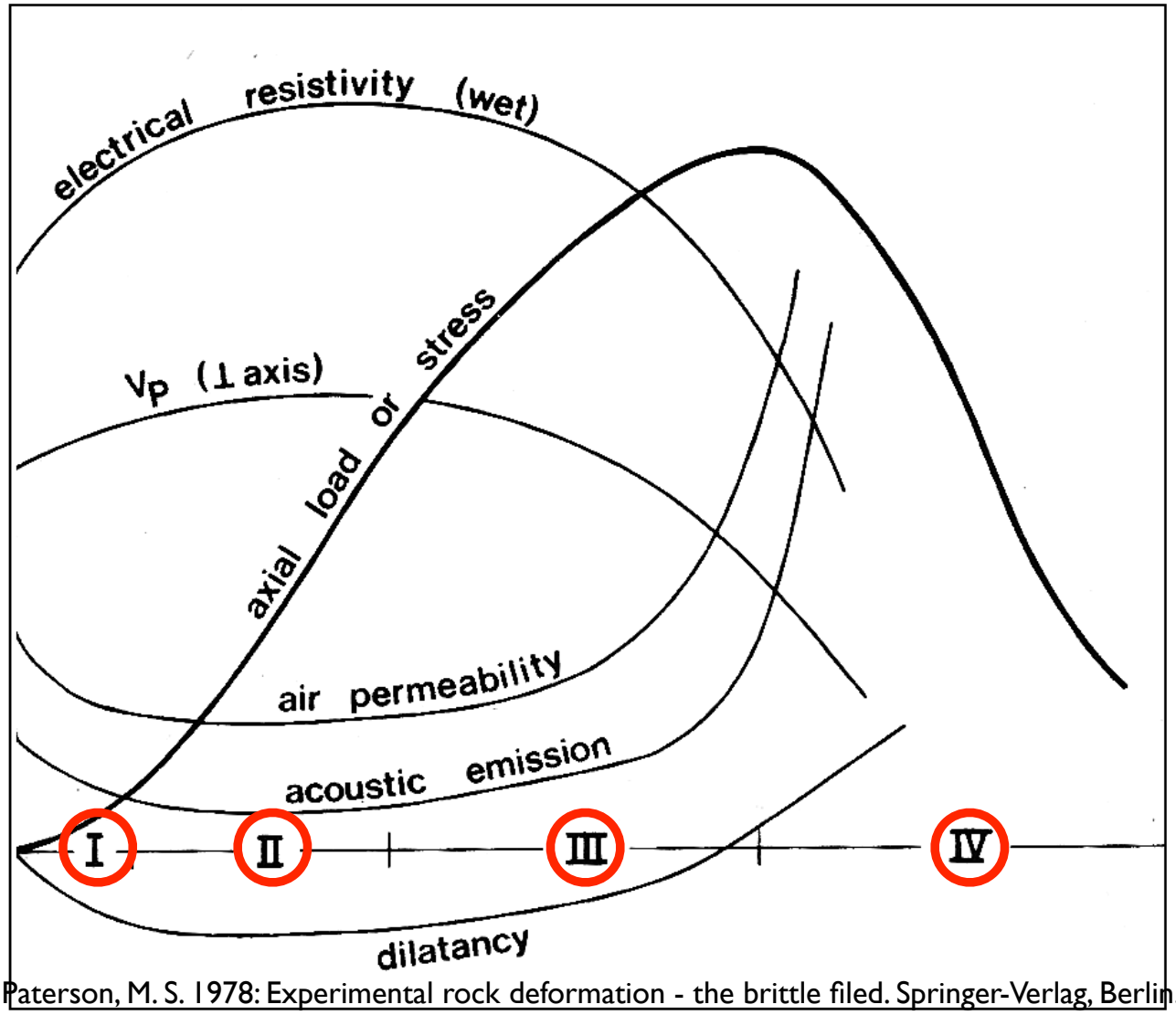

stages

Paterson, M. S. 1978: Experimental rock deformation - the brittle filed. Springer-Verlag, Berlin.

Accoustic emissions

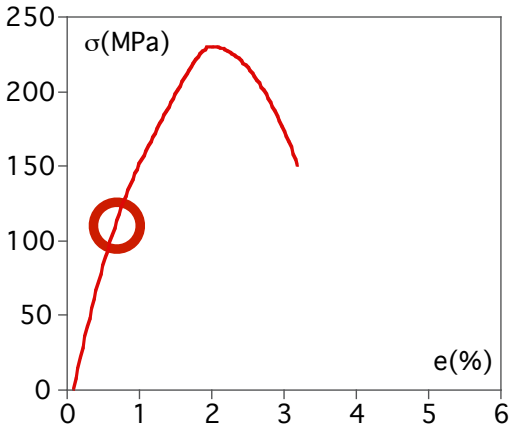

Increase of rate of accoustic emissions in Westerly granite(pc=400 MPa)

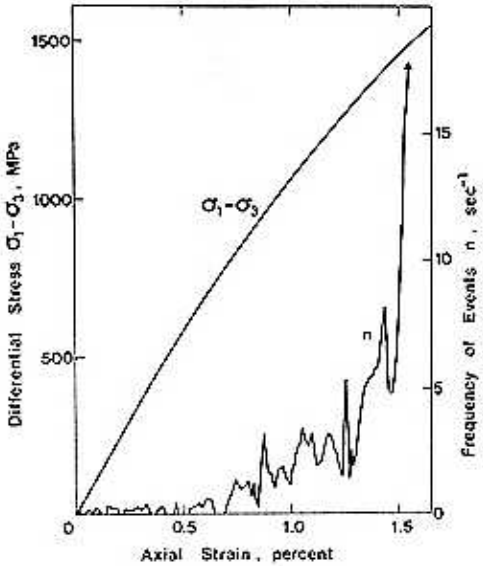

Paterson, M. S. 1978: Experimental rock deformation - the brittle filed. Springer-Verlag, Berlin.

Location of events:

static cracking
(below 95%
random process

dynamic cracking
above 95% fracture stress)
clustering along fault

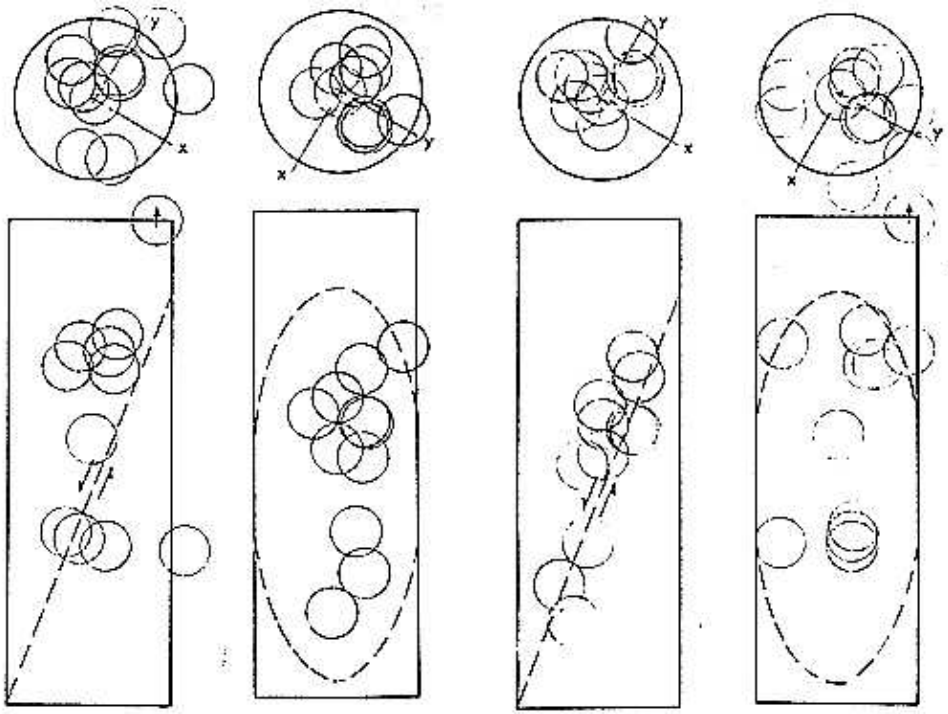

Scholz, C. H. 1968: Experimental study of the fracturing process in brittle rock. J. geophys. Res. 73, 1447-1449.
(Figure 4 and 5 interchanged)

Pre - failure conditions

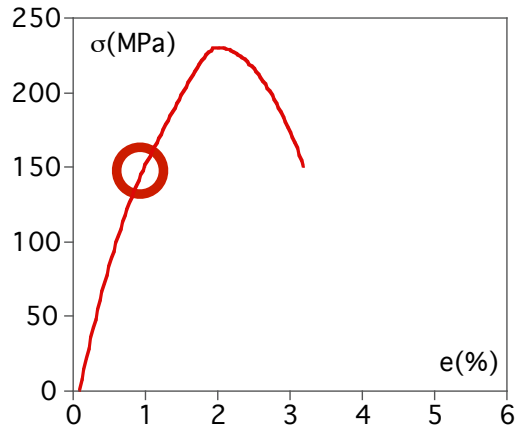

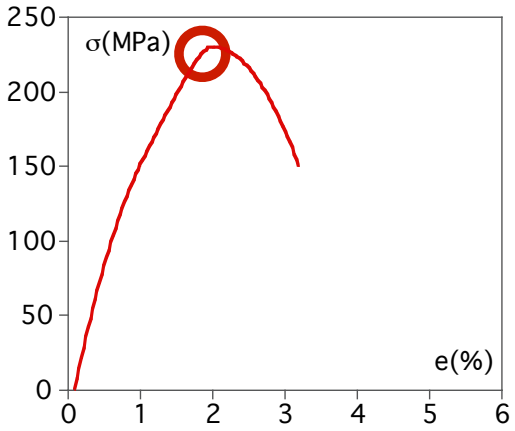

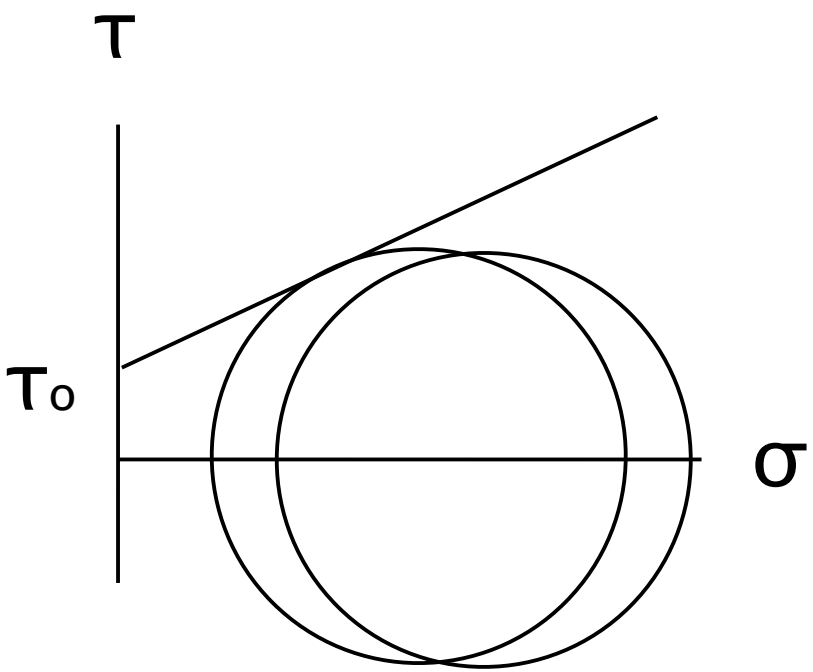

dilatancy

pore pressure

Microfracturing - dilatancy

Microfracturing of sandstone 50 ·127 mm cylinders

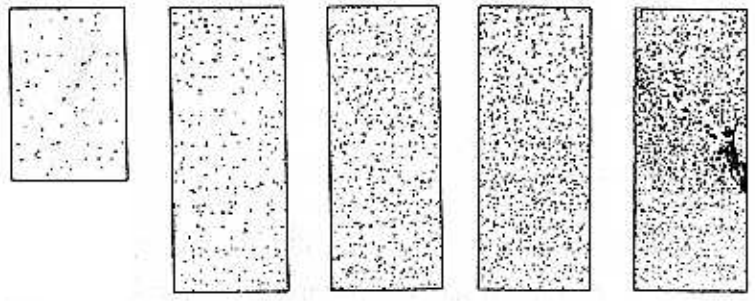

0% 25% 50% 83% 100%
of maximum stress (vertical, pc=0)

Sangha, C.M., Talbot, C.J., Dhir, R.K., 1974. Microfracturing of a sandstone in uniaxial compression. Int. J. Rock Mech. Min. Sci., Abstr. Vol. 11, 107-113

Microfracturing of gabbro 50 ·100mm cylinders

0% 62% 82% 90% 100% $\sigma_{ultimate}$

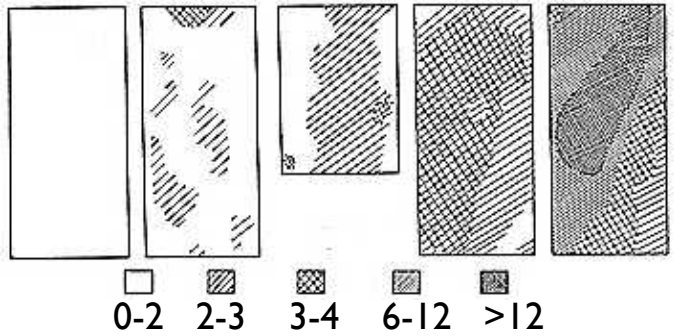

0-2 2-3 3-4 6-12 >12

Optical reflectivity ratio (= microcrack density)
w/r to average reflectivity (pc = 130 MPa

Chen Rong, Yao Xiao-Xin, Xie Hung-Sen, 1979. Studies of fracture of gabbro. Int. J. Rock Mech. Min. Sci., Abstr. Vol. 16, 187-193

Dilatancy of pyrophyllite blocks 30 ·30 ·33 mm

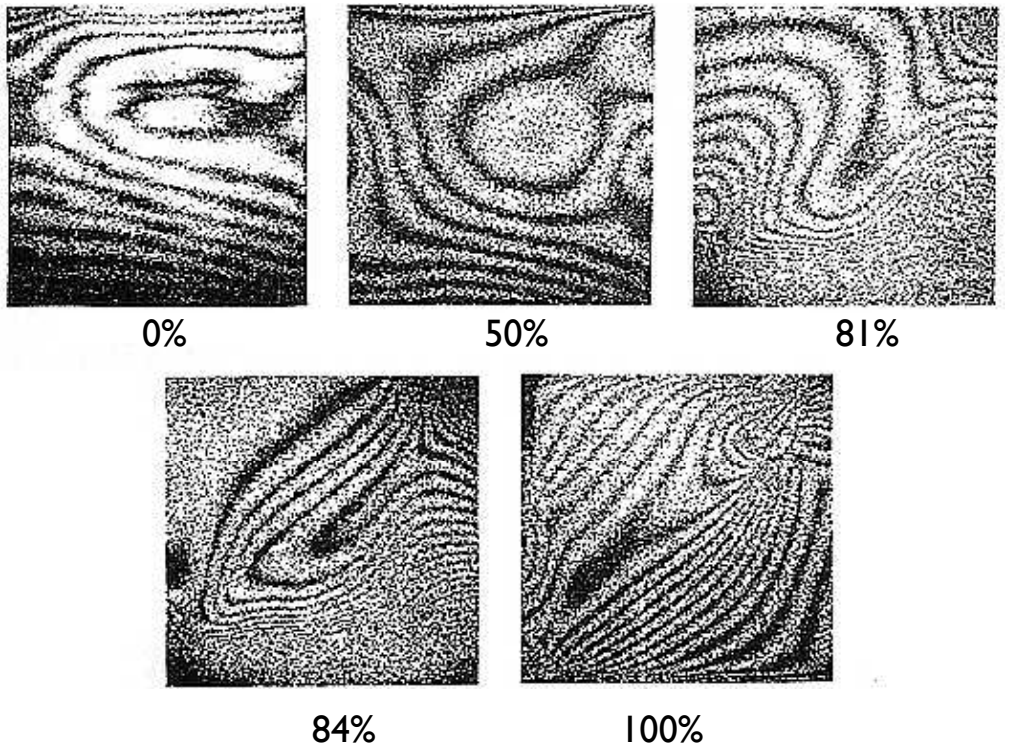

0% 50% 81%

84% 100%

Doubly exposed holograms; % of $\sigma_{ultimate}$ (vertical)

Sobolev G, Spetzler H., Salov, B., 1978.
Precursors to failure in rocks while undergoing anelastic deformation.
JGR 83, 1775-1784

Dilatancy

Axial loading, pc=100MPa
Westerley granite

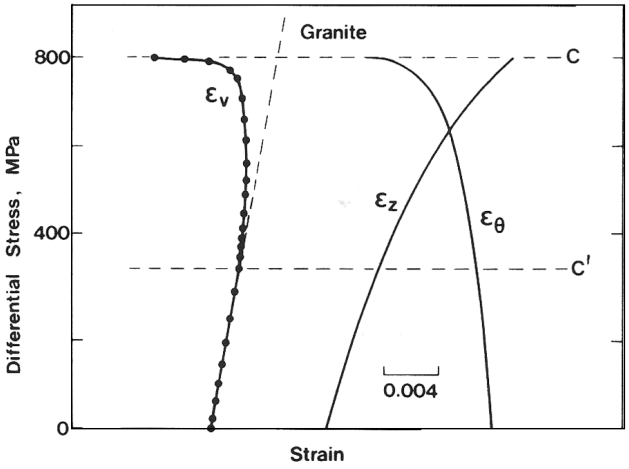

macroscopic failure stress

stress at onset of dilatancy

differential stress vs strain

εv	volumteric strain
εz	axial strain
εθ	circumferential strain

Paterson, M. S. 1978: Experimental rock deformation - the brittle filed. Springer-Verlag, Berlin.

at fault tip: rotation kinkband model

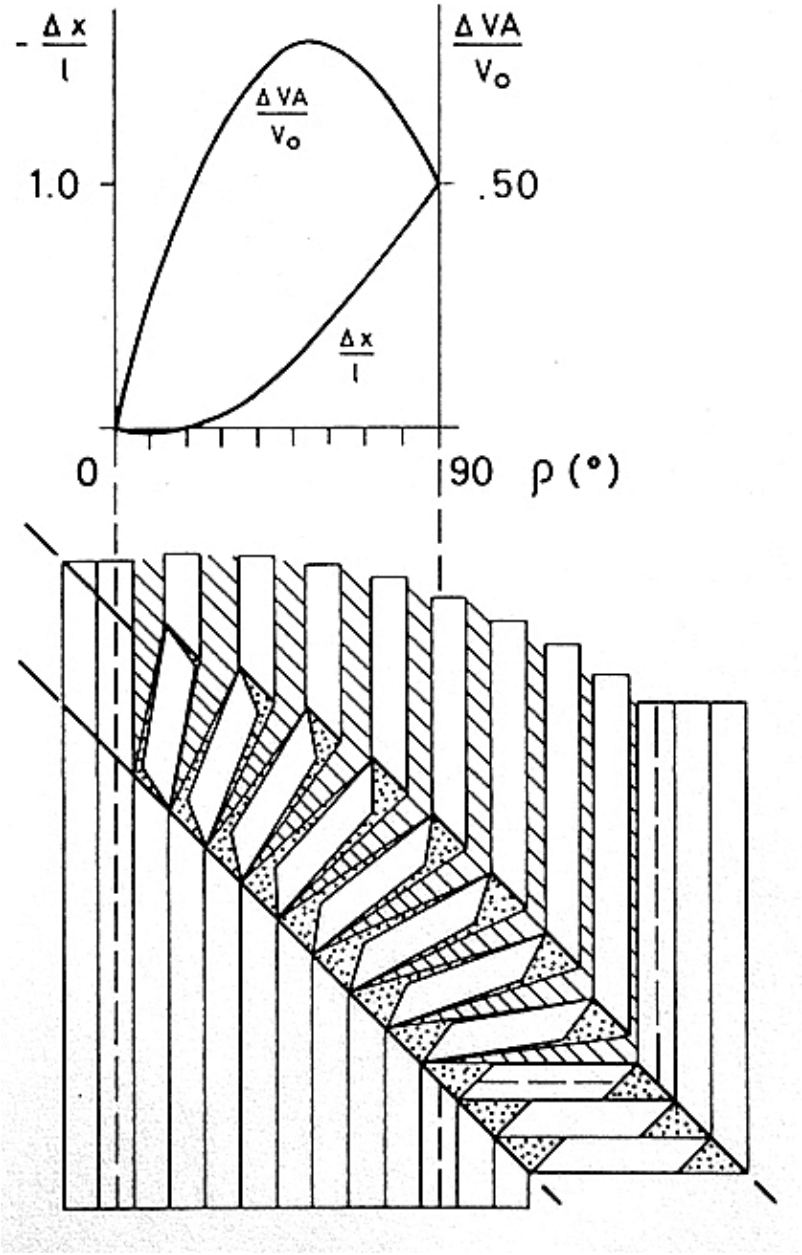

Fracture - Stress at failure

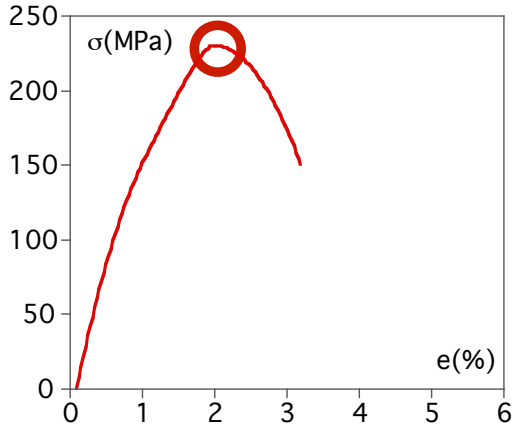

Factors influencing fracture strength

- mineral composition
- porosity
- density
- microstructure
- state of alteration, weathering
- deformation history
- microcrack distribution

General failure criterion:

$$\Delta\sigma = f(p_c, p_p, T, \dot{\varepsilon}/\dot{Y}, \ldots)$$

7

Fracture process - failure criteria for fracture

Deformationsprozesse in der Erde (7) (6b)

Fracture process - Failure criterion

nature ⟷ experiment

theory

macro

homogeneity

micro

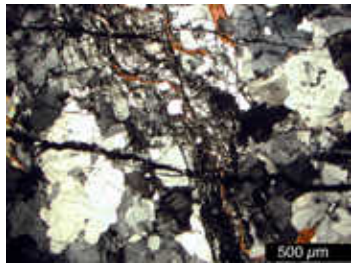

Deformationsprozesse in der Erde (7)

Fracture process

nature
macro

experiment
micro

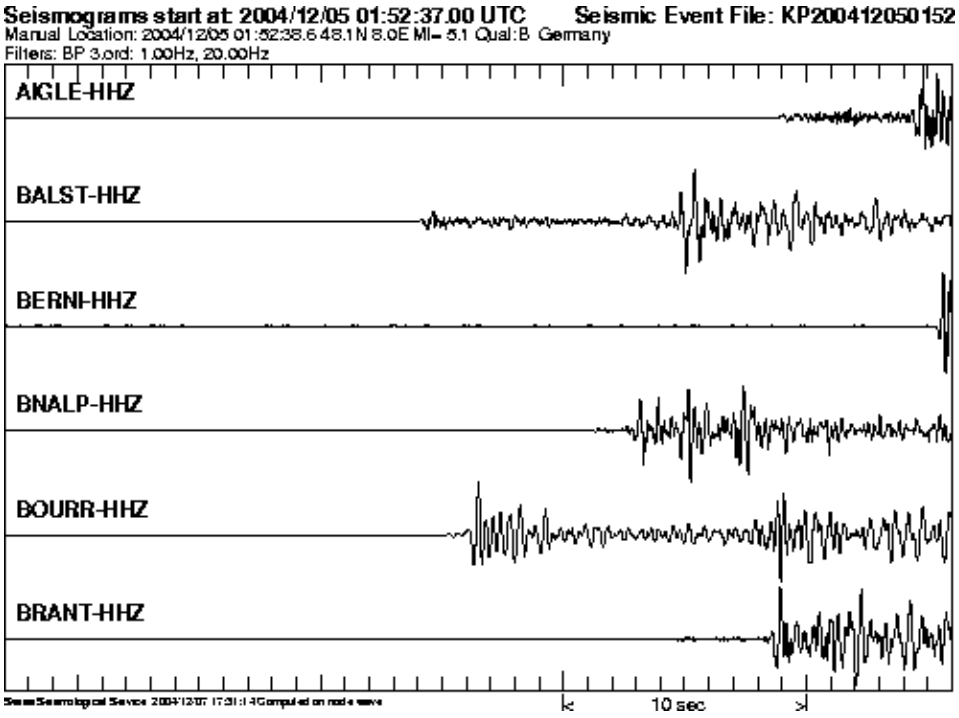

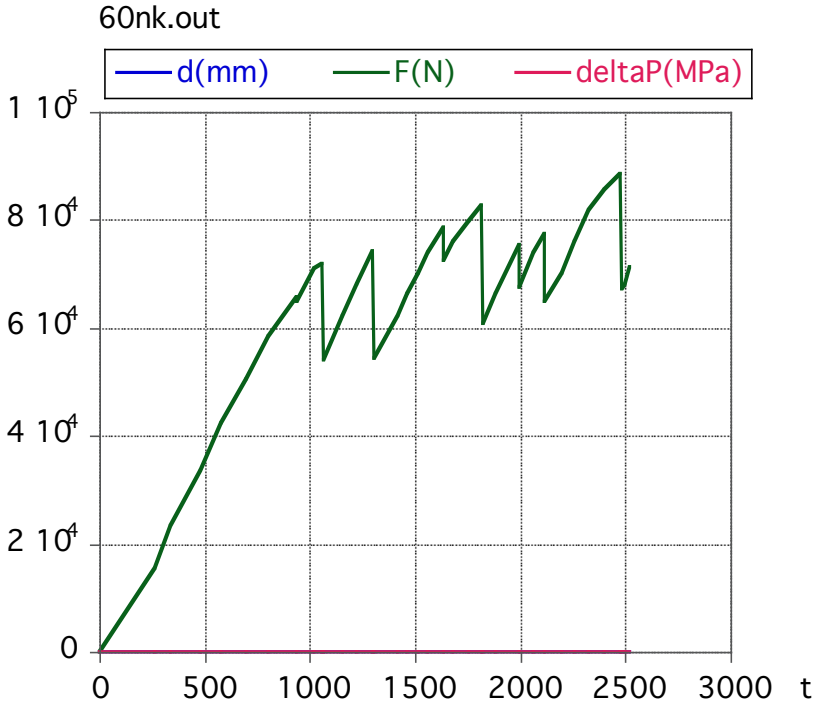

Fracture process in experiments

in stress strain curve:

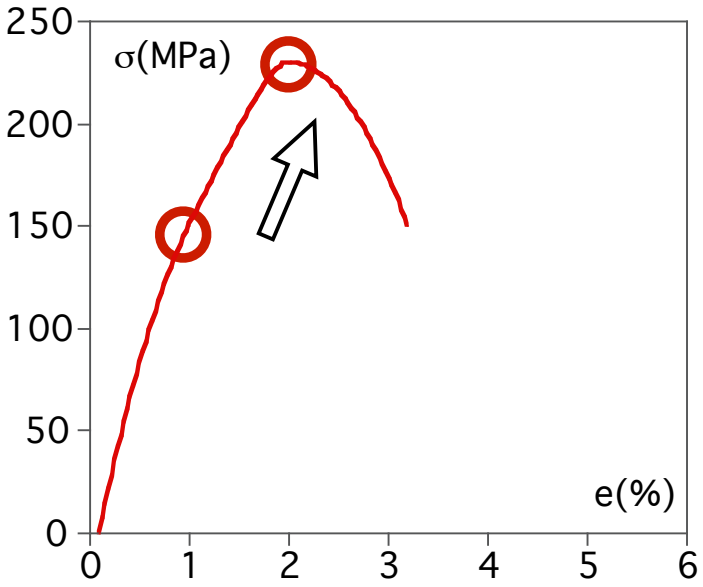

in Mohr space:
(no strain, no time)

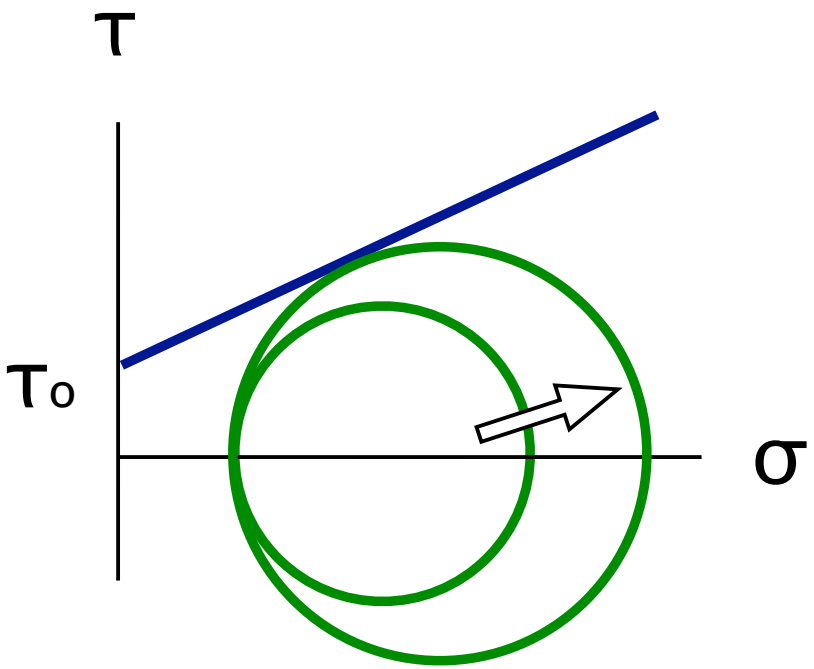

Fracture process in experiments

Mechanisms of brittle fracture

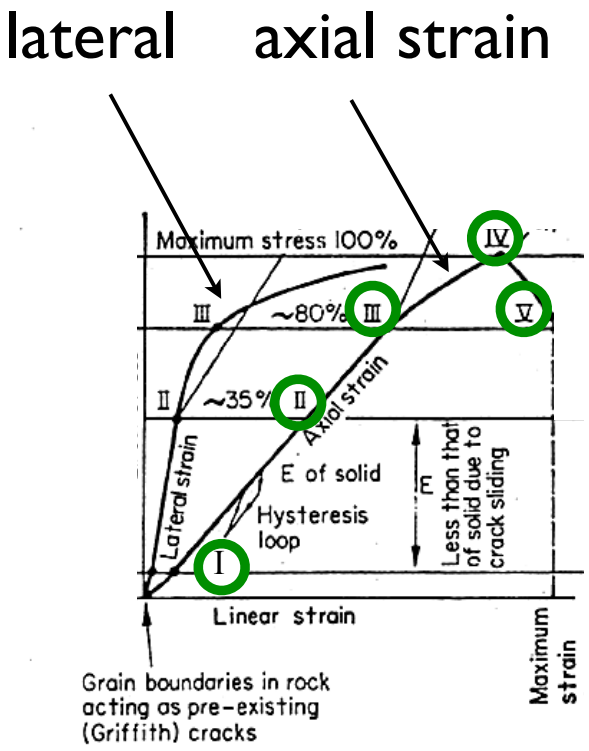

points on curve:

I. crack closure

II. fracture initiation

III. critical energy release

IV. strength failure

V. rupture

Fracture process in experiments

Mechanisms of brittle fracture

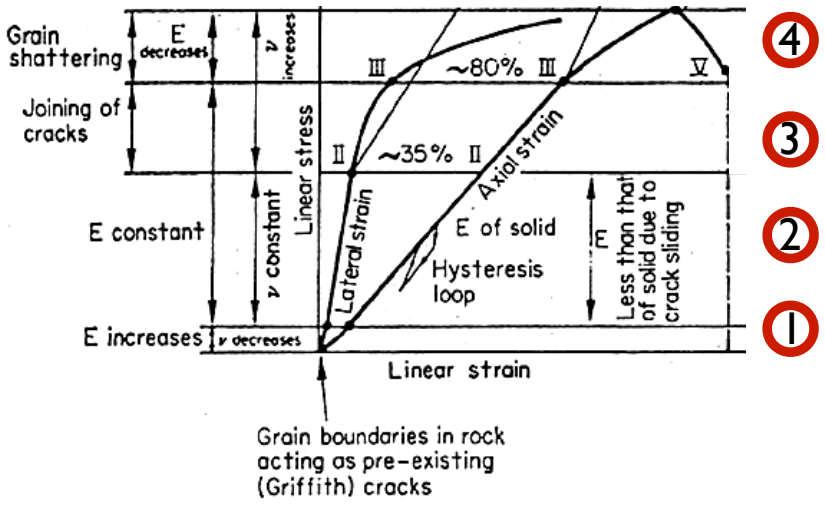

segments of curve (stages):

1. closing of cracks
2. linear elastic deformation
3. stable fracture propagation
4. unstable fract. propagation

Mechanisms of brittle fracture

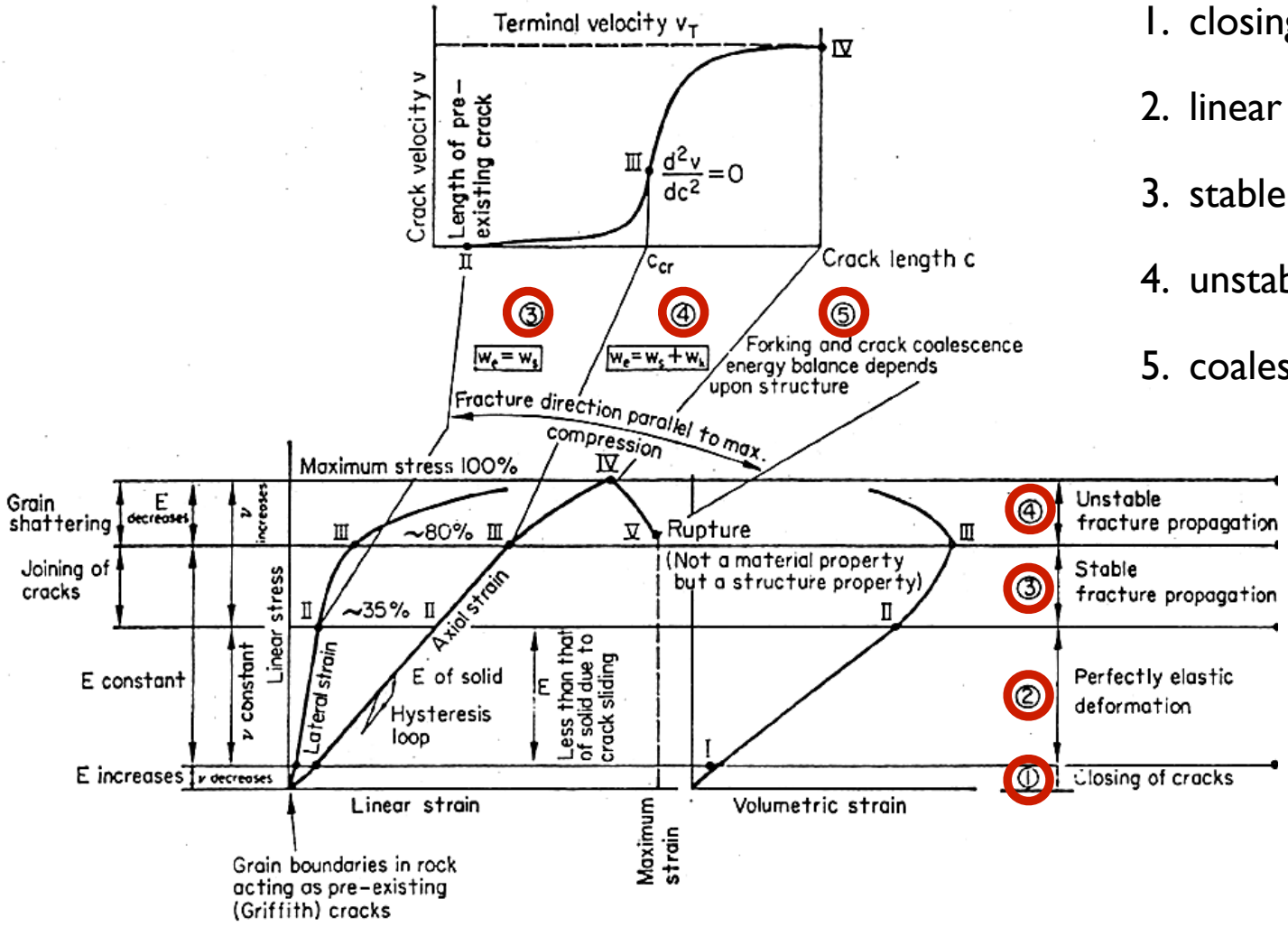

1. closing of cracks
2. linear elastic deformation
3. stable fracture propagation
4. unstable fract. propagation
5. coalescence of cracks

Precursors

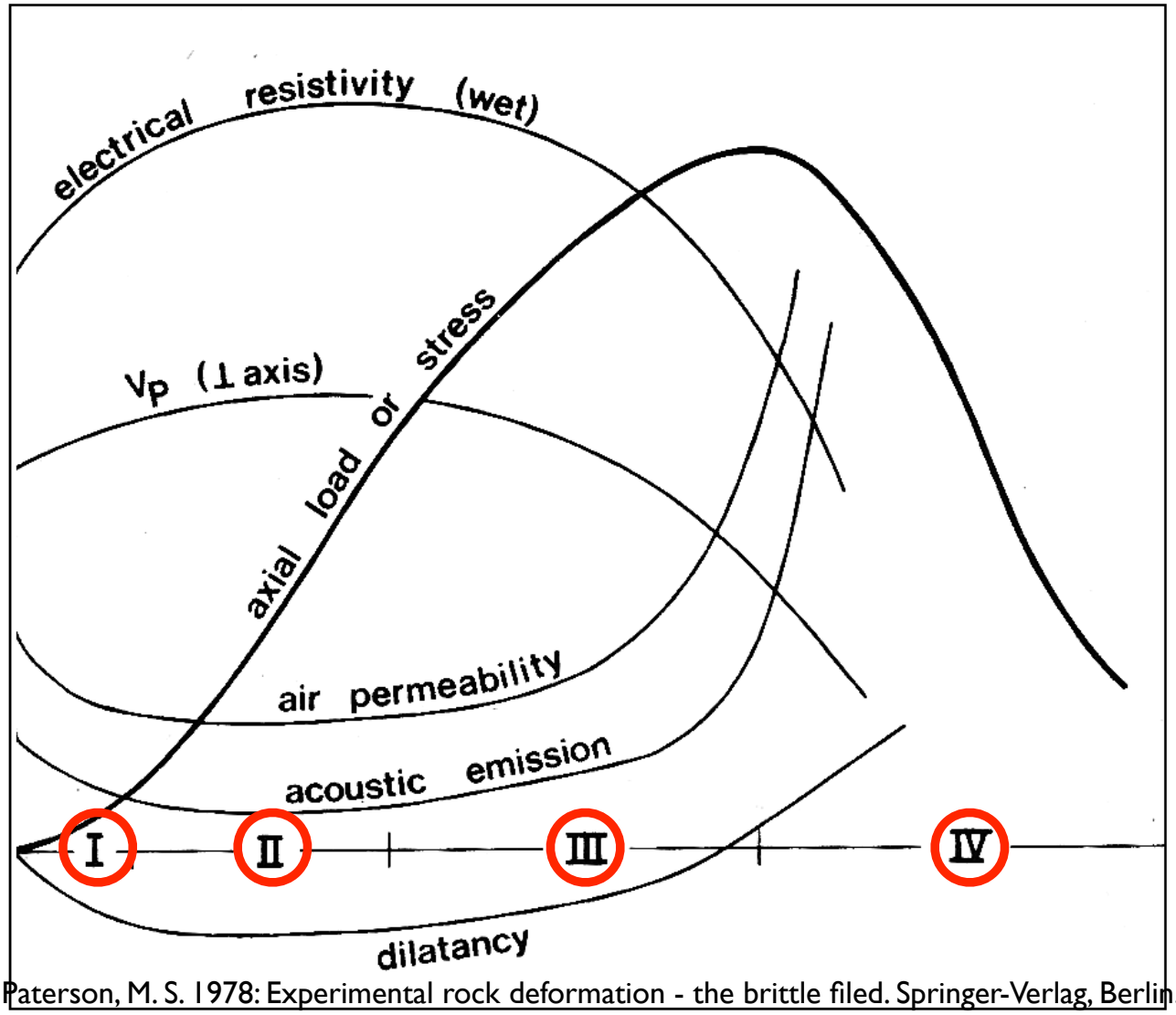

stages

Paterson, M. S. 1978: Experimental rock deformation - the brittle filed. Springer-Verlag, Berlin.

Accoustic emissions

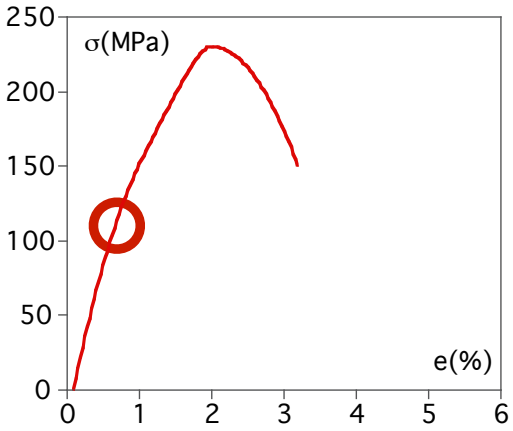

Increase of rate of accoustic emissions in Westerly granite(pc=400 MPa)

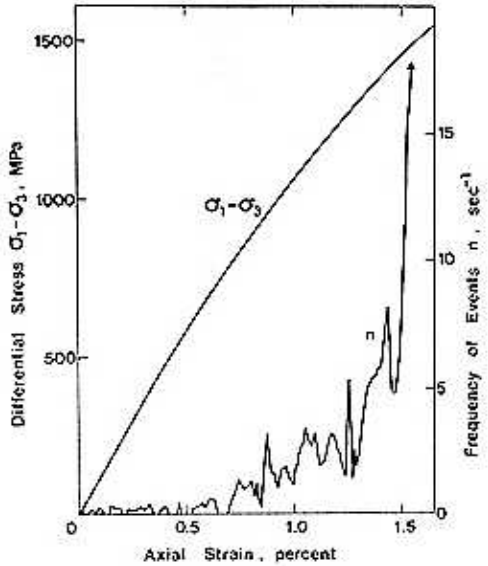

Paterson, M. S. 1978: Experimental rock deformation - the brittle filed. Springer-Verlag, Berlin.

Location of events:

static cracking
(below 95%
random process

dynamic cracking
above 95% fracture stress)
clustering along fault

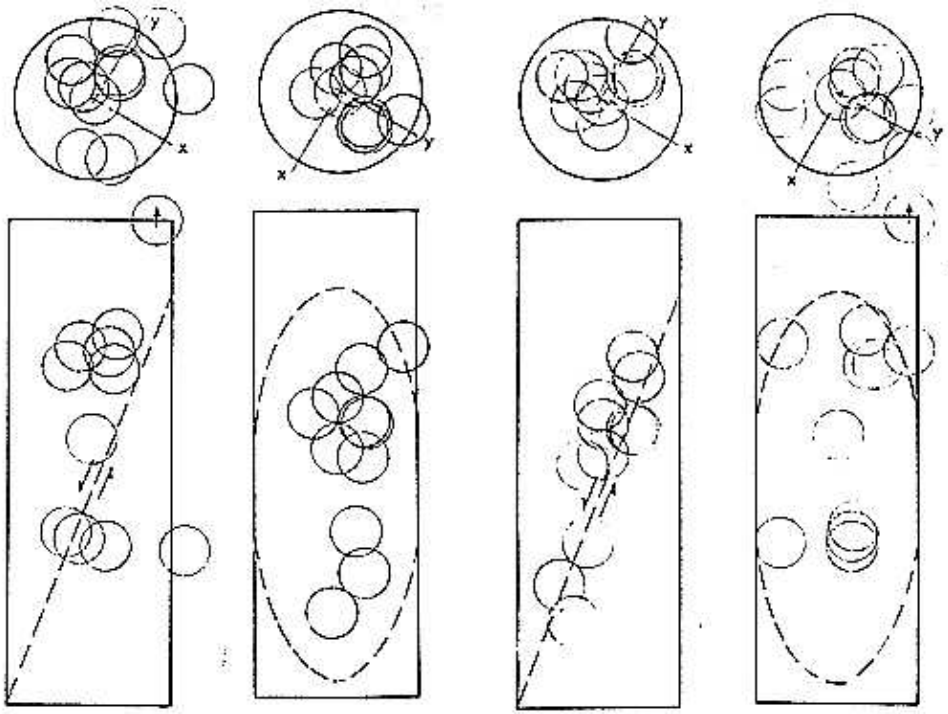

Scholz, C. H. 1968: Experimental study of the fracturing process in brittle rock. J. geophys. Res. 73, 1447-1449.
(Figure 4 and 5 interchanged)

Pre - failure conditions

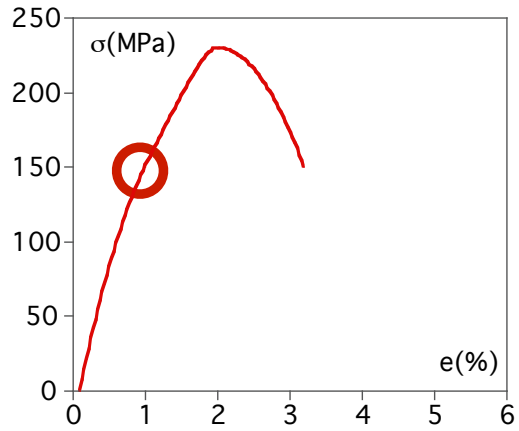

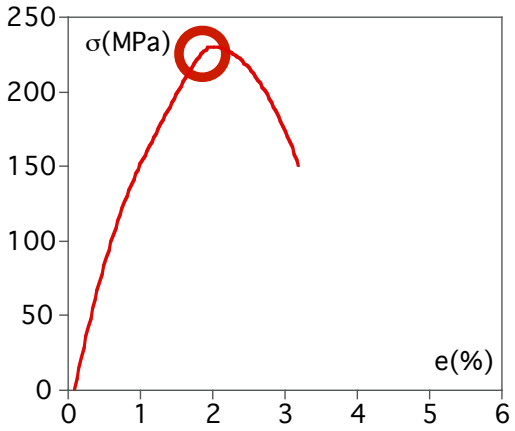

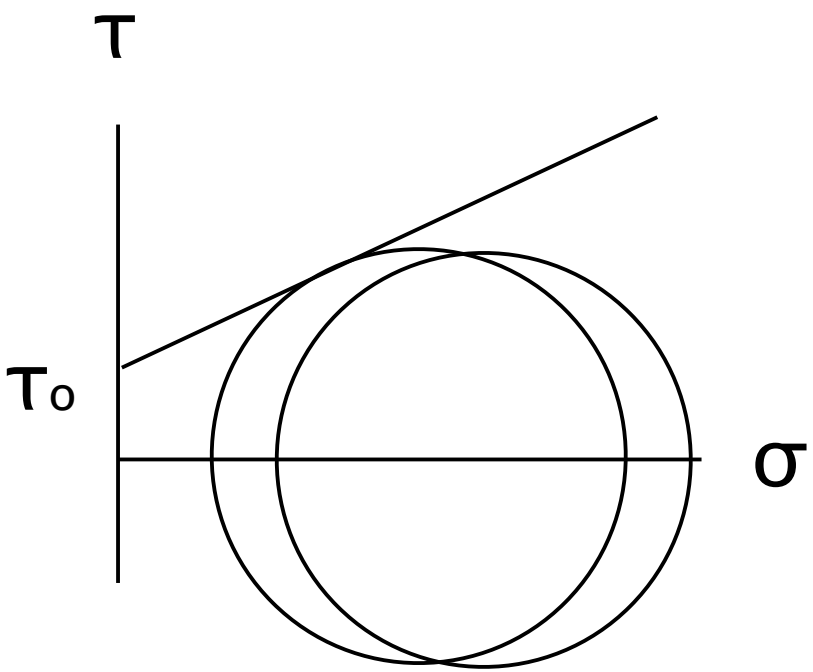

dilatancy

pore pressure

Microfracturing - dilatancy

Microfracturing of sandstone 50 ·127 mm cylinders

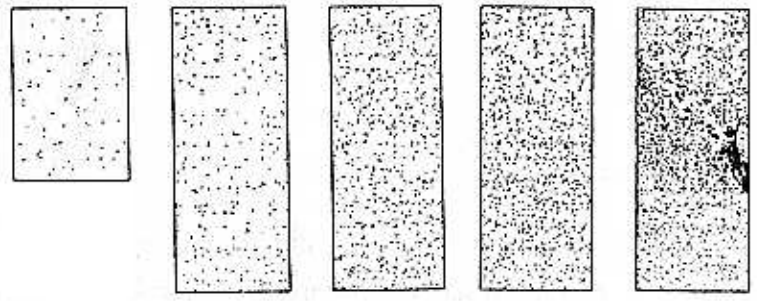

Sangha, C.M., Talbot, C.J., Dhir, R.K., 1974. Microfracturing of a sandstone in uniaxial compression. Int. J. Rock Mech. Min. Sci., Abstr. Vol. 11, 107-113

Microfracturing of gabbro 50 ·100mm cylinders

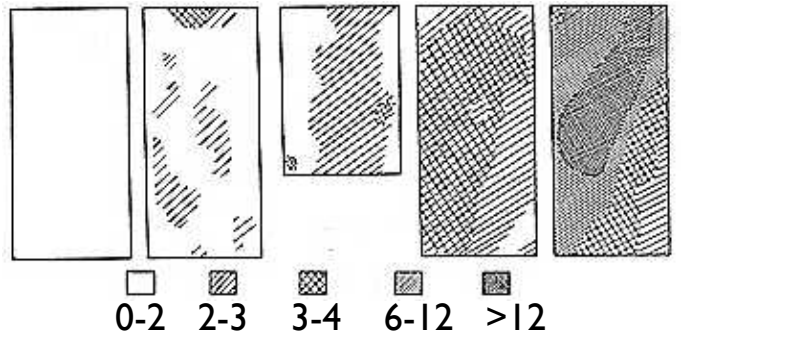

Optical reflectivity ratio (= microcrack density) w/r to average reflectivity (pc = 130 MPa

Chen Rong, Yao Xiao-Xin, Xie Hung-Sen, 1979. Studies of fracture of gabbro. Int. J. Rock Mech. Min. Sci., Abstr. Vol. 16, 187-193

Dilatancy of pyrophyllite blocks 30 ·30 ·33 mm

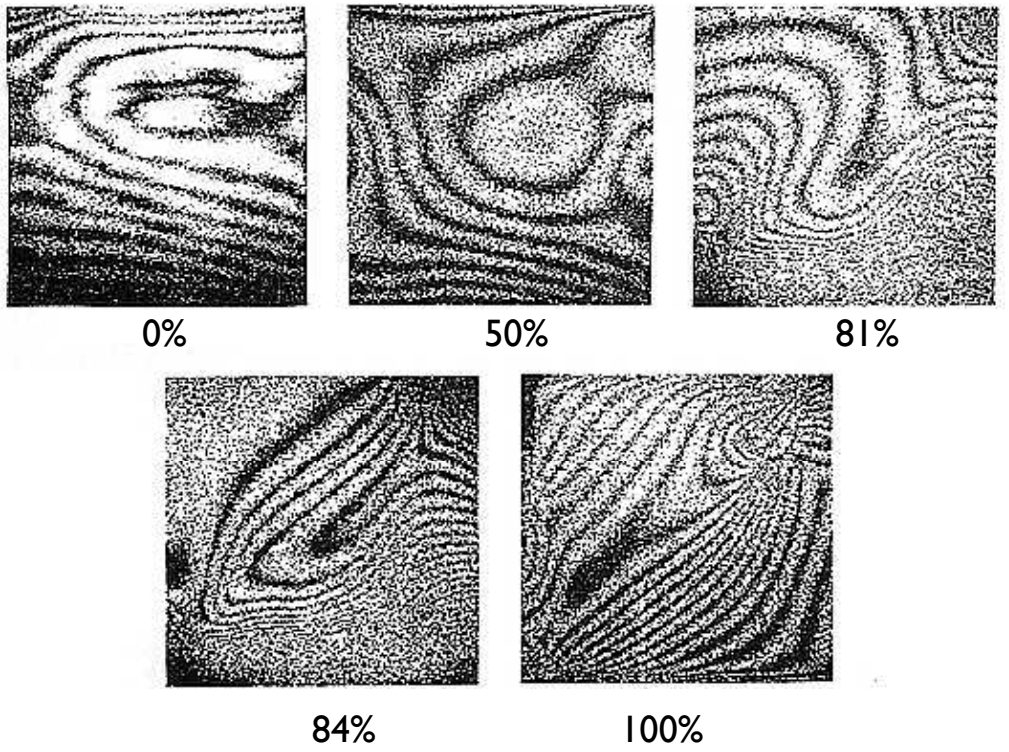

Doubly exposed holograms; % of σultimate (vertical)

Sobolev G, Spetzler H., Salov, B., 1978.
Precursors to failure in rocks while undergoing anelastic deformation.
JGR 83, 1775-1784

Dilatancy

Axial loading, pc=100MPa
Westerley granite

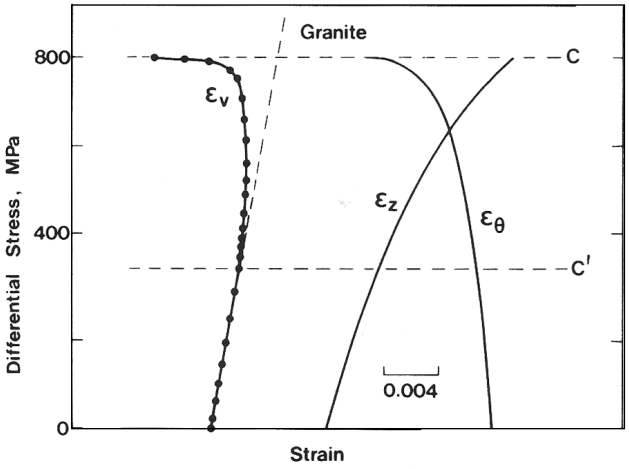

macroscopic failure stress

stress at onset of dilatancy

differential stress vs strain

εv	volumteric strain
εz	axial strain
εθ	circumferential strain

Paterson, M. S. 1978: Experimental rock deformation - the brittle filed. Springer-Verlag, Berlin.

at fault tip: rotation kinkband model

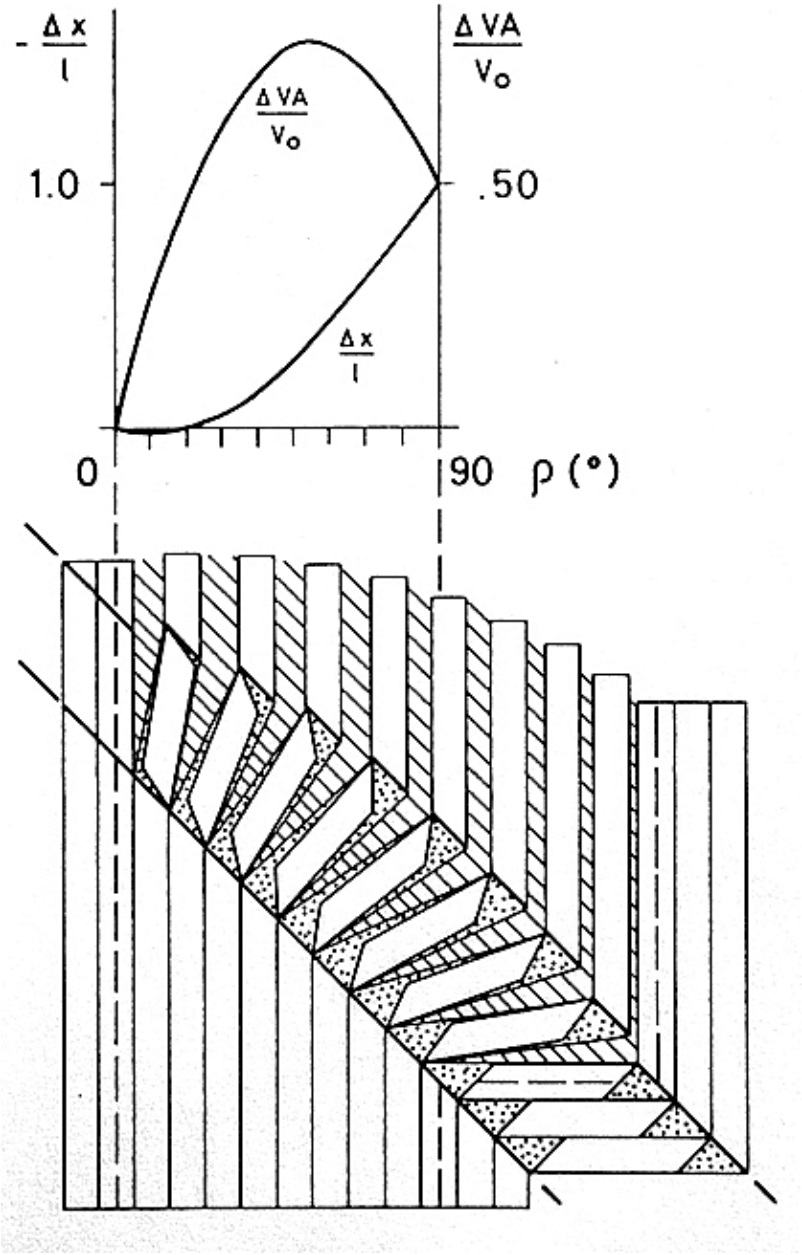

Fracture - Stress at failure

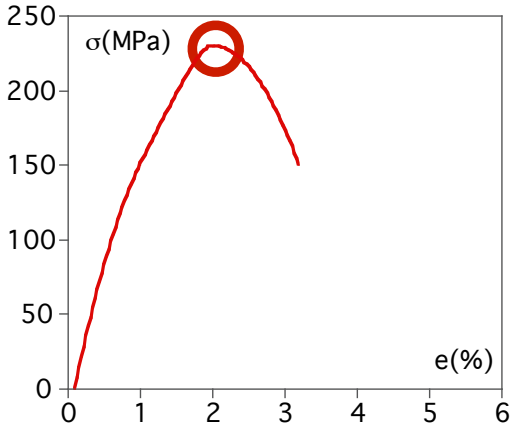

Factors influencing fracture strength

- mineral composition
- porosity
- density
- microstructure
- state of alteration, weathering
- deformation history
- microcrack distribution

General failure criterion:

$$\Delta\sigma = f(p_c, p_p, T, \dot{\varepsilon}/\dot{Y}, \ldots)$$

Failure by fracture:

2 types of fracture:

1. extension (Brazil test)	tensile stress	a) intrusion fracture (pore fluid) b) internal stress concentration (inclusion, crack)
2. shear (Triaxial testing)	compressive stresses	

Brittle failure in granite

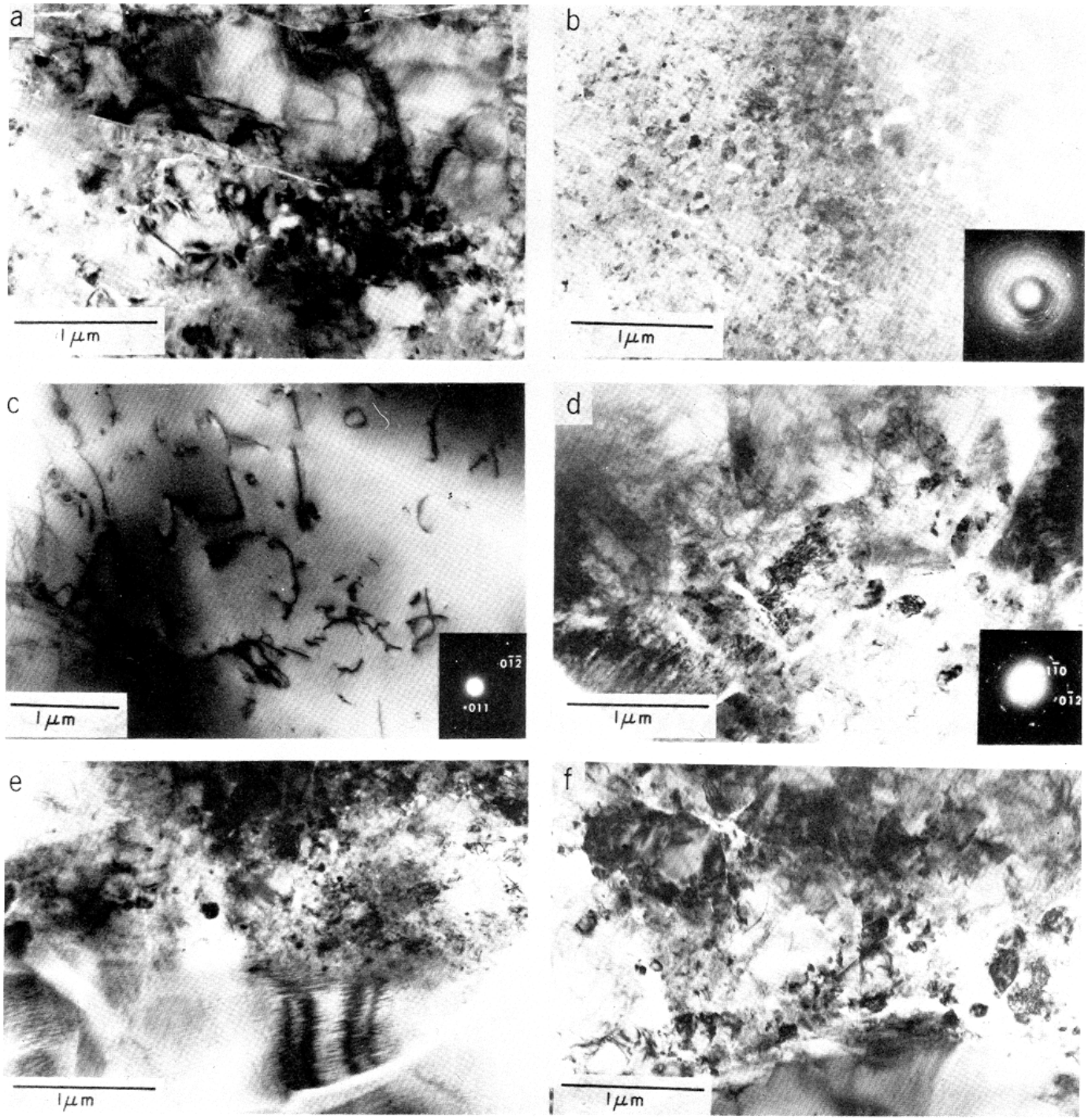

Brittle failure in granite

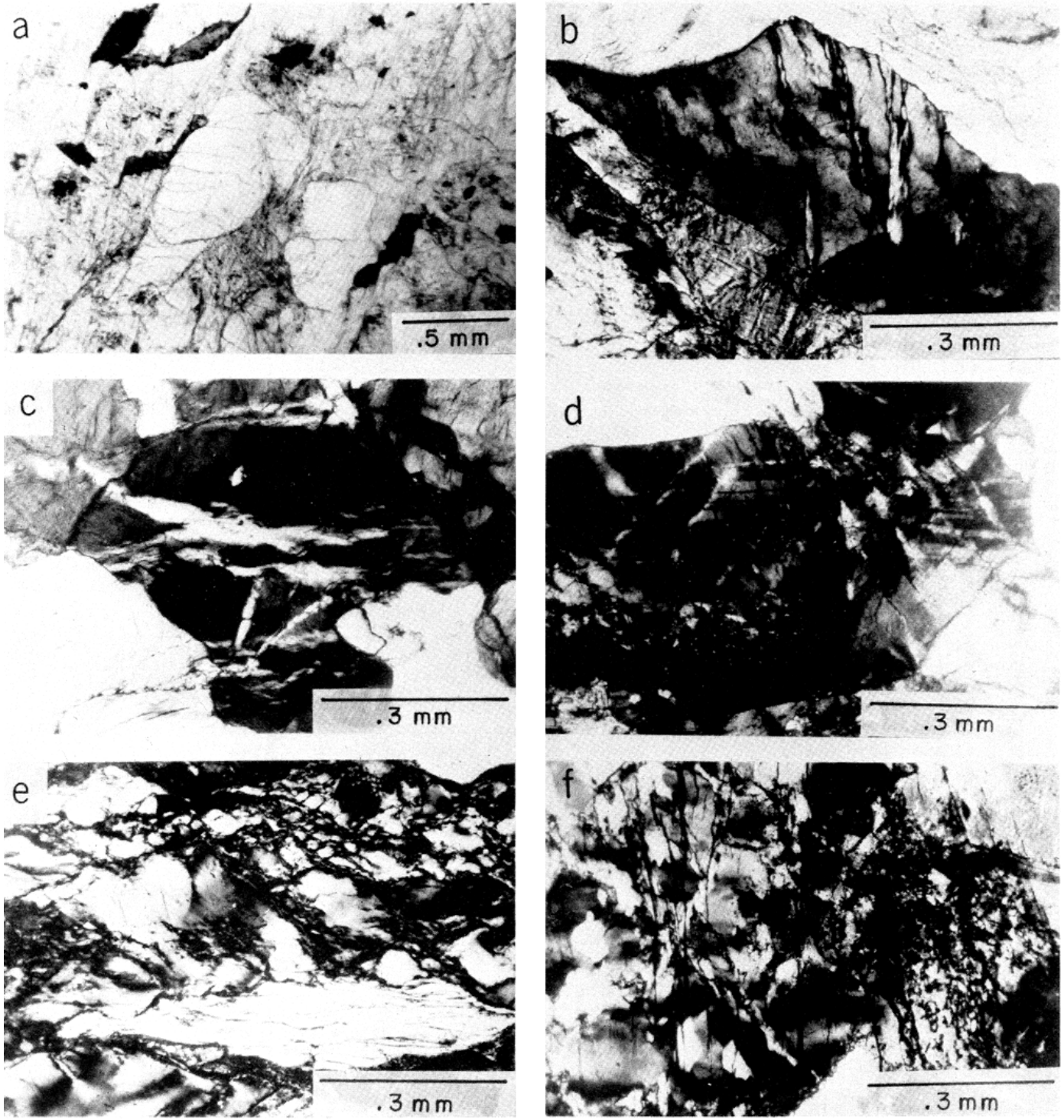

Brittle failure in granite

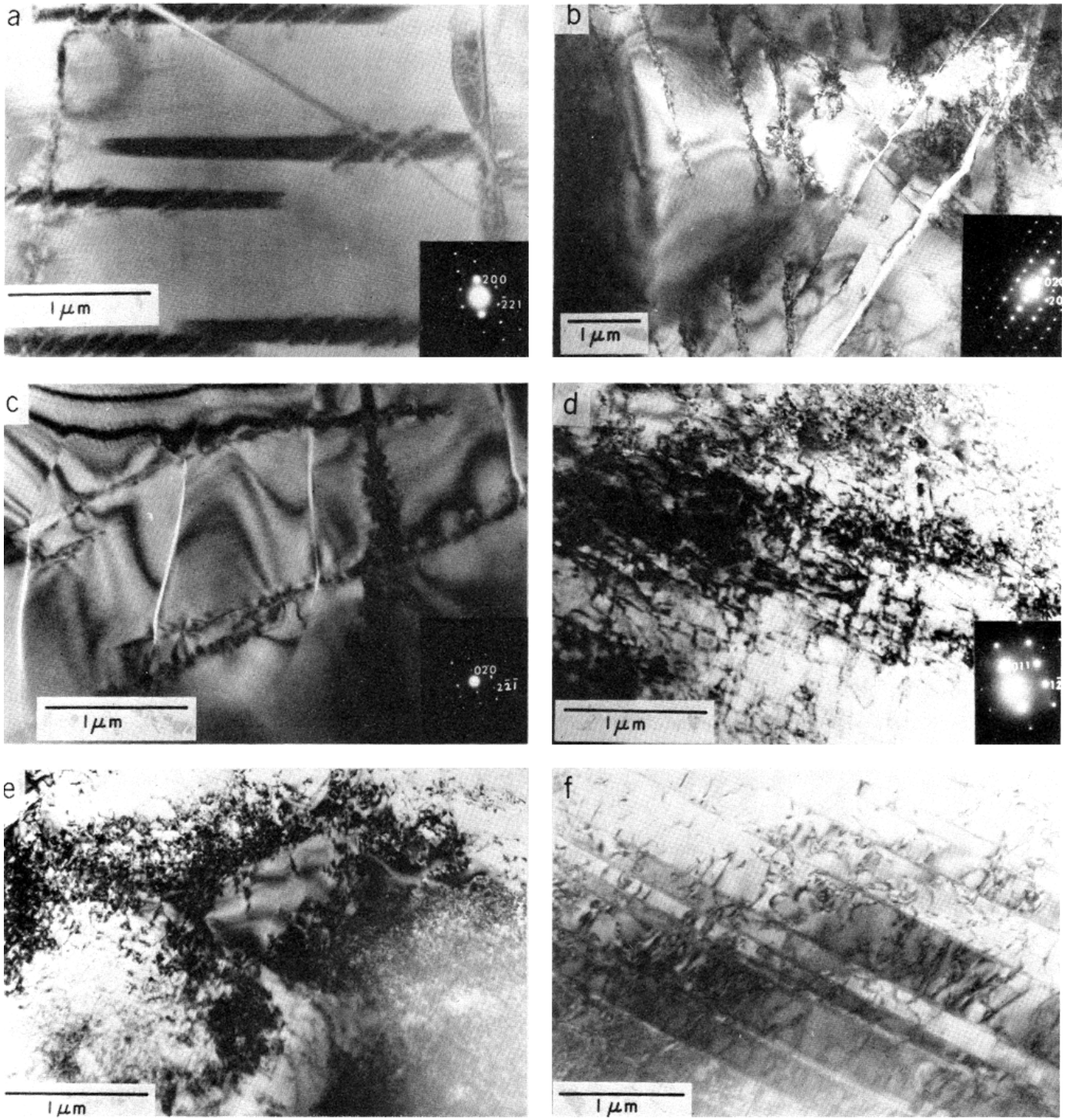

Brittle failure in granite

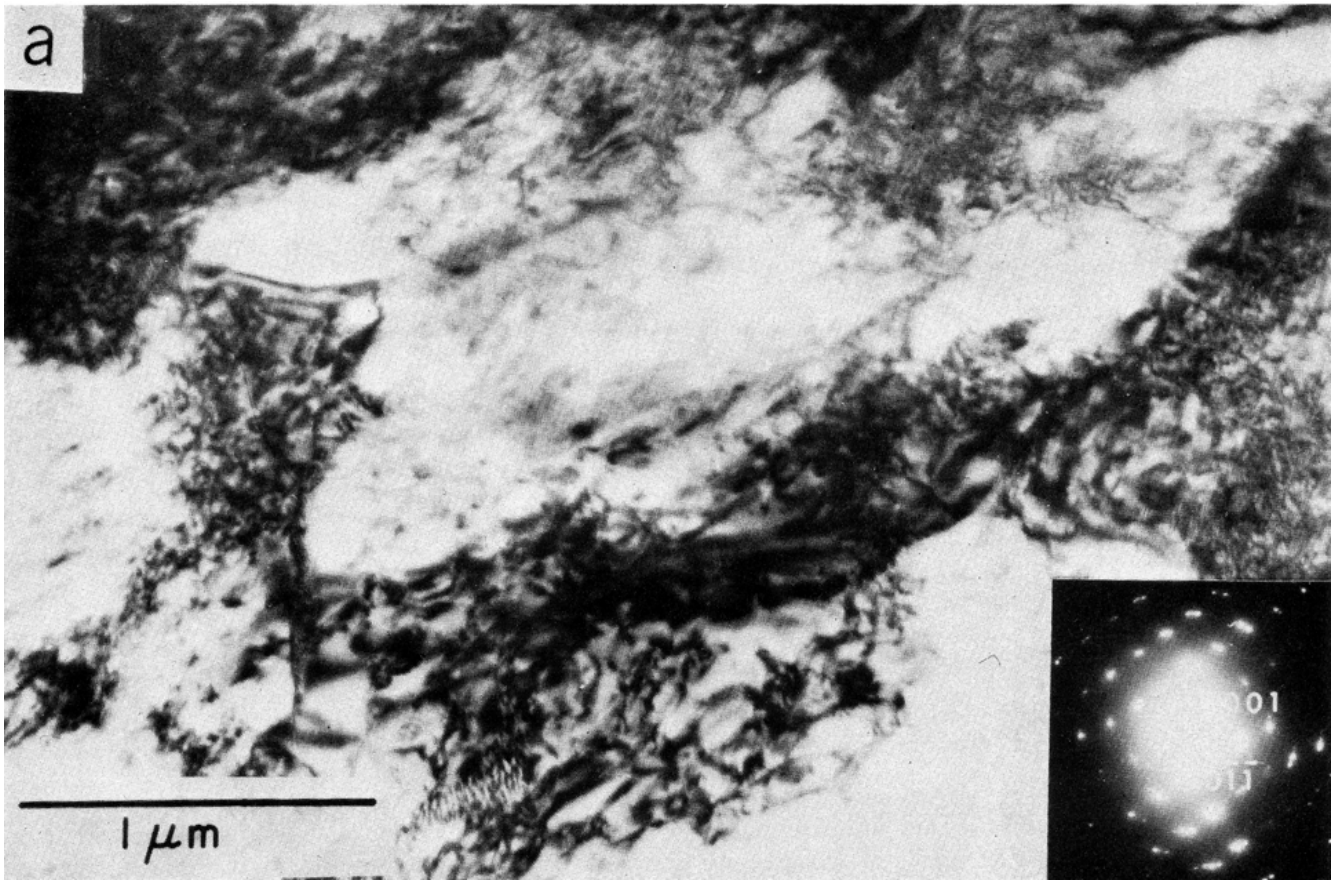

quartz: high dislocation density

Brittle failure in granite

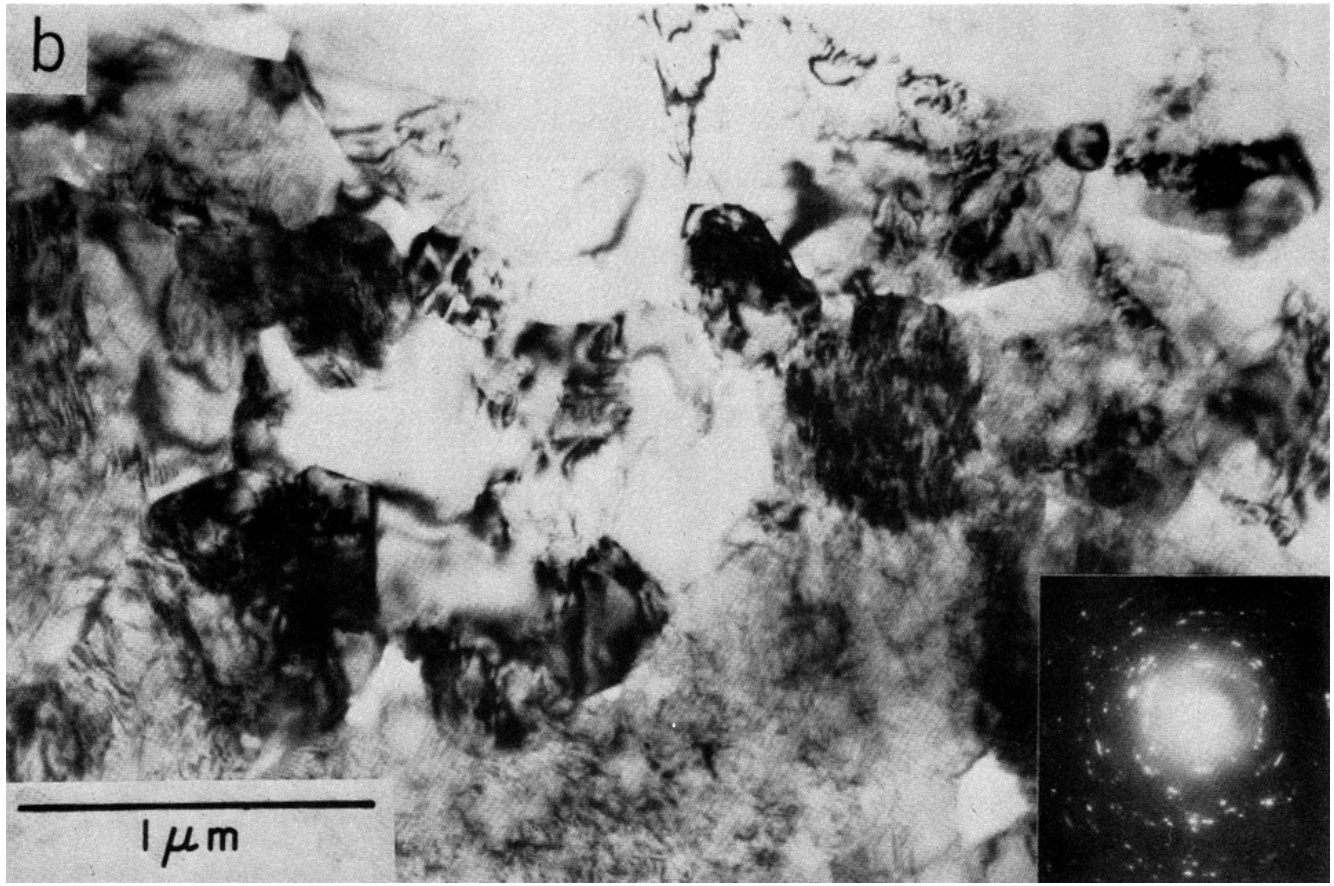

feldspar: formation of cells

Brittle failure in granite

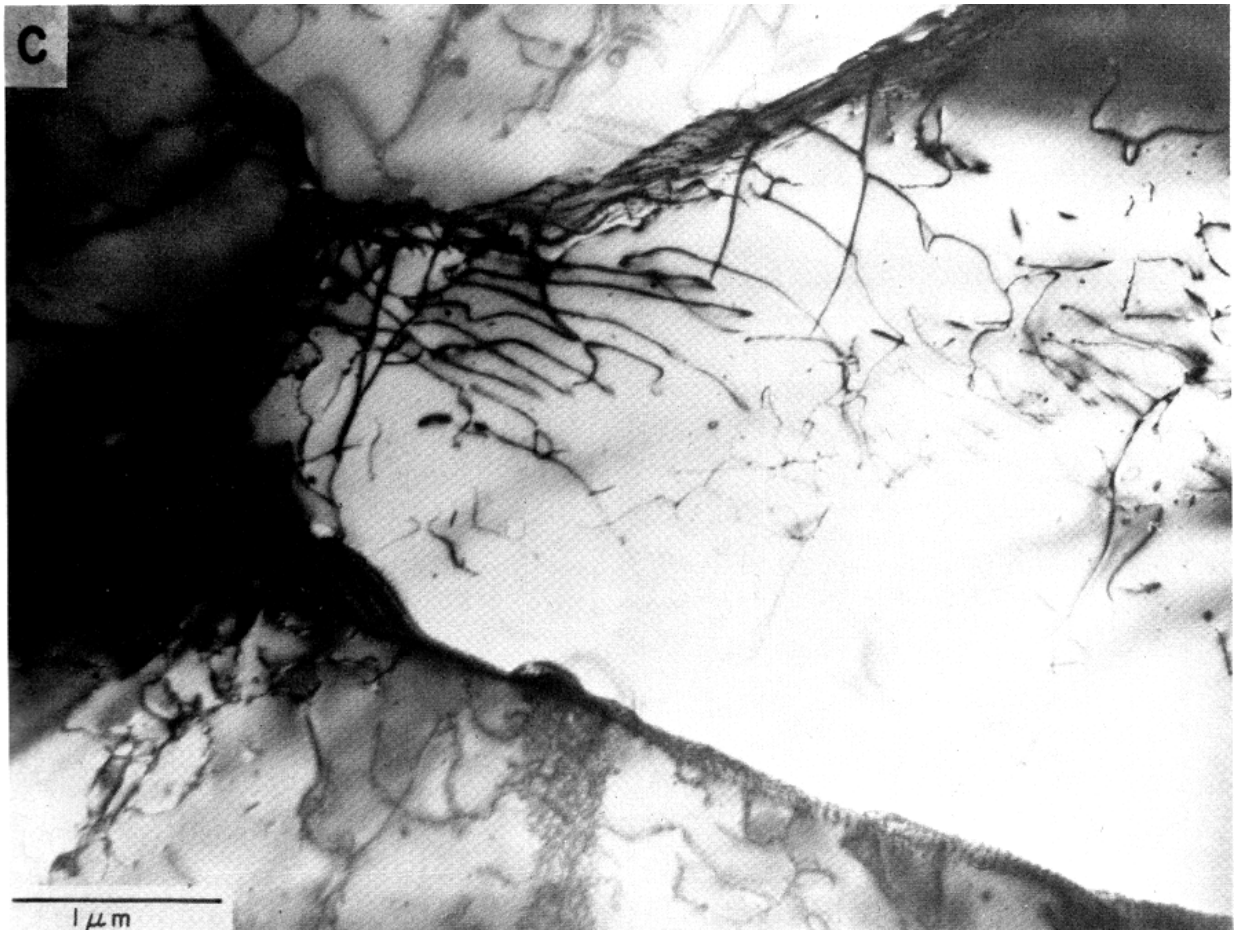

quartz: subgrains formation > creep

Brittle failure in granite

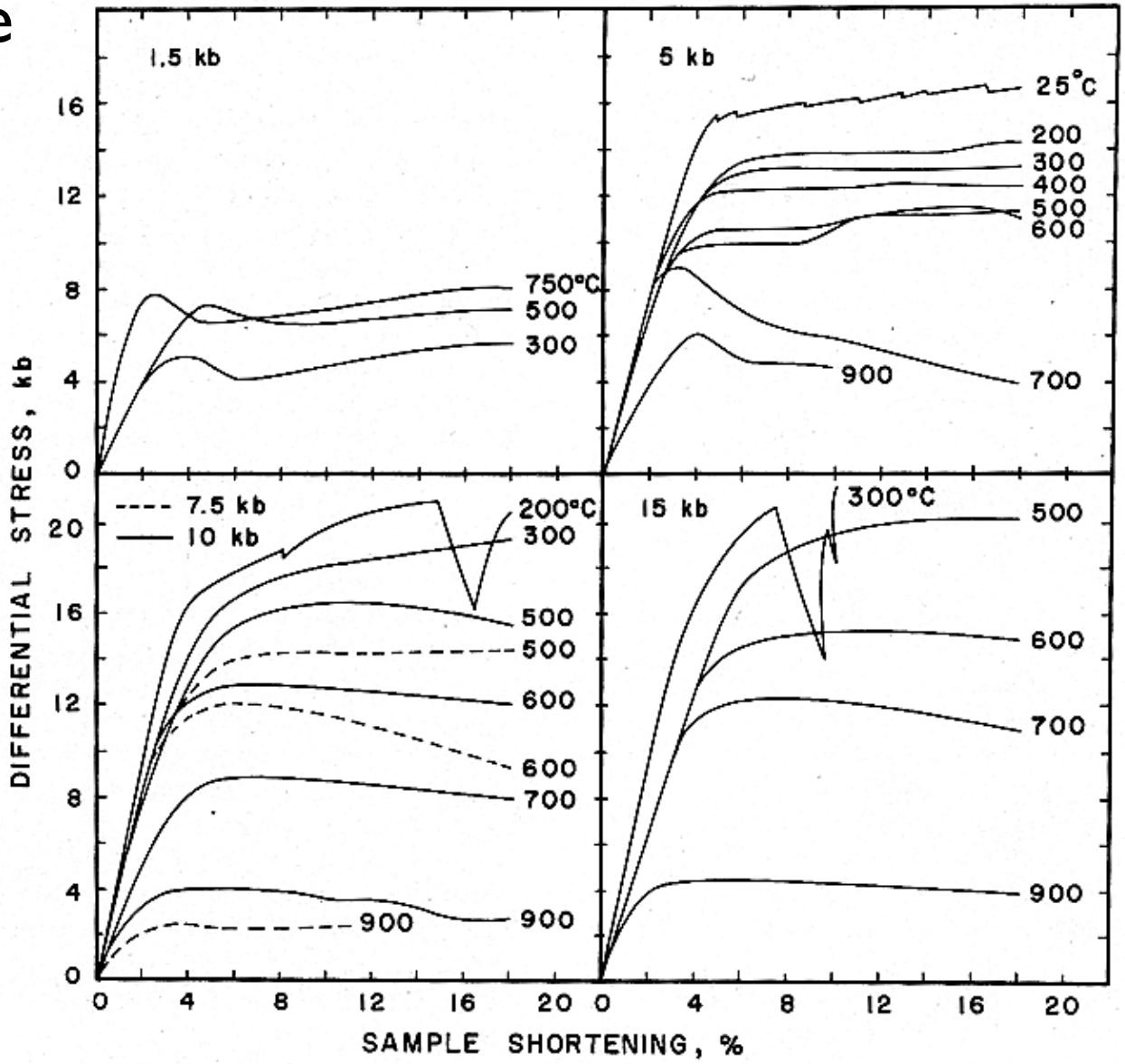

Fig. 6. Stress-strain curves for representative experiments. These curves have not been corrected for the strength of the sodium chloride confining medium or the thin metal jacket around the sample or for the nonuniform shortening of the sample; this correction should be less than 1 kbar. The curves are shown only out to 18% strain.

Brittle failure in granite

Summary:

high T (900°):
- no dependence of strength on pc

medium T (700°):
- slight dependence of strength on pc
  (cell formation)

low T (500°):
- strength depends on pc
  = friction dependent behaviour

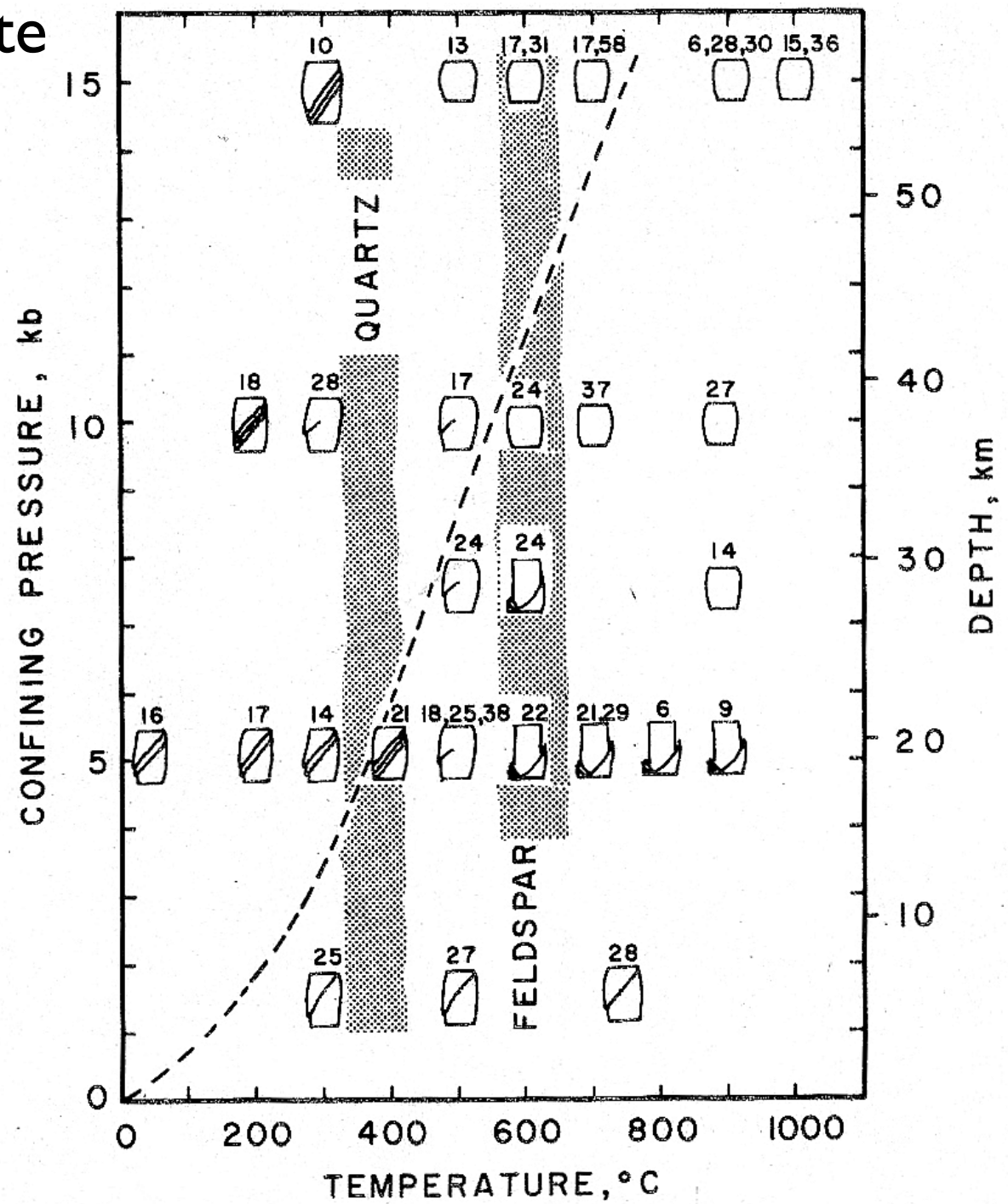

Tullis, J. & Yund, R.A., 1977:
Experimental deformation of dry
Westerly granite. J.G.R. 82, 5705-5718

Failure by fracture:

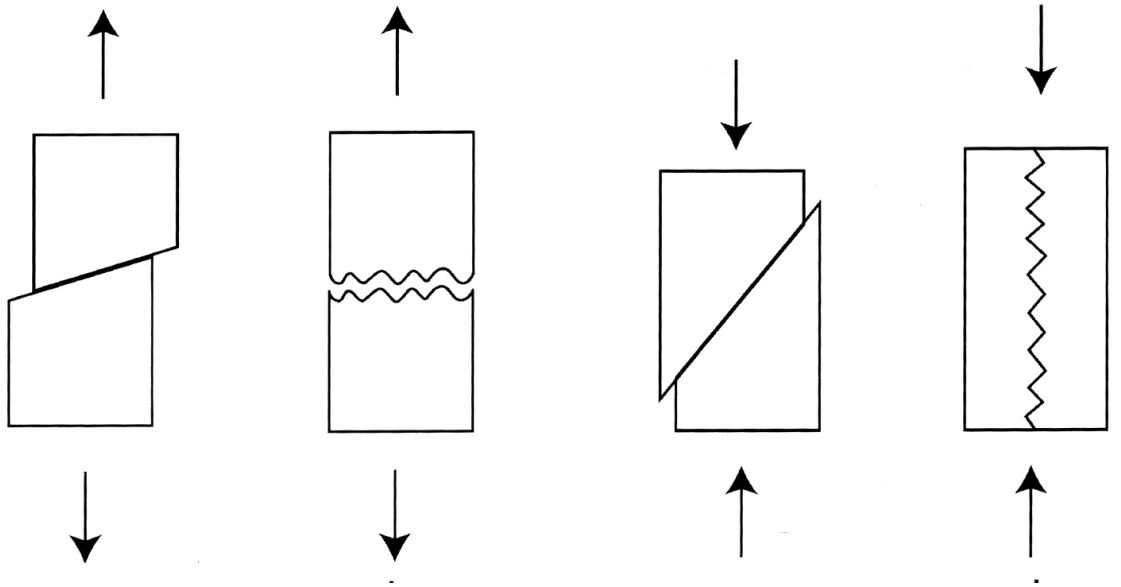

2 types of fracture:

1. extension — tensile stress
   a) intrusion fracture (pore fluid)
   b) internal stress concentration (inclusion, crack)
   (Brazil test)

2. shear — compressive stresses
   (Triaxial testing)

General failure criterion for fracture:

$$\sigma_1 = f(\sigma_2, \sigma_3)$$

example: differential stress at failure depends on cohesion and confining pressure:

$$\Delta\sigma = f(\sigma_0, \sigma 3)$$

$$(\sigma_1 - \sigma_3) = \sigma_0 + \sigma_3 \cdot \tan(\Psi)$$

$$(1 < \tan(\Psi) < 10)$$

$$|\tau| = \tau_0 + \sigma_n \cdot \tan(\varphi)$$

$$(0.5 < \tan(\varphi) < 1.5)$$

General failure criterion for fracture:

$$\Delta\sigma = f(\sigma_0, \sigma 3)$$

$$|\tau| = \tau_0 + \sigma_n \cdot \tan(\varphi)$$

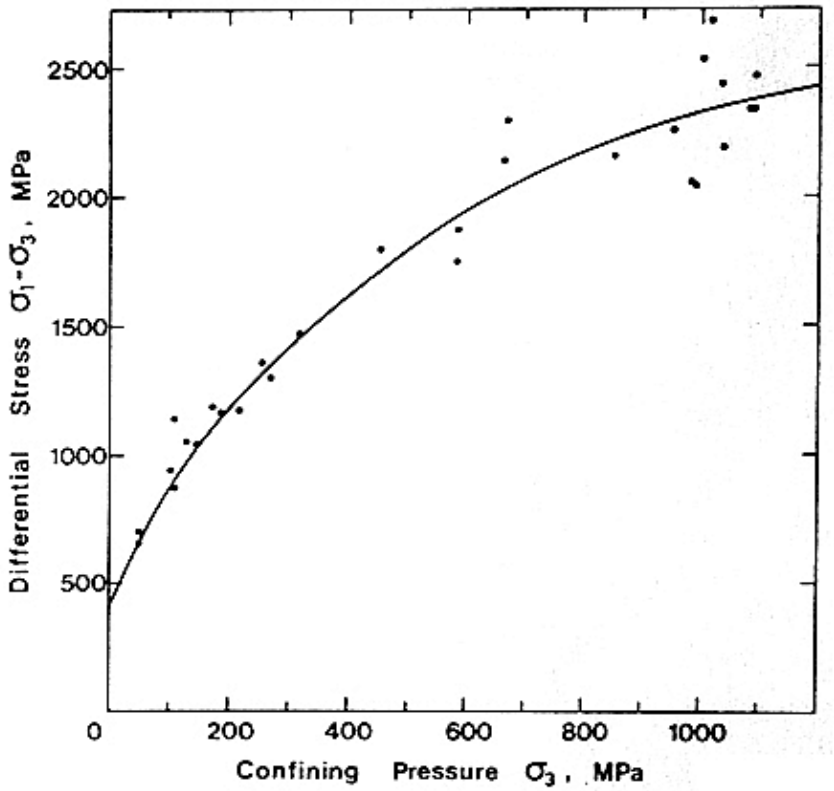

Fig. 9. Dependence of differential stress at failure in compression on confining pressure for granite, illustrating non-linearity. (After Byerlee, 1967a)

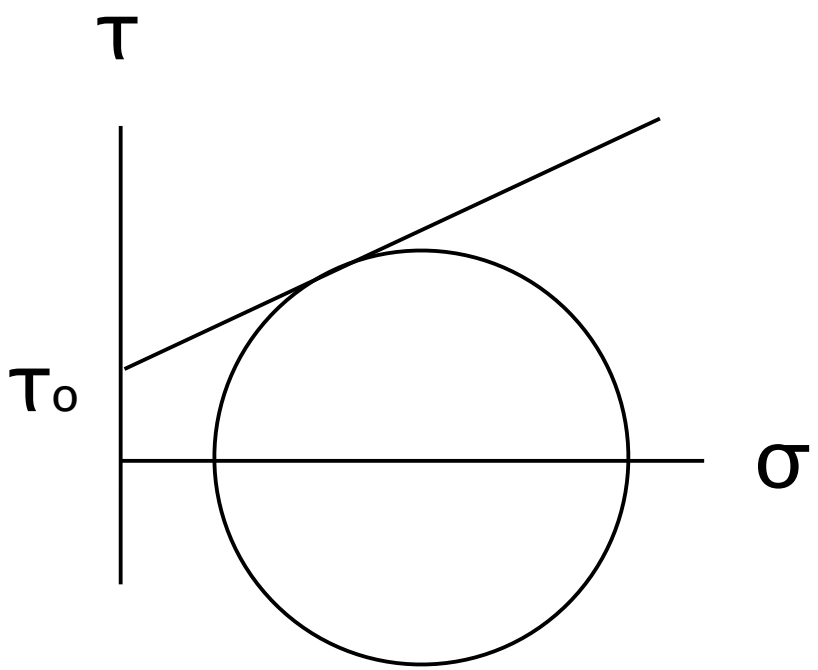

Paterson, M. S. 1978: Experimental rock deformation
- the brittle filed. Springer-Verlag, Berlin.

Influence of strain rate:

Fig. 11.
a Uniaxial compressive strength as a function of strain rate for four different rock types. The marble and sandstone data are from the compilation of Sano, Ito and Terada (1981). The granite and shale data are from Masud, Mizutani and Yamada (1987) and Chong et al. (1980), respectively.

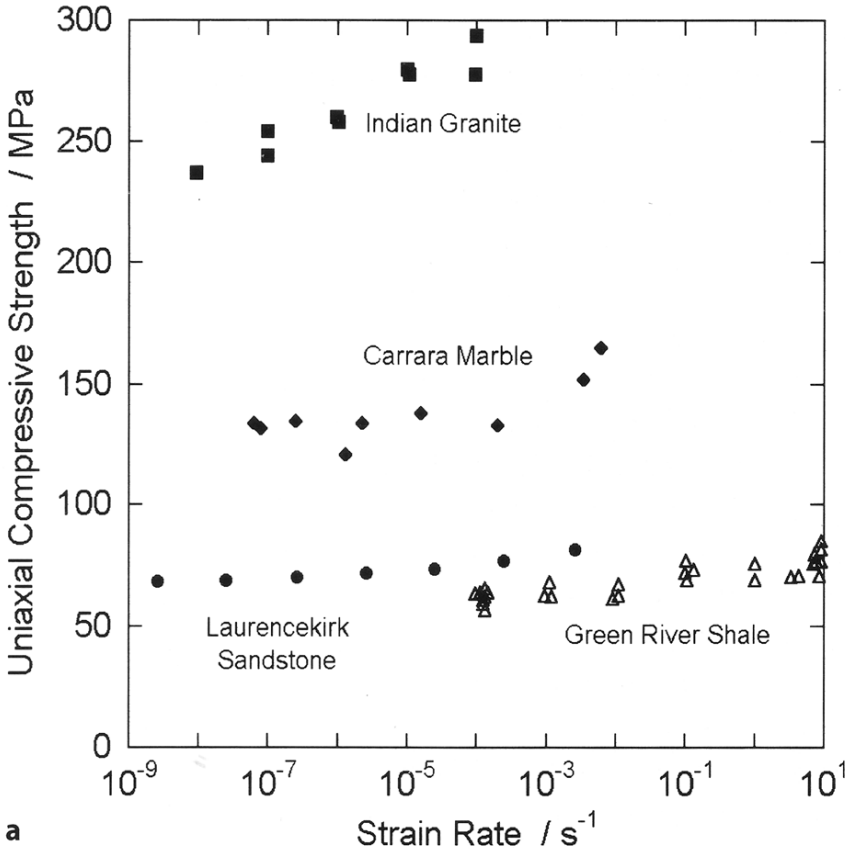

Paterson, M. S. & Teng-fong Wong (2005):
Experimental rock deformation - the brittle filed.
Springer-Verlag, Berlin.

Influence of temperature:

b Influence of temperature on peak differential stress at confining pressures shown. The data for room pressure and 50 MPa are for Charcoal granodiorite at a strain rate of 10^{-4} s^{-1} (Friedman et al. 1979). The data for 80 MPa, 250 MPa and 400 MPa are for Westerly granite at a strain rate of 10^{-5} s^{-1} (Wong 1982b)

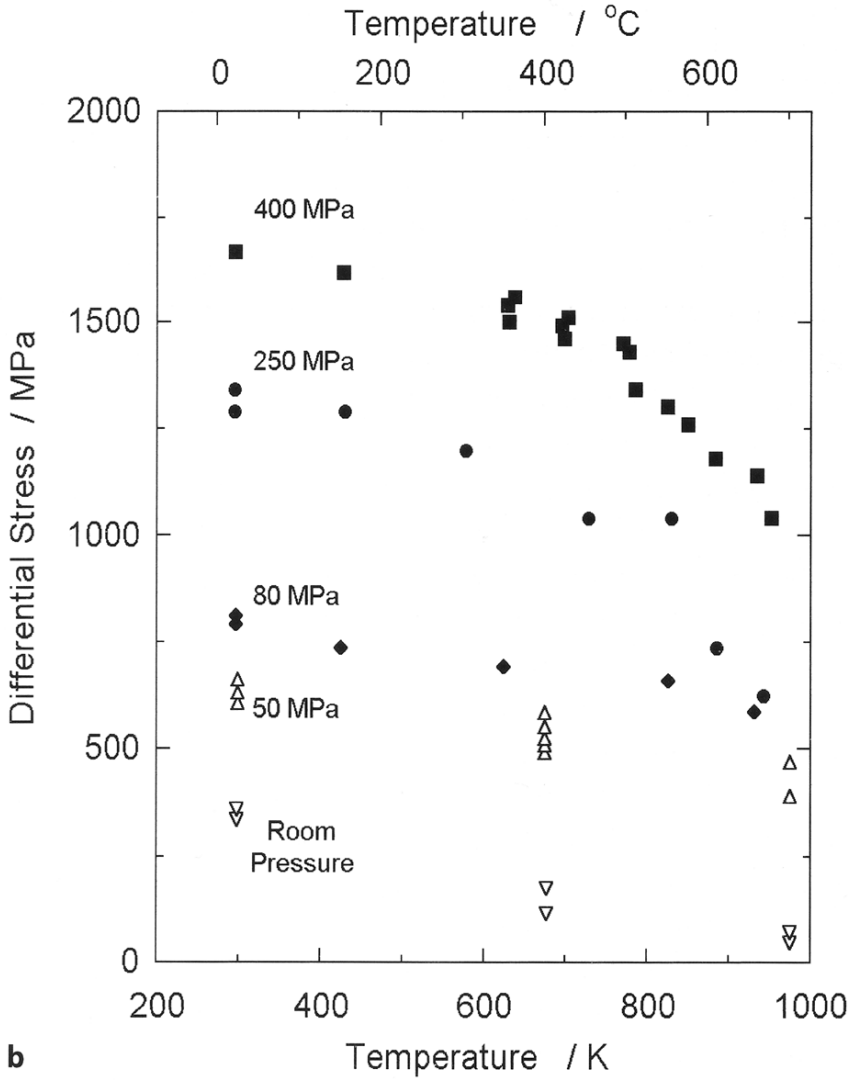

Paterson, M. S. & Teng-fong Wong (2005):
Experimental rock deformation - the brittle filed.
Springer-Verlag, Berlin.

Influence of shape and size:

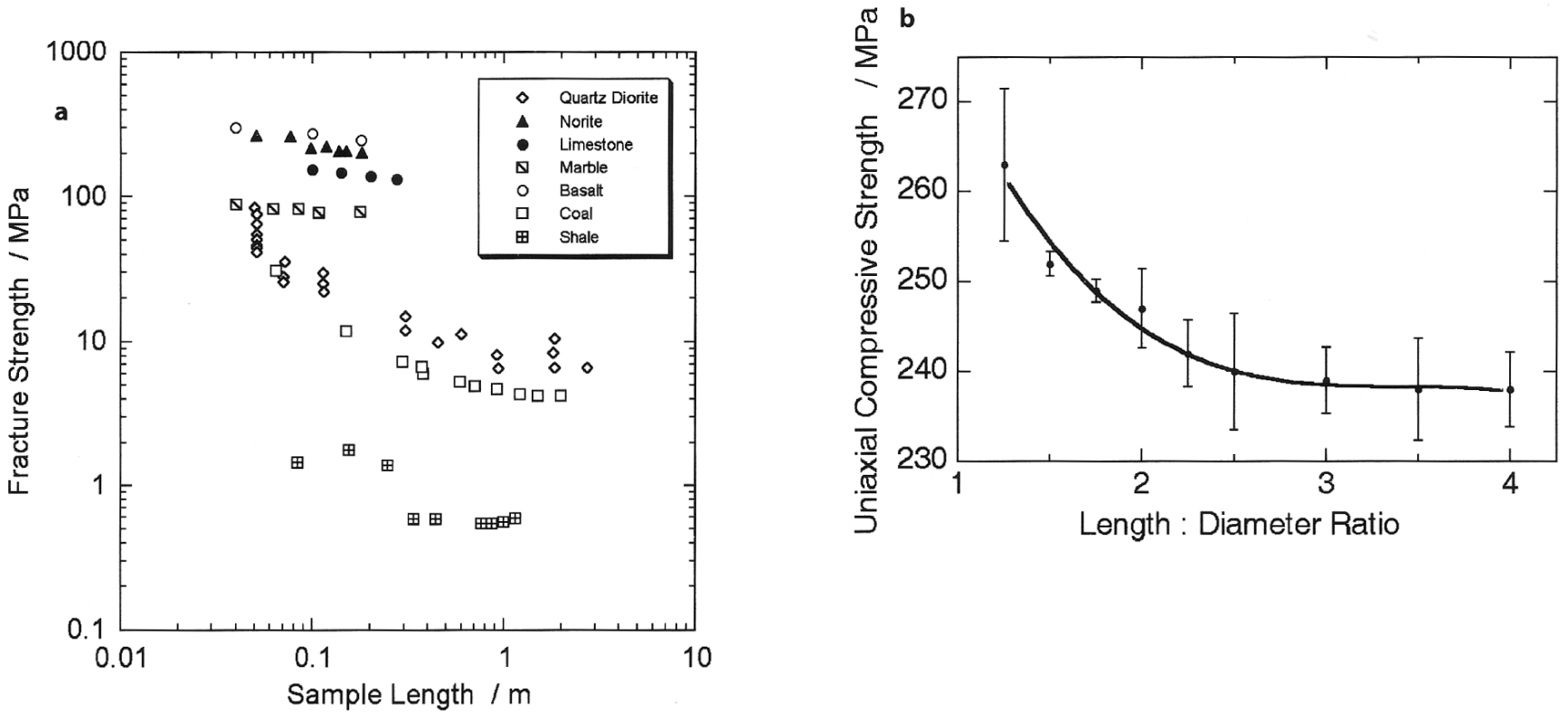

Fig. 12. a Effect of sample size on peak differential stress at fracture (after Lockner 1995). **b** Dependence of uniaxial compressive strength on length : diameter ratio for Westerly granite (after Mogi 1966).

Paterson, M. S. & Teng-fong Wong (2005):
Experimental rock deformation - the brittle filed.
Springer-Verlag, Berlin.

Influence of stress field (stress concentrations):

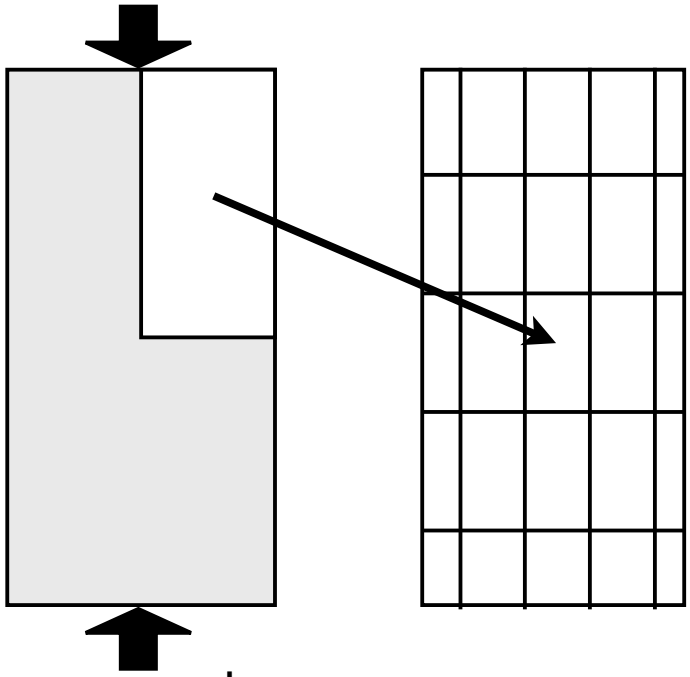

stress trajectories in cylinder
σ1 vertical
σ3 radial

(finite element calculation for 1/4 of cylinder)

σ1 contours:

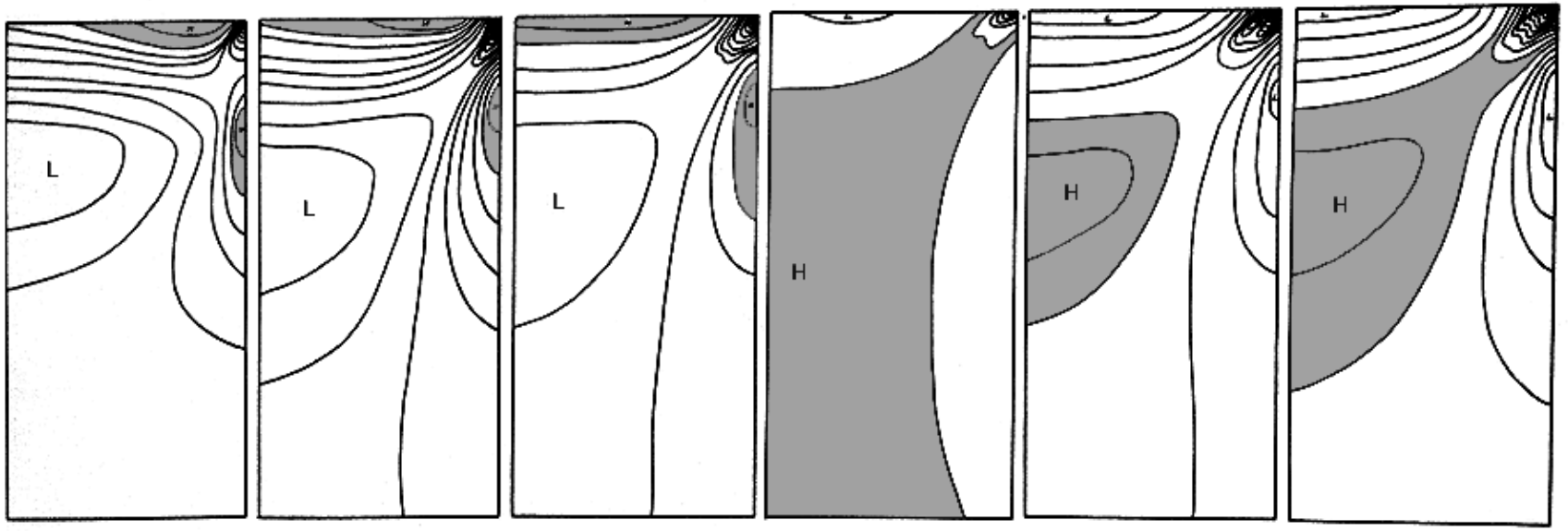

σ1/σ3: 1.0 1.33 2.0 3.33 4.00 ∞

Influence of stress field (shape of sample):

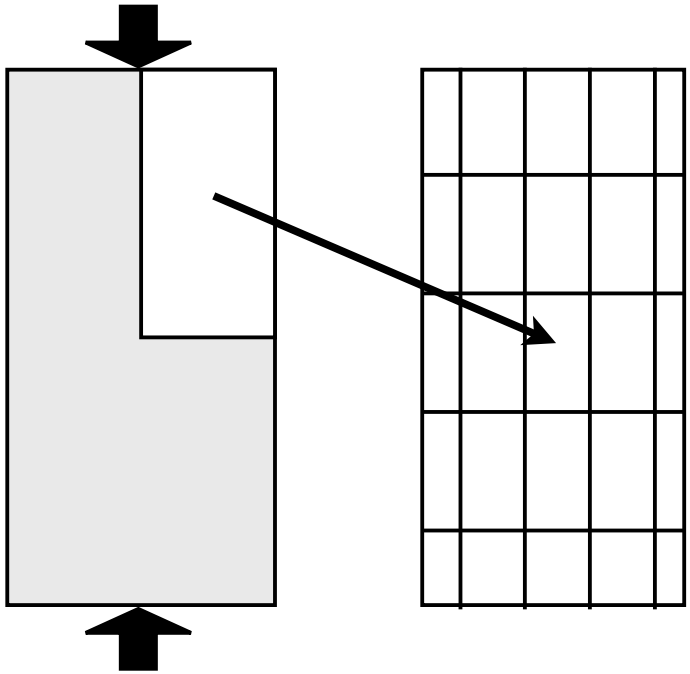

stress trajectories in cylinder
σ1 vertical
σ3 radial

(finite element calculation for 1/4 of cylinder)

contours of σ1/σ3:
(ratio > 4 = grey)

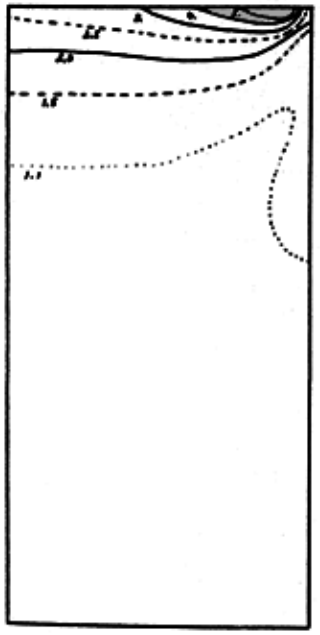

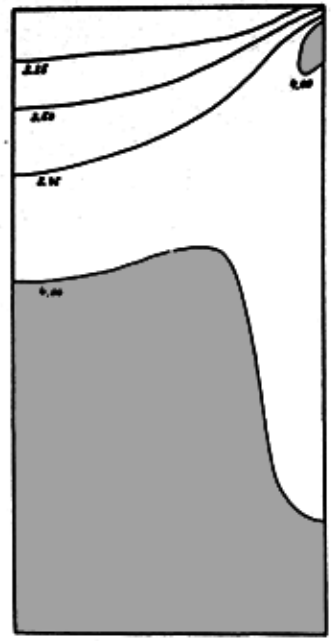

for applied σ1/σ3: 1.0 (hydrostatic) 4.00 (axial load)

Influence of true triaxial conditions:

$$\tau_{oct} = 1/3 \sqrt{[(\sigma_1-\sigma_2)^2 + (\sigma_2-\sigma_3)^2 + (\sigma_3-\sigma_1)^2]}$$

$$p_m = 1/3 (\sigma_1 + \sigma_2 + \sigma_3)$$

$$\tau_{oct} = A \cdot (\sigma_1 + \sigma_3)^n$$

$(0.56 < n < 0.89)$

Van Mises criterion:

$$\sqrt{(J^2)} = K$$

Tresca criterion:

$$(\sigma_1-\sigma_3) = 2\,\overline{K}$$

Fig. 13.
Data from "true" triaxial tests of Westerly granite, plotted as the peak value of σ_1 as function of σ_2 at σ_3 values shown. Data points connected by the *solid line* were from conventional triaxial tests (after Haimson and Chang 2000)

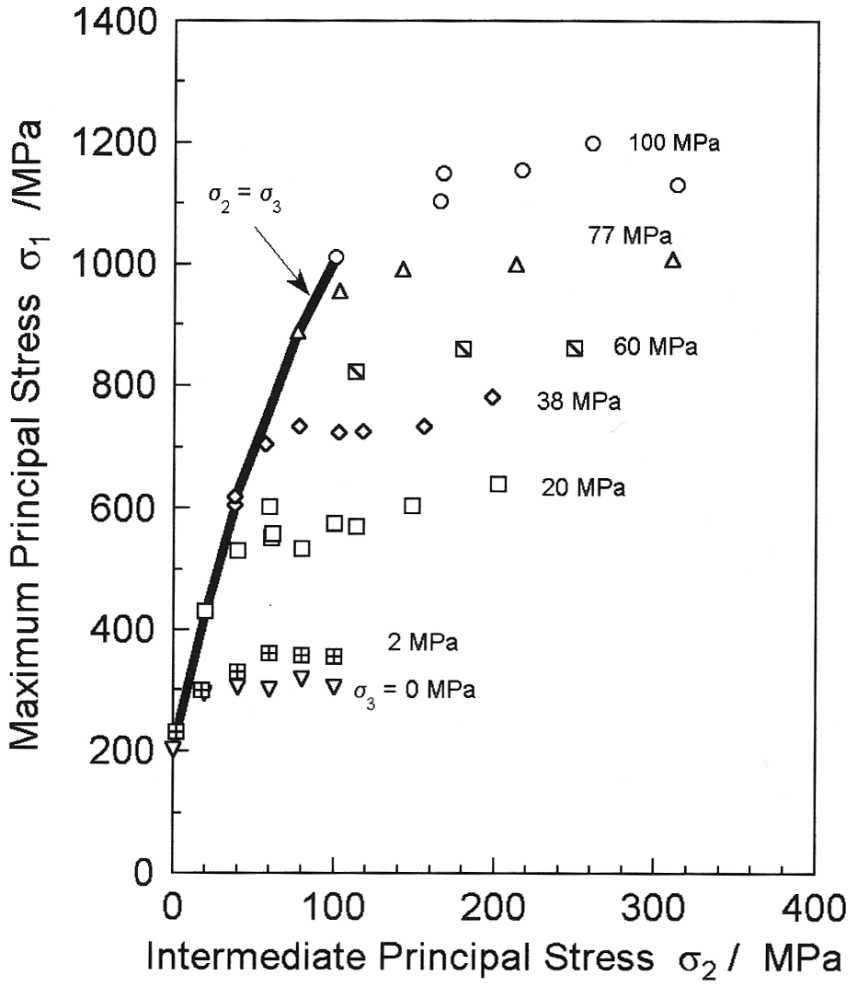

Paterson, M. S. & Teng-fong Wong (2005):
Experimental rock deformation - the brittle filed.
Springer-Verlag, Berlin.

Stress concentration factor (Inglis, 1913)

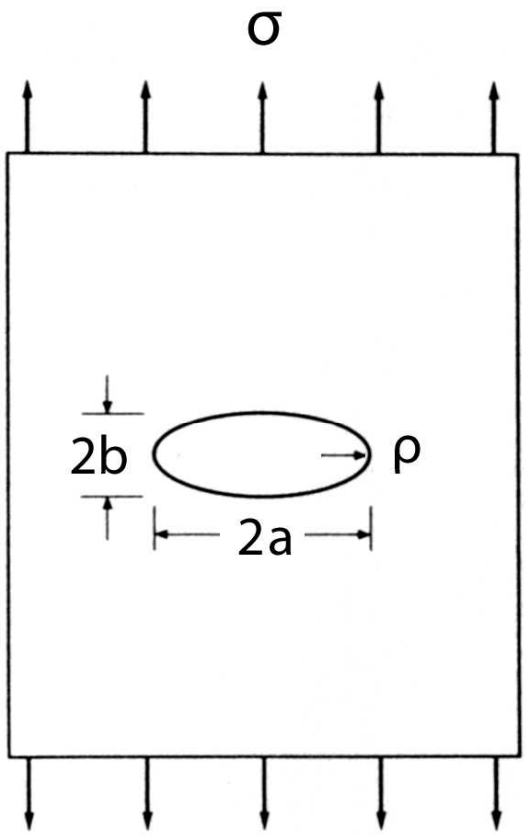

$$\sigma_{max} / \sigma = 1 + 2a/b$$

σ_{max}	max. stress at end of major axis
σ	applied stress
2a	major axis
2b	minor axis
ρ	radius of curvature

Stress concentration:

$$\sigma_{max} / \sigma = 1 + 2a/b$$

Curvature:

$$\rho = b^2/a$$

$$\sigma_{max} = \sigma [1 + 2\sqrt{(a/\rho)}]$$

For $a >> \rho$:

$$\sigma_{max} \approx 2\sigma \sqrt{(a/\rho)}$$

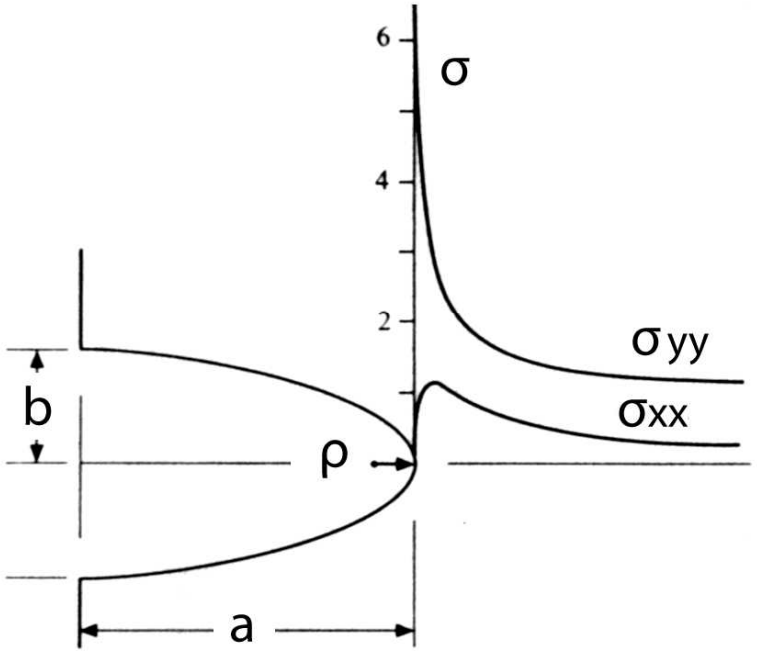

Griffith cracks (Griffith, 1920)

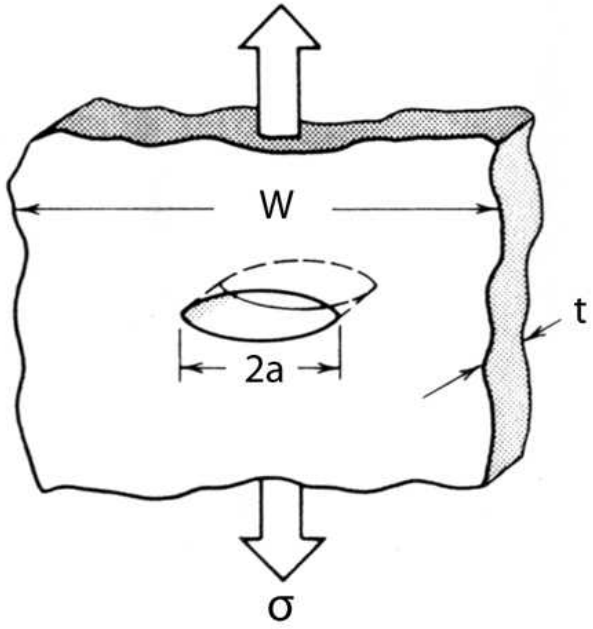

$$U - U_0 = - \pi \sigma^2 a^2 t / E + 4at\Upsilon_s$$

U	potential energy of body with crack
U_0	potential energy of body without crack
σ	applied stress
a	one half crack length
t	thickness
E	module of elasticity
Υ_s	specific surface energy

$$U - U_0 = - \pi \sigma^2 a^2 t / E + 4at\Upsilon_s$$

Rewriting:

$$U = 4at\Upsilon_s - \pi \sigma^2 a^2 t / E + U_0$$

Equilibrium, i.e., stable crack length:
First derivative:

$$\partial U/\partial a = 0$$
$$\partial U/\partial a = 4t\Upsilon_s - 2\pi \sigma^2 at / E = 0$$

note:
$\partial U_0/\partial a = 0$ since U_0 does not depend on a

$$\partial U/\partial a = 4t\Upsilon_s - 2\pi \sigma^2 at / E = 0$$

Equilibrium condition:

$$2t\Upsilon_s = \pi \sigma^2 at / E$$

Nature of equlibrium:
Second derivative:

$$\partial U^2/\partial a^2 = 0$$

$$\partial U^2/\partial a^2 = -2\pi \sigma^2 t / E$$

Negative, i.e., crack will grow

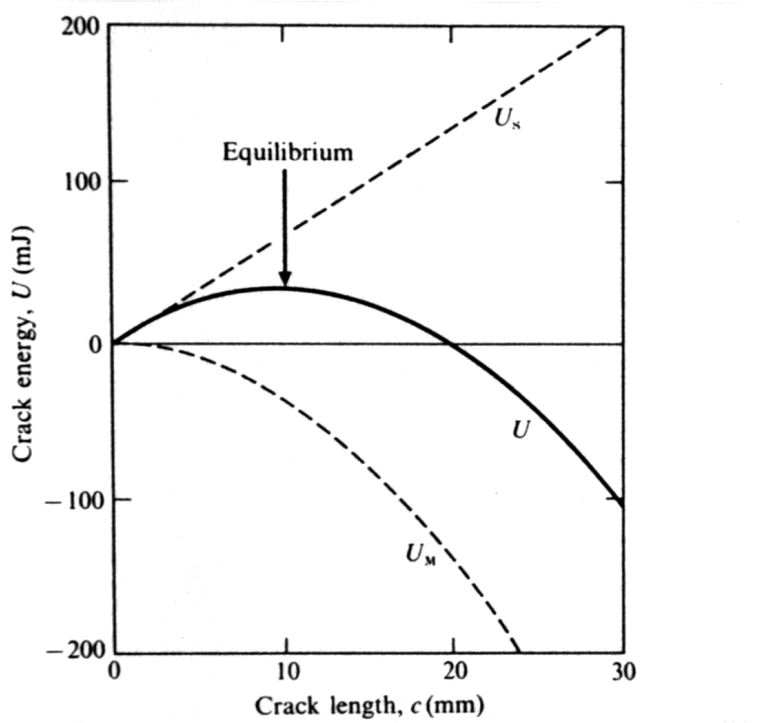

Energetics of Griffith crack in uniform tension, plane stress. Data for glass from Griffith: $\gamma = 1.75\,\mathrm{J\,m^{-2}}$, $E = 62\,\mathrm{GPa}$, $\sigma_A = 2.63\,\mathrm{MPa}$ (chosen to give equilibrium at $c_0 = 10$ mm).

$2t\gamma_s = \pi \sigma^2 a t / E$

Griffith:

$\sigma = \sqrt{(2E \gamma_s / \pi a)}$ for plane stress

$\sigma = \sqrt{(2E \gamma_s / \pi a(1-\nu^2))}$ for plane strain

ν Poisson's ratio $\approx$ 0.25 to 0.33:

$\sigma \approx \sqrt{(2E \gamma_s / \pi a)}$ for plane strain also...

Fracture modes

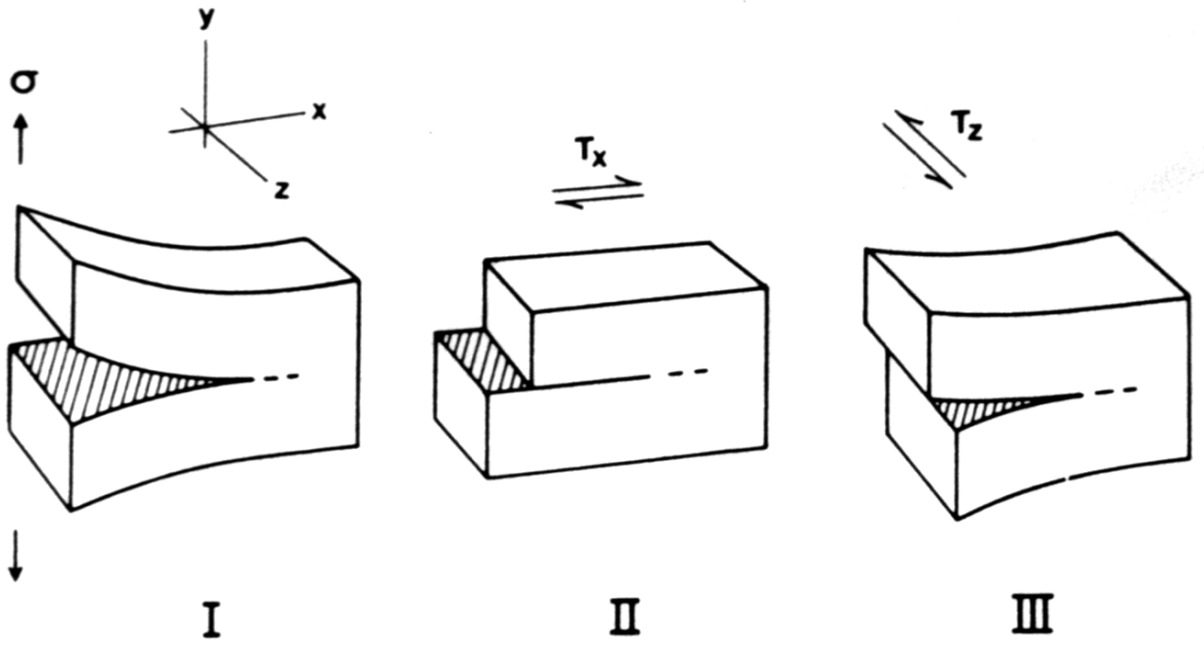

mode I – opening or tensile mode, where the crack surfaces move directly apart

mode II – sliding or in-plane shear mode, where the crack surfaces slide over one another in a

mode III – tearing or antiplane shear mode, where the crack surfaces move relative to one another and parallel to the leading edge of the crack

- plane strain – thin plate and $\sigma z = 0$; 2D strain / 3D stress
- plane stress – thick sections; 2D stress / 3D strain

Coulomb OK? Orientation of failure/fracture surface

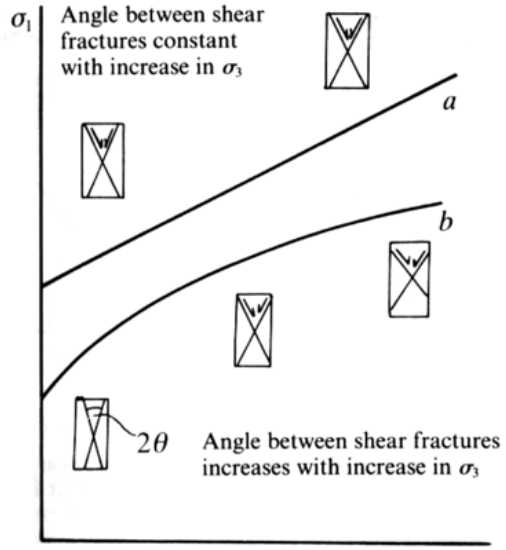

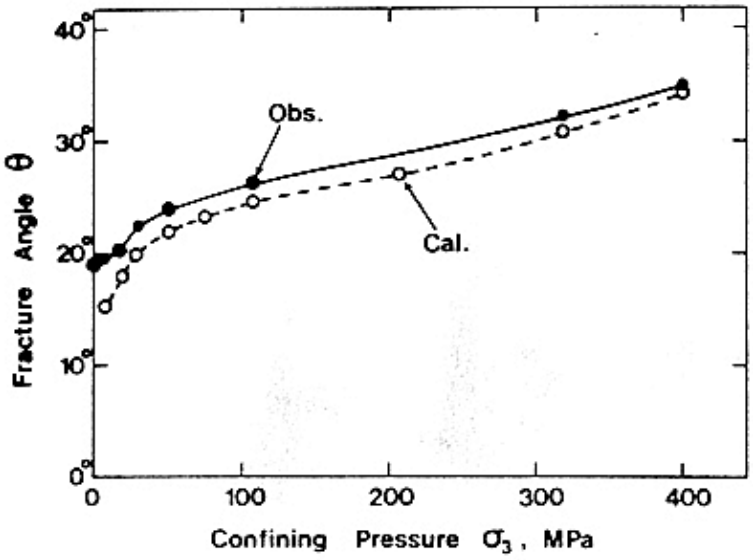

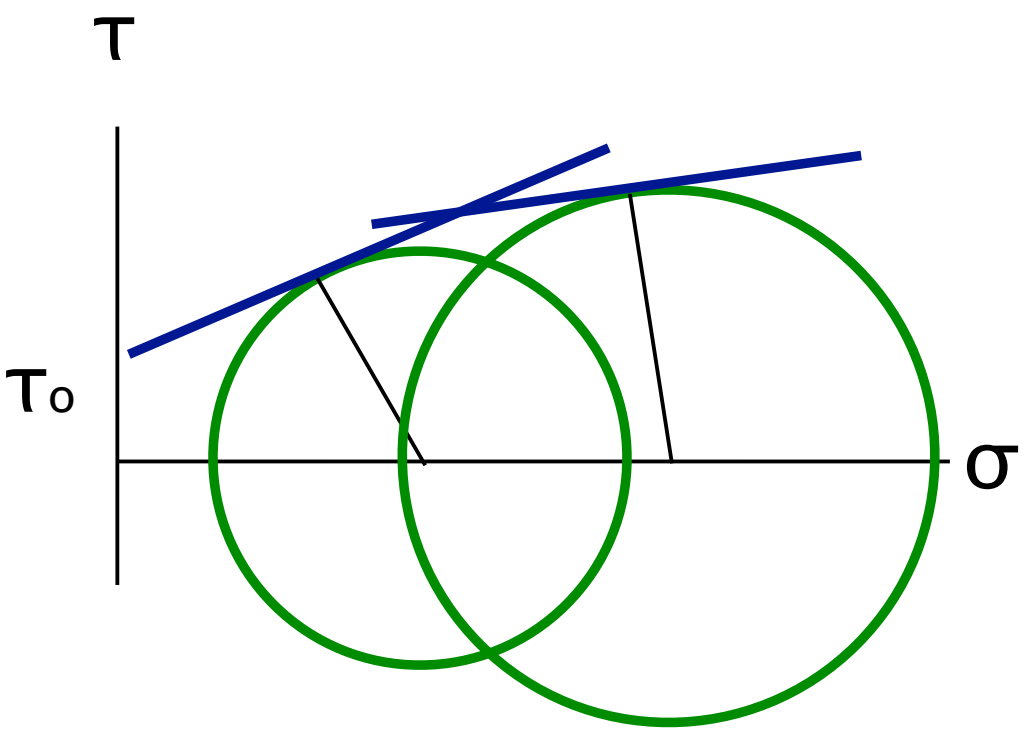

τ/σ = max

2φ (low pc) < 2φ (high pc)

Paterson, M. S. 1978: Experimental rock deformation - the brittle filed. Springer-Verlag, Berlin.

Coulomb OK? Stress at failure

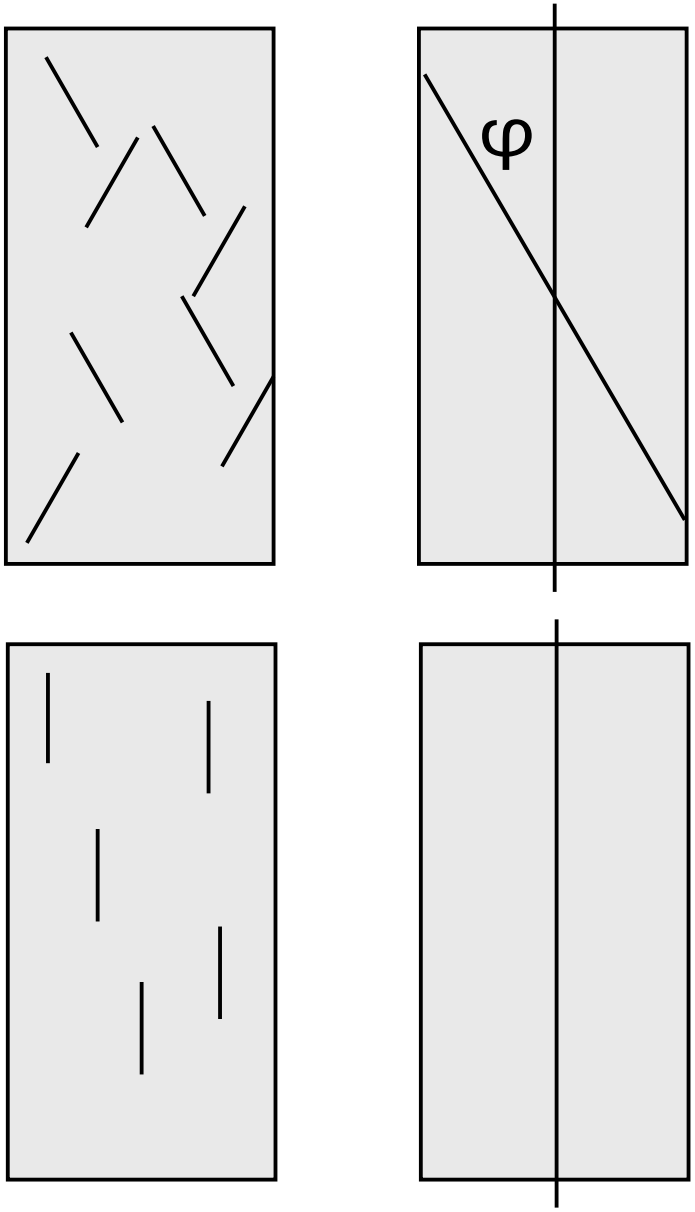

prediction by Coulomb- Mohr
failure along surface where
τ/σ = max

in reality at low pc
extension cracks

Influence of anisotropy

$\Delta\sigma_{failure} = f(\sigma 3, orientation)$

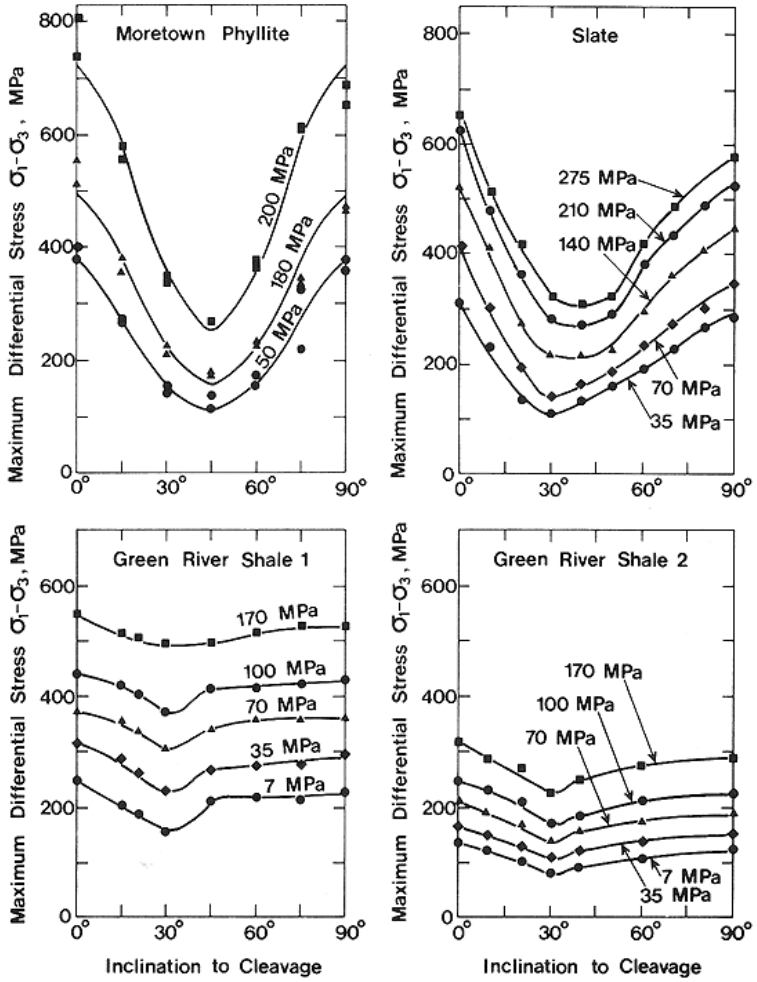

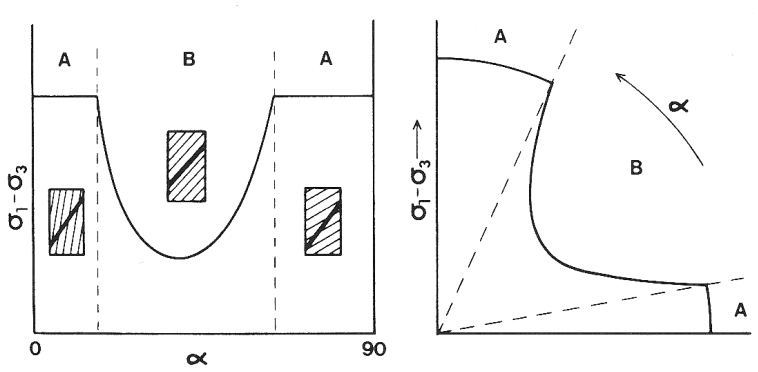

Cartesian plot Polar plot

Differential stress at failure as function of α

Paterson, M. S. 1978: Experimental rock deformation - the brittle filed. Springer-Verlag, Berlin.

Extended bibliography

Ashby, M. F. & Verrall, R. A. 1977: Micromechanics of flow and fracture, and their relevance to the rheology of the upper mantle. Phil. Trans. R. Soc. Lond. A. 288, 59-95.

Bieniawski, Z. T. 1967: Mechanism of brittle fracture of rock. Part I - Theory of the fracture process. Int. J. Rock Mech. Min. Sci. 4, 399-406.

Brace, W. F. 1971: Micromechanics in rock systems. In: Structure, Solid Mechanics and Engineering Design (Ed. by Te'eni, M.). Wiley Interscience, New York,

Brace, W. F., et al. 1966: Dilatancy in the Fracture of crystalline rocks. J. geophys. Res. 71, 3939-3953.

Byerlee, J. D. 1978: Friction of rocks. Pageophys. 116, 615-626.

Chen Rong, Yao Xiao-Xin, Xie Hung-Sen, 1979. Studies of fracture of gabbro. Int. J. Rock Mech. Min. Sci., Abstr. Vol. 16, 187-193

Cook, N. G. W. 1981: Stiff testing machines, stickslip sliding, and the stability of rock deformation. Geophys. Monograph 24,

Friedman, M. & Higgs, N. G. 1981: Calcite fabrics in experimental shear zones. Geophys. Monograoh 24, 11-28.

Gangi, A. F. 1978: Variation of whole- and fractured-porous-rock permeability with confining pressure. Int. J. rock Mech. & Min. Sci. & Geomech. Abstr. 15, 249-257.

Griffith, A. A. 1920: The phenomenon of rupture and flow in solids. Phil. Trans. Roy. Soc. Lond. A 221, 163-198.

Handin, J. 1969: On the Coulomb-Mohr failure criterion. J. geophys. Res. 74, 5343-5348.

Hertzberg, R. W. 1976: Deformation and fracture mechanics of engineering materials. John Wiley & Sons, New York.

Inglis, C. E. 1913: Stresses in a plate due to the presence of cracks and shatrp corner. Trans. Inst. Naval Archit. 55, 219.

Karman, T. v. 1911: Festigkeitsversuche unter allseitigem Druck. Z. Verein dtsch. Ing. 55, 1749-1757.

Krahn, J. & Morgenstern, N. 1979: The ultimate frictional resistance of rock discontinuities. Int. J. rock Mech. Min. Sci. & Geomech. Abstr. 16, 127-133.
Lawn, B. 1993: Fracture of brittle solids. Cambridge University Press, Cambridge.
Logan, J. M., et al. 1979: Experimental study onf simulated gouge and their application to studies of natural fault zones. Proc. of Conf. VIII: Analysis of actual fault zones in bedrock. Geol. Survey Open File report U.S.79-1239,
Logan, J. M., et al. 1981: Laboratory studies on natural gouge from the U.S. geological survey Dry Lake valley no.1 well, San Andreas fault zone. Geophys. Monograph 24, 121-134.
Marone, C. & Scholz, C. H. 1989: Particle-size distribution and microstructures within simulated fault gouge. J. struct. Geol. 11, 799-814.
Mohr, O. 1900: Welche Umstände bedingen die Elastizitätsgrenze und den Bruch eines Materials ? Z. Verein dtsch. Ing. 44, 1524-1530, 1572-1577.
Paterson, M. S. 1978: Experimental rock deformation - the brittle filed. Springer-Verlag, Berlin.
Paterson, M. S. & Teng-fong Wong, 2005: Experimental rock deformation - (...) Springer-Verlag, Berlin.
Sangha, C.M., Talbot, C.J., Dhir, R.K., 1974. Microfracturing of a sandstone in uniaxial compression. Int. J. Rock Mech. Min. Sci., Abstr. Vol. 11, 107-113
Scholz, C. H. 1968: Experimental study of the fracturing process in brittle rock. J. G. R. 73, 1447-1449.
Segall, P. & Pollard, D. D. 1980: Mechanics of discontinuous faults. J. geophys. Res. 85, 4337-4350.
Shimamoto, T. & Logan, J. M. 1981: Effects of simulated fault gouge on the sliding behaviour of Tennessee sandstone: nonclay gouges. J. geophys. Res. 86, 2902-2914.
Sobolev G, Spetzler H., Salov,B., 1978.
Precursors to failure in rocks while undergoing anelastic deformation. JGR 83, 1775-1784
Teufel, L. W. & Logan, J. K. 1978: Effect of displacement rate oon the real area of contact anfd temperatures generated during frictional sliding of Tennesse sandstaone. Pageophys. 116, 840-865.
Tullis, J. & Yund, R.A., 1977: Experimental deformation of dry Westerly granite. J.G.R. 82, 5705-5718

8

Cataclasites: grain size, shape and fractals

Deformationsprozesse in der Erde (8) (8b)

cataclasites: grain size, shape and fractals

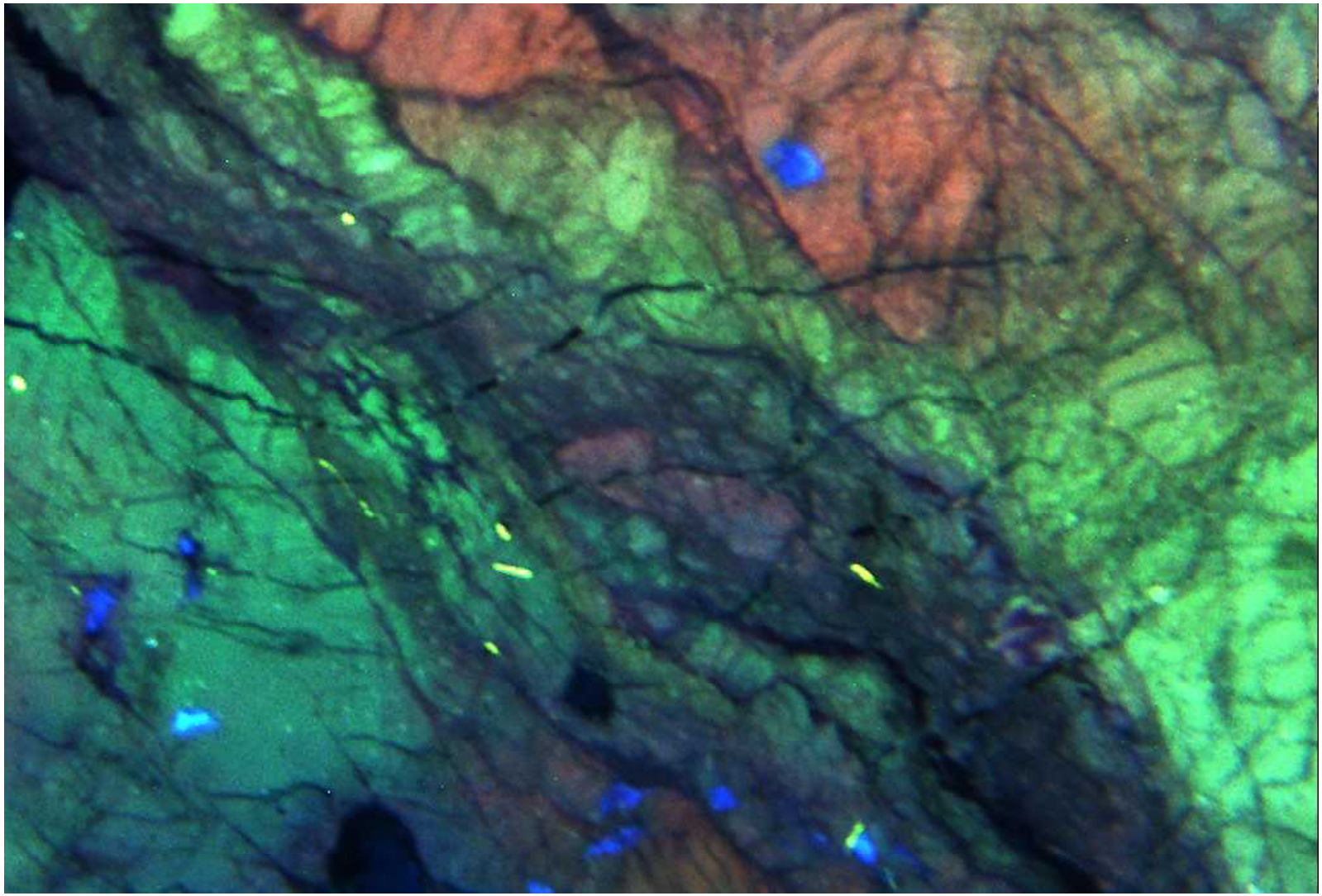

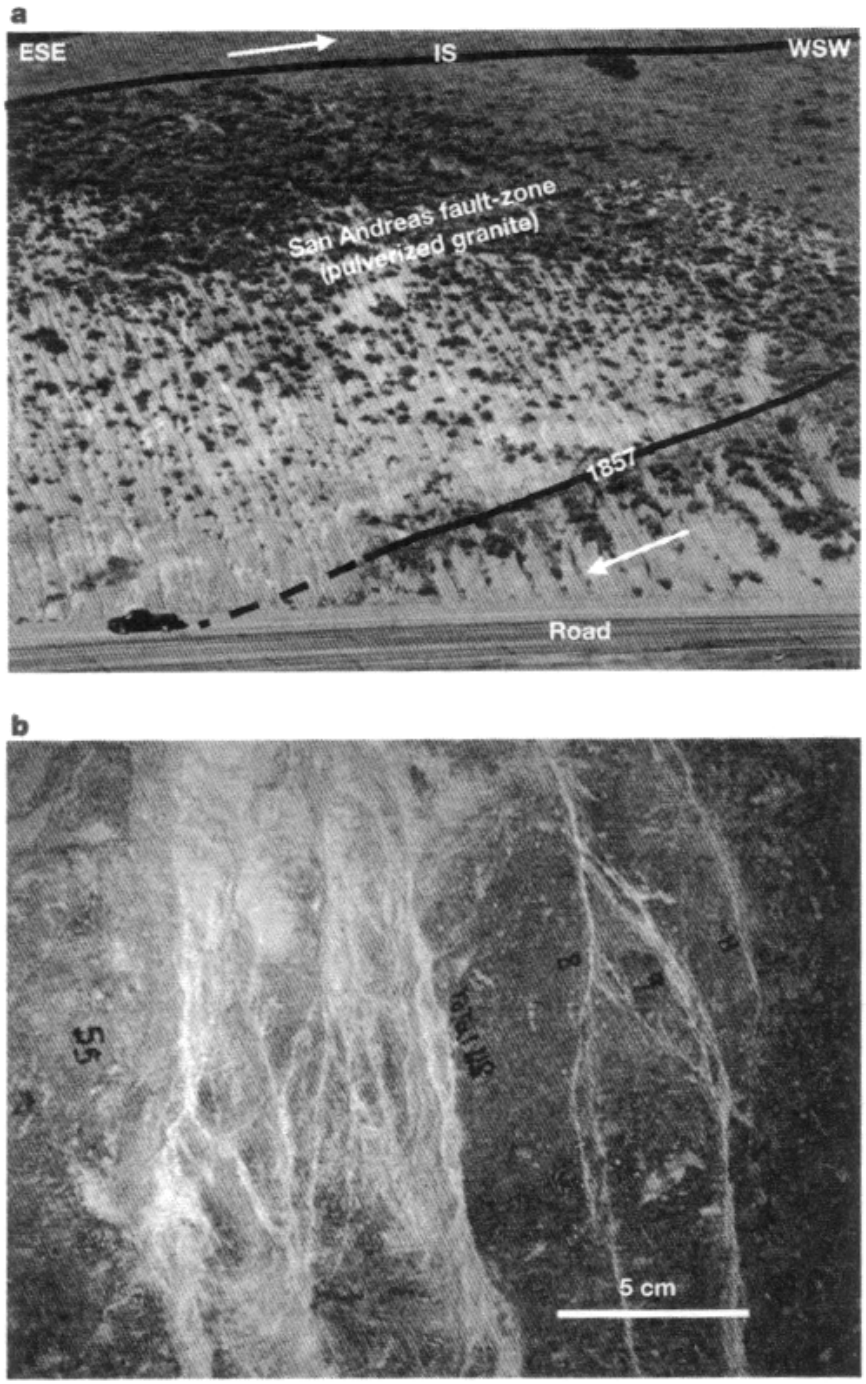

Wilson et al. 2005, Nature 434, p.749

Figure 1 Field setting of the investigated faults. **a**, The San Andreas fault-zone at Tejon Pass, California. The car is shown for scale. IS, inactive fault segment; 1857, slipping segment of the 1857 earthquake. Note the gouge zone 70–100 m wide with badland morphology of the pulverized granite. This exposure and its extensions were mapped, and hundreds of gouge samples were collected. **b**, Close-up view of the fractured zone of the Bosman fault (text). The white striations are coalescing fractures filled with gouge powder (rock flour) that cut across the solid, dark quartzite.

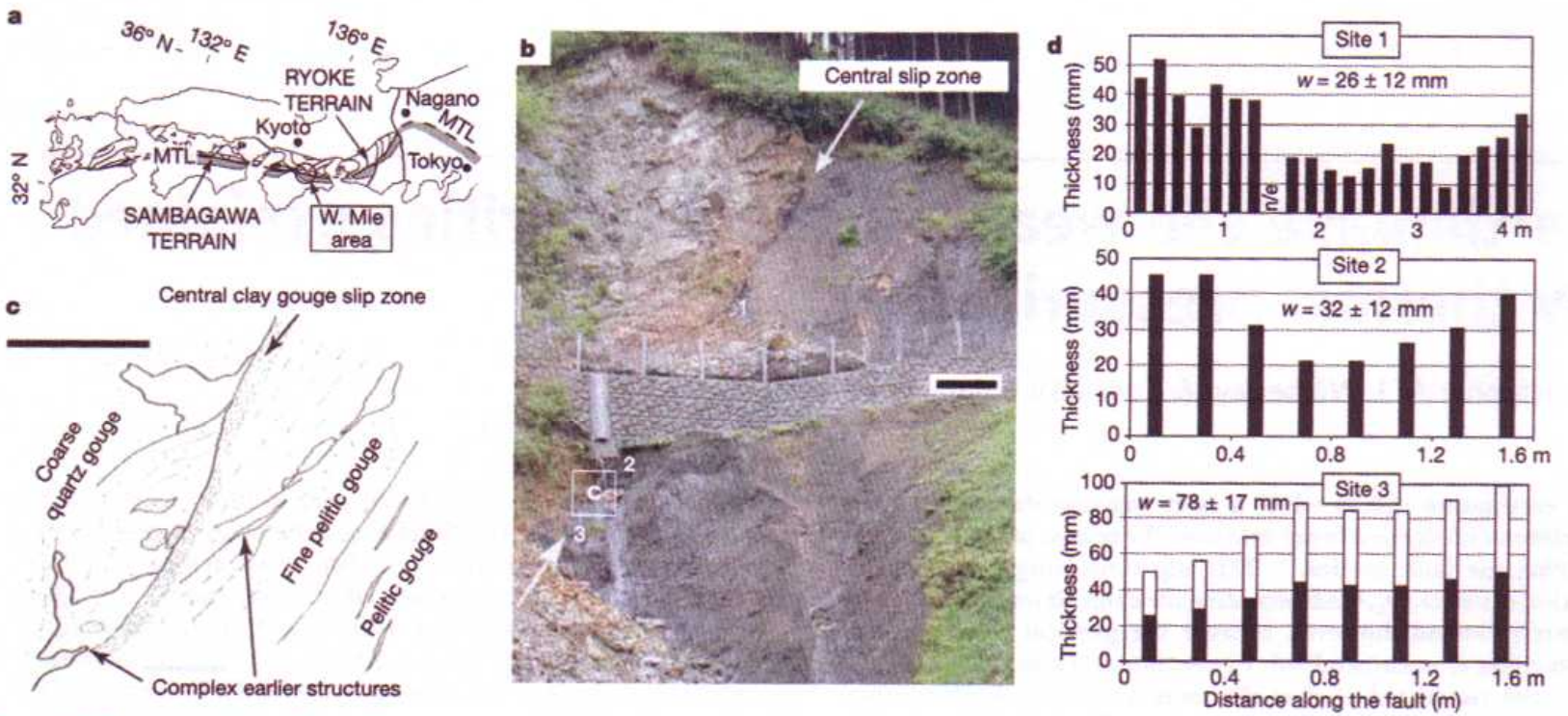

Figure 1 | The nature of a localized slip zone in a large geological fault. **a**, The Median Tectonic Line (MTL) in southwestern Japan. **b**, View facing east of the MTL fault zone in western Mie (scale bar, 2 m). **c**, Sketch of the details of the slip zone and its vicinity (scale bar, 0.3 m). **d**, Variation in slip zone widths w along the exposed slip zone in three different sites (shown in **b**), with average and one standard deviation shown for each site. At site 3, the gradational nature of one edge is indicated by the white part of the bar.

Wibberley & Shimamoto 2005, Nature 436, p.689

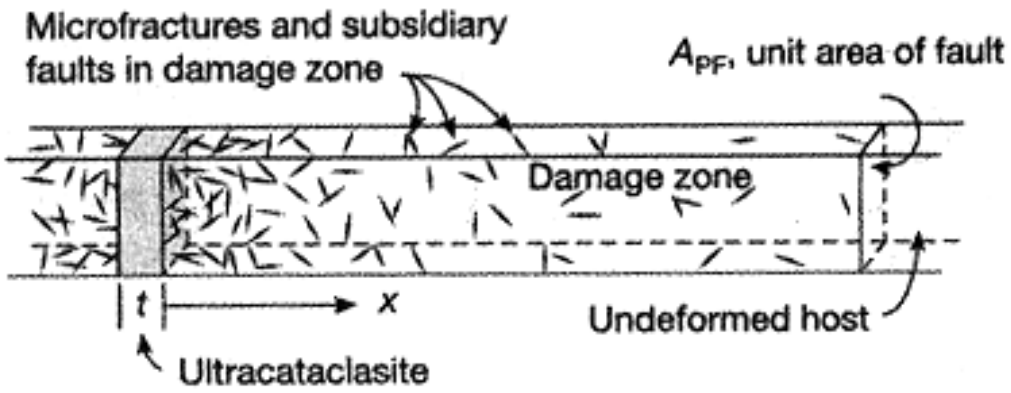

Figure 2 | Structural model of the Punchbowl fault zone for calculating fracture surface area. Domains of damaged rock containing subsidiary faults and microfractures are bounded by undeformed host rock. The central core of the fault contains an ultracataclasite layer of thickness t. Total fracture surface area, $S_T = S_{UC} + S_{SF} + S_{MF}$, is determined within the column of rock across the entire fault zone of cross-sectional area $A_{PF} = 1\,m^2$. Calculations assume damage is symmetric about the ultracataclasite layer.

Chester et al. 2005, Nature 437, p.133

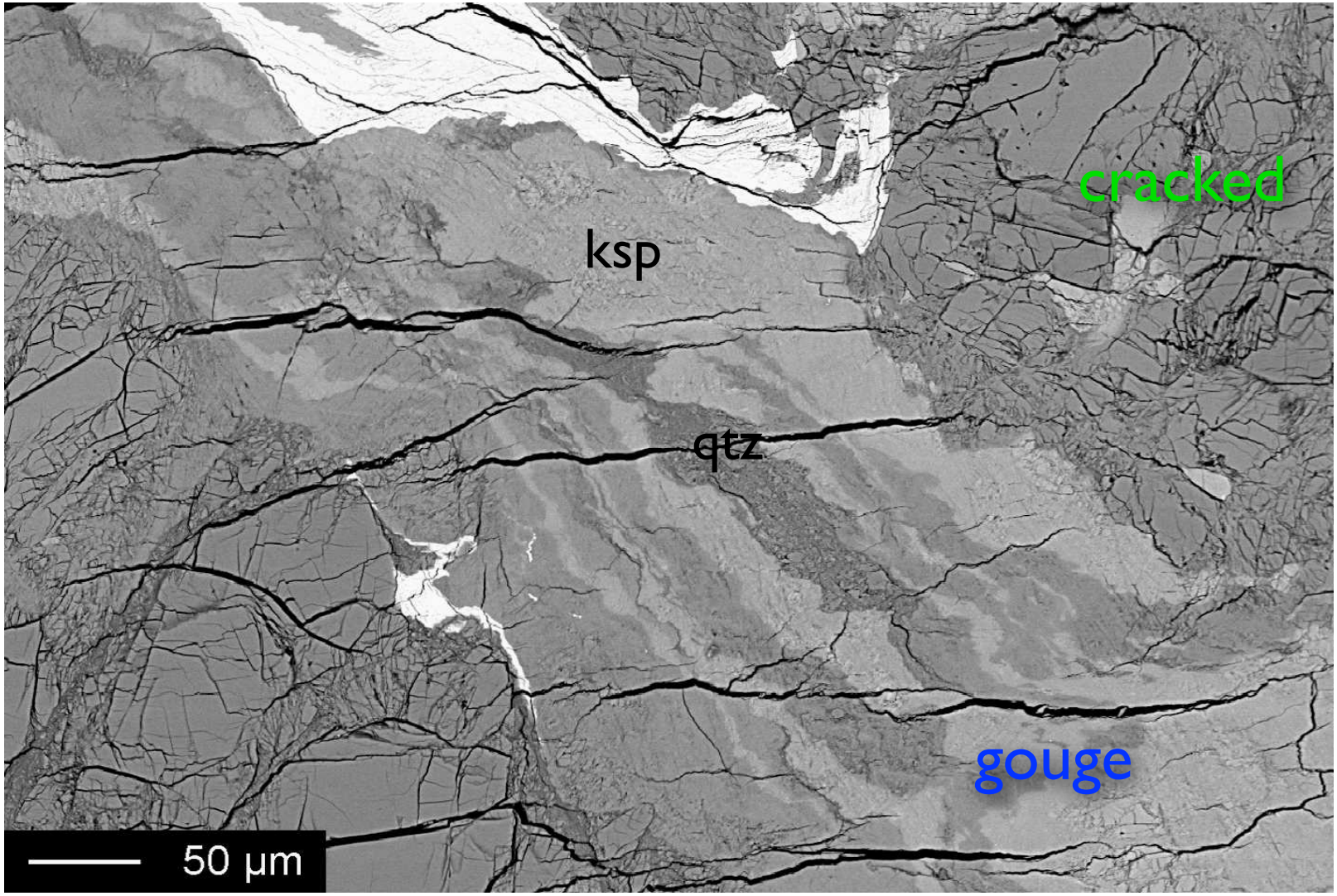

experimentally produced fault rock

General idea:

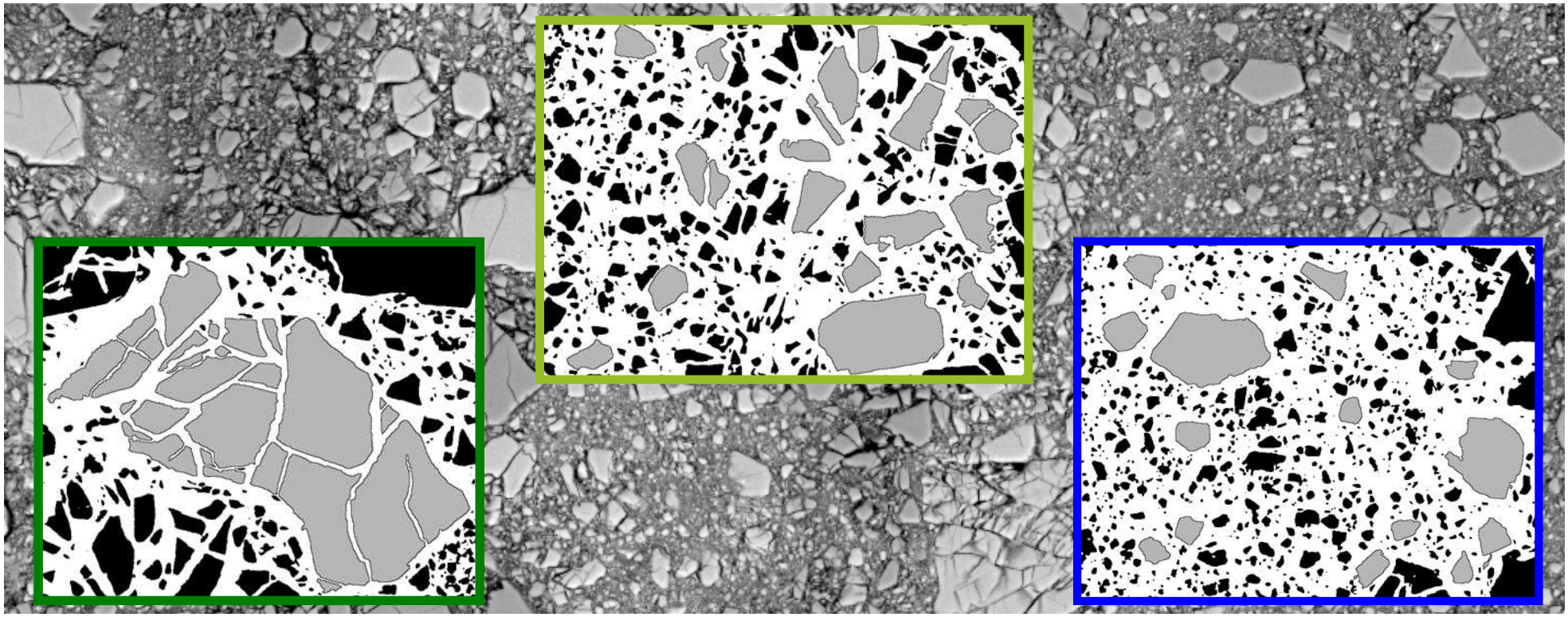

intact rock - faulting - healing - intact rock

cracked in situ - cracked moved - - - - - - gouge

phase mixing

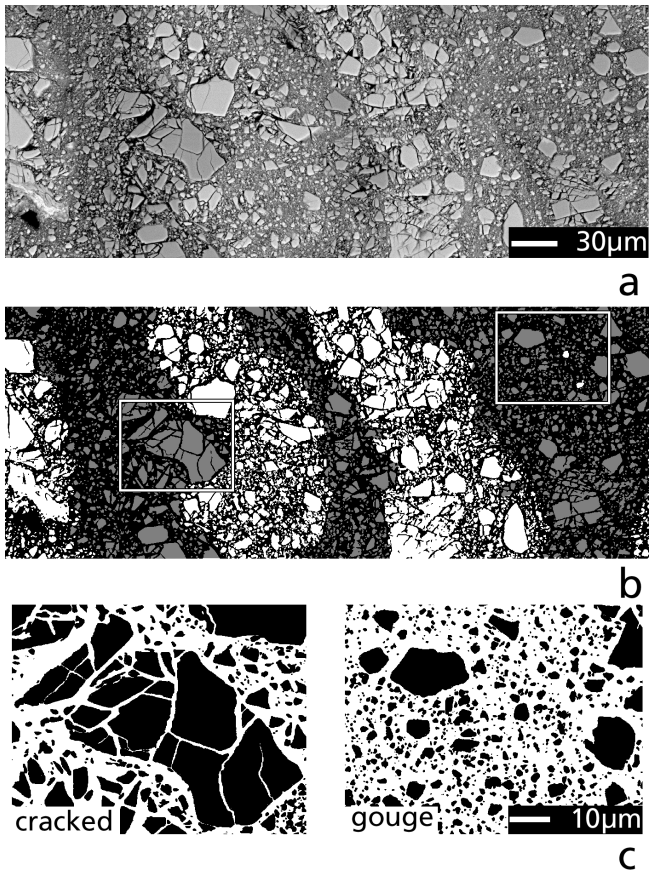

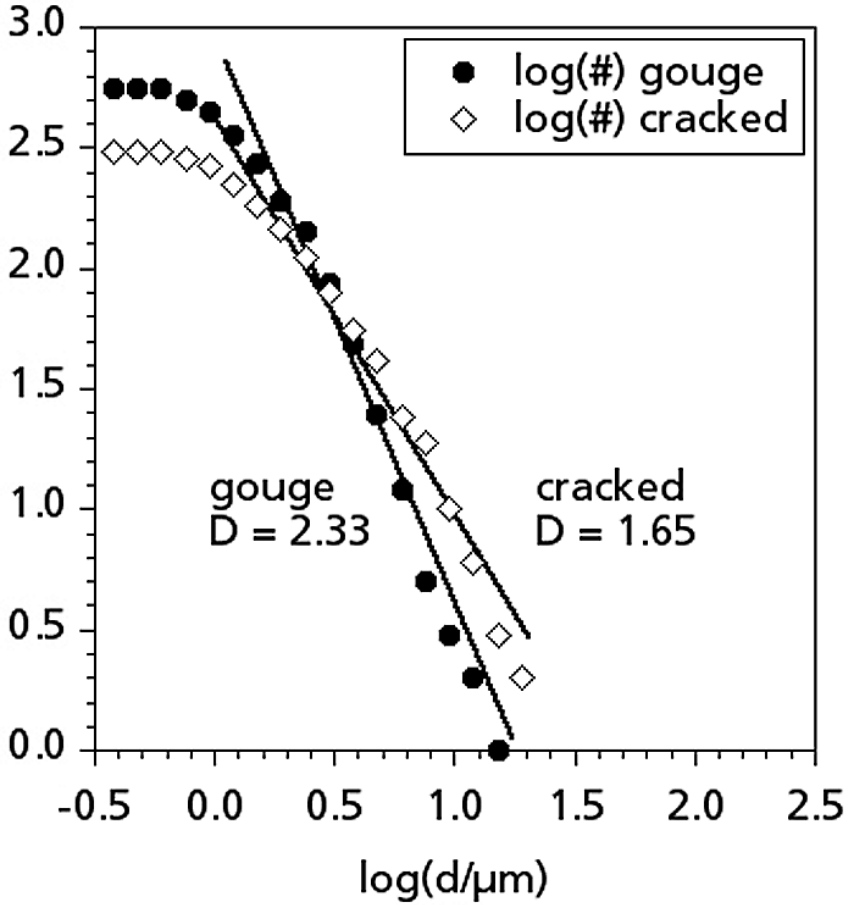

experimentally produced fault rock

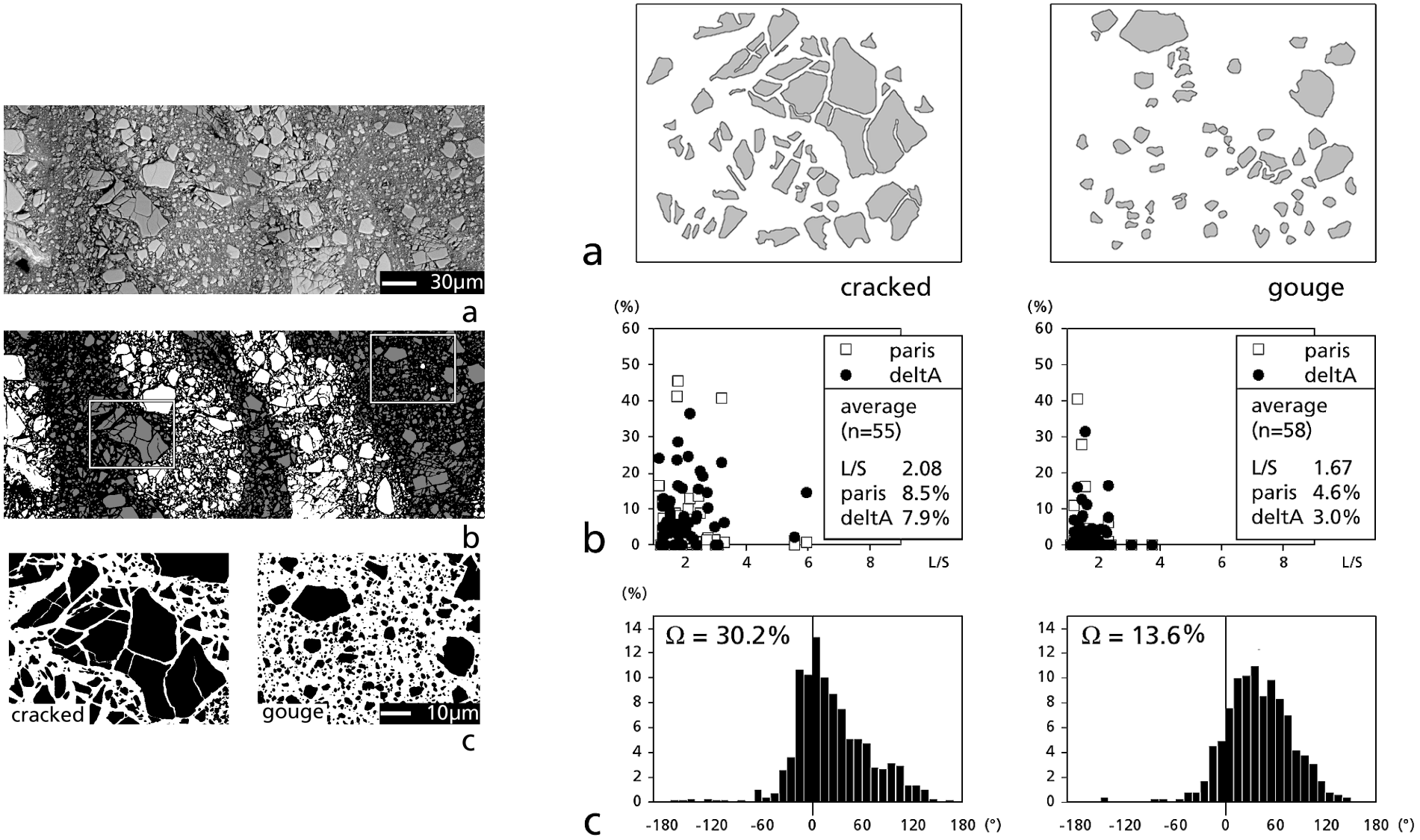

experimentally produced fault rock

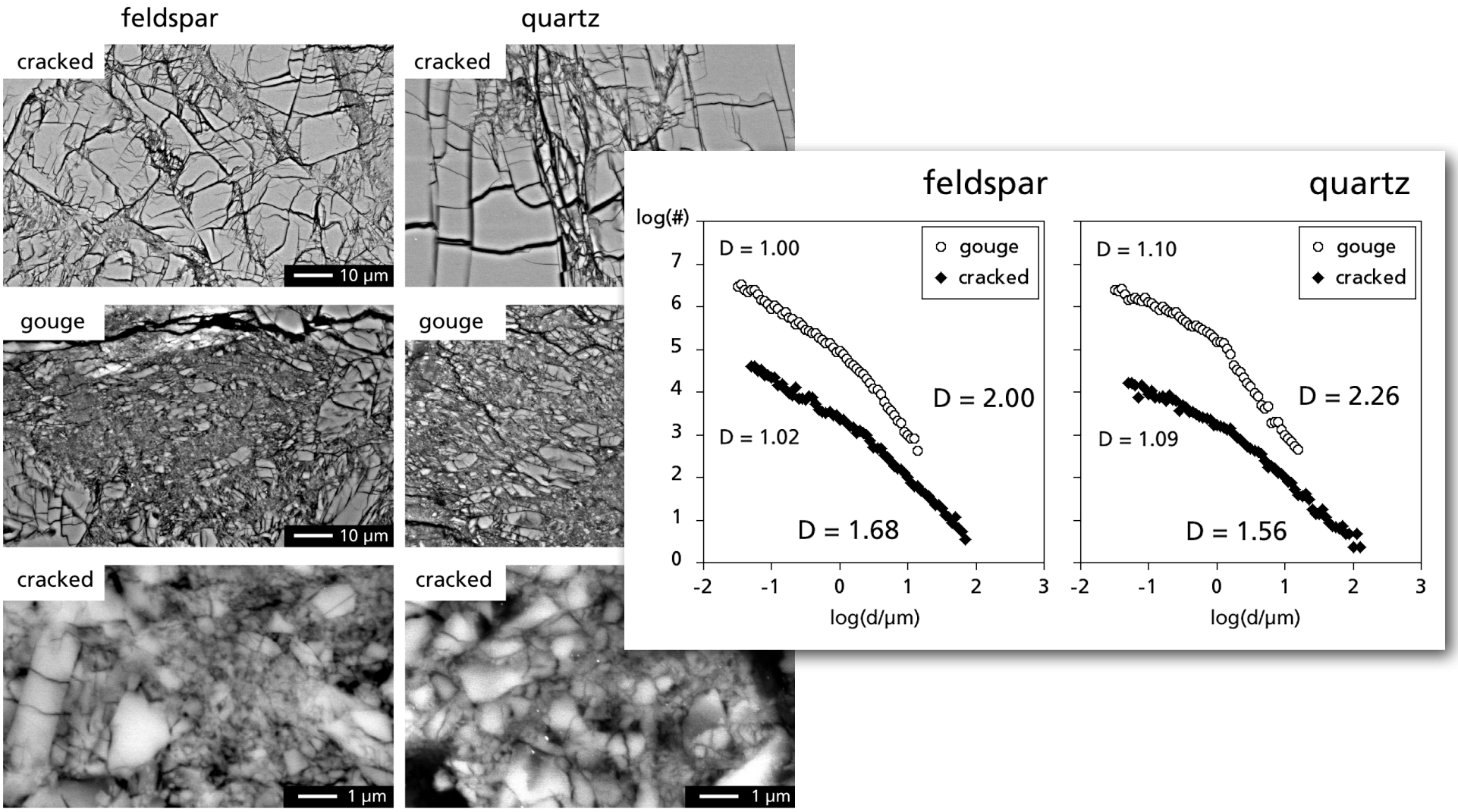
feldspar
quartz
cracked
cracked
10 µm
gouge
gouge
10 µm
cracked
cracked
1 µm
1 µm
feldspar
quartz
log(#)
D = 1.00
gouge
cracked
D = 2.00
D = 1.02
D = 1.68
D = 1.10
gouge
cracked
D = 2.26
D = 1.09
D = 1.56
log(d/µm)
log(d/µm)

Spatial distribution of grain size distribution
D-mapping

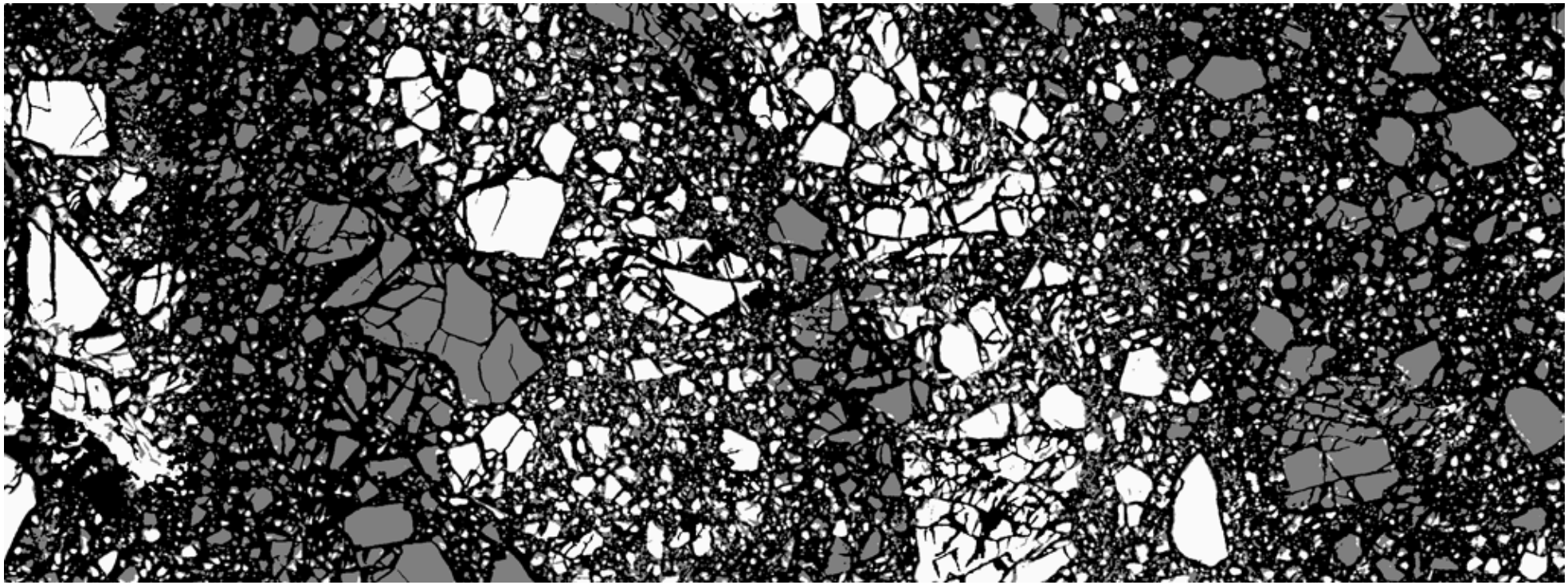

	area of matrix	measured D
qtz fractured (grey)	38%	1.6
qtz gouge (grey)	68%	2.0

Grain size distribution - "Fractal dimension"

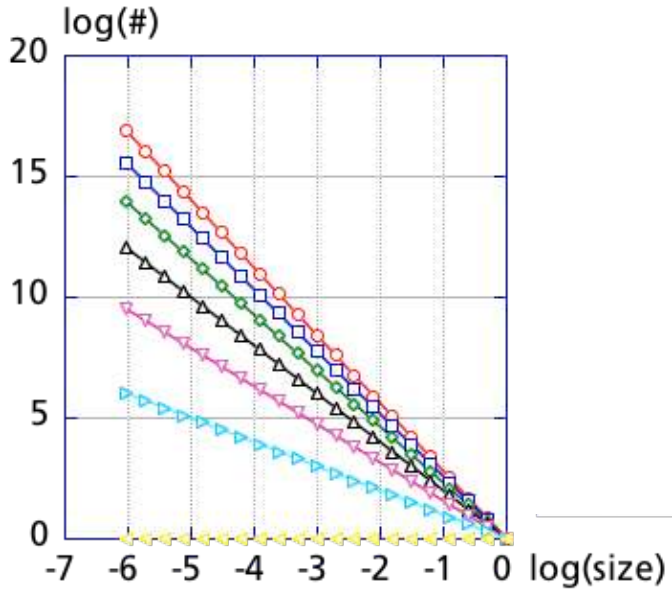

	D
1	2.8074
2	2.5850
3	2.3219
4	2.0000
5	1.5850
6	1.0000
7	0.0000

$E = 3-D$

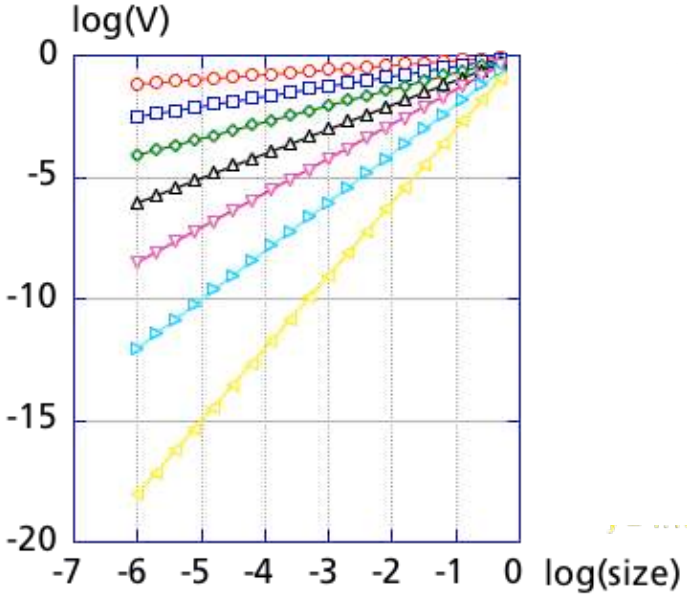

	E
1	0.1926
2	0.4150
3	0.6781
4	1.0000
5	1.4150
6	2.0000
7	3.0000

Grain size distribution 2D - 3D

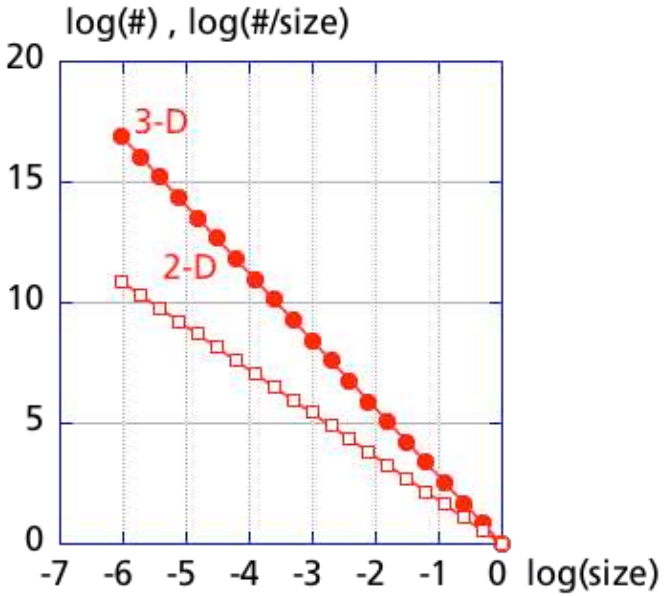

probability of sectioning cube
is inverse proportional to size:

D(3D) - 1.00 = D(2D)

Grain size distribution

D	area% (size<1/8) (chessboard)	area% (size<1/16)
2.81	66.99	58.62
2.58	42.19	31.64
2.32	24.41	15.26
2.00	12.50	6.25
1.58	5.27	1.98
1.00	1.56	0.39
0.00	0.20	0.02

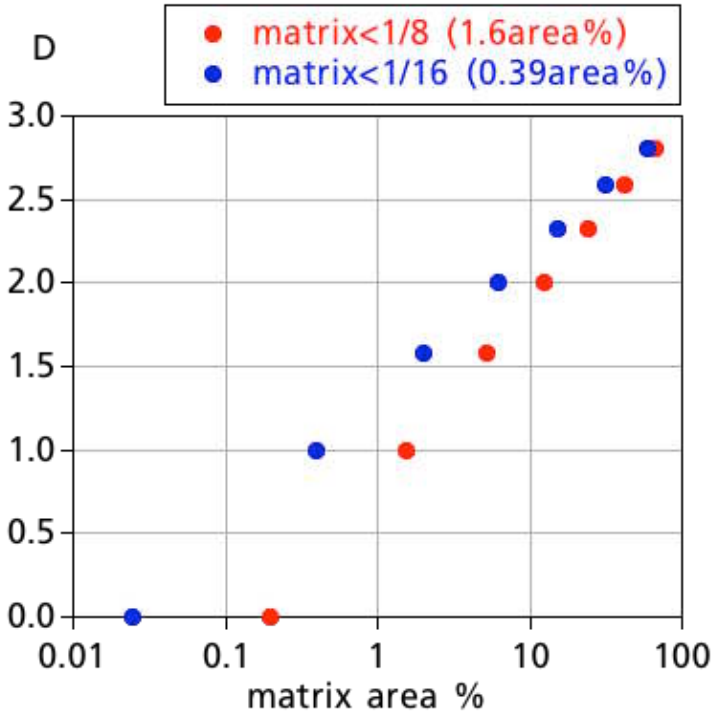

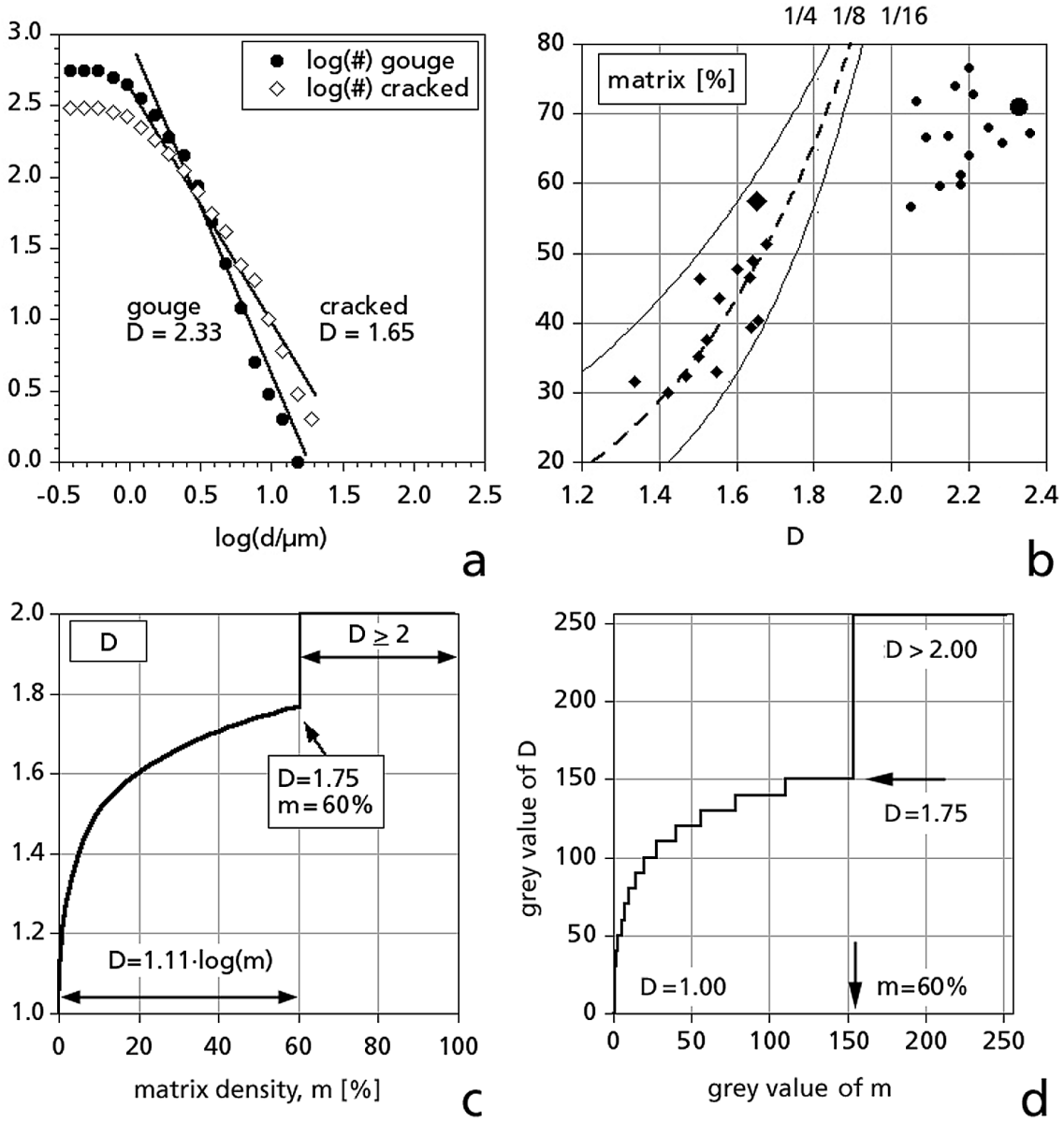
log(#) gouge
log(#) cracked
gouge
D = 2.33
cracked
D = 1.65
log(d/µm)
a
1/4 1/8 1/16
matrix [%]
D
b
D
D ≥ 2
D=1.75
m=60%
D=1.11·log(m)
matrix density, m [%]
c
D > 2.00
D=1.75
D=1.00
m=60%
grey value of D
grey value of m
d

D-map

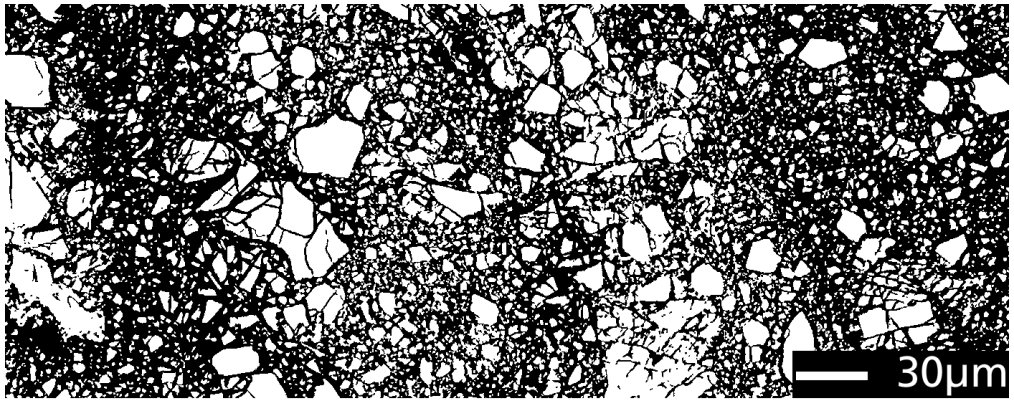

a

b

matrix 0% 50% 100%

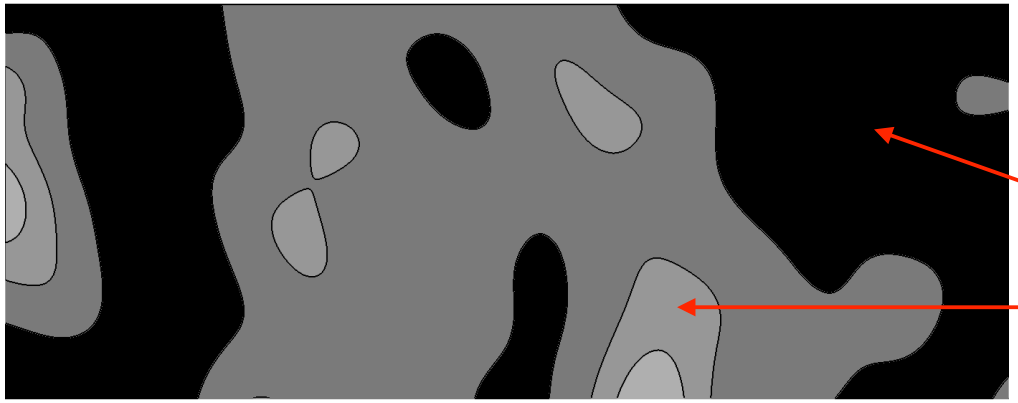

c

D 1.55 1.65 1.75 > 2.00

high D

low D

D-map

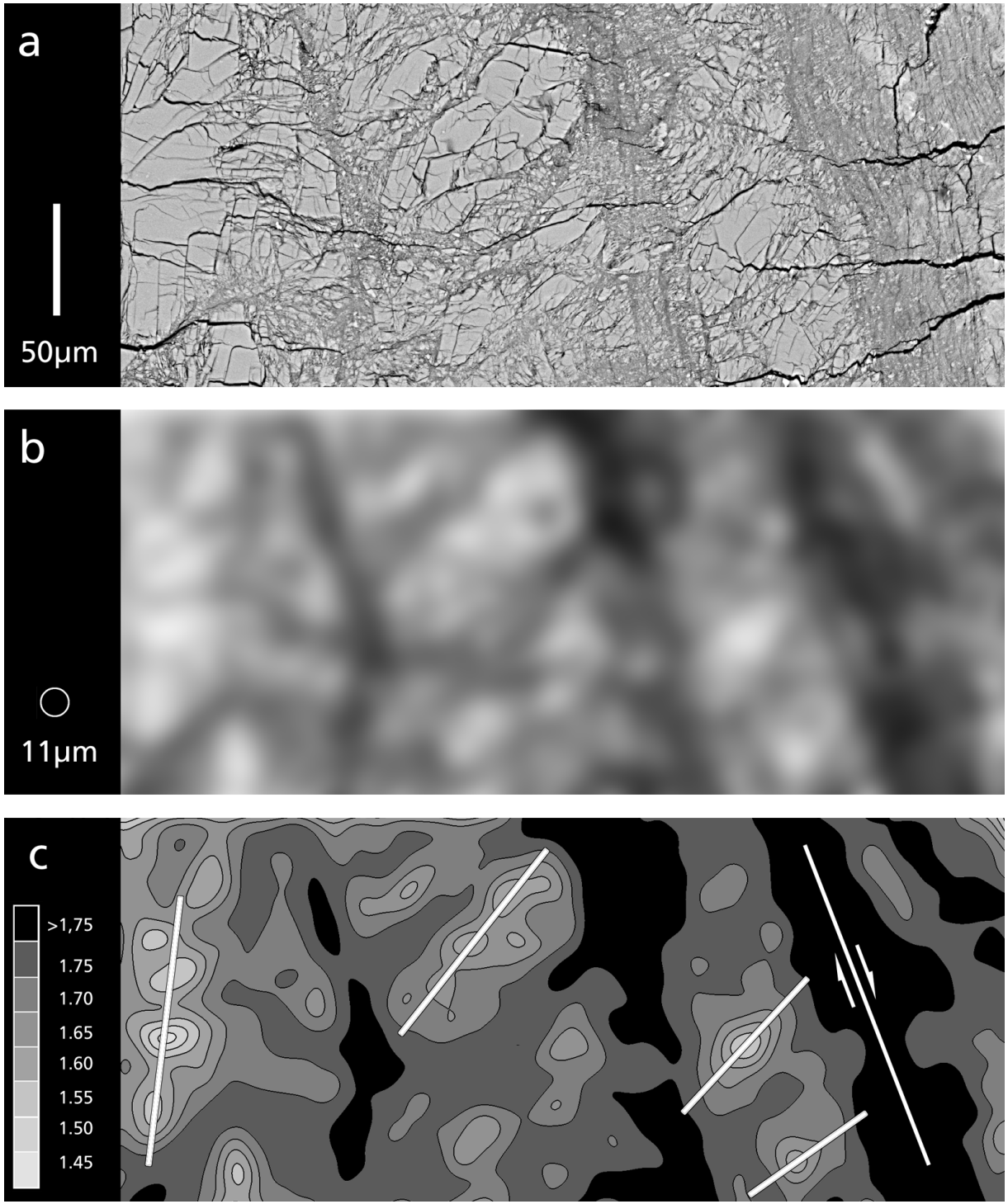

D-map

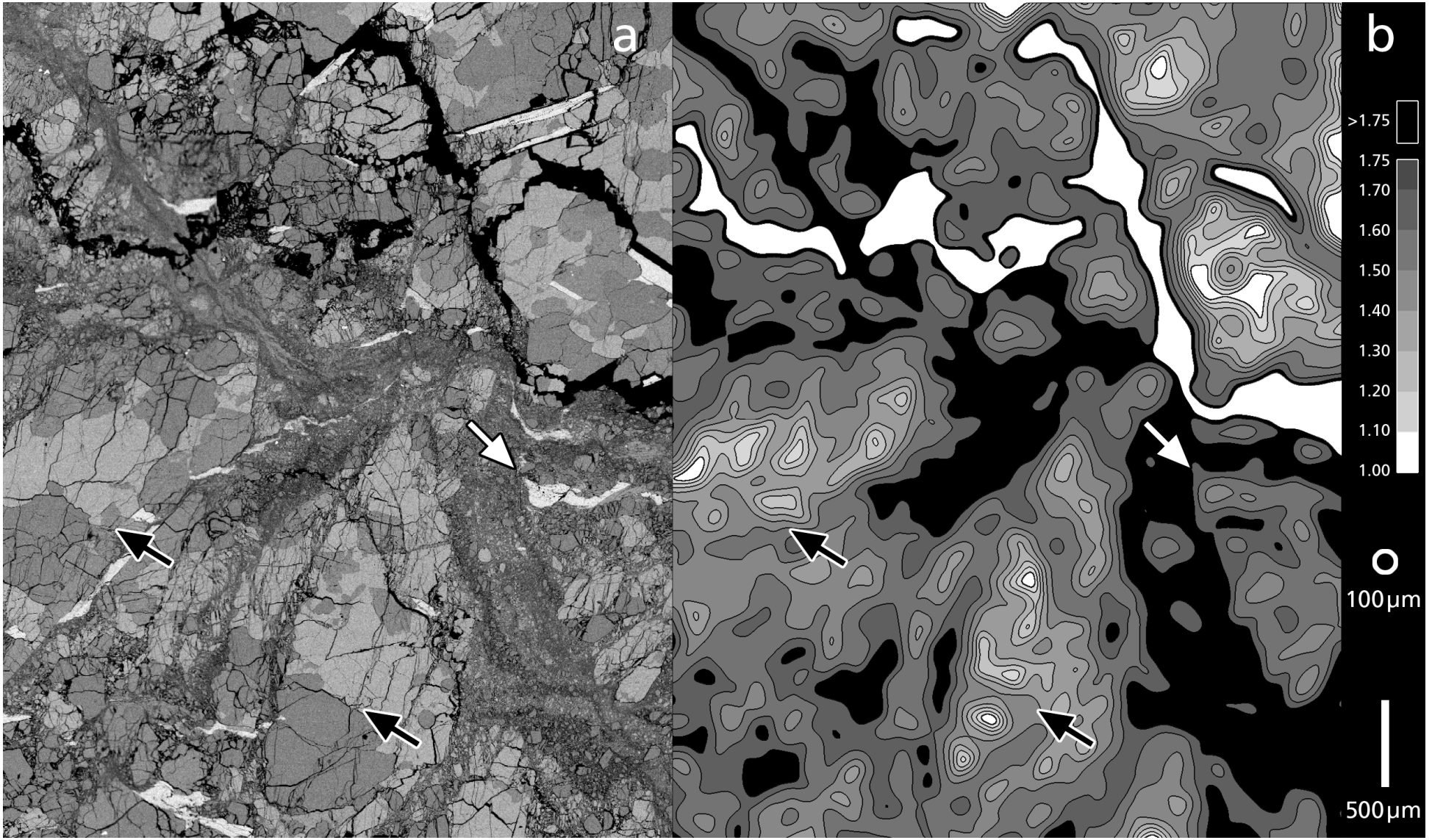

Grain size distribution of Nojima fault rock

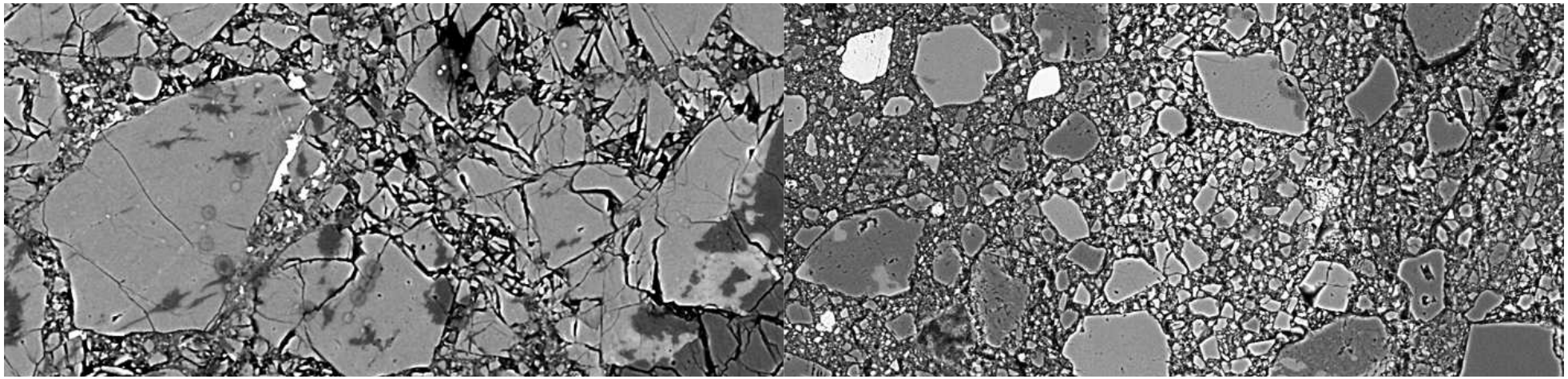

CRACKED

GOUGE

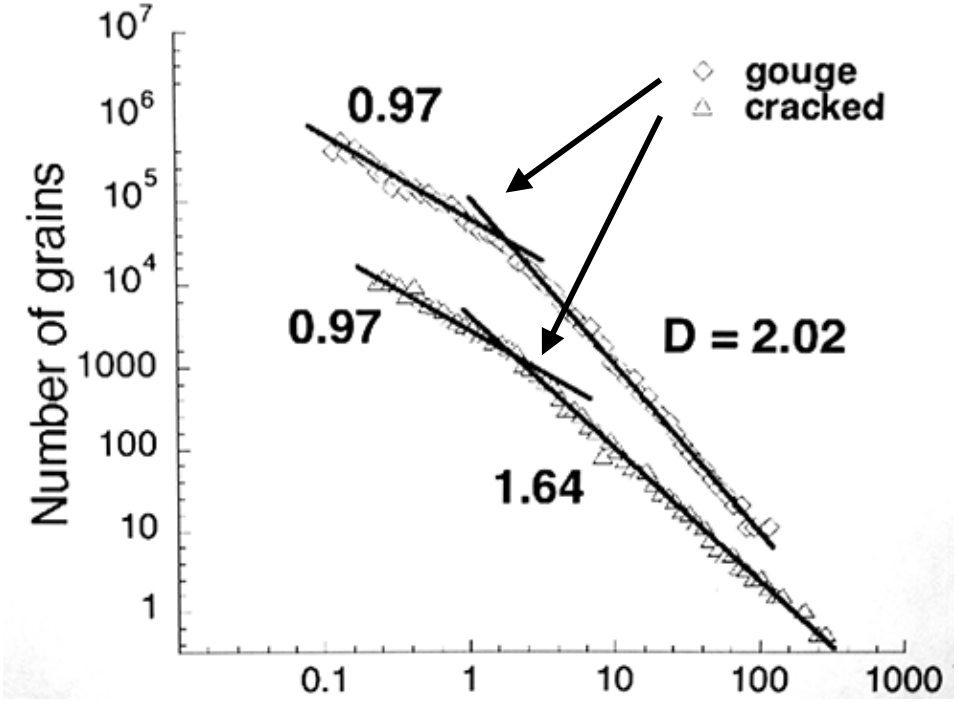

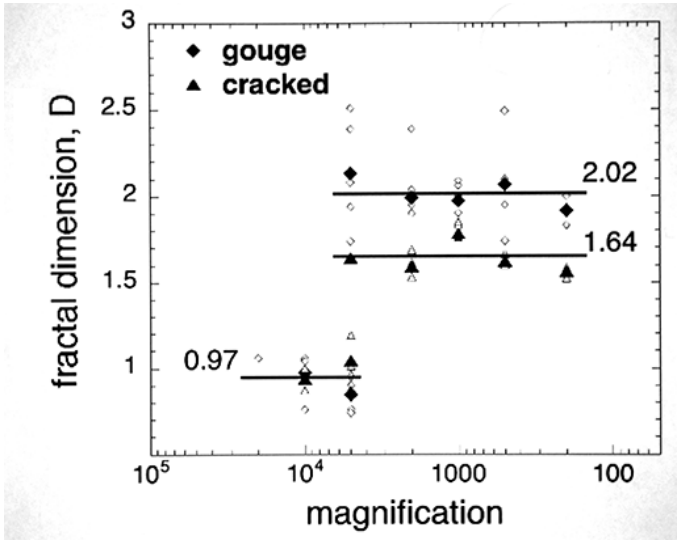

Grain size (μm)

=> Shape descriptors based on:

"excess" perimeter	PARIS factor (%) deltP (%)
"excess" area	deltA (%)
convex/concave vertices	histogram of angles mean, range, angles < 0°

cracked in situ
cracked moved
gouge

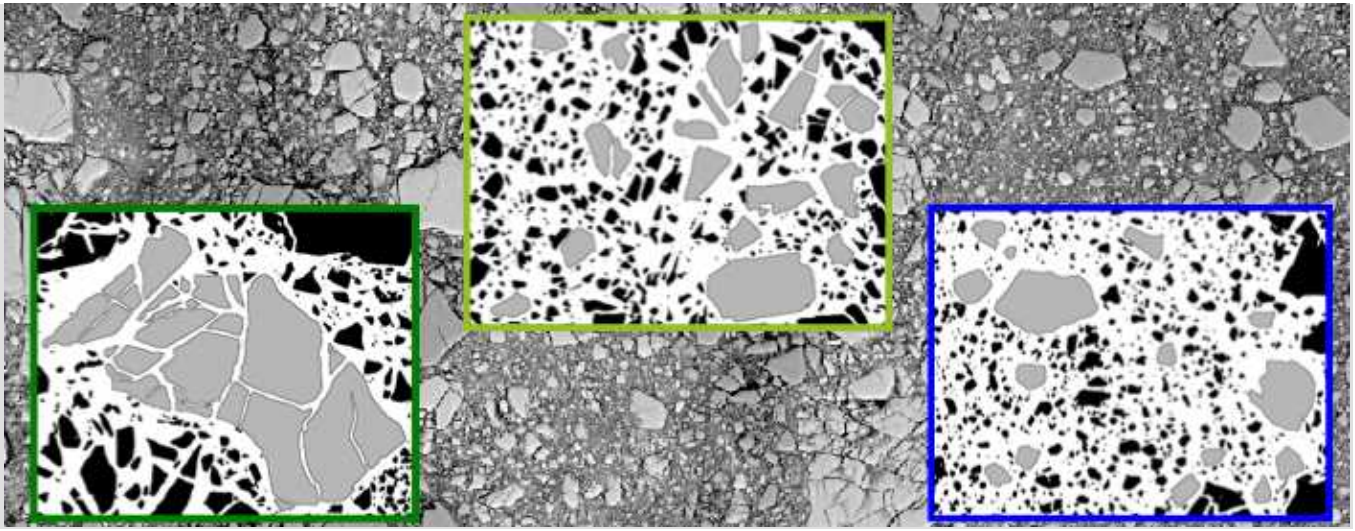

Shape

LONG AXIS	L	longest projection
SHORT AXIS	S	shortest projection
PERIMETER	P	length of original outline
AREA	A	area of original shape
EQUIVALENT PERIMETER	P_{equ}	perimeter of circle with same area $= 2\pi R_{equ}$; where $R_{equ} = \sqrt{(A/\pi)}$

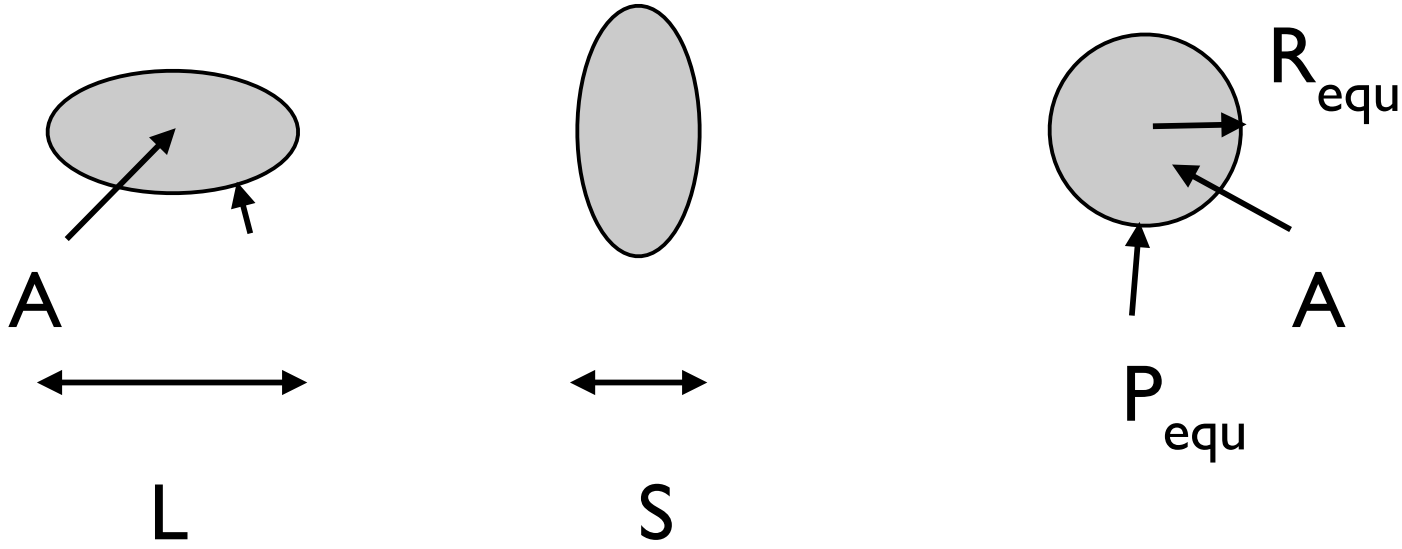

Shape

PERIMETER OF ENVELOPE	E	length of outline of envelope
AREA OF ENVELOPE	AE	area of outline envelope

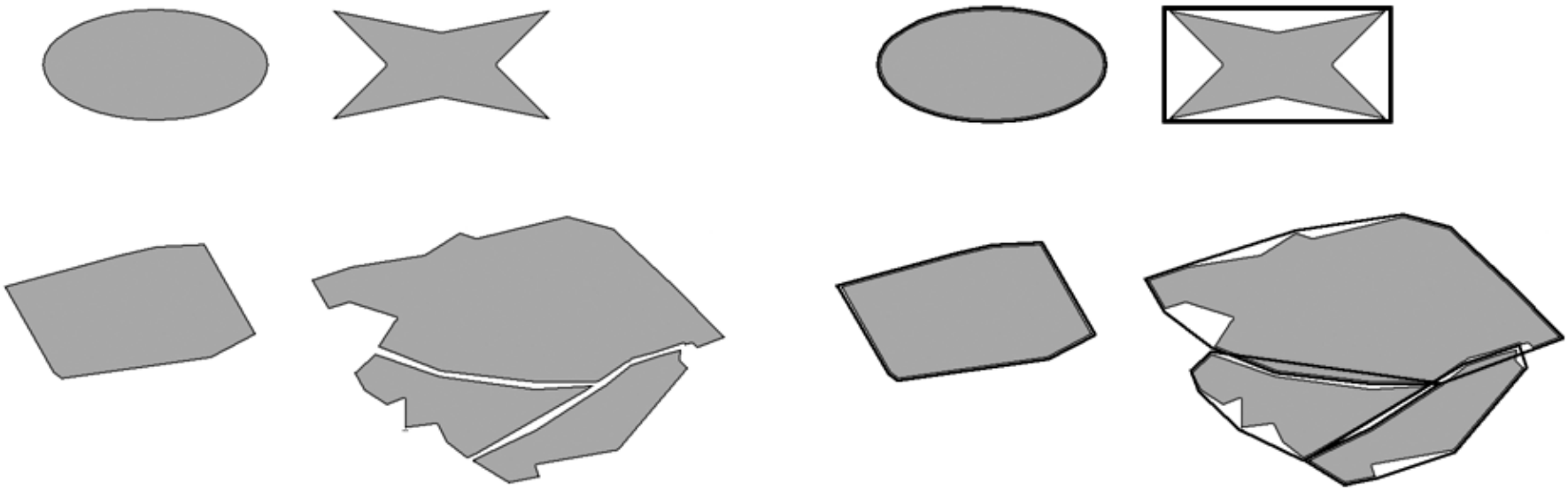

Shape

SHAPE FACTOR F P / P_{equ} (so-called "fractal dimension")

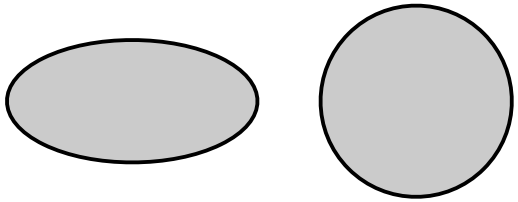

EXCESS PERIMETER
PARIS(%) $2 \cdot ((P-E) / E) \cdot 100$
deltP(%) $((P-E) / P) \cdot 100$

EXCESS AREA
deltA(%) $((AE-A) / AE) \cdot 100$

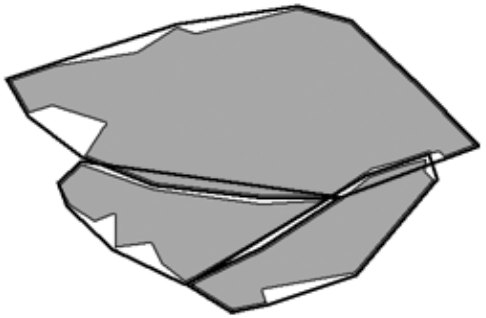

Angles

ANGLE AT VERTEX:

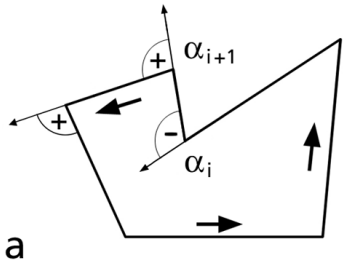

a

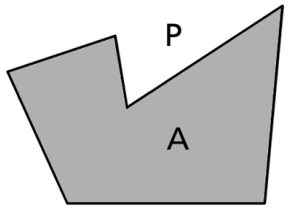

PE

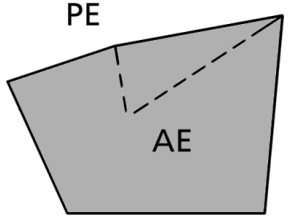

b

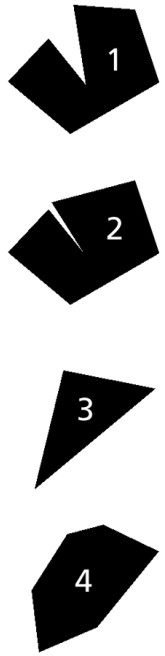

c

SUM OF ANGLES OF POLYGON
$\sum\alpha = 360°$

POSITIVE ANGLES = CLOSING
CONVEX $\alpha > 0°$
CONCAVE $\alpha < 0°$

MEAN $\sum [h(\alpha) \cdot \alpha]$ where $\sum h(\alpha) = 1.00$

ANGLE < 0° $\sum [h(\alpha) \cdot \alpha]$ for $\alpha < 0°$

EXTREMA α_{max} and α_{min}

RANGE $\alpha_{max} - \alpha_{min}$

Shape

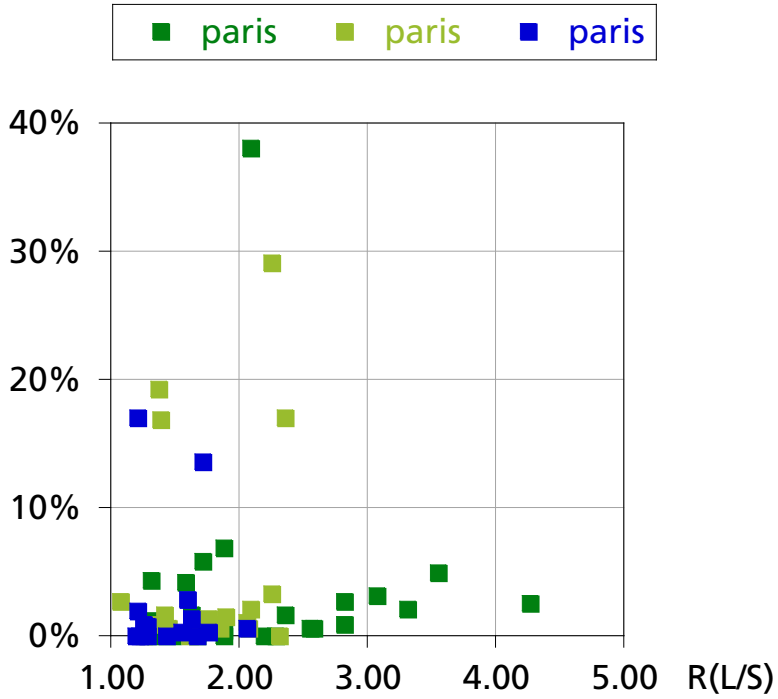

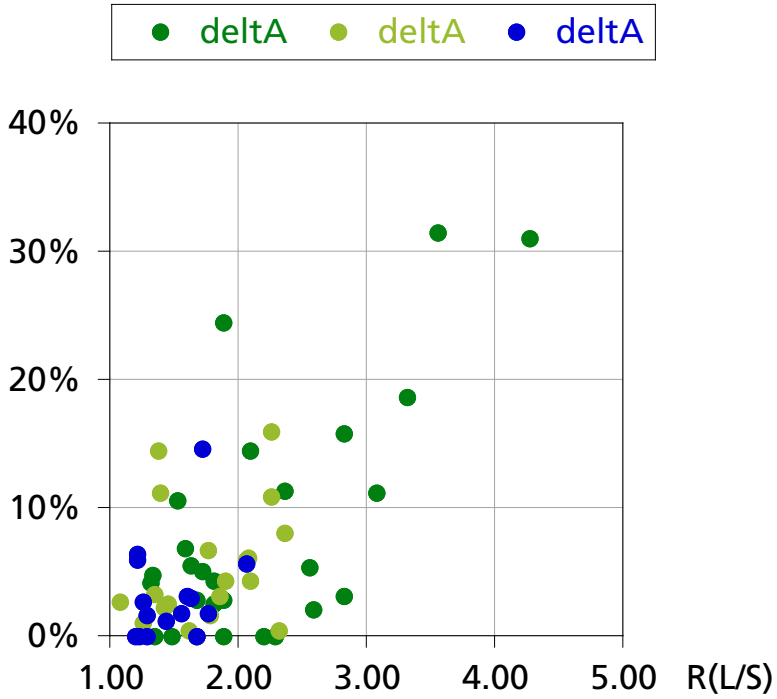

measures of concavity / lobateness vs. aspect ratio:

paris = indented surface area %

deltA = excess area of envelope %

cracked in situ

cracked moved

gouge

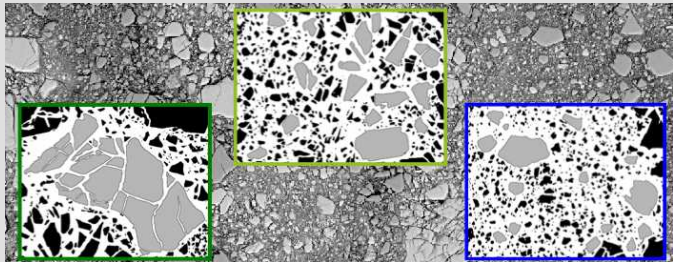

Angles

positive = convex
negative = concave

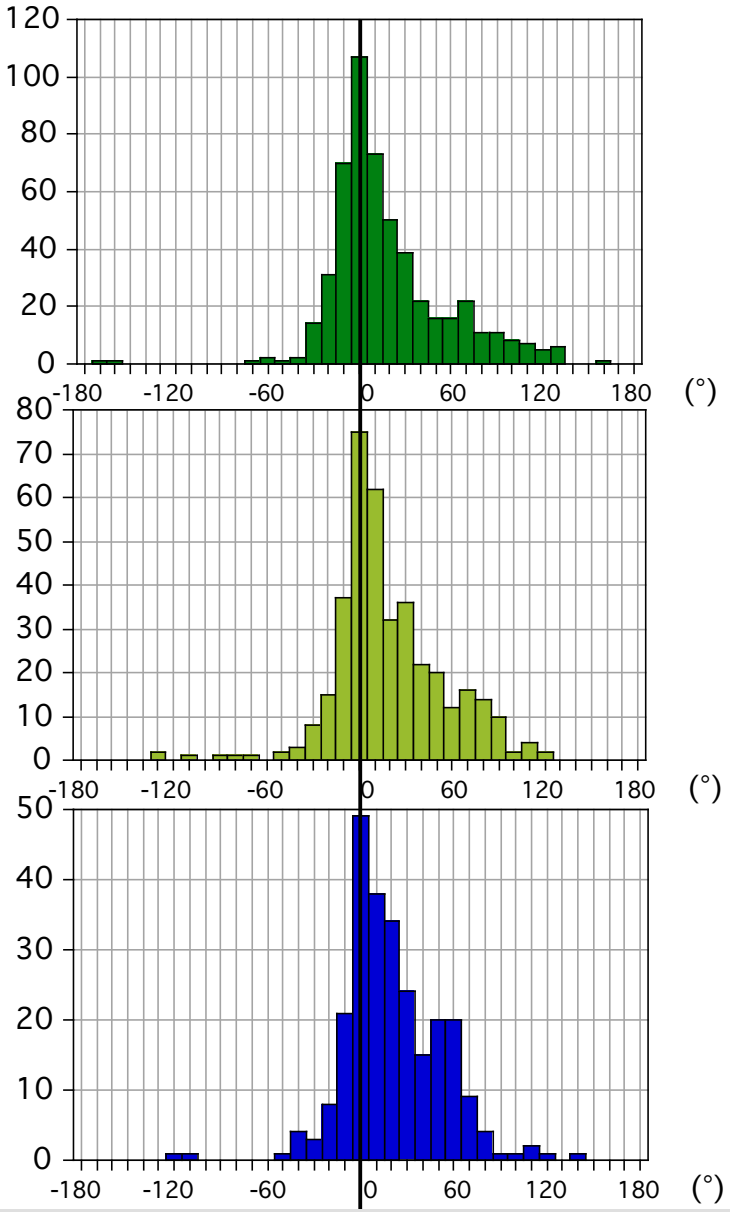

	% <0°	median	std.dev.
cracked in situ	28.4	8.943	38.009
cracked moved	24.0	11.916	35.524
gouge	17.8	16.144	32.144

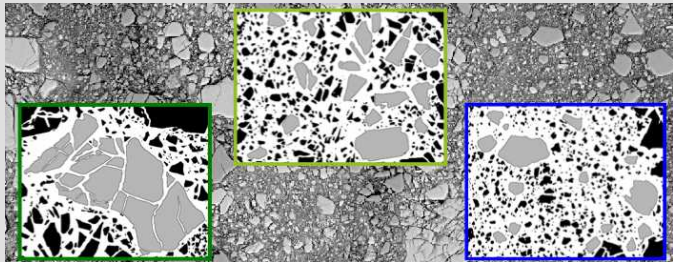

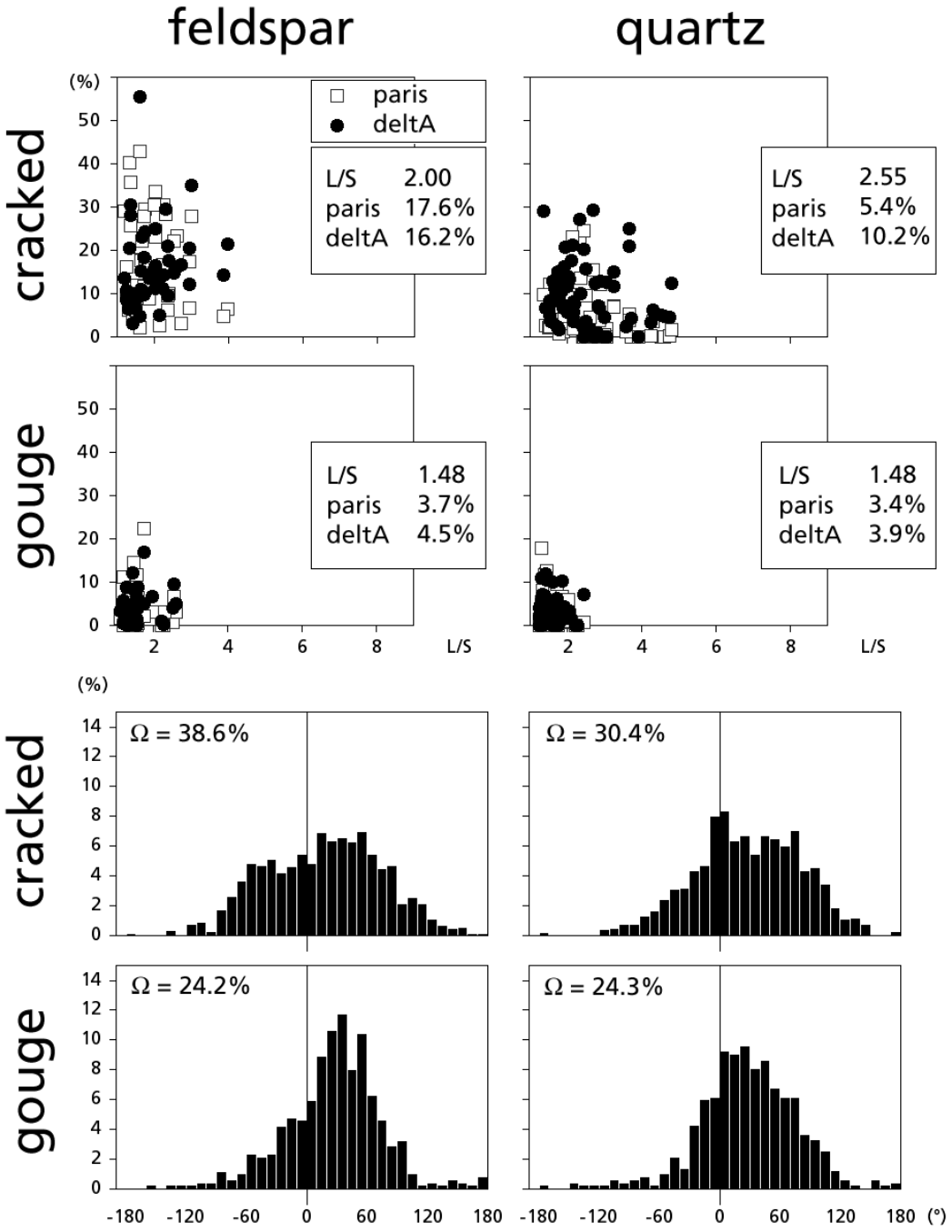
feldspar
quartz
cracked
gouge
(%)
paris
deltA
L/S 2.00
paris 17.6%
deltA 16.2%
L/S 2.55
paris 5.4%
deltA 10.2%
L/S 1.48
paris 3.7%
deltA 4.5%
L/S 1.48
paris 3.4%
deltA 3.9%
L/S
Ω = 38.6%
Ω = 30.4%
Ω = 24.2%
Ω = 24.3%
(°)

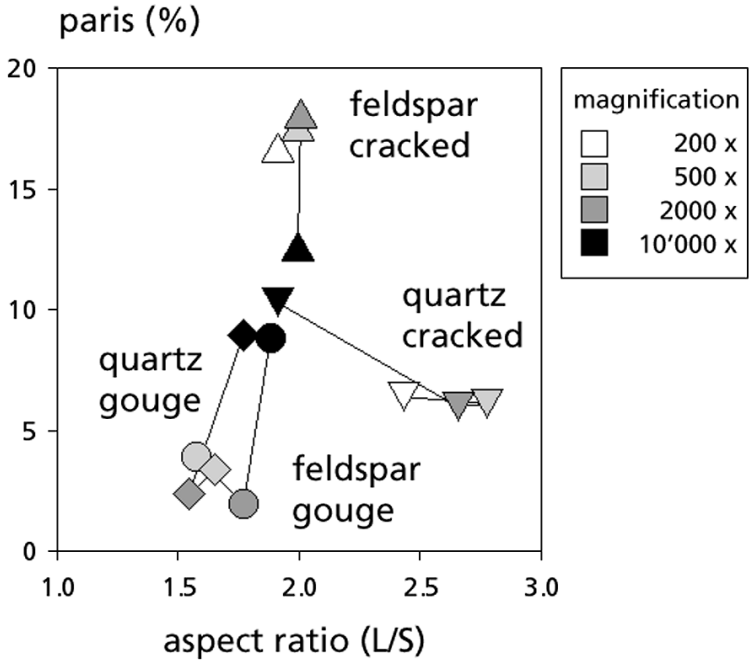
paris (%)
feldspar cracked
quartz cracked
quartz gouge
feldspar gouge
magnification
200 x
500 x
2000 x
10'000 x
aspect ratio (L/S)

Shapes & angles of Nojima fault rock

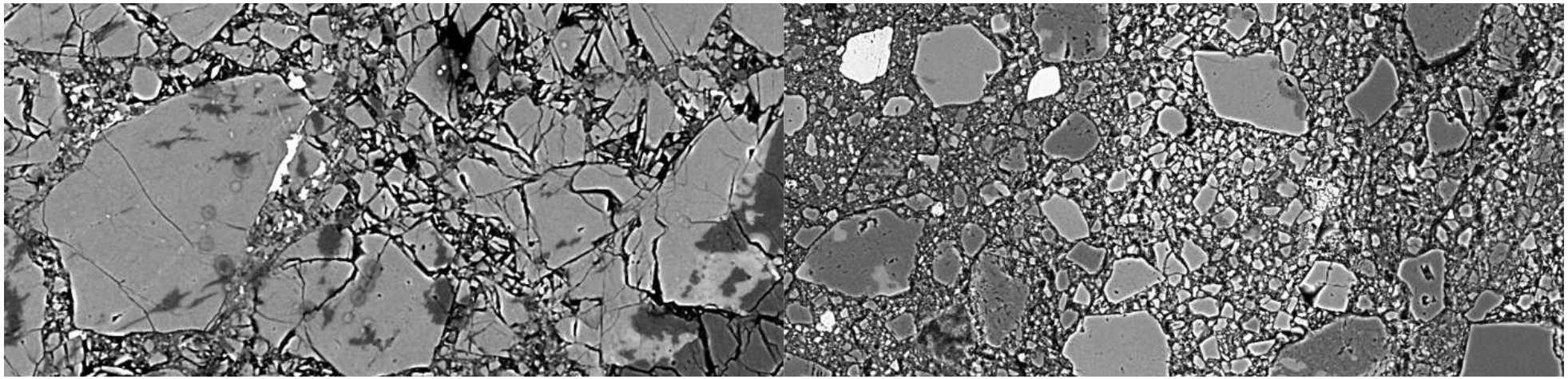

CRACKED

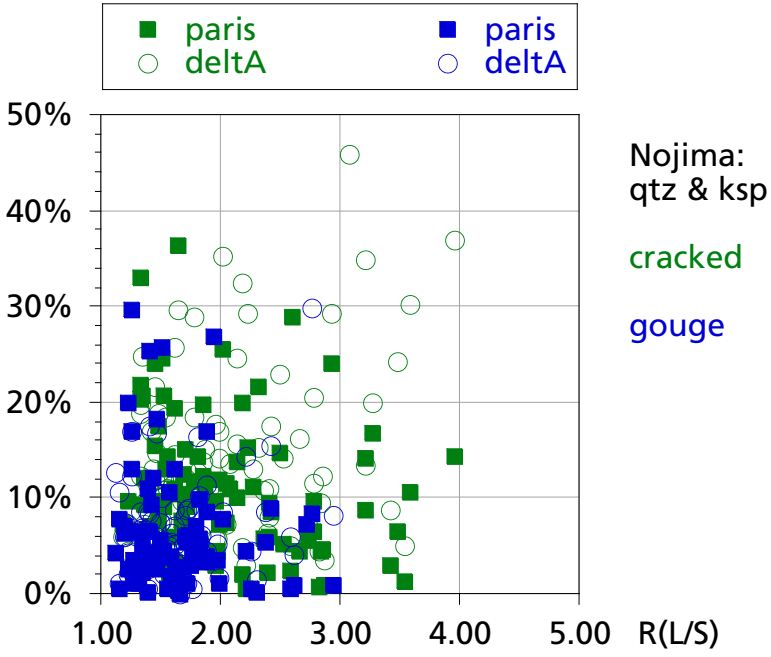

Nojima:
qtz & ksp

cracked

gouge

GOUGE

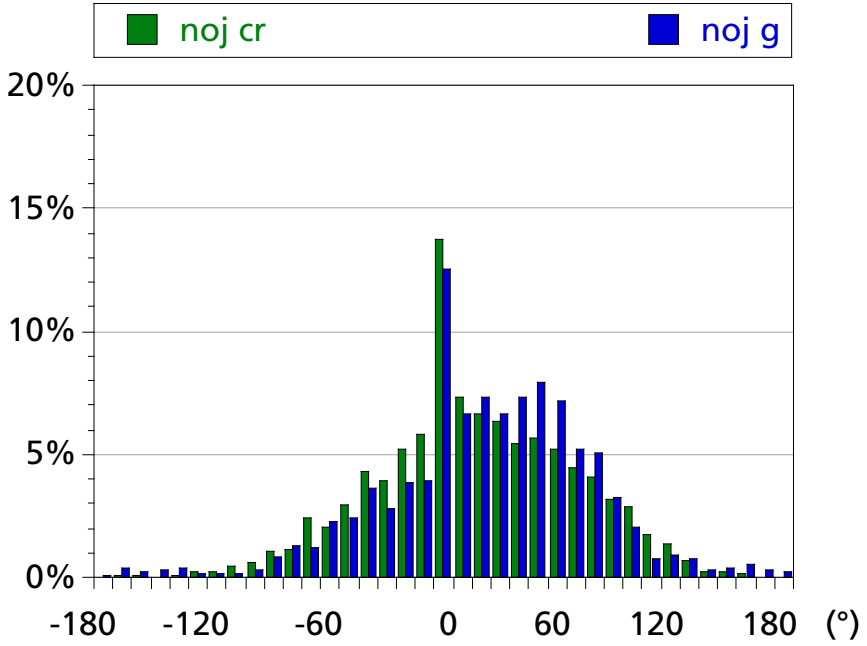

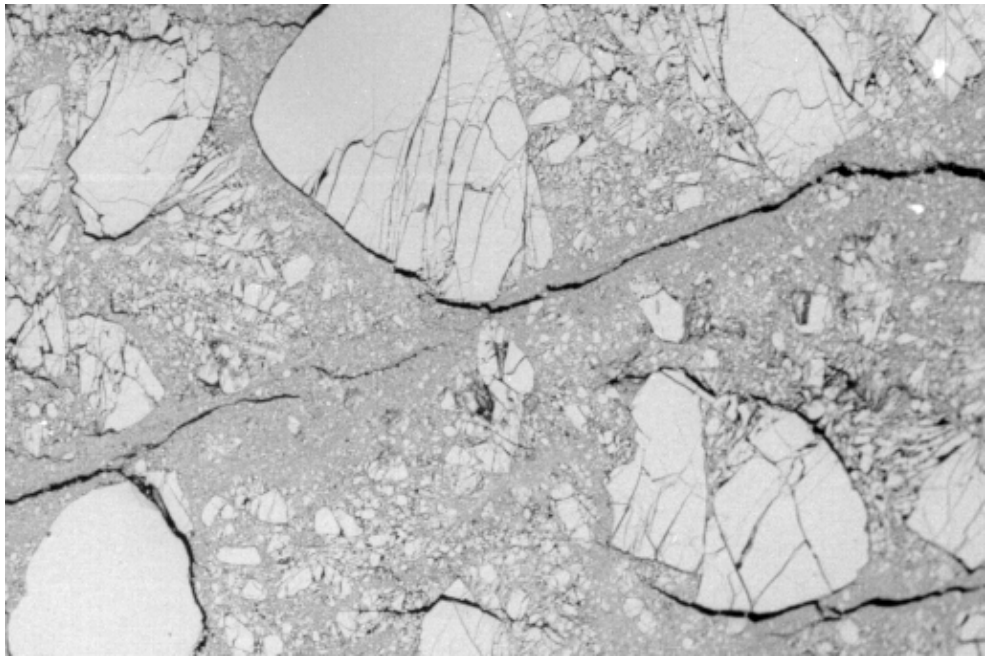

PROBLEMS:

define area of homogeneity

magnification (cascade)

differentiate shape - shape descriptor

grain size

linear? - log?

2-D? - 3-D?

cut-off grain size

....

Example: quartz gouge: load cycling 100MPa Y=1.3

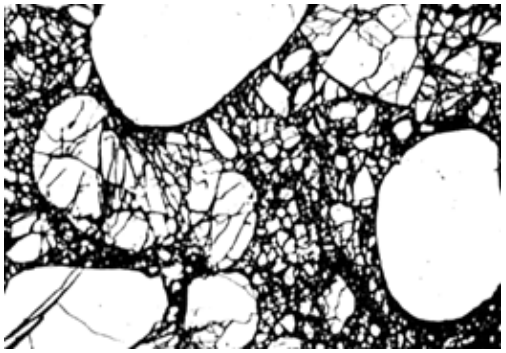

50x

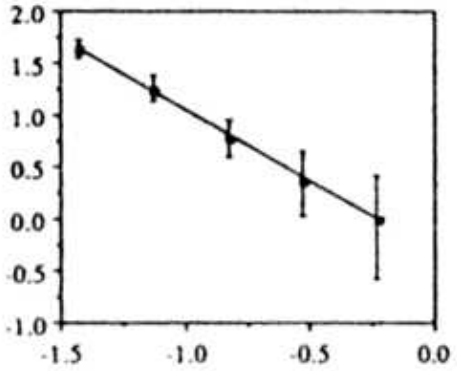

D=1.38±0.21

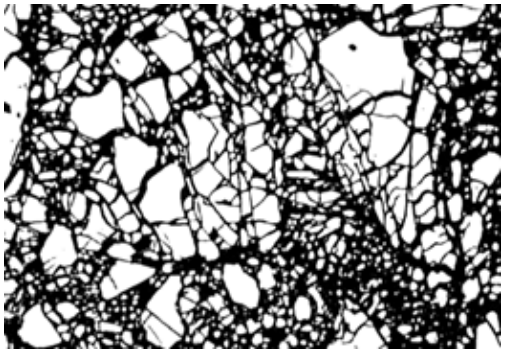

200x

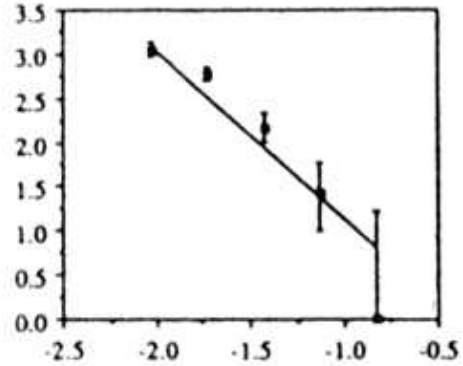

D=1.35±0.21

800x

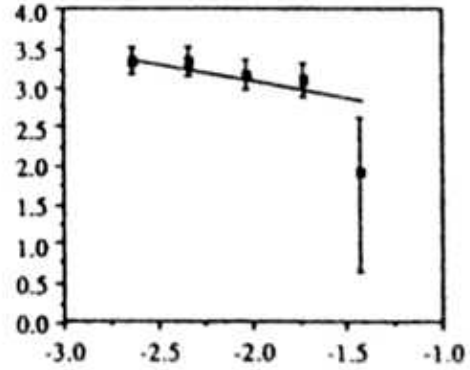

D=0.36±0.26

load cycling 20MPa Y= 2.3

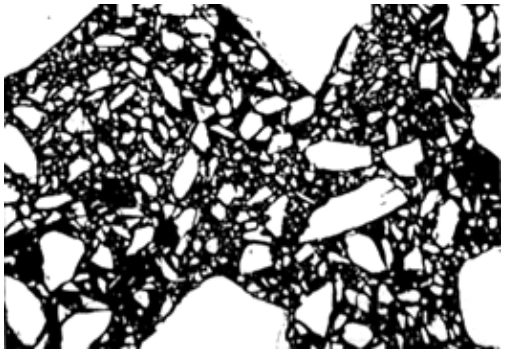

50x

200x

load cycling 100MPa Y= 2.9

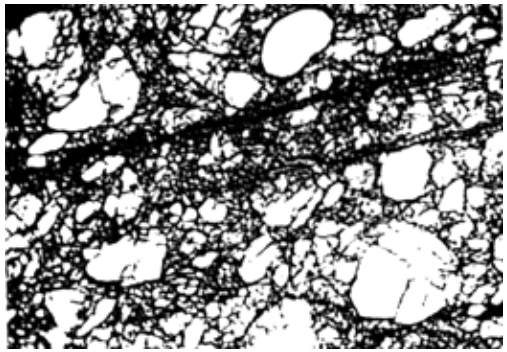

30x

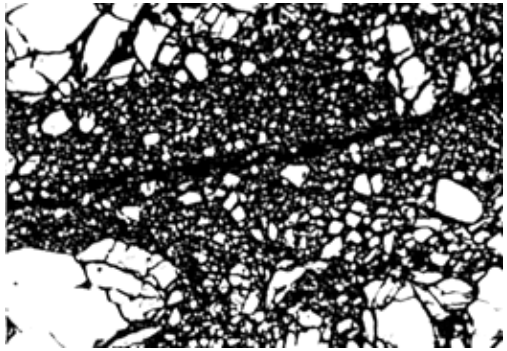

300x

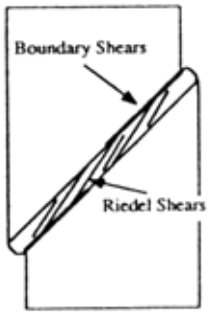

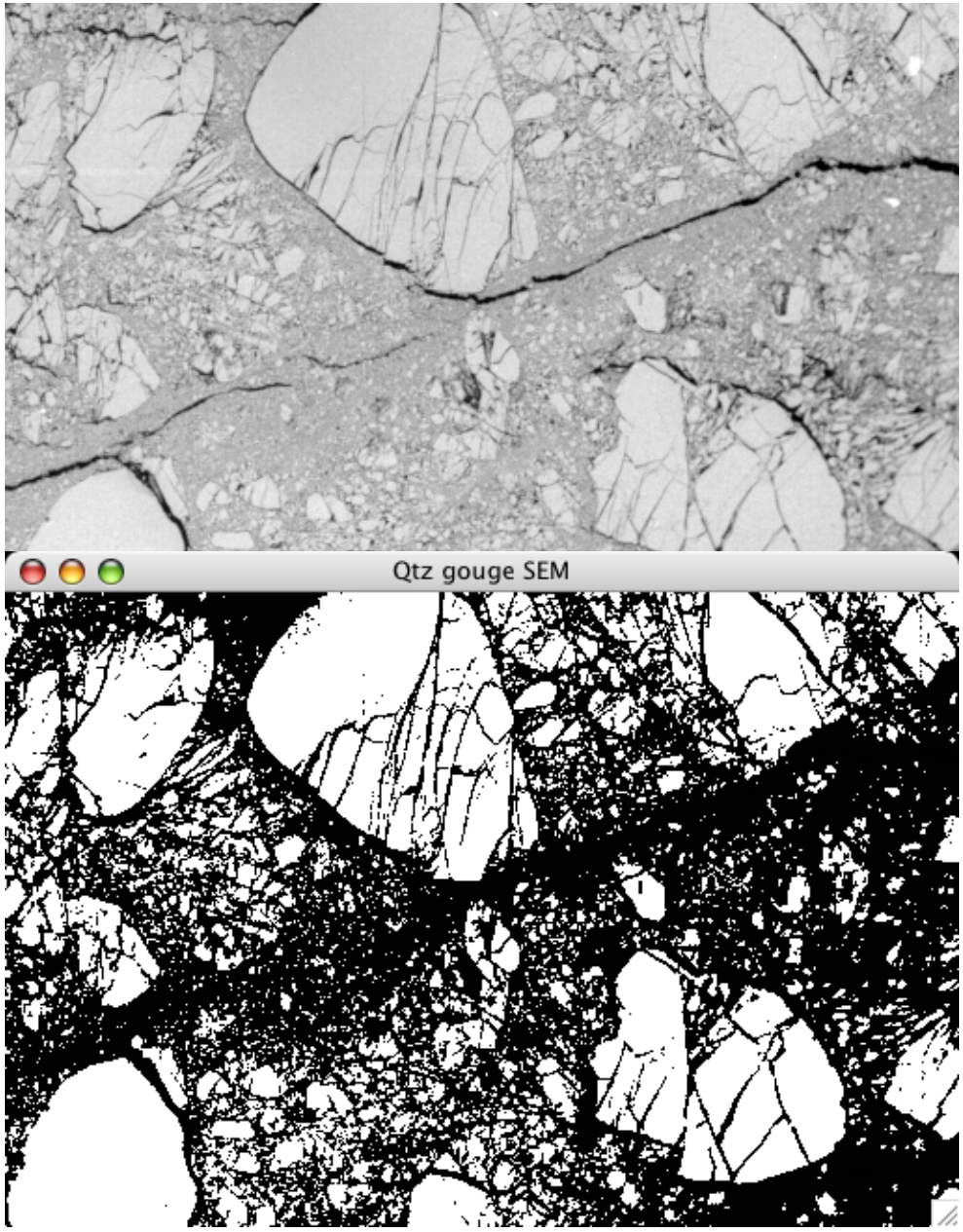

image SXM / NIH Image

threshold (level=60)

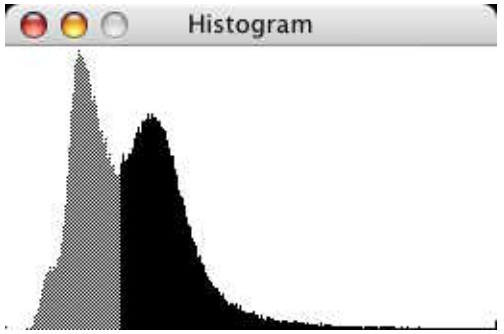

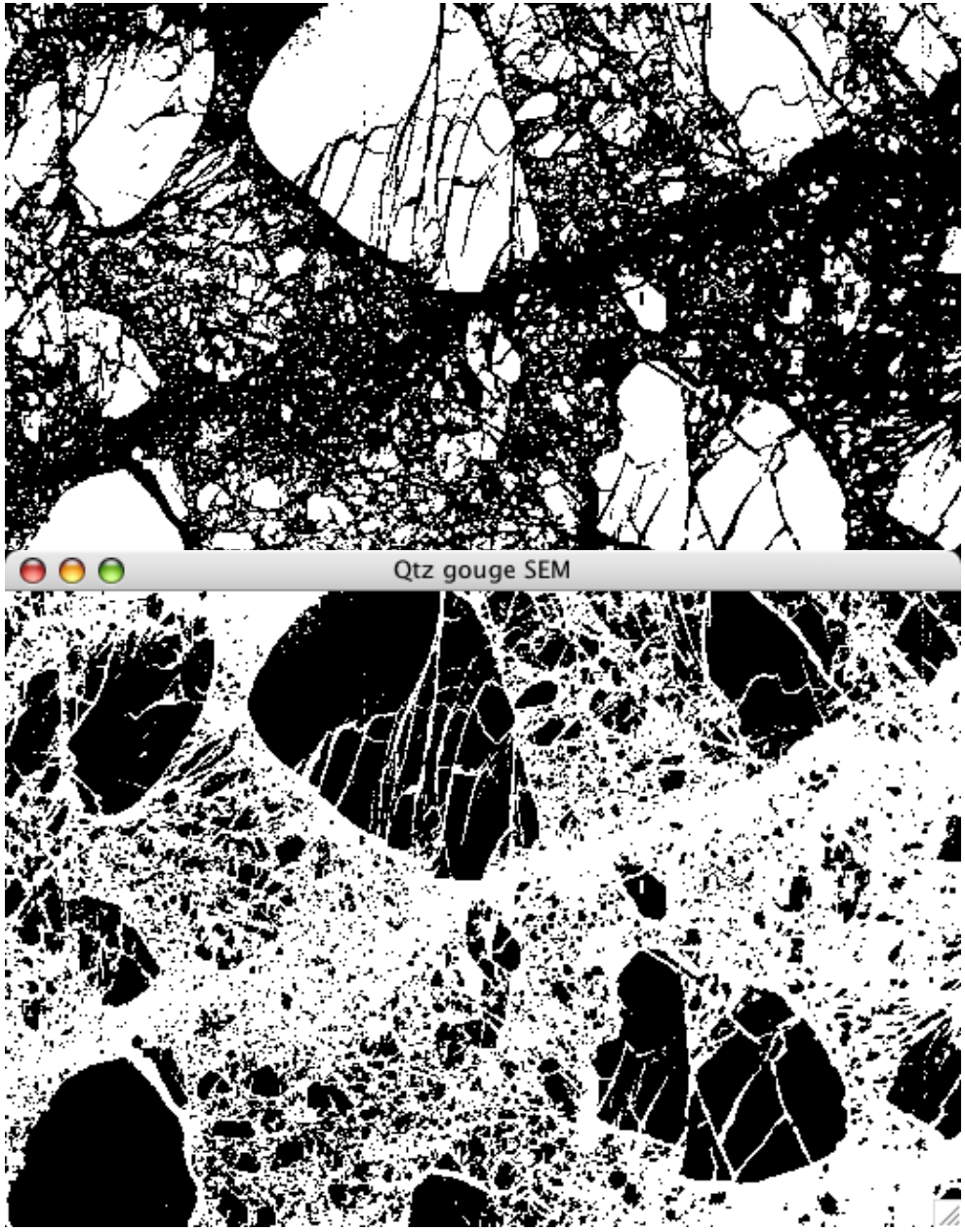

image SXM / NIH Image

invert (area=black)

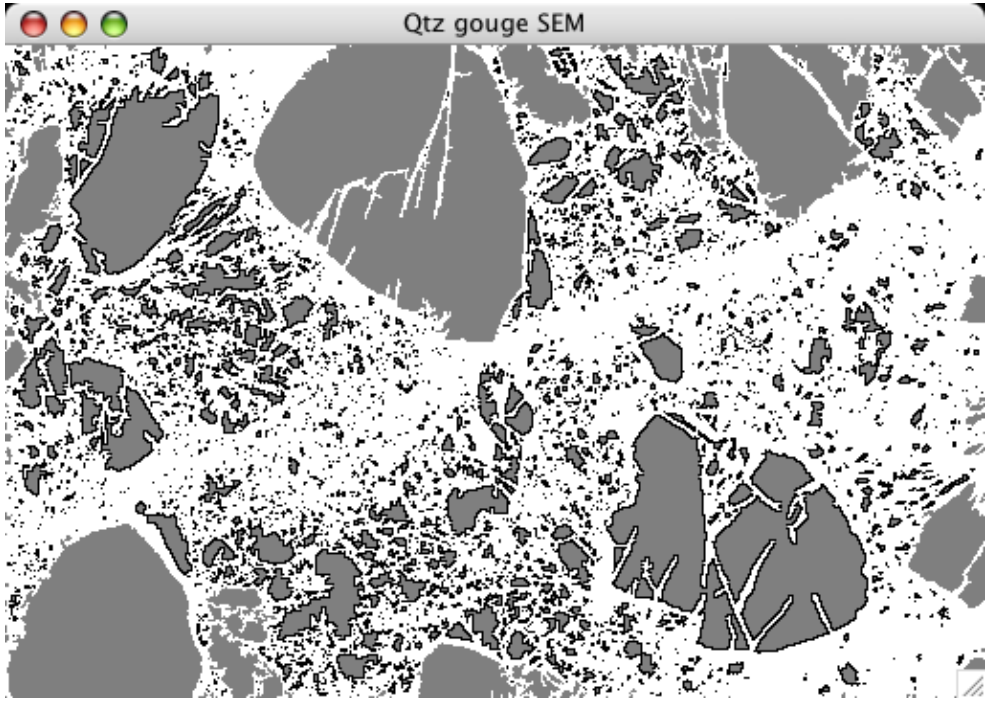

image SXM / NIH Image:

analyze options
- area
- perimeter

export results

➡ Kaleidagraph:

Results

#	Area	Len
1.	101.000	54.527
2.	85.000	72.569
3.	1.000	2.828
4.	7.000	10.485
5.	1.000	2.828
6.	15.000	15.314
7.	2.000	5.657
8.	1.000	2.828
9.	1.000	2.828
10.	2.000	4.828
11.	2.000	4.828
12.	27.000	27.799
13.	533.000	269.262

Qtz gouge SEM (Meas)

	0 #	1 Area	2 Len
0			
1	1.0000	101.00	54.527
2	2.0000	85.000	72.569
3	3.0000	1.0000	2.8280
4	4.0000	7.0000	10.485
5	5.0000	1.0000	2.8280
6	6.0000	15.000	15.314
7	7.0000	2.0000	5.6570
8	8.0000	1.0000	2.8280
9	9.0000	1.0000	2.8280
10	10.000	2.0000	4.8280
11	11.000	2.0000	4.8280
12	12.000	27.000	27.799
13	13.000	533.00	269.26

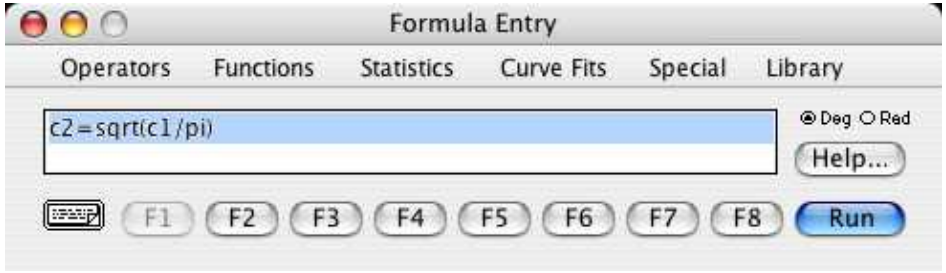

Kaleidagraph:

calculate equivalent radius

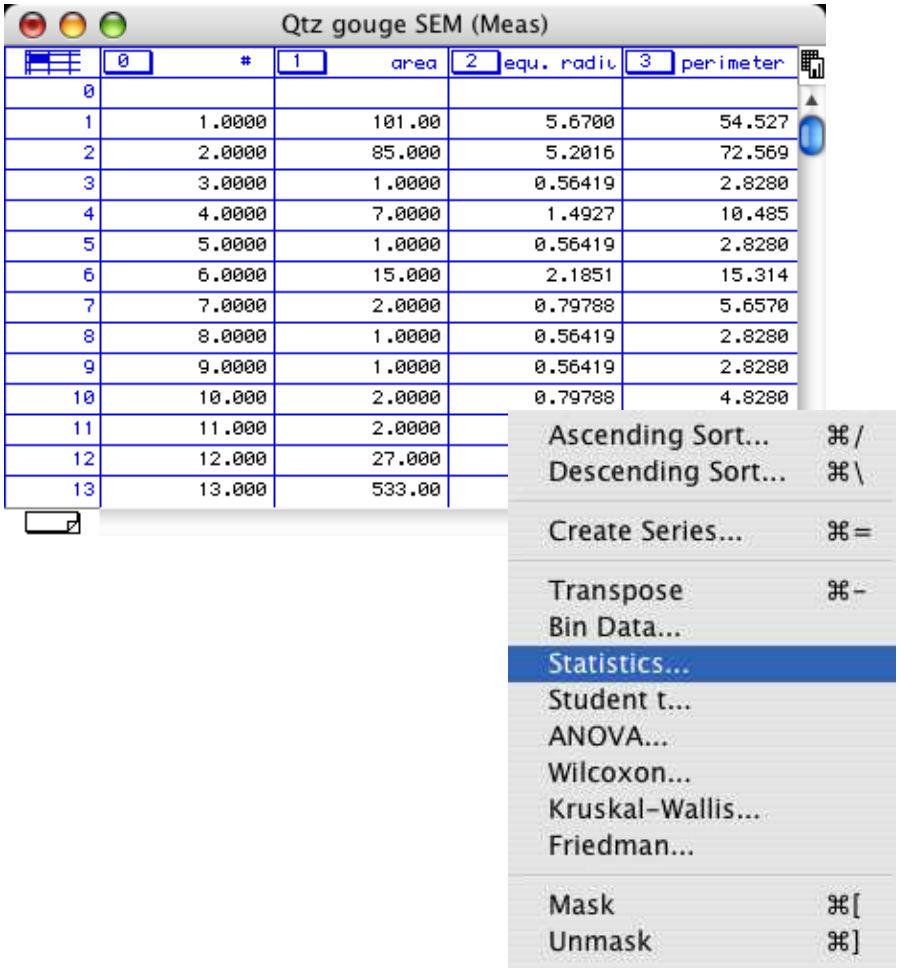

Statistics:

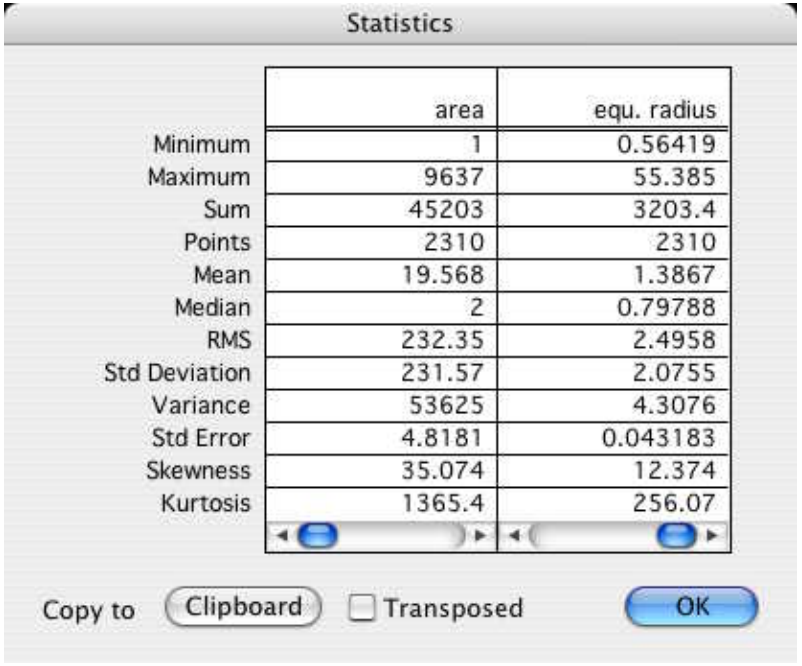

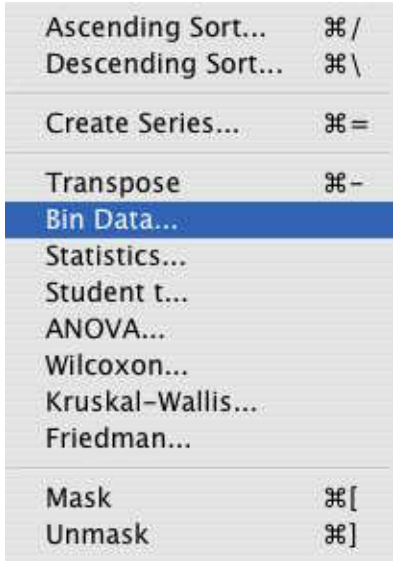

Kaleidagraph:

prepare histograms

(copy to clipboard)
(copy to new file)

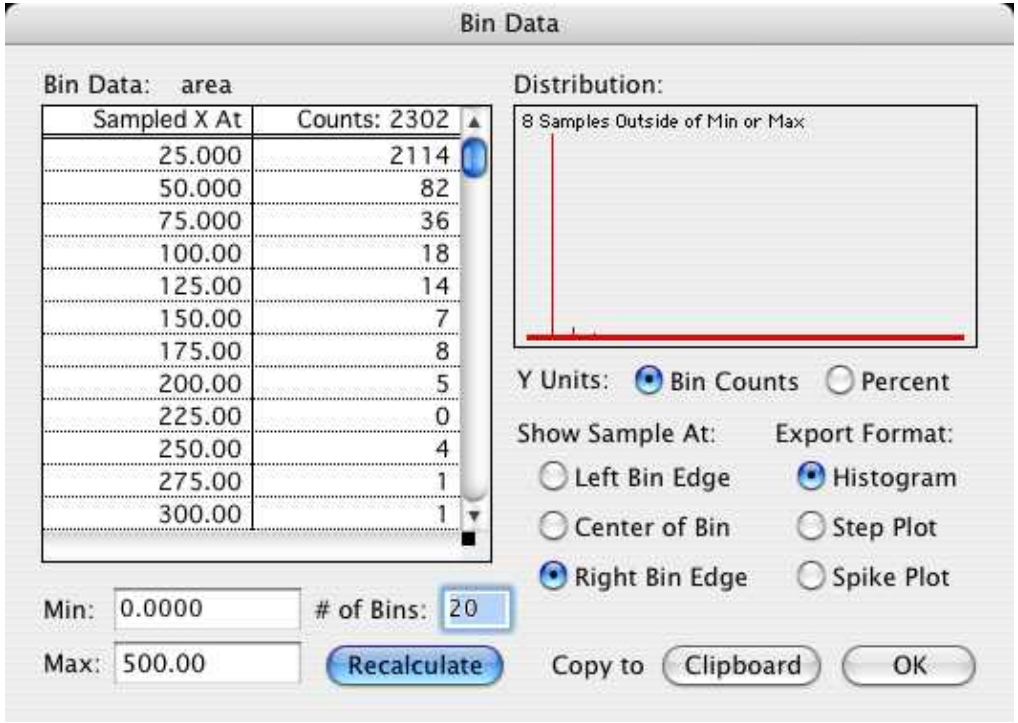

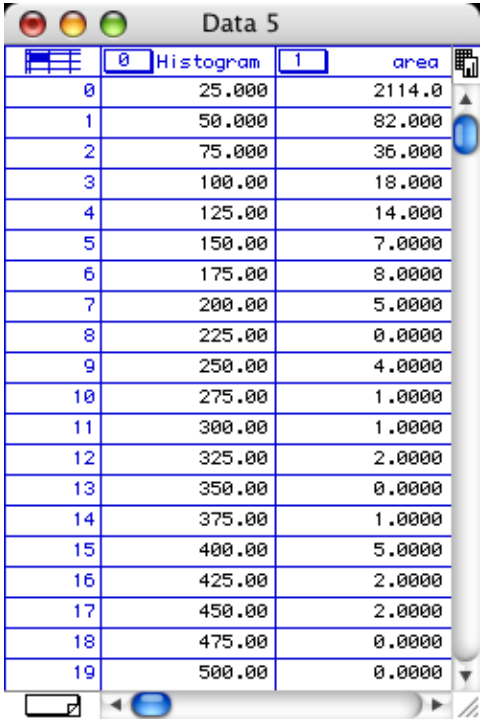

Data 5

	0 area	1 no.	2 equ.radius	3 no.
0	25.000	2114.0	1.0000	1407.0
1	50.000	82.000	2.0000	575.00
2	75.000	36.000	3.0000	160.00
3	100.00	18.000	4.0000	56.000
4	125.00	14.000	5.0000	36.000
5	150.00	7.0000	6.0000	25.000
6	175.00	8.0000	7.0000	14.000
7	200.00	5.0000	8.0000	11.000
8	225.00	0.0000	9.0000	4.0000
9	250.00	4.0000	10.000	4.0000
10	275.00	1.0000	11.000	2.0000
11	300.00	1.0000	12.000	8.0000
12	325.00	2.0000	13.000	1.0000
13	350.00	0.0000	14.000	2.0000
14	375.00	1.0000	15.000	0.0000
15	400.00	5.0000	16.000	0.0000
16	425.00	2.0000	17.000	1.0000
17	450.00	2.0000	18.000	0.0000
18	475.00	0.0000	19.000	0.0000
19	500.00	0.0000	20.000	1.0000

Kaleidagraph:

prepare histograms

(copy to clipboard)
(copy to new file)

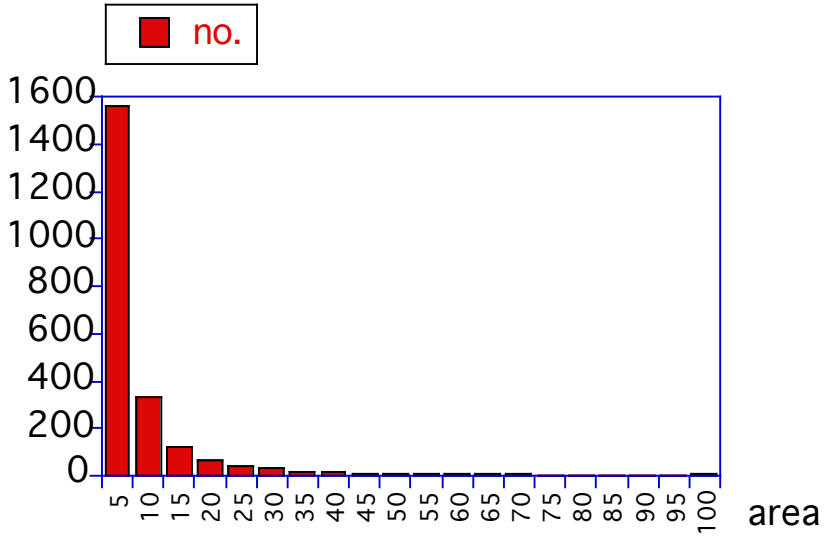

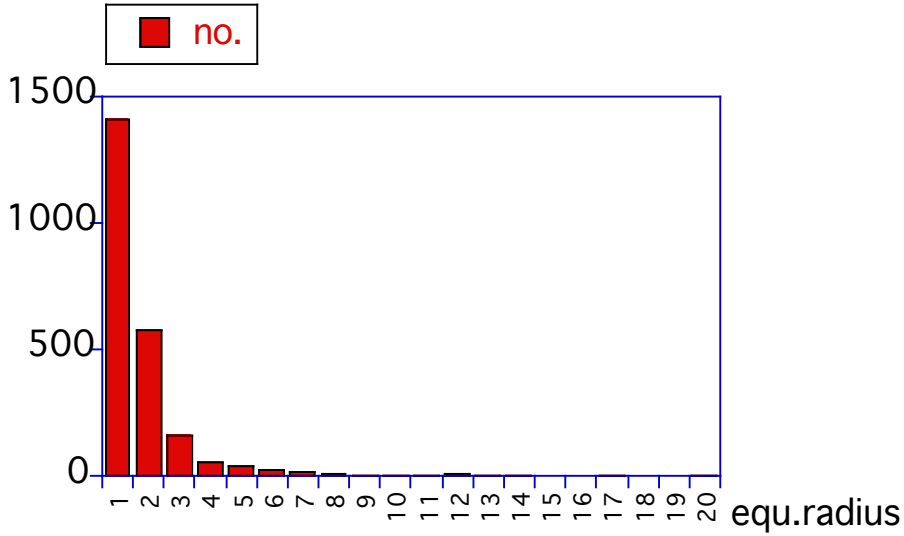

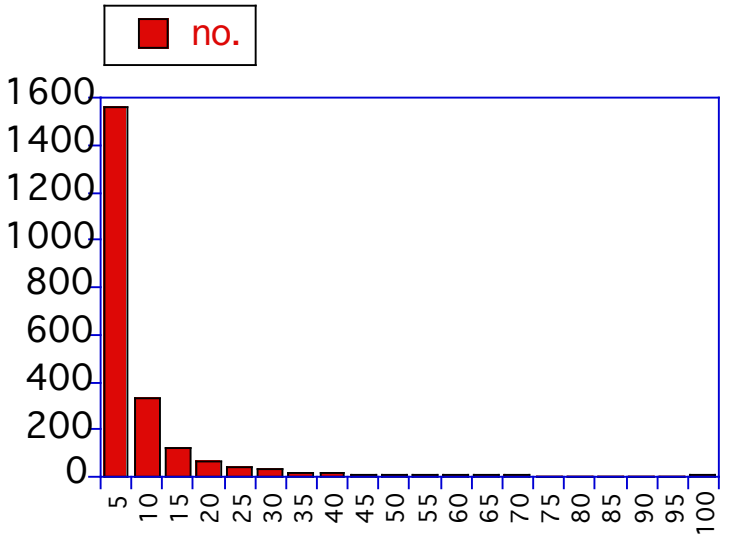

linear bins, linear counts
(quadratic measure)

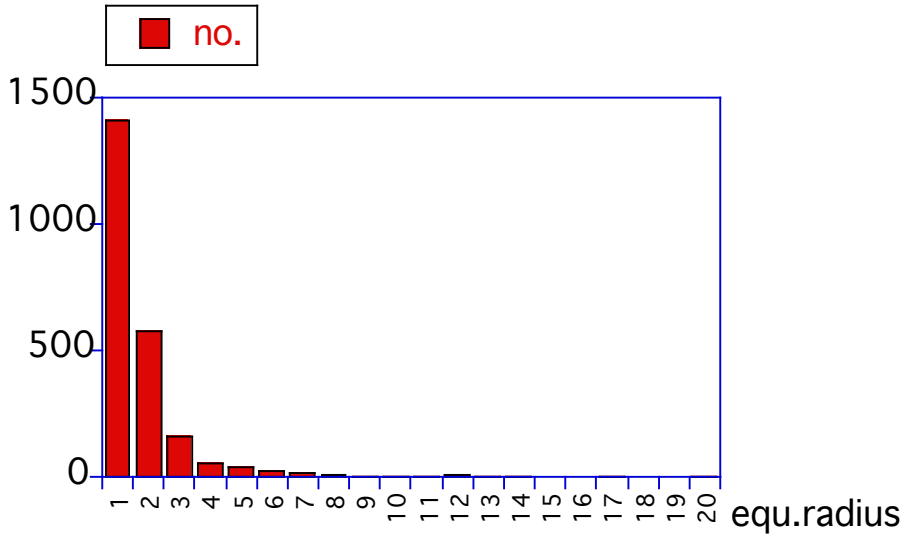

linear bins, linear counts
(linear measure)

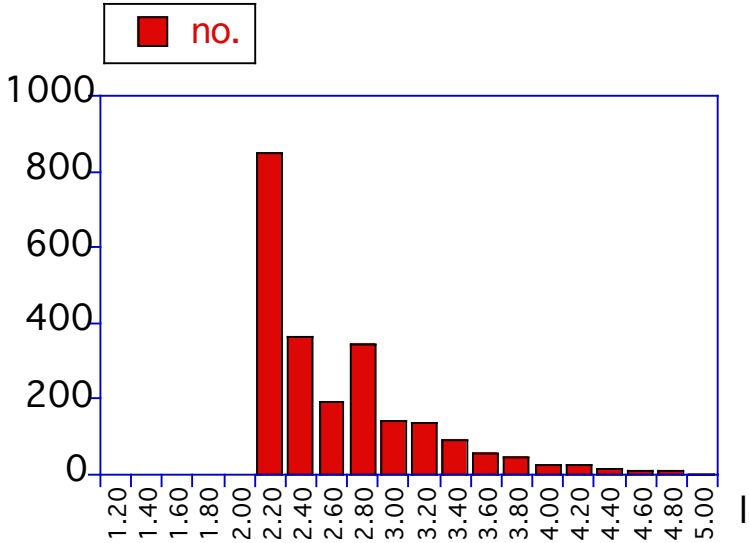

logarithmic bins, linear counts
(increasing bin width)

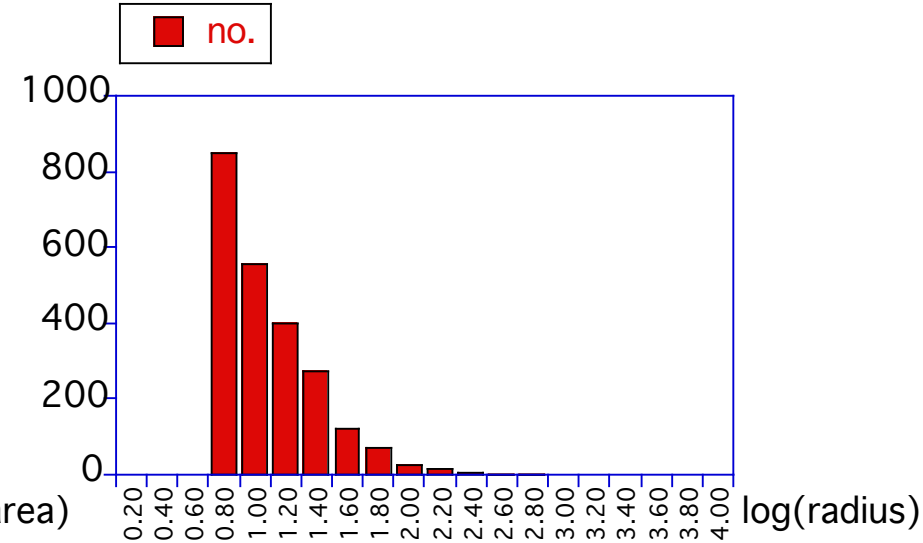

logarithmic bins, linear counts
(increasing bin width)

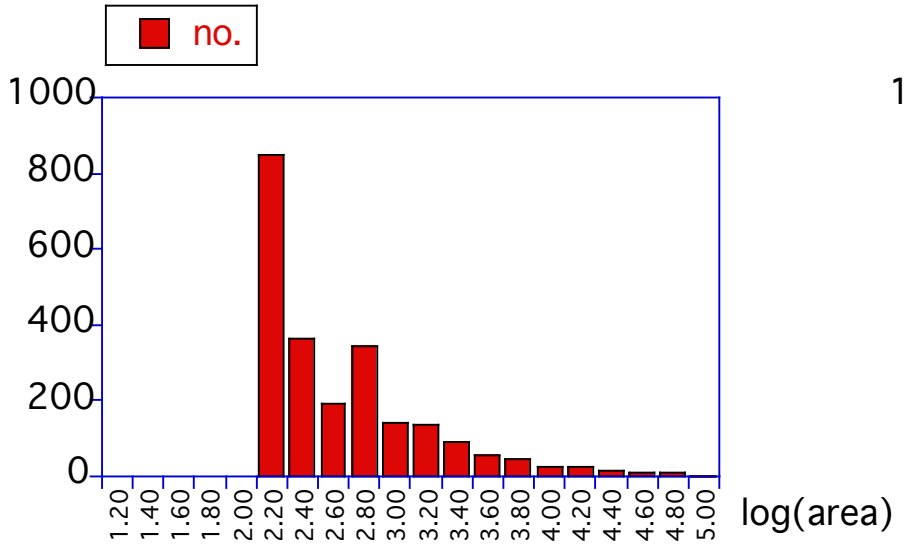

logarithmic bins, linear counts
(increasing bin width)

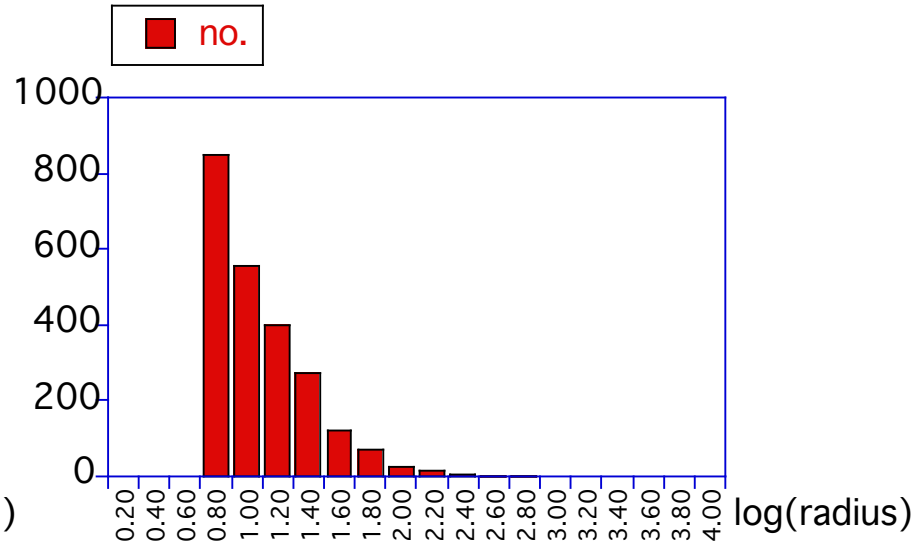

logarithmic bins, linear counts
(increasing bin width)

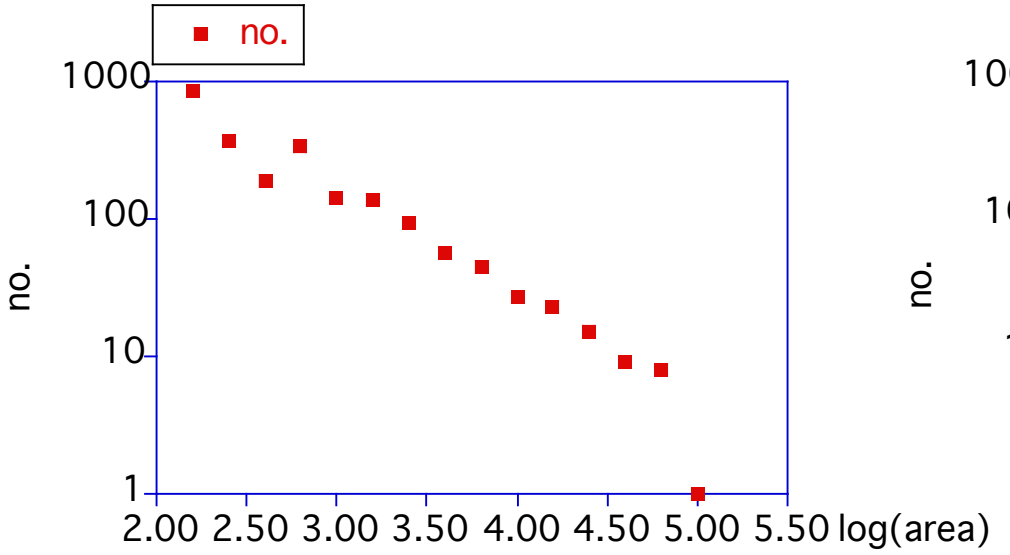

log bins, log counts
(quadratic measure)

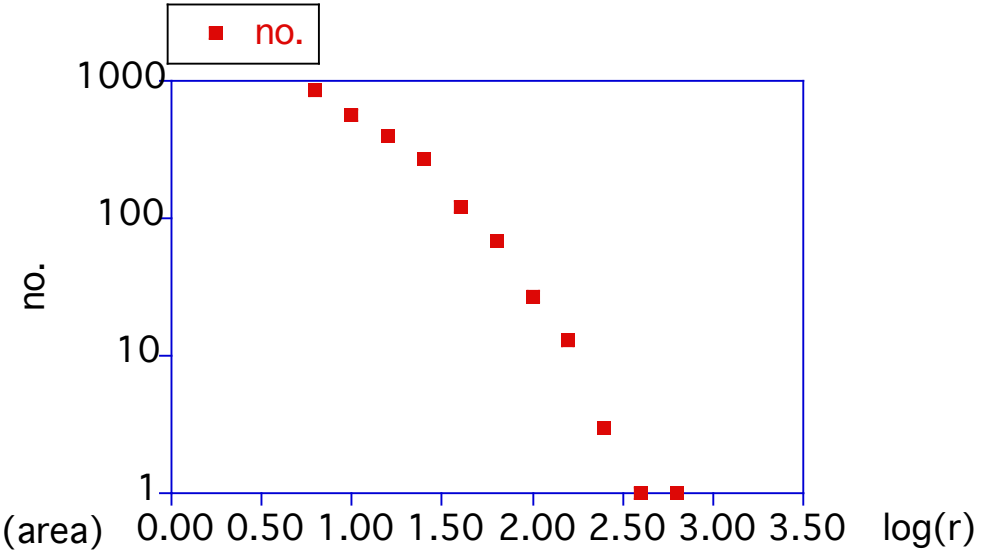

log bins, log counts
(linear measure)

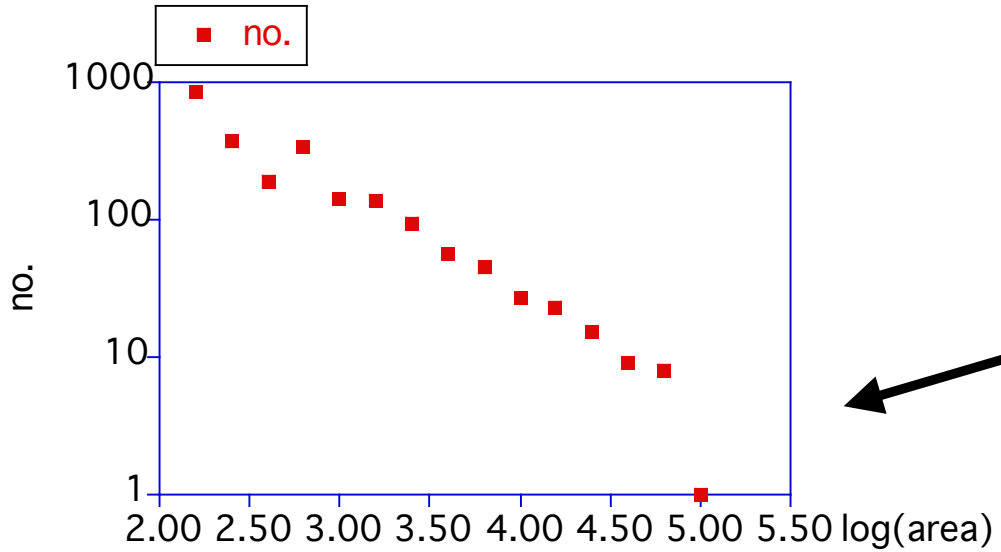

log bins, log counts

ATTENTION !

no. IN size range vs log. size range

no. ABOVE size range vs log. size range

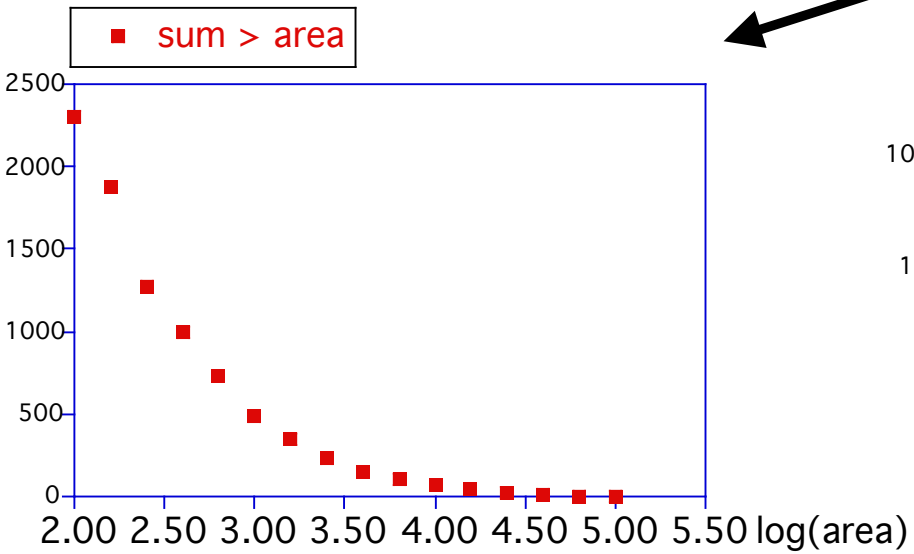

log bins, linear cumulative counts
(no of area > area)

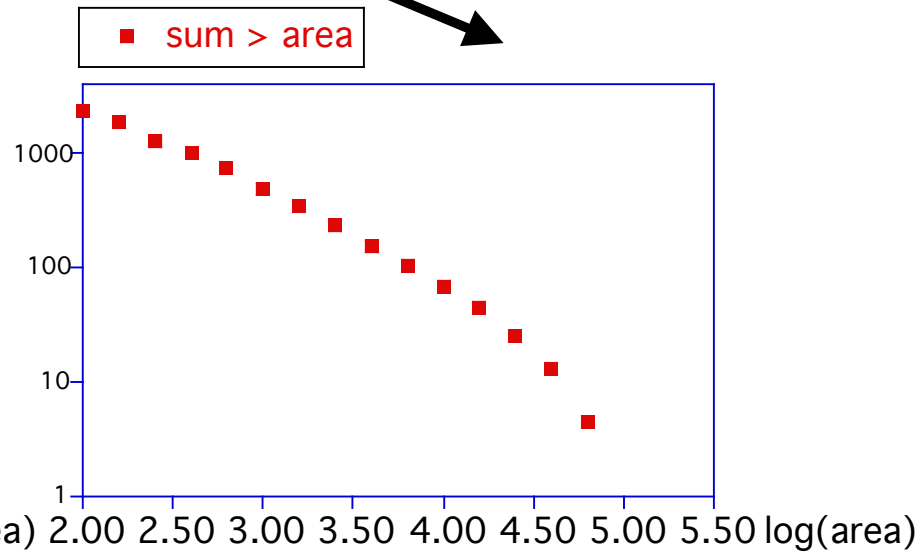

log bins, log cumulative counts
(no of area > area)

ATTENTION !

no. IN size range vs log. size range

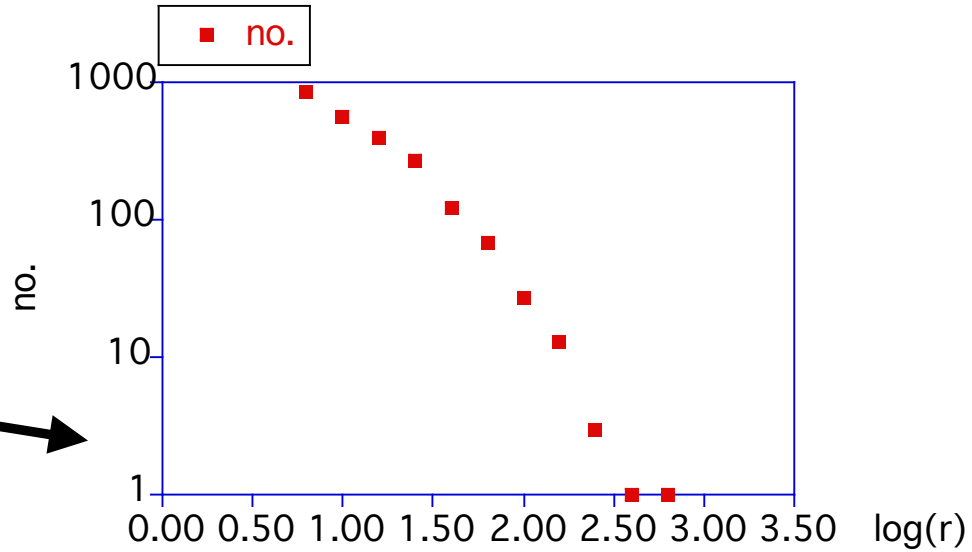

log bins, log counts

no. ABOVE size range vs log. size range

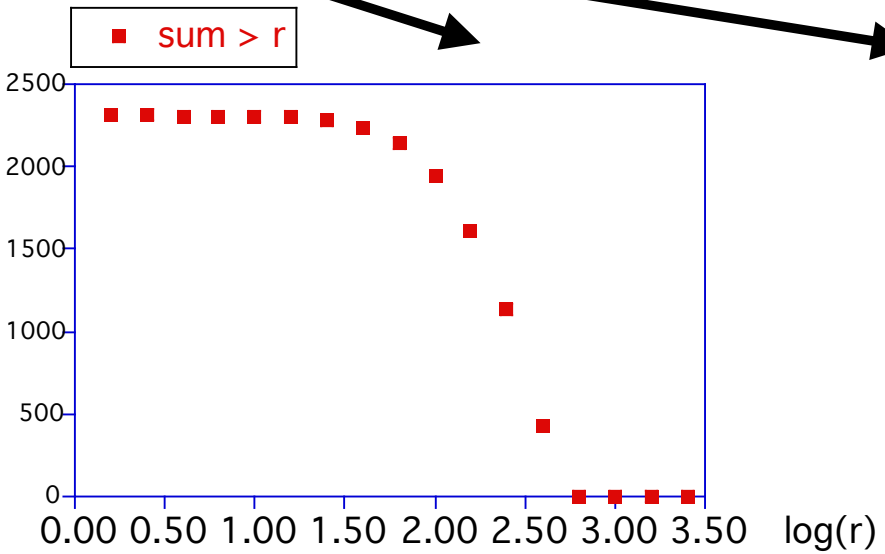

log bins, linear cumulative counts
(no of r > r)

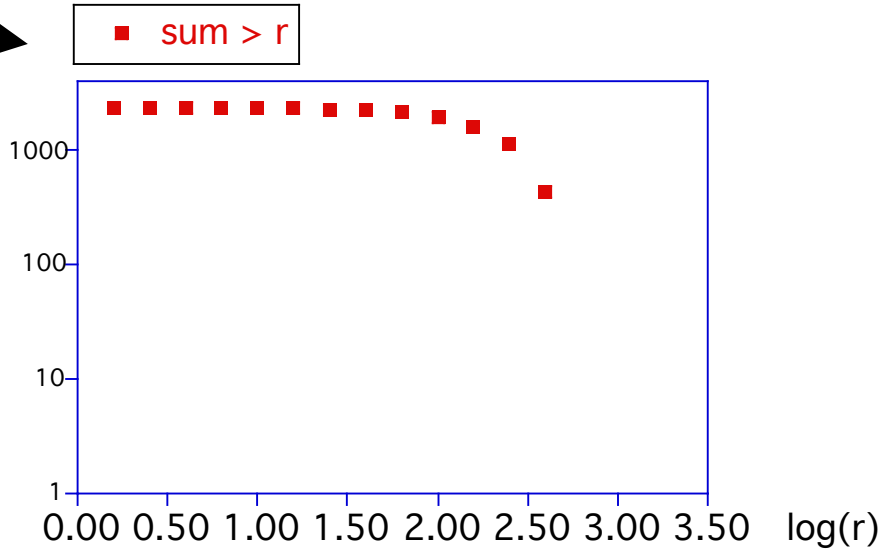

log bins, log cumulative counts
(no of r > r)

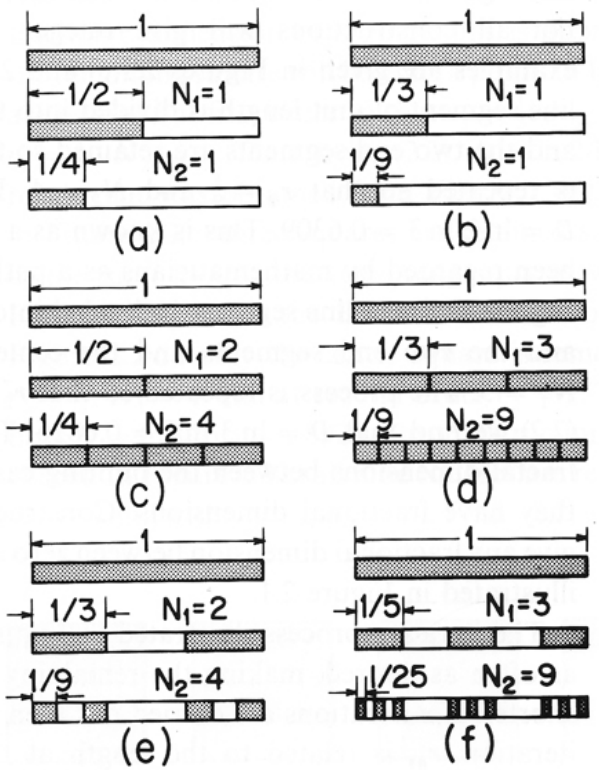

Figure 2.1. At order one a line segment of unit length is divided into an integer number of equal-sized smaller segments. A fraction of these segments is retained. The construction is repeated at higher orders. The first two orders are illustrated. (a) A line segment is divided into two parts and one is retained; $D = \ln 1/\ln 2 = 0$ (fractal dimension of a point). (b) A line segment is divided into three parts and one is retained; $D = \ln 1/\ln 3 = 0$ (fractal dimension of a point). (c) A line segment is divided into two parts and both are retained; $D = \ln 2/\ln 2 = 1$ (fractal dimension of a line). (d) A line segment is divided into three parts and all three are retained; $D = \ln 3/\ln 3 = 1$ (fractal dimension of a line). (e) A line segment is divided into three parts and two are retained; $D = \ln 2/\ln 3 = 0.6309$ (non-integer fractal dimension; this construction is also known as a Cantor set). (f) A line segment is divided into five parts and three are retained; $D = \ln 3/\ln 5 = 0.6826$ (non-integer fractal dimension).

Donald L. Turcotte:
Fractals and chaos in geology and geophysics
Cambridge Univ.Press, 1992

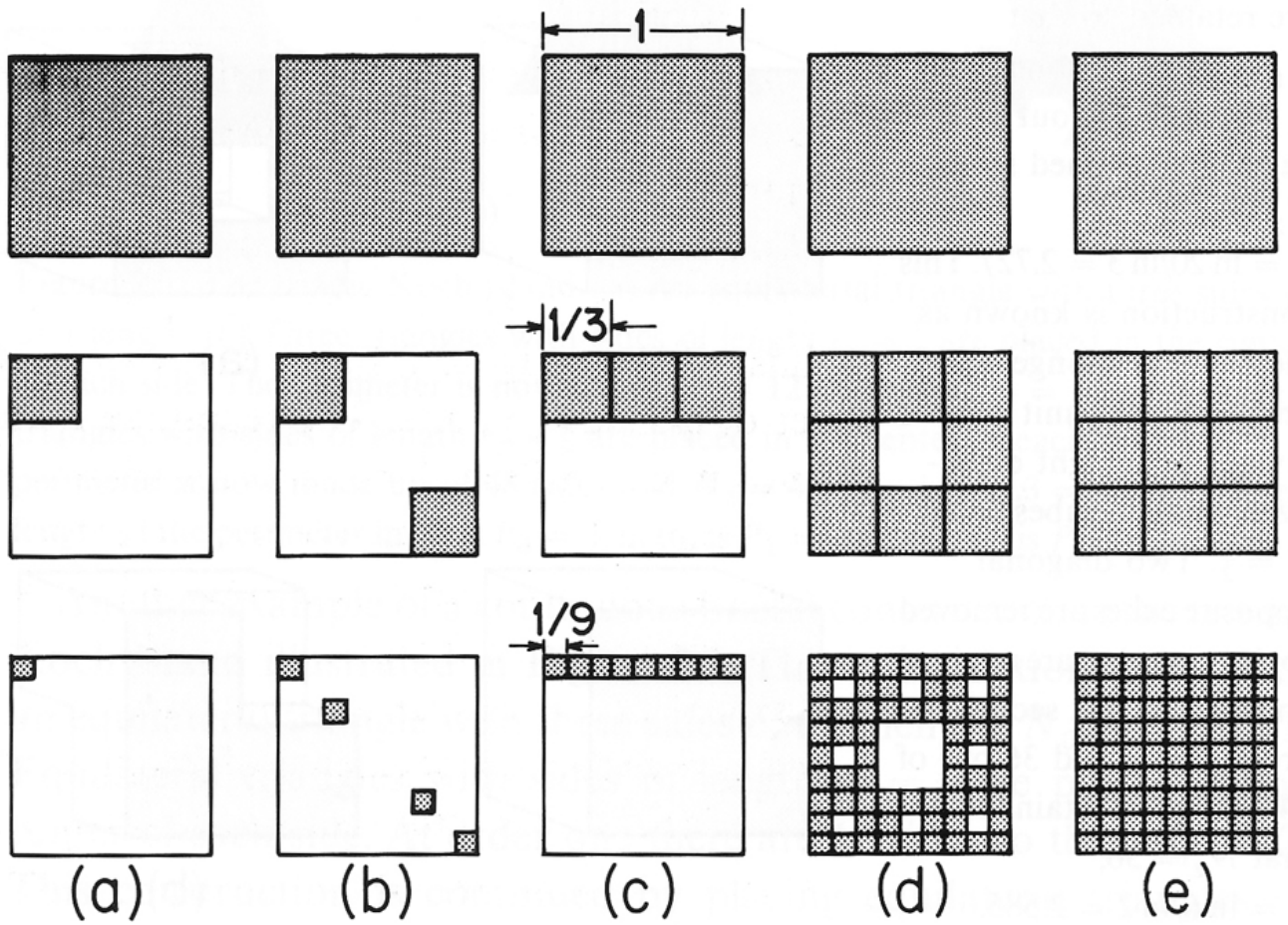

Figure 2.2. At order one the unit square is divided into nine equal-sized smaller squares with $r_1 = \frac{1}{3}$. At order two the remaining squares are divided into nine smaller equal-sized squares with $r_2 = \frac{1}{9}$. Five examples are given in which various numbers of squares, N, are retained. (a) $N_1 = 1$, $N_2 = 1$, $D = \ln 1/\ln 3 = 0$. (b) $N_1 = 2$, $N_2 = 4$, $D = \ln 2/\ln 3 = 0.6309$. (c) $N_1 = 3$, $N_2 = 9$, $D = \ln 3/\ln 3 = 1$. (d) $N_1 = 8$, $N_2 = 64$, $D = \ln 8/\ln 3 = 1.8928$ (also known as a Sierpinski carpet). (e) $N_1 = 9, N_2 = 81$, $D = \ln 9/\ln 3 = 2$.

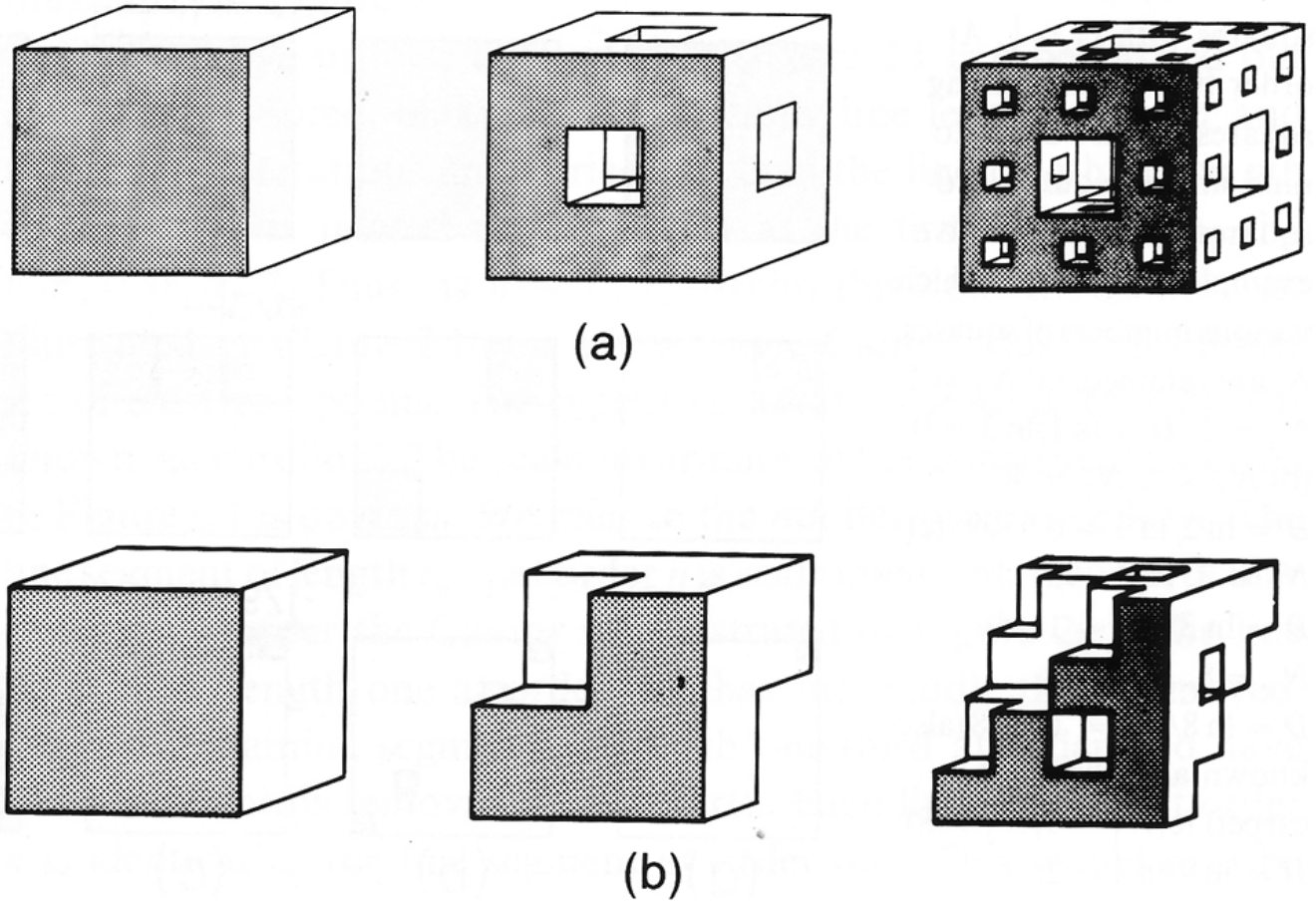

Figure 2.3. (a) At first order the unit cube is divided into 27 equal-sized smaller cubes with $r_1 = \frac{1}{3}$, 20 cubes are retained so that $N_1 = 20$. At second order $r_2 = \frac{1}{9}$ and 400 out of 729 cubes are retained so that $N_2 = 400$; $D = \ln 20/\ln 3 = 2.727$. This construction is known as the Menger sponge. (b) At first order the unit cube is divided into eight equal-sized smaller cubes with $r_1 = \frac{1}{2}$. Two diagonal opposite cubes are removed so that six cubes are retained and $N_1 = 6$. At second order $r_2 = \frac{1}{4}$ and 36 out of 64 cubes are retained so that $N_2 = 36$; $D = \ln 6/\ln 2 = 2.585$.

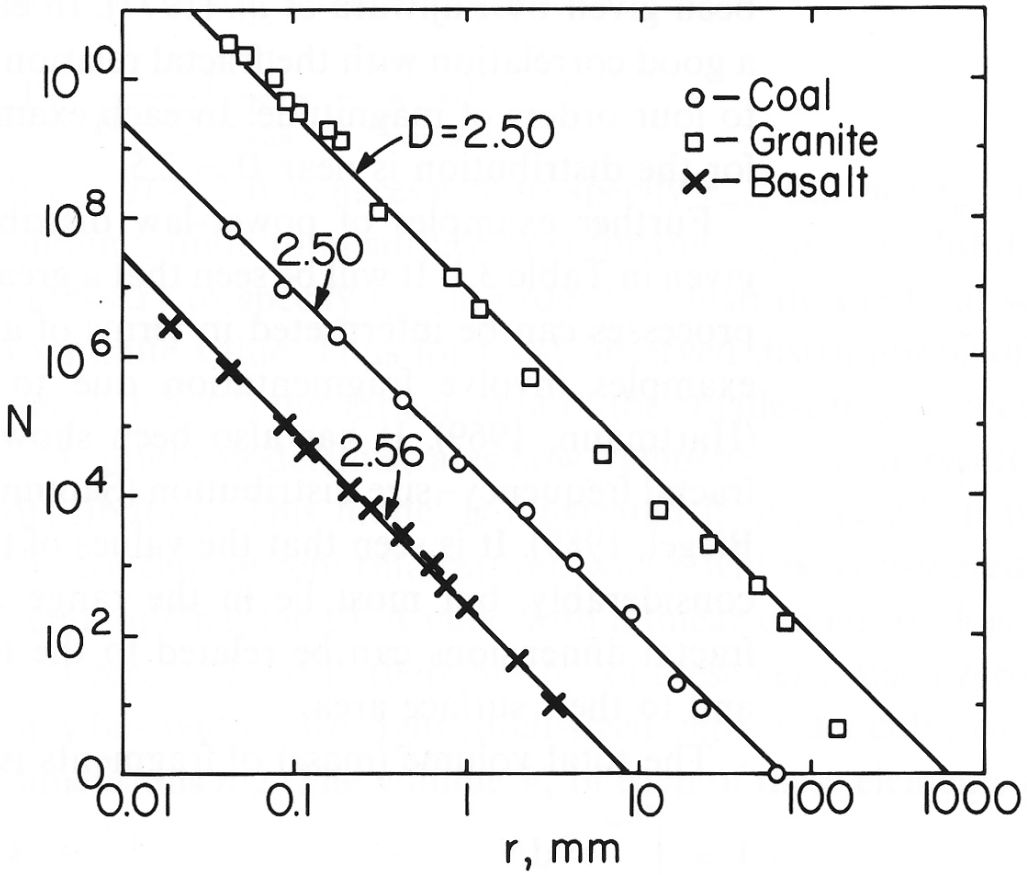

Figure 3.1. Since fragments have a variety of shapes, the cube root of volume is an objective measure of size. The number N of fragments with cube root of volume greater than r is given as a function of r for broken coal (Bennett, 1936), broken granite from a 61 kt underground nuclear detonation (Schoutens, 1979), and impact ejecta due to a 2.6 km s^{-1} polycarbonate projectile impacting on basalt (Fujiwara *et al.*, 1977). The best-fit fractal distribution from (2.6) is shown for each data set.

Figure 3.2. Idealized model for fractal fragmentation. A zero-order cubic cell with dimensions h is divided into eight zero-order cubic elements each with dimensions $h/2$. The probability that a zero-order cell will be fragmented into eight zero-order elements is f. The fragments with dimensions $h/2$ become first-order cells; each of these have a probability f of being fragmented into first-order elements with dimensions $h/4$. The process is repeated to higher orders. The basic structure is fractal.

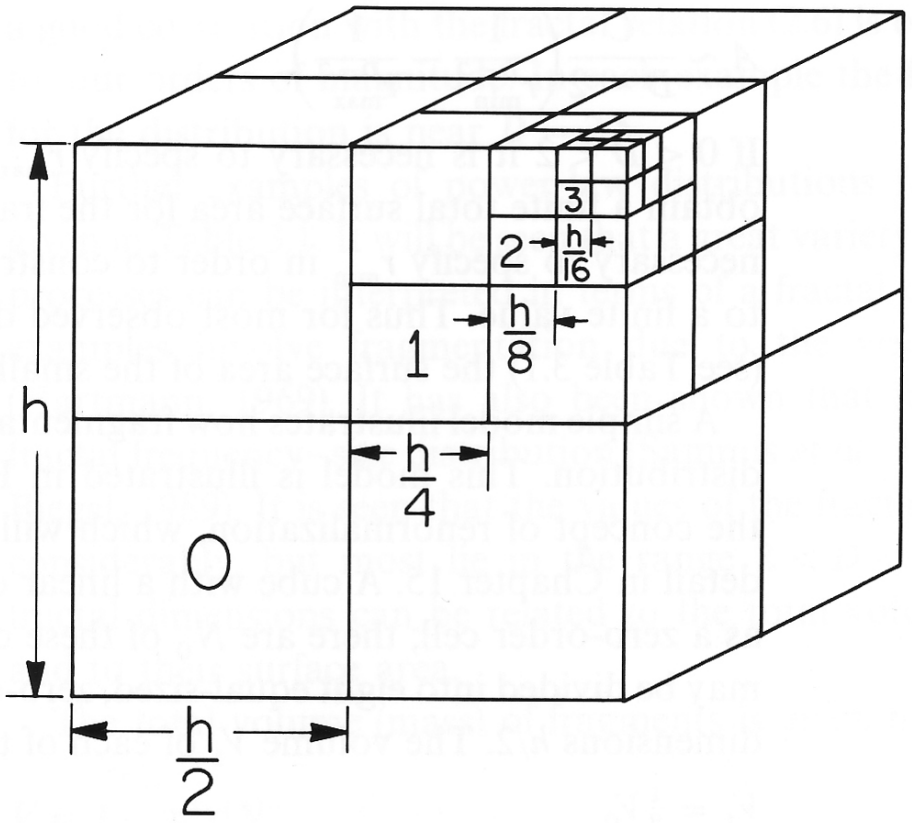

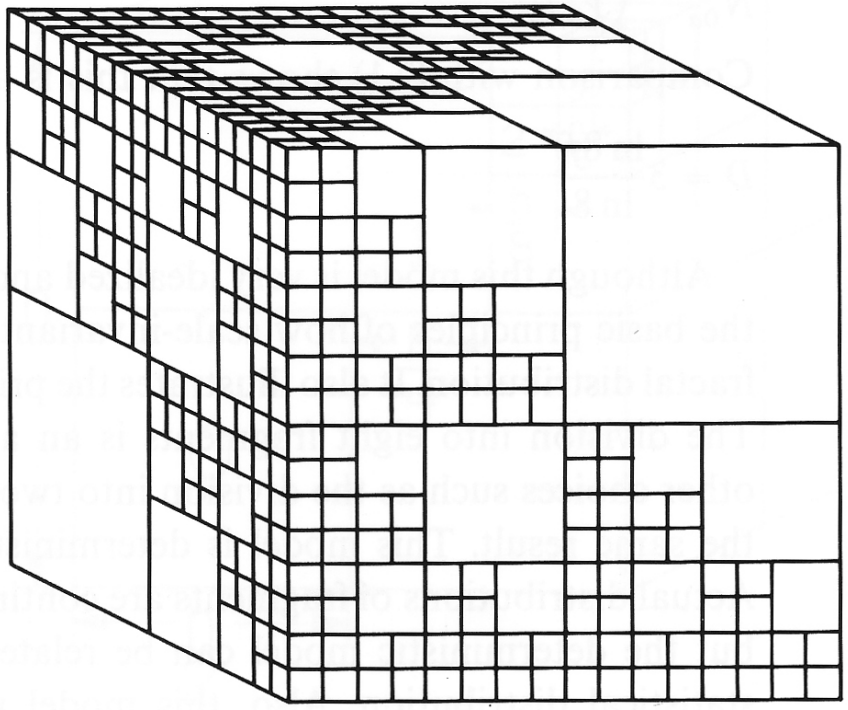

Figure 3.3. Illustration of a fractal model for fragmentation. Two diagonally opposite cubes are retained at each scale. With $r_1 = h/2$, $N_1 = 2$ and $r_2 = h/4$, $N_2 = 12$ we have $D = \ln 6/\ln 2 = 2.5850$.

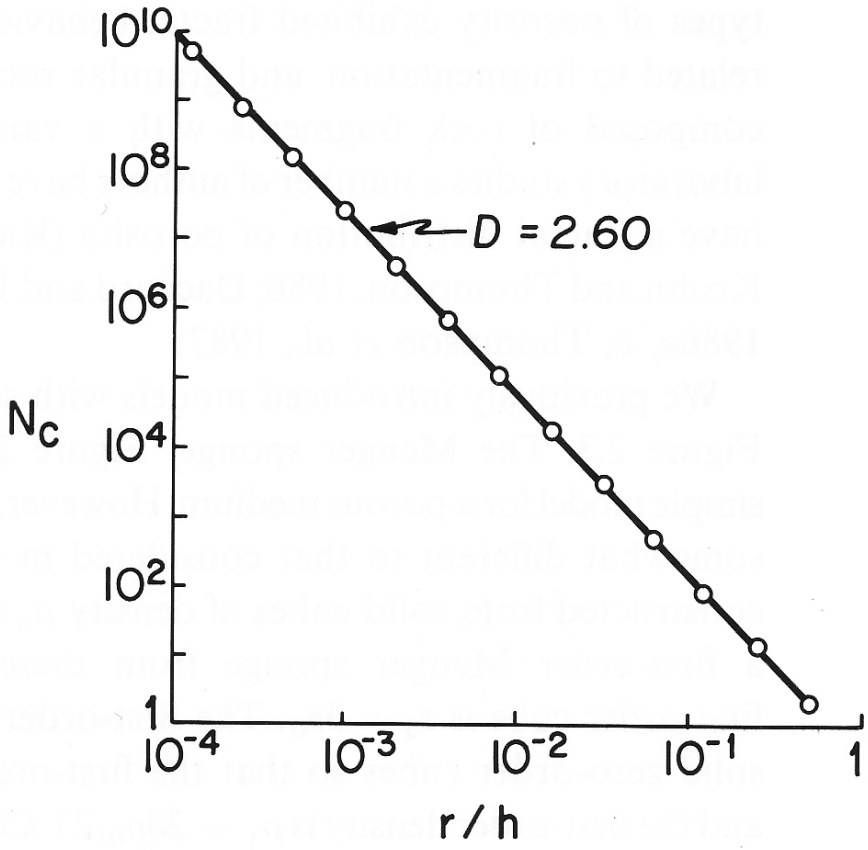

Figure 3.4. Cumulative statistics for the fragmentation model illustrated in Figure 3.3. Correlation with (2.6) gives $D = 2.60$.

G.C. Rowling & L.B. Goodwin (2003)
Cataclasis and particuate flow in faulted, poorly lithified sediments
JSG, 25, 317-331

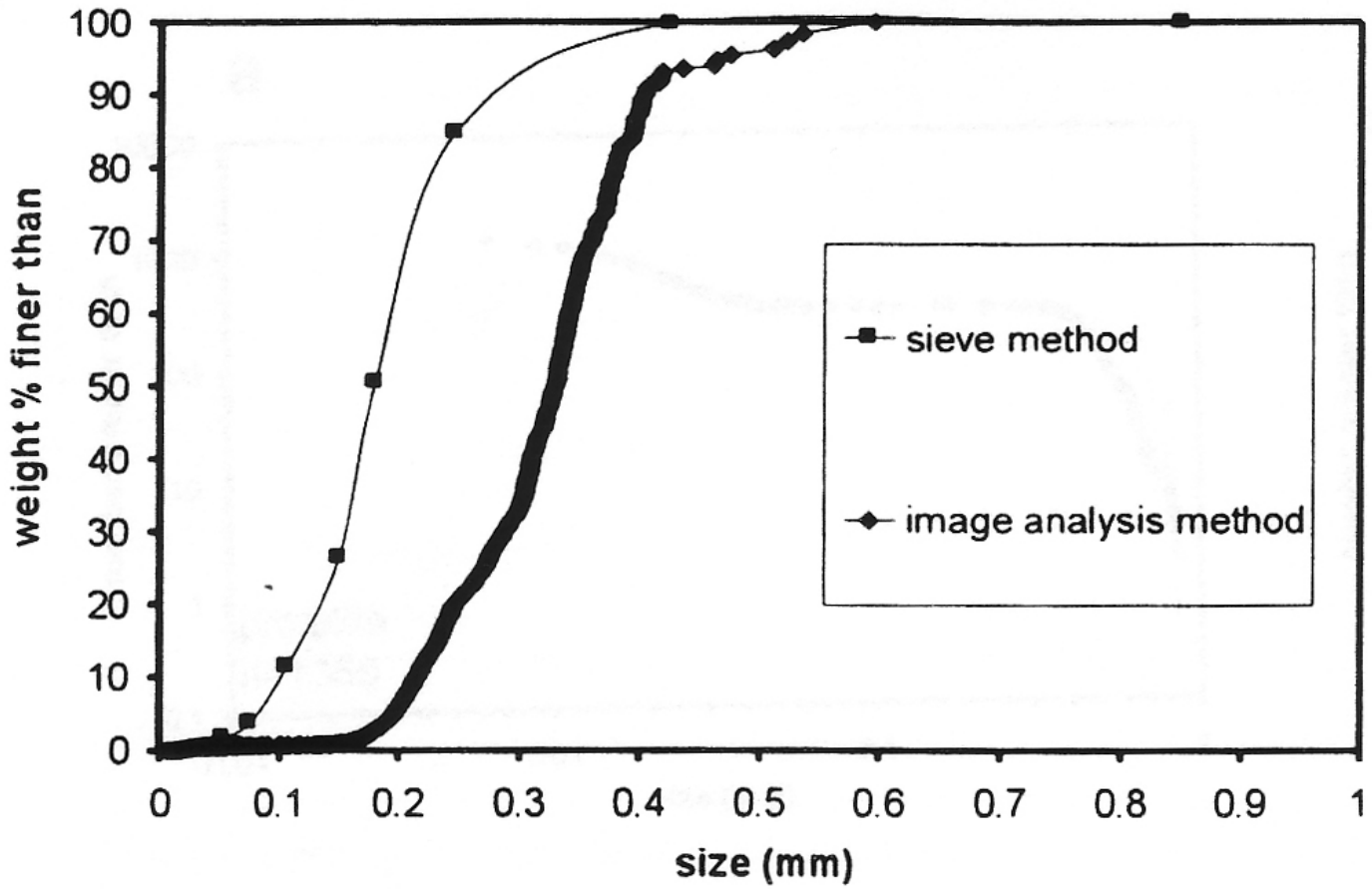

Fig. 8. Crushed quartz sand PSDs by weight determined by sieving and image analysis methods. Image analysis distribution by number was converted to distribution by weight by calculating equivalent spherical sizes from nominal section diameters and assuming a density for all particles of 2.65 g/cm^3.

8

Cataclasites: grain size, shape and fractals

Deformationsprozesse in der Erde (8)

Cataclasites: grain size, shape and fractals

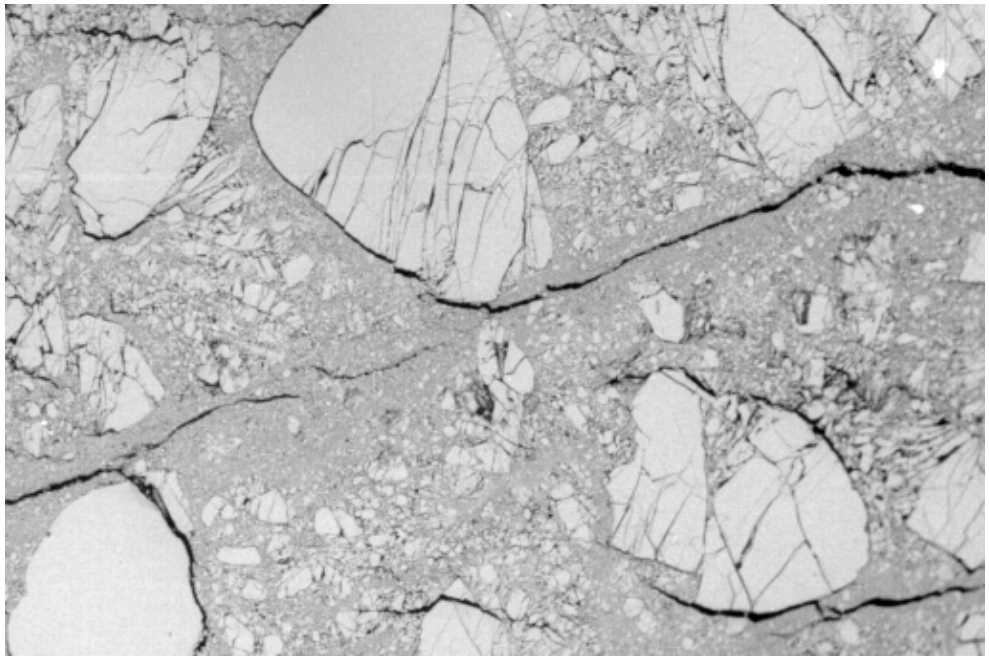

fault gouge

SEM

segmentation

image analysis of particles:

➡ shape, size, ...

➡ grain size distribution

➡ fractal dimension

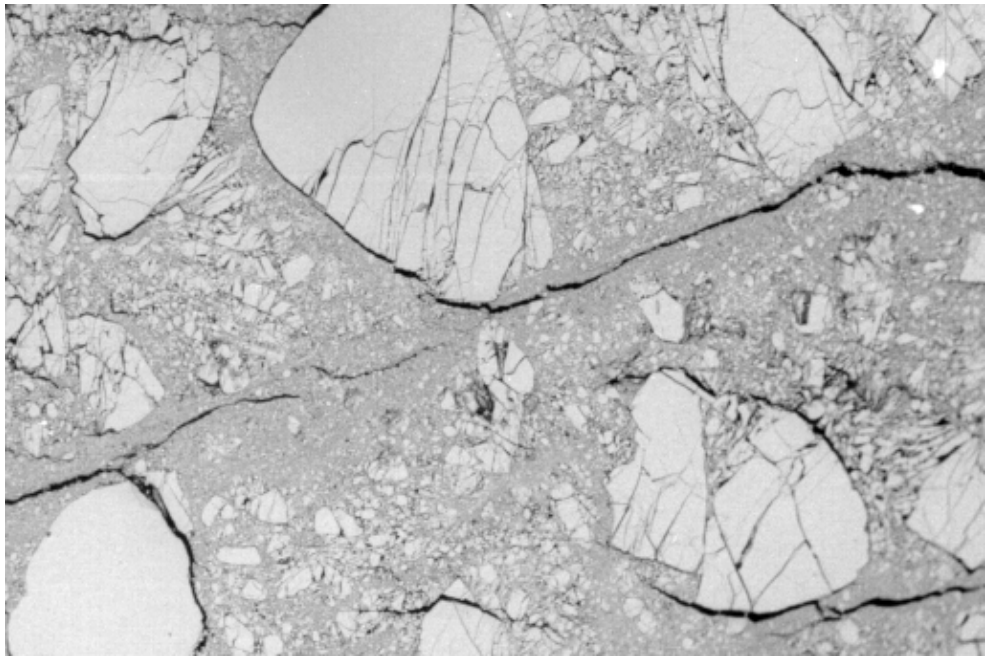

PROBLEMS:

define area of homogeneity

magnification (cascade)

differentiate shape - shape descriptor

grain size

linear? - log?

2-D? - 3-D?

cut-off grain size

....

Example: quartz gouge: load cycling 100MPa Y=1.3

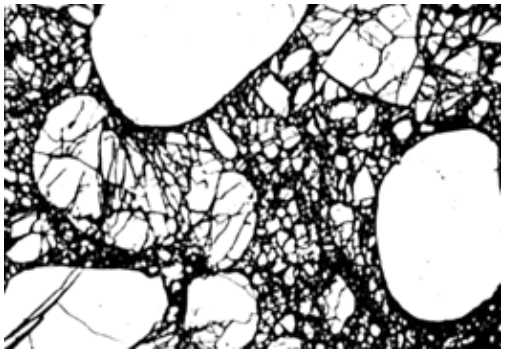

50x

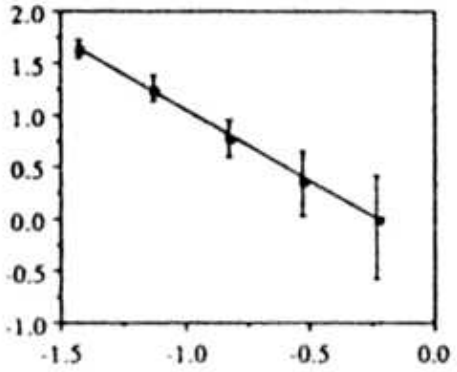

D=1.38±0.21

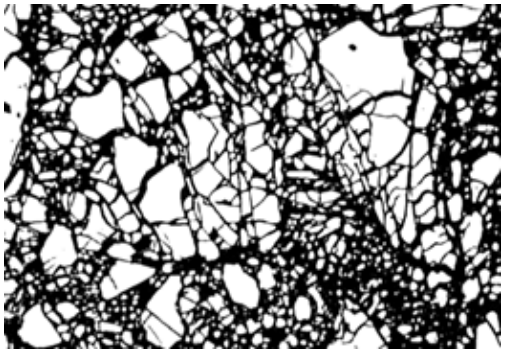

200x

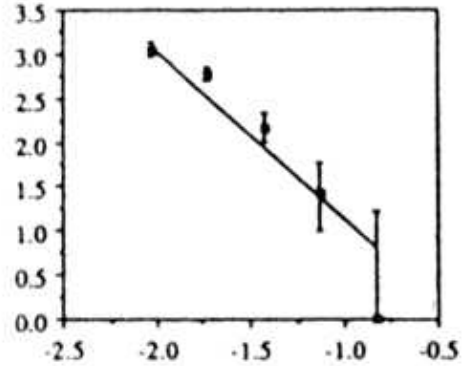

D=1.35±0.21

800x

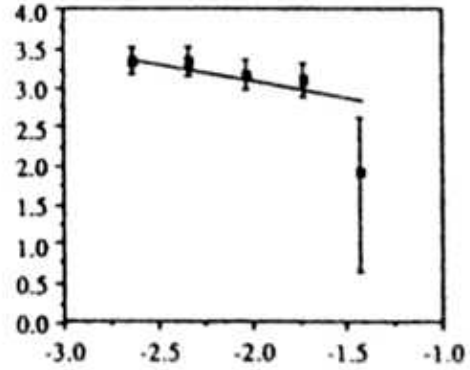

D=0.36±0.26

load cycling 20MPa Y= 2.3

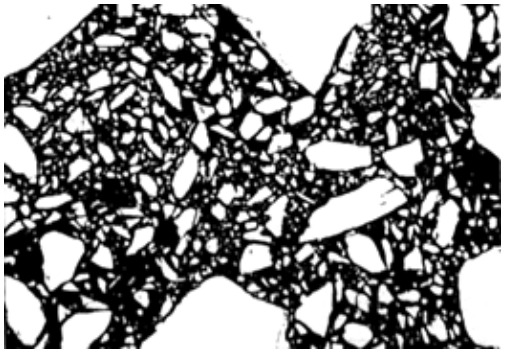

50x

200x

load cycling 100MPa Y= 2.9

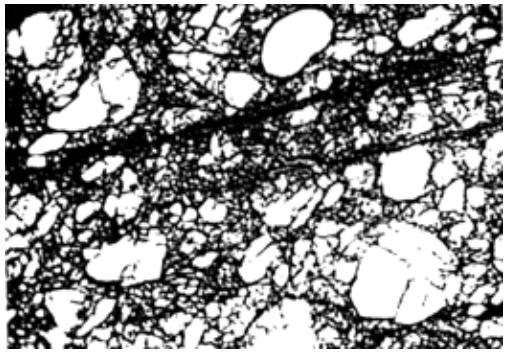

30x

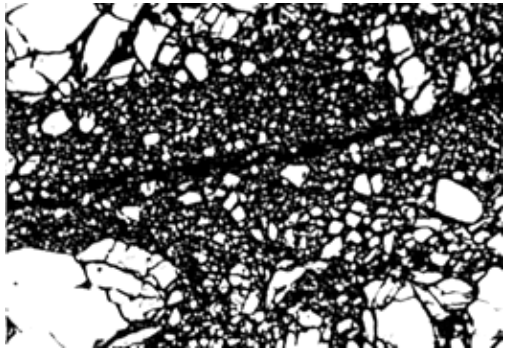

300x

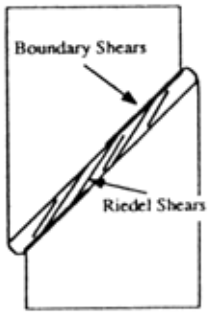

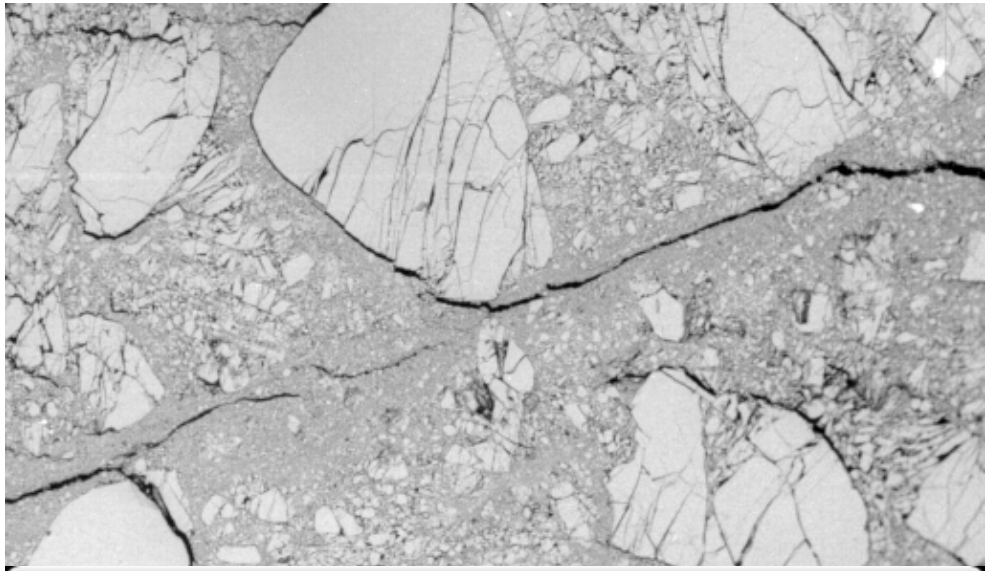

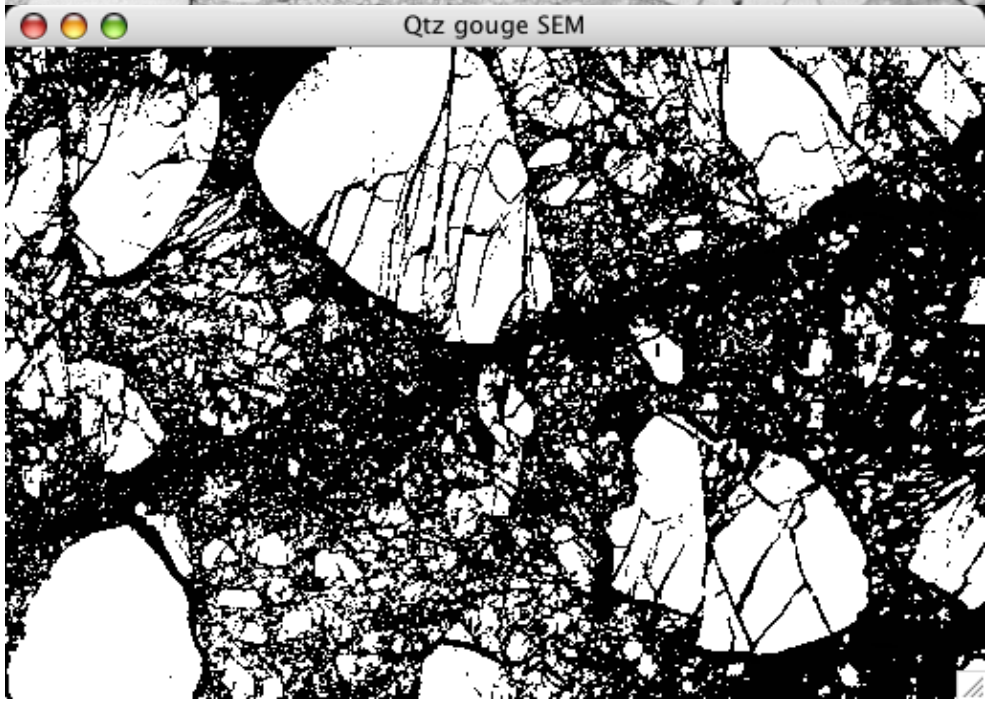

image SXM / NIH Image

threshold (level=60)

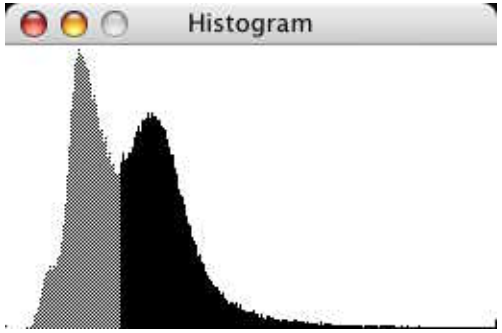

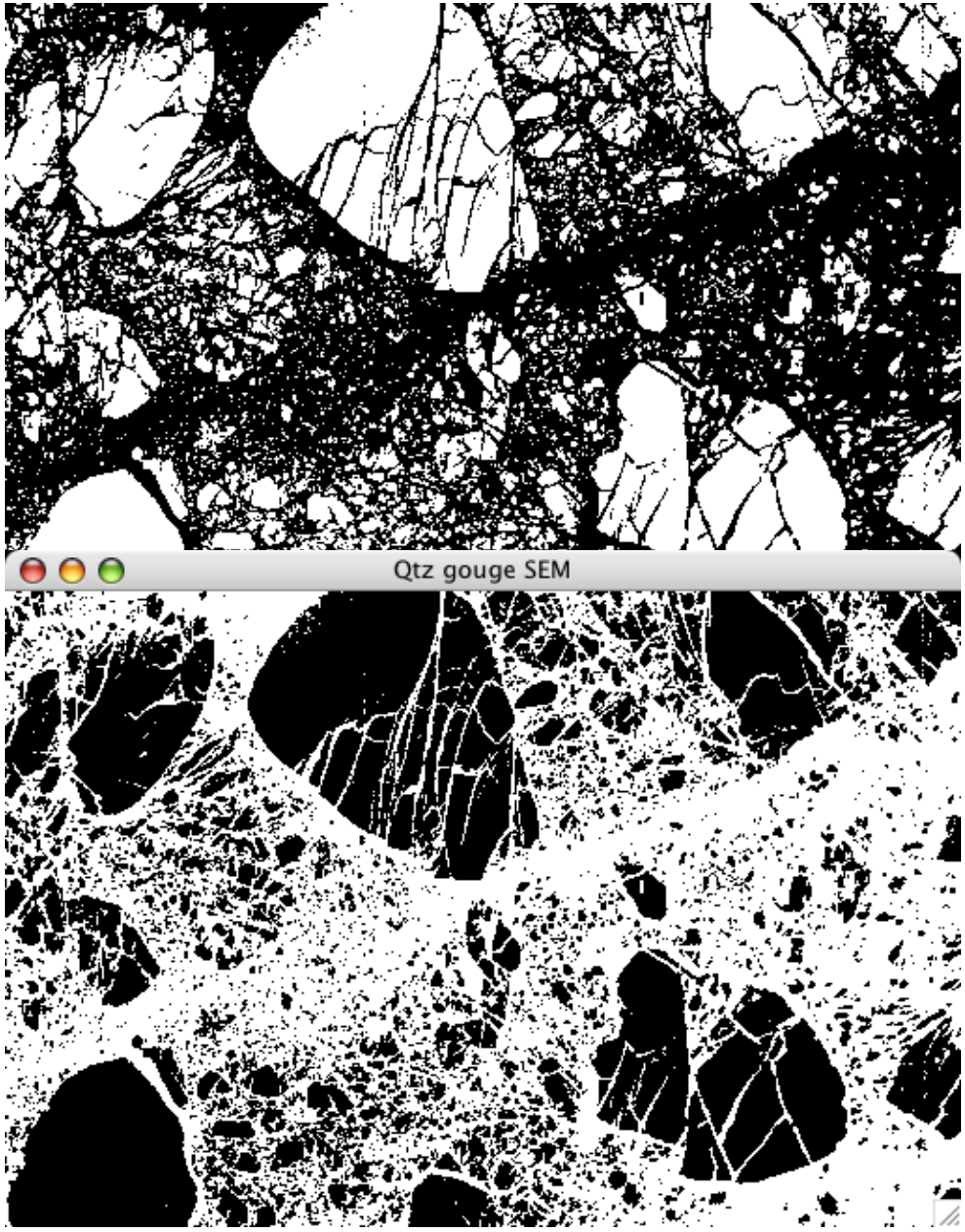

image SXM / NIH Image

invert (area=black)

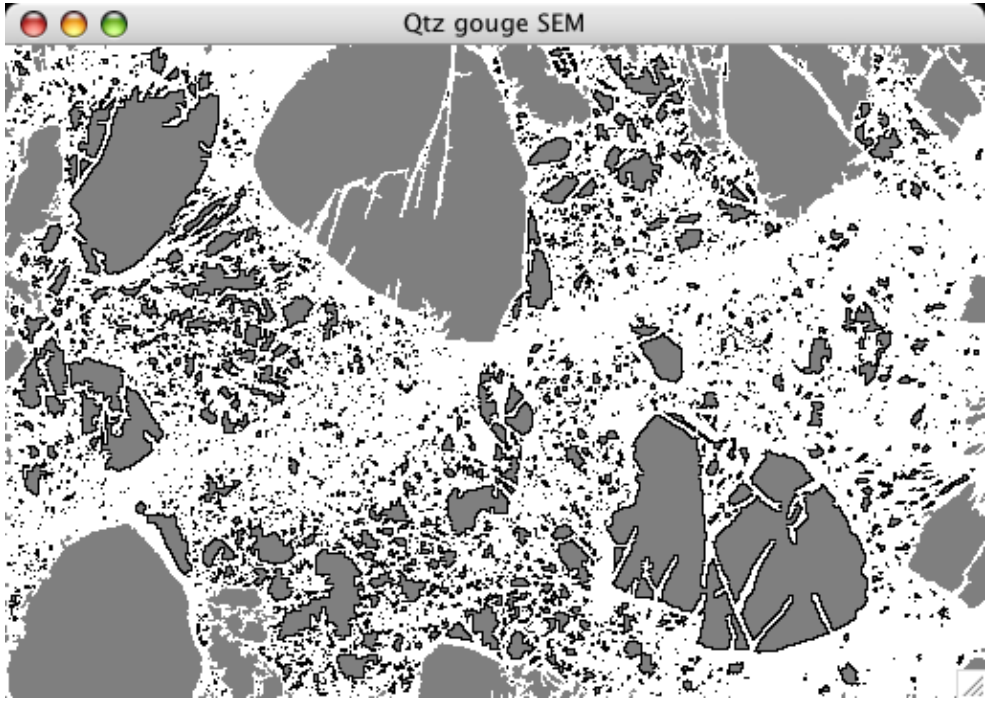

image SXM / NIH Image:

analyze options
- area
- perimeter

export results

➡ Kaleidagraph:

Results

#	Area	Len
1.	101.000	54.527
2.	85.000	72.569
3.	1.000	2.828
4.	7.000	10.485
5.	1.000	2.828
6.	15.000	15.314
7.	2.000	5.657
8.	1.000	2.828
9.	1.000	2.828
10.	2.000	4.828
11.	2.000	4.828
12.	27.000	27.799
13.	533.000	269.262

Qtz gouge SEM (Meas)

	0 #	1 Area	2 Len
0			
1	1.0000	101.00	54.527
2	2.0000	85.000	72.569
3	3.0000	1.0000	2.8280
4	4.0000	7.0000	10.485
5	5.0000	1.0000	2.8280
6	6.0000	15.000	15.314
7	7.0000	2.0000	5.6570
8	8.0000	1.0000	2.8280
9	9.0000	1.0000	2.8280
10	10.000	2.0000	4.8280
11	11.000	2.0000	4.8280
12	12.000	27.000	27.799
13	13.000	533.00	269.26

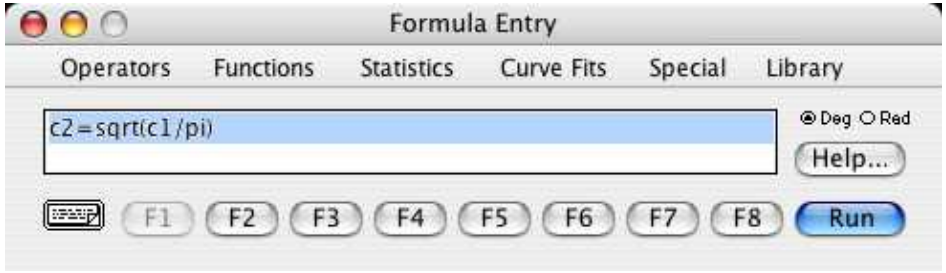

Kaleidagraph:

calculate equivalent radius

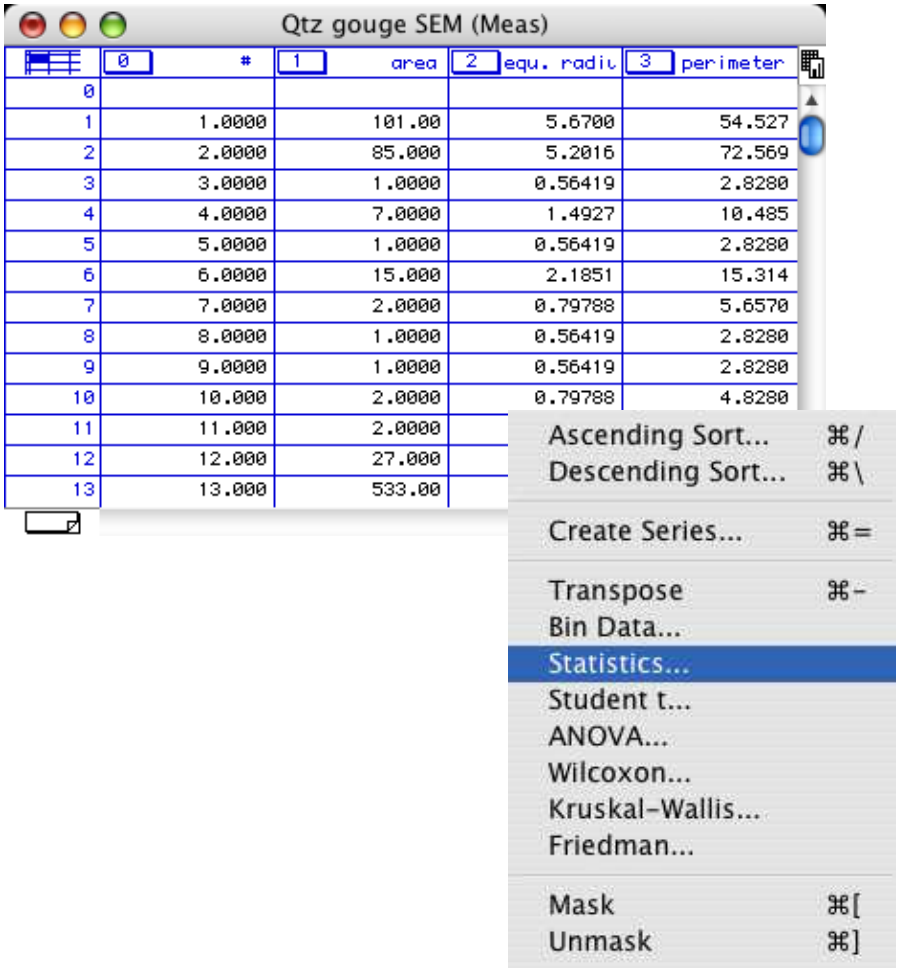

Statistics:

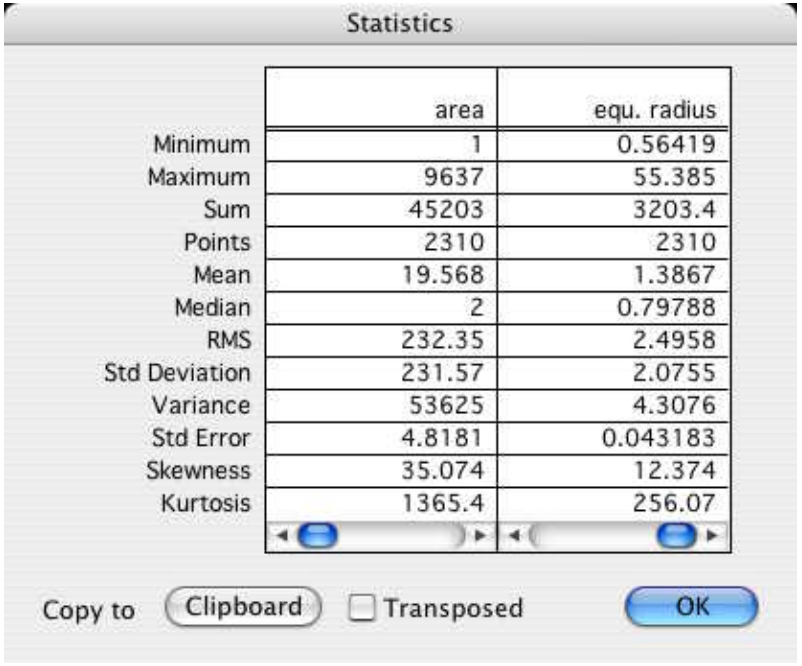

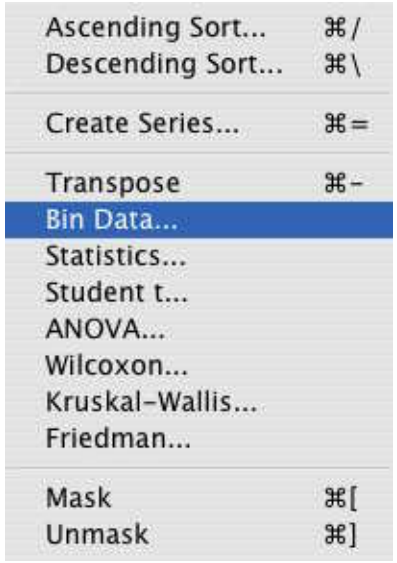

Kaleidagraph:

prepare histograms

(copy to clipboard)
(copy to new file)

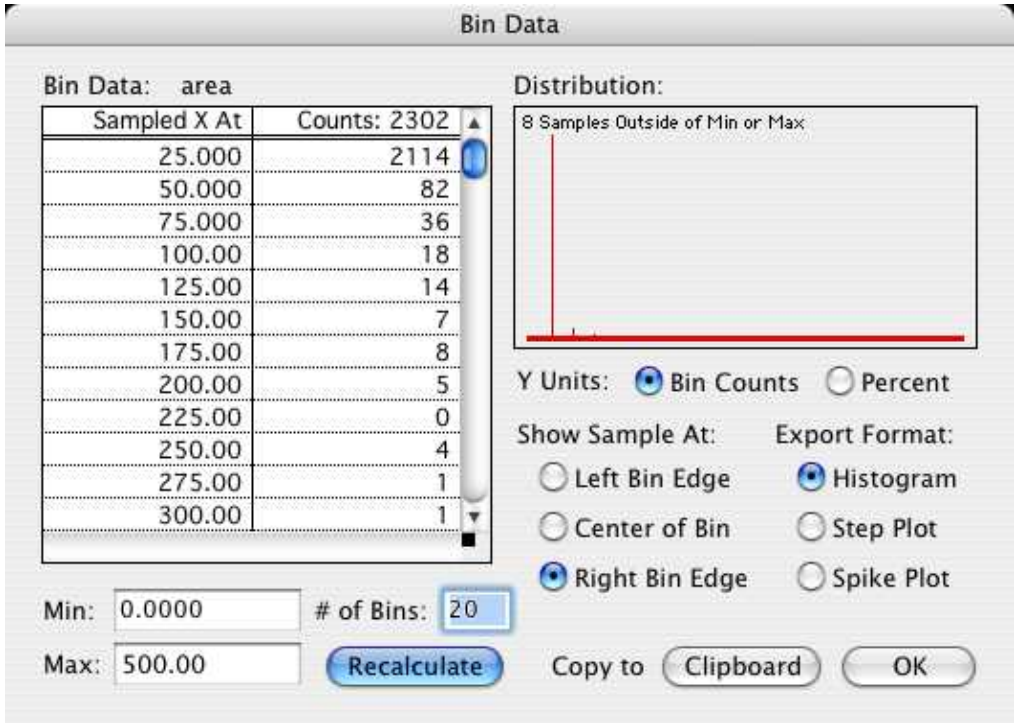

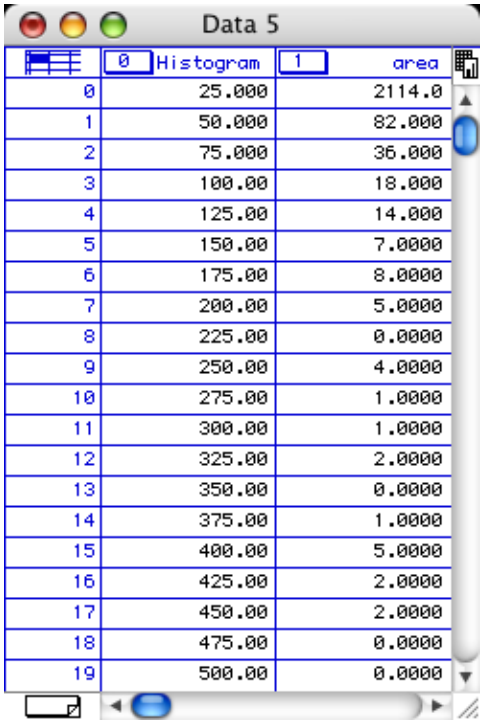

Data 5

	0 area	1 no.	2 equ.radius	3 no.
0	25.000	2114.0	1.0000	1407.0
1	50.000	82.000	2.0000	575.00
2	75.000	36.000	3.0000	160.00
3	100.00	18.000	4.0000	56.000
4	125.00	14.000	5.0000	36.000
5	150.00	7.0000	6.0000	25.000
6	175.00	8.0000	7.0000	14.000
7	200.00	5.0000	8.0000	11.000
8	225.00	0.0000	9.0000	4.0000
9	250.00	4.0000	10.000	4.0000
10	275.00	1.0000	11.000	2.0000
11	300.00	1.0000	12.000	8.0000
12	325.00	2.0000	13.000	1.0000
13	350.00	0.0000	14.000	2.0000
14	375.00	1.0000	15.000	0.0000
15	400.00	5.0000	16.000	0.0000
16	425.00	2.0000	17.000	1.0000
17	450.00	2.0000	18.000	0.0000
18	475.00	0.0000	19.000	0.0000
19	500.00	0.0000	20.000	1.0000

Kaleidagraph:

prepare histograms

(copy to clipboard)
(copy to new file)

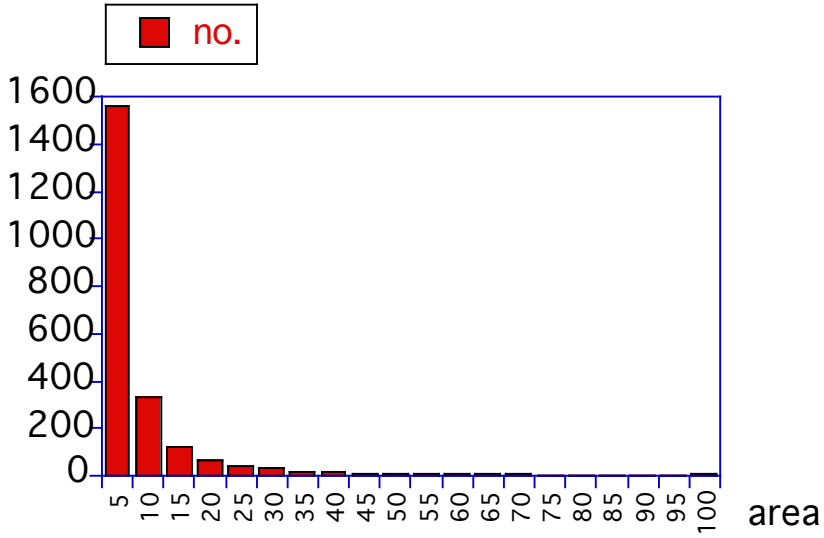

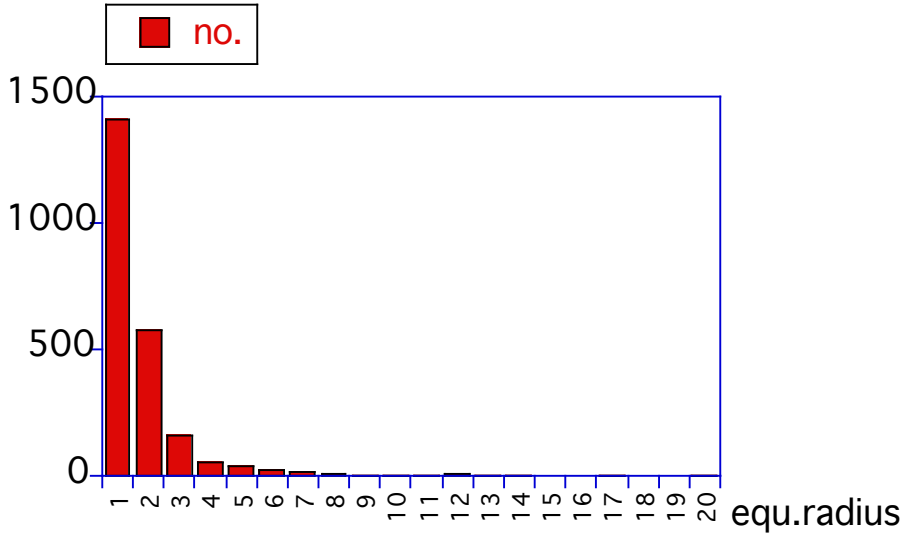

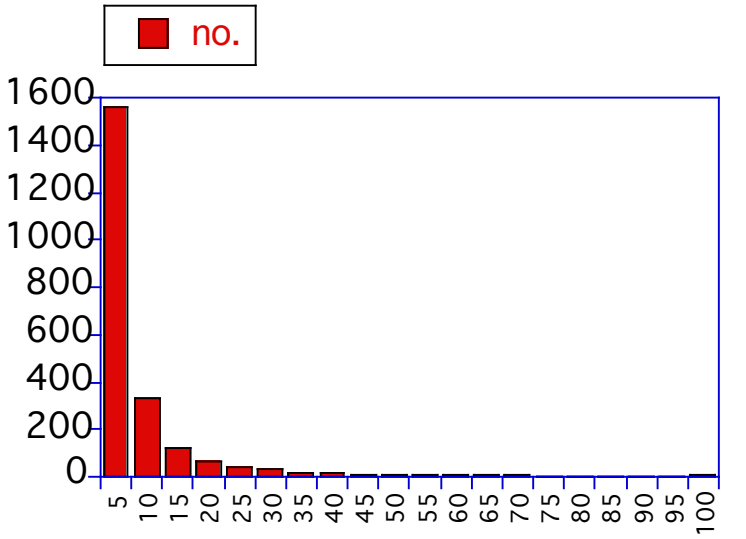

linear bins, linear counts
(quadratic measure)

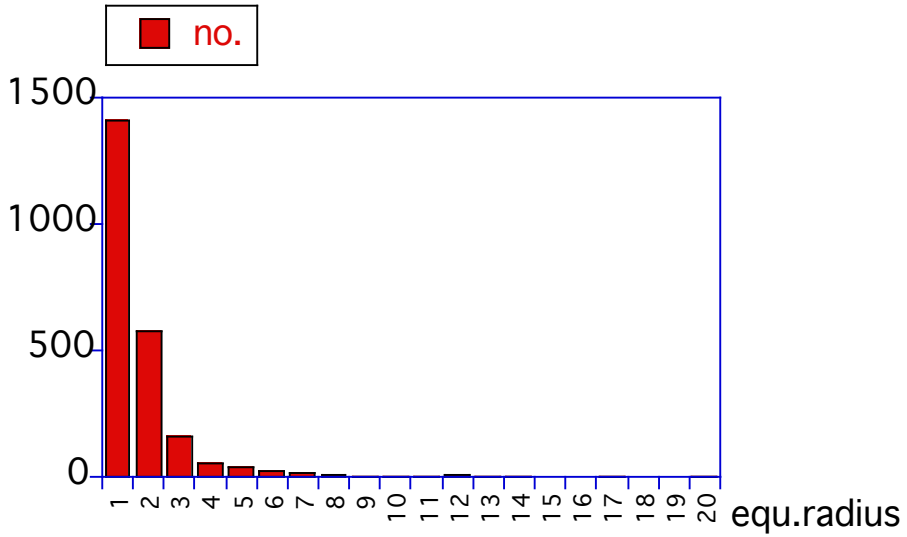

linear bins, linear counts
(linear measure)

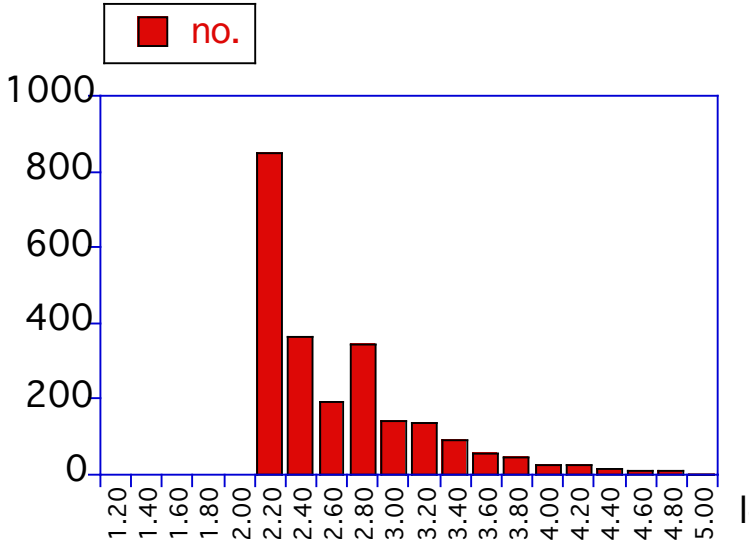

logarithmic bins, linear counts
(increasing bin width)

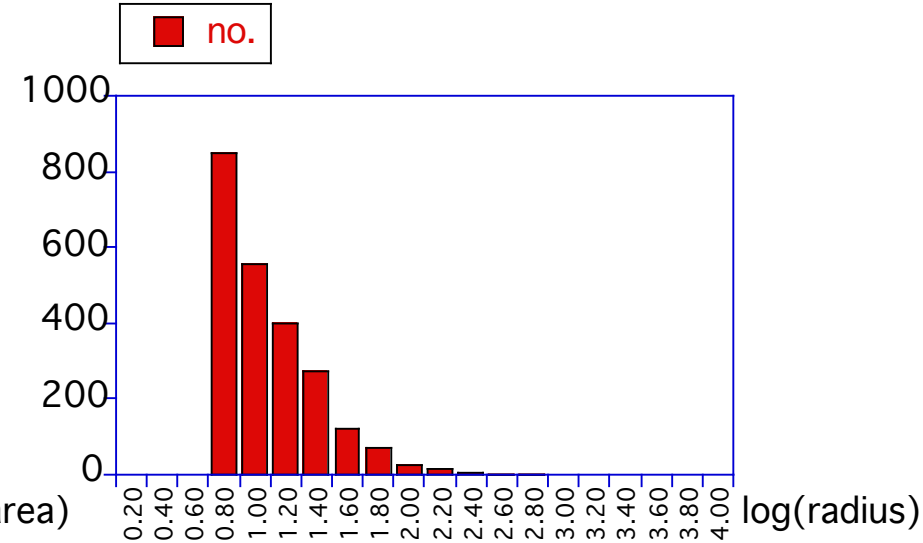

logarithmic bins, linear counts
(increasing bin width)

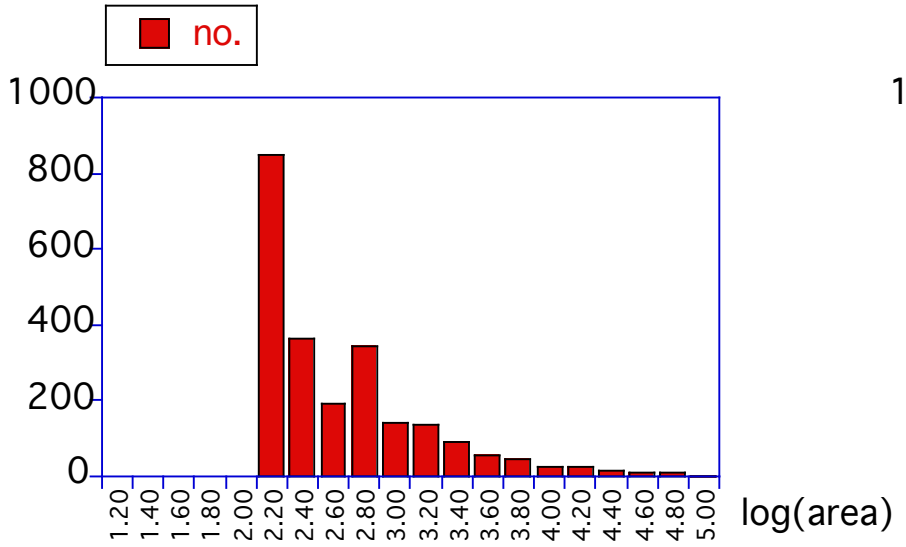

logarithmic bins, linear counts
(increasing bin width)

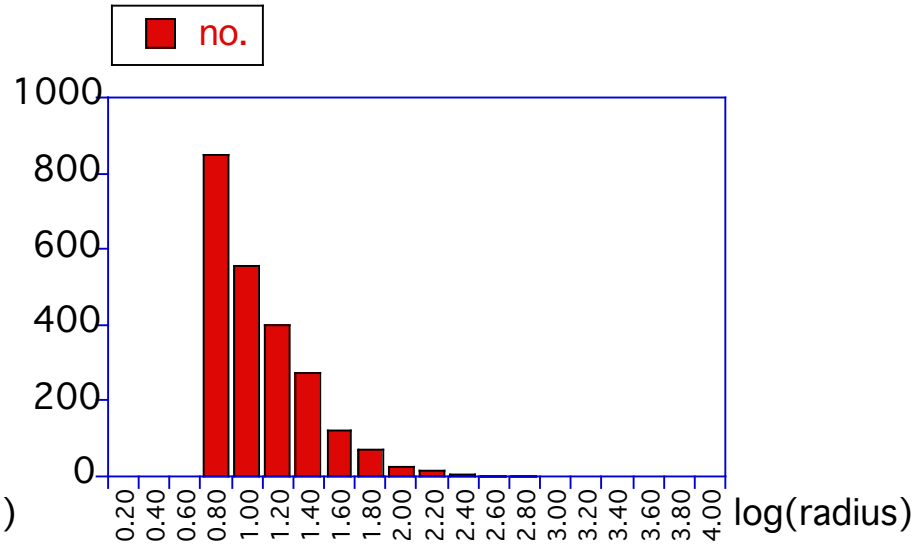

logarithmic bins, linear counts
(increasing bin width)

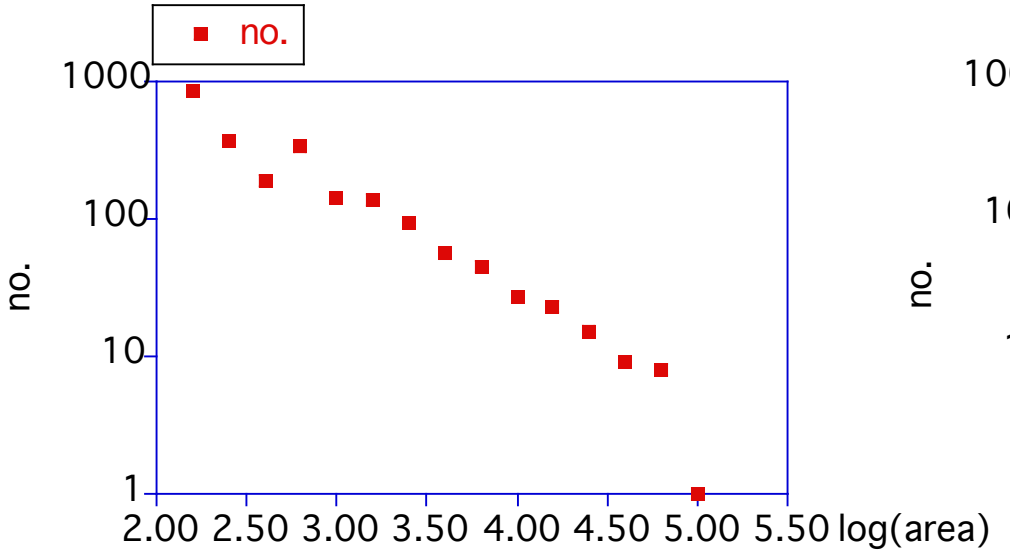

log bins, log counts
(quadratic measure)

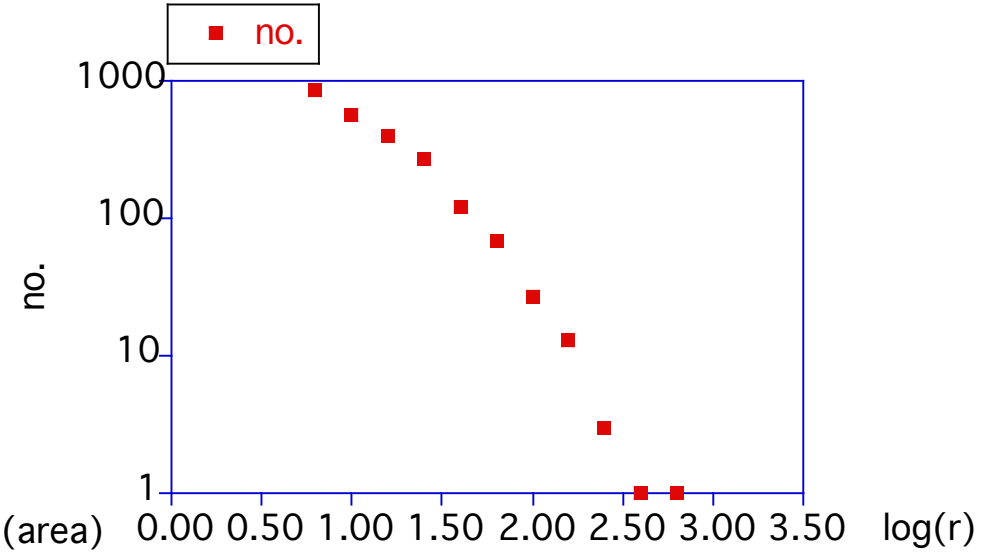

log bins, log counts
(linear measure)

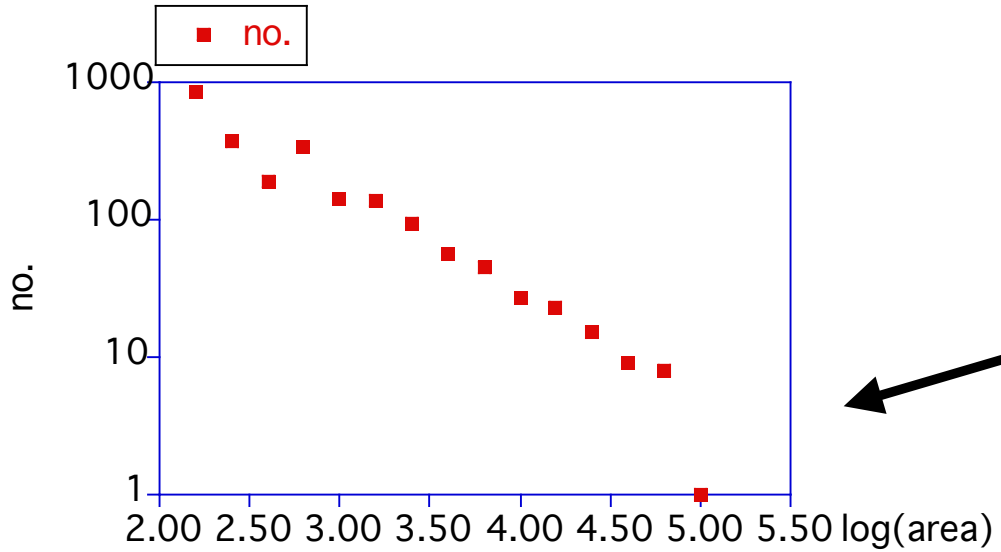

log bins, log counts

ATTENTION !

no. IN size range vs log. size range

no. ABOVE size range vs log. size range

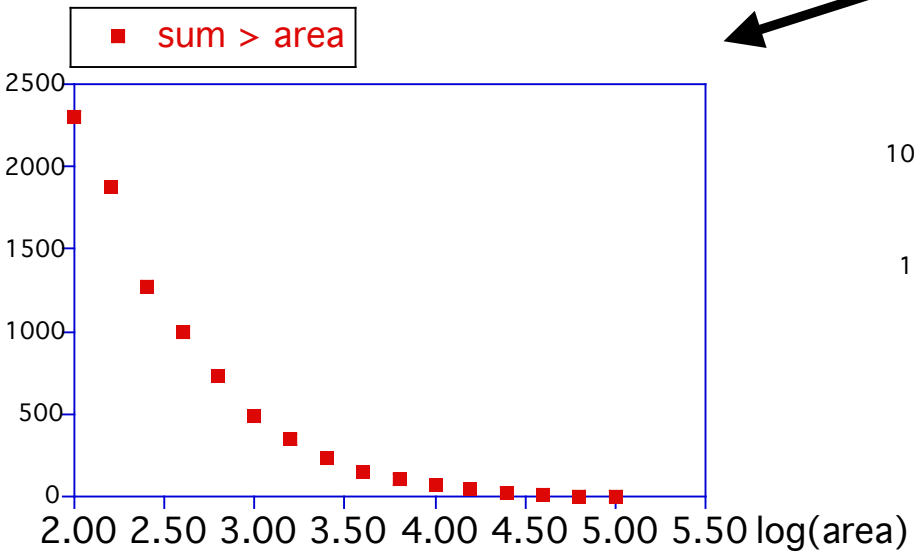

log bins, linear cumulative counts
(no of area > area)

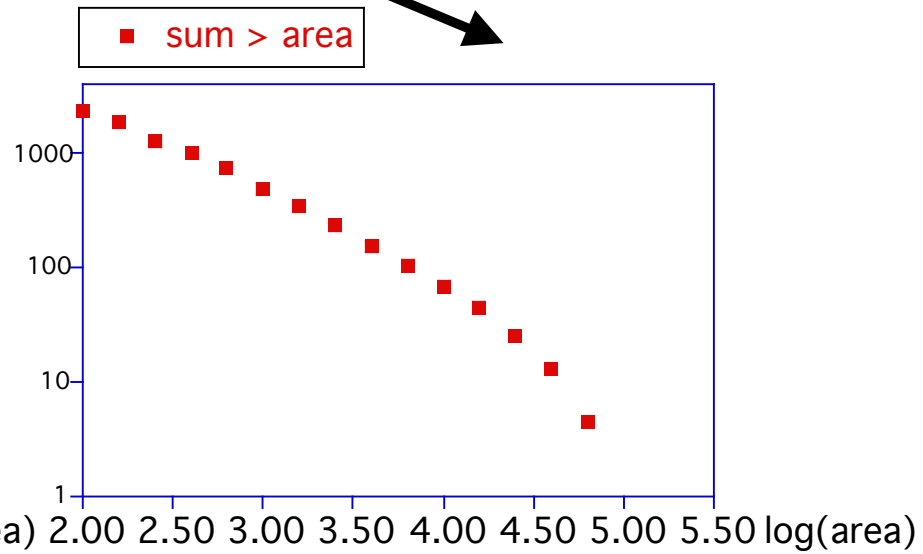

log bins, log cumulative counts
(no of area > area)

ATTENTION !

no. IN size range vs log. size range

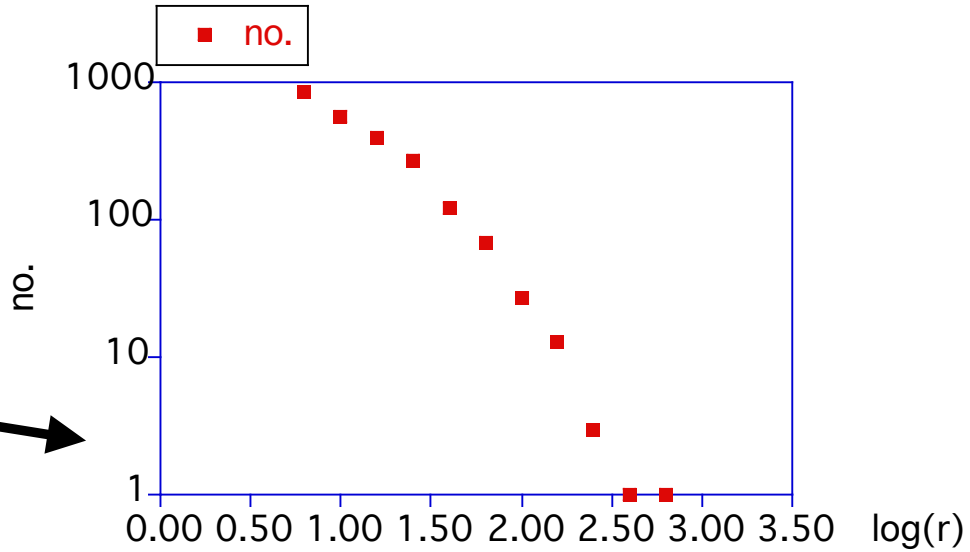

log bins, log counts

no. ABOVE size range vs log. size range

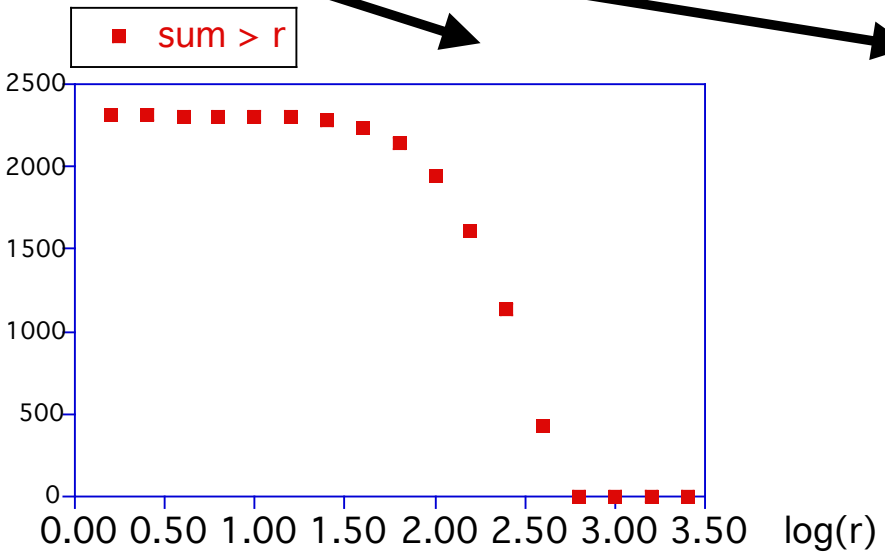

log bins, linear cumulative counts
(no of r > r)

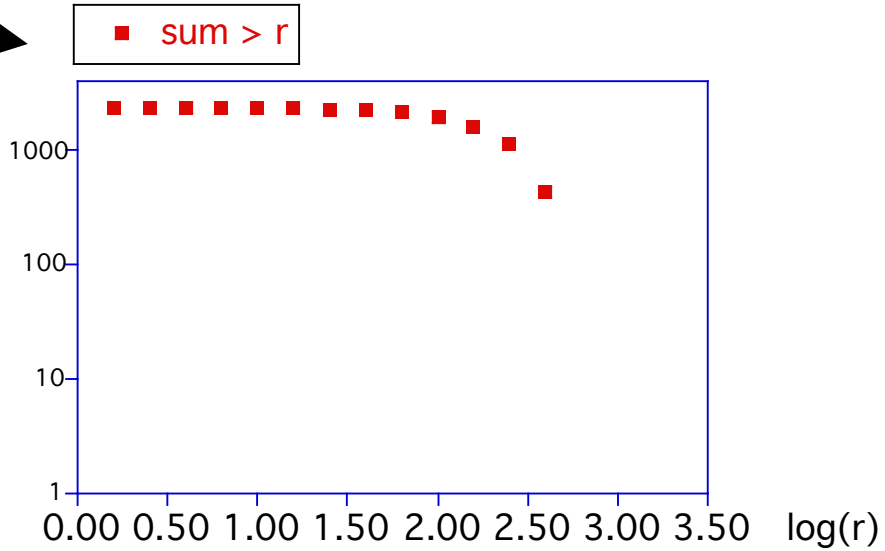

log bins, log cumulative counts
(no of r > r)

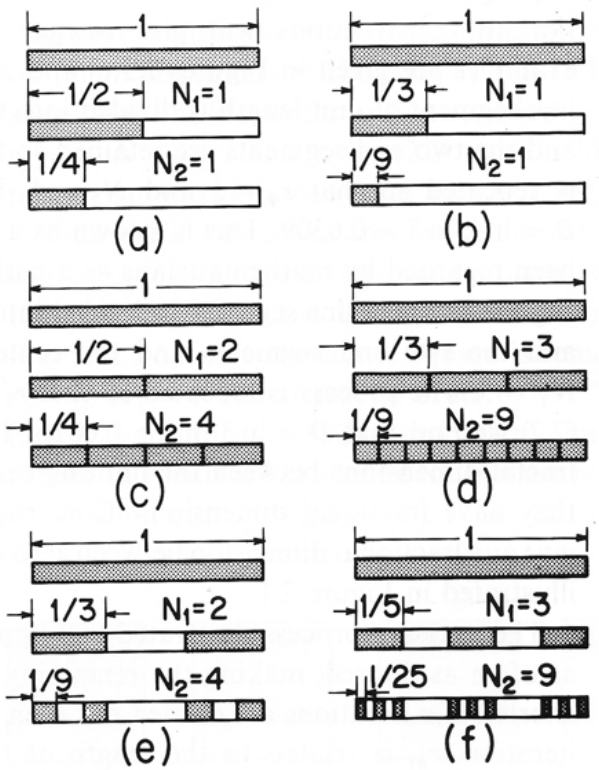

Figure 2.1. At order one a line segment of unit length is divided into an integer number of equal-sized smaller segments. A fraction of these segments is retained. The construction is repeated at higher orders. The first two orders are illustrated. (a) A line segment is divided into two parts and one is retained; $D = \ln 1/\ln 2 = 0$ (fractal dimension of a point). (b) A line segment is divided into three parts and one is retained; $D = \ln 1/\ln 3 = 0$ (fractal dimension of a point). (c) A line segment is divided into two parts and both are retained; $D = \ln 2/\ln 2 = 1$ (fractal dimension of a line). (d) A line segment is divided into three parts and all three are retained; $D = \ln 3/\ln 3 = 1$ (fractal dimension of a line). (e) A line segment is divided into three parts and two are retained; $D = \ln 2/\ln 3 = 0.6309$ (non-integer fractal dimension; this construction is also known as a Cantor set). (f) A line segment is divided into five parts and three are retained; $D = \ln 3/\ln 5 = 0.6826$ (non-integer fractal dimension).

Donald L. Turcotte:
Fractals and chaos in geology and geophysics
Cambridge Univ.Press, 1992

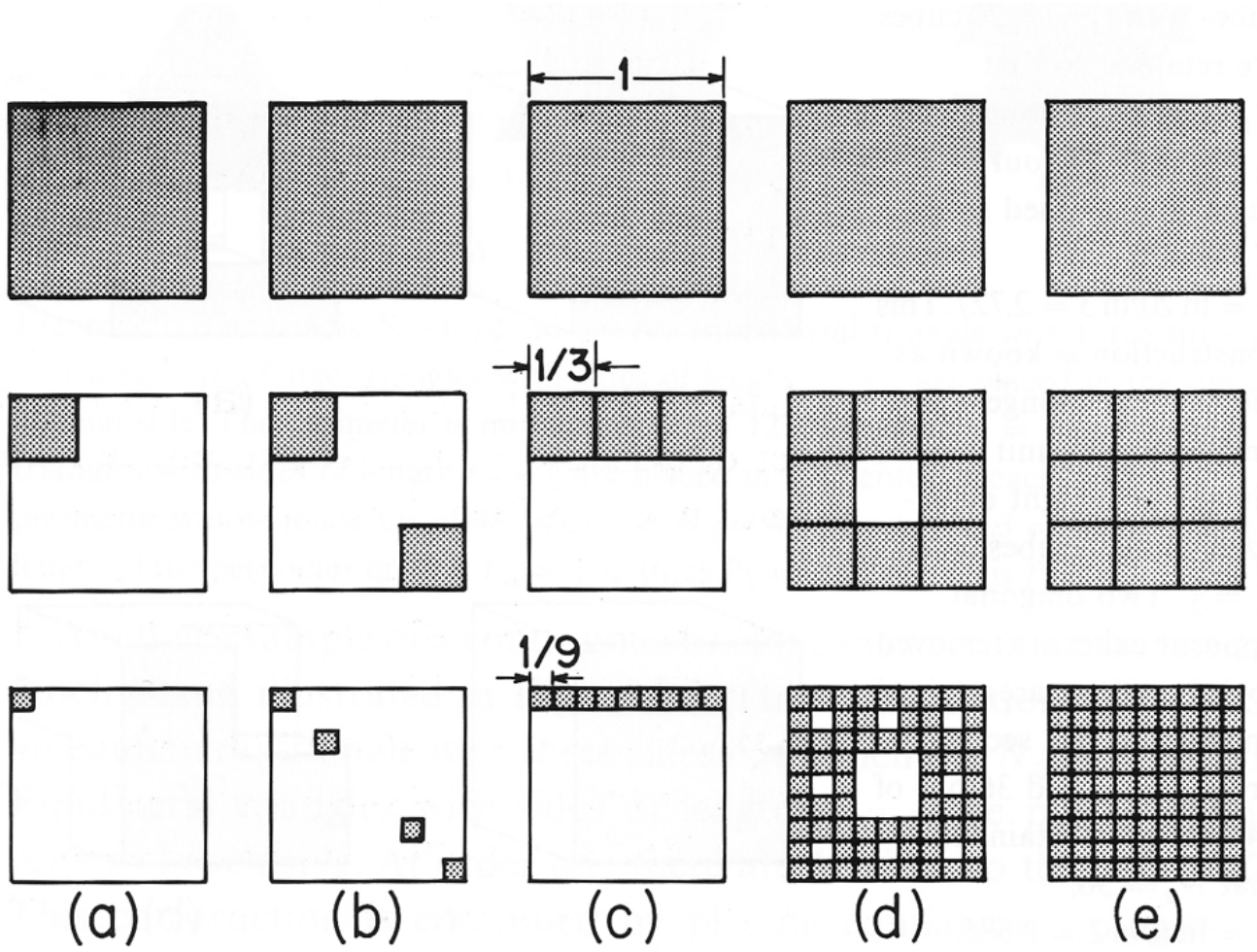

Figure 2.2. At order one the unit square is divided into nine equal-sized smaller squares with $r_1 = \frac{1}{3}$. At order two the remaining squares are divided into nine smaller equal-sized squares with $r_2 = \frac{1}{9}$. Five examples are given in which various numbers of squares, N, are retained. (a) $N_1 = 1$, $N_2 = 1$, $D = \ln 1/\ln 3 = 0$. (b) $N_1 = 2$, $N_2 = 4$, $D = \ln 2/\ln 3 = 0.6309$. (c) $N_1 = 3$, $N_2 = 9$, $D = \ln 3/\ln 3 = 1$. (d) $N_1 = 8$, $N_2 = 64$, $D = \ln 8/\ln 3 = 1.8928$ (also known as a Sierpinski carpet). (e) $N_1 = 9, N_2 = 81$, $D = \ln 9/\ln 3 = 2$.

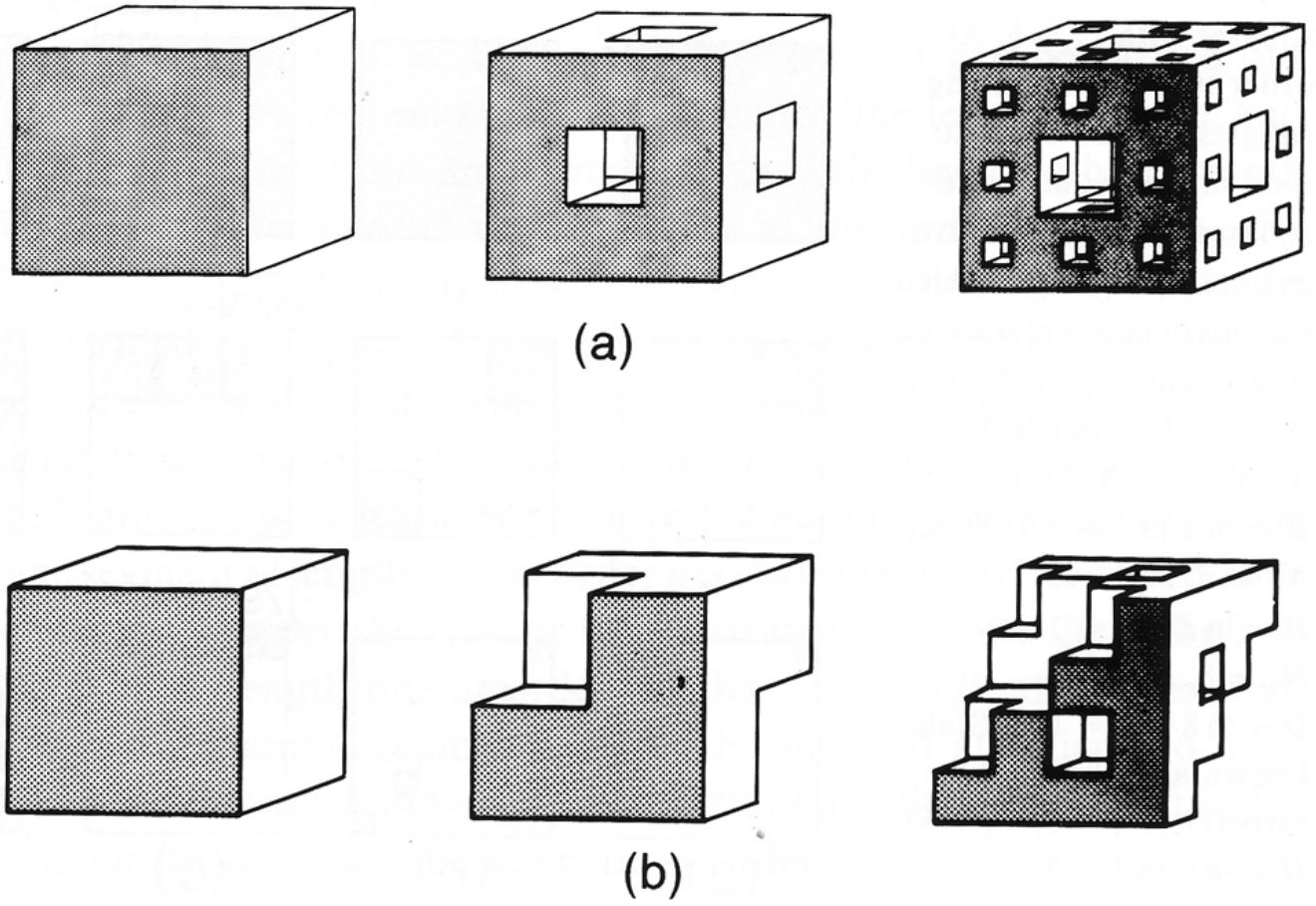

Figure 2.3. (a) At first order the unit cube is divided into 27 equal-sized smaller cubes with $r_1 = \frac{1}{3}$, 20 cubes are retained so that $N_1 = 20$. At second order $r_2 = \frac{1}{9}$ and 400 out of 729 cubes are retained so that $N_2 = 400$;
$D = \ln 20/\ln 3 = 2.727$. This construction is known as the Menger sponge. (b) At first order the unit cube is divided into eight equal-sized smaller cubes with $r_1 = \frac{1}{2}$. Two diagonal opposite cubes are removed so that six cubes are retained and $N_1 = 6$. At second order $r_2 = \frac{1}{4}$ and 36 out of 64 cubes are retained so that $N_2 = 36$;
$D = \ln 6/\ln 2 = 2.585$.

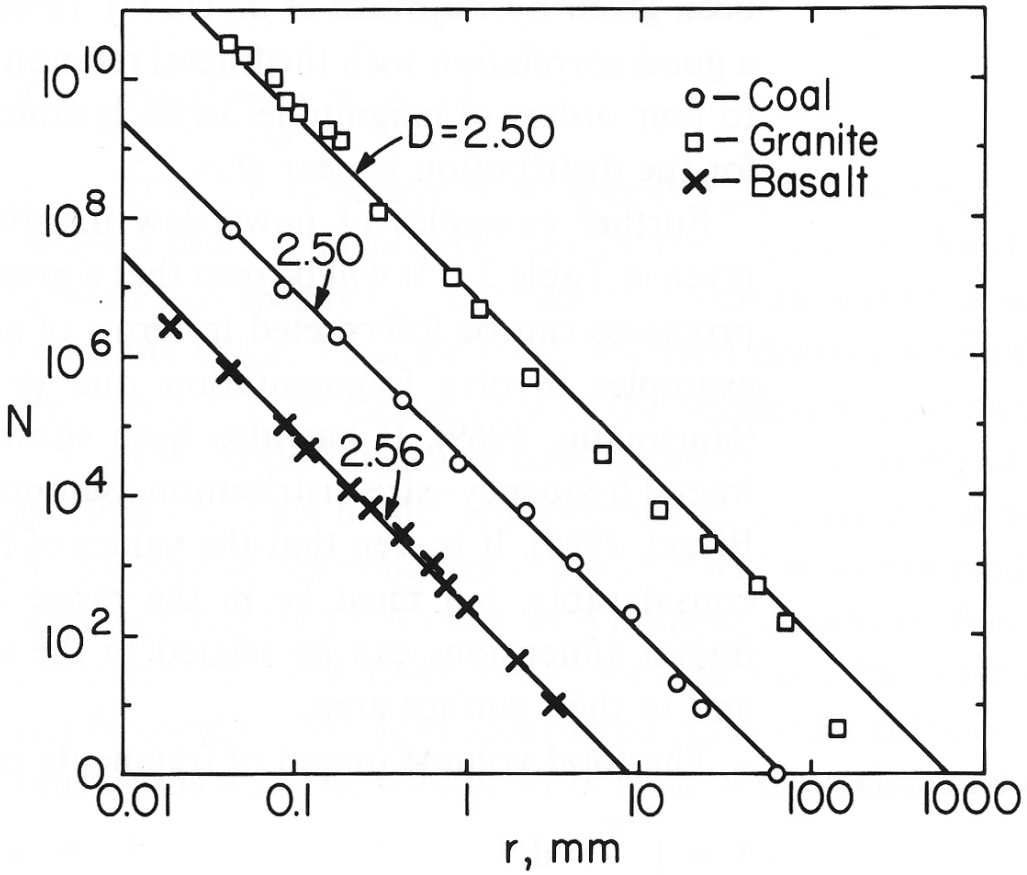

Figure 3.1. Since fragments have a variety of shapes, the cube root of volume is an objective measure of size. The number N of fragments with cube root of volume greater than r is given as a function of r for broken coal (Bennett, 1936), broken granite from a 61 kt underground nuclear detonation (Schoutens, 1979), and impact ejecta due to a 2.6 km s^{-1} polycarbonate projectile impacting on basalt (Fujiwara *et al.*, 1977). The best-fit fractal distribution from (2.6) is shown for each data set.

Figure 3.2. Idealized model for fractal fragmentation. A zero-order cubic cell with dimensions h is divided into eight zero-order cubic elements each with dimensions $h/2$. The probability that a zero-order cell will be fragmented into eight zero-order elements is f. The fragments with dimensions $h/2$ become first-order cells; each of these have a probability f of being fragmented into first-order elements with dimensions $h/4$. The process is repeated to higher orders. The basic structure is fractal.

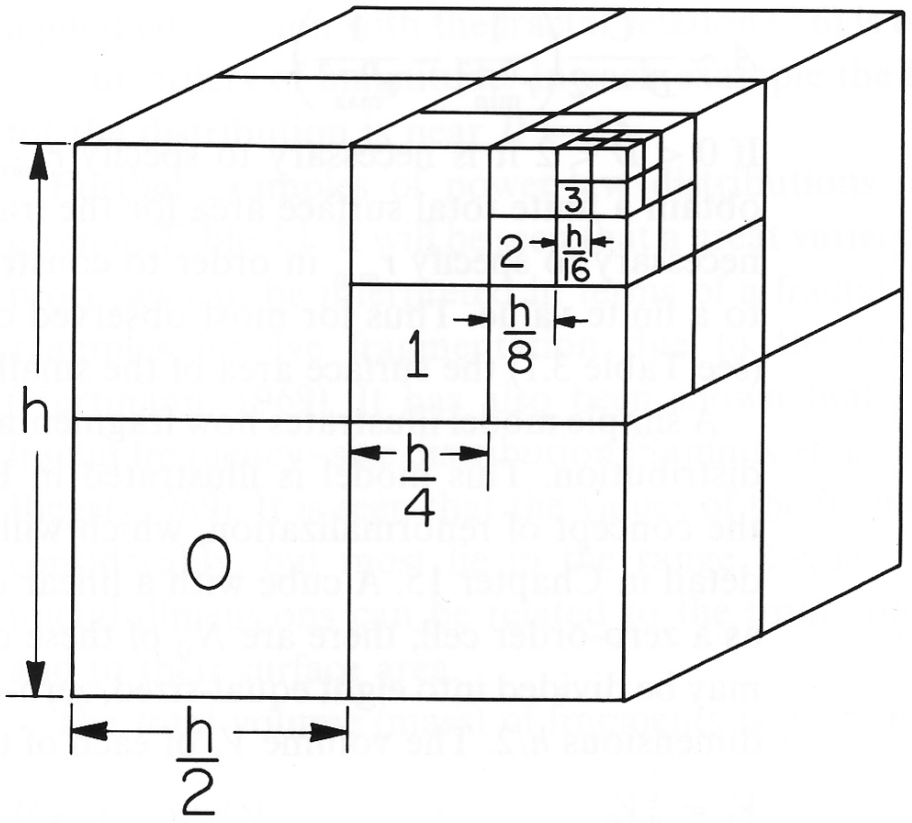

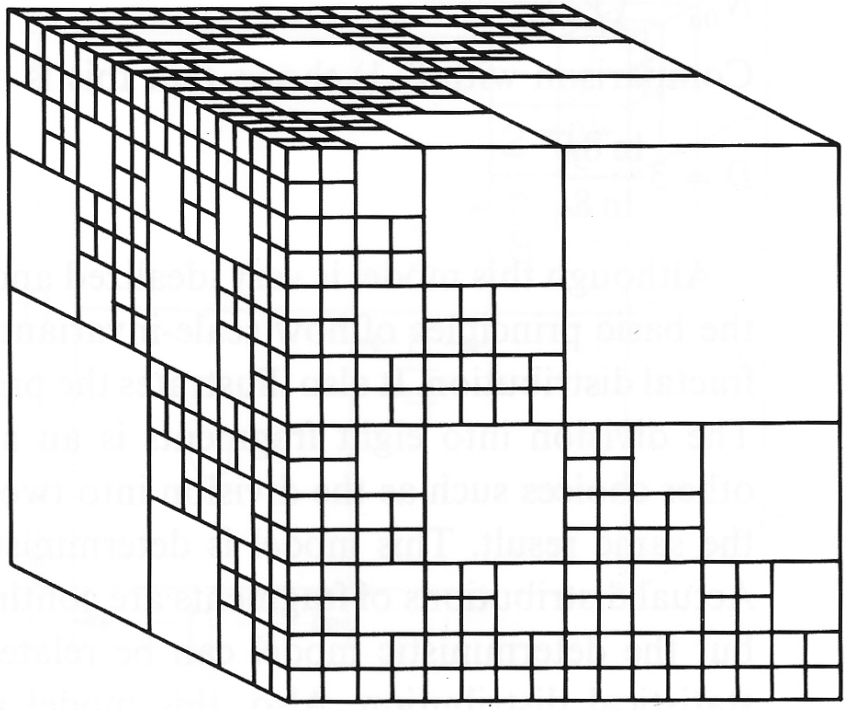

Figure 3.3. Illustration of a fractal model for fragmentation. Two diagonally opposite cubes are retained at each scale. With $r_1 = h/2$, $N_1 = 2$ and $r_2 = h/4$, $N_2 = 12$ we have $D = \ln 6/\ln 2 = 2.5850$.

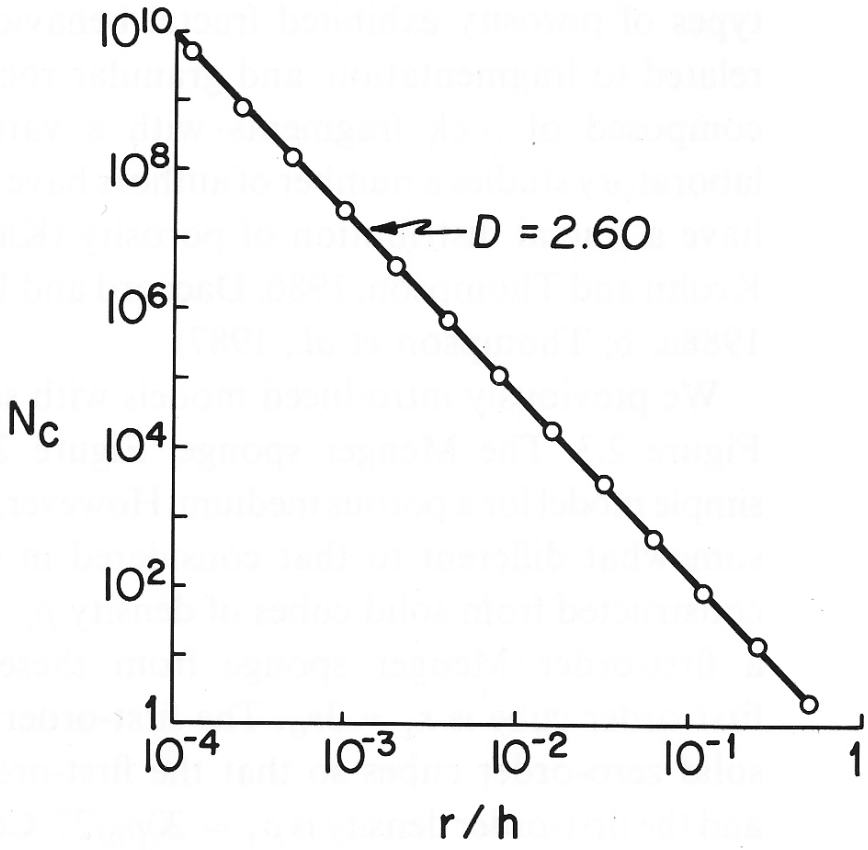

Figure 3.4. Cumulative statistics for the fragmentation model illustrated in Figure 3.3. Correlation with (2.6) gives $D = 2.60$.

G.C. Rowling & L.B. Goodwin (2003)
Cataclasis and particuate flow in faulted, poorly lithified sediments
JSG, 25, 317-331

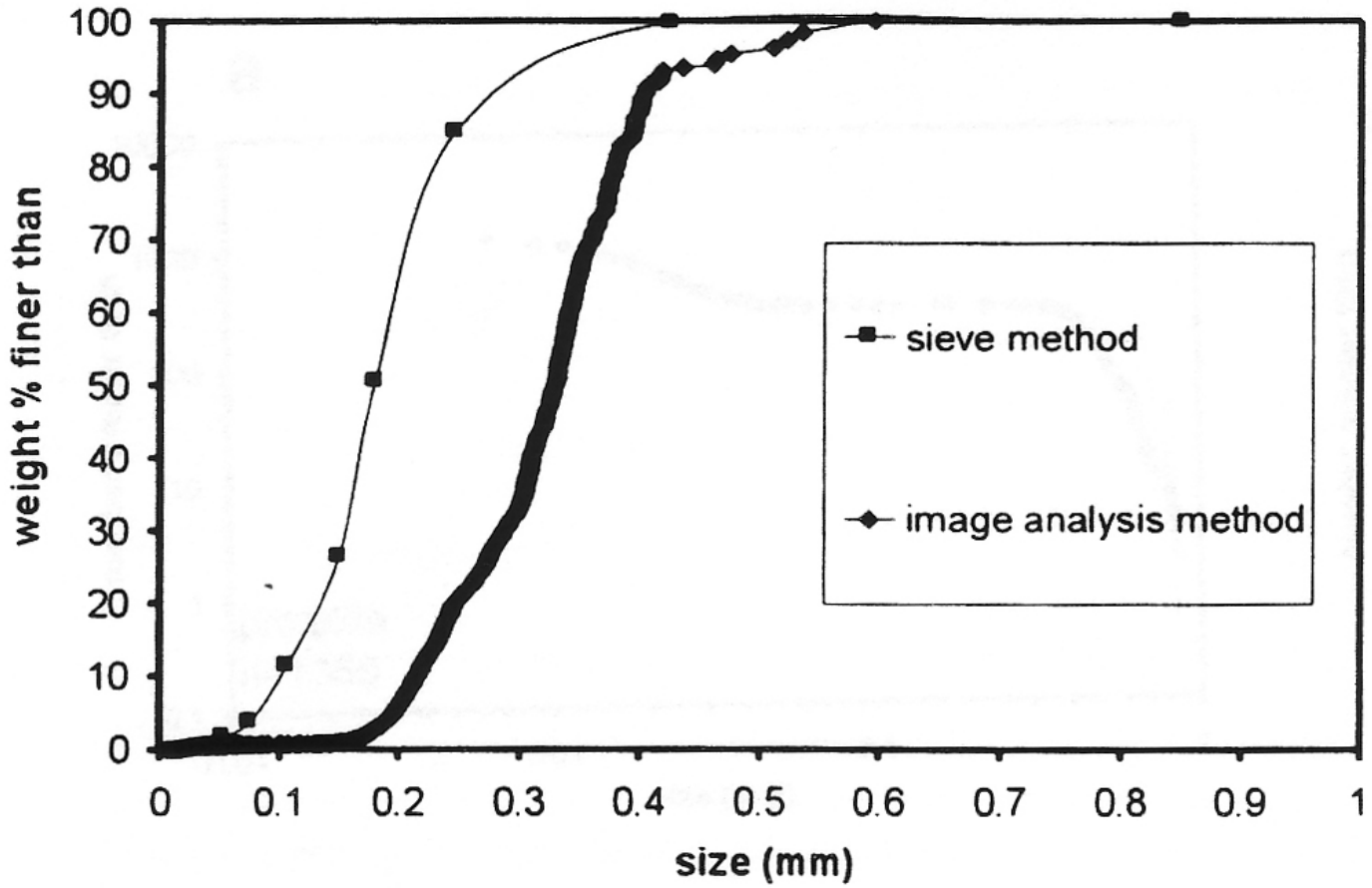

Fig. 8. Crushed quartz sand PSDs by weight determined by sieving and image analysis methods. Image analysis distribution by number was converted to distribution by weight by calculating equivalent spherical sizes from nominal section diameters and assuming a density for all particles of 2.65 g/cm^3.

9

Griffith failure

Deformationsprozesse in der Erde (9)

Griffith failure

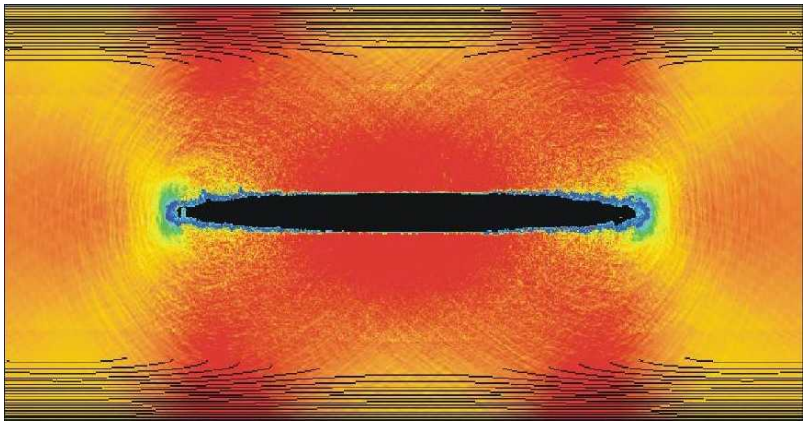

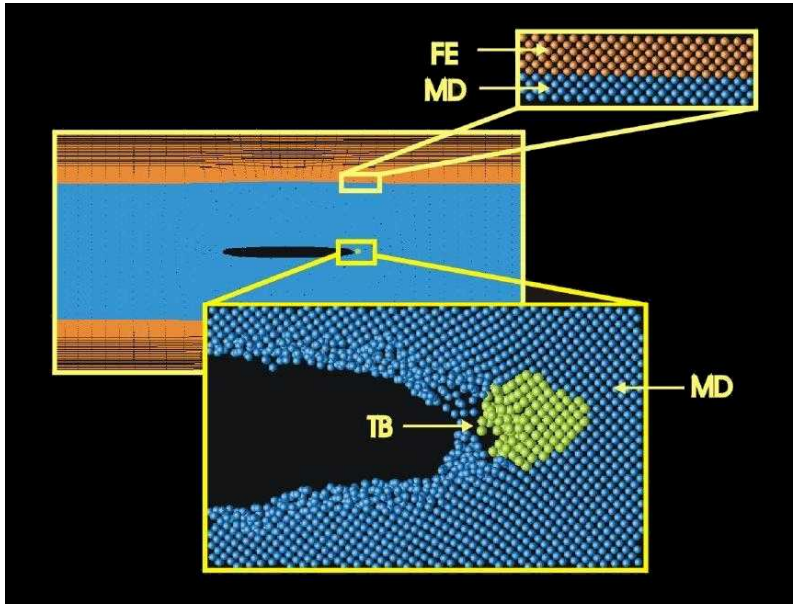

Mode of failure

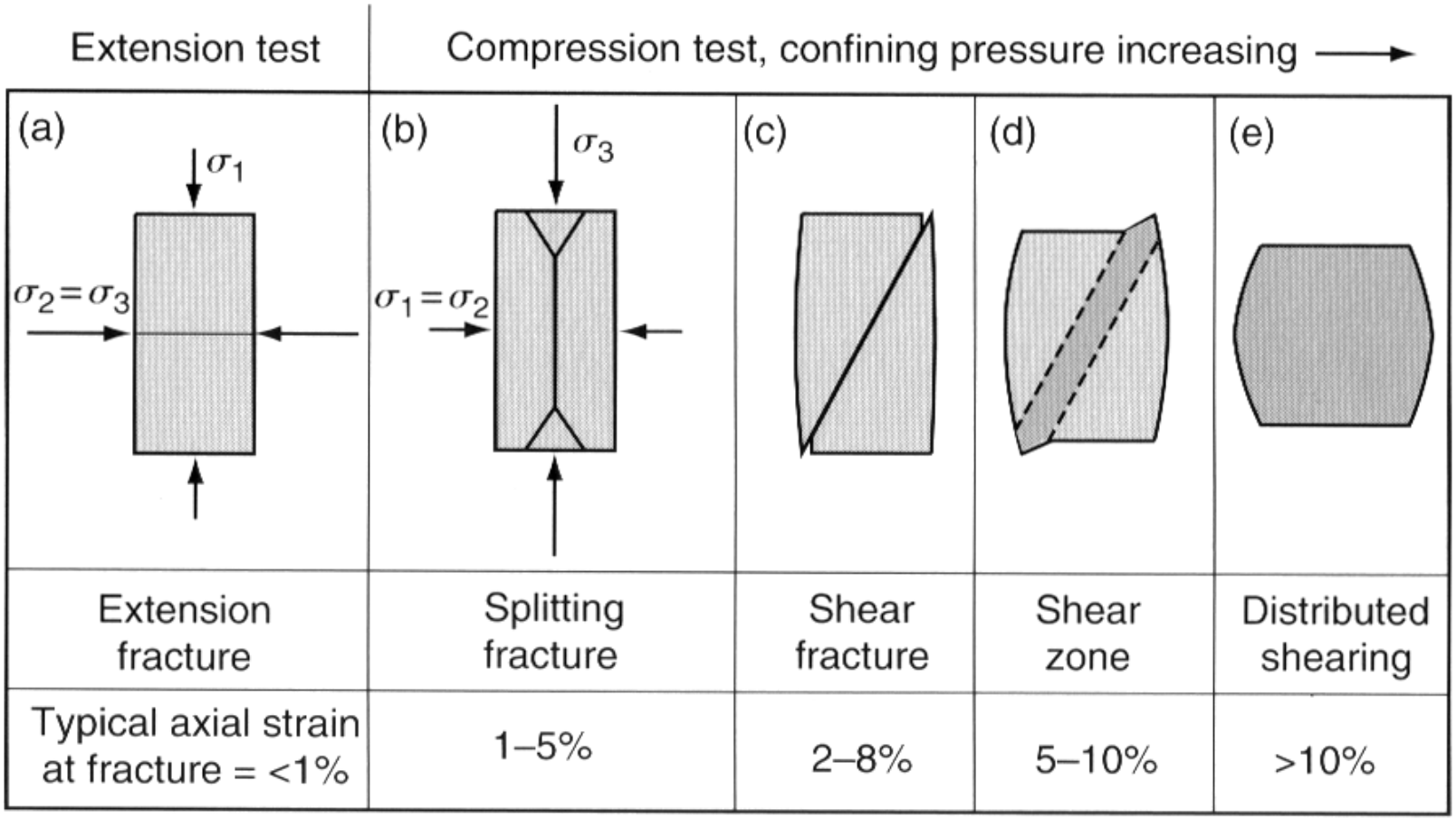

Fig 9.1 Schematic representation of brittle failure styles in triaxial tests. (a) Extension test. (b)–(e) Compression test with confining pressure increasing to the right. Reprinted from Griggs and Handin (1960a) with permission of The Geological Society of America.

Pollard, D.D. & Fletcher, R.C., 2005

Concept of virtual work

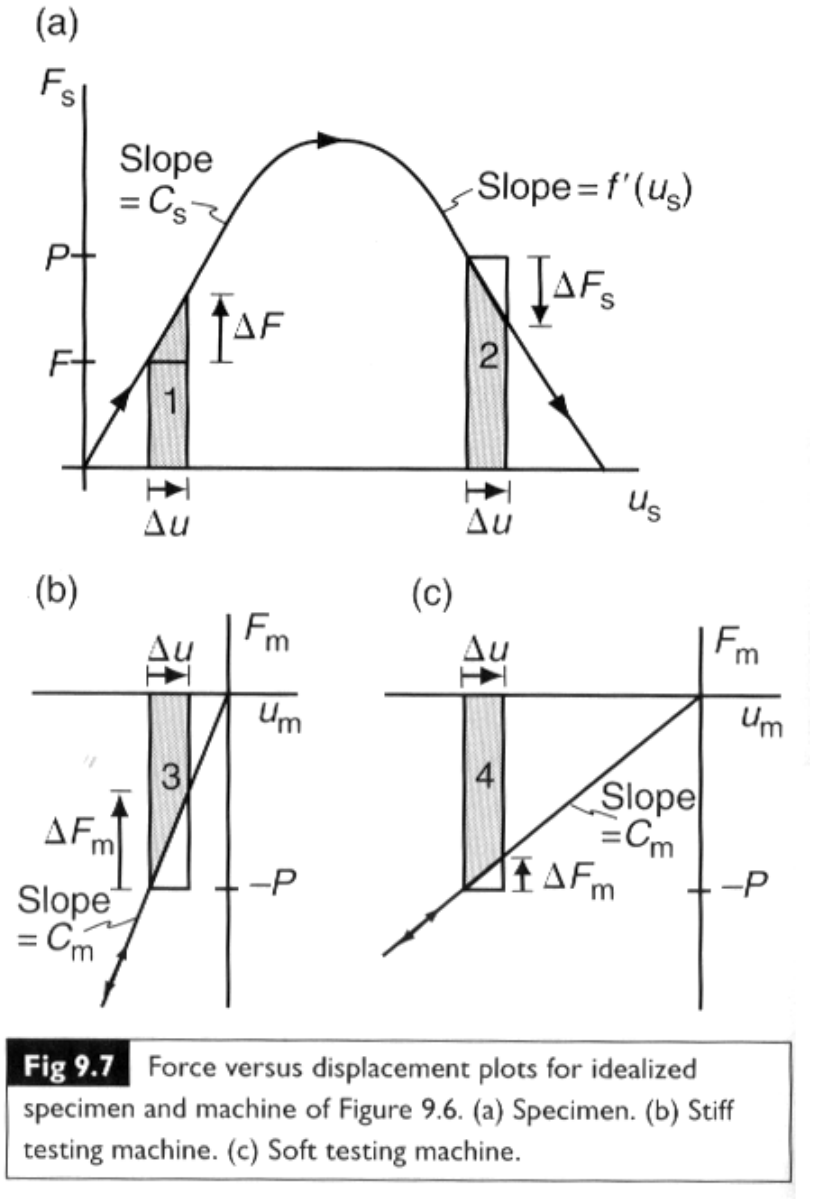

Fig 9.7 Force versus displacement plots for idealized specimen and machine of Figure 9.6. (a) Specimen. (b) Stiff testing machine. (c) Soft testing machine.

Pollard, D.D. & Fletcher, R.C., 2005

stiff machine = stable:
Cm > Cs

soft machine = unstable:
Cm < Cs

Failure surface

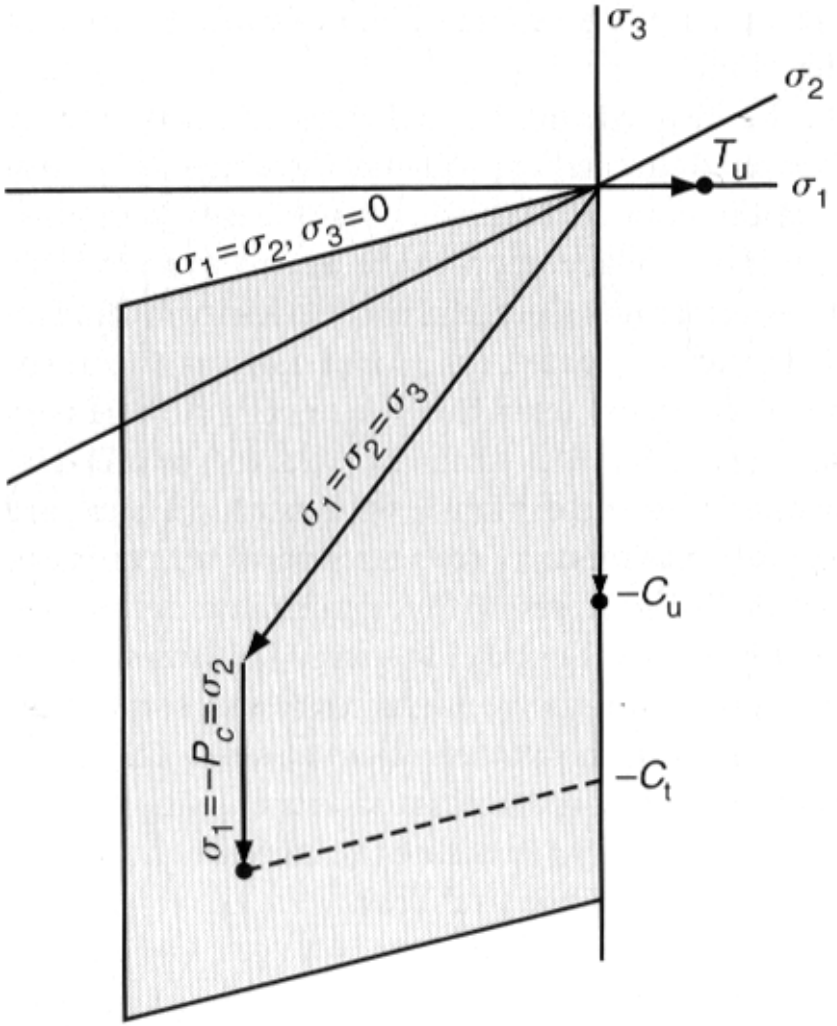

Fig 9.10 Plot in principal stress space with uniaxial tensile and compressive strengths, T_u and C_u, and triaxial compressive strength, C_t.

Pollard, D.D. & Fletcher, R.C., 2005

Effective pressure (Terzaghi)

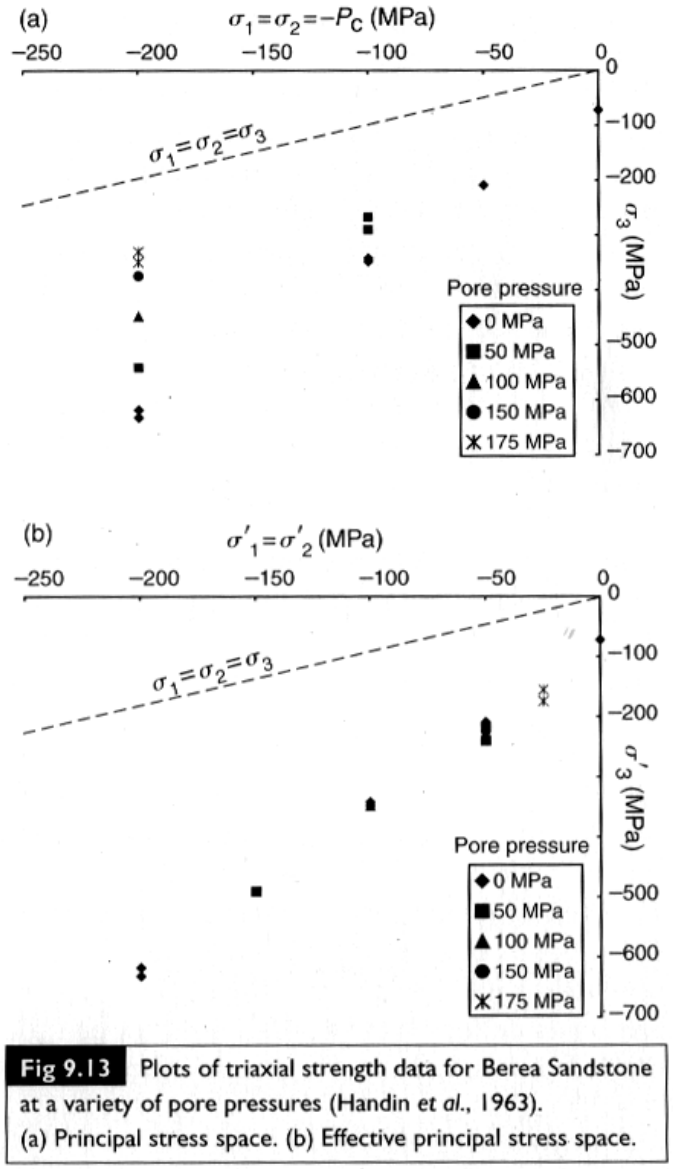

Fig 9.13 Plots of triaxial strength data for Berea Sandstone at a variety of pore pressures (Handin *et al.*, 1963). (a) Principal stress space. (b) Effective principal stress space.

Pollard, D.D. & Fletcher, R.C., 2005

Strength of perfect crystal

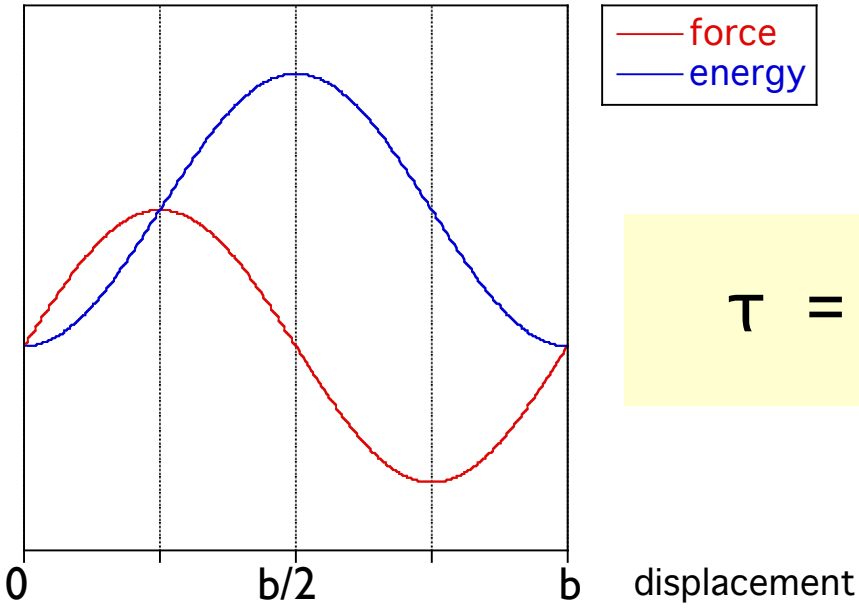

$$\tau = \tau_m \sin(2\pi x / b)$$

τ	applied stress
b	distance between equilibrium position
x	distance atoms are moved
τ_m	max. theoretical strength of crystal

$$\tau = \tau_m \sin(2\pi x / b)$$

Hooke's law: $\tau = G \cdot \Upsilon$

approximations for small x:
$\Upsilon \approx x/a$; $\sin(2\pi x / b) \approx (2\pi x / b)$

$G \cdot x/a \approx \tau_m (2\pi x / b)$

$\tau_m \approx G \cdot b / 2\pi a$

For most crystals: $a \approx b$

$\tau_m \approx G / 2\pi$

Maximum theoretical shear strength:

$$\tau_m \approx G / 2\pi$$

material	theory G/2π (GPa)	experimental yield strength (MPa)
Copper	19.6	0.49
Iron	33.9	27.5
Beryllium (basal slip)	49.3	1.37
Beryllium (prism slip)	49.3	52.0

Theoretical cohesive strength of perfect crystal

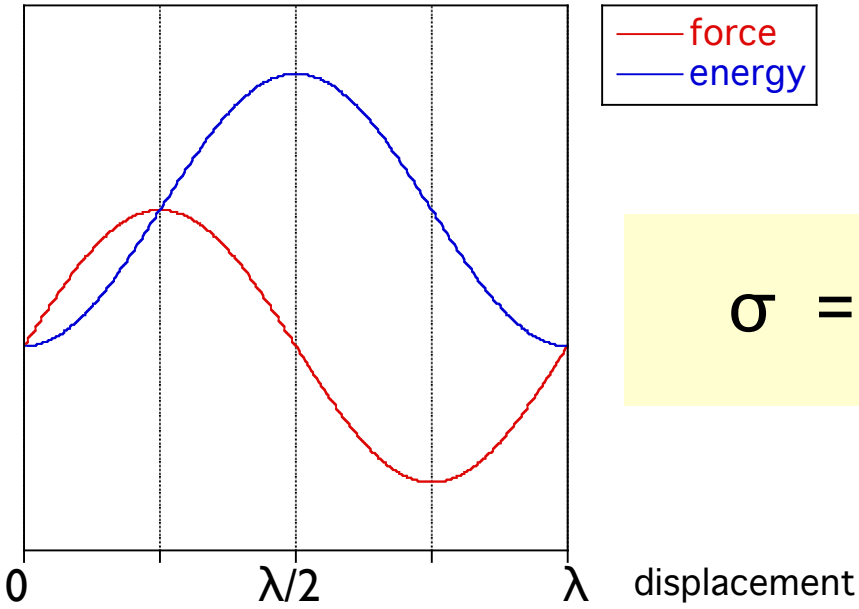

$$\sigma = \sigma_c \sin(2\pi x / \lambda)$$

σ applied stress

x distance atoms are moved

σ_c max. theoretical cohesive strength

$x << \lambda$

$$\sigma = \sigma_c \sin(2\pi x / \lambda)$$

For small x:

$$\sigma = \sigma_c \cdot 2\pi x / \lambda$$

Slope of curve:

$$d\sigma/dx = \sigma_c \cdot 2\pi / \lambda \qquad (1)$$

Hooke's law: $\sigma = E \cdot (x/a_0)$

E modulus of elasticity
a_0 equilibrium atomic separation

Differentiating Hooke's law:

$$d\sigma / dx = E / a_0 \qquad (2)$$

Combining (1) and (2)

$$\sigma_c = E\lambda / 2\pi a_0 \qquad (3)$$

For $a_0 \approx \lambda/2$:

$$\sigma_c \approx E / \pi$$

Maximum theoretical cohesive strength:

$\sigma_c \approx E / \pi$

	theory	experimental	
material	E (GPa)	σ_f (MPa)	E/σ_f
Silica fibers	97.1	24.1	4
Ausformed steel	200.1	3.13	64
Piano wire	200.1	2.75	73

Energy of fracture process:

fracture work: $\int_0^{\lambda/2} \sigma_c \sin(2\pi x / \lambda)\, dx = \sigma_c \lambda/\pi$

work done to create two new fracture surfaces 2Υ

Insert in:

$$\sigma_c = E\lambda / 2\pi a_0 \qquad (3)$$

$$\sigma_c = \sqrt{(E \cdot \Upsilon / a_0)}$$

see Hertzberg (1976)

Stress concentration factor (Inglis, 1913)

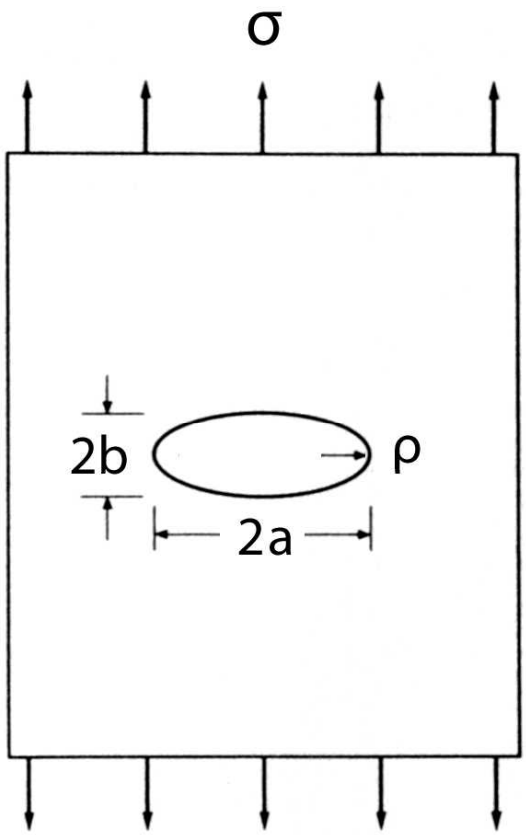

$$\sigma_{max} / \sigma = 1 + 2a/b$$

σ_{max}	max. stress at end of major axis
σ	applied stress
2a	major axis
2b	minor axis
ρ	radius of curvature

$\sigma_{max} / \sigma = 1 + 2a/b$

Curvature:

$\rho = b^2/a$

$\sigma_{max} = \sigma [1 + 2\sqrt{(a/\rho)}]$

For $a >> \rho$:

$\sigma_{max} \approx 2\sigma \sqrt{(a/\rho)}$

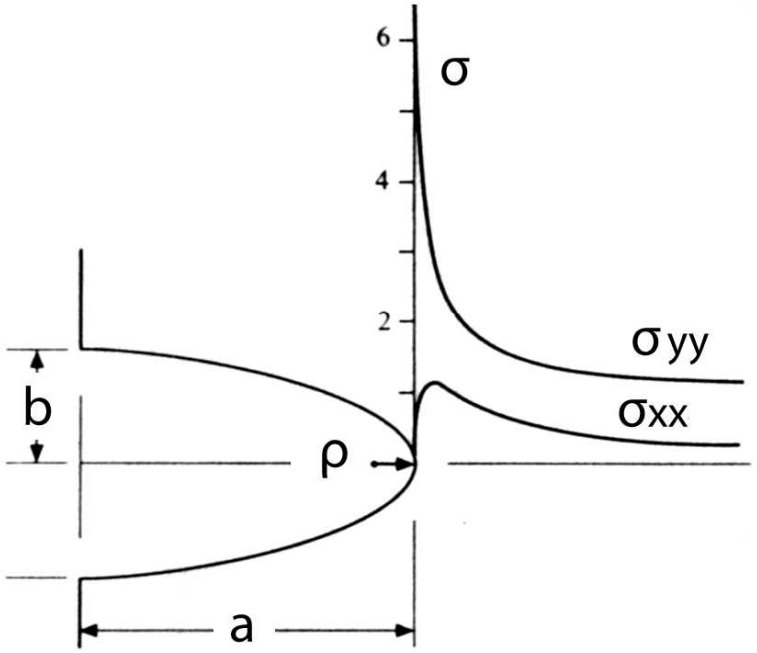

Griffith cracks (Griffith, 1920)

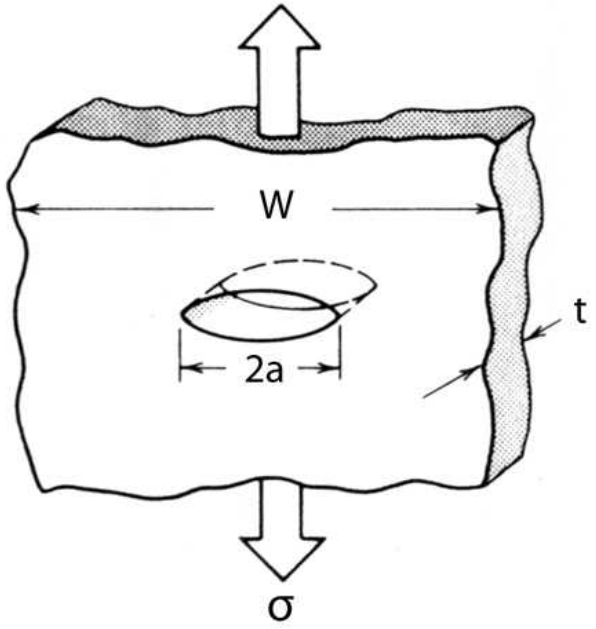

$$U - U_0 = - \pi \sigma^2 a^2 t / E + 4at\Upsilon_s$$

U	potential energy of body with crack
U_0	potential energy of body without crack
σ	applied stress
a	one half crack length
t	thickness
E	module of elasticity
Υ_s	specific surface energy

$$U - U_0 = - \pi \sigma^2 a^2 t / E + 4at\Upsilon_s$$

Rewriting:

$$U = 4at\Upsilon_s - \pi \sigma^2 a^2 t / E + U_0$$

Equilibrium, i.e., stable crack length:
First derivative:

$$\partial U/\partial a = 0$$
$$\partial U/\partial a = 4t\Upsilon_s - 2\pi \sigma^2 at / E = 0$$

note:
$\partial U_0/\partial a = 0$ since U_0 does not depend on a

$$\partial U/\partial a = 4t\Upsilon_s - 2\pi \sigma^2 at / E = 0$$

Equilibrium condition:

$$2t\Upsilon_s = \pi \sigma^2 at / E$$

Nature of equlibrium:
Second derivative:

$$\partial U^2/\partial a^2 = 0$$

$$\partial U^2/\partial a^2 = -2\pi \sigma^2 t / E$$

Negative, i.e., crack will grow

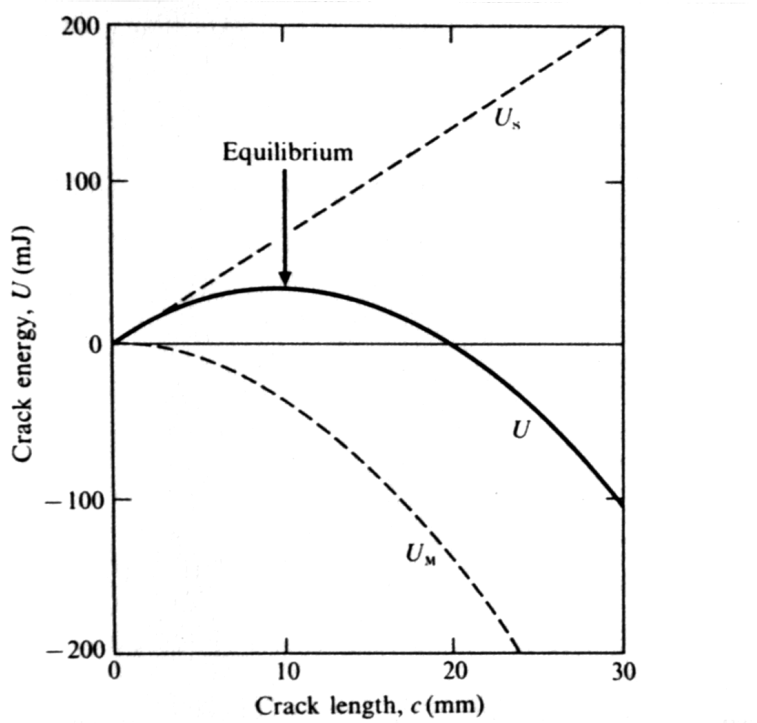

Energetics of Griffith crack in uniform tension, plane stress. Data for glass from Griffith: $\gamma = 1.75\,\mathrm{J\,m^{-2}}$, $E = 62\,\mathrm{GPa}$, $\sigma_A = 2.63\,\mathrm{MPa}$ (chosen to give equilibrium at $c_0 = 10$ mm).

$2t\Upsilon_s = \pi \sigma^2 at / E$

Griffith:

$\sigma = \sqrt{(2E \Upsilon_s / \pi a)}$ for plane stress

$\sigma = \sqrt{(2E \Upsilon_s / \pi a(1-\nu^2))}$ for plane strain

ν Poisson's ratio $\approx$ 0.25 to 0.33:

$\sigma \approx \sqrt{(2E \Upsilon_s / \pi a)}$ for plane strain also...

Fracture modes

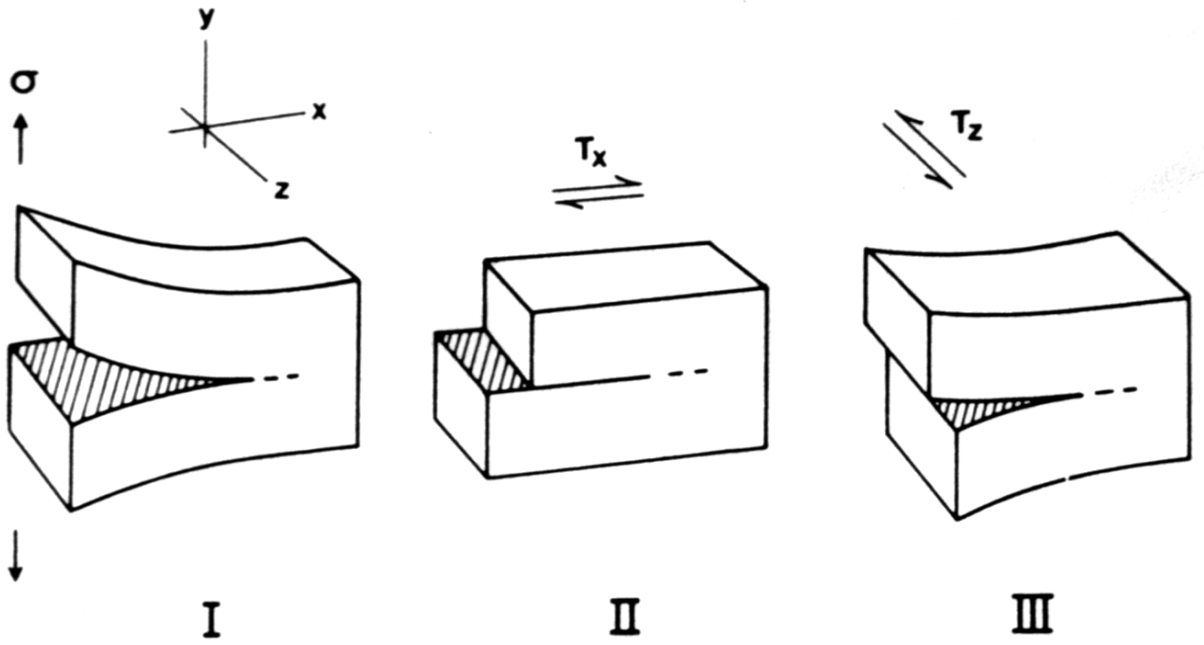

mode I – opening or tensile mode, where the crack surfaces move directly apart

mode II – sliding or in-plane shear mode, where the crack surfaces slide over one another in a

mode III – tearing or antiplane shear mode, where the crack surfaces move relative to one another and parallel to the leading edge of the crack

- plane strain – thin plate and $\sigma z = 0$; 2D strain / 3D stress
- plane stress – thick sections; 2D stress / 3D strain

Crack interaction (Segall & Pollard, 1980)

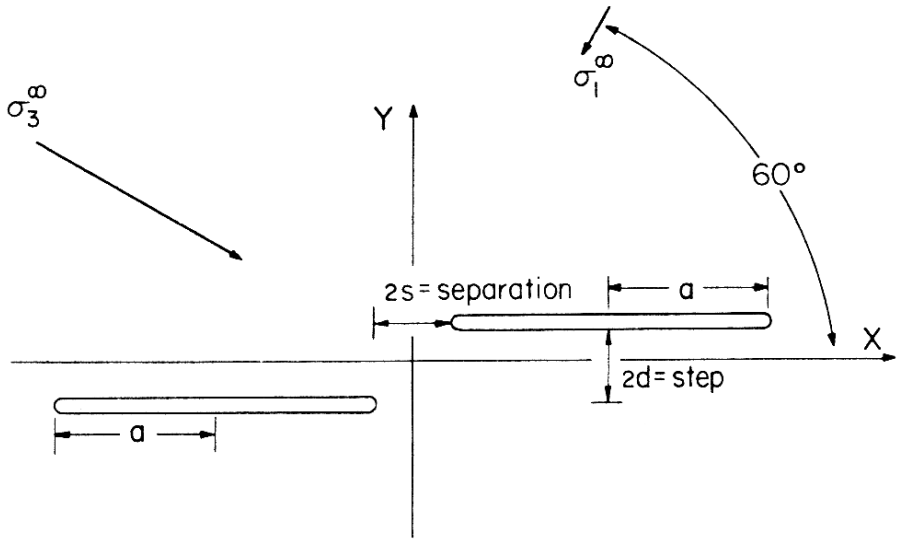

Fig. 6. Definitions of echelon crack geometry. Two cracks of half-length a are parallel to X direction; $2d$ is step between cracks, and $2s$ is separation between crack tips. Far-field stresses used in computations are also shown; $\sigma_3^\infty = 5\sigma_1^\infty$.

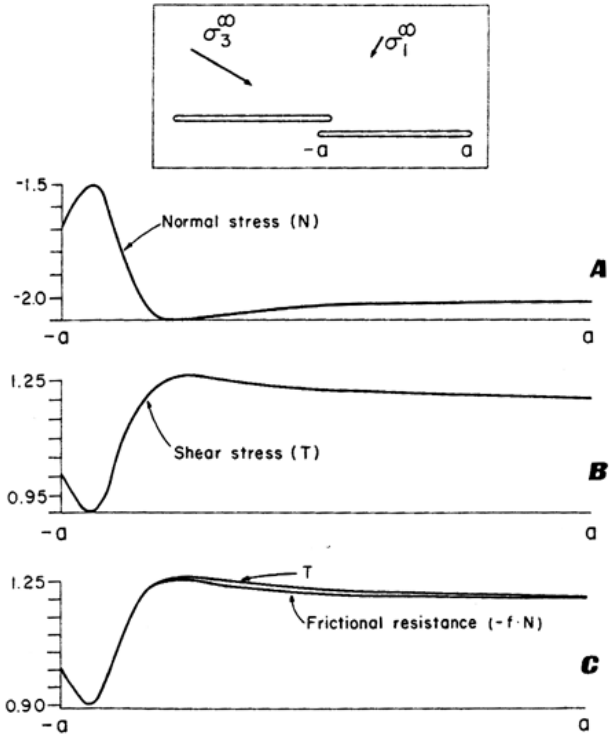

Fig. 8. Tractions acting on rightmost crack of a right-stepping echelon pair of cracks having $d/a = s/a = -0.09$. Applied stresses are same as in Figure 6. Inset: scale illustration of crack geometry, showing overlap and applied stress state. (*a*) Distribution of normal tractions N on right crack from $-a$ to a; negative values indicate compression. (*b*) Distribution of shear tractions T on right crack from $-a$ to a. (*c*) Replot of shear traction and frictional resistance ($-f \cdot N$) illustrating slip occurring over entire segment. Small discrepancy between the two curves is due to numerical error.

Crack interaction (Segall & Pollard, 1980)

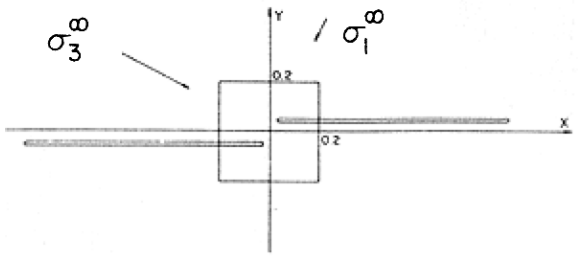

mean stress

mean stress

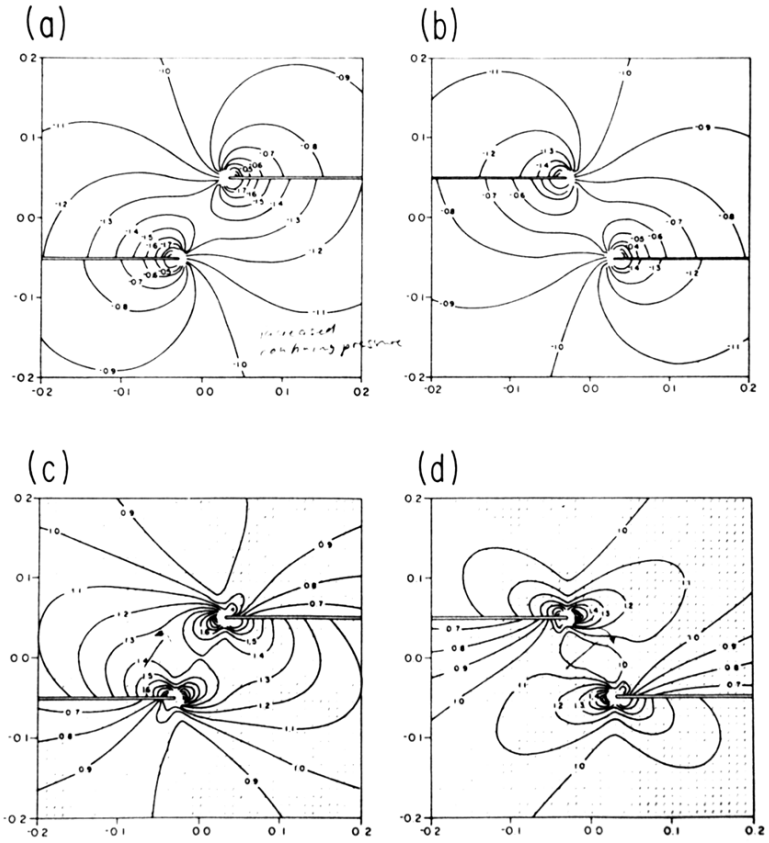

shear stress

shear stress

Crack interaction (Segall & Pollard, 1980)

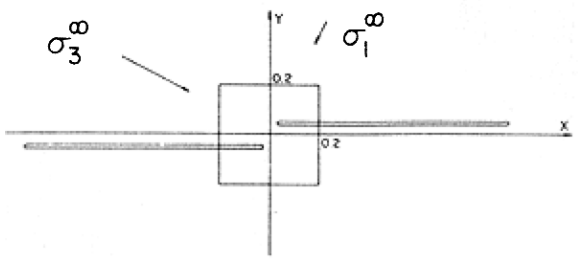

max.tension max.tension

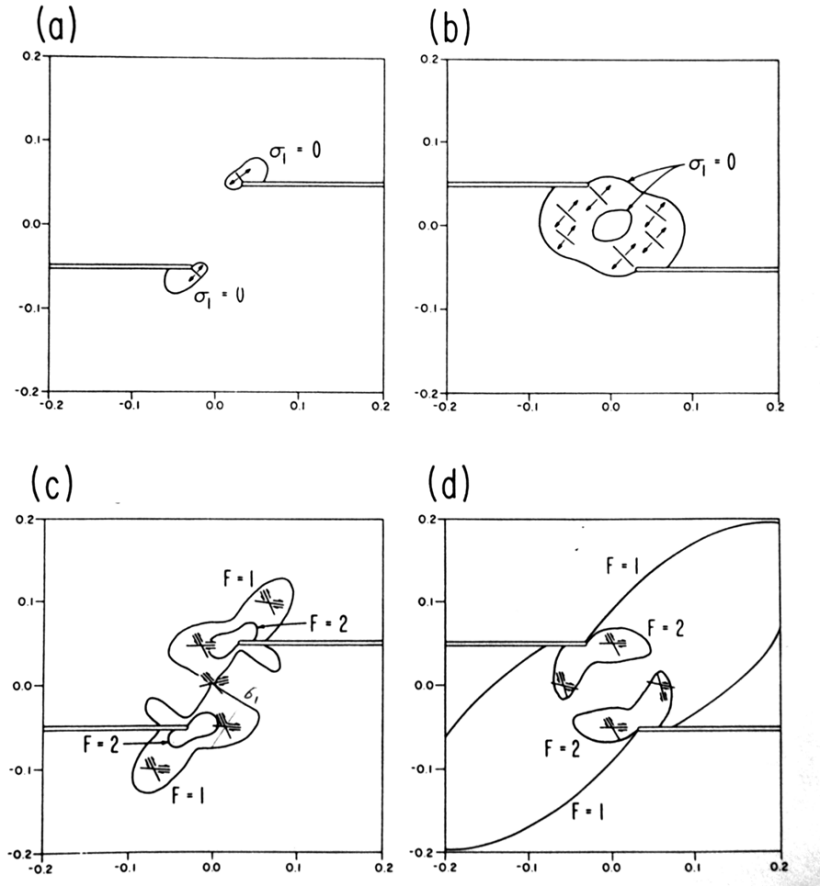

local shear failure local shear failure

web sites:

http://en.wikipedia.org/wiki/Fracture_mechanics

books:

Pollard, D.D. & Fletcher, R.C., 2005, Fundamentals of Structural Geology, Cambridge University Press

Hertzberg, R.W., 1976, Deformation and Fracture Mechanics of Engineering Materials, John Wiley

Jaeger, J.C. & Cook, N.G.W., 1969, Fundamentals of Rock Mechanics, Chapman & Hall

articles:

Segall, P. & Pollard, D.D., 1980, JGR 85, p.4337-4350

Griffith, A.A., 1920, Phil. Trans. Roy. Soc. Lond., 221, 163-198

Inglis, C.E., 1913, Proc. Naval Architects, 219-241

10
Pressure solution

Deformationsprozesse in der Erde (10)

Pressure solution

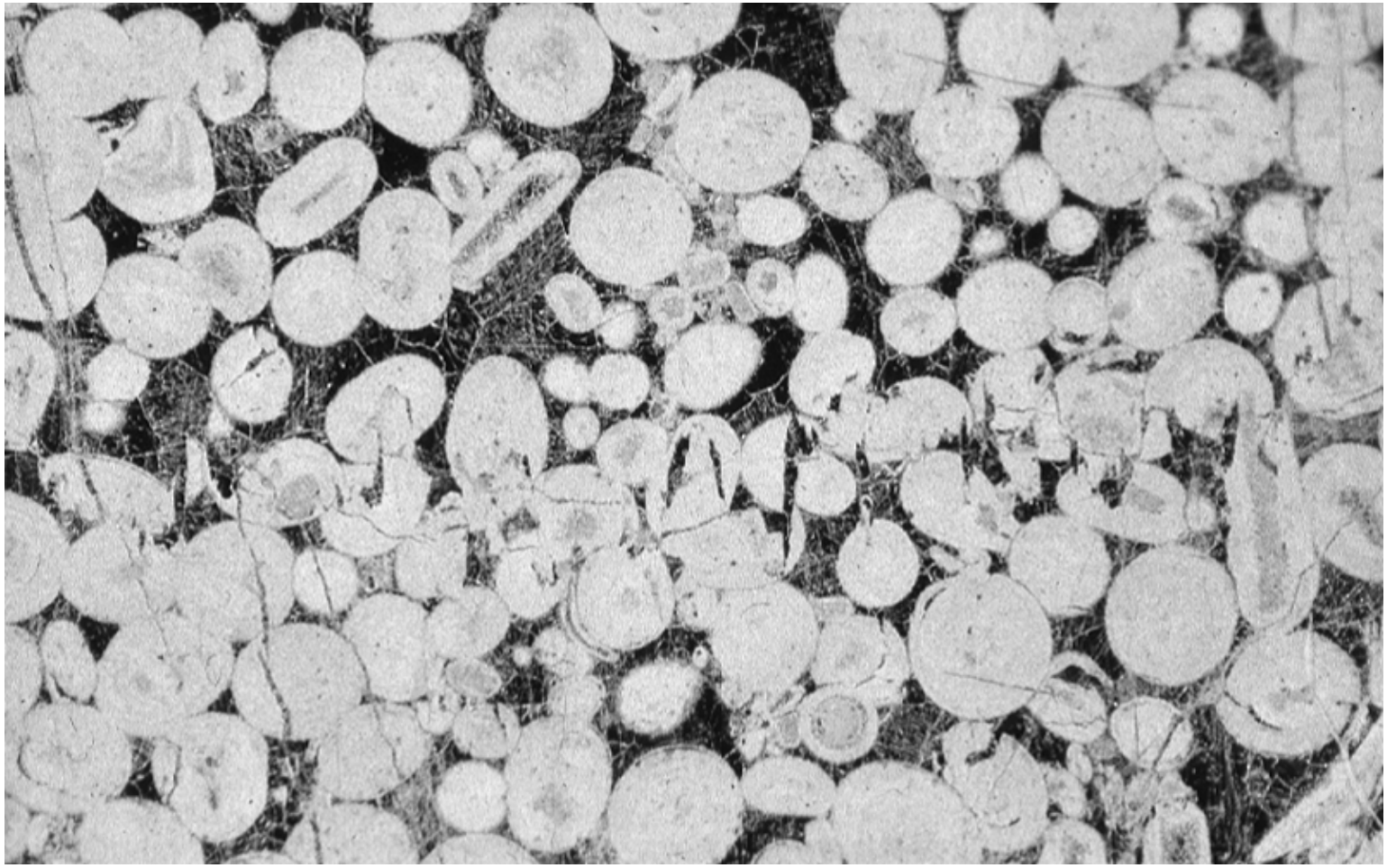

Pressure solution is an important deformation mechanism in rocks under conditions of low grade metamorphism. It leads to structures that are characterized by

solution → mass transfer → precipitation

Definition

Pressure solution:

A phenomenon of diffusive mass transfer in polycrystalline material in response to variations of normal stress. When solid state grain boundaray diffusion is rate controlling, (...) this process is known as Coble creep. Pressure soluton may formally be treated as Coble creep (Elliot (1973).

If fluid phase is present along grain boundaries and in pores then the solvent will provide pathways of relatively high diffusivity (Atkinson & Rutter, 1975). This predicts significant strain rates at low temperature and a diffusion controlled deformation mechanism (Rutter, 1976)

GEOMETRY & KINEMATIC DESCRIPTION

Kink folds, Chaines Subalpine (Panozzo, 1984)

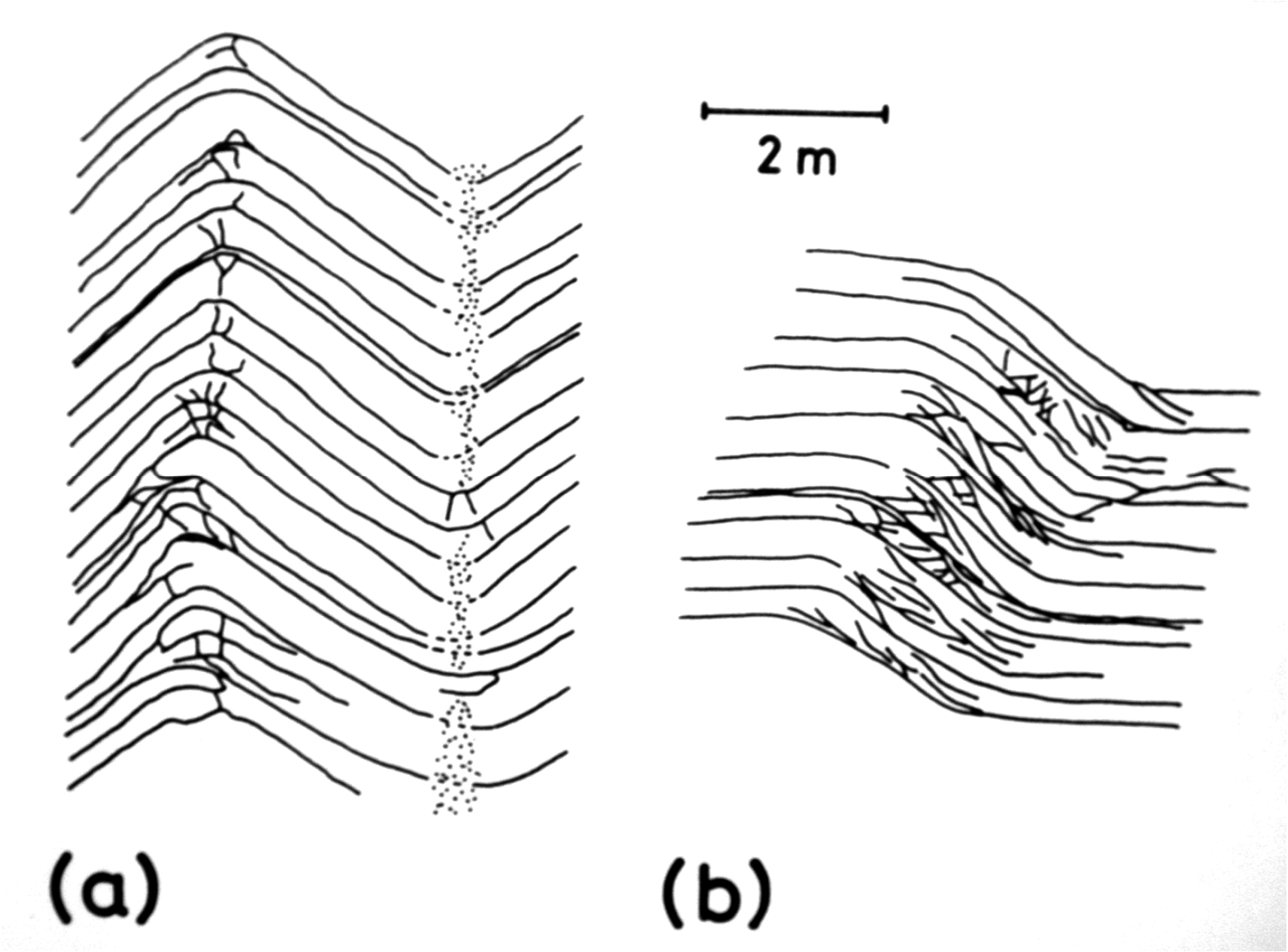

Stylolites in carbonates, Chaines Subalpine (Panozzo, 1984)

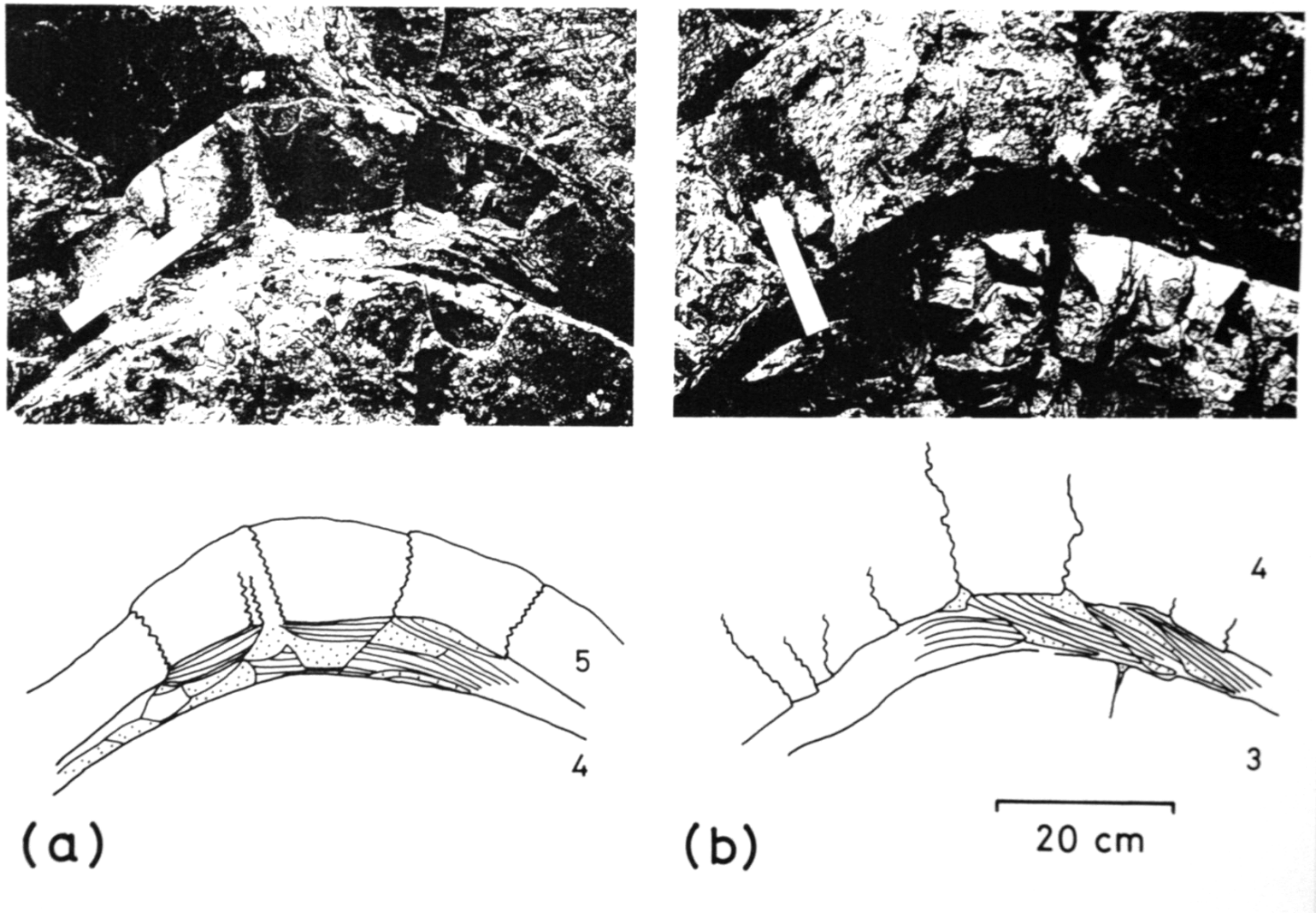

Stylolites in carbonates, Chaines Subalpine (Panozzo, 1984)

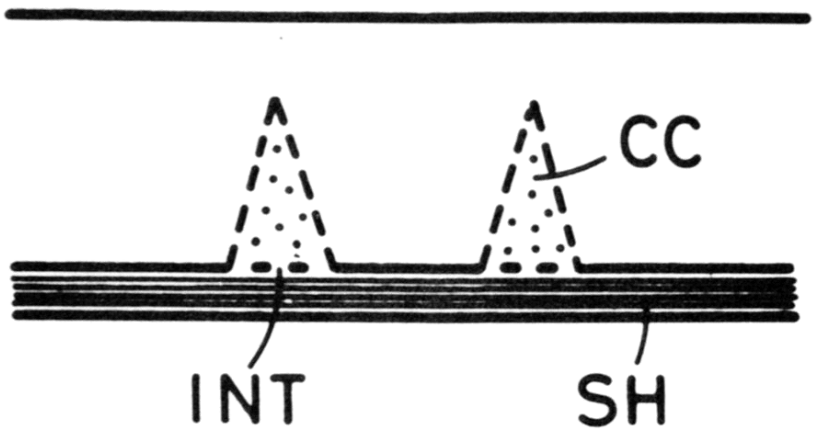

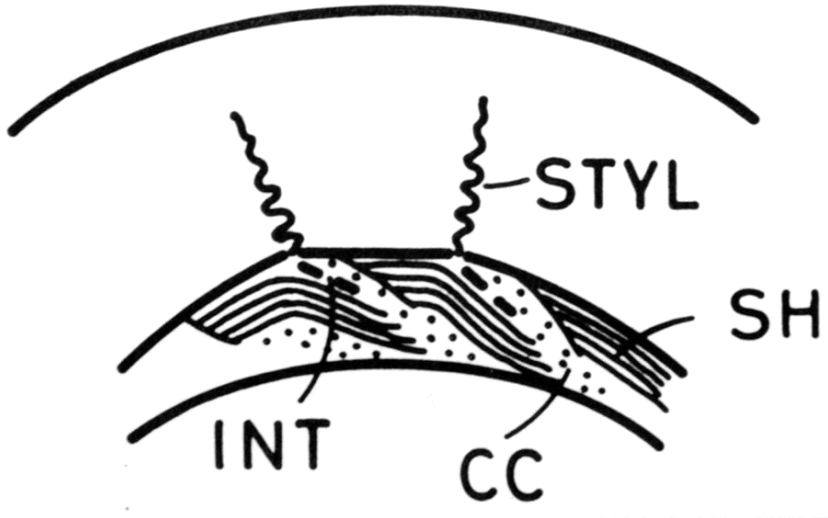

Schrägstylolithe (Plessman, 1972)

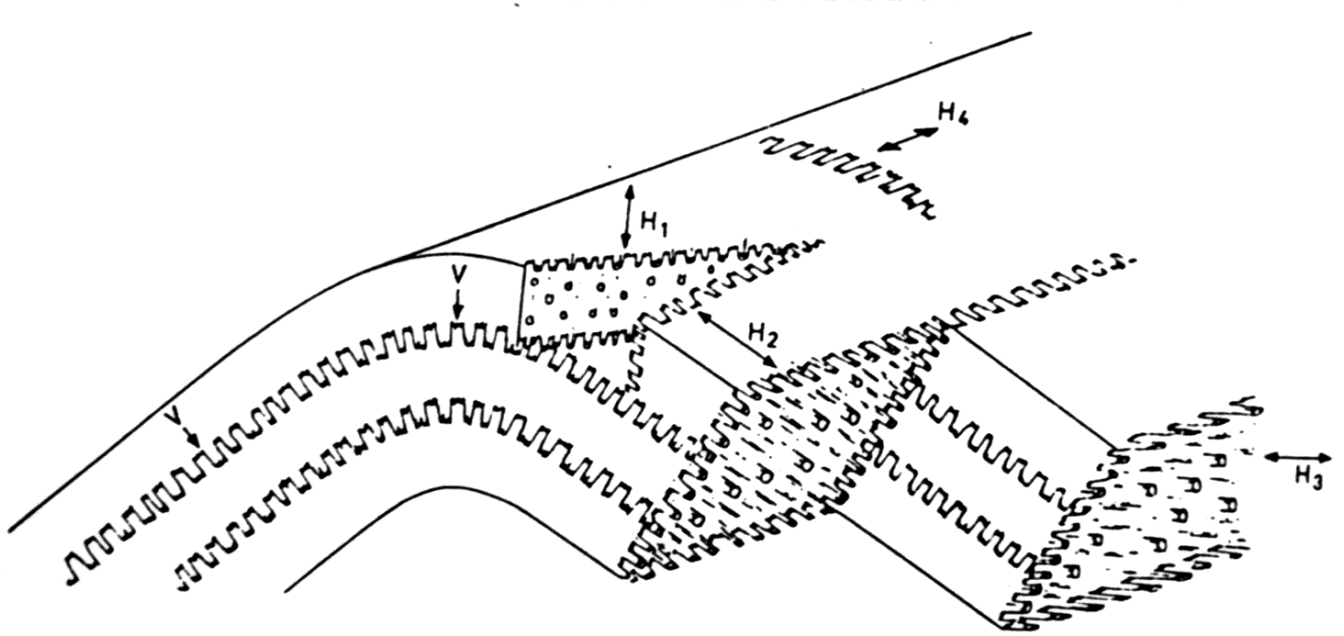

Abb. 5. Schematischer Überblick über die Richtungen und Altersfolgen von Stylolithen im Faltenjura. — V = Vertikalzapfen, möglicherweise sehr früh nach der Sedimentation senkrecht zur Schichtung angelegt (Überlagerungsdruck), später durch Faltung verstellt. H_1 = H-Zapfen, die in das regionale Bild Mitteleuropas passen (um N—S). H_2 = Stylolithen, die senkrecht zur Faltenachse angelegt und später bei weitergehender Faltung mit verstellt wurden. H_3 = H-Zapfen, die jünger als H_2 sind und neu in horizontaler Richtung entstehen. H_4 = Vermutlich am Ende der Faltung infolge blockierter Querdehnung ($B' \perp B$) gebildet.

Slickensides - crystal fibres (Durney & Ramsay, 1973)

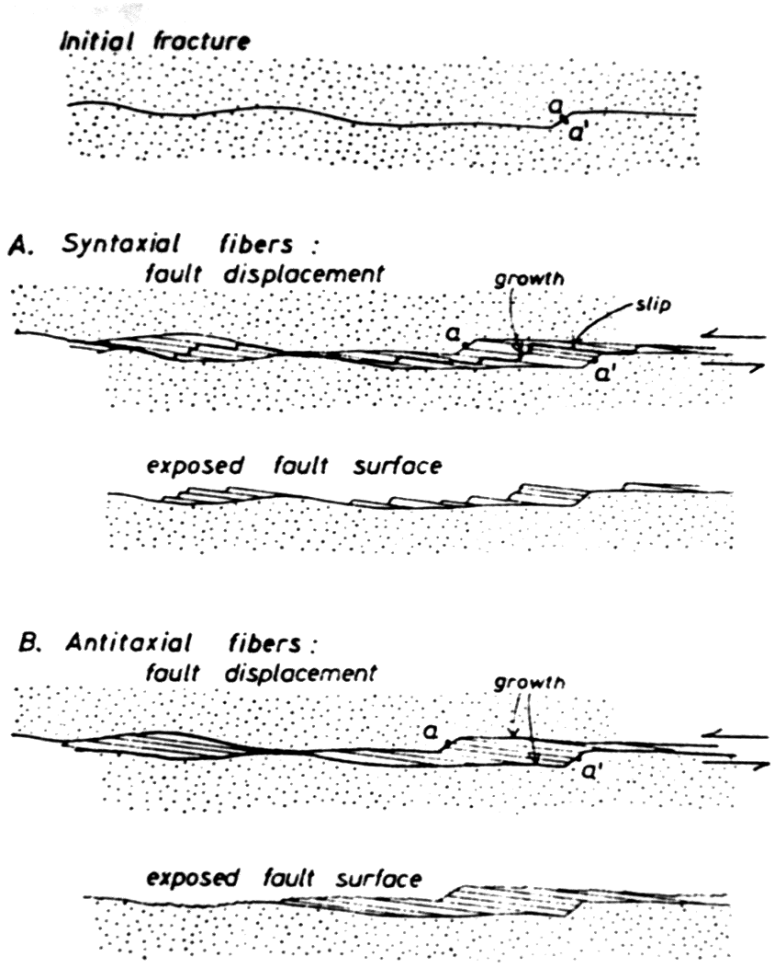

Tension veins (Price & Cosgrove, 1990, Durney & Ramsay, 1973)

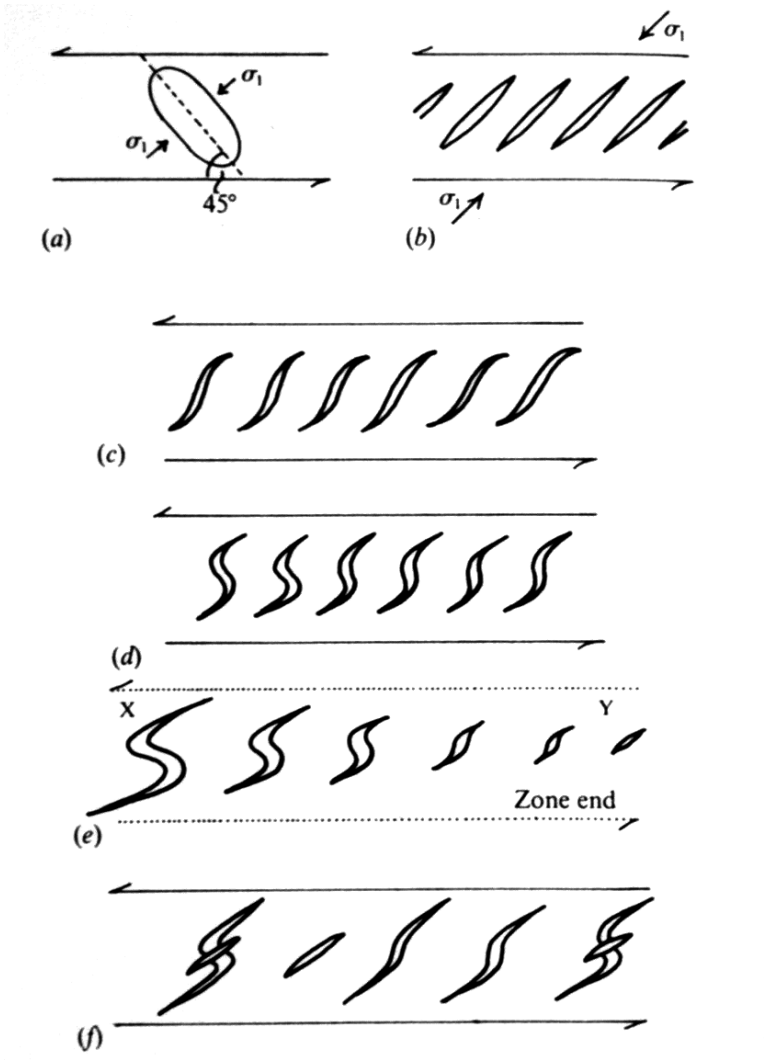

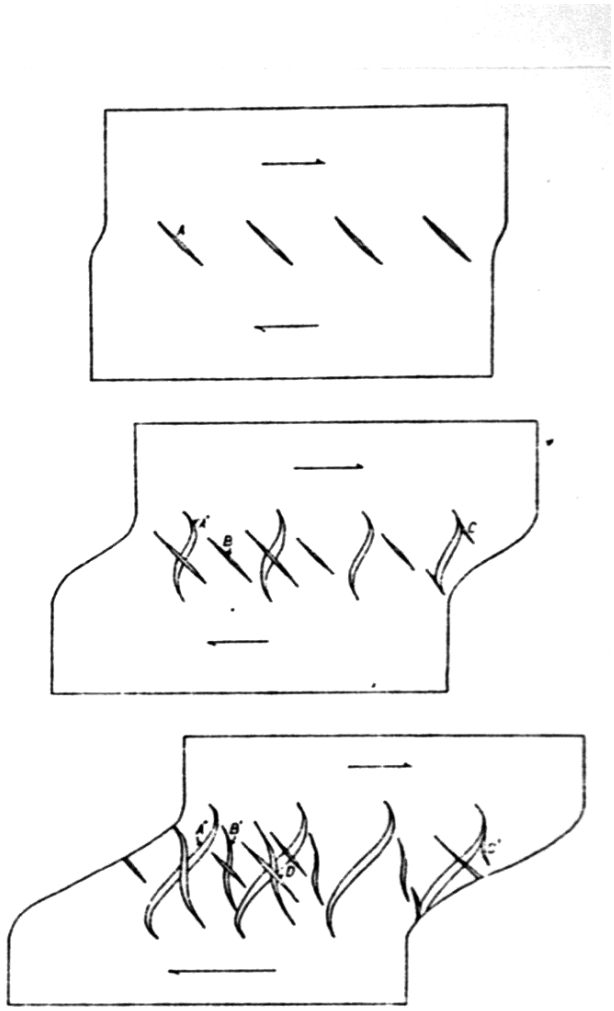

STRAIN INTERPRETATION

Fibrous vein filing, Durney & Ramsay, 1973)

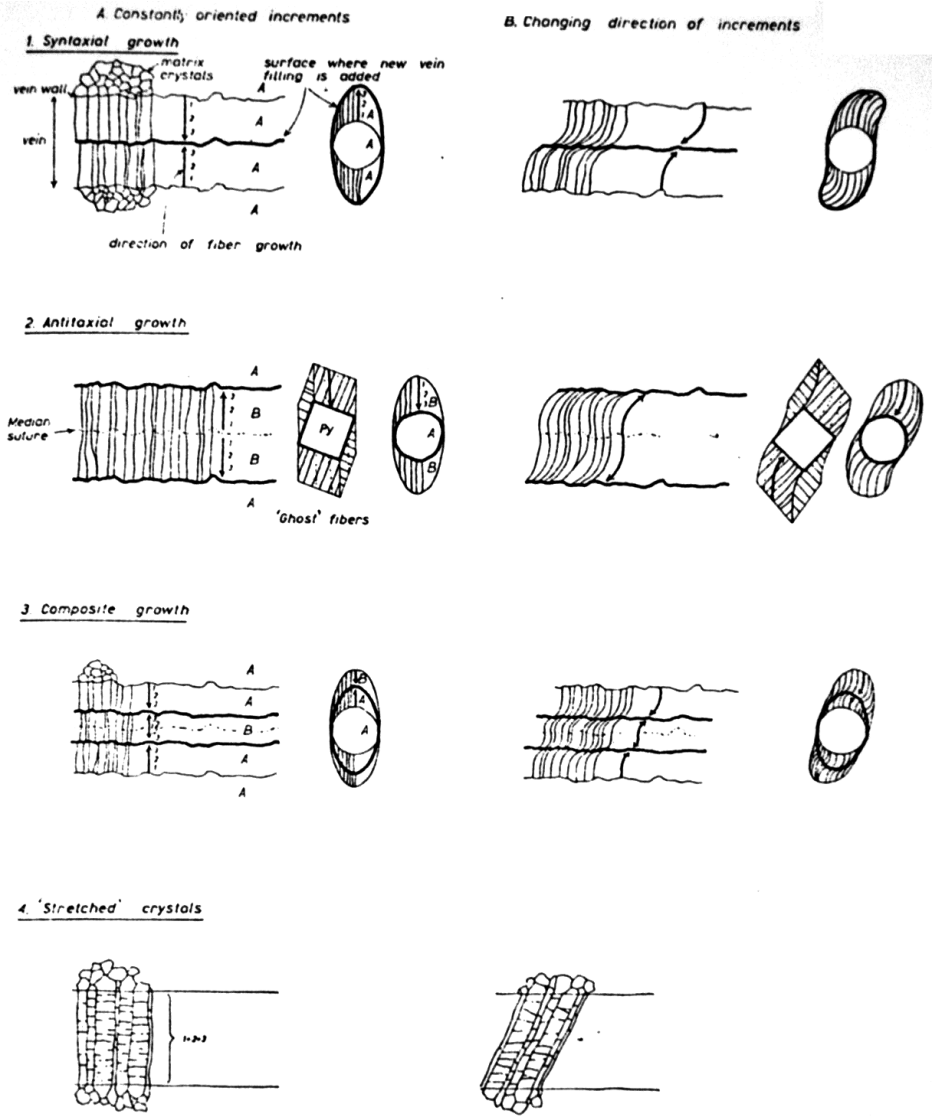

Chocolate tablet structure (Ramsay & Huber, 1983)

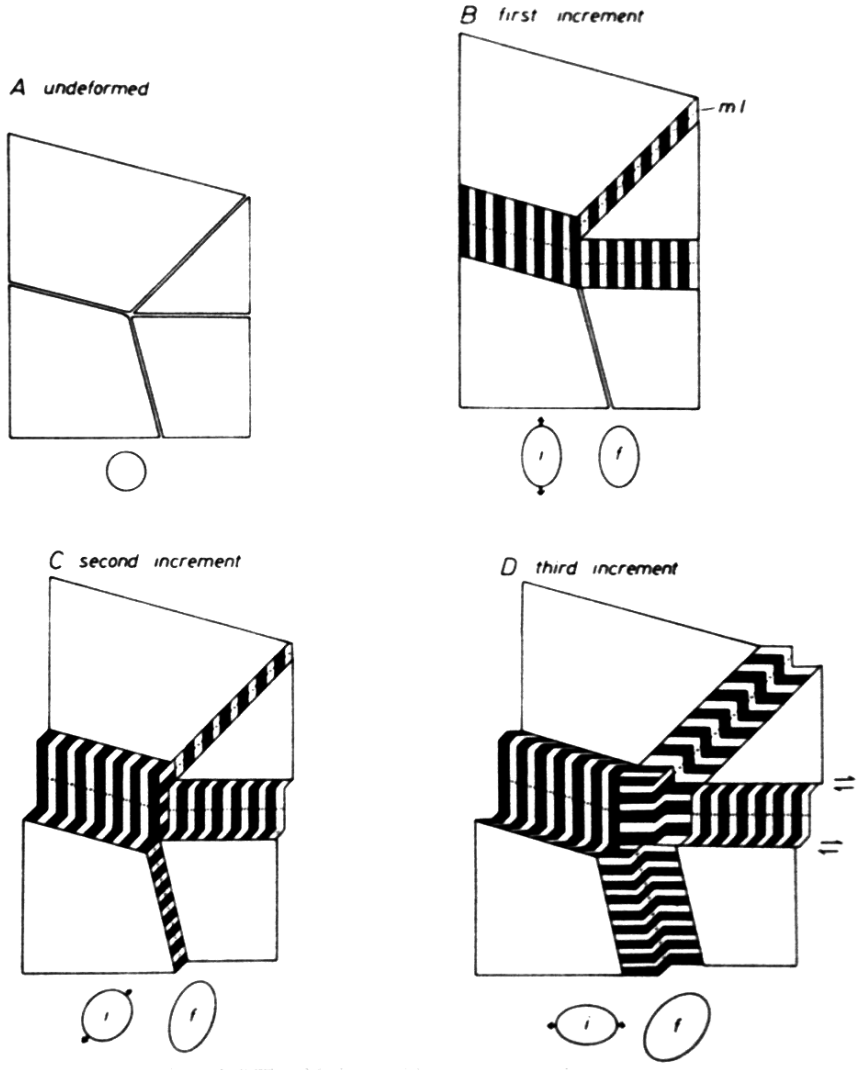

Pressure shadows (Ramsay & Huber, 1973)

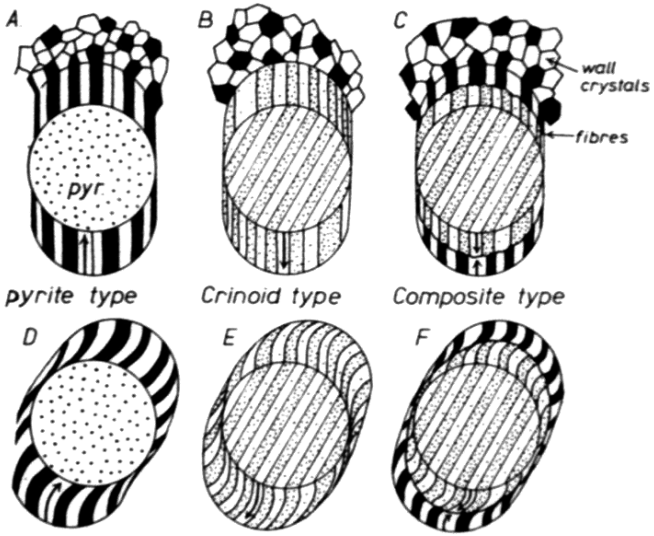

DEFORMATION HISTORY

Pressure shadows (Etchecopar & Malavielle, 1987)

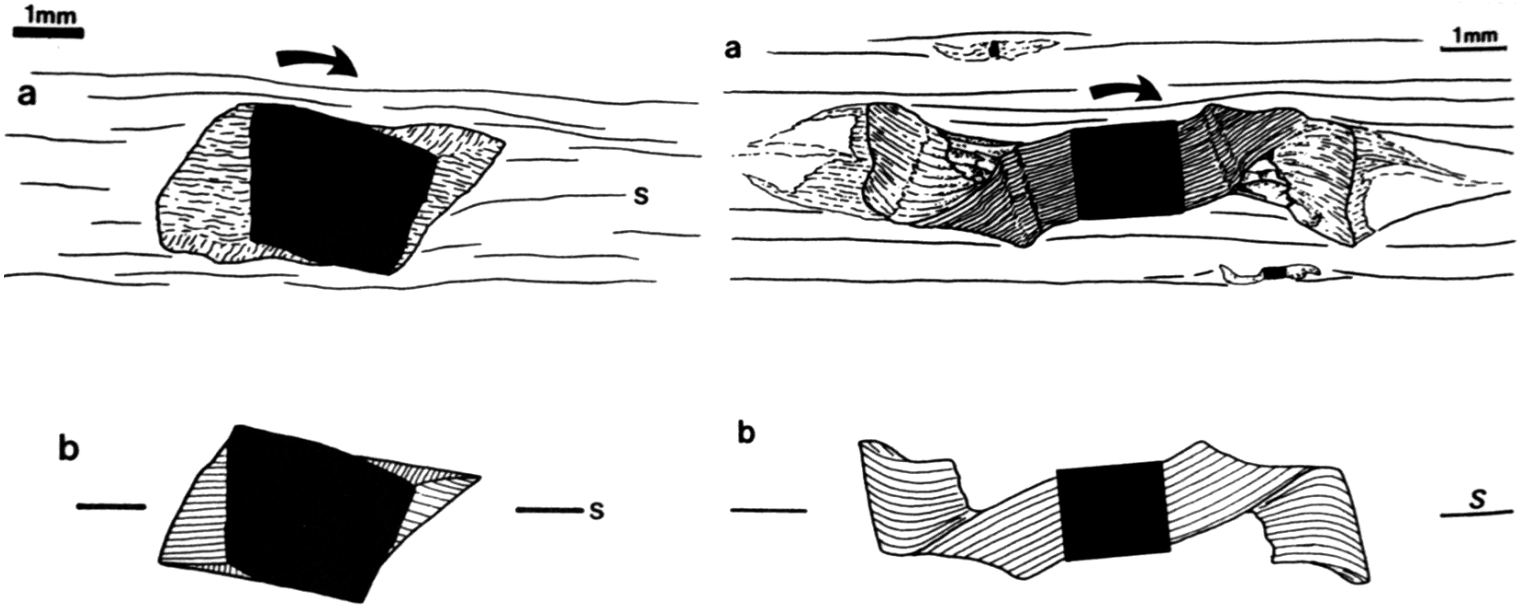

Crack - seal (Gratier, 1984)

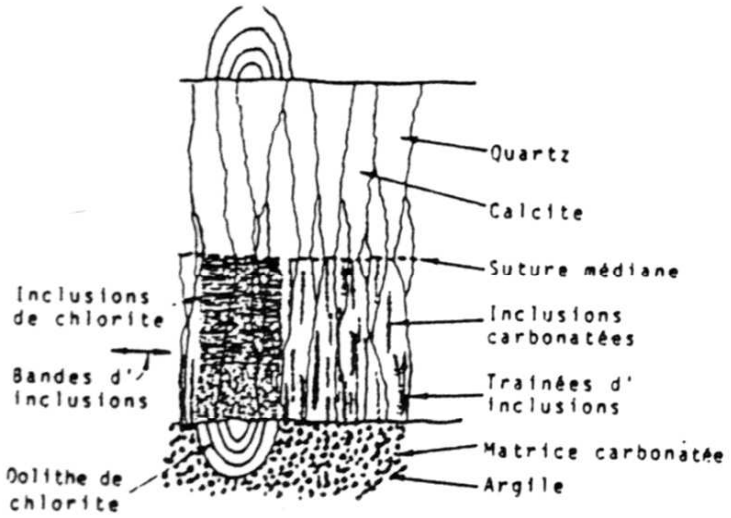

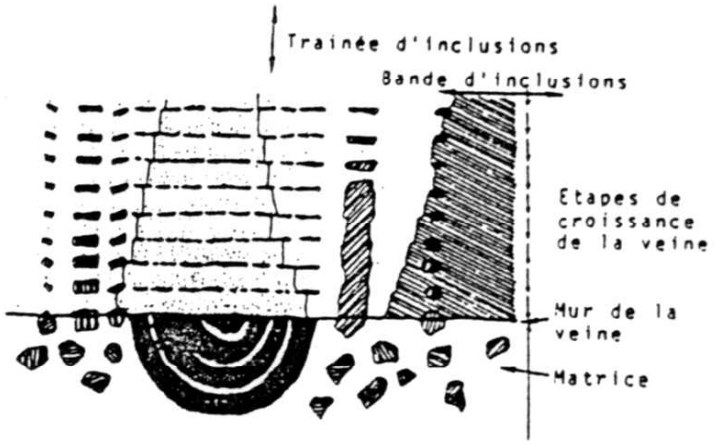

Deformation history (Casey, Dietrich & Ramsay, 1983)

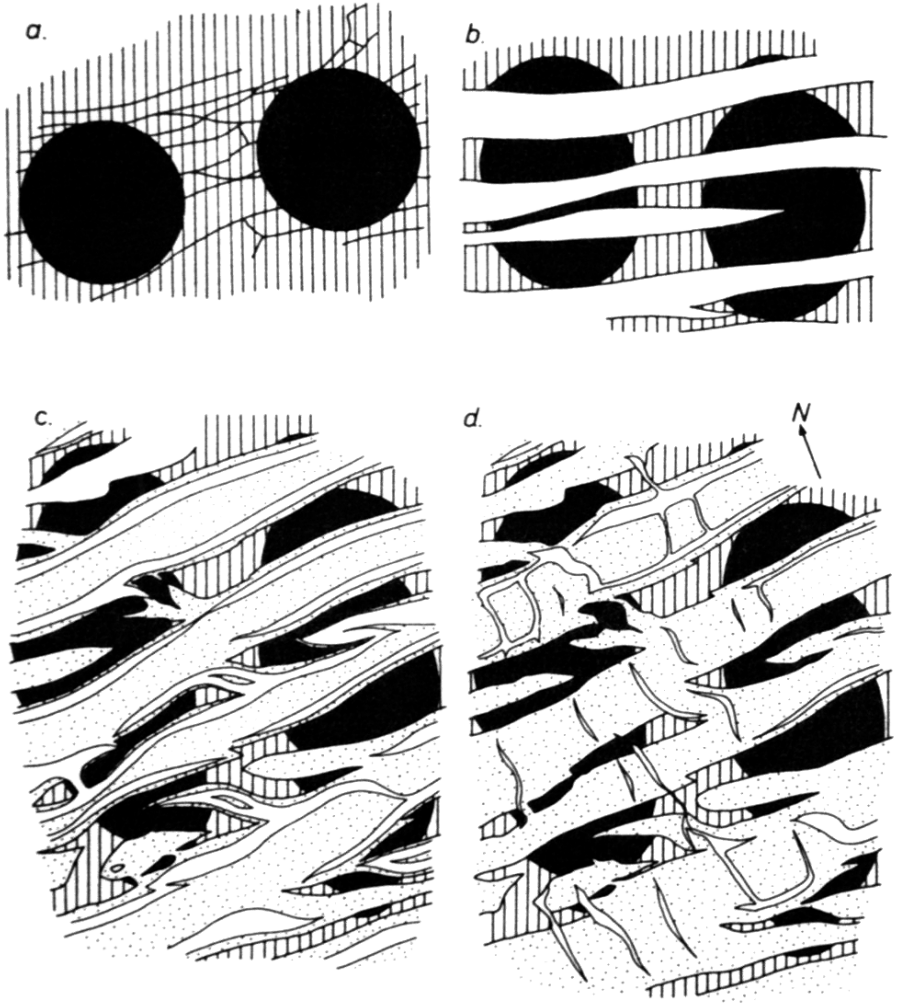

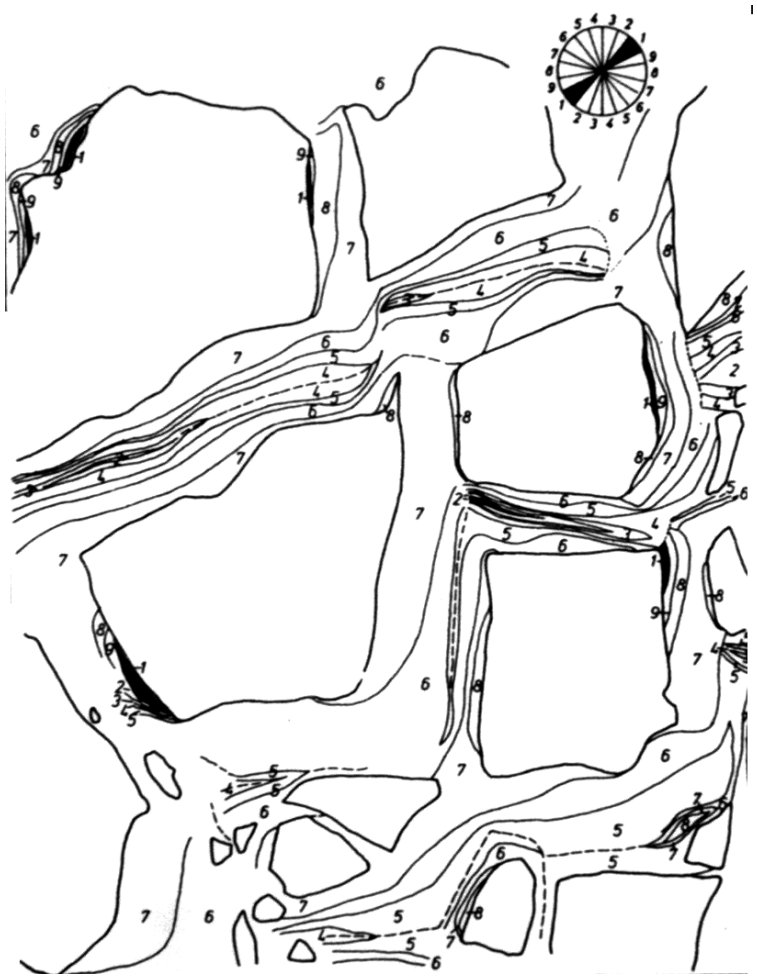

MICROSTRUCTURES

Stylolites = source

Extension cracks = sink

Source & sink

(thin section +Pol)

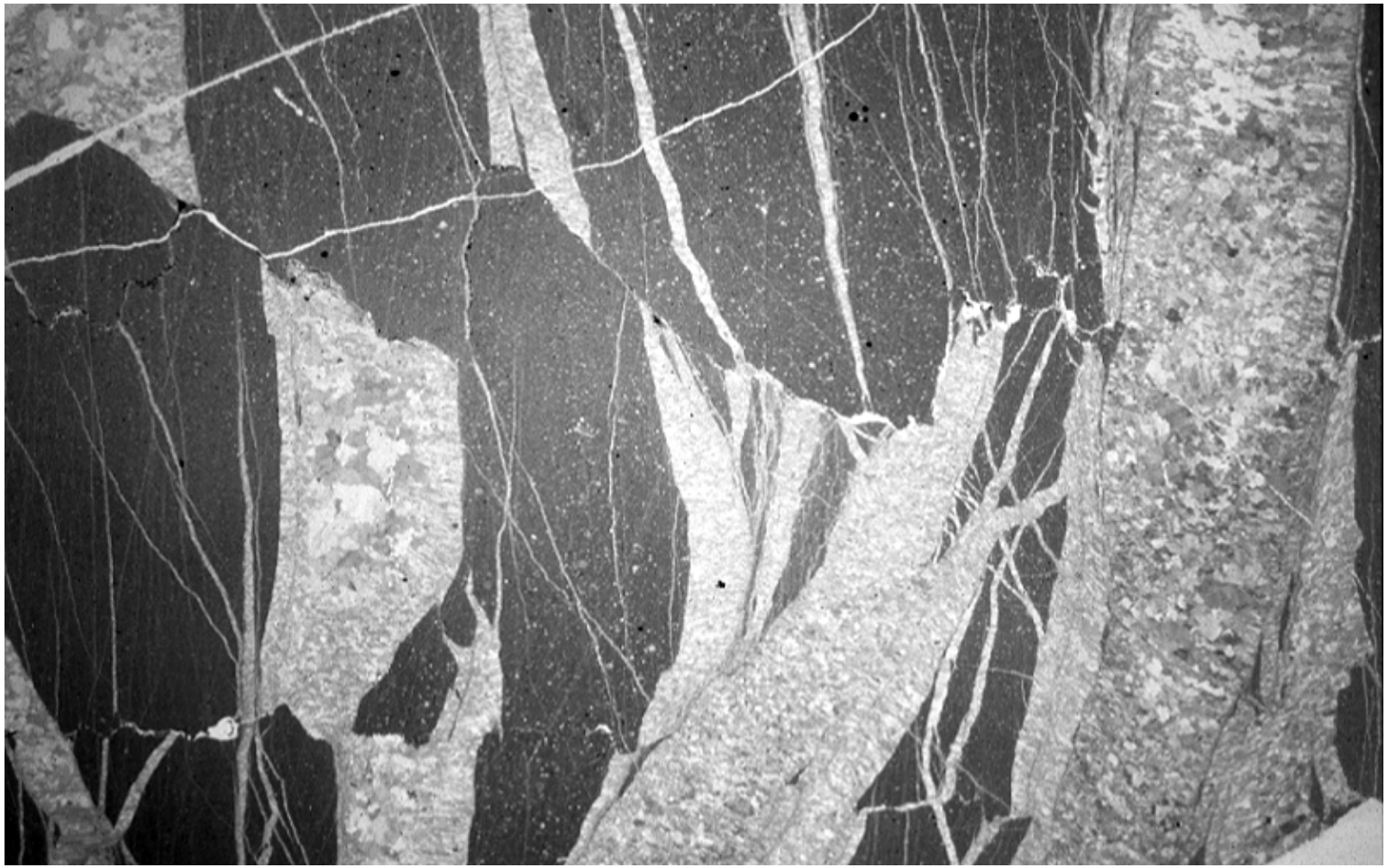

pressure solution:

diagenetic tectonic (polished surface)

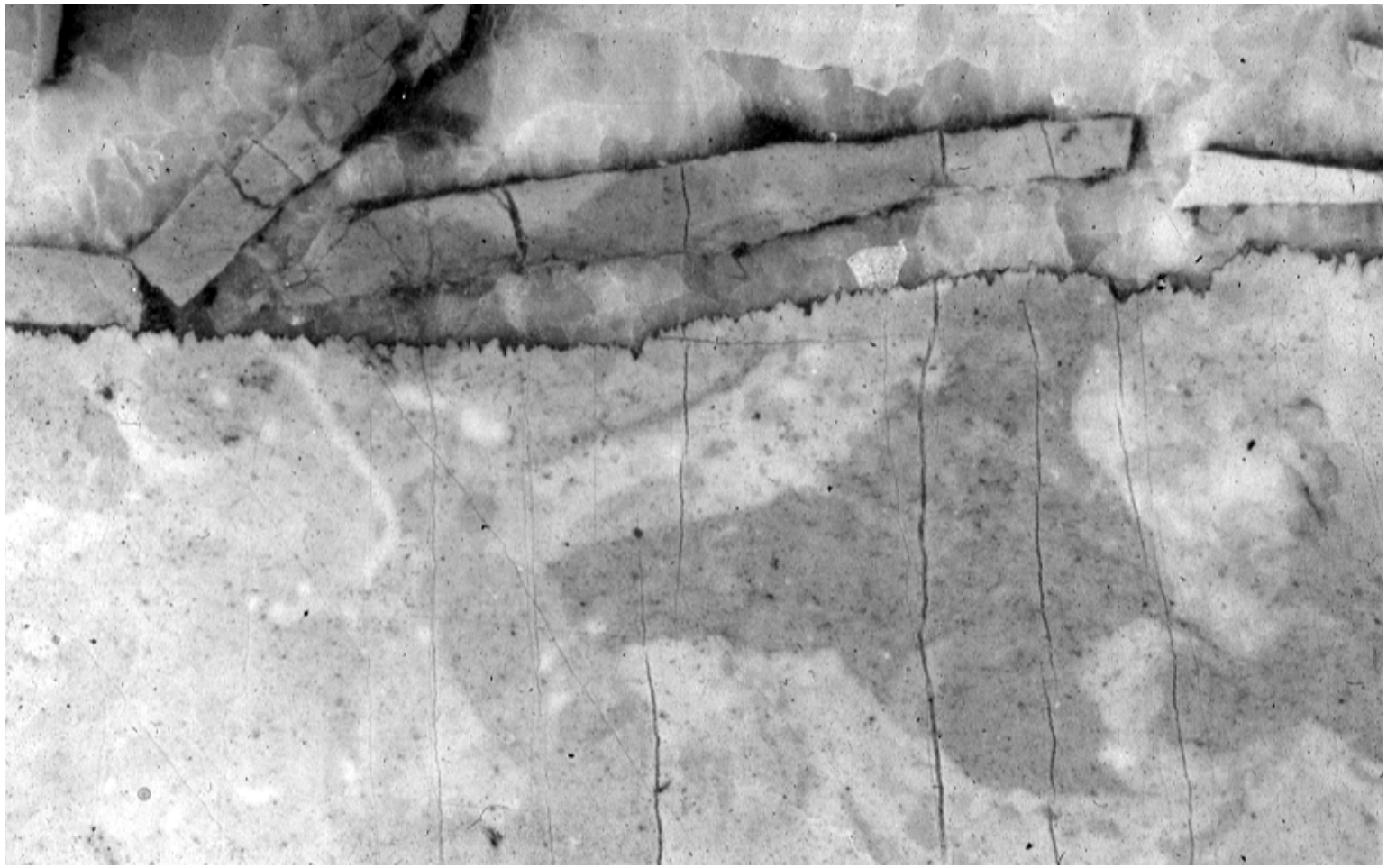

pressure
solutiondiagenetic tectonic (thin section +Pol)

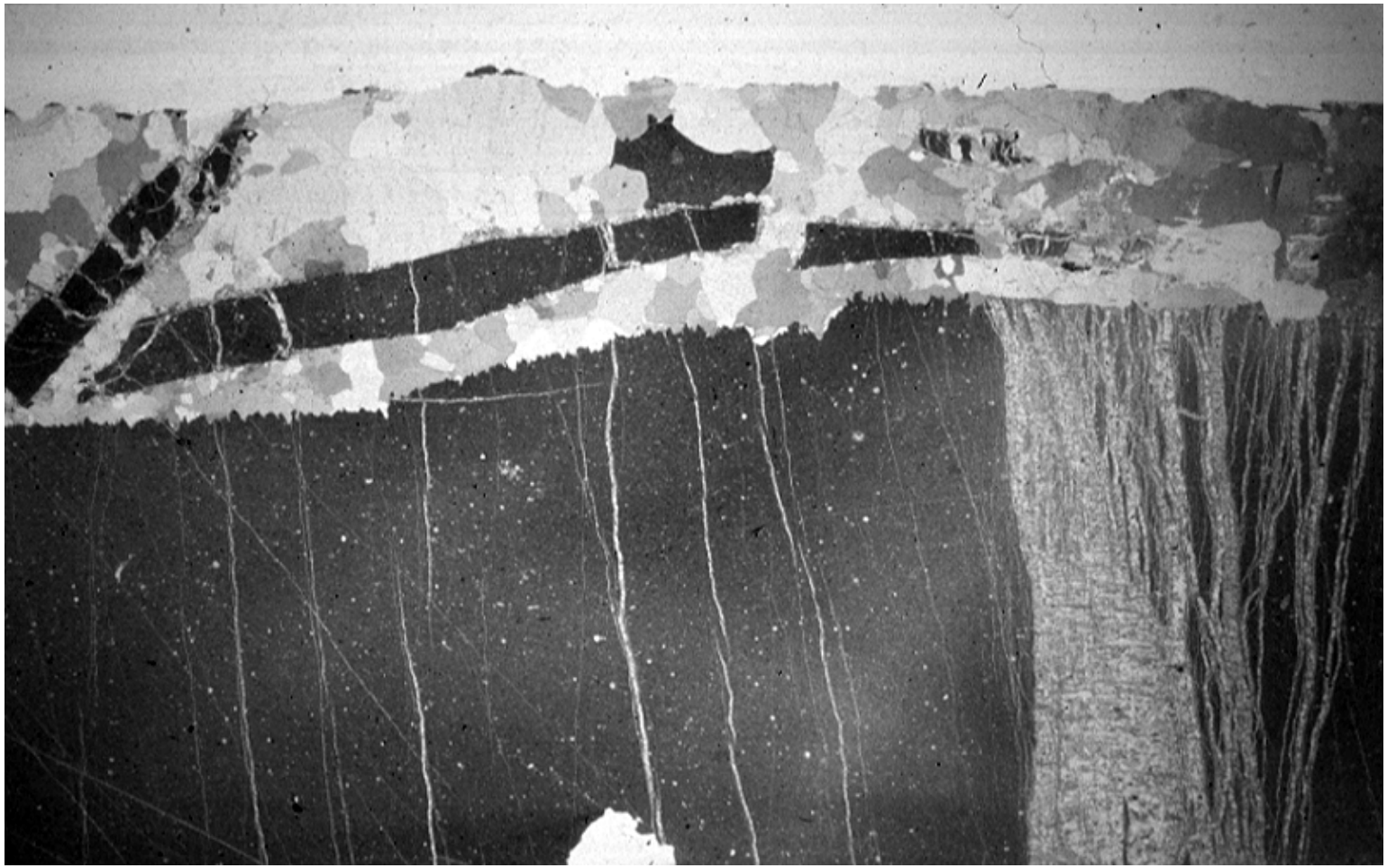

EXPERIMENTS

Boer, R.B. de, 1977 - Thermodynamics of pressure solution

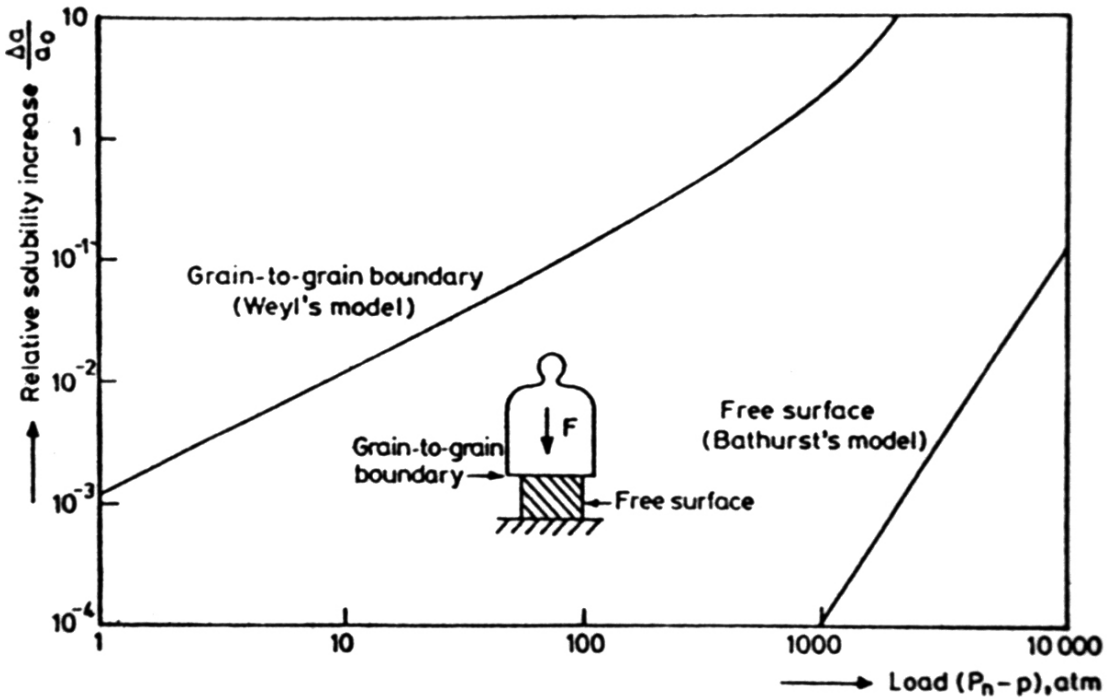

Rutter, E.H., 1976
The kinetics of rock deformation by pressure solution

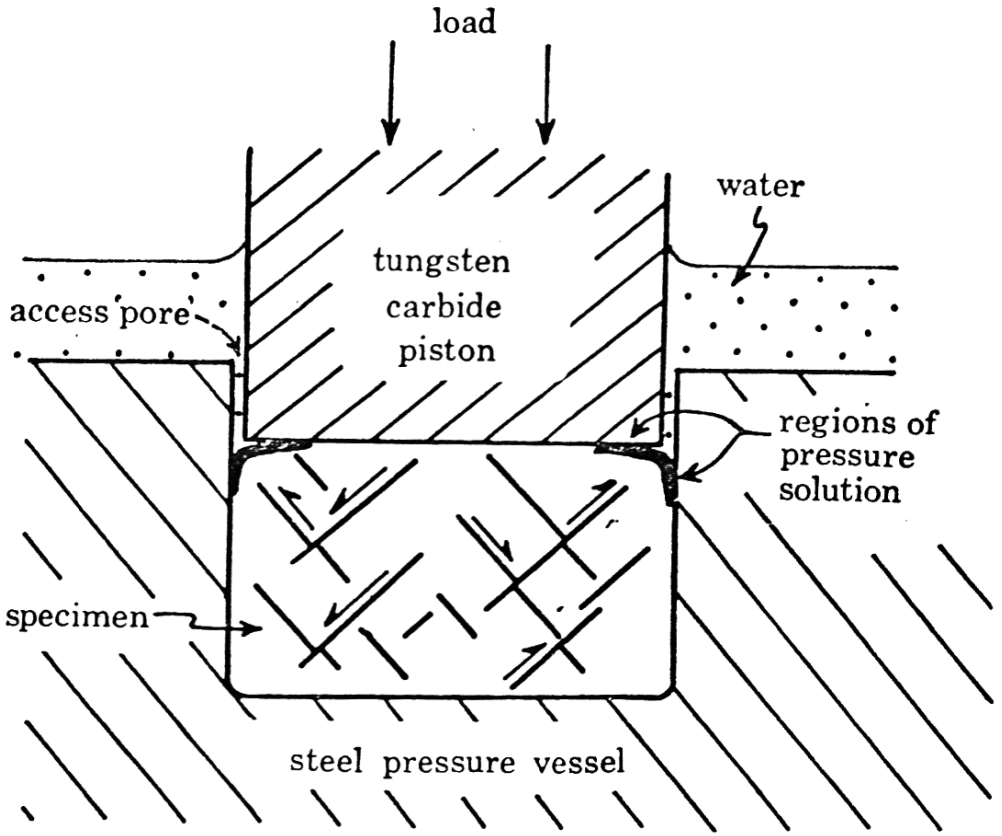

Dissolution (Engelder, 1982, Sprunt & Nur, 1977)

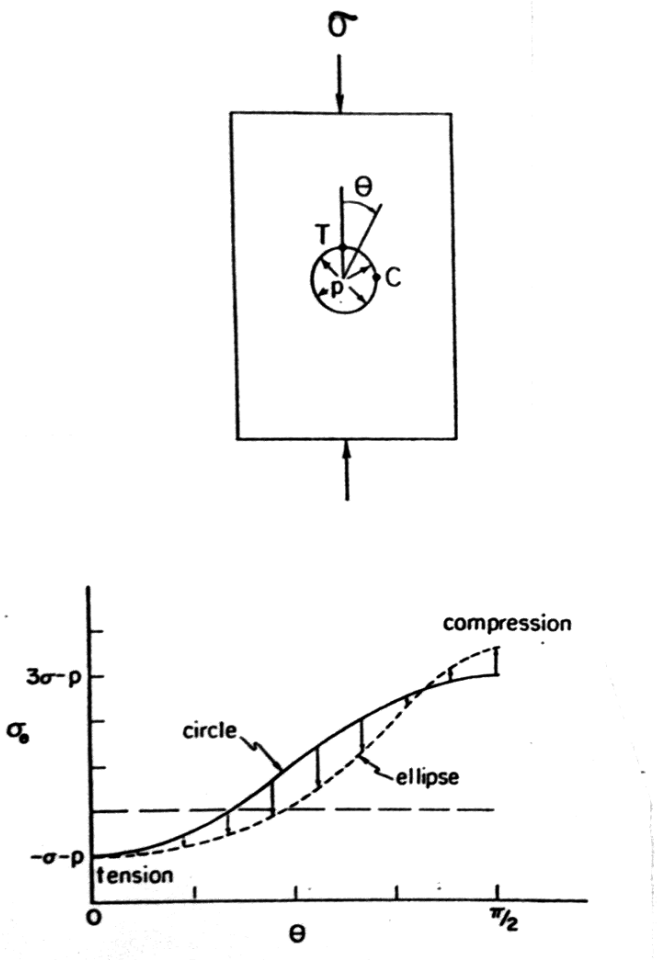

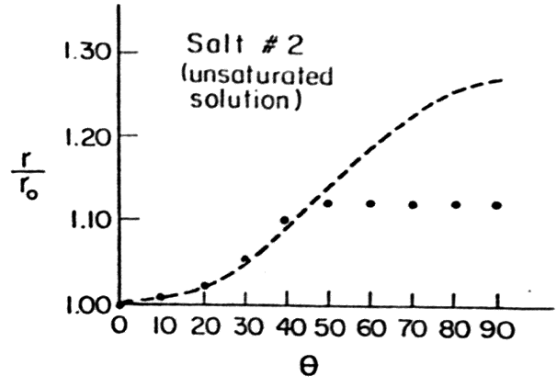

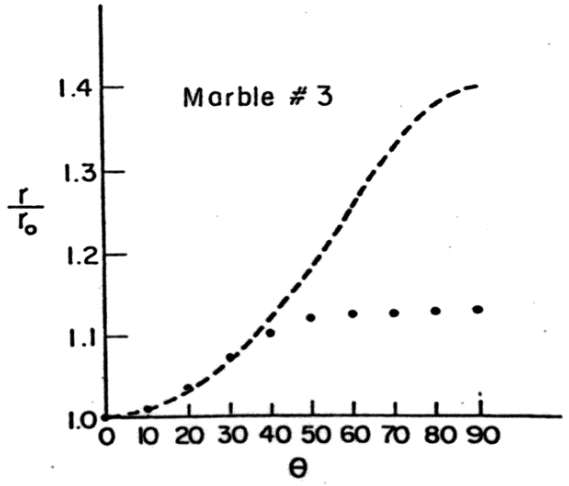

Dissolution (Engelder, 1982, Sprunt & Nur, 1977)

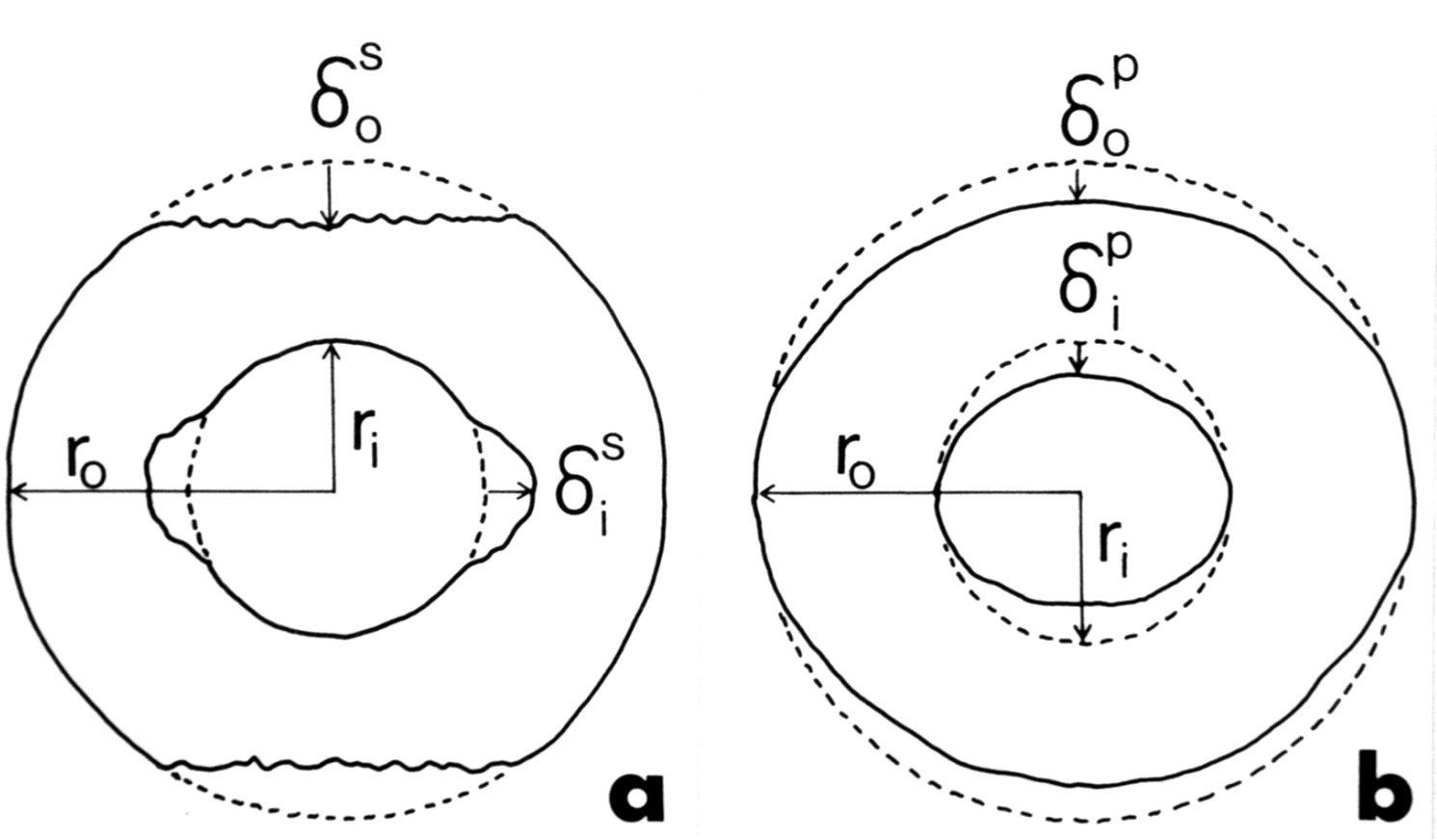

PRESSURE SOLUTION - THEORY

Kamb, 1961

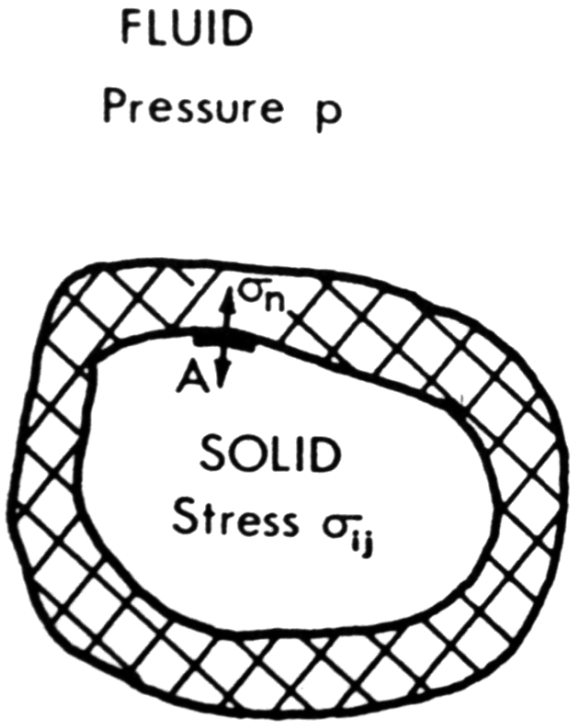

Creep mechanisms

pro memoria:
Nabarro, .R.N., 1948
Deformation of crystals by the motion of single atoms

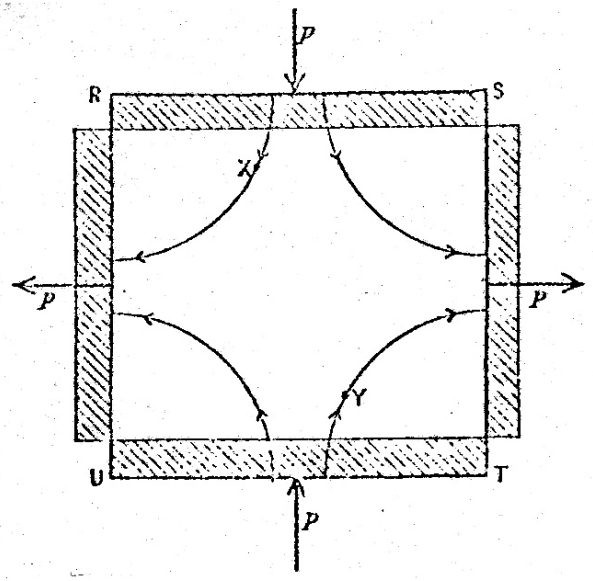

diffusion through bulk

Pressure solution = Coble creep

Elliott, D., 1973 - Diffusion flow laws in metamorphic rocks

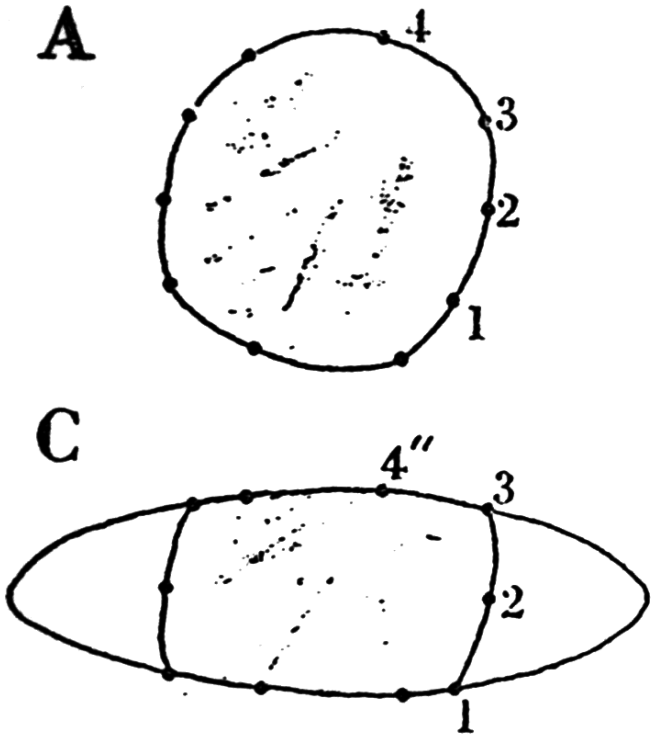

Pressure solution - deformation mechanism map

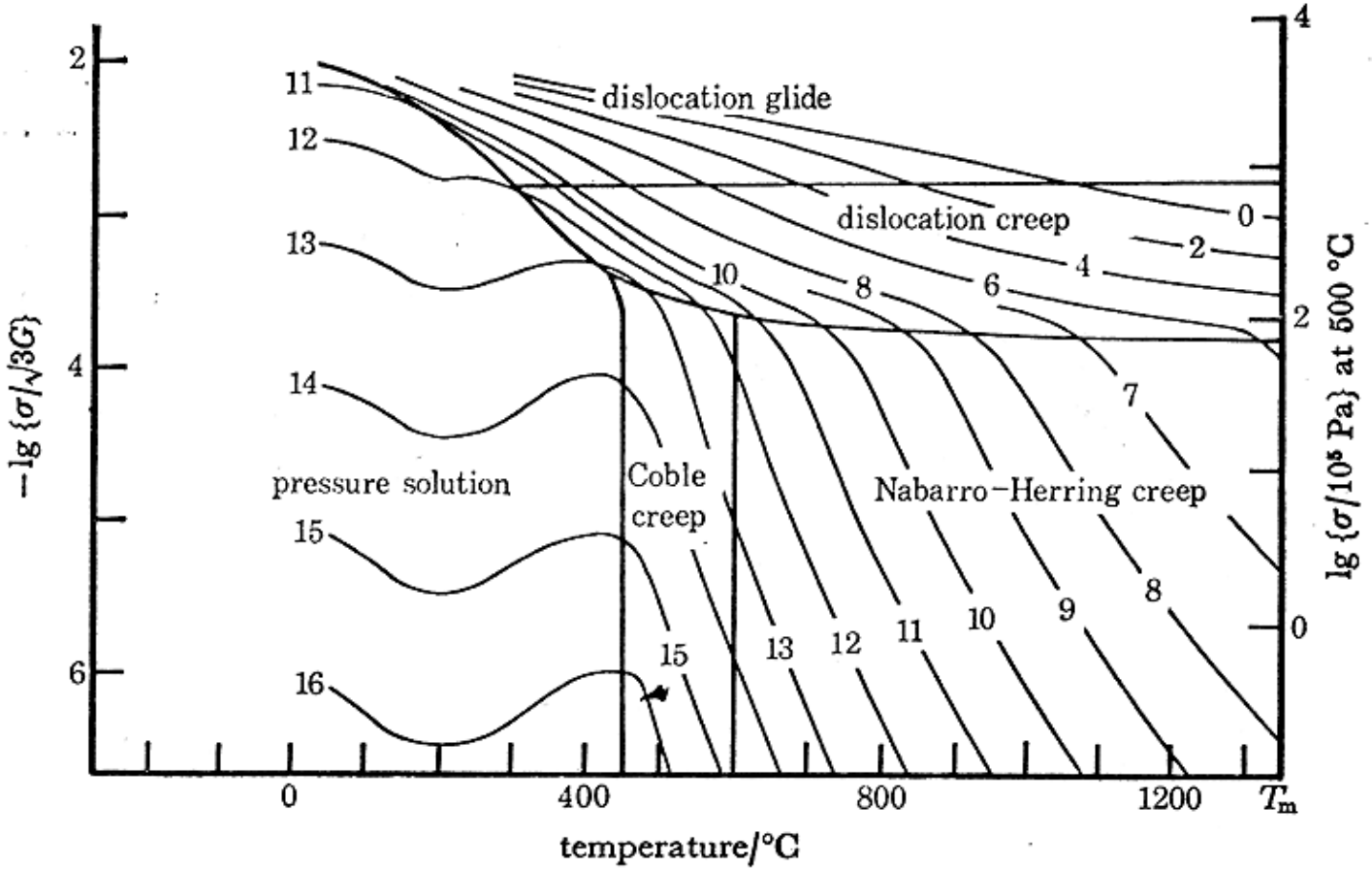

Deformation mechanism map for calcite modified by the addition of a pressure solution field. $d = 100\ \mu m$; $V = 37\ cm^3$.

Rutter, E.H., (1976) The kinetics of rock deformation by pressure solution, Phil. Trans. R. Soc. Lond., A, 283, 203-219

MICROMECHANICS

Geometry of stylolites

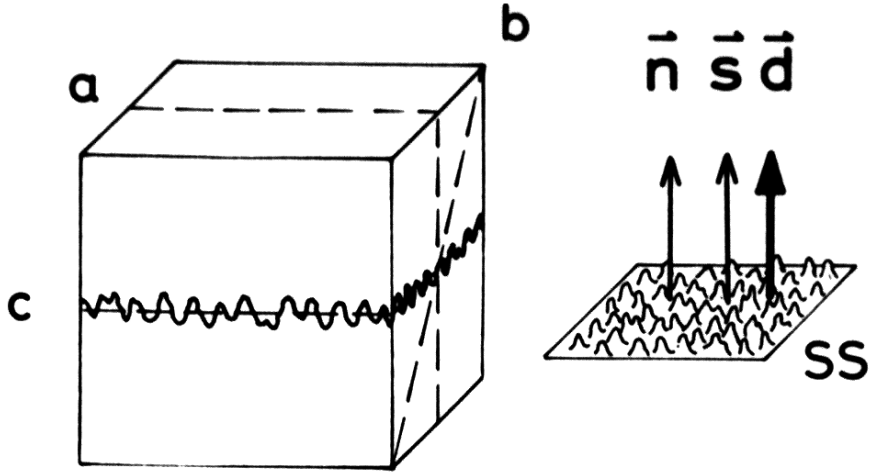

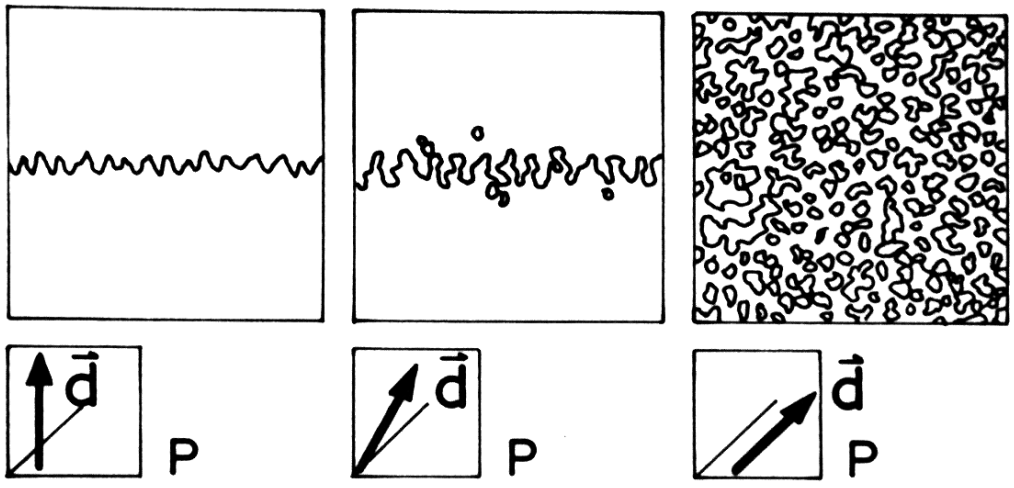

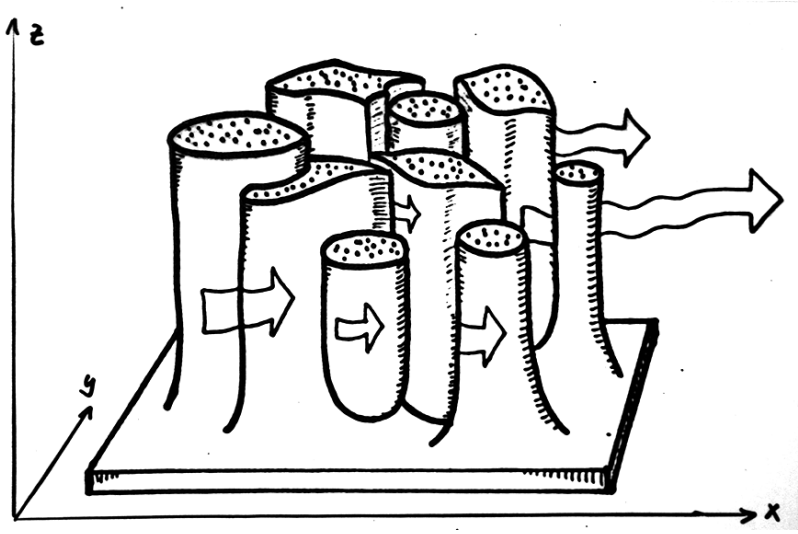

Weyl, P.K., 1959 - Pressure solution and the force of crystallization

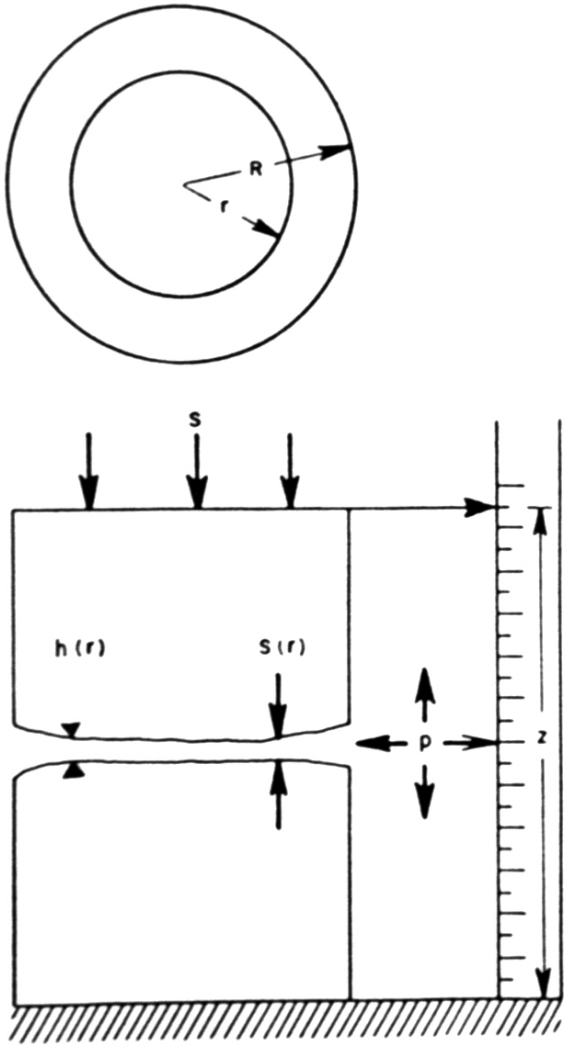

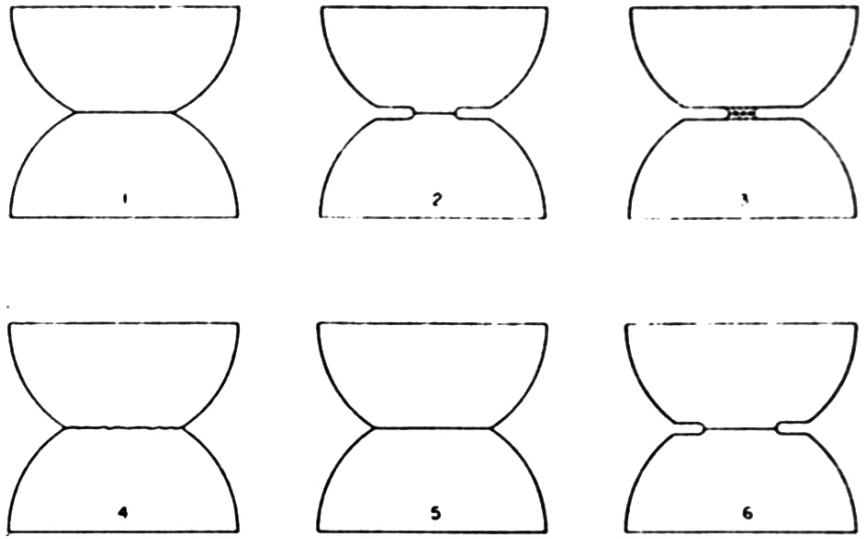

Weyl, P.K., 1959 - Pressure solution and the force of crystallization

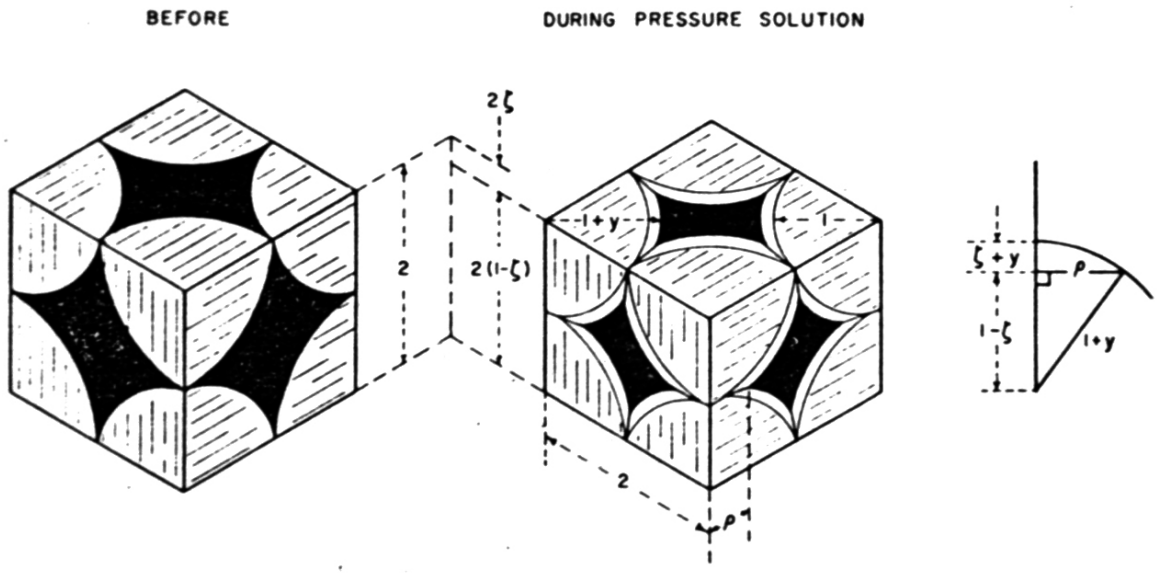

Anti-crack model (Fletcher & Pollard, 1981)

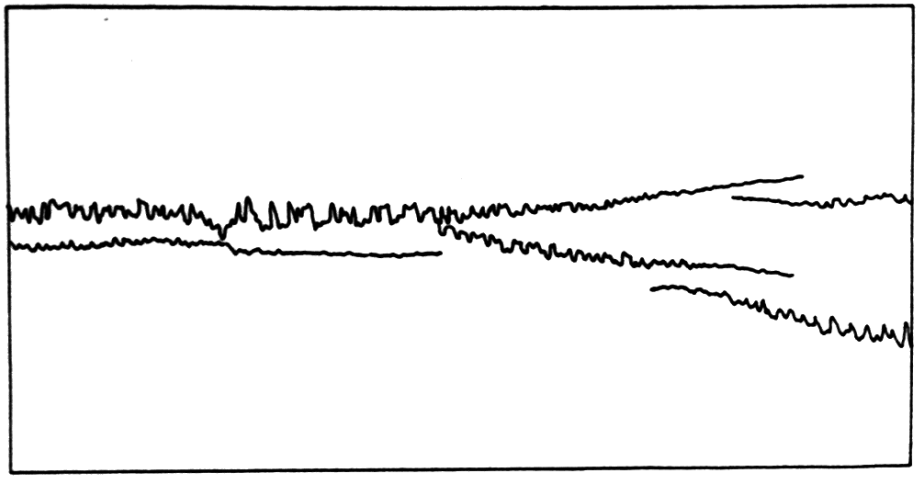

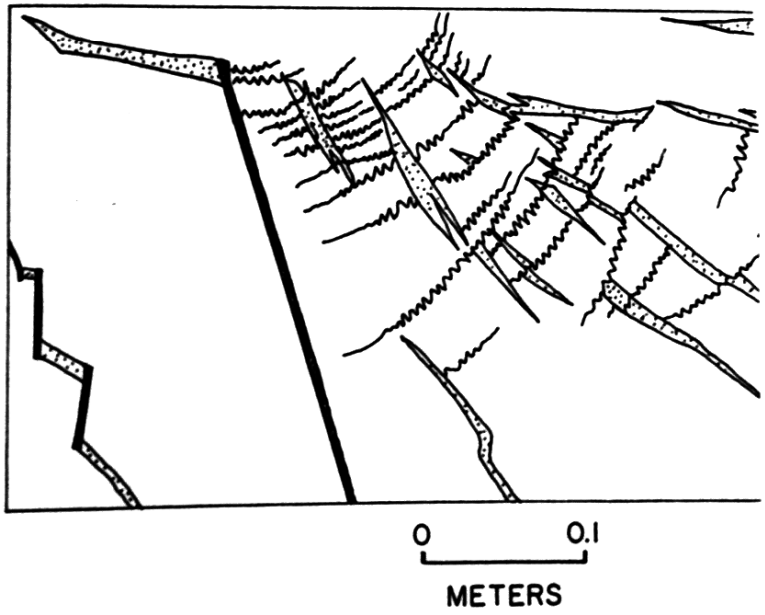

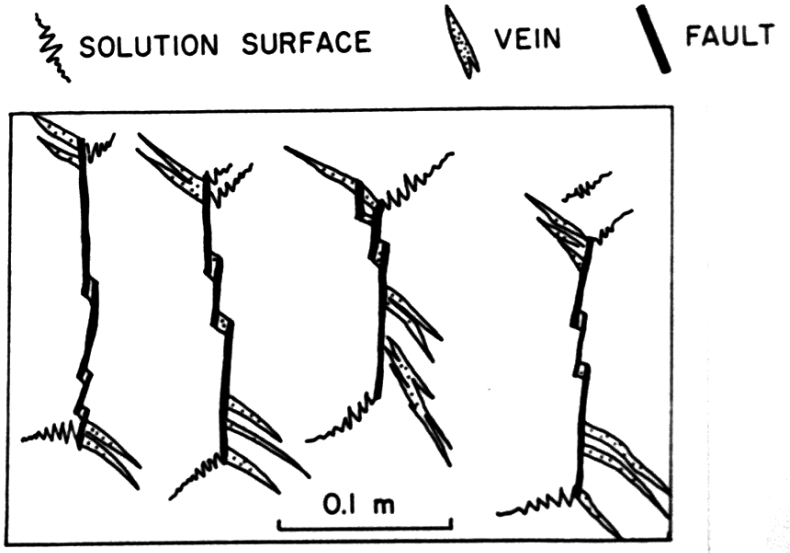

PRESSURE SOLUTION - LARGE SCALE

Pressure solution cleavage (Alvarez et al., 1976)

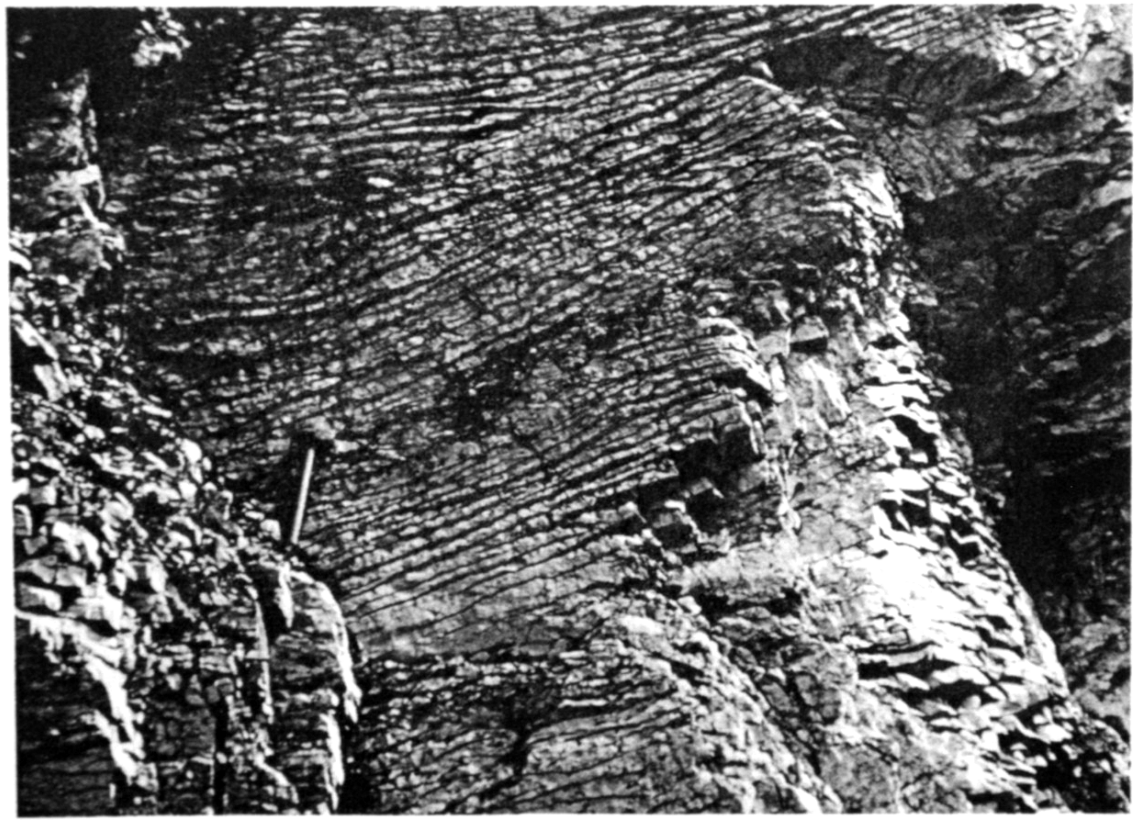

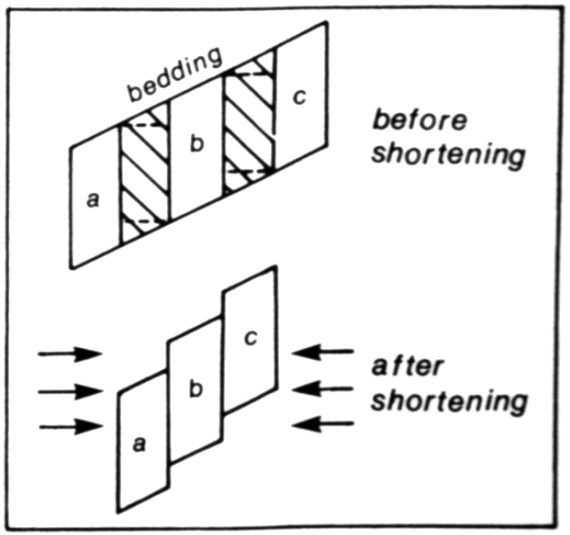

Pressure solution - “viscous component of folding” Laubscher (1975)

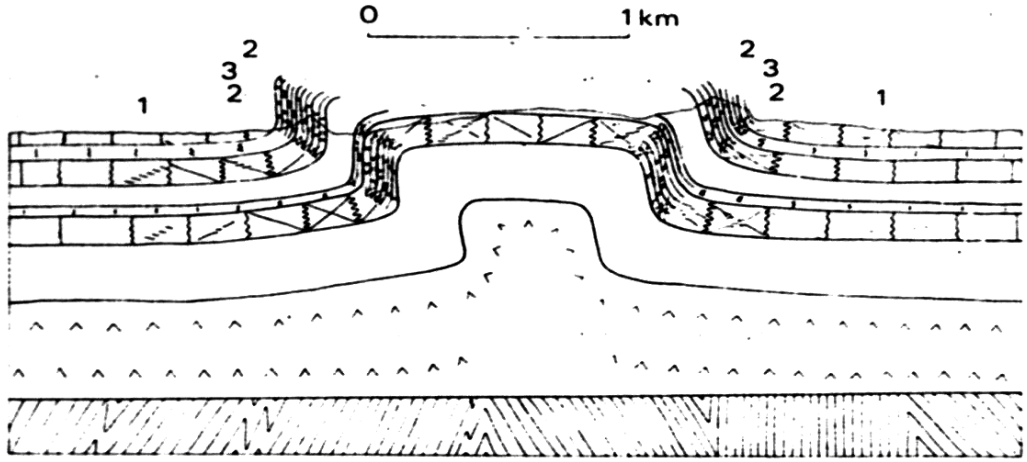

Polarisation

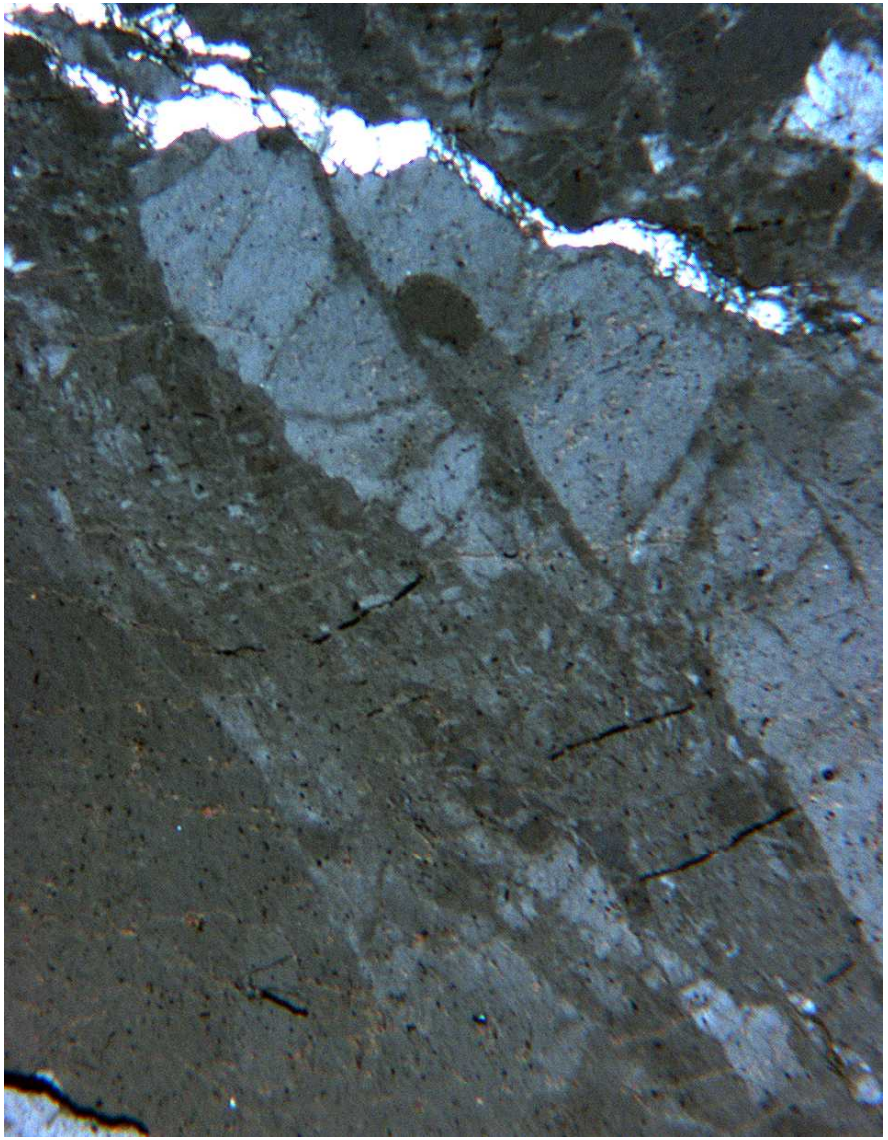

SEM

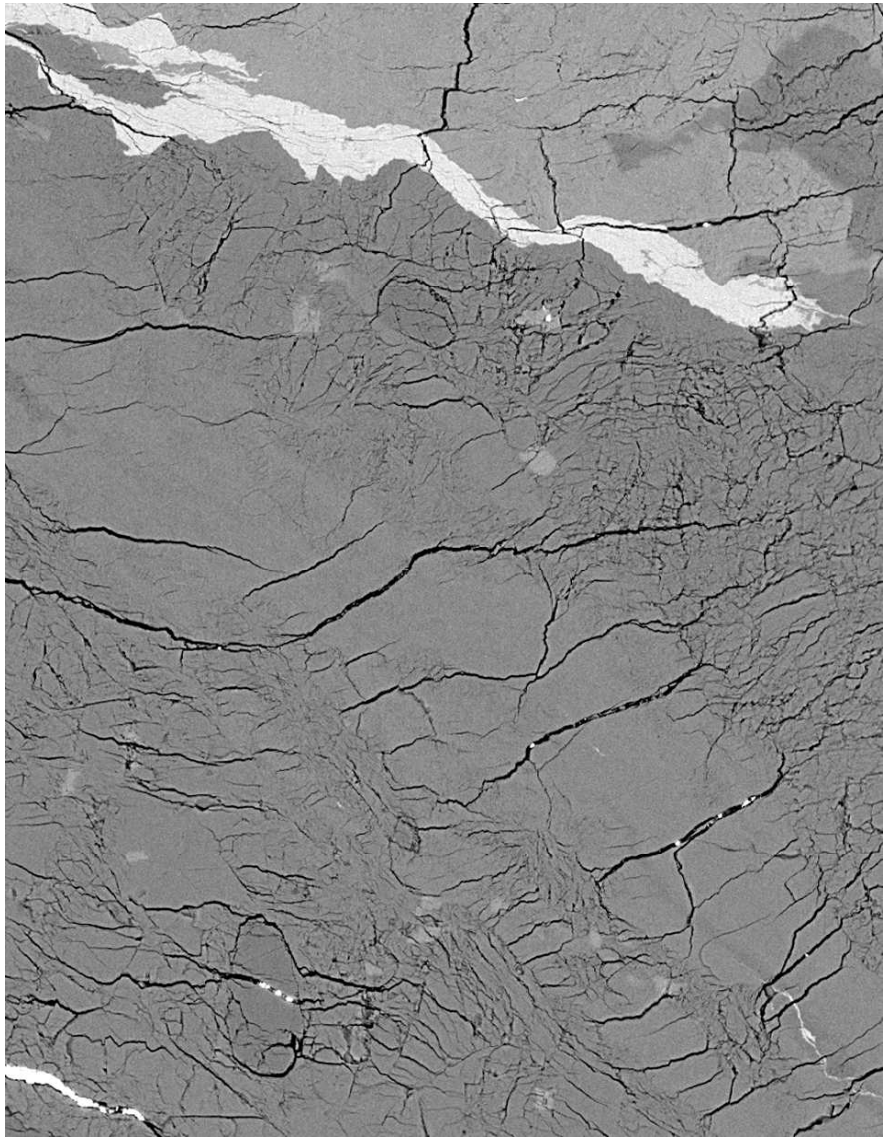

SEM

Cathodoluminescence CL

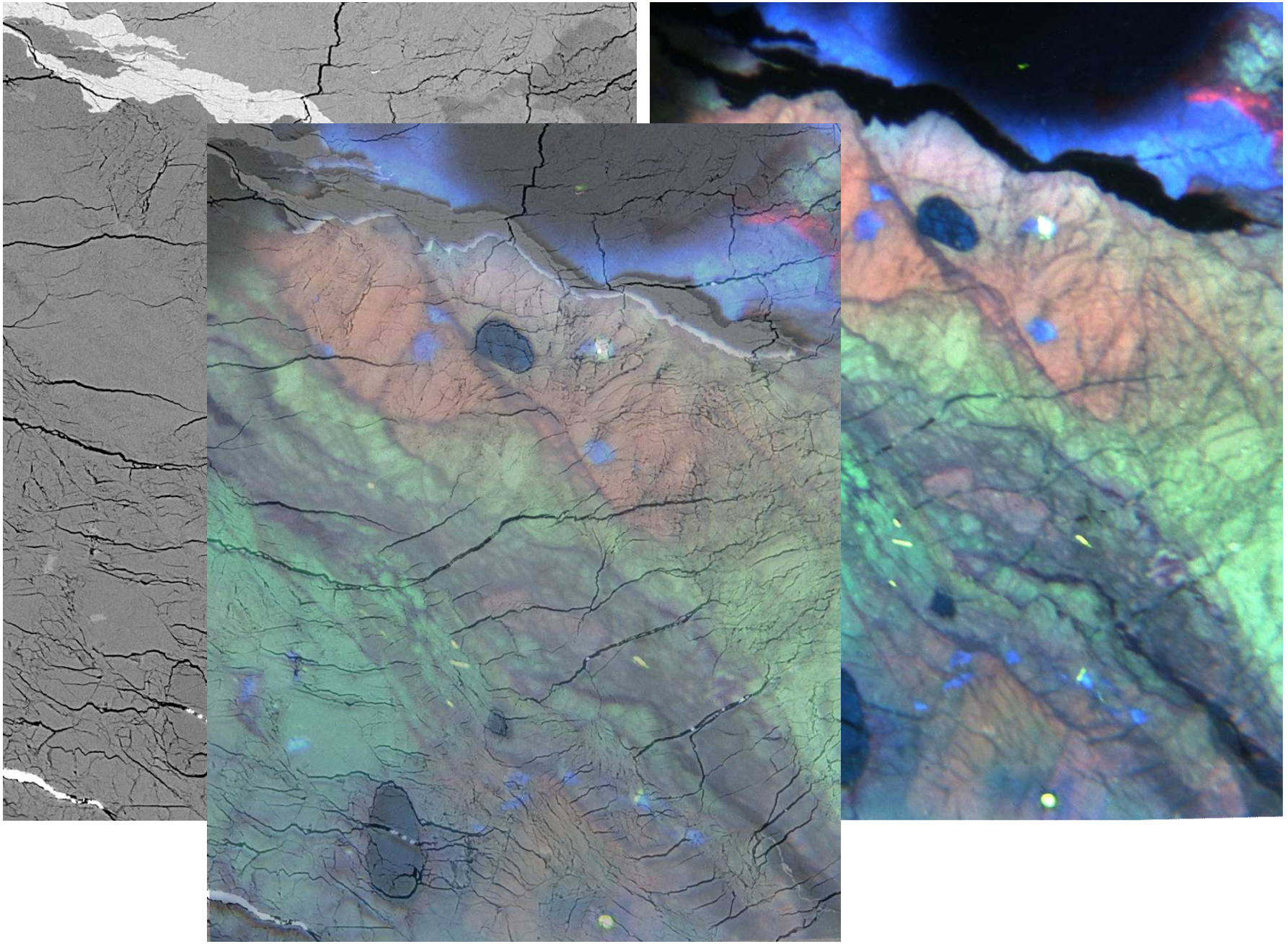

Cathodoluminescence CL SEM

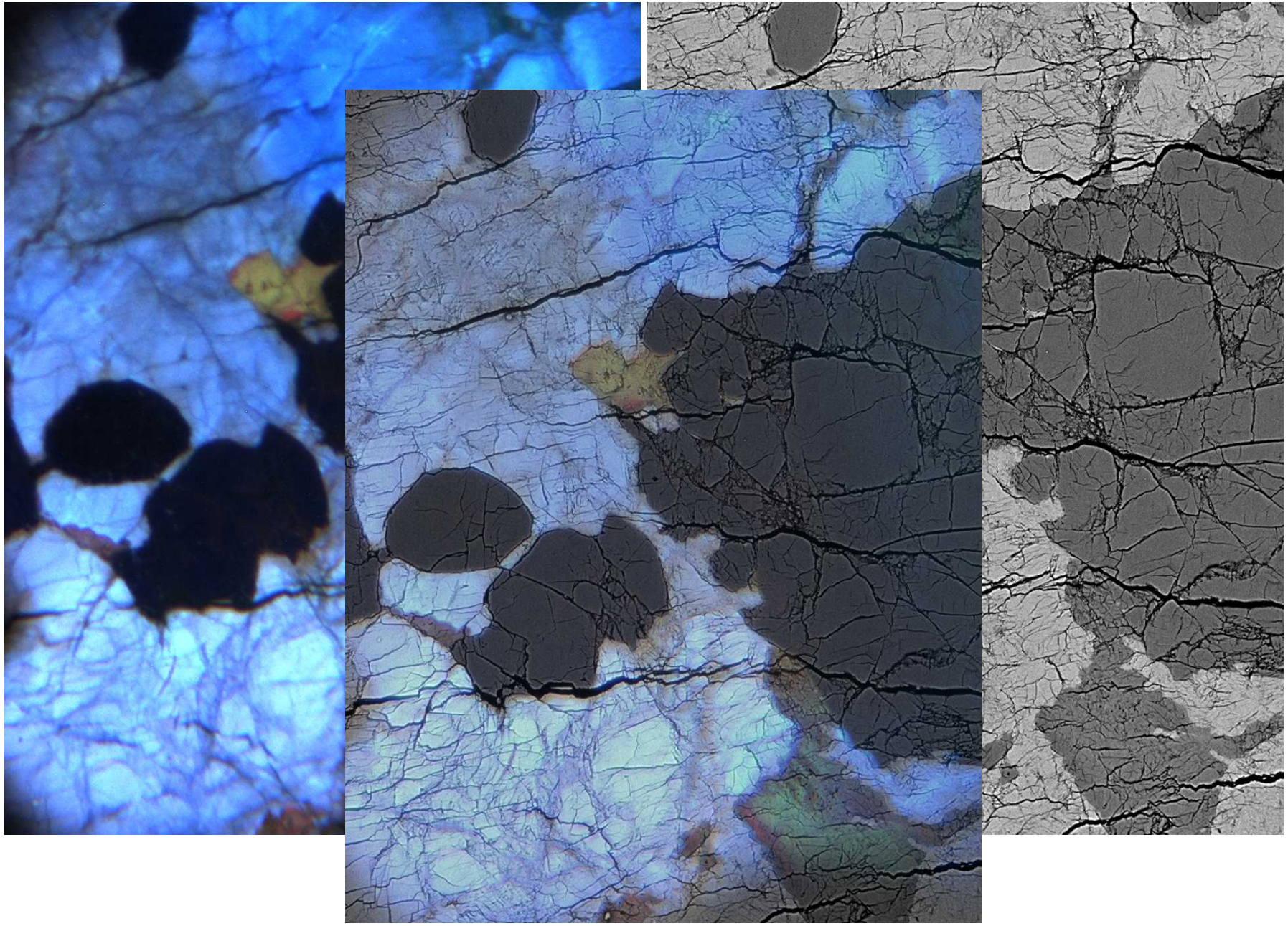

Cathodoluminescence CL SEM

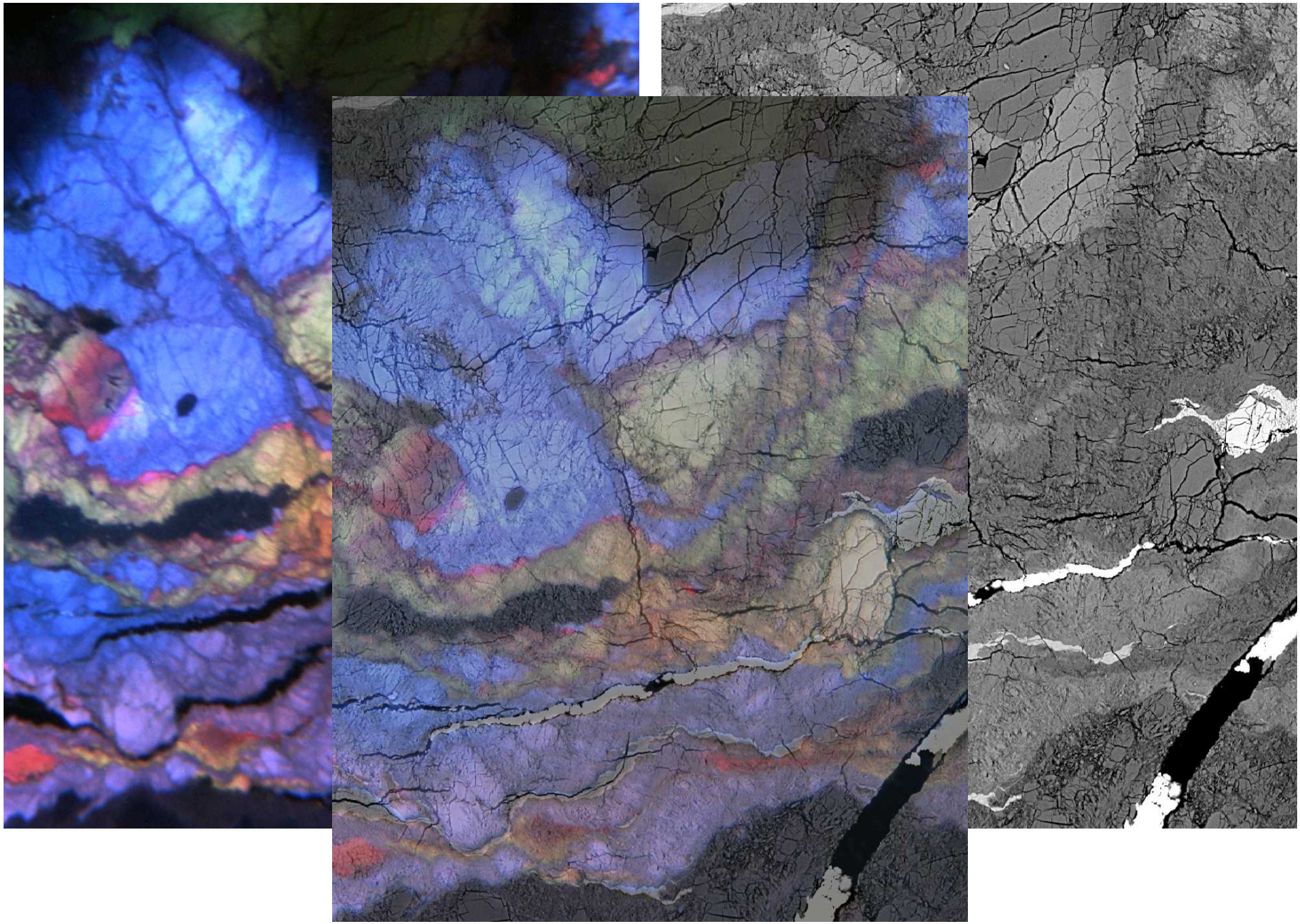

REFERENCES

Alvarez, W., et al. 1976: Formation of spaced cleavage and folds in brittle limestone by dissolution. Geology 4, 698-701.

Angevine, C. L., et al. 1982: Pressure solution lithification as a mechanism for the stick slip behaviour of faults. Tectonics 1, 151-160.

Casey, M., et al. 1983: Method for determining deformation history for chocolate tablet boudinage with fibrous crystals. Tectonophysics 92, 211-240.

DeBoer, R. B. 1977: On the thermodynamics of pressure solution - interaction between chemical and material forces. Geochimica et Cosmocimica Acta 41, 249-256.

Dewers, T. & Ortoleva, P. 1989: Mechano-chemical coupling in stressed rocks. Geochimica et Cosmocimica Acta 53, 1243-1258.

Durney, D. W. 1972: Solution-trnasfer, an important geological deformation mechanism. Nature 235, 315-317.

Durney, D. W. & Ramsay, J. G. 1973: Incremental strains measured by syntectonic crystal growth. In: Gravity and Tectonics (Ed. by DeJong, K.A. & Scholten, R.). John Wiley & Sons, New York, 67-96.

Elliott, D. 1973: Diffusion flow laws in metamorphic rocks. Bull. Geol. Soc. Am. 84, 2645-2664.

Engelder, T. 1982: A natural example of the simultaneous operation of free-face dissolution and pressure solution. Geoch. cosmochim. Acta 46, 69-74.

Etchecopar, A. & Malavieille, J. 1987: Computer models of pressure shadows: a method for strain measurements and shear-sense determination. J. struct. Geol. 9, 667-677.

Fletcher, R. C. & Pollard, D. D. 1981: Anticrack model for pressure solution surfaces. Geology 9, 419-424.

Gratier, J. P. 1983: Estimation of volume change by comparative chemical analyses in heterogeneously deformed rocks (folds with mass transfer). J. Struct. Geology 5, 329-339.

Gratier, J. P. 1984: La déformation des roches par dissolution-cristallisation. Ph.D., I.R.I.G.M., Grenoble.

Gratier, J. P. 1984: La déformation des roches par dissolution-cristallisation. Ph.D., I.R.I.G.M., Grenoble.
Kamb, W. B. 1961: The thermodynamic theory of nonhydrostatically stressed solids. J.G.R. 66,
Kerrich, R. 1977: An historical review and synthesis of research on pressure solution. Zbl. Geol. Paläontol. Teil I 5/6, 512-550.
Laubscher, H. P. 1975: Viscous components in Jura folding. Tectonophysics 27, 239-254.
Panozzo, R. H. 1980: Kinetics of solution and transport processes in porous rocks. In Center for Tectonophysics, Texas A&M University.
Panozzo, R. H. 1984: Deformation mechanisms associated with mesoscopic kinkbands, Jura Mountains (Switzerland) and Chaînes Subalpines (France). Ph.D., Texas A&M University.
Paterson, M. S. 1973: Nonhydrostatic thermodynamics and its geological applications. Rev. Geophys. Space Phys. 11, 355-390.
Plessmann, W. 1972: Horizontal-Stylolithen im französisch-schweizerischen Tafel- und Faltenjura und ihre Einpassung in den regionalen Rahmen. Geol. Rdsch. 61, 332-347.
Price, N. G. & Cosgrove, J. W. 1990: Analysis of geological structures. Cambridge University Press, Cambridge.
Ramsay, J. G. 1980: The crack-seal mechanism of rock deformation. Nature 284, 135-139.
Ramsay, J. G. & Huber, M. I. 1983: The techniques of modern structural geology, Vol. 1: Strain Analysis. Academic Press, London.
Robin, P. Y. 1978: Pressure solution at grain to grain contacts. Geochim. Cosmo. Acta 43, 1383-1389.
Rutter, E. H. 1976: The kinetic of rock deformation by pressure solution. Phil. Trans. Roy. Soc. Lond. A 283, 43-54.
Rutter, E. H. 1983: Pressure solution in nature, theory and experiment. J. Geol. Sci. Lond. 140, 725-740.
Sprunt, E. S. & Nur, A. 1977: Experimental study of the effects of stress on solution rate. J. geophys. Res. 82, 3013-3022.
Stephansson, O. 1974: Stress-induced diffusion during folding. Tectonophysics 22, 233-251.
Weyl, P. K. 1959: Pressure solution and the force of crystallisation, a phenomenological theory. J. geophys. Res. 64, 2001-2025.

11
Flow and fracture

Deformationsprozesse in der Erde (11)

Flow and fracture

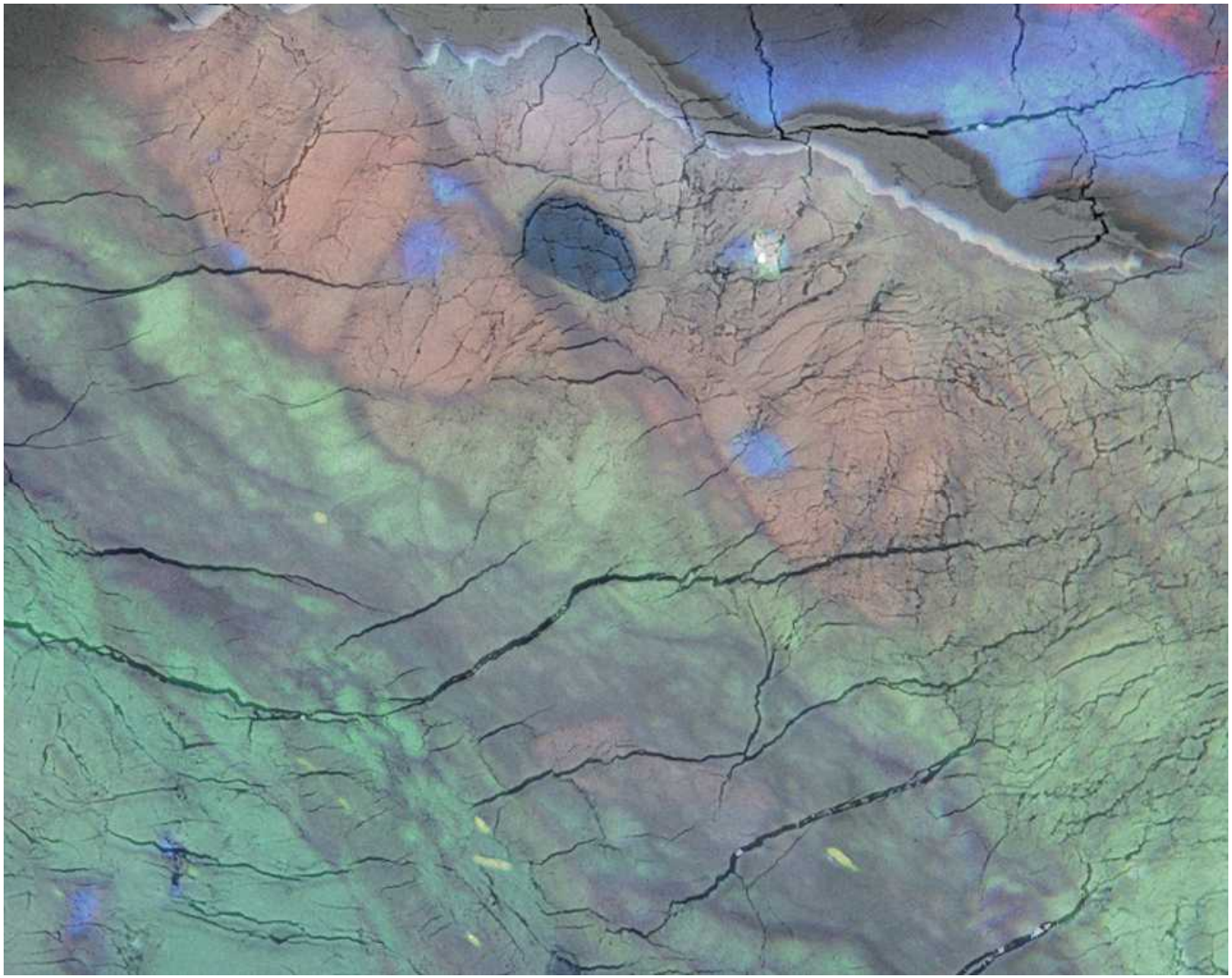

Ashby, M.F. & Verrall, R.A., 1977 Micromechanisms of flow and fracture

TABLE 4. LOW-TEMPERATURE FRACTURE OF DUNITE AND PERIDOTITE

T/°C	T/T_M	σ_1/MPa	σ_3/MPa	σ_t/MPa	$10^3\sigma_t/\mu$	reference
25	0.14	500	2300	650	8.1	Griggs *et al.* (1960)
25	0.14	500	2000	500	6.2	
150	0.2	100	510	400	5.0	Handin (1966)
150	0.2	100	450	350	4.5	

Ashby, M.F. & Verrall, R.A., 1977 Micromechanisms of flow and fracture

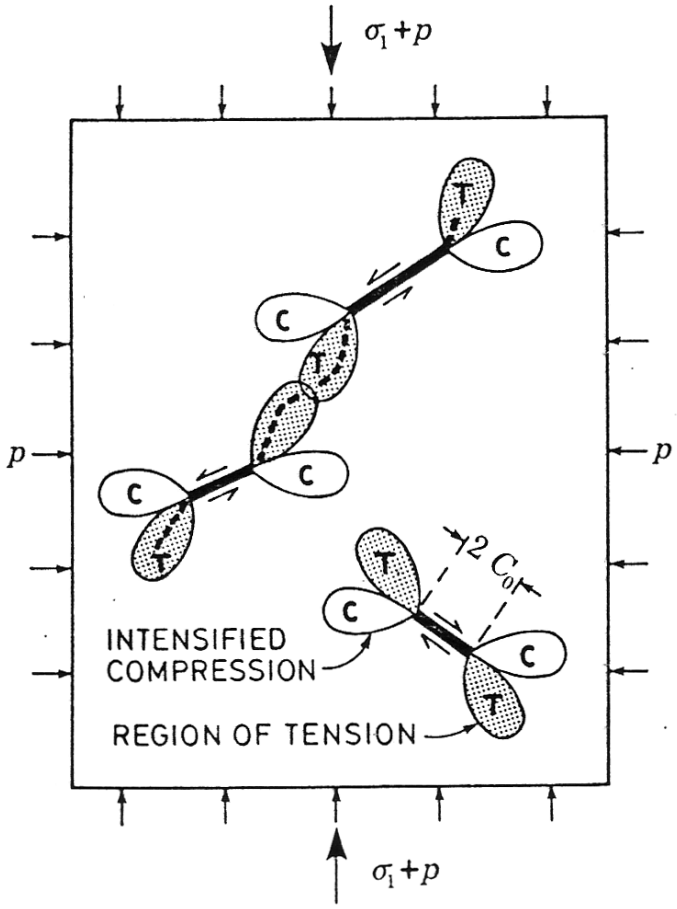

Ashby, M.F. & Verrall, R.A., 1977 Micromechanisms of flow and fracture

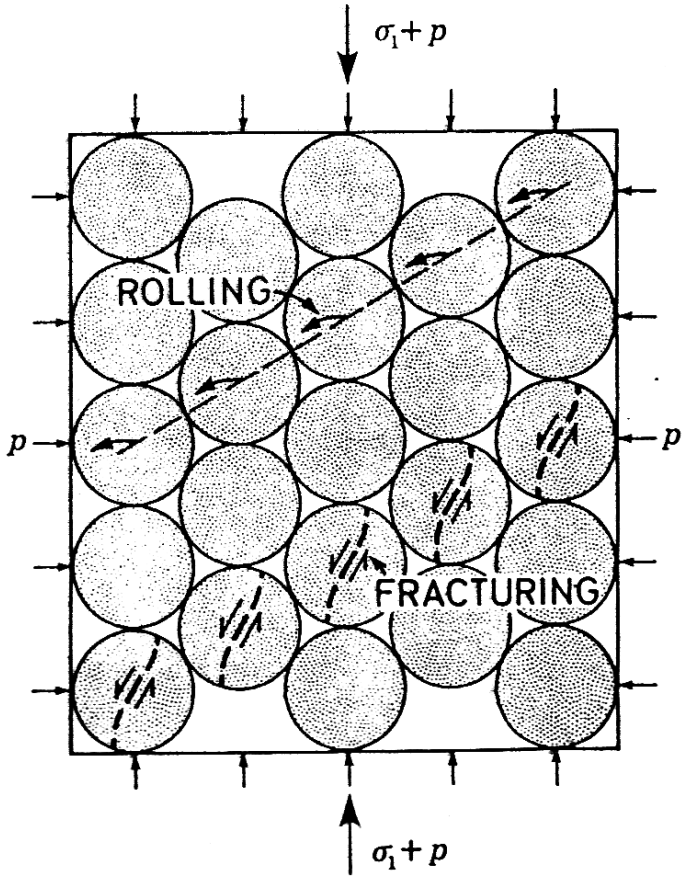

Ashby, M.F. & Verrall, R.A., 1977 Micromechanisms of flow and fracture

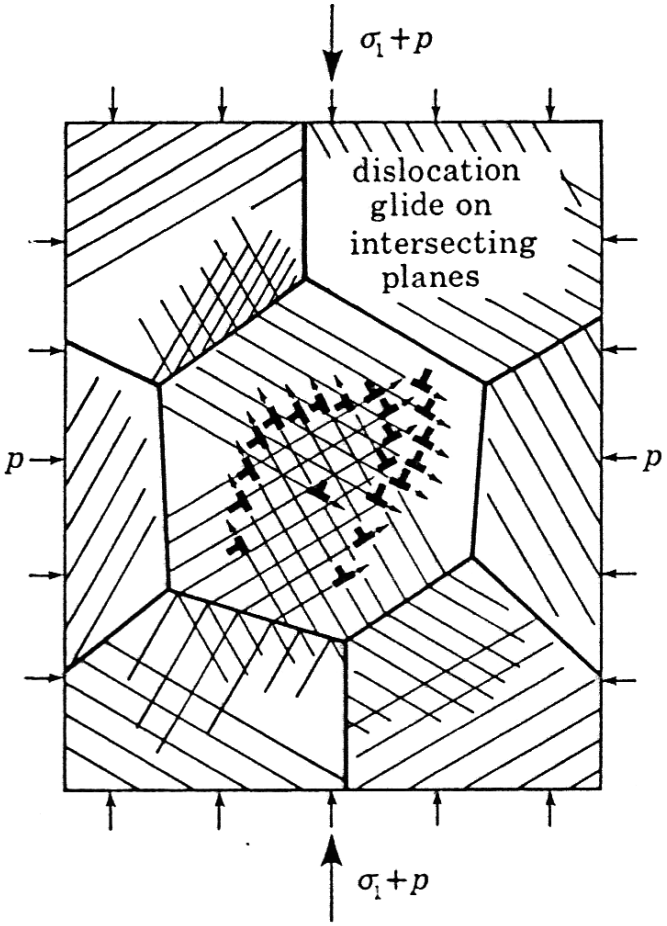

Ashby, M.F. & Verrall, R.A., 1977 Micromechanisms of flow and fracture

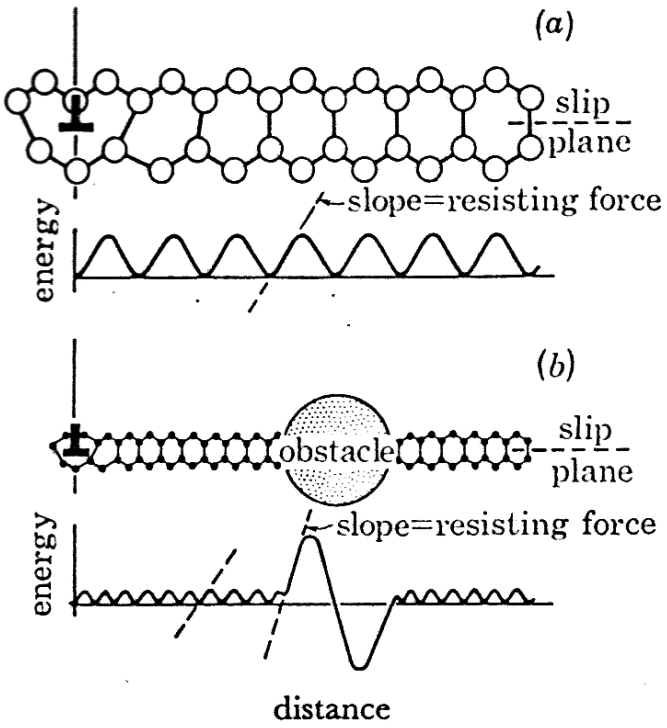

Ashby, M.F. & Verrall, R.A., 1977 Micromechanisms of flow and fracture

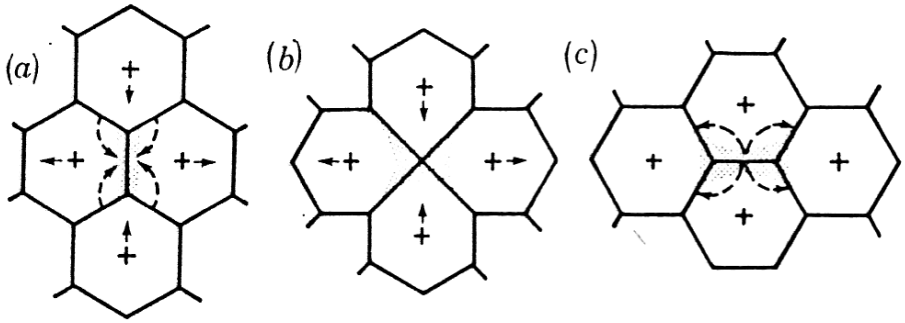

Ashby, M.F. & Verrall, R.A., 1977 Micromechanisms of flow and fracture

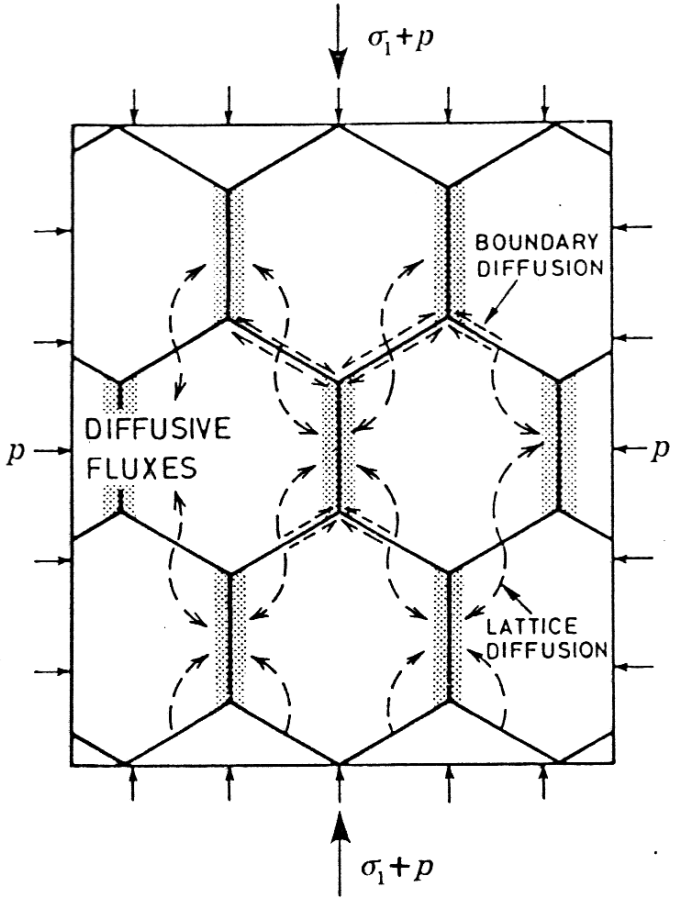

Ashby, M.F. & Verrall, R.A., 1977 Micromechanisms of flow and fracture

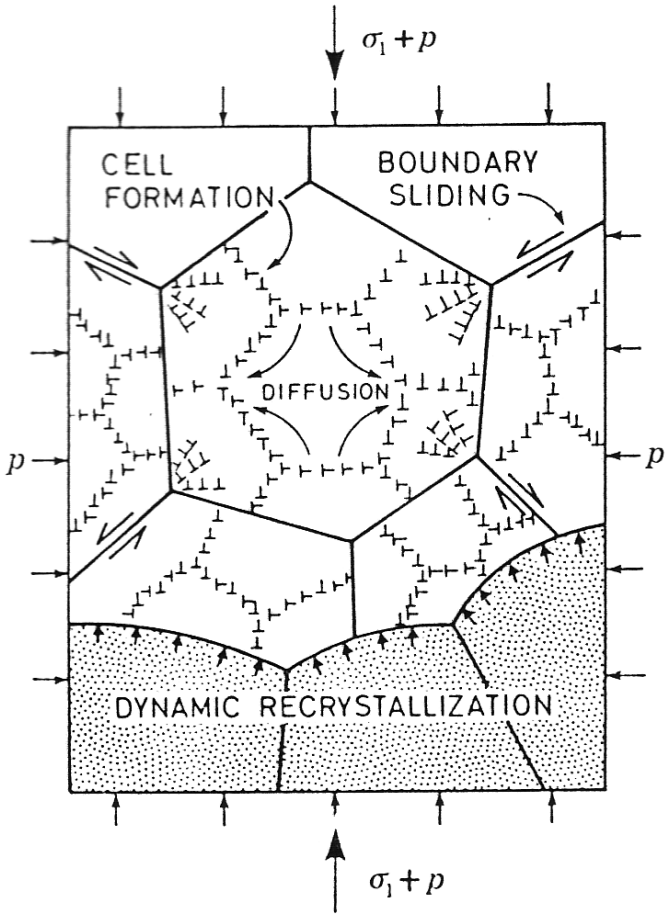

Ashby, M.F. & Verrall, R.A., 1977 Micromechanisms of flow and fracture

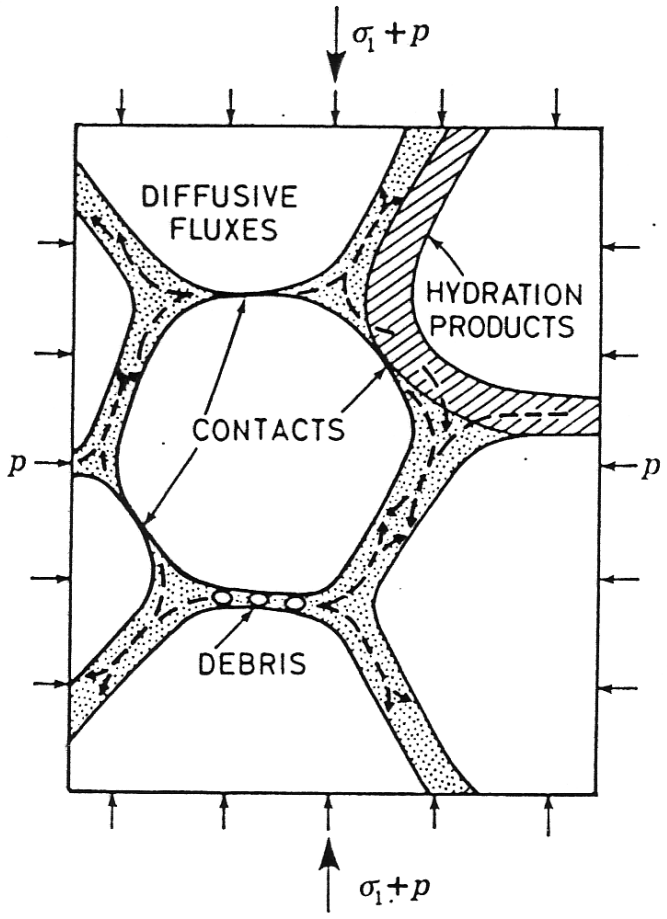

Ashby, M.F. & Verrall, R.A., 1977 Micromechanisms of flow and fracture

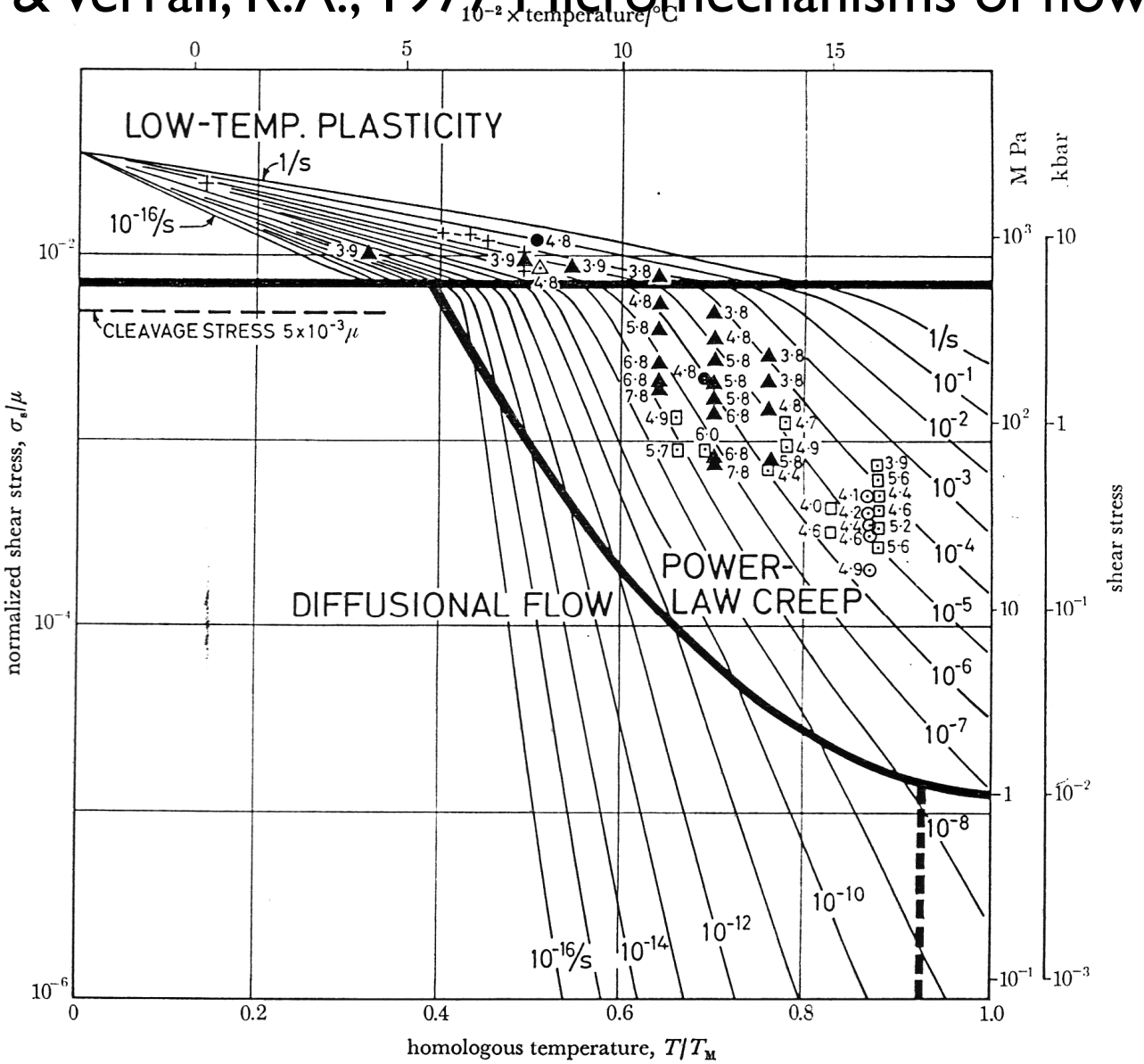

FIGURE 14. A map for olivine with a grain size of 0.1 mm; zero pressure. The symbols identify experimental points, and are labelled with the negative of the logarithm to the base 10 of the observed shear strain-rate. Cleavage was suppressed to show the plasticity field; if a realistic value for σ_i were used, the diagram would be truncated at the level marked 'cleavage stress $5\times10^{-3}\mu$'. Data: +, Evans (1976) hardness data; ▲, Carter & Ave' Lallemant (1970) (peridotite, 15 kbar); ●, Durham *et al.* (1976); △, Phakey *et al.* (1972) (single crystals, hard direction); ⊙, Kohlstedt & Goetze (1974); ⊡, Durham & Goetze (1976).

Ashby, M.F. & Verrall, R.A., 1977 Micromechanisms of flow and fracture

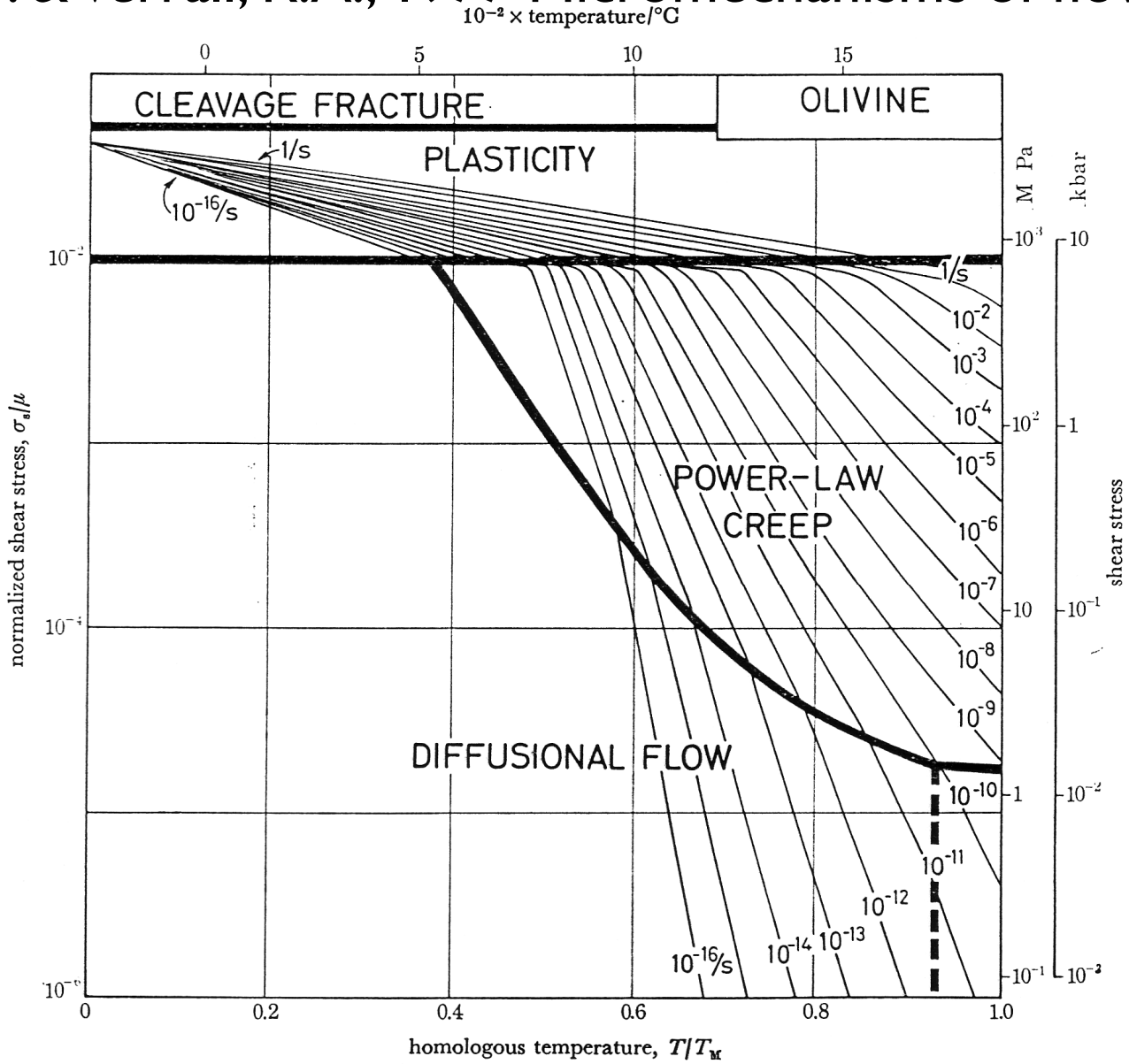

FIGURE 15. A map for olivine, based on the same data as figure 14, but with a pressure of 0.1 K^0 (81 kbar) applied. The cleavage stress has been raised by a factor of about 10 to $5 \times 10^{-3}\mu$; the stress required for plasticity has increased by a factor of about 1.5 and the creep rates have decreased by a factor of about 10^3.

Ashby, M.F. & Verrall, R.A., 1977 Micromechanisms of flow and fracture

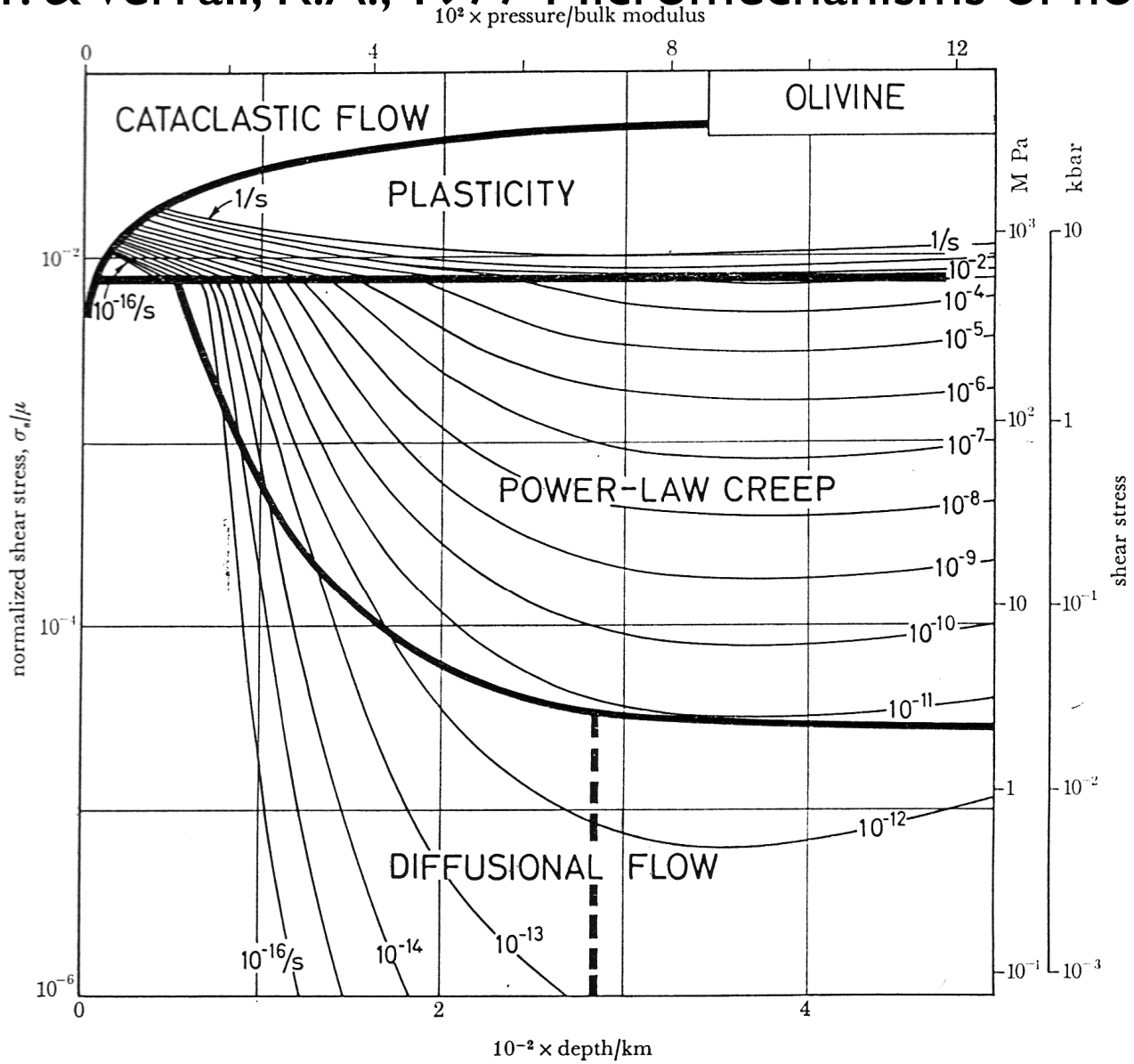

FIGURE 17. Olivine under upper-mantle conditions with $V^* = 0$; cleavage stress $= 5 \times 10^{-3}\mu$. In this figure, depth (below the Earth's surface) has replaced temperature as the abscissa; temperature and pressure are both related directly to it. The figure shows that, to a depth of about 30 km, cataclastic flow is the dominant mechanism. Below this, plasticity and creep replace fracturing as the dominant mechanisms.

Ashby, M.F. & Verrall, R.A., 1977 Micromechanisms of flow and fracture

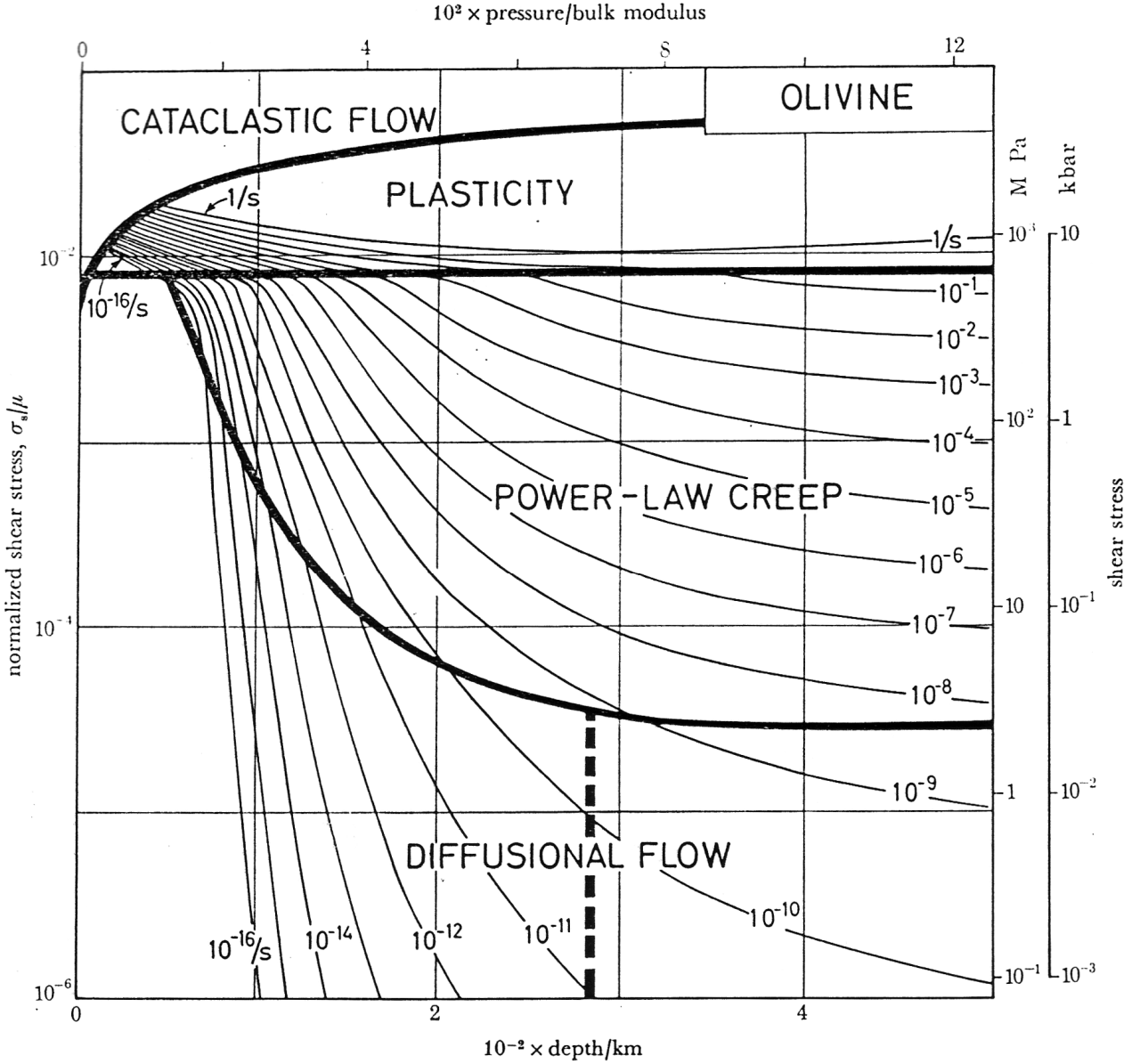

FIGURE 18. Olivine under upper-mantle conditions with $V^* = \Omega_i$. The creep rates are slower by a factor of between 10^2 and 10^3 than those of figure 17. Note that the strain-rate contours are almost flat below 200 km.

Ashby, M.F. & Verrall, R.A., 1977 Micromechanisms of flow and fracture

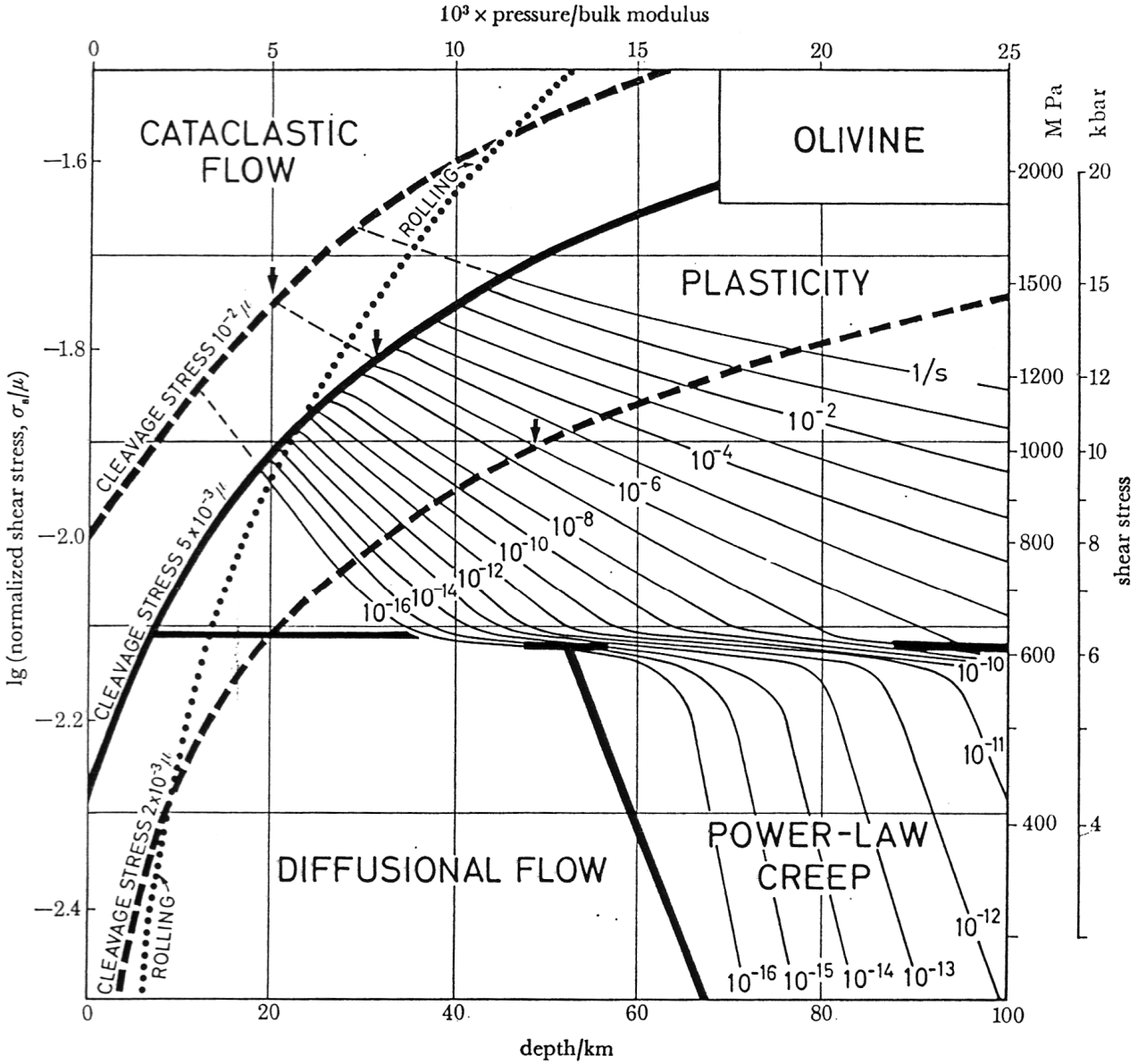

FIGURE 19. An enlarged portion of figure 18, illustrating the transition from cataclastic flow to plastic flow. The depth at which this transition occurs depends on the strain-rate and on the fracture stress, σ_f. It also depends on the temperature profile in the mantle, and will be different in regions where descending plates cool the mantle locally.

12
Flow laws & deformation mechanism maps

Deformationsprozesse in der Erde (12)

Flow laws & deformation mechanism maps

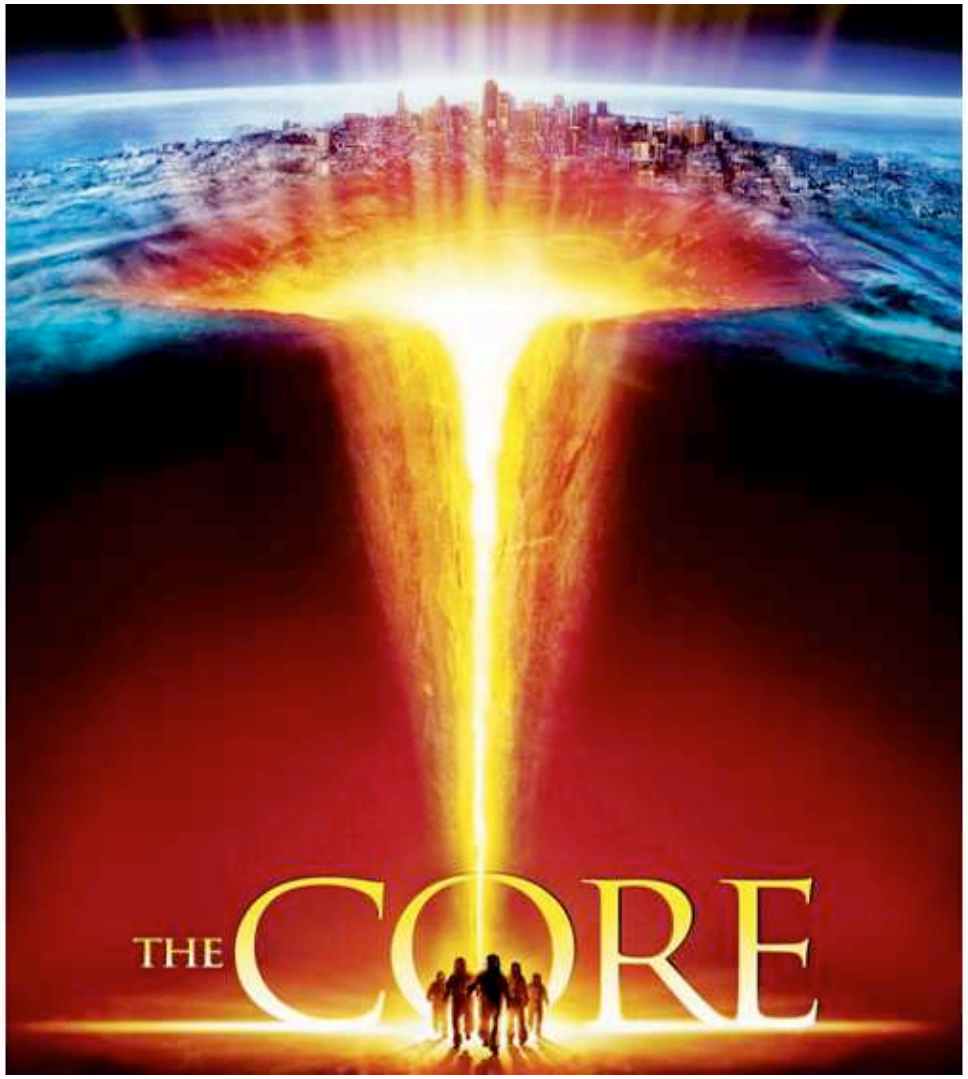

Deformation Mechanism Map

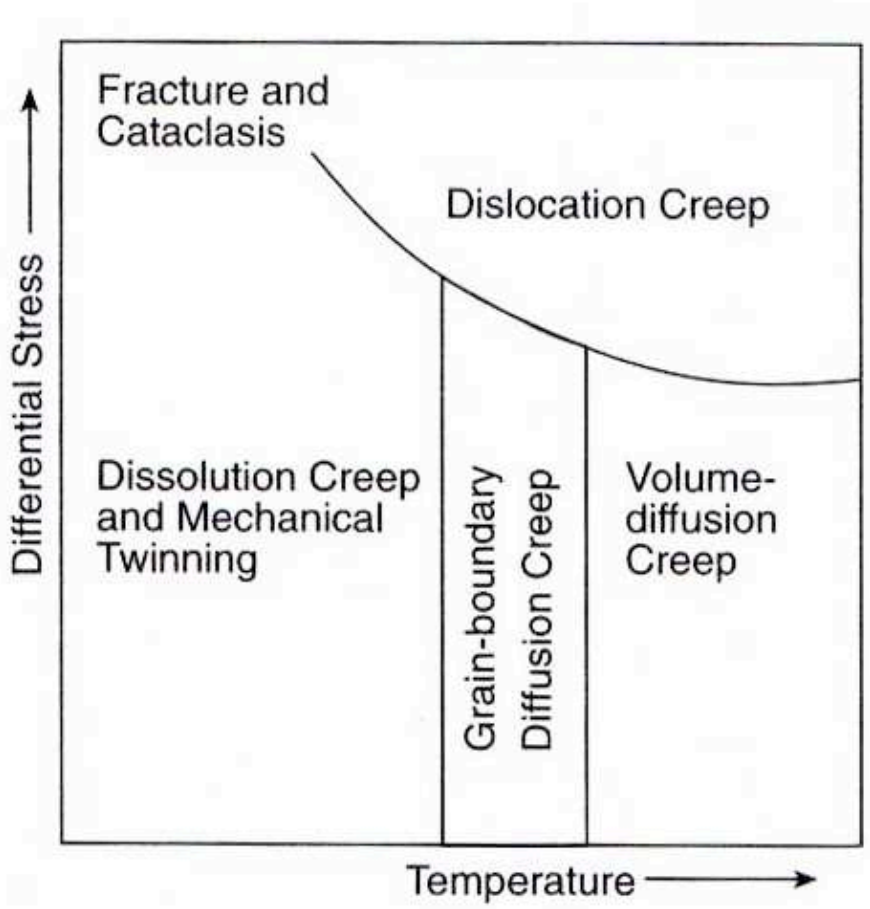

Simplified deformation mechanism map showing mineral response relative to temperature and differential stress (from Davis and Reynolds, Structural Geology of Rocks and Regions, 1996).

Deformation Mechanism Map

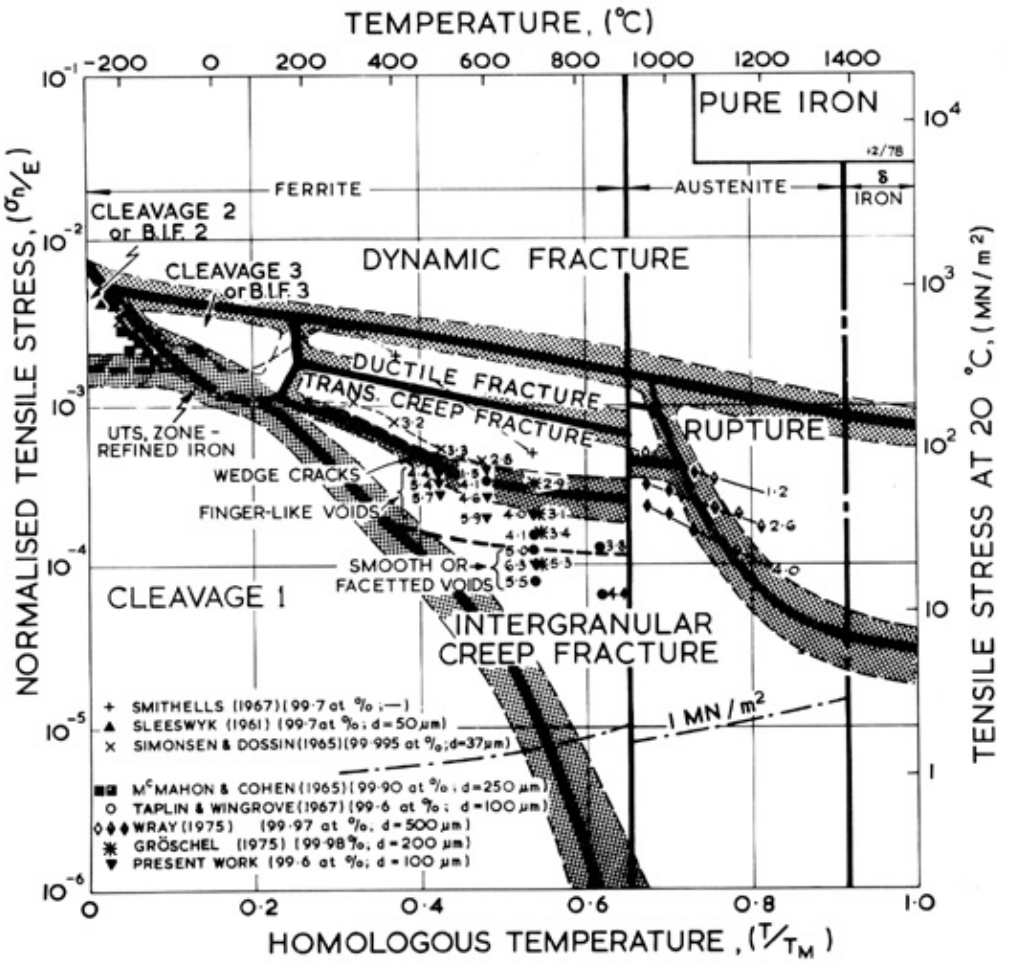

The fracture mechanism map for nominally pure iron. It shows mechanism fields of cleavage, ductile fracture, transgranular creep fracture, intergranular creep fracture, and rupture. The numbers against data points are $\log_{10} t$. When the iron is slowly cooled from 1200 K, cleavage is suppressed, and brittle intergranular fracture (BIF) appears in its place. Shading indicates a mixed mode of fracture.

Deformation Mechanism Map

Ashby, M.F. (1972)
A first report on deformation mechanism maps.
Acta Met. 20, 887-897.

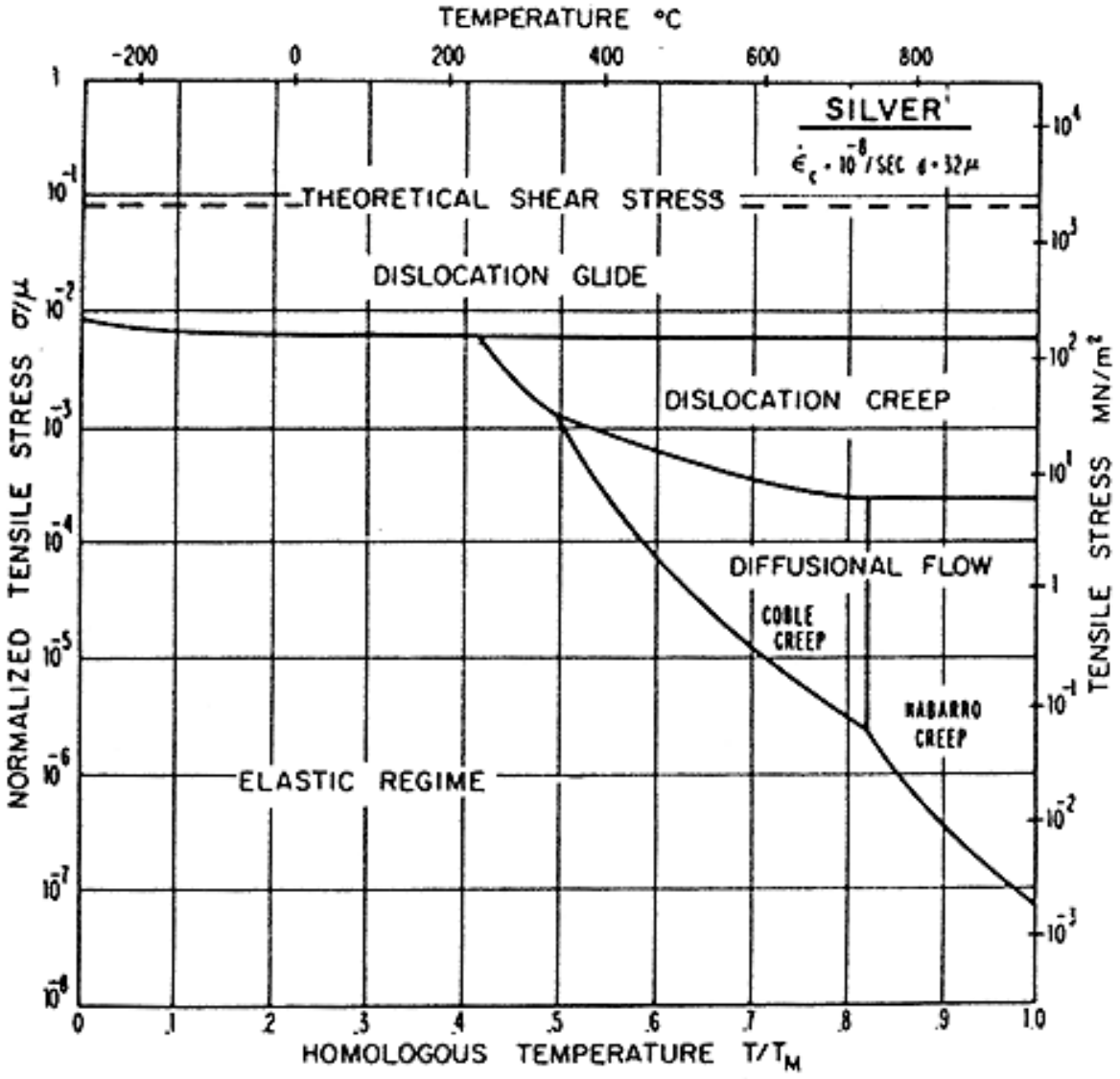

FIG. 1. A deformation–mechanism map for pure silver, of grain size 32 μ, and for a critical strain rate $\dot{\epsilon}_c$ of 10^{-8}/sec.

Deformation Mechanism Map

Ashby, M.F. (1972)
A first report on deformation mechanism maps.
Acta Met. 20, 887-897.

1 Defectless flow

theoretical strength

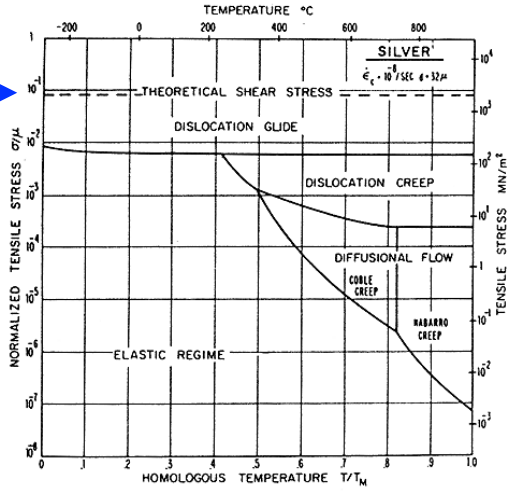

FIG. 1. A deformation–mechanism map for pure silver, of grain size 32 μ, and for a critical strain rate $\dot{\varepsilon}_c$ of 10^{-8}/sec.

$$\left.\begin{aligned} \dot{\varepsilon}_1 = \infty \qquad & \frac{\sigma}{\mu} \geq \frac{\sigma^{TH}}{\mu} \\ \dot{\varepsilon}_1 = 0 \qquad & \frac{\sigma}{\mu} < \frac{\sigma^{TH}}{\mu} \end{aligned}\right\}$$

Deformation Mechanism Map

Ashby, M.F. (1972)
A first report on deformation mechanism maps.
Acta Met. 20, 887-897.

2 Dislocation glide

dislocation glide

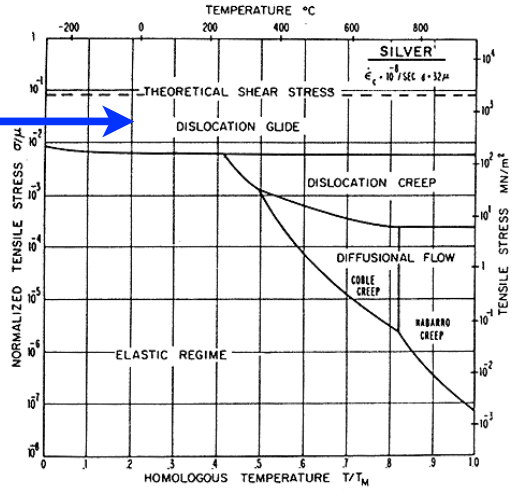

FIG. 1. A deformation–mechanism map for pure silver, of grain size 32 μ, and for a critical strain rate $\dot{\varepsilon}_c$ of 10^{-8}/sec.

$$\dot{\varepsilon}_2 = \dot{\varepsilon}_0 \exp - \frac{\{S - \sigma\}}{kT} ba \qquad \frac{\sigma}{\mu} \geq \frac{\sigma_0}{\mu}$$

$$\dot{\varepsilon}_2 = 0 \qquad \frac{\sigma}{\mu} < \frac{\sigma_0}{\mu}$$

Deformation Mechanism Map

Ashby, M.F. (1972)
A first report on deformation mechanism maps.
Acta Met. 20, 887-897.

3, 4 Diffusional creep

3 Coble creep

4 Nabarro-Herring creep

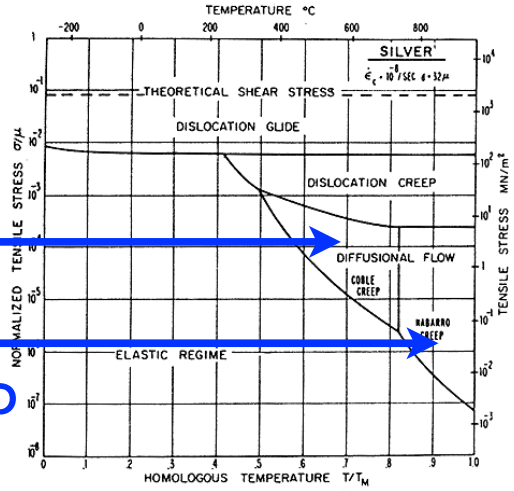

FIG. 1. A deformation–mechanism map for pure silver, of grain size 32 μ, and for a critical strain rate $\dot{\varepsilon}_c$ of 10^{-8}/sec.

$$\dot{\varepsilon}_{3,4} = 14 \frac{\sigma\Omega}{kT} \frac{1}{d^2} D_v \left\{ 1 + \frac{\pi\delta}{d} \frac{D_B}{D_v} \right\}$$

Deformation Mechanism Map

Ashby, M.F. (1972)
A first report on deformation mechanism maps.
Acta Met. 20, 887-897.

3, 4 Diffusional creep

3 Coble creep

4 Nabarro-Herring creep

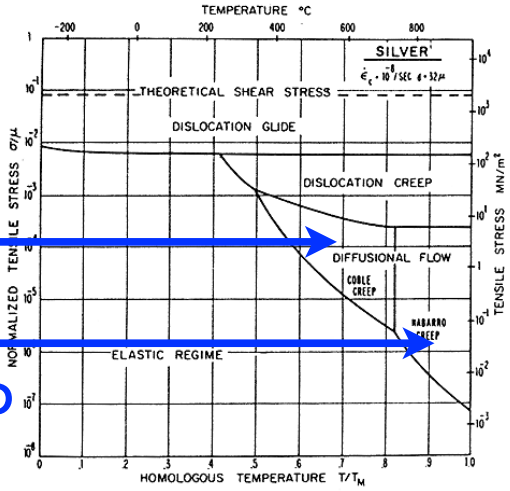

FIG. 1. A deformation–mechanism map for pure silver, of grain size 32 μ, and for a critical strain rate $\dot{\varepsilon}_c$ of 10^{-8}/sec.

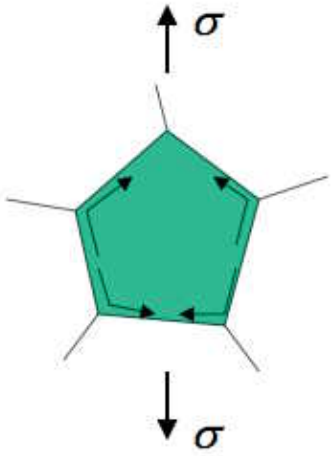

$$\dot{\varepsilon}_C = A\frac{\delta D_{GB}}{d^3}\frac{\sigma\Omega}{kT}$$

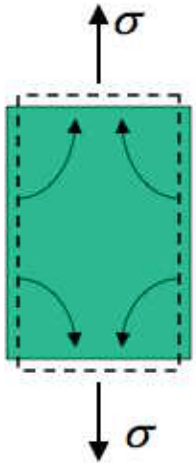

$$\dot{\varepsilon}_{NH} = A\frac{D}{d^2}\frac{\sigma\Omega}{kT}$$

Deformation Mechanism Map

Ashby, M.F. (1972)
A first report on deformation mechanism maps.
Acta Met. 20, 887-897.

5 Dislocation creep

dislocation creep

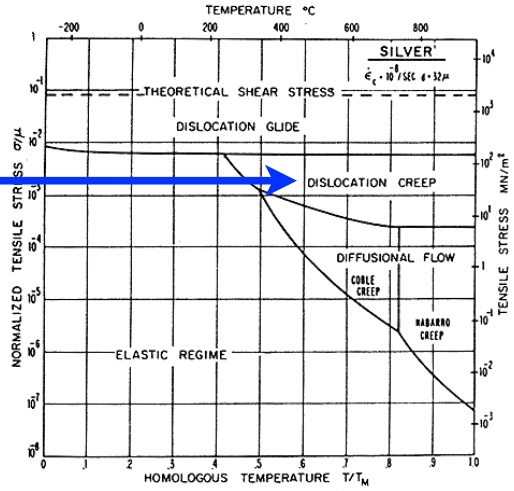

FIG. 1. A deformation–mechanism map for pure silver, of grain size 32 μ, and for a critical strain rate $\dot{\varepsilon}_c$ of 10^{-8}/sec.

$$\dot{\varepsilon}_5 = A \frac{D_v \mu b}{kT} \left(\frac{\sigma}{\mu}\right)^n$$

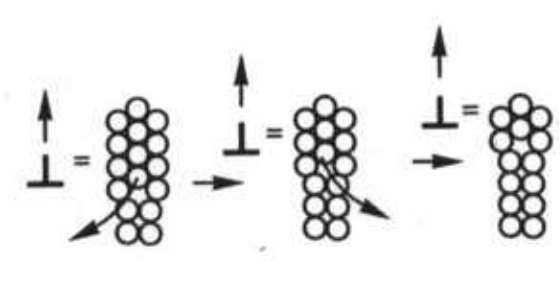

$$\dot{\varepsilon}_D = A \frac{DGb}{kT} \left(\frac{\sigma}{G}\right)^n$$

Mechanical data for nonobtainium from experiments

STEP 1: derive flow stress from stress-strain plots for various temperatures and strain rates

NOTE:
The data presented in the following is for nonobtainium IX, i.e., not for the material used in terranauting...

Mechanical data for nonobtainium from experiments

Test at constant temperature (1200°C)

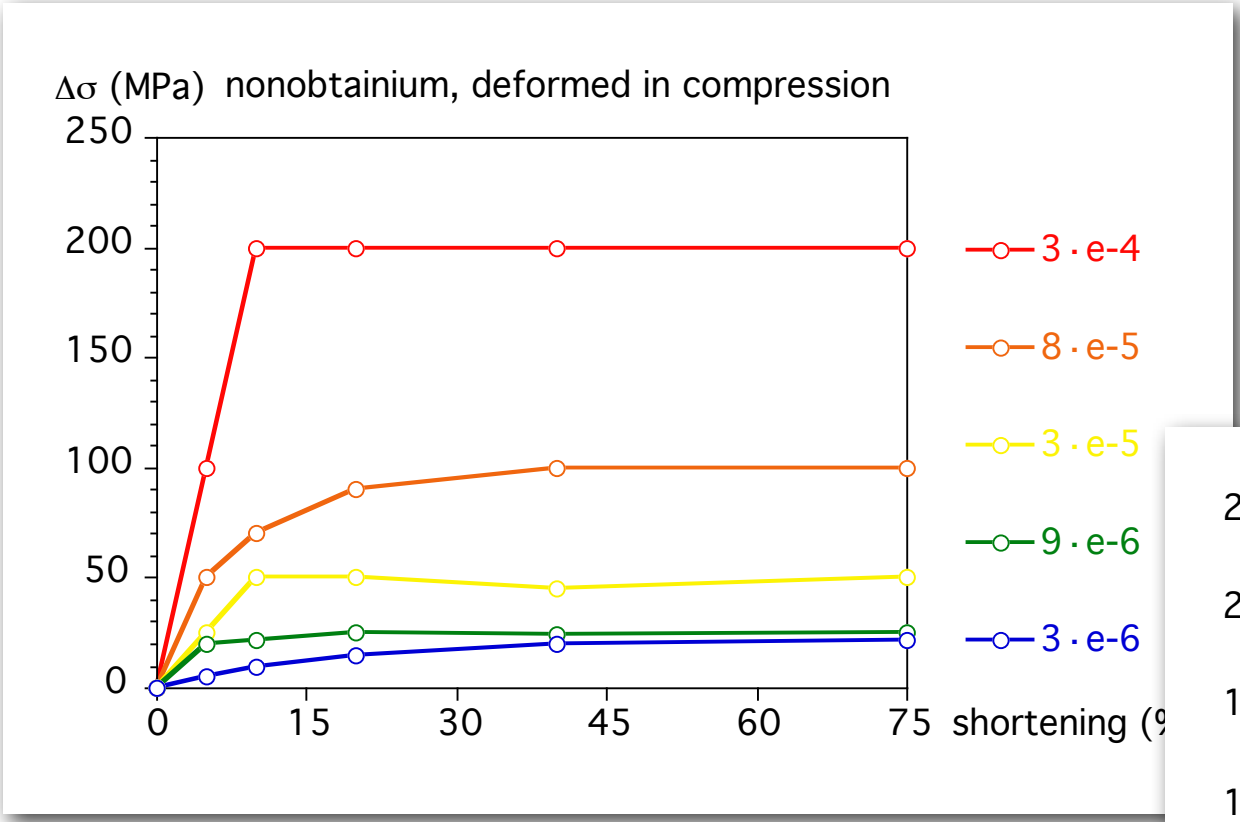

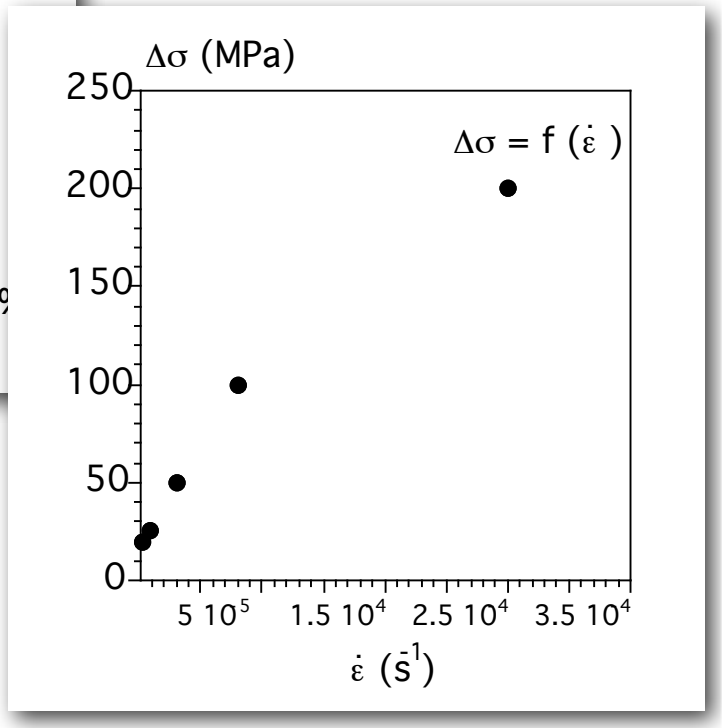

Mechanical data for nonobtainium from experiments

Test at constant strain rate ($3 \cdot 10^{-6} s^{-1}$)

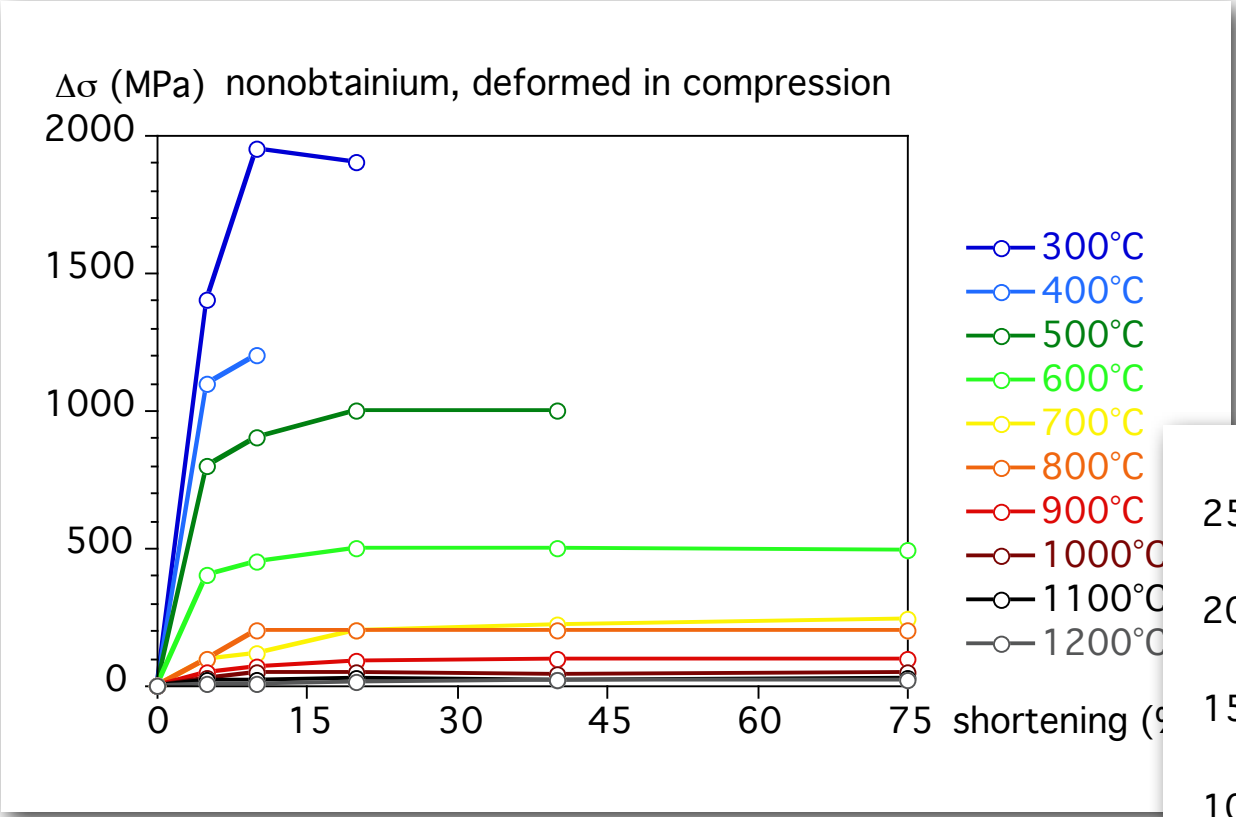

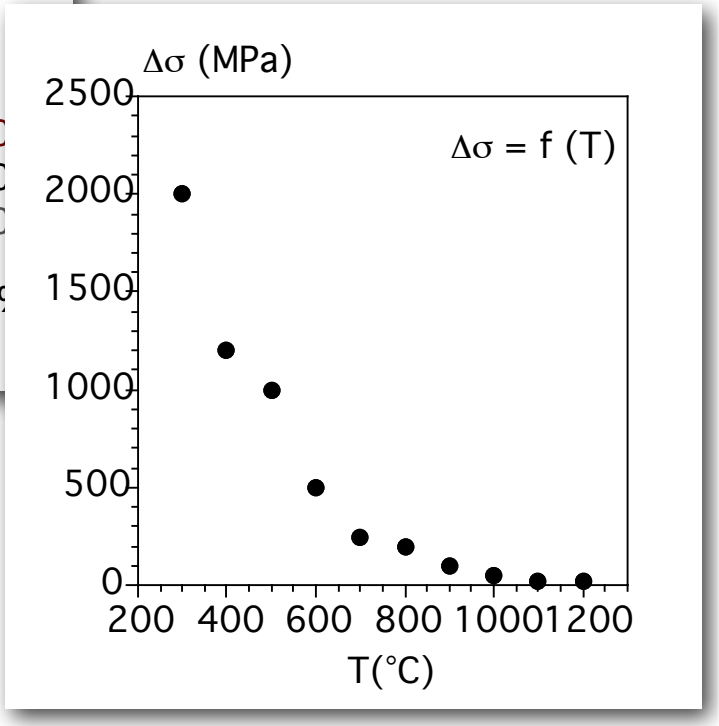

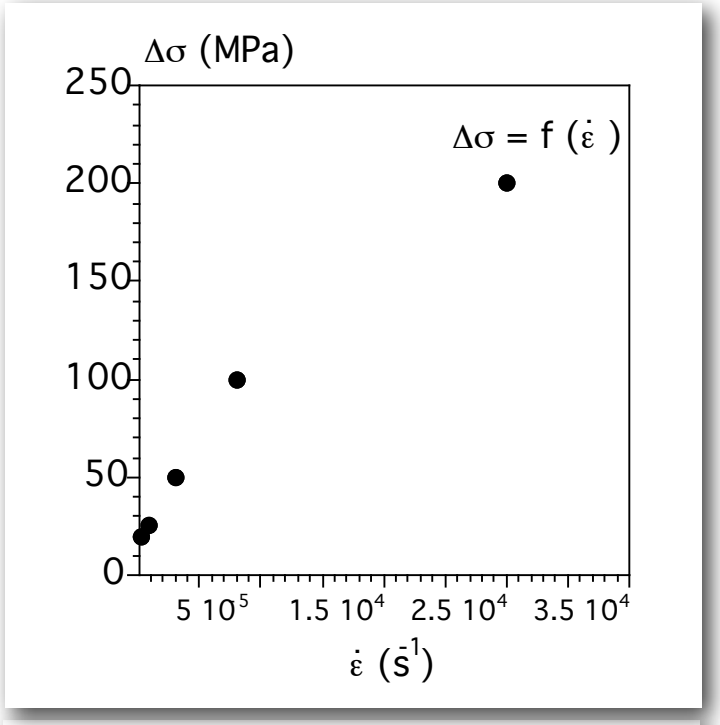

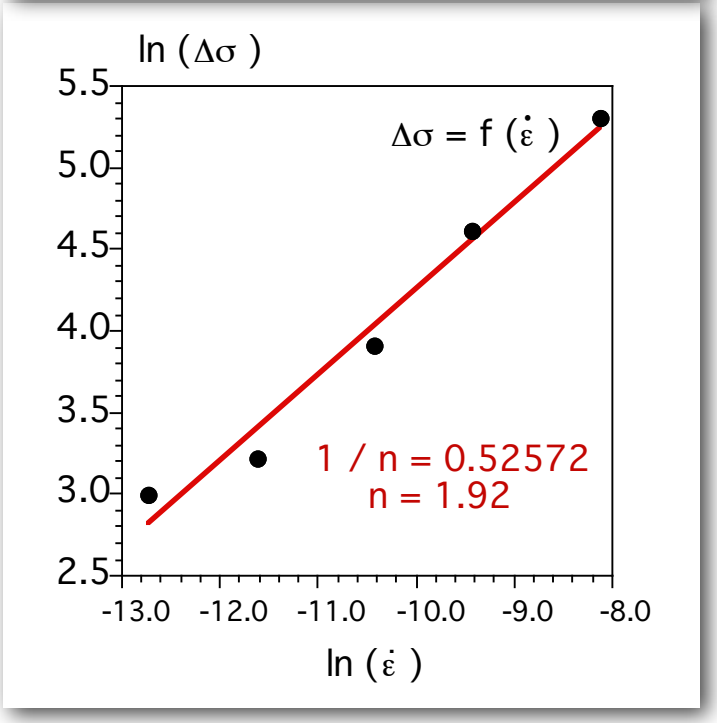

STEP 2:
Use log-log plots of steady state differential stress versus strain rate plots to derive stress exponent n (slope = 1/n)

ε	ln(ε)	Δσ(MPa)	ln Δσ
3. e-06	-12.717	20.00	2.9957
9. e-06	-11.618	25.00	3.2189
3. e-05	-10.414	50.00	3.9120
8. e-05	-9.4335	100.00	4.6052
3. e-04	-8.1117	200.00	5.2983

Test at constant temperature (1200°C)

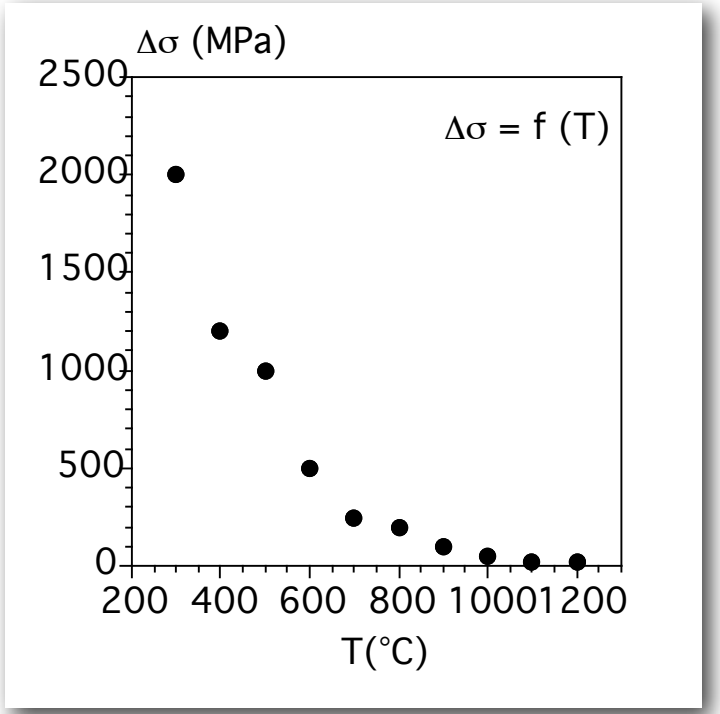

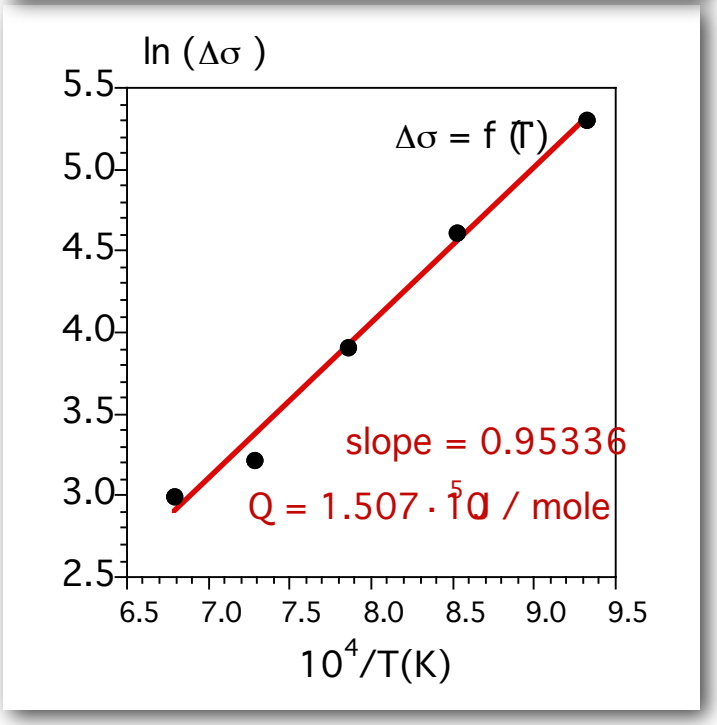

STEP 3:
Use Arrhenius plot of steady state differential stress vs. inverse temperature to obtain activation energy Q
(slope = $Q/n \cdot R$)

T(°C)	10000/T(K)	Δσ(MPa)	ln Δσ
1200.0	6.7889	20.00	2.9957
1100.0	7.2833	25.00	3.2189
1000.0	7.8555	50.00	3.9120
900.00	8.5251	100.00	4.6052
800.00	9.3197	200.00	5.2983

Test at constant strain rate ($3 \cdot 10^{-6}$ s^{-1})

STEP 4: Select appropriate flow law

exponential $\dot{\varepsilon} = A \cdot \exp(-Q / RT) \cdot \exp(\sigma / \sigma 0)$

power law $\dot{\varepsilon} = A \cdot \exp(-Q / RT) \cdot \sigma^n$

grain size sensistive $\dot{\varepsilon} = A \cdot \exp(-Q / RT) \cdot d^m \cdot \sigma^n$

$\dot{\varepsilon}$ = strain rate (s^{-1}),
Q = activation energy (kJ/mol),
R = Gas constant (8.314 J/ (molK))
T = temperature (K),
σ = flow stress (MPa),
d = grain size (µm)
n = stress expeonent (n>0),
m = grain size exponent (m<0)

exponential $\dot{\varepsilon} = A \cdot \exp(-Q / RT) \cdot \exp(\sigma / \sigma 0)$

power law $\dot{\varepsilon} = A \cdot \exp(-Q / RT) \cdot \sigma^n$

grain size sensistive $\dot{\varepsilon} = A \cdot \exp(-Q / RT) \cdot d^m \cdot \sigma^n$

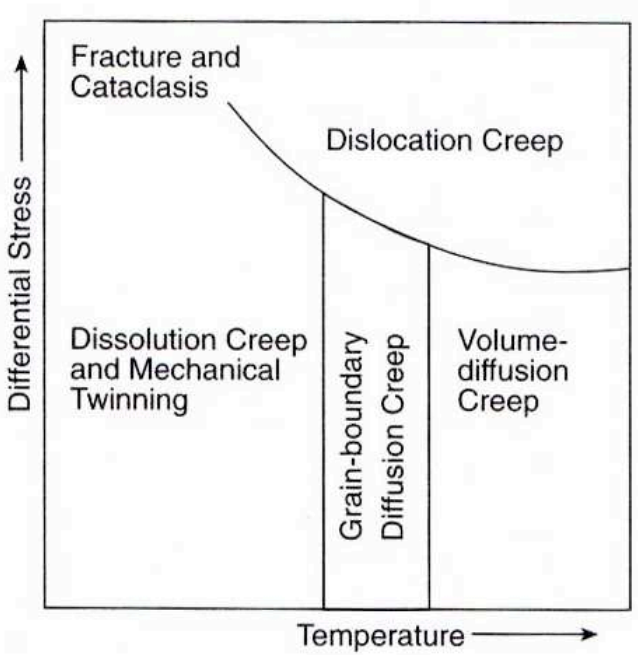

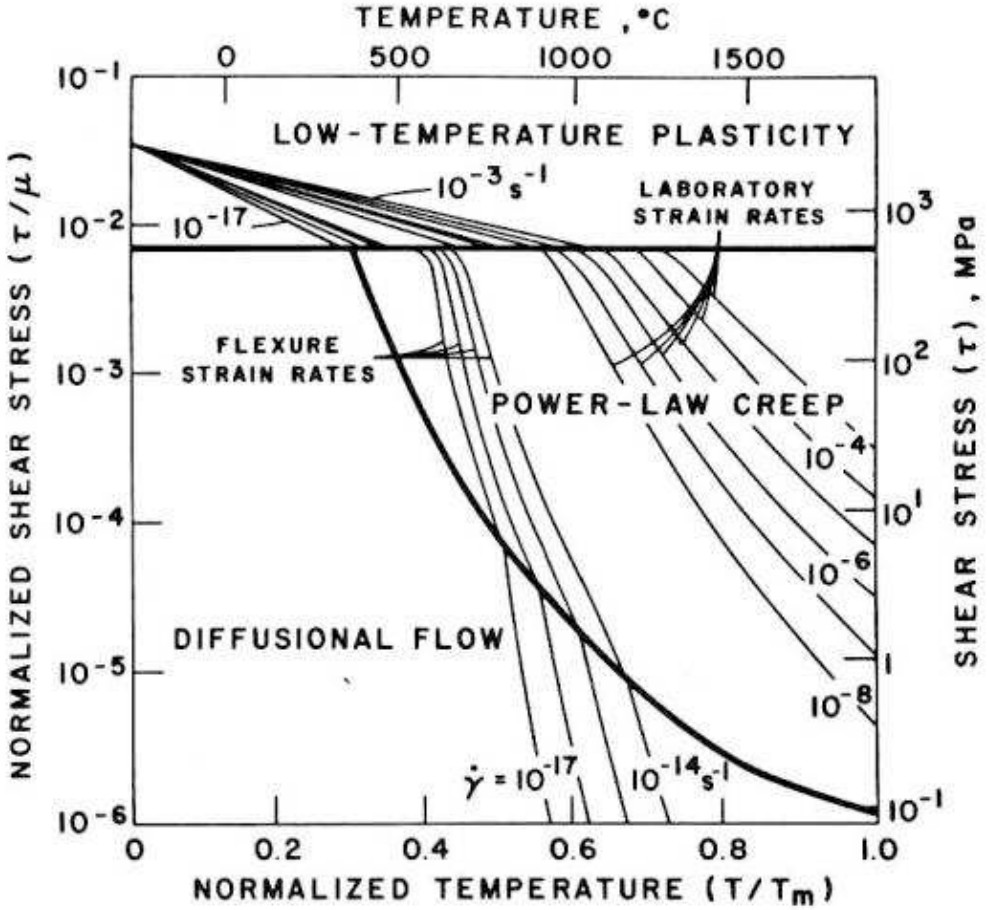

STEP 4: (Select appropriate data)

Wherever possible the shear modulus was calculated as

$$\mu = \sqrt{\tfrac{1}{2}c_{44}(c_{11} - c_{12})}$$

TABLE 2

	Peierls stress $\tau_p \times 10^9$ (dyn/cm²)	Activation energy for kink nucleation $u_k \times 10^{12}$ (eV)	Preexponential factor $\dot{\gamma}_0'$ (/sec)	References
Molybdenum	4.13	0.62	10^4	4
Tantalum	3.34	0.31	10^4	4
Tungsten	4.1	0.6	10^4	*
α-iron	4.5	0.31	10^4	4

* No data available. Data for molybdenum used for tungsten calculation.

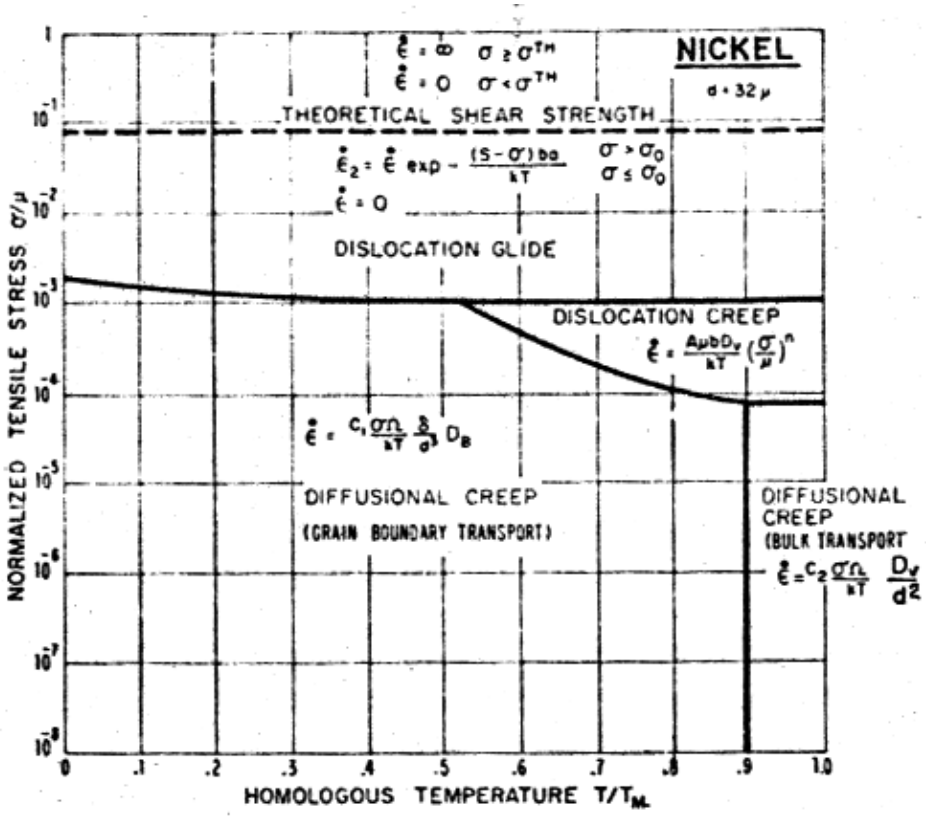

FIG. 2. Mechanism fields for pure nickel with a grain size of 32 μ. The fields are labeled with the appropriate constitutive equation. Field boundaries are obtained by equating constitutive equations.

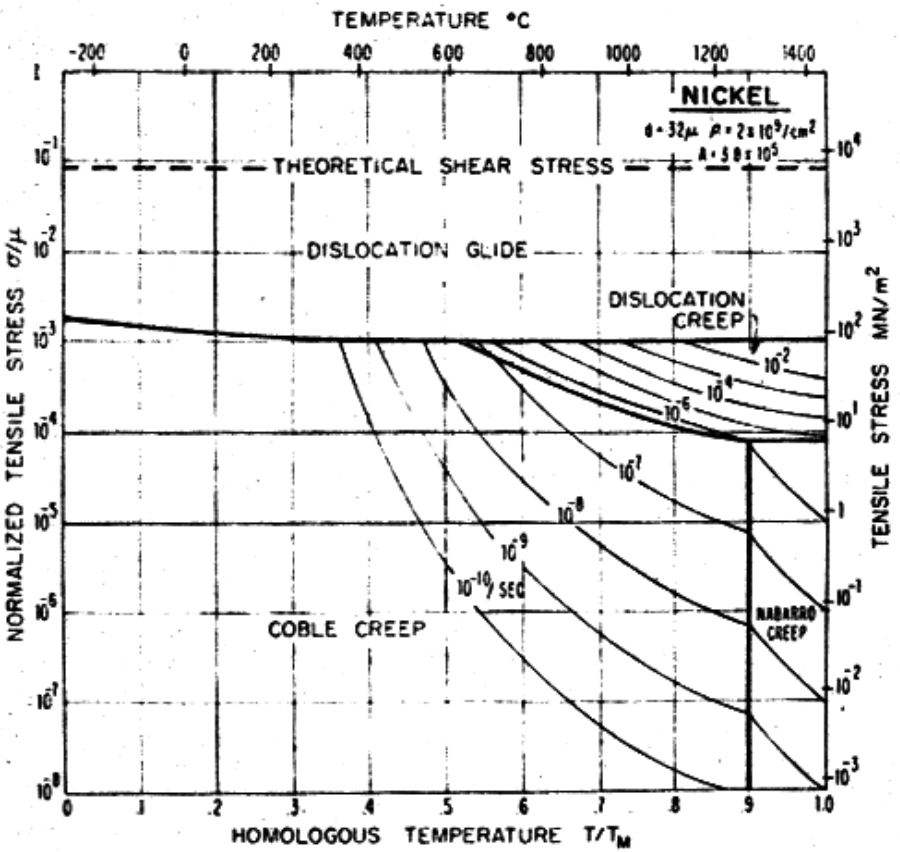

FIG. 3. A complete map for pure nickel with a grain size of 32 μ.

STEP 5: Plot files

Use GnuPlot and "Non.dem" and "DataNon"
Start gnuplot and type: load "Non.dem"
Open "DataNon" in an editor and test influence of Q, n, A and m by changing the values.
Obtain different plots by permutating the plot-blocks in "Non.dem"

```
#------Plotting block 1¬
¬
plotΔ    r1(x,per6) with l -1,\¬
Δ    r2(x,per6) with l 0,\¬
Δ    r3(x,per6) with l 1,\¬
Δ    r4(x,per6,pd) with l 2,\¬
        test1a23(x,per6) with l 3,\¬
Δ    test1a24(x,per6,pd) with l 9¬
```

```
#------Creating output------¬
¬
#set terminal postscript eps¬
#set terminal postscript color¬
#set output "output.eps"¬
#replot¬
¬
reset
```

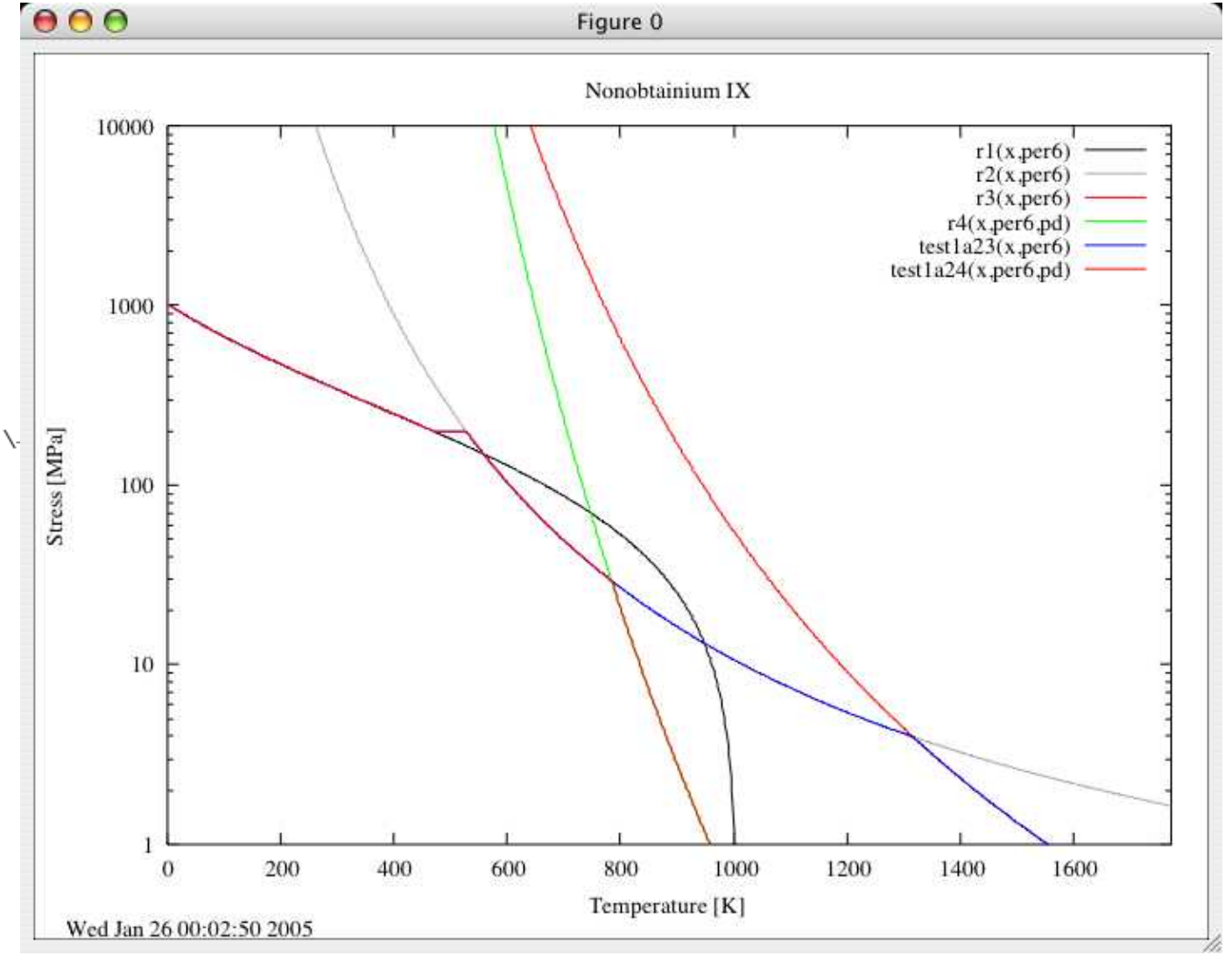

```
#------Plotting block 3¬
¬
plotΔ     test1a23(x,per3) with l 3,\¬
Δ    test1a24(x,per3,pd) with l 3,\¬
Δ     test1a23(x,per6) with l 4,\¬
Δ    test1a24(x,per6,pd) with l 4,\¬
Δ     test1a23(x,per9) with l 5,\¬
Δ    test1a24(x,per9,pd) with l 5,\¬
Δ     test1a23(x,per12) with l 6,\¬
Δ    test1a24(x,per12,pd) with l 6,\¬
Δ     test1a23(x,per15) with l 7,\¬
Δ    test1a24(x,per15,pd) with l 7
    ¬
```

```
#------Creating output------¬
¬
#set terminal postscript eps¬
#set terminal postscript color¬
#set output "output.eps"¬
#replot¬
¬
reset
```

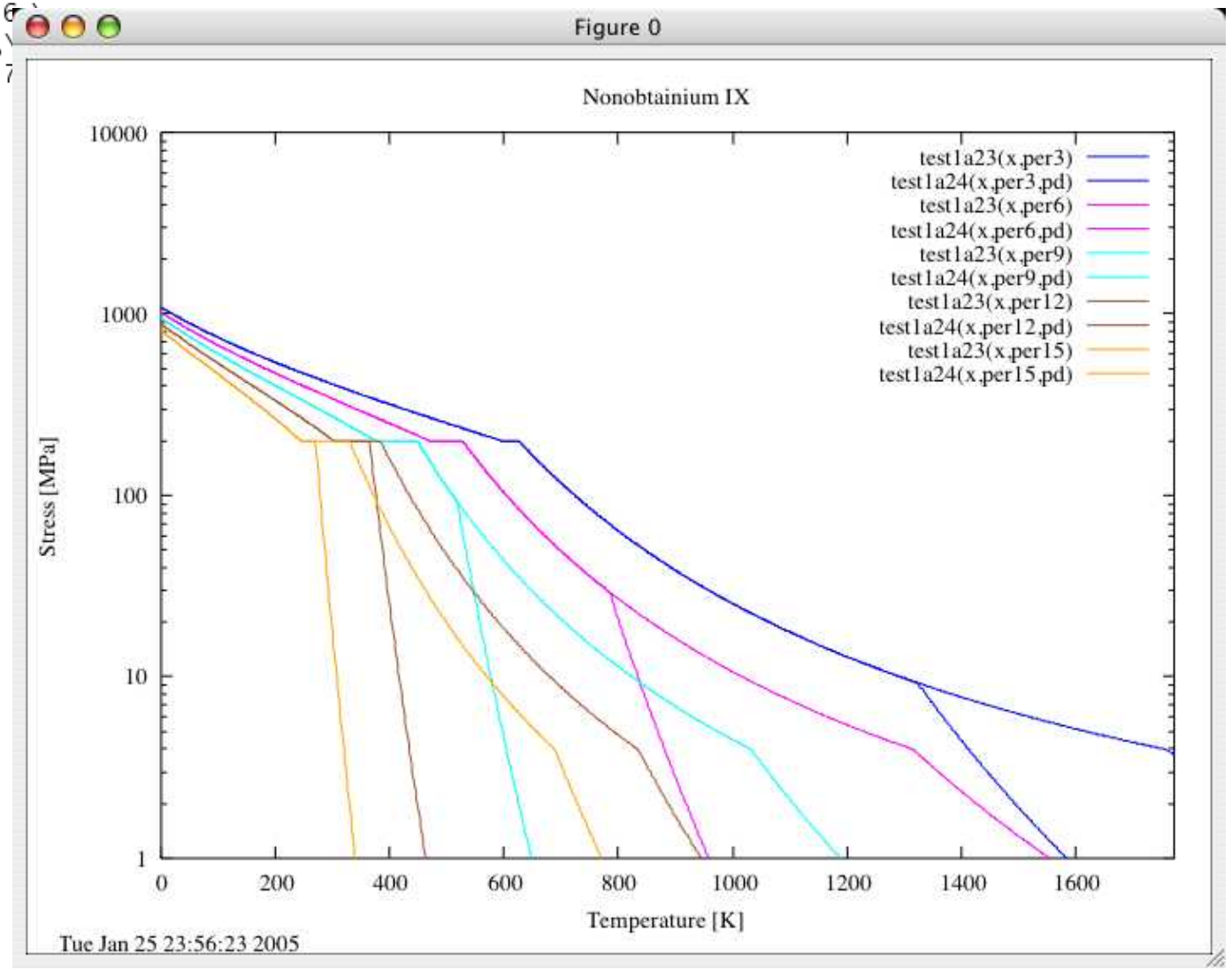

influence of grain size

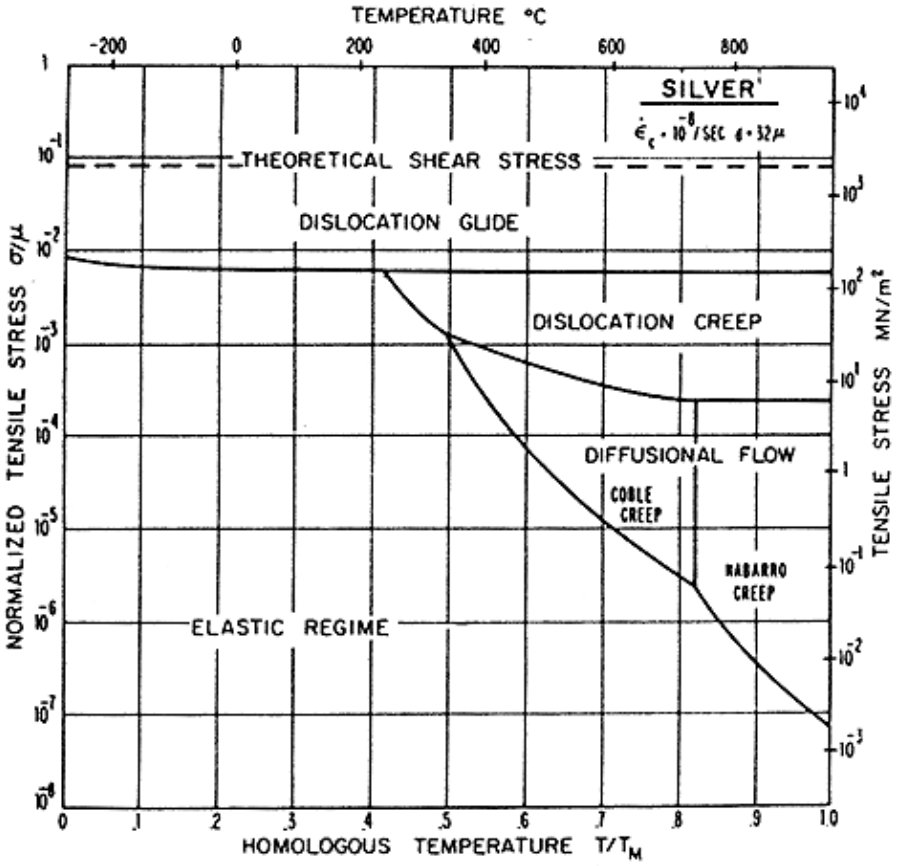

FIG. 1. A deformation–mechanism map for pure silver, of grain size 32 μ, and for a critical strain rate $\dot{\epsilon}_c$ of 10^{-8}/sec.

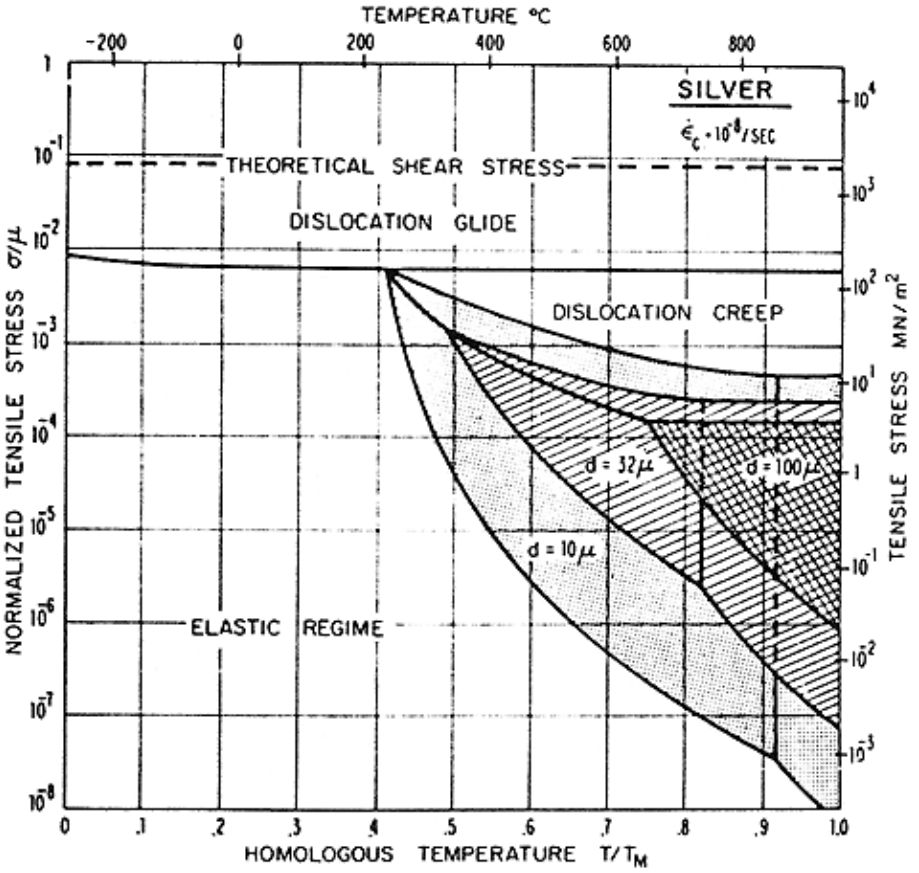

FIG. 6. Changing the grain size d, expands or contracts the diffusional-flow fields. It also has a small effect on the dislocation glide field (not shown).

Ashby, M.F., (1972) A first report on deformation mechanism maps, Acta Met., 20, 887

pressure solution

	Deformation-rate		Factor (geometry or proportionality)	Thermodynamic term	Grainsize term	Filmthickness Grainboundary-width	Diffusion coefficient	Stress
Nabarro (1948)	$\frac{dS}{dt}$	=	$K \propto$	$\frac{a^3}{kT}$	$(A)^{-2}$		D	P
Coble (1963)	$\dot{\varepsilon}$	=	148	$\frac{\Omega}{kT}$	$(GS)^{-3}$	w	D_b	σ
Elliott (1973)	$\dot{\varepsilon}_{gb}$	=	$K \bar{\pi}$	$\frac{\Omega}{kT}$	$(X)^{-3}$	$h \left(\frac{a}{b}\right)^{3/2}$	D_{gb}	σ
Rutter (1976)	$\dot{\varepsilon}$	=	$32 \frac{C}{\rho}$	$\frac{V}{RT}$	$(d)^{-3}$	w	D_b	σ_a
Weyl (1959)	$\frac{d\zeta}{dt}$	=	$\frac{32}{\pi} b$		$(a)^{-3}$	$\frac{m}{\rho^4}$	D	Σ

pressure solution

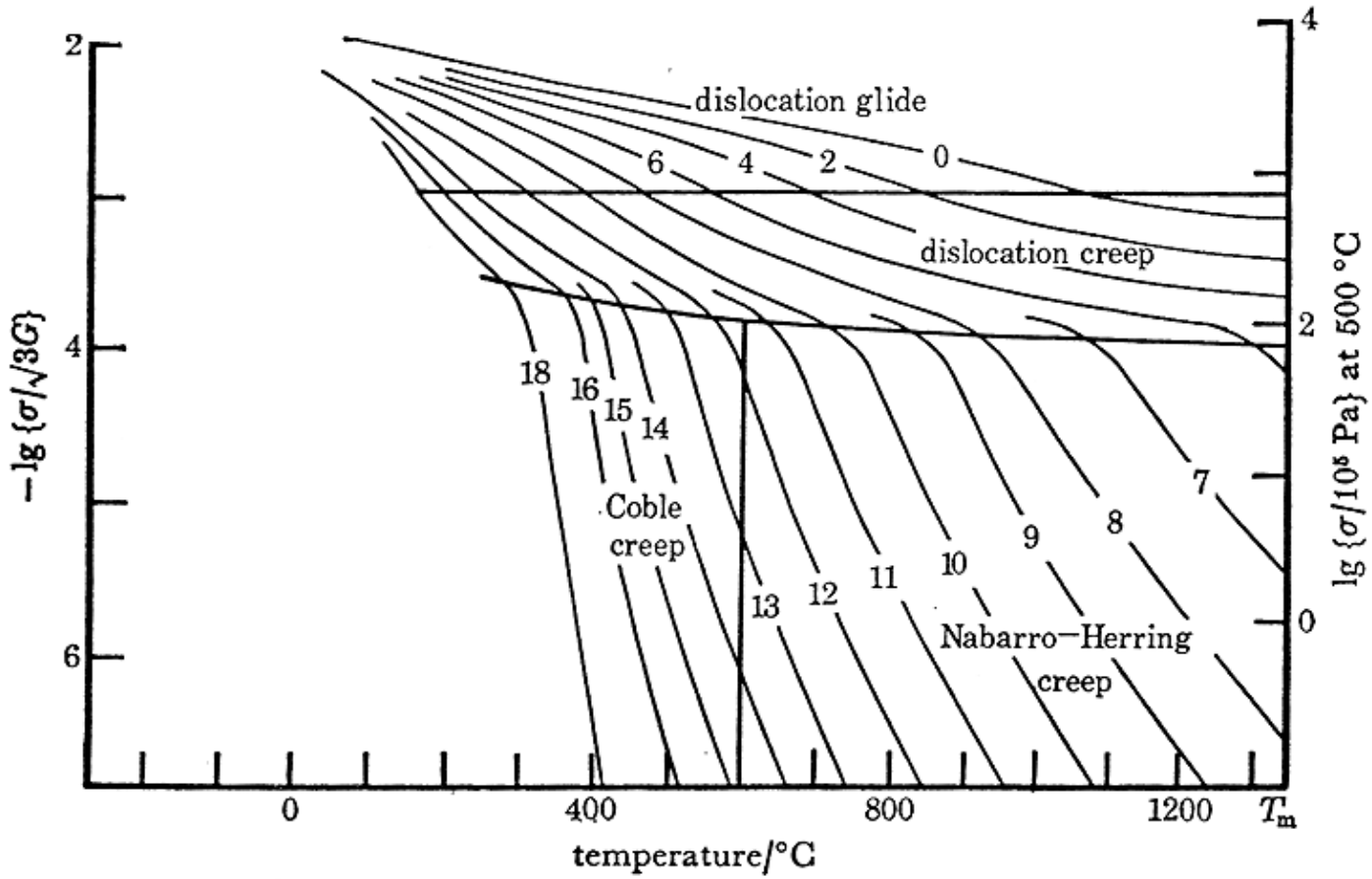

Deformation mechanism map for calcite without pressure solution. Contours of $-\lg$ strain rate are shown. σ is differential stress $(\sigma_{11}-\sigma_{33})$. $d = 100\ \mu\mathrm{m}$; $V = 37\ \mathrm{cm}^3$.

Rutter, E.H., (1976) The kinetics of rock deformation by pressure solution, Phil. Trans. R. Soc. Lond., A, 283, 203-219

pressure solution

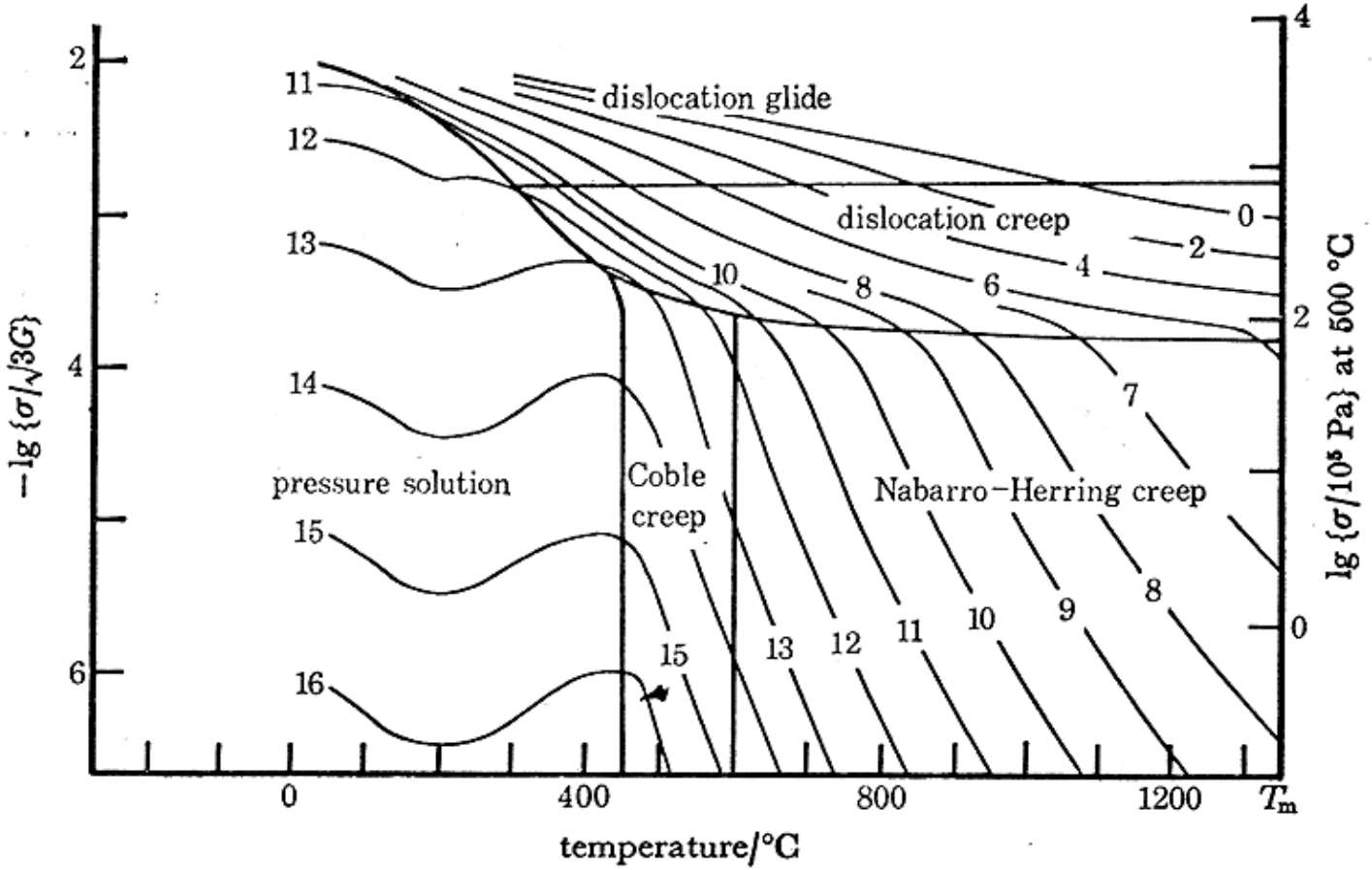

Deformation mechanism map for calcite modified by the addition of a pressure solution field. $d = 100\ \mu m$; $V = 37\ cm^3$.

Deformation Mechanism Map

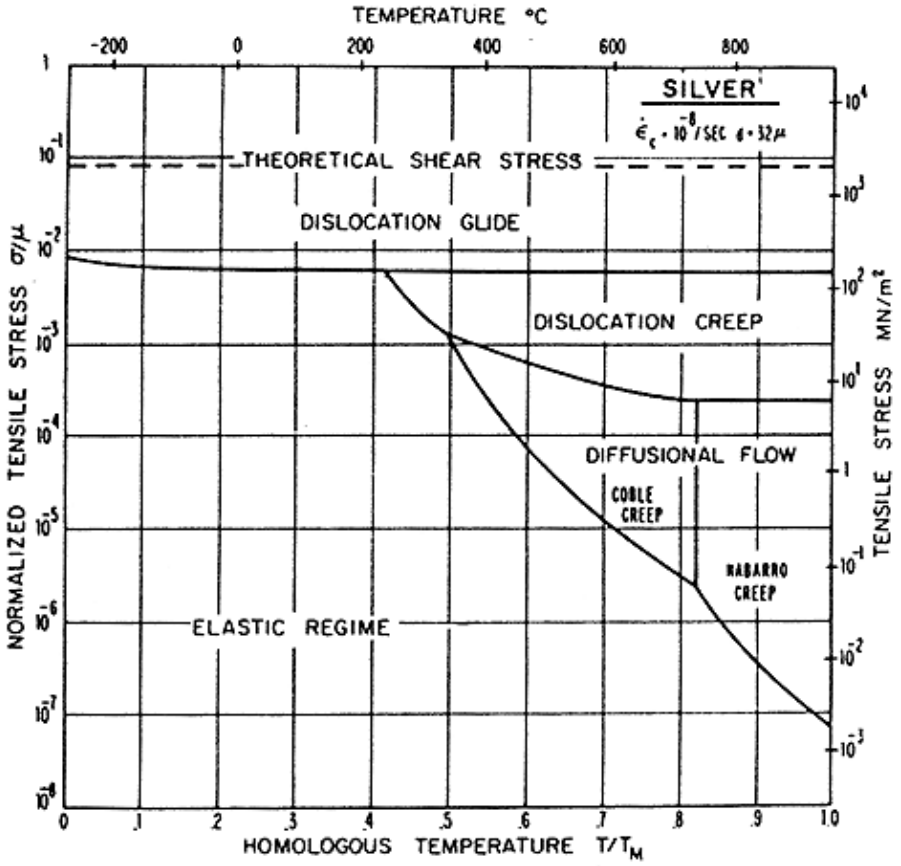

FIG. 1. A deformation–mechanism map for pure silver, of grain size 32 μ, and for a critical strain rate $\dot{\epsilon}_c$ of 10^{-8}/sec.

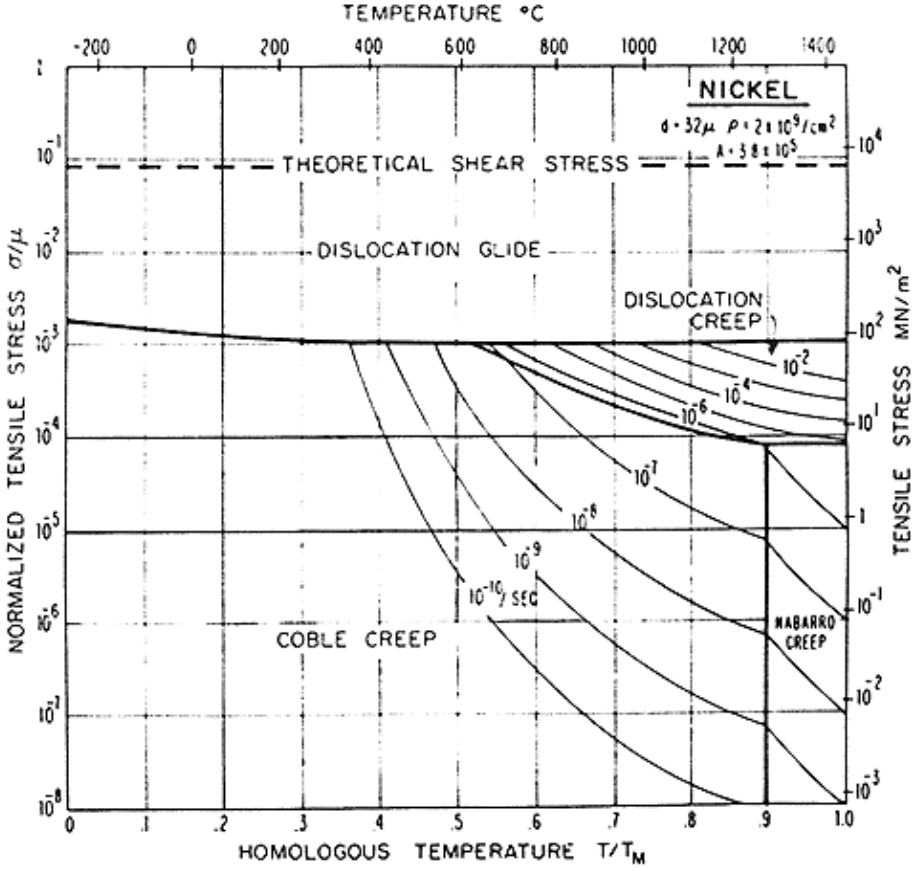

FIG. 3. A complete map for pure nickel with a grain size of 32 μ.

Deformation Mechanism Map

1-For high stress regime

exponential flow law $\dot{\varepsilon} = A \cdot \exp(Q / RT) \cdot \exp(\sigma / \sigma 0)$

$\sigma 0 = 100.0 \quad \sigma = 100.0$

$Q = 50000.0$

$A = 10^4$

$T = 400 - 1200K$

$\dot{\varepsilon}$ c4=10^4*exp(50000/(8.314*c0))*exp(1)

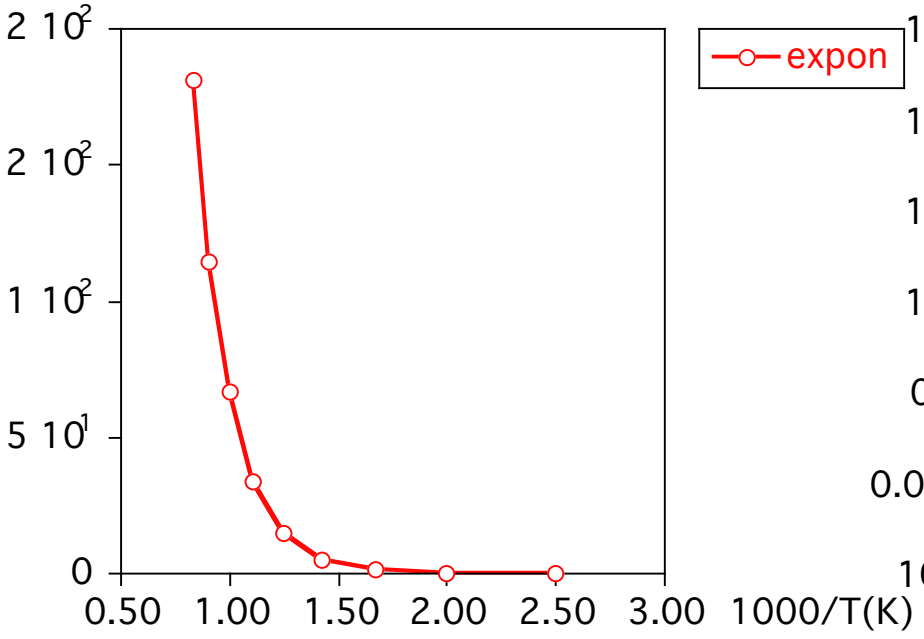

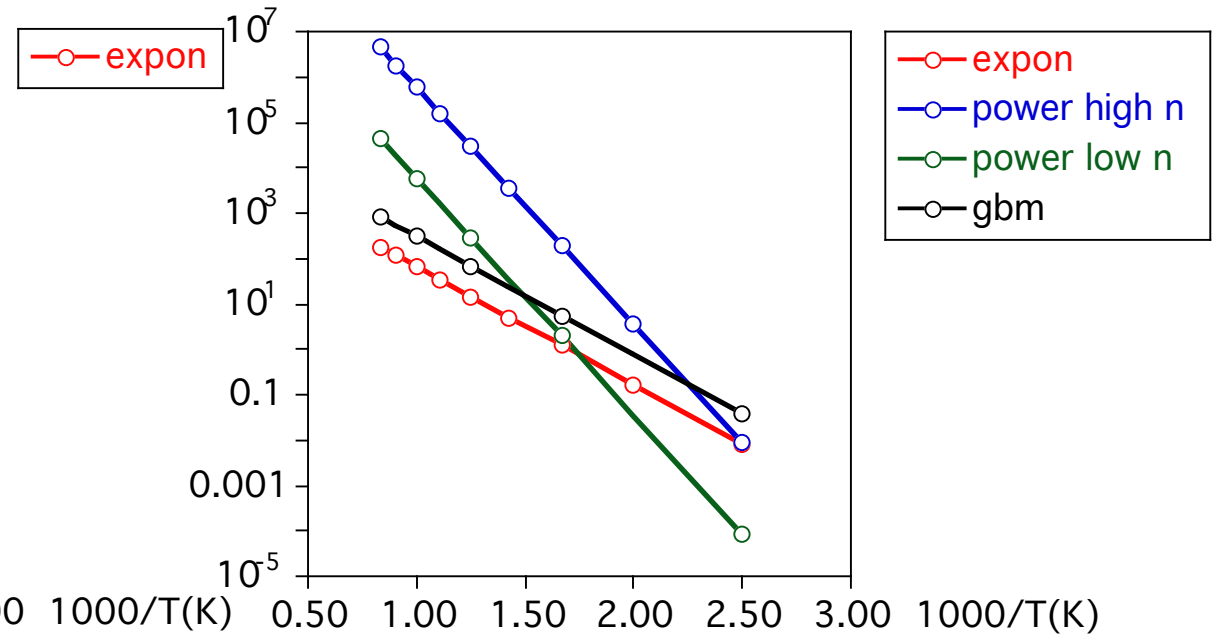

Deformation Mechanism Map

2-For intermediate stress regime
power law with high n value

$$\dot{\varepsilon} = A \cdot \exp(-Q / RT) \cdot \sigma^n$$

n = 8.0

Q = 100000.0 σ = 100.0

A = 10^{-5}

T = 400 - 1200K

$\dot{\varepsilon}$ c1=10^-5*exp(-100000/(8.314*c0))*100^8

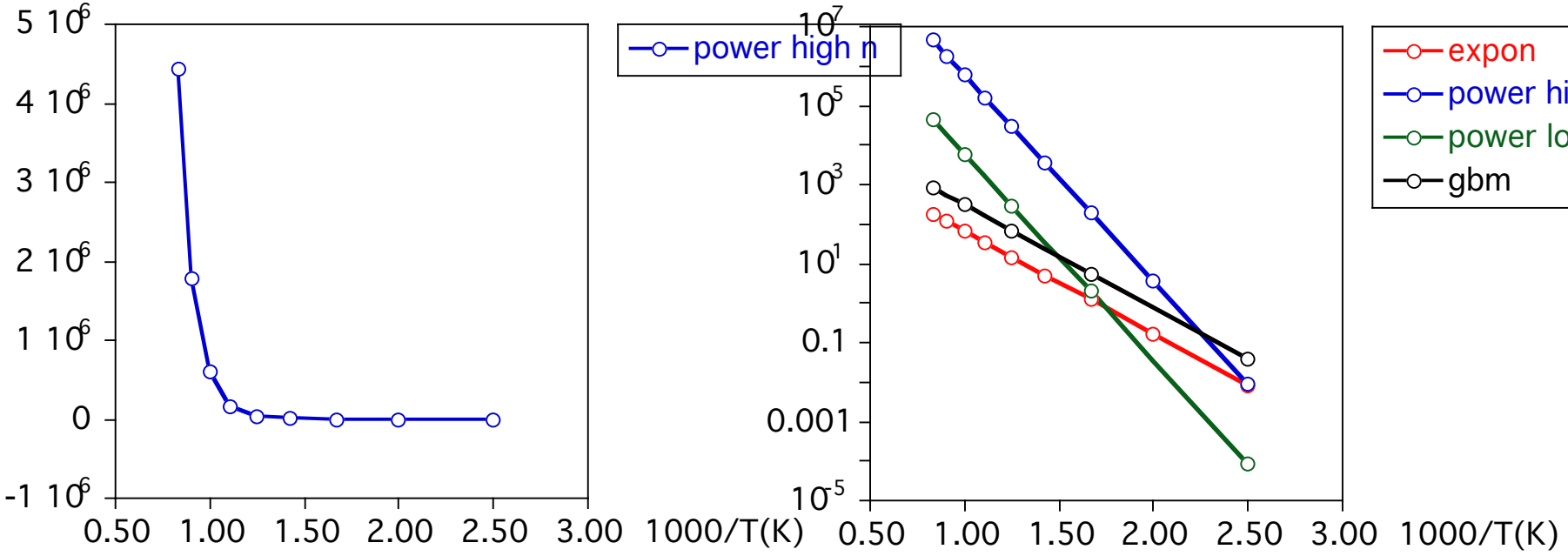

Deformation Mechanism Map

3-For low stress regime
power law with low n value
n = 3.0
Q = 100000.0 σ = 100.0
A = 10^3
T = 400 - 1200K

$$\dot{\varepsilon} = A \cdot \exp(-Q / RT) \cdot \sigma^n$$

$\dot{\varepsilon}$ c2=10^3*exp(-100000/(8.314*c0))*100^3

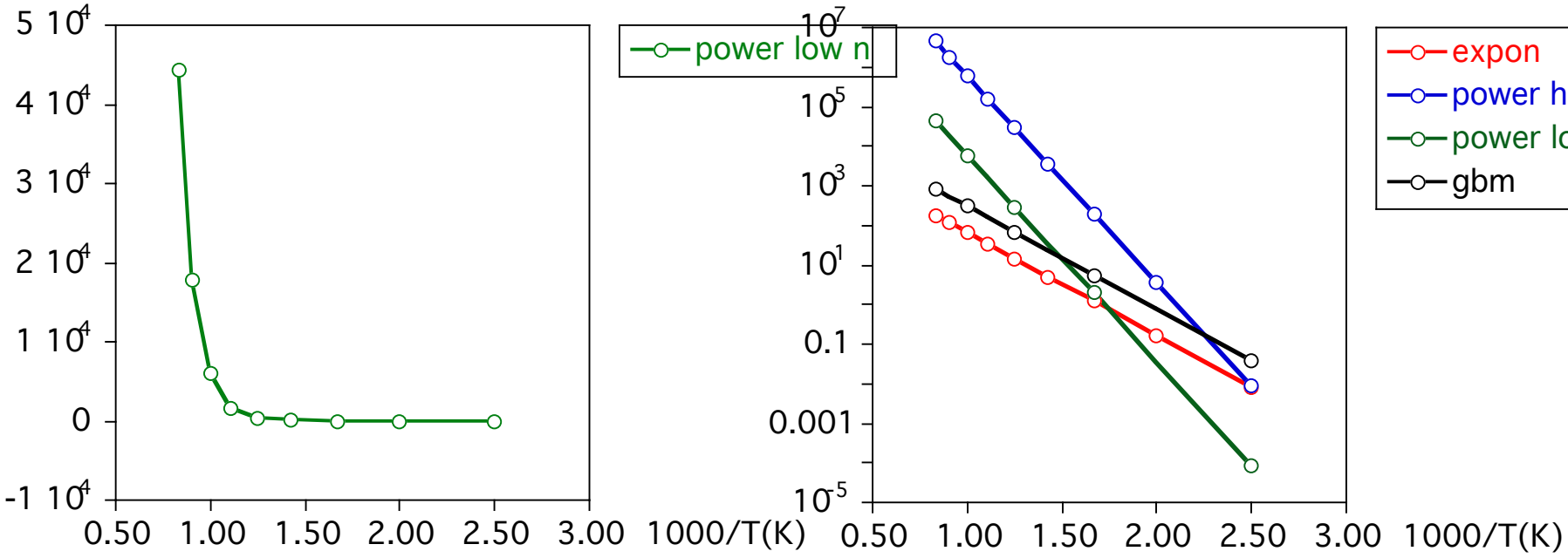

Deformation Mechanism Map

4-For grain site sensitive flow
powerlaw with $\dot{\varepsilon} = A \cdot \exp(-Q / RT) \cdot d^{m} \cdot \sigma^{n}$
very low n value (n=1.0), grain size dependence m=-3.0 d=2
Q = 50000.0 σ = 100.0
A = 10^{-5}
T = 400 - 1200K
$\dot{\varepsilon}$ c3=10^4*exp(-50000/(8.314*c0))*100*2^-3